SCCER SoE

SWISS COMPETENCE CENTER for ENERGY RESEARCH
SUPPLY of ELECTRICITY

SCCER-SoE Science Report

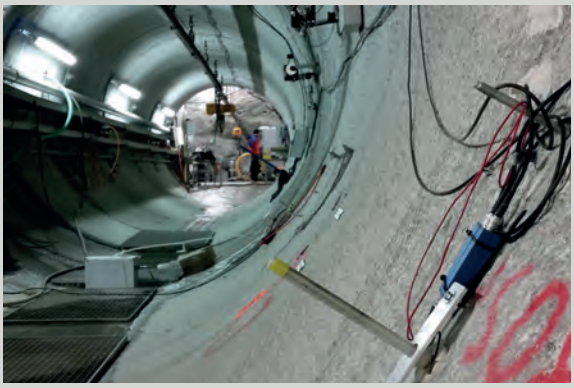

2017

In cooperation with the CTI

Energy funding programme
Swiss Competence Centers for Energy Research

Schweizerische Eidgenossenschaft
Confédération suisse
Confederazione Svizzera
Confederaziun svizra

Swiss Confederation

Commission for Technology and Innovation CTI

Imprint

Editor

Swiss Competence Center for Energy Research – Supply of Electricity (SCCER-SoE)

Address

SCCER-SoE
Gianfranco Guidati & Ueli Wieland
c/o ETH Zurich
Sonneggstrasse 5
8092 Zurich

Website

www.sccer-soe.ch

Copyright Cover Pictures

Hydropower (left): AEW Energie AG
Geo-energy (right): ETH Zurich

Date of Issue

28 September 2017

Content

Editorial

The Swiss Competence Center for Energy Research – Supply of Electricity (SCCER-SoE) has been established in 2013 to ensure that the academic community works closely with industry to provide the required research advancement, develop innovative technologies and robust solutions, and ultimately ensure the future provision of electricity and energy to the Swiss country and the transition to a competitive carbon-free economy.

The specific targets are geo-energies and hydropower, the two resources identified by the Energy Strategy 2050 to provide a substantial band-electricity contribution to enable the exit from nuclear power, with the target of up to 7 % electricity production from deep geothermal energy and a 10 % increase of hydropower production.

The SCCER-SoE initiated in 2017 its second implementation phase. About 260 scientists, engineers, researchers, doctoral and master students and professors are now associated to the SCCER-SoE, working together in inter-disciplinary projects to realize the identified innovation roadmap. Among these, over 95 doctoral students are now working in the SCCER-SoE, providing a substantial component of the future capacity building of Switzerland.

The SCCER-SoE Annual Conference 2017, held on 14 and 15 September at the WSL in Birmensdorf, aimed at providing a comprehensive overview of the R&D conducted by the SCCER-SoE and its associated projects, and to confront the scientific agenda with the needs and views of stakeholders from industry, public institutions, federal offices and policy makers.

Nearly 140 posters were presented and discussed at the conference, covering all aspects of the scientific portfolio of the SCCER-SoE. These posters are collected in this volume and presented according to the work packages and tasks to which they are associated.

These are exciting times for energy research in Switzerland. The Energy Law 2016 has been confirmed by the public referendum, providing the basis for the implementation of the Energy Strategy 2050. The SCCER-SoE will continue with the development of integrative solutions, testing and installation of innovative technologies, technology assessment and scenario modelling.

In the second phase, we are expanding the overall R&D portfolio, with a wider perimeter for geo-energies, adding new targets on usage of hydrothermal resources for direct heating and heat storage; a refocusing of the hydropower area with four tasks and five key overarching targets; a clearer innovation agenda, now including innovative technologies and computational energy innovation; a more integrated approach to the future supply of electricity, with an expanded scope of the risk assessment activities and of the evaluation of global electricity resources and technologies, new resources and a closer integration with the SCCER CREST on the socio-economic-political drivers of electricity supply, and two new SCCER Joint Activities, on Scenario and Modeling and on Socio-political conditions of the extension of hydropower and geothermal energy. Finally, we are expanding the focus on pilot and demonstration projects, conducted with industry partners, to validate the technologies and proposed solutions; seven pilot and demonstration projects are now pursued, covering the whole portfolio of technologies and energy sources of the SCCER-SoE.

The Annual Conference 2017 shows a vibrant and integrated scientific community, and the scientific level of the presentations proves that we are on the good way to complete the implementation of the geo-energy and hydropower R&D roadmaps.

We look forward to the future progress of our program!

Domenico Giardini
Head of the SCCER-SoE

Work Package 1: Geo-energies

To enable the large-scale exploitation of deep geothermal energy for electricity generation in Switzerland, solutions must be found for two fundamental and coupled problems: (a) How do we create an efficient heat exchanger in the hot underground that can produce energy for decades while (b) at the same time keeping the nuisance and risk posed by induced earthquakes to acceptable levels?

There is general agreement that only by enhancing the permeability of the underground in a controlled way, can these goals potentially be met. In the Geo-energies Roadmap we showed that in order to make progress in answering these questions as rapidly as possible without compromising safety three overarching and complementary approaches need to be tackled by the SCCER-SoE:

- Advance the capability to quantitatively model the stimulation process and reservoir operation
- Advance stimulation process understanding and validation in underground lab experiments
- Develop petrothermal P&D projects

For Phase II, strong focus was put on working towards pilots and demonstrators. Since petrothermal P&D projects continue to be delayed due to appeals and the effects of an unfavorable market environment, we directed a large effort towards accelerating stimulation process understanding and validation via underground lab experiments, in order to at least partially compensate for the lack of P&D data. Additional partial compensation for the lack of petrothermal P&D, with direct involvement in actual project development and implementation, results from the new activity on seasonal high temperature heat storage and direct heat production. In close collaboration with industrial partners in the Geneva area, we work on this novel technology to reduce CO_2 emissions from the domestic heating sector, which will also give us direct access to perform research in wells to be drilled within the next few months.

Last but not least we also progressed on the third option to utilize the underground in support of the Energy Strategy 2050, namely the sequestration of CO_2. ELEGANCY, a SFOE funded P&D project, embedded in a larger European framework, has the mission to provide clean hydrogen for heat and mobility based on steam-methane-reforming. CO_2 storage is an essential part of this concept. Underground experiments at the Mt Terri Lab will study the potential CO_2 migration through a fault in the caprock and the effects of fault activation. This is complemented by lab experiments on rock samples, modelling of injection and CO_2 migration and the identification of suitable regions in the Swiss sedimentary basin.

Highlights 2017

Deep Underground Laboratory Experiment at Grimsel Test Site completed

Two hydraulic stimulation experimental campaigns were successfully performed (hydro-shearing in February 2017, hydro-fracturing in May 2017). The key goal was to generate high-quality data on the interacting physical processes during stimulation, in order to provide the basis for a more rigorous understanding and engineering of the stimulation process. It is widely believed that this experiment has been the by far most detailed, best instrumented, and most comprehensive of its kind to date. Extensive pre-experiment characterization of the rock volume provided an accurate and comprehensive baseline data set that has been missing for most other experiments and pilots. This formed the basis for both a risk assessment study and for experiment planning. Among the experimental highlights are (a) recorded magnitudes of micro-seismicity during the experiment were well below the estimated worst case magnitudes from the risk study, (b) permeability was successfully stimulated by orders of magnitude in all structures, and (c) first preliminary interpretations show significant innovation potential, e.g., for remote fluid pressure propagation monitoring using seismic wave velocities.

Geneva heat storage and utilization project enters the exploration phase

The SCCER-SoE's partner University of Geneva has been heavily involved in the prospection phase of Geneva's "Geothermie 2020" program that now enters a concrete exploration phase with the first well to be drilled within fall of 2017. This program enables us to participate in all phases of geothermal project development from prospecting through resource assessment to possible implementation. Although entirely being designed towards heat storage and utilization, we consider this as a unique "stepping stone" opportunity for preparing for deep geothermal power pilot and demonstration projects.

Overall progress

Our portfolio of individual projects and clusters of projects continues to make significant progress with many smaller "highlights". As examples this includes: innovative numerical methods to assess the seismic properties of fractured rock masses as a possible future tool for exploration (UniL & USI); theoretical and experimental progress on quantifying hydraulic stimulation processes (new APs at EPFL plus ETHZ, UniNE, USI); quantification of thermal anomalies associated with flow in fracture zones and linking this to geologic and geophysical parameters, at an analogue site at Grimsel pass and in numerical simulation (UniBE & UniL); on-track progress in building, maintaining, and filling the novel geodata-infrastructure, including a new initiative to update the Swiss heat flow map (swisstopo with ETHZ and regional partners); participation in the new ACT/H2020 project ELEGANCY as a means for stronger support of research towards CCS technologies in Switzerland (various partners).

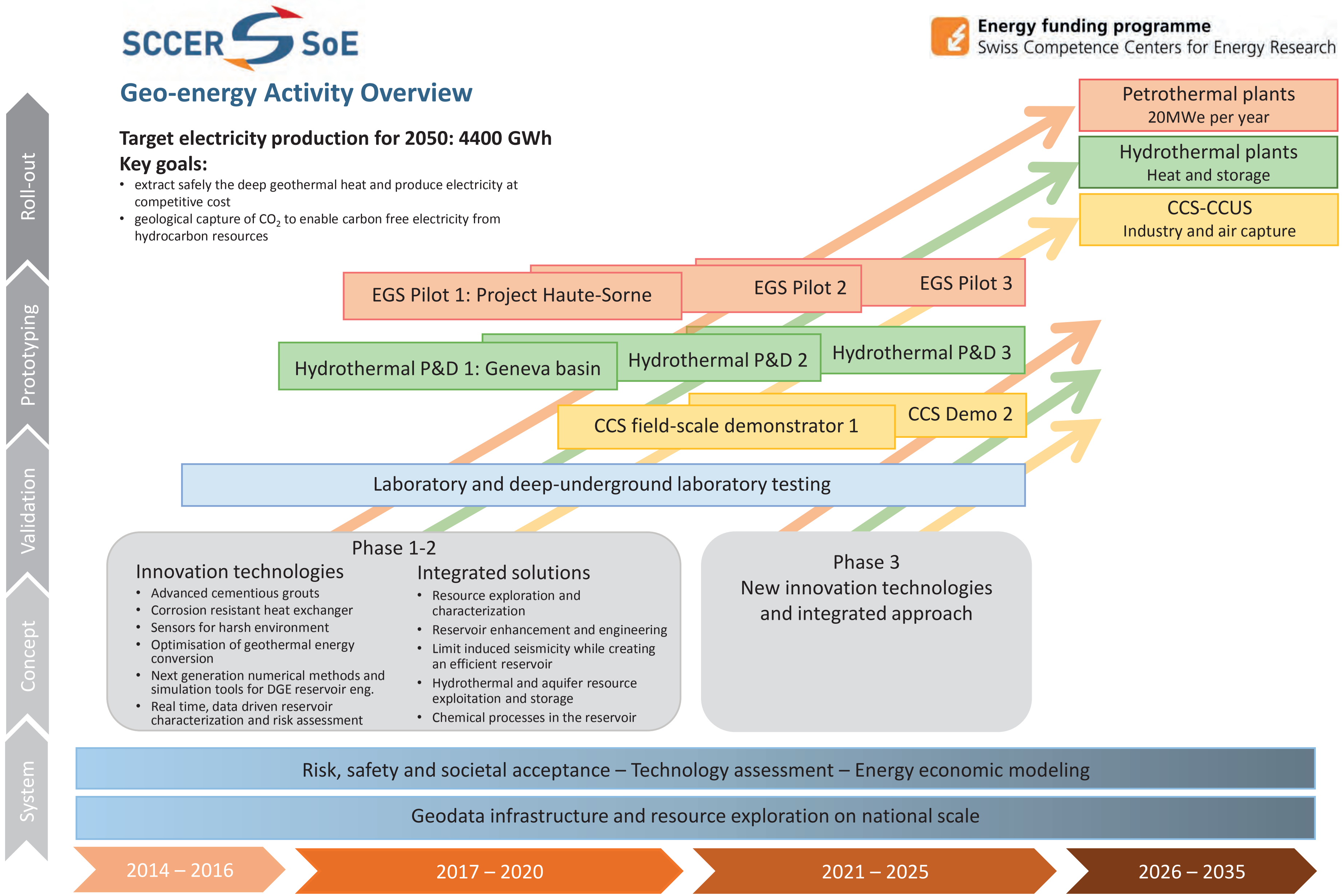
SCCER SoE
Energy funding programme
Swiss Competence Centers for Energy Research
Geo-energy Activity Overview
Target electricity production for 2050: 4400 GWh
Key goals:
• extract safely the deep geothermal heat and produce electricity at competitive cost
• geological capture of CO_2 to enable carbon free electricity from hydrocarbon resources
Roll-out
Prototyping
Validation
Concept
System
Petrothermal plants
20MWe per year
Hydrothermal plants
Heat and storage
CCS-CCUS
Industry and air capture
EGS Pilot 1: Project Haute-Sorne
EGS Pilot 2
EGS Pilot 3
Hydrothermal P&D 1: Geneva basin
Hydrothermal P&D 2
Hydrothermal P&D 3
CCS field-scale demonstrator 1
CCS Demo 2
Laboratory and deep-underground laboratory testing
Phase 1-2
Innovation technologies
• Advanced cementious grouts
• Corrosion resistant heat exchanger
• Sensors for harsh environment
• Optimisation of geothermal energy conversion
• Next generation numerical methods and simulation tools for DGE reservoir eng.
• Real time, data driven reservoir characterization and risk assessment
Integrated solutions
• Resource exploration and characterization
• Reservoir enhancement and engineering
• Limit induced seismicity while creating an efficient reservoir
• Hydrothermal and aquifer resource exploitation and storage
• Chemical processes in the reservoir
Phase 3
New innovation technologies and integrated approach
Risk, safety and societal acceptance – Technology assessment – Energy economic modeling
Geodata infrastructure and resource exploration on national scale
2014 – 2016
2017 – 2020
2021 – 2025
2026 – 2035

Task 1.1

Title

Resource exploration and characterization

Projects (presented on the following pages)

Porosity evolution of bioclastic beds during early diagenesis: Upper Muschelkalk, Switzerland
A. Adams, L. W. Diamond

Anhydrite-dissolution porosity in the Upper Muschelkalk aquifer, NE-Swiss Molasse Basin: implications for geo- energy and gas storage
L. Aschwanden, A. Adams, L. W. Diamond, M. Mazurek

Seismic transmissivity of fractures from full-waveform sonic log measurements
N. D. Barbosa, E. Caspari, J. Germán Rubino, T. Zahner, A. Greenwood, L. Baron, K. Holliger

Geothermal prospection in the Greater Geneva Basin (Switzerland and France): Multidisciplinary approach
M. Brentini, N. Clerc, E. Rusillon, A. Moscariello

Geophysical characterization of a hydrothermally active fault zone in crystalline rocks – GDP 1 borehole, Grimsel Pass project
E. Caspari, L. Baron, T. Zahner, A. Greenwood, E. Toschini, D. Egli, K. Holliger

Attenuation in fluid-saturated fractured porous media – quasi-static numerical upscaling vs dynamic wave propagation modeling
E. Caspari, M. Novikov, V. Lisitsa, N. Barbosa, B. Quintal, J. Germán Rubino, K. Holliger

Fault structure and porosity distribution in an active hydrothermal system
D. Egli, R. Baumann, S. Küng, A. Berger, L. Baron, M. Herwegh

Characterization and imaging of a fractured crystalline hydrothermal fault zone from hydrophone VSP data
A. Greenwood, E. Caspari, J. Hunziker, L. Baron, K. Holliger

Gravity survey in the Geneva Basin for deep geothermal and heat storage projects
L. Guglielmetti, G. Mijic, A. Moscariello, D. Dupuy, P. Radogna

VSP Survey at the Thonex Well, Geneva
L. Guglielmetti, A. Moscariello, M. Francois, C. Nawratil de Bono, C. Dezayes, B. Adnand, P. Corubolo, F. Poletto

Seismic attenuation in porous rocks containing stochastic fracture networks
J. Hunziker, M. Favino, E. Caspari, B. Quintal, J. Germán Rubino, R. Krause, K. Holliger

Towards fracture characterization using tube waves
J. Hunziker, S. Minato, E. Caspari, A. Greenwood, K. Holliger

Importance of the dolomitiziation of Upper Jurassic carbonate rocks for geothermal prospection in the Geneva Basin (Switzerland & France)
Y. Makhloufi, E. Rusillon, M. Brentini, M. Meyer, E. Samankassou

SCCER SoE
SWISS COMPETENCE CENTER for ENERGY RESEARCH
SUPPLY of ELECTRICITY

SCCER-SoE Annual Conference 2017

In cooperation with the CTI
Energy
Swiss Competence Centers for Energy Research
Swiss Confederation
Commission for Technology and Innovation CTI

Porosity evolution of bioclastic beds during early diagenesis: Upper Muschelkalk, Switzerland

A.Adams[1]; L.W. Diamond[1]

1) Rock-Water Interaction Group, Institute of Geological Sciences, University of Bern, Baltzerstrasse 1+3, CH-3012 Bern, Switzerland

1. Introduction

The Middle Triassic Upper Muschelkalk of the Swiss Molasse Basin is under study as a potential gas storage reservoir and for geothermal energy production. It is characterized by a porous upper dolomitic unit (Trigonodus Dolomit) and a tight lower calcitic unit (Hauptmuschelkalk). Porosities of the Swiss Hauptmuschelkalk are <5% on average, however in Germany the Hauptmuschelkalk reaches porosities over 20%.

Using cathodoluminescence (CL), UV-fluorescence (UV-F), stable isotopes and point counting, four diagenetic environments were identified in boreholes across northern Switzerland. The same paragenetic sequence occurred at all depths in each borehole. The results shed light on the improbability of any porous bioclastic beds in Switzerland.

2. Results

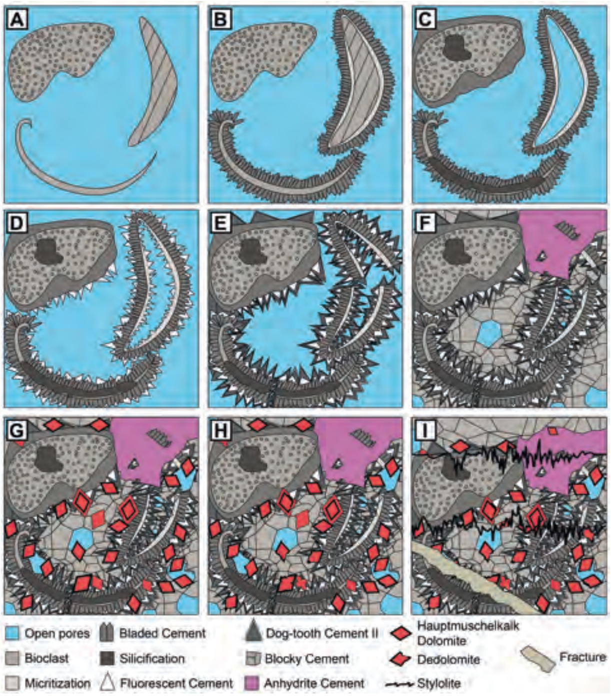

Figure 1) Schematic diagrams of early diagenesis

Marine diagenesis
A) Initial deposition of a crinoid (left), aragonitic bivalve (right) and brachiopod (bottom).
B) Micritization and bladed cement.

Mixing-zone diagenesis
C) Silicification and inclusion-rich syntaxial cement.
D) Leaching and fluorescent dog-tooth cement.

Meteoric diagenesis
E) Dull and bright dog-tooth cement, and compaction.
F) Blocky cement and anhydrite cement.

Shallow burial diagenesis
G) Dissolution and subsequent Hauptmuschelkalk dolomitization.
H) Dedolomitization.
I) Stylolitization and fracturing cutting all features.

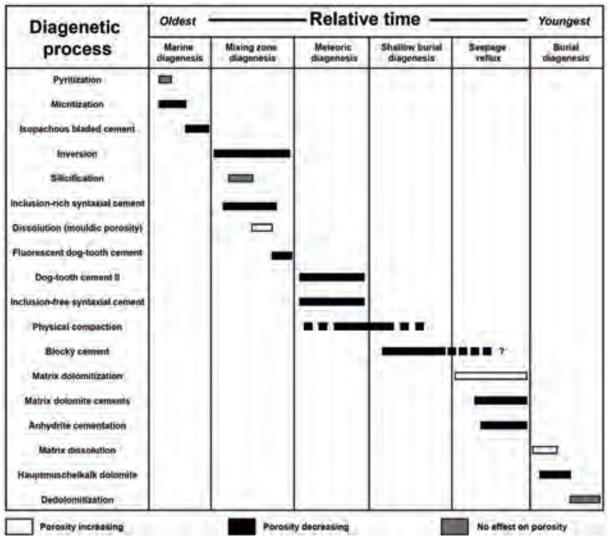

Figure 2) Summary of early diagenetic events

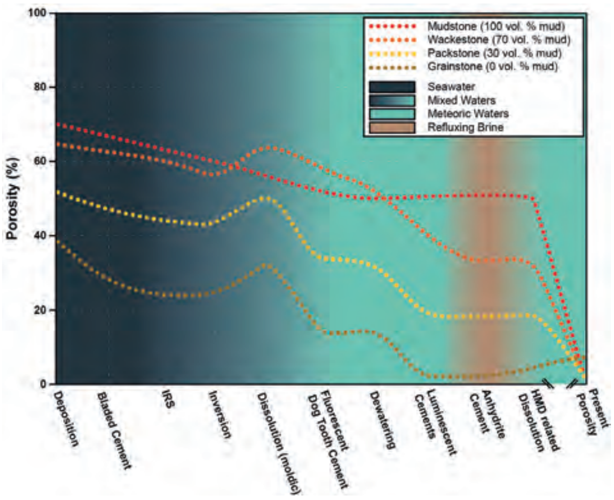

Figure 3) Quantification of porosity in relation to early diagenetic events

Porosities of bioclastic beds were calculated based on thin-section point counting and a fixed mud vol. % with a porosity of 70%. Background colours refer to pore fluids during diagenesis.

3. Conclusions and Outlook

- Early diagenesis of the Upper Muschelkalk resulted from 18 diagenetic events prior to stylolitization.
- Meteoric cementation caused the most significant occlusion, often by a more than 50% relative reduction in porosity.
- Bioclast hosted and derived porosities were already <5% prior to significant burial.
- More suitable reservoir conditions may exist where there was less influence from meteoric waters. This however, may prove to be only in southern Germany.

SCCER SoE
SWISS COMPETENCE CENTER for ENERGY RESEARCH
SUPPLY of ELECTRICITY

70 NRP Energy Turnaround
National Research Programme

SCCER-SoE Annual Conference 2017

Anhydrite-dissolution porosity in the Upper Muschelkalk aquifer, NE-Swiss Molasse Basin: implications for geo-energy and gas storage

In cooperation with the CTI
Energy
Swiss Competence Centers for Energy Research
Swiss Confederation
Commission for Technology and Innovation CTI

L. Aschwanden, A. Adams, L.W. Diamond, M. Mazurek

Rock-Water Interaction Group, Institute of Geological Sciences, University of Bern, Baltzerstrasse 1+3, CH-3012 Bern, Switzerland

Introduction

In the Swiss Molasse Basin (SMB; Fig. 1), deep saline aquifers are one of the options under investigation for geothermal energy production and for geological storage of gas. Particularly the Middle Triassic dolomites within the Upper Muschelkalk (Trigonodus Dolomit) show encouraging aquifer properties along the northern margin of the SMB.

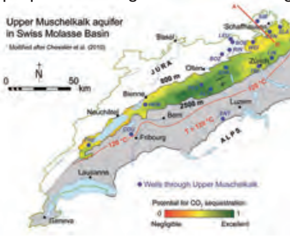

Fig. 1: *CO_2 storage potential of the Upper Muschelkalk aquifer in the Swiss Molasse Basin within the technically favoured depth range for CO_2 storage (800-2500 m). The 120 °C isotherm (red line) marks the minimal temperature required to produce geothermal electricity.*

Matrix porosity and permeability are locally high (<25% and <100 mD, respectively), in part due to beds rich in cm-dm scale cavities left by the dissolution of eogenetic anhydrite nodules (Fig. 2). However, the spatial distribution of anhydrite-dissolution pores is not well known as the basin is underexplored. The present study reconstructs the genesis and evolution of these pores, thus providing conceptual understanding to support ongoing exploration.

Fig. 2: *Drill-core section of the Trigonodus Dolomit at the BEN borehole. The cm-dm scale cavities originate from the dissolution of eogenetic anhydrite nodules.*

Methods

The reconstruction of the genesis and evolution of the anhydrite-dissolution cavities is based on drill-core samples from various boreholes across the Swiss Molasse Basin and it includes:

- Standard petrographic investigations
- Analyses of stable and radiogenic isotopes (i.e. δ^2H, $\delta^{18}O$, and $^{87}Sr/^{86}Sr$) of rock-forming (dolomite) and pore-filling (quartz, calcite and kaolinite) minerals
- Fluid inclusion studies of pore-filling quartz and calcite

Petrography

Some of the anhydrite-dissolution cavities have been affected by two events of mineral precipitation: (1) precipitation of quartz during anhydrite dissolution; (2) a second, younger event in which calcite and kaolinite co-precipitated.

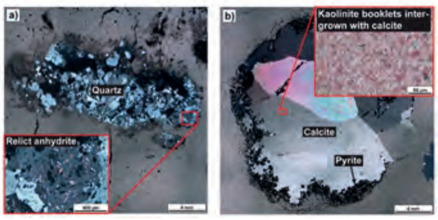

Fig. 3: *Thin-section microphotographs of a) pore-filling quartz with solid inclusions of relict anhydrite and b) of paragenetically younger pore-filling calcite intergrown with kaolinite.*

Fluid inclusion studies

Primary saline water and methane inclusions were trapped simultaneously in both quartz and younger calcite. Homogenisation temperatures are therefore equivalent to trapping temperatures (Fig. 4a).

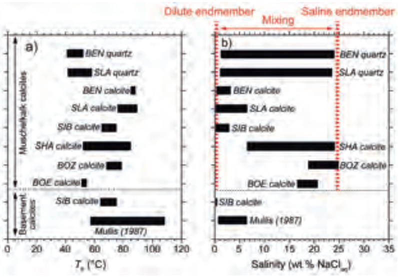

Fig. 4: *Microthermometric results of primary fluid inclusions in pore-filling minerals. Salinity is based on ice-melting temperatures.*

Isotope analyses

Pore- and fracture-filling calcite in the Upper Muschelkalk yield high $^{87}Sr/^{86}Sr$ ratios relative to the dolomite matrix. These high values overlap with the $^{87}Sr/^{86}Sr$ signatures of basement water and calcite fracture-fillings.

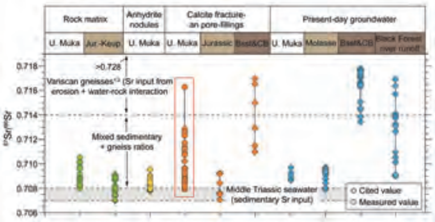

Fig. 5: *Strontium isotope ratios for rock matrix, anhydrite nodules, secondary pore- and fracture fillings and the recent groundwater in the Muschelkalk and in its overlying (beige) and underlying (brown) units (Bsst: Buntsandstein; CB: Variscan gneiss basement; Pearson et al., 1991; Nagra, 2001; McArthur et al., 2001; Durand et al., 2005).*

Isotope analyses

Stable and radiogenic isotopes show that the original hypersaline porewater of the Muschelkalk was diluted by infiltration of meteoric water containing radiogenic Sr. This water overlaps with the $\delta^{18}O$-δ^2H of basement waters.

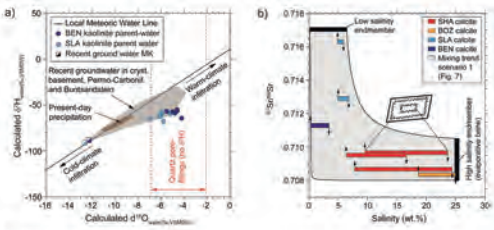

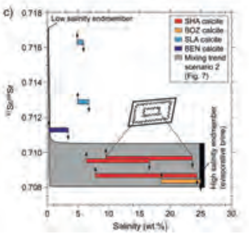

Fig. 6: *a) Isotope signatures of the parent-water of quartz and kaolinite pore-fillings calculated on the basis of fluid inclusion trapping temperatures. The clear petrographic evidence that calcite and kaolinite partly co-precipitated is taken as evidence that the temperatures of mineral formation derived from the primary fluid inclusions in calcite are also valid for kaolinite. b,c) Fluid inclusion salinities in calcite pore- and fracture-fillings as a function of the mineral's $^{87}Sr/^{86}Sr$ ratio. The grey areas represent calculated mixing trends for the two infiltration scenarios outlined in the next section.*

Discussion

- Fluid inclusion and isotope evidence shows that anhydrite was dissolved by influx of meteoric water with high $^{87}Sr/^{86}Sr$ ratios.
- The only feasible sources of radiogenic Sr in the local stratigraphy are the underlying Buntsandstein and Variscan gneiss basement (Fig. 7).

➞ Two scenarios are conceivable for the path of infiltration (Fig. 7)

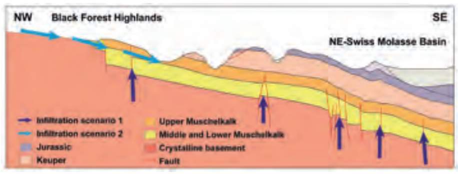

Fig. 7: *Water modified by the interaction with crystalline basement rocks could have infiltrated the Upper Muschelkalk according to two different scenarios: (1) fluid ascent along cross-formational faults or (2) lateral recharge of metoric runoff from the Black Forest Highlands, where the basement rocks are exhumed (see Fig. 1 to locate the profile; modified after Müller et al., 2002).*

➞ Calculated mixing trends for calcite parent-waters show that mixing of a hypersaline, strontium-rich brine with low-salinity, strontium-poor meteoric runoff from the Black Forest Highlands cannot explain the intermediate salinity of primary fluid inclusions in the radiogenic secondary calcites at the BEN and SLA wells. In contrast, mixing with strontium-enriched basement water explains the observations.

Conclusions

Anhydrite-dissolution porosity in the Muschelkalk was caused by the incursion of groundwater from the underlying crystalline basement and/or the Buntsandstein, which ascended along cross-formational faults. Accordingly, anhydrite-dissolution porosity is spatially restricted to the vicinity of deep-seated tectonic structures, which hydraulically connect the crystalline basement and the Muschelkalk. This finding should aid in focussing geothermal and gas-storage exploration in the Swiss Molasse Basin.

SCCER SoE
SWISS COMPETENCE CENTER for ENERGY RESEARCH
SUPPLY of ELECTRICITY

SCCER-SoE Annual Conference 2017

UNIL | Université de Lausanne

In cooperation with the CTI
Energy
Swiss Competence Centers for Energy Research
Swiss Confederation
Commission for Technology and Innovation CTI

Seismic transmissivity of fractures from full-waveform sonic log measurements

Nicolás D. Barbosa[1], Eva Caspari[1], J. Germán Rubino[2], Tobias Zahner[1], Andrew Greenwood[1], Ludovic Baron[1], and Klaus Holliger[1]

1- University of Lausanne
2- CONICET, Centro Atómico Bariloche

Introduction

The identification and proper characterization of fractures is of increasing concern in many domains ranging from hydrocarbon exploration to CO_2 sequestration and nuclear waste storage. In the case of fractured crystalline rocks, such as those prevailing in petrothermal reservoirs, the impact of the fractures on the mechanical and hydraulic properties is particularly strong. Acoustic attributes from full-waveform sonic (FWS) logs are suitable for the identification of fractures. However, the quantitative determination of their mechanical and hydraulic properties is not straightforward as FWS measurements represent averages over intervals that tend to be much larger than the fracture thickness. In this work, we propose a novel methodology to determine the transmission coefficient associated with a single thin layer, such as a fracture, or a vein based on attenuation and phase velocity estimations from FWS. This quantity can be then directly related to the normal compliance of the thin layer, which is a key mechanical parameter.

FWS data acquisition

FWS data were acquired at the Grimsel Felslabor INJ2 borehole using a single transmitter and three receivers at nominal frequencies of 3, 15, and 25 kHz. In order to increase the signal-to-noise ratio, we performed multiple static measurements at each position and subsequently stacked them. In addition, by considering multiple source-receiver offset configurations, we can estimate the geometrical spreading correction associated to the probed borehole environment. To this end, we have considered two tool configurations, "short" and "long" (Fig. 1).

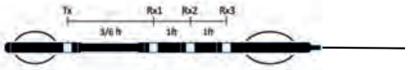

Fig.1: Sonic log tool with one transmitter (Tx) and three receivers (Rx1, Rx2, Rx3). The offset to the source of the first receiver is 3 and 6 ft for the "short" and "long" tool configurations, respectively.

Velocity and attenuation estimation from FWS data

In order to compute P-wave attenuation and velocity, we have separated the head P-wave arrival from later arrivals using a tapered time window. For each interval between receivers, we have determined phase velocities v_p by calculating the phase difference $\Delta\varphi$ from the unwrapped phase spectrum of the corresponding recorded signals

$$v_p(\omega)=\frac{\omega\Delta r}{\Delta\varphi(\omega)}, \qquad (1)$$

where ω is the angular frequency and Δr the distance between receivers. Fig. 2 shows the phase velocity profile in the upper section of the borehole. Some velocity dispersion is evident from the difference between the velocities for 15 and 25 kHz. Notice that the presence of fractures, slightly reduces the effective velocity of the medium. Some erratic behavior of the velocity profile has been attributed to damaged zones in the borehole based on televiewer images.

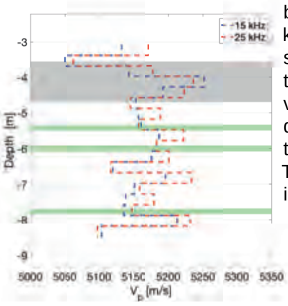

Fig. 2: Velocity profile computed from 15 and 25 kHz measurements. Grey zone corresponds to ductile shear zones. Green features are fractures.

The raw attenuation Q_p^{-1} for a given receiver interval can, in turn, be computed as

$$Q_p^{-1}(\omega)=\ln\left(\frac{A(\omega,r_i)G_{i+1}}{A(\omega,r_{i+1})G_i}\right)\frac{2v_p(\omega)}{\omega\Delta r}, \qquad (2)$$

where $A(\omega, r_i)$ is the head P-wave spectrum at the ith-receiver and G_i is the geometrical spreading function, which depends on frequency, position, and source-receiver offset.

Transmission losses determination

The attenuation in Eq. 2 can be expressed as

$$Q_p^{-1}(\omega)=Q^{-1}_{sprd}(\omega)+Q^{-1}_{intr}(\omega)+Q^{-1}_{transm}(\omega), \qquad (3)$$

where $1/Q_{sprd}$, $1/Q_{intr}$, and $1/Q_{transm}$, refer to the attenuation associated with the geometrical spreading, the intrinsic loss of the formation, and the transmission loss associated to the presence of interfaces and layers in the formation.

Assuming that, in Eq. 3, only Q_{sprd} depends on the offset between the source and receivers and that $G_i=(1/r_i)^\gamma$, we can use the raw attenuation measurements from different tool configurations (Fig.1) to estimate the geometrical spreading correction (Fig. 3).

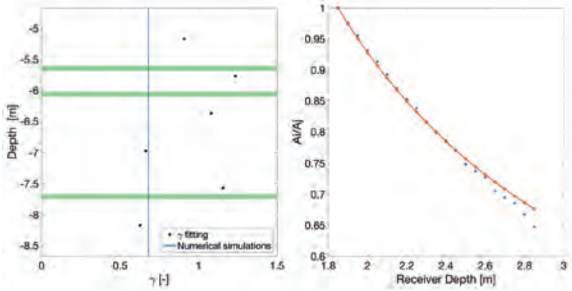

Fig.3: Geometrical spreading correction factor γ obtained from the combination of long and short offset configurations at 25 kHz (left) and from numerically simulated log data (right). For the numerical simulations, the parameters of the medium were chosen based on measurements on core samples characterizing the host granodiorite and using sonic velocities for P- and S-waves.

The attenuation depth profiles after geometrical spreading correction are shown in Fig. 4. From the standard deviation of the fitting of γ, we have defined a range of possible values of corrected attenuation. From the attenuation depth profile, we identify a reference value for the background intrinsic attenuation.

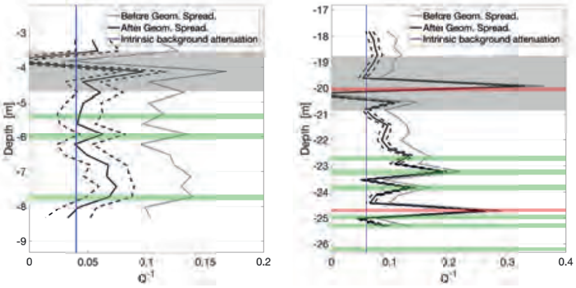

Fig.4: Attenuation profile for 25 kHz sonic log data. Blue curve is identified as the intrinsic background attenuation. Grey, red and green zones correspond to ductile shear, dyke, and fracture sections, respectively.

For each receiver interval, we can compute an effective P-wavenumber from the attenuation and velocity estimations as

$$k_p^{eff}(\omega)=\frac{\omega}{v_p(\omega)}\left(1-i\frac{Q_p^{-1}(\omega)}{2}\right). \qquad (4)$$

In addition, the background reference velocity and attenuation can be used to obtain a P-wavenumber of the background rock k^b_p. Finally, the transmission coefficient of a thin layer can be approximated as

$$A_t(\omega)=e^{i\left(k_p^b-k_p^{eff}\right)\Delta r}, \qquad (5)$$

from which normal compliance values can be estimated. This effective quantity of the thin layer responsible of the transmission losses, can be used to obtain information on the material composing it. We have verified this for the dykes and veins for which the estimated velocities are close to those found in the literature for lamprophyres and quartz, respectively.

Conclusions

We have presented a novel approach that allows us to estimate the transmissivity of a single thin layer using FWS log data. The advantage of estimating transmission coefficients of thin-layer-type structures such as veins or fractures, is that it allows us to isolate and quantify their mechanical properties.

Acknowledgements

This work has been completed within the Swiss Competence Center on Energy Research – Supply of Electricity with the support of the Swiss Commission for Technology and Innovation.

SCCER SoE
SWISS COMPETENCE CENTER for ENERGY RESEARCH
SUPPLY of ELECTRICITY

Swiss Competence Center on Supply for Electricity
Annual Conference 2017

In cooperation with the CTI
Energy
Swiss Competence Centers for Energy Research
Swiss Confederation
Commission for Technology and Innovation CTI

Geothermal prospection in the Greater Geneva Basin (Switzerland and France): Multidisciplinary approach

Maud Brentini (*), Nicolas Clerc (*), Elme Rusillon (*), Andrea Moscariello (*)

(*) Department of Earth Sciences, University of Geneva, 13 rue des Maraîchers, 1205 Geneva (maud.brentini@unige.ch)

Introduction

G eneva
E nergy
O bjectif
T ectonic
H ydraulic
E lectricity
R esources
M ultidisciplinary
I nvestigation
E valuation
2 0 2 0

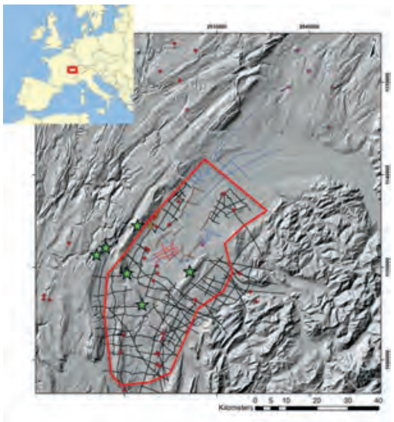

The GEothermie2020 program, managed by the State of Geneva and implemented by the SIG (Services Industriels de Genève), aims at developing geothermal energy resources in the Greater Geneva Basin (GGB).). A reservoir assessment has been then performed in the Greater Geneva Basin to evaluate the geothermal resources potential of low to medium enthalpy. For this purpose, a detail structural analysis of the basin has been carried out simultaneously with a reservoir appraisal study including petrophysical properties assessment in a consistent sedimentological and stratigraphical frame.

This multi-disciplinary study has been organized in 4 steps:
(1) Investigation of the surrounding outcrops to understand the stratigraphy and lateral facies distribution of the sedimentary sequence from Permo-Carboniferous to Lower Cretaceous units
(2) Development of 3D geological models derived from 2D seismic and well data focusing on the structural scheme of the basin to constrain better the tectonic influence on facies distribution and to assess potential hydraulic connectivity through faults between reservoir units
(3) Evaluation of the distribution, geometry, sedimentology and petrophysical properties of potential reservoir units from well data
(4) Identification and selection of the most promising reservoir units for in-depth rock type characterization and 3D modeling.

Stratigraphic framework

Challenge

- Harmonization of the stratigraphy of the Geneva Basin
- Establishment of composite logs
- Correlation with national stratigraphy (HARMOS)
- Implementation of stratigraphic catalog

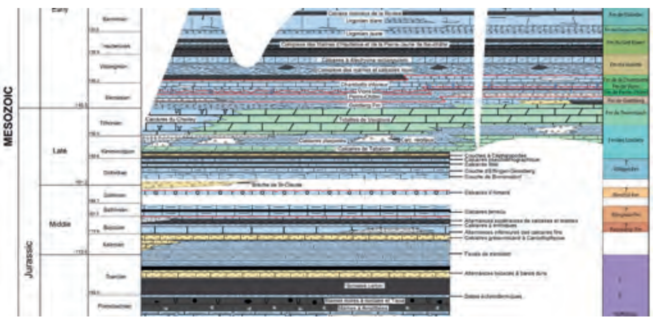

Main issues

- Heterogeneities and discrepancies of data
- Important lateral variabilities

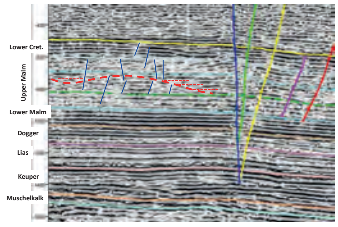

Massive calcareous Upper Malm units:

- Often chaotic / discontinuous seismic facies
  → *fracture-enhanced permeability zones?*
- Dome-shape structures surrounded by onlapping reflectors within the Kimeridgian interval
  → *reef structures?*

Current fault framework interpretation from 2D seismic data in the Geneva and surrounding basins reveals strike-slip fault segments oscillating between two main directions: SSE-NNE in the southern and central parts & E-W in the northern part and toward the foothills of the Jura.
Intra-basinal smaller scale thrust faults appear restricted to the more britlle calcareous-prone units of the Upper Jurassic and Lower Cretaceous units whereas deeper (marl-prone) Mesozoic units deform in a more ductile manner.

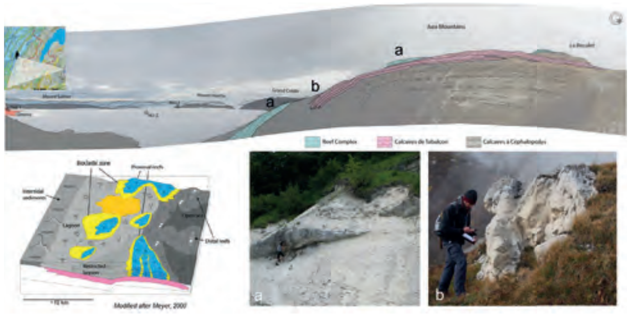

The Kimmeridgian Reef complex

- Most promising geothermal reservoir
- Complexe facies architecture and petrophysical properties distribution
- Prevailing microporosity
- Increasing fracture density in the Reef complex and in dolomitized intervals
- Identification of zones of fracture-enhanced permeability on seismic data and outcrops

Conclusion

✓ Definion of a stratigraphic catalog with a clear stratigraphic framework for the GGB.
✓ Lateral extent and precise orientation of seismic-scale faults remains challenging with current 2D seismic dataset
✓ Better understanding of the distribution and properties of productive reservoir facies as well as hydraulic connectivity zones within the study area.
✓ Petrophysical investigations revealed that the Kimmeridgian-Tithonian Reef Complex and the underlying Calcaires de Tabalcon units are the most promising geothermal reservoir targets
✓ Kimmeridgian reef buildups are tentatively interpreted on 2D seismic as being responsible for the dome-shape structures observed across the basin.
✓ Consistent knowledge for future geothermal exploration pushes toward the successful development of this sustainable energy resource in the GGB.

REPUBLIQUE ET CANTON DE GENEVE
Departement de l'environnement, des transports et de l'agriculture
Service de géologie, sols et déchets

SIG

GEOTHERMIE 2020

UNIVERSITÉ DE GENÈVE
FACULTÉ DES SCIENCES
Department of Earth Sciences

SCCER SoE
SWISS COMPETENCE CENTER for ENERGY RESEARCH
SUPPLY of ELECTRICITY

SCCER-SoE Annual Conference 2017

In cooperation with the CTI
Energy
Swiss Competence Centers for Energy Research
Commission for Technology and Innovation CTI
70 NRP Energy Turnaround
National Research Programme

Geophysical characterization of a hydrothermally active fault zone in crystalline rocks – GDP 1 borehole, Grimsel Pass project

Eva Caspari[1], Ludovic Baron[1], Andrew Greenwood[1], Tobias Zahner[1], Enea Toschini[1], Daniel Egli[2] and Klaus Holliger[1],
University of Lausanne and University of Bern

Motivation

A shallow near-vertical hydrothermally active fault zone embedded in sheared and fractured crystalline rocks of the Central Aar massif (Switzerland), has been drilled and geophysically explored in view of its potential analogies to planned deep natural geothermal reservoirs in the Alpine Foreland. The geophysical well logs collected in 2015 (open hole) and 2016 (screened hole) characterize the petrophysical variations of the Grimsel Breccia Fault (GBF) due to ductile and brittle deformation in the fault core and the surrounding damage zones. Open fracture porosity estimates obtained from the nuclear and borehole radar logs correlate well with the petrophysical variations observed.

Borehole logging data

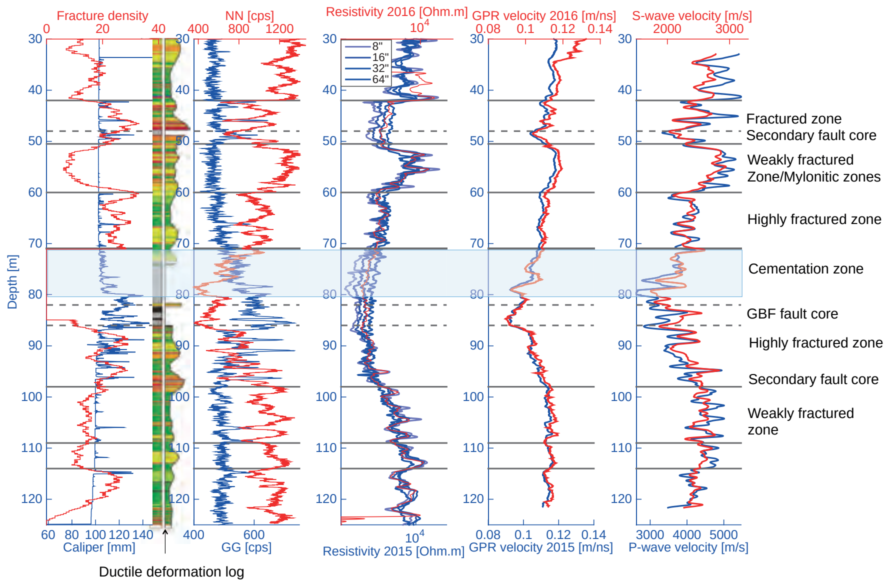

A selection of geophysical logging data acquired during 2015 (open hole) and 2016 (screened casing) is shown alongside fracture density and relative deformation intensity logs (first column) obtained from core analysis and televiewer data. The geophysical logging data comprise nuclear (neutron-neutron NN and gamma-gamma GG) and resisitivity logs and borehole ground-penetrating radar (GPR) and sonic (P- and S-wave) velocities. The main trend is consistent for all logs and correlates well with the degree of deformation and fracturing of the formation and the GBF fault core is clearly delineated. The resistivity logs have low values in the highly fractured zones. This is expected since they are directly sensitive to the water content of the formation (electrolytical conductivity) and thus to open fracture porosity. However, large variabilities of the resistivity logs can be observed in zones of low fracture denisty (e.g. 50-60 m depth). This, together with the overall low resistivity values for a granitic formation within these zones, is indicative of the presence of surface conductivity, most likely due to the abundance of mica in the mylonites.

Porosity and density estimates

Borehole radar, neutron-neutron and resistivity logs are suitable for the estimation of porosity and the gamma-gamma log is classically utilized to derive densities. However, the GG log is strongly affected by the large variations in borehole diameter, depicted by the caliper log, which caused calibration issues and thus reliable density estimates are not possible. To constrain the density, Archimedes-type density measurements (Lab dens) performed on core samples taken at 20-30 cm intervals over the entire borehole length are utilized. The upper bound of density is well constrained by low cleavage and non fractured Grimsel Granite samples taken at 55 and 120 m depth. However, the lower bound is less reliable due to the incohesive quality of the core material (not suitable for core measurements) and core loss in the highly fractured parts of the borehole.

Porosity is first derived form GPR velocities using the so-called Complex Refractive Index Method (CRIM), which requires a representative dielectric constant of the rock matrix ε. The porosity estimate is then subsequently converted into density using a grain density typical for granitic formations. To constrain the transformations, an upper and lower dielectric constant is chosen iteratively so that lab densities from competent samples fall between the resulting calculated density logs (GPR dens $\varepsilon=5.8$ and $\varepsilon=6.2$). The support volume of the BHR data is around 2 m, and thus, smoothens out the strong fluctuations due to intense fracturing observed in the other well logs. To obtain a porosity and density log on a smaller scale the NN measurement is utilized. For this, the NN log is calibrated with the GPR porosity in the intact formation (NN GPR por), or porosity lab measurements (NN Lab por), both leading to similar estimates. The calculated porosity logs are then subsequently converted into density logs (NN GPR dens, NN Lab dens). The resistivity log, which samples different support volumes of the formation depending on the chosen spacing, could not be converted into porosity due to the strong influence of surface conductivity, which overrides the response due to open fracture porosity.

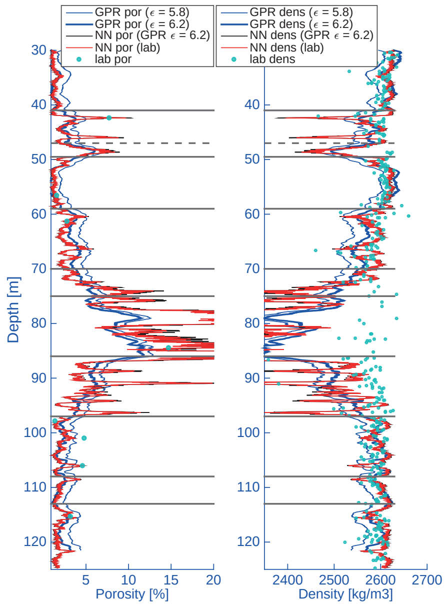

Acknowledgements

This work was supported by the Swiss National Science Foundation through the National Research Programme 70 “Energy Turnaround” and completed within the Swiss Competence Center on Energy Research - Supply of Electricity (SCCER-SoE), with the support of the Swiss Commission for Technology and Innovation. We thank Yannick Forth and Jörg Renner from the Ruhr-University Bochum for Archimedes-type density measurements.

SCCER SoE
SWISS COMPETENCE CENTER for ENERGY RESEARCH
SUPPLY of ELECTRICITY

SCCER-SoE Annual Conference 2017

In cooperation with the CTI
Energy Swiss Competence Centers for Energy Research
Swiss Confederation
Commission for Technology and Innovation CTI

Attenuation in fluid-saturated fractured porous media: quasi-static numerical upscaling vs dynamic wave propagation modeling

Eva Caspari[1], Mikhail Novikov[2], Vadim Lisitsa[2], Beatriz Quintal[1], Nicolas Barbosa[1], J. Germán Rubino[3] and Klaus Holliger[1]
[1]University of Lausanne, Switzerland, [2]Institute of Petroleum Geology and Geophysics, Novosibirsk, Russia, [3]CONICET, Centro Atómico Bariloche – CNEA, Argentina

1. Motivation

Fractures are of great interest in earth sciences and in civil engineering since they significantly influence the elastic and hydraulic properties of geological formations. Seismic attributes are commonly used to detect and characterise fracture zones. One such attribute which recently gained increased attention is seismic attenuation. However, several mechanisms can cause wave attenuation and velocity dispersion in fluid-saturated fractured porous media comprising, on the one hand, pressure diffusion phenomena, such as fracture-to-background (FB) and fracture-to-fracture (FF) wave-induced flow (WIFF), and, on the other hand, dynamic effects, such as scattering and Biot global flow. In this study, we compare attenuation estimates from wave propagation simulations with corresponding estimates from a numerical upscaling approach. The former captures all aforementioned attenuation mechanisms and their interplay, though detailed interpretations tend to be difficult. The latter only accounts for pressure diffusion phenomena and thus will be guiding the physical interpretation. Understanding the interplay of attenuation mechanisms is an essential first step for estimating petrophysical properties form seismic measurements.

2. Numerical methods

Numerical upscaing based on Biot's quasi-static equations (QS)

Oscillatory compression and shear tests (Rubino et al. 2016):

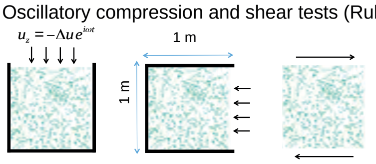

Pressure diffusion:
FB-WIFF
FF-WIFF

Wave propagation transmission based on Biot's dynamic equations (WP)

Transmission experiment (Novikov et al. 2017, Masson et al. 2006):

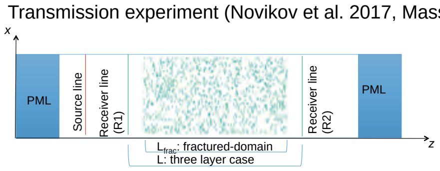

Pressure diffusion
Scattering
Biot global flow
Transmission losses

Domain size: 2 - 5 wavelengths (20 correlation lengths of the medium)

3. Fractured medium

Background: stiff porous matrix

Fractures: compliant porous inclusions with a width of 4 mm and a length of 30 mm

Perpendicular — Intersecting — Parallel

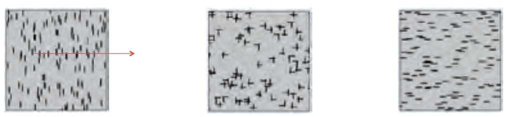

Attenuation mechanisms

	Perpendicular	Intersecting	Parallel
	Scattering	Scattering	Scattering
	FB WIFF	FF WIFF	
	Biot global flow (B+F)	Biot global flow (F)	Biot global flow (F)

Permeability

	Perpendicular	Intersecting	Parallel
Host	10^{-10} m^2 - 10^{-17} m^2	10^{-17} m^2	10^{-17} m^2
Fracture	10^{-9} m^2	10^{-9} m^2 - 10^{-14} m^2	10^{-8} m^2 - 10^{-14} m^2

References:
Masson, YJ, SR Pride, & KT Nihei, 2006. Finite difference modeling of Biot's poroelastic equations at seismic frequencies, Journal of Geophysical Research: Solid Earth , 111 (B10).
Novikov, M., E. Caspari, V. Lisitsa, B. Quintal, J. G. Rubino & K. Holliger, 2017. Attenuation in fluid-Saturated fractured porous media— Quasi static numerical upscaling and wave propagation modeling: In proceedings of the 6th Biot Conference on Poromechanics, pp. 1499-1506
Rubino, J.G., E. Caspari, T.M. Müller, M. Milani, N. Barbosa & K. Holliger, 2016. Numerical upscaling in 2-D heterogeneous poroelastic rocks: Anisotropic attenuation and dispersion of seismic waves, Journal of Geophysical Research: Solid Earth, 121 (9), 6698-6721.

4. Modeling results

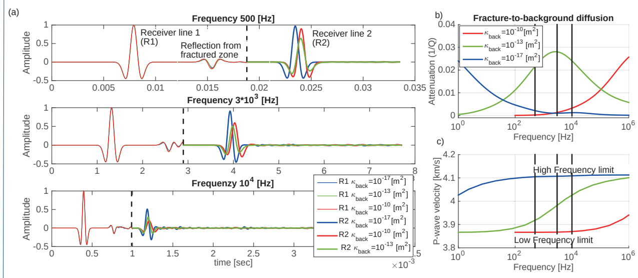

Figure 1: Example for the perpendicular case a) Transmission experiment: Recorded averaged waveforms at receiver line 1 and 2 for three central frequencies and permeabilities. The black dashed line separates the two recordings. b) Resulting P-wave attenuation and c) phase velocity as function of frequency from the oscillatory tests. The black lines correspond to the central frequencies of the signals shown in a).

5. Attenuation and velocity estimation

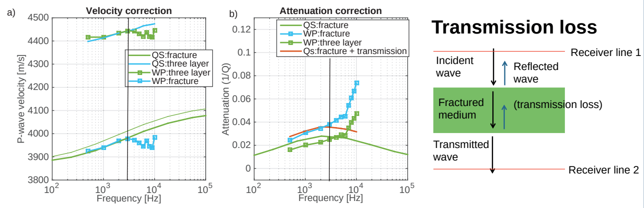

Figure 2: a) Effective velocities of the fractured domain and the three layer case for the transmission experiment (WP) and oscillatory test (QS). The black line indicates the onset of scattering. b) Attenuation estimate for the fractured domain and the three layer case.

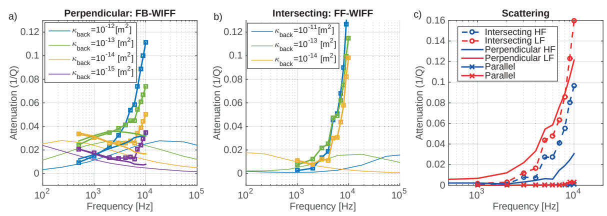

Figure 3: Attenuation comparison for a) perpendicular case (FB-WIFF) and b) intersecting case (FF-WIFF) and c) scattering in the low- and high-frequency limits for all three types of the fractured medium.

6. Conclusions

To interpret wave propagation results in terms of intrinsic attenuation caused by a fractured medium, we have to account for the travel path of the wave and amplitude reductions due to transmission losses. After correcting for these effects the good agreement between the transmission experiment and oscillatory test, indicates that, at low frequencies pressure diffusion phenomena are dominant, whereas at higher frequencies scattering attenuation starts to control the response. The magnitude of scattering attenuation varies considerably depending on the arrangement of fractures and the effective compliance of the fractured medium, which in turn is strongly influenced by the pressure diffusion phenomena.

Acknowledgements: This work has been completed within the Swiss Competence Center on Energy Research - Supply of Electricity, with the support of the Swiss Commission for Technology and Innovation. V. Lisitsa and M. Novikov are thankful to the Russian Foundation for Basic Research grants no. 16-05-00800, 17-05-00250, 17-05-00579 for financial support of the research. Simulations of seismic wave propagation were performed on clusters of the Siberian Supercomputer Center.

SCCER-SoE Annual Conference 2017

SCCER SoE
SWISS COMPETENCE CENTER for ENERGY RESEARCH
SUPPLY of ELECTRICITY

70 NRP Energy Turnaround
National Research Programme

In cooperation with the CTI
Energy
Swiss Competence Centers for Energy Research

Schweizerische Eidgenossenschaft
Confédération suisse
Confederazione Svizzera
Confederaziun svizra

Swiss Confederation

Commission for Technology and Innovation CTI

Fault structure and porosity distribution in an active hydrothermal system

Daniel Egli[1], Rahel Baumann[1], Sulamith Küng[1], Alfons Berger[1], Ludovic Baron[2] & Marco Herwegh[1]

[1]Institute of Geological Sciences, University of Bern (daniel.egli@geo.unibe.ch), [2]Institut des sciences de la Terre, Université de Lausanne

Motivation and approach

The geometry of fracture networks and matrix porosity of fault rocks are key parameters controlling the permeability and ultimately the fluid flux along fault zones. On the example of a long-lived and still active fault-bound hydrothermal system (Grimsel breccia fault; Hoffmann et al., 2004; Belgrano et al., 2016) in the crystalline basement of the Aar Massif (Swiss Alps), this study aims at understanding the extent, occurrence, dynamics and evolution of natural fluid pathways along faults and their characteristics in hydrothermal zones in particular. Better understanding of such naturally porous and permeable rocks is of prime importance for the successful exploration of natural hydrothermal systems. On the basis of structural data collected from an inclined 125 m long drillhole, the corresponding drill core and surface mapping, we evaluate the porosity, permeability and fracture distribution around a central water-bearing breccia zone from the micrometre to decametre scale and its significance for past and present fluid circulation.

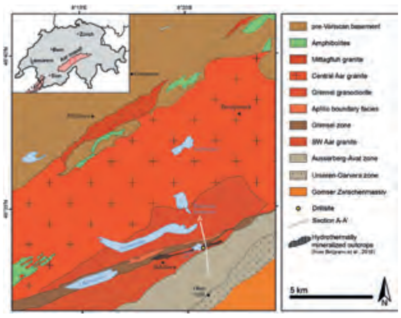

Geologic map of the central Aar massif, modified after Berger et al., (2016).

Large-scale temperature distribution and fractures

a) Geologic cross-section along the Transitgas AG tunnel below Grimsel Pass showing the drillhole (projected into section), rock-wall temperatures and main ductile high strain zones, b) Elevated fracture density along the cross-section correlates with ductile high strain zones, but only one of these zones shows hydrothermal inflow. c) Lower hemisphere equal-area pole plots of mapped fractures reflect the regional ENE-WSW main structural trend.

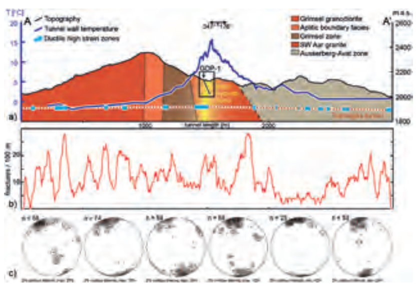

Matrix porosity measurements

Porosity data from the matrix- and microfracture-porosity measurements show a correlation between deformation intensity and matrix porosity ranging from <1vol% to >20vol%. Comparable to the macroscopic fractures, the micro-porosity is strongly controlled by the intensity of precursory deformation. Fault core rock analyses yield highly elevated matrix porosity.

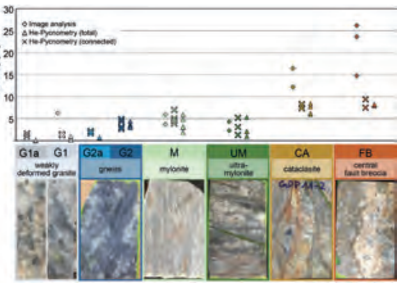

Meso-scale fracture distribution

The main fracture orientation is controlled by a regional ENE-WSW trend forming sub-parallel high-strain zones interconnected by NW-SE trending fracture sets. There is a strong correlation between ductile deformation intensity and fracture density/porosity. Increased fracture density and high fracture volume suggest two secondary fault cores north and south of the central fracture zone. Clusters of intersection lines might represent a network of focused linear flow-paths along the main trend of the hydrothermal zone.

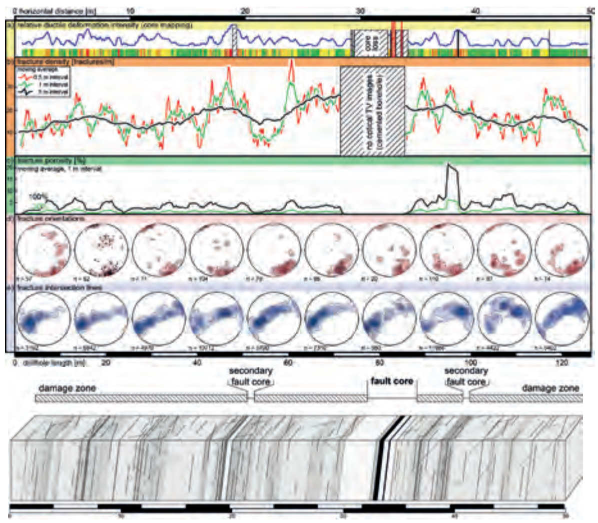

Schematic block-diagram of the examined deformation zone indicating the variable and alternating grade of ductile deformation, the observed fracture pattern as well as the central fault core and secondary fault cores.

Discussion

Fracturing is controlled by regularly spaced variations in ductile deformation intensity ranging from granite to ultramylonite. The variable degree of ductile precursory deformation shows a range of matrix porosity values between <0.1 and 7% and thus forms a succession of subparallel sealing and high-porosity structures bridged by a dense fracture network. Fluid flow is therefore directly related to the combined effect of fractures and enhanced fault-related matrix porosity. In this specific setting, the width of the damage zone exceeds the distance between the large scale faults that can be observed on the surface and which are characterized by a regular increase in fracture density. However, of several such parallel fault zones, the Grimsel breccia fault is the only one showing enhanced heat flow. This suggests a key importance of matrix porosity within fault core rocks (breccia & fault gouge) for the transport of hydrothermal fluids as an enhanced fracture network alone is not providing sufficient permeability in the case of this natural hydrothermal system.

Acknowledgments

This project is part of the NRP70 program and is funded by the Swiss National Science Foundation. We thank Swisstopo, the Swiss Federal Office of Energy, NAGRA and the Kraftwerke Oberhasli AG for additional financial and practical support.

References

Belgrano, T.M., Herwegh, M. & Berger, A. 2016: Inherited structural controls on fault geometry, architecture and hydrothermal activity: an example from Grimsel Pass, Switzerland. Swiss Journal of Geosciences.

Berger, A., I. Mercolli, and E. Gnos 2016: Geological map of the Aar Massif, Tavetsch and Gotthard nappes 1:100000, Landesgeologie der Schweiz.

Hoffmann, B.A., Helfer, M., Diamond, L.W., Villa, I.M., Frei, R. & Eikenberg, J. 2004: Topography-driven hydrothermal breccia mineralization of Pliocene age at Grimsel Pass, Aar massif, Central Swiss Alps. Schweiz. Mineral. Petrogr. Mitt., 84, 271–302.

SCCER SoE

SWISS COMPETENCE CENTER for ENERGY RESEARCH
SUPPLY of ELECTRICITY

UNIL | Université de Lausanne

SCCER-SoE Annual Conference 2017

Characterization and imaging of a fractured crystalline hydrothermal fault zone from hydrophone VSP data

A. Greenwood, E. Caspari, J. Hunziker, L. Baron, and K. Holliger.

In cooperation with the CTI
Energy
Swiss Competence Centers for Energy Research
Swiss Confederation
Commission for Technology and Innovation CTI
70 NRP Energy Turnaround
National Research Programme

Borehole hydrophones for fracture characterisation

Petrothermal reservoirs with sufficient potential for electric power generation prevail at depths between 4-6 km. At these depths, current drilling techniques return limited rock samples for fracture and fluid pathway analysis. Thus, there is a large dependence on borehole geophysical techniques to determine the fracture characteristics, hydraulic properties and the extent of targets drilled. Borehole hydrophones record pressure waves originating from seismic body-waves passing the borehole. However, due to the high sensitivity of hydrophones and their suspension in the fluid column, they are susceptible to strong coherent noise trapped within the water column known as tube-waves. Tube-waves are generated at large impedance contrasts in the borehole wall such as open fractures. As such, hydrophones are well suited to identify and characterise hydraulically open fractures and to map deformation zones. For these reasons, we analyse hydrophone-based vertical seismic profiling (VSP) experiments along the GDP1 borehole, which penetrates the Grimsel Breccia Fault (GBF) as well as the embedding fractured granitic rocks. The GBF has been exhumed from a depth of 3-4 km and is considered to exhibit pertinent analogies to a deep fractured petrothermal target.

Tube-waves

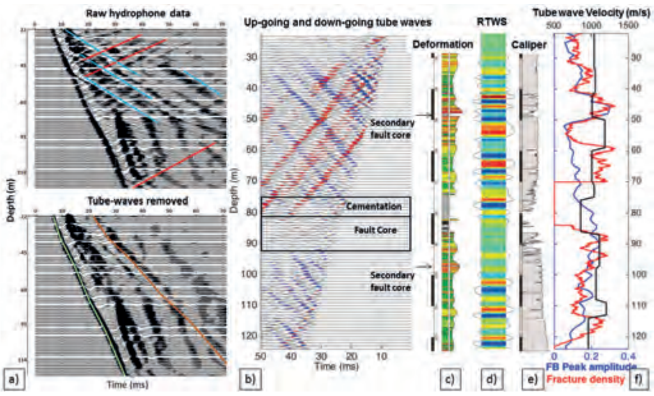

Figure 1 *(a) Zero-offset VSP data before (top) and after (bottom) up- and down-going tube-wave (red and blue lines, respectively) removal through f-k filtering, (b) superposition of up- and down-going tube-waves extracted from the data shown in (a), (c) relative deformation intensity log from core analysis, (d) reflected tube-wave stack (RTWS), (e) calliper log, and (f) first-arrival amplitudes (blue), fracture density from televiewer data (red) and tube-wave velocity (black). The black box denotes the main fault core and black arrows identify two secondary fault cores.*

Channel waves

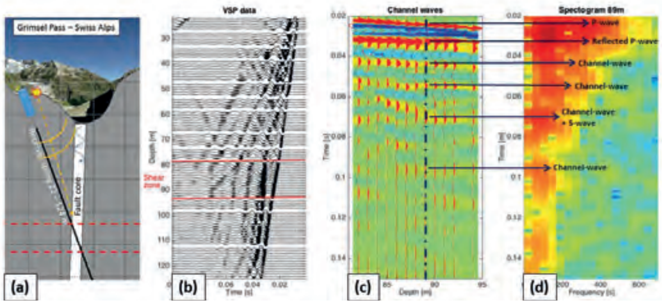

Figure 3 *(a) Simplified cross-section of the GBF showing the deeply incised topography, the geometry of the borehole intersecting the main fault core, the location of the seismic source and borehole hydrophone receivers and a schematic of channel waves generated within the GBF due to its high impedance contrast with regard to its embedding environment. (b) Zero-offset hydrophone VSP data with the GBF main fault core highlighted by the red rectangle. (c) Seismic traces from the main fault core (red rectangle). (d) Dispersion analysis of the seismic trace at depth 89 m indicated by the dashed line in (c). Identified within the spectrogram are the first arriving P-wave, the strongly reflected P-wave, later arriving channel waves and a channel wave overlapped by a down-going S-wave. Note the decrease in channel wave frequency with time.*

Seismic imaging

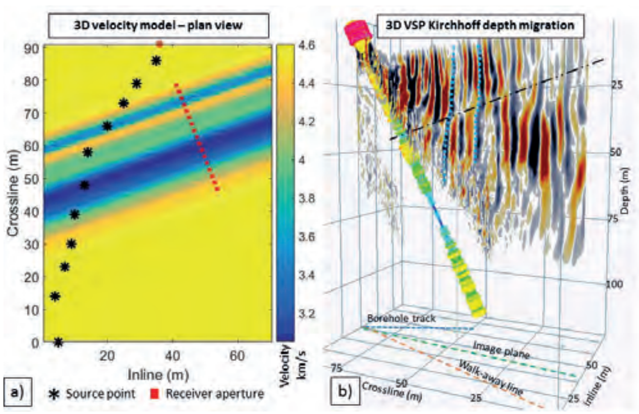

Figure 2 *(a) Plan view of the 3D velocity model derived from smoothed zero-offset VSP interval velocities, surface projection of walk-away sources and extent of hydrophone string, and (b) pre-stack depth migration (PSDM) image taken on a plane bisecting the borehole plane and walk-away VSP source line. Neutron-neutron data is displayed along the borehole track identifying the main fault core (blue) and upper secondary fault (green), which is bisected by a sub-horizontal structural lineation (dashed black line). Reflections from the top and bottom of the main fault core are indicated by blue dashed lines.*

Conclusions and outlook

The Grimsel breccia fault, as well as its embedding fractured crystalline environment, have been characterized using hydrophone VSP and well log data. Fractures indicating brittle deformation are accurately mapped by the reflected tube-wave stack (Figure 1d). This is also supported by the presence of unusually high amplitudes of the first arrivals at the fracture locations (Figure 1f). In addition, the main fault core similarly causes high-amplitude first-arrivals. However, there is an absence of observable tube-waves within the fault core due to borehole breakouts, which inhibit tube-wave propagation and thus uniquely identifies the main deformation zone (Figure 1b).

The generation of a laterally changing 3D velocity model from zero-offset VSP interval velocities and the implementation of 3D pre-stack depth migration, necessitated by out-of-plane source points, has been successful in seismically imaging the near-vertical fault structures (Figure 2) and a potential, as of yet unknown, sub-horizontal structure, which bisects the borehole coincidentally at the upper secondary fault core.

The creation of channel waves requires a large impedance contrast to the surrounding formation, such as a breccia embedded in crystalline rock. Thus, the identification of these wavefields clearly identifies the GBF core, whilst the decrease of frequency observed in Figure 3 is indicative of geometrical dispersion. The modelling and analysis of dispersion to further characteritze the GBF is an avenue of future work, as is the determination of the shear modulus from tube-wave velocities and the modelling of fracture properties from tube-waves (Poster Hunziker et al).

Acknowledgements *We thank: Daniel Egli, from the University of Bern for structural deformation and fracture density measurements and Yannick Forth and Jörg Renner from the Ruhr-University Bochum for Archimedes-type density measurements. This work was supported by the Swiss National Science Foundation through the National Research Programme 70 "Energy Turnaround" and completed within the Swiss Competence Center on Energy Research - Supply of Electricity (SCCER-SoE), with the support of the Swiss Commission for Technology and Innovation.*

SCCER SoE
SWISS COMPETENCE CENTER for ENERGY RESEARCH
SUPPLY of ELECTRICITY

SCCER-SoE Annual Conference 2017

In cooperation with the CTI
Energy
Swiss Competence Centers for Energy Research
Commission for Technology and Innovation CTI

Gravity survey in the Geneva Basin for deep geothermal and heat storage projects

Luca Guglielmetti[1], Goran Mijic[1], Andrea Moscariello[1], David Dupuy[2], Piervittorio Radogna[2]
[1]Earth Science Department, University of Geneva;[2] Geo2X SA

Abstract: A gravity survay has been carried out in the Geneva area with the goal to collect new high resolution data in three main areas on interest for the geothermal development in Geneva.
1227 new stations have been collected in the Bernex, Thonex and Allondon area. The approach is to produce 3D density models for the study sites and integrate them to the exisiting geoohysical data (2D seismic, VSP and CSEM) to develop integrated models produced by the joint interpretation of the different datasets to reduce the exploration risk of future geothermal projects.

Design: The acquisition has been designed taking into account the results of the forward gravity modelling of the the 3D geological model from GeoMol which provided some geometrical contraints of the different formations at depth. Density values were retrieved by different data sources. Particular attention has been devoted to the presence of faults which could have an important geophysical signature and that could affect the compartimentalization of the poten

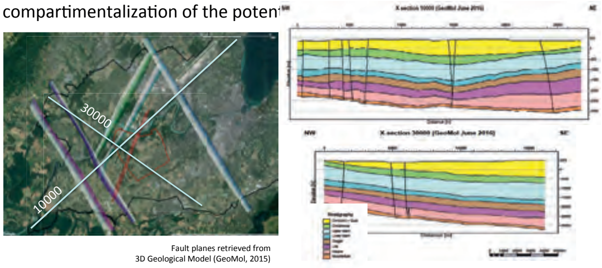

Fault planes retrieved from
3D Geological Model (GeoMol, 2015)

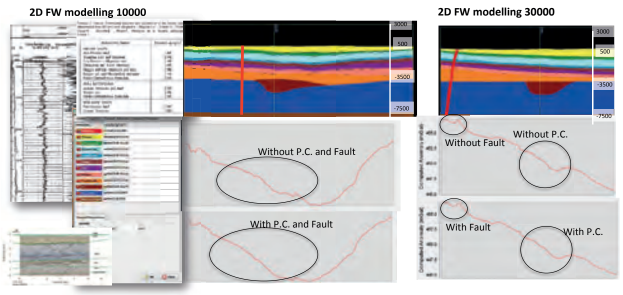

Acquisition

1227 New Stations (black dots)
3 Areas:
- Bernex
- Allondon
- Thonex

52 field working days

Average distance between stations: 200m
Average distance when crossing expected fault: 50-100m
Average Distance at Allondon: 150m
Average distance in Thonex: 50m

All new stations have been correlated to the existing SwissTopo and SIG data (red and green dots)

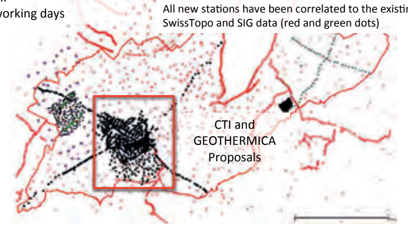

Field Acquisition

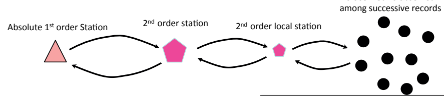

Daily QC + Processing (GravProcess)

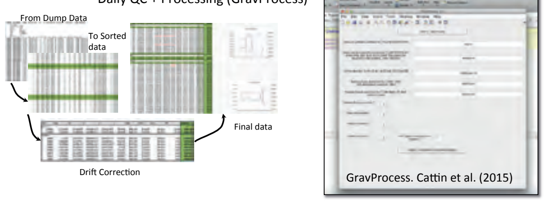

Processing (ongoing):

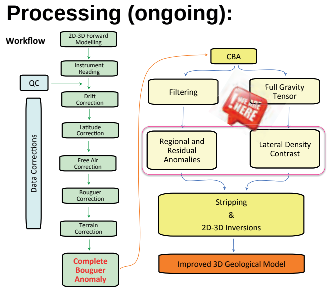

Good quality data

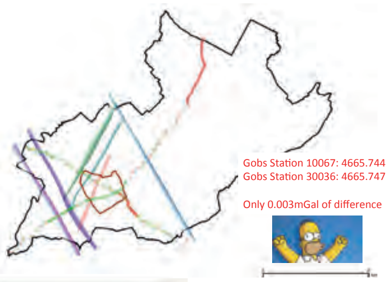

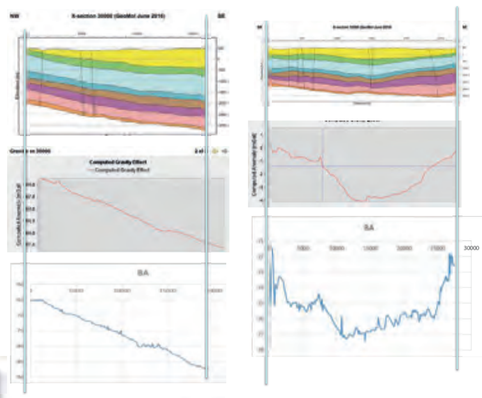

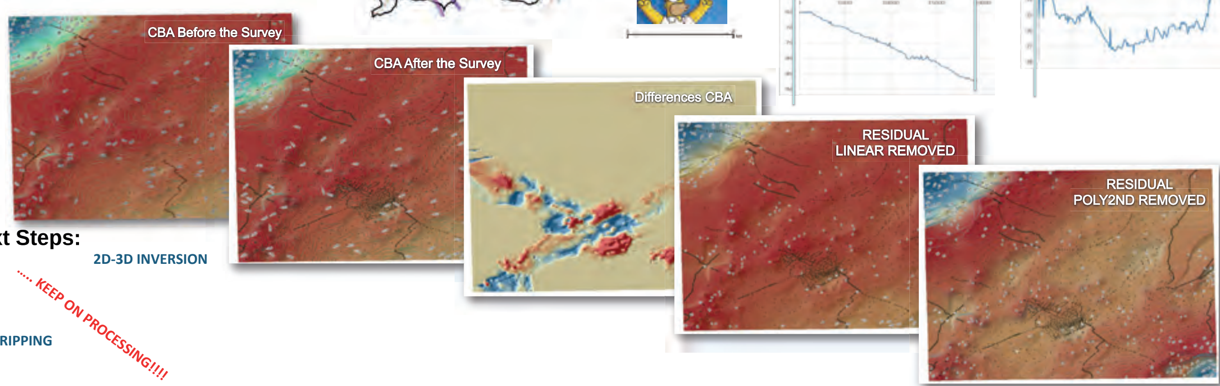

Next Steps:

2D-3D INVERSION

….. KEEP ON PROCESSING!!!!

STRIPPING

GRAVITY TENSORS

SCCER SoE

SWISS COMPETENCE CENTER for ENERGY RESEARCH
SUPPLY of ELECTRICITY

SCCER-SoE Annual Conference 2017

In cooperation with the CTI

Energy
Swiss Competence Centers for Energy Research

Schweizerische Eidgenossenschaft
Confédération suisse
Confederazione Svizzera
Confederaziun svizra

Swiss Confederation

Commission for Technology and Innovation CTI

VSP survey at the Thonex Well - Geneva

L. Guglielmetti[1], A. Moscariello[1], M. Francois[2], C. Nawratil de Bono[2], C. Dezayes[3], B. Adnand[3], P. Corubolo[4], F. Poletto[4]

[1]Earth Science Department, University of Geneva;[2] Services Industriles de Geneve; [3] BRGM; [4]INOGS Trieste

Abstract: In the frameowrk of the Geothermie 2020 program and the FP7 IMAGE project a VS suvrey has been carried out in the Thonex geothermal well in 2016. The main goals were:

- Acquire a detailed velocity model to improve the GeoMol 3D Model
- Characterize the carbonate formations
- Highlight fault zones
- Develop an acquisition approach which can be applied for further wells

The collected data show an overall good quality and helped constraining the velocity model of the main potential geothermal reservoirs and highlight some anisotropies in the Molasse sediments which can reflect a layered structure of the deposits.

The Thonex Geothermal Well

- The Thonex well was drilled in 1993 with the goal to tap a deep thermal acquifers in the Jurassic formations to provide heat for district heating.
- A TVD of 2530m was reached with a deviated geometry towards NE (MD 2690m)
- Ground water was tapped in the Upper Jurassic reef limestones, but at rates below expectations.
- Well testing via air lift indicated a stabilized flowrate of 11 m3/h, originating from Upper Jurassic limestones at a depth of about 1900 m and a fluid temperature of 70°C as evidenced by production logging. The geothermal gradient, measured at 3.12°C/100
- The well is now accessible only down to 1500m MD

Local Geology and Stratigraphy

The Greater Geneva region is a Swiss-French transnational zone located at the southwestern extremity of the North Alpine foreland Molasse basin. It consists of a thick sedimentary cover of Mesozoic age, principally composed of carbonate and marl formations, overlying a crystalline basement often incised by depressions filled with Permo-Carboniferous sediments.

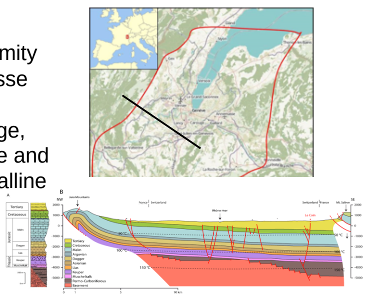

Synthetic stratigraphic log (A) and geological cross-section (B) across the Greater Geneva Basin (modified after PGG report, 2011)

3D Geological horizons from GeoMol Model

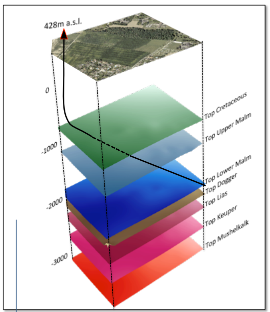

Well Stratigraphy

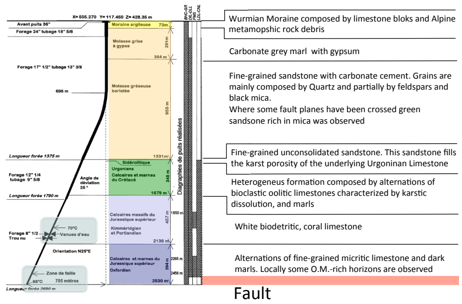

Design

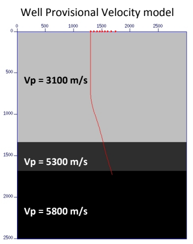

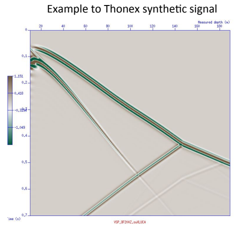

Walk above VSP obtained by moving the source above the well in order to cover the well path, overlap the sections, obtain gathers suitable to separate the VSP wavefields

Design supported by:
1. Ray tracing
2. Synthetic data processing

Layout with gathers of 24 traces and 5 source positions

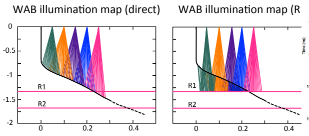

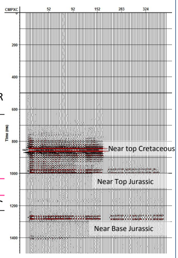

Example of WAB synthetic subset-data processing (separated reflections)

Acquisition and Field QC

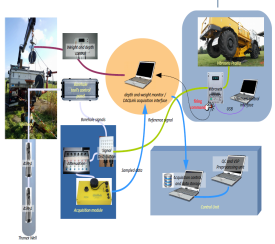

Receivers
Two Avalon ASR-1 Borehole Geophones containing 3C orthogonal receivers

Record length	20 sec.
Sampling rate	1 ms

Source
One Prakla vibrator driven by Seismic Source force II control

Sweep parameters

Minimum frequency	8Hz
Maximum frequency	120 Hz
Sweep per level	3
Sweep duration	14 sec.
Sweep taper	0.3 sec
Peak Force	80%

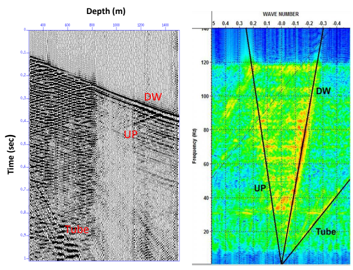

DW- Down-going wave
UP- Up-going wave

- Good quality data below 800m depth (0.25ms)
- Poor quality data above 800: condition of the casing or cement bond

Example showing data quality

Processing

Main processing steps:

- Header adjustment
- Source receiver offset calculation
- Frequency analysis
- Band-pass filtering (8-12-110-120 Hz)
- First Break (FB) picking
- Velocity analysis
- Wavefield separation
  - Mean scaling in 20ms window centered on the FB
  - Median filter (7 traces)
  - FK filter design
  - FK filter for upgoing enhancement
  - Two Way Time (TWT) with and without NMO verticalization
  - Predictive deconvolution
  - Wave shaping deconvolution
  - Spherical divergence recovering
  - Corridor mute and corridor stack
- Kirchhoff migration

Location of the VSP offsets

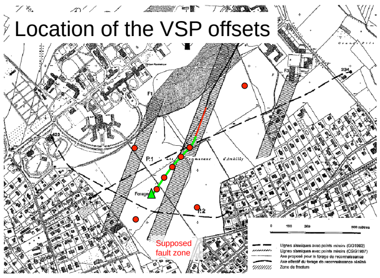

Results

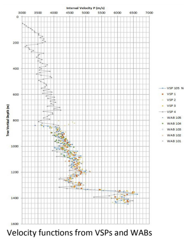

Velocity functions from VSPs and WABs

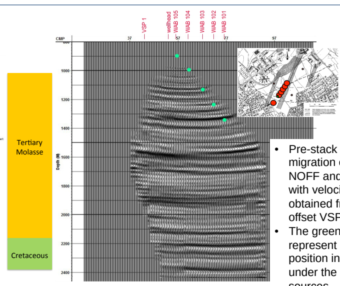

- Pre-stack depth migration of WAB, NOFF and VSP-1 data with velocity model obtained from near offset VSP
- The green dots represent the sensor position in the well under the different sources

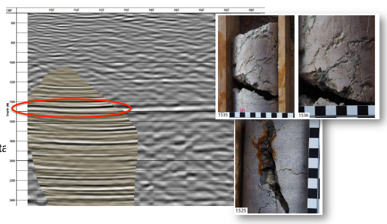

Superposition of depth conversion Thonex-2 reflection seismic line with pre-stack depth migration of WAB, NOFF and VSP1 and core samples collected at the depth of 1525-1536m

Conclusions:

- Overall good quality data even though some noisy signal in the upper 700m due to casing is observed
- Good coherence between offsets velocity models
- Some important reflections on the WAB are observed at 1500 (Karst), 1800, 2100 and 2300m strongly improving the resolution of vintage 2D seismic lines

SCCER SoE
SWISS COMPETENCE CENTER for ENERGY RESEARCH
SUPPLY of ELECTRICITY

SCCER-SoE Annual Conference 2017

In cooperation with the CTI

Seismic attenuation in porous rocks containing stochastic fracture networks

Jürg Hunziker, Marco Favino°*, Eva Caspari*, Beatriz Quintal*, J. Germán Rubino§, Rolf Krause° and Klaus Holliger**

*Université de Lausanne, Switzerland // °Università della Svizzera italiana, Switzerland // §CONICET Centro Atómico Bariloche, Argentina

Introduction

Direct imaging of fractures with seismic waves is generally not possible as the seismic wavelengths tend to be much larger than the aperture of the fractures. To overcome this limitation, we study the attenuation of seismic waves in fractured rocks due to fluid pressure diffusion (FPD) with the goal to use the attenuation, expressed as the inverse of the quality factor $1/Q$, to characterize fracture networks. To this end, we perform numerical upscaling experiments on 2D rock samples featuring stochastic fracture networks. Fractured samples are simulated as poroelastic media. We apply compression and shear tests (Rubino et al., 2009) based on Biot's quasi-static poroelastic equations (Biot, 1941) to obtain P- and S-wave attenuation, respectively.

Fracture Model

A fractured sample is generated by drawing the fracture length from a distribution similar to the one of de Dreuzy et al. (2001):

$$n(l,L) = d_c L^2 (a-1) \frac{l^{-a}}{l_{\min}^{-a+1}} \quad \text{for } l \in [l_{\min}, l_{\max}]$$

The fracture thickness is kept constant at 0.5 mm and the length of the sample L is 0.4 m. The fracture length is varying between l_{min} = 0.01 m and l_{max} = 0.2 m. Instead of the fracture density d_c, which defines the amount of fracture center points per unit area, we use the fracture density d_a, which defines how much area of the sample is covered by fractures. We simulate different samples by changing the fracture density d_a and the characteristic exponent a:

a = 1.5; d_a = 1.5% **a = 3; d_a = 1.5%** **a = 3; d_a = 3%**

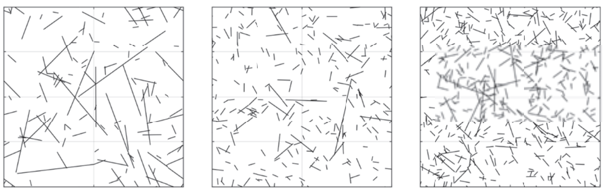

The characteristic exponent a controls the appearance of long fractures relative to short ones. A small value of a represents a distribution with more long fractures, whereas a large a represents a distribution with only very few long fractures. Fractures are considered to be connected if they overlap at least partially.

Results

After having carried out the compression and the shear tests at different frequencies, we obtain the P- and S-wave attenuation due to FPD. For each combination of a and d_a, we generate 20 different samples. The attenuation for the 20 samples generated for a = 1.5 and d_a = 1.5% is shown below with gray curves. The bold black curve is the median of these 20 attenuation curves.

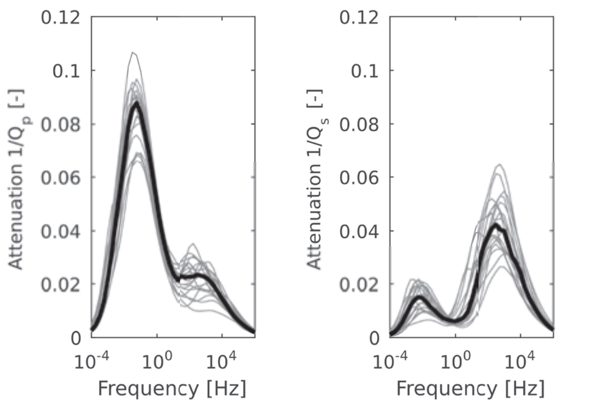

The low-frequency attenuation peak corresponds to FPD from the fracture into the background, while the high-frequency peak is due to FPD within connected fractures (Rubino et al., 2013). We observe, that for P-waves the fracture-to-background process is dominant, while for S-waves the fracture-to-fracture process is more important.

Executing these two tests for five different fracture densities d_a, three different values of the characteristic exponent a, 20 different samples for each combination and 41 different frequencies, results in 24'600 simulations. We have summarized all these information by plotting the mean and the range of the magnitude of the two attenuation peaks as a function of fracture connections:

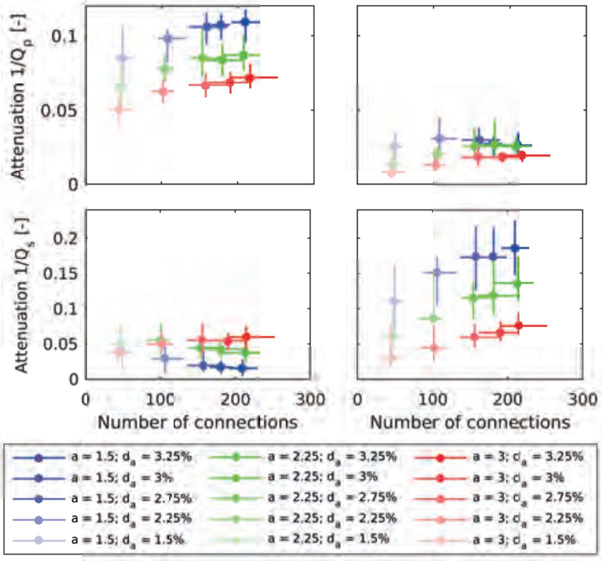

We observe, that the attenuation changes with the amount of fracture connections. Thus, seismic attenuation due to FPD is sensitive to the local connectivity. However, global connectivity, i.e. the presence of a fully connected fluid path, is more difficult to detect. For a detailed interpretation of the data see Hunziker et al. (2017).

Conclusions and Outlook

Our numerical experiments indicate that seismic attenuation due to fluid pressure diffusion is sensitive to the local connectivity of the fractures. Information about the global connectivity is more difficult to extract.

In the future, we aim to investigate the attenuation behavior of anisotropic fracture networks and simulations in 3D. We also aim to study a combination of seismic and resistivity measurements in order to obtain more detailed connectivity information.

References

Biot, M. A. (1941), General theory for three-dimensional consolidation, *Journal of Applied Physics*, 12, 155–164.

de Dreuzy, J.-R., P. Davy, and O. Bour (2001), Hydraulic properties of two-dimensional random fracture networks following a power law length distribution: 1. Effective connectivity, *Water Resources Research*, 37, 2065–2078.

Hunziker, J., Favino, M., Caspari, E., Quintal, B., Rubino, J. G., Krause, R., and Holliger, K. (2017), Seismic attenuation and modulus dispersion in porous rocks containing stochastic fracture networks, *Journal of Geophysical Research*, under revision.

Rubino, J. G., C. L. Ravazzoli, and J. E. Santos (2009), Equivalent viscoelastic solids for heterogeneous fluid-saturated porous rocks, *Geophysics*, 74, N1–N13.

Rubino, J. G., L. Guarracino, T. M. Müller, and K. Holliger (2013), Do seismic waves sense fracture connectivity?, *Geophysical Research Letters*, 40, 692–696.

SCCER SoE
SWISS COMPETENCE CENTER for ENERGY RESEARCH
SUPPLY of ELECTRICITY

SCCER-SoE Annual Conference 2017

Unil | Université de Lausanne

TU Delft
Delft University of Technology

In cooperation with the CTI
Energy
Swiss Competence Centers for Energy Research
Swiss Confederation
Commission for Technology and Innovation CTI

Towards fracture characterization using tube waves

Jürg Hunziker, Shohei Minato°, Eva Caspari*, Andrew Greenwood* and Klaus Holliger**
**Université de Lausanne, Switzerland // °Technische Universiteit Delft, The Netherlands*

Introduction

Tube waves are generated and reflected at intersections between a borehole and one or more fractures. Their amplitude depends notably on the fracture compliance and the hydraulic transmissivity of the fracture. Therefore, tube waves have significant potential for characterizing fractures in terms of their mechanical and hydraulic properties. The main ingredient of a corresponding inversion algorithm is an accurate and efficient solver of the forward problem. For this purpose, we test the analytical tube wave model described by Minato and Ghose (2017).

Tube wave generation

When a P-wave hits a fracture intersecting a borehole, the fracture is compressed. This induces fluid flow from the fracture into the borehole, which in turn generates a tube wave in the borehole.

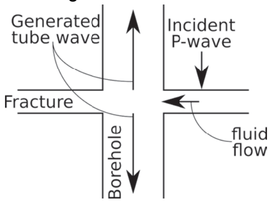

Minato and Ghose (2017) describe the generation of a tube wave due to this mechanism with the tube wave potential Φ_g

$$\phi_g(z) = \sum_{i=1}^{N} \frac{2}{\rho_f c_T} \frac{p_t^{(i)}}{p_{inc}^{(i)}} \delta(z - z_i),$$

where N is the number of fractures in the medium, ρ_f the density of the fluid, c_T the speed of the tube wave and δ the Dirac function. Depth is denoted by z and the sub- or superscripts i give the properties of the ith fracture. The pressure fields of the tube wave p_t and the incoming P-wave p_{inc} are given by

$$p_t^{(i)}(\omega) = \sigma_0 \frac{j\omega c_T \rho_f Z \alpha_{eff}}{k_r \alpha_f} \frac{H_1(\zeta R)}{R \, H_0(\zeta R)} \quad \text{and} \quad p_{inc}^{(i)}(\omega) = \sigma_0 \frac{\rho_f c_T^2}{\rho V_S^2} \left(\frac{1 - 2V_S^2/V_P^2}{1 - c_T^2/V_P^2} \right),$$

where σ_0 is the amplitude of the normally incident plane P-wave, ω the angular frequency, k_r the radial wavenumber in the rigid, non-deformable fracture, α_f the fluid velocity, Z the fracture compliance, α_{eff} the effective fluid velocity in the fracture (including the fracture compliance), and R the borehole radius. H_n denotes the Hankel function of the first kind and order n and ζ the effective radial wavenumber.

Tube wave scattering

When a tube wave propagating through a borehole encounters a fracture, fluid flow from the borehole into the fracture is triggered. This leads to reflection and transmission of tube waves.

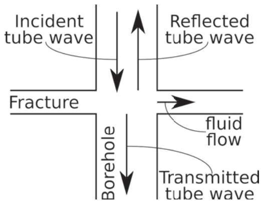

Minato and Ghose (2017) describe this with the scattering potential Φ_s

$$\phi_s(z) = j\omega \sum_{i=1}^{N} \eta^{(i)} \delta(z - z_i),$$

where j is the imaginary unit and η the interface compliance given by

$$\eta = -\frac{2\zeta}{R} \frac{L_0}{k_r^2 \alpha_f^2 \rho_f} \frac{H_1(\zeta R)}{H_0(\zeta R)},$$

with L_0 denoting the fracture aperture.

Results

We start by considering a simple model with two identical fractures with an aperture L_0 of 2 mm.

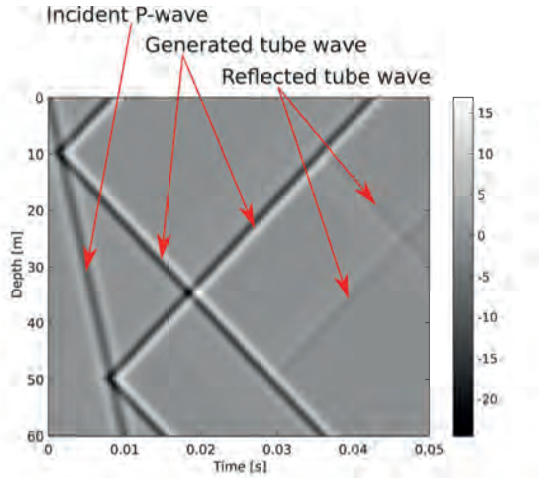

Next, we consider a more realistic model of a fractured rock mass based on evidence from the GDP1 borehole on the Grimsel Pass. The locations of the fractures are inferred from the caliper log while their mechanical and hydraulic properties are chosen to be uniform. Despite these simplifications, the overall resemblance between the observed and simulated tube wave records is remarkably close, which in turn indicates that the problem might be amenable to a global inversion approach.

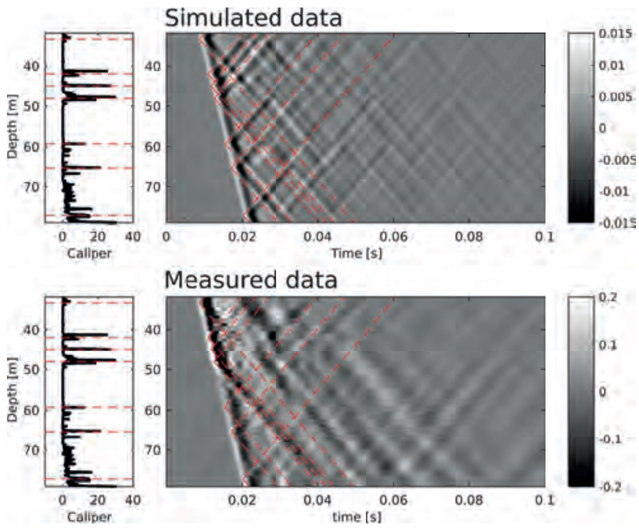

Conclusions

We have implemented a new method for tube wave modeling and applied it to a simplified model of the fractured crystalline rocks penetrated by the GDP1 borehole on the Grimsel Pass. The results are encouraging and indicate that the inversion of tube wave data might allow for the characterization of fractures in terms of their mechanical and hydraulic properties.

Reference

Minato, S. and R. Ghose (2017), Low-frequency guided waves in a fluid-filled borehole: Simultaneous effects of generation and scattering due to multiple fractures, *Journal of Applied Physics*, 121, 104902.

SCCER SoE
SWISS COMPETENCE CENTER for ENERGY RESEARCH
SUPPLY of ELECTRICITY

SCCER-SoE Annual Conference 2017

In cooperation with the CTI
Energy
Swiss Competence Centers for Energy Research
Commission for Technology and Innovation CTI

Importance of dolomitiziation of the Upper Jurassic carbonate rocks for geothermal prospection in the Geneva Basin (Switzerland & France)

Makhloufi Y., Rusillon E.*, Brentini M.*, Meyer, M., Samankassou E.**
(yasin.makhloufi@unige.ch)
* UNIVERSITÉ DE GENÈVE

Introduction and geological context

The Canton of Geneva is currently exploring the opportunities for geothermal energy exploitation in the Geneva Basin (GB) sub-surface. It has been shown that the Upper Jurassic, and more particularly the Kimmerdigian limestones, are affected by dolomitization processes (e.g. Charollais, 1996, 2013; Deville, 1988; Fookes, 1995; Meyer, 2000; Mouchet, 1998; Rameil, 2008; Strasser, 2015). Such diagenetic processes are often associated with important modifications in the reservoir properties of the rock by poro-genesis or poro-necrosis mechanisms. Dolomitized limestones already proved to be productive reservoir for geothermal exploitation in time-equivalent deposits in South-Germany.

Based on field analogues and sub-surface data (Fig. A), our main objectives are: (1) to provide a detailed diagenetic history of the Kimmeridgian units in the GB, (2) to discuss the origin of the dolomitization processes when encountered and finally, (3) to propose a diagenetic model to allow our results to be used during further exploration of the basin and compared with petrophysical characterization of the reservoir units.

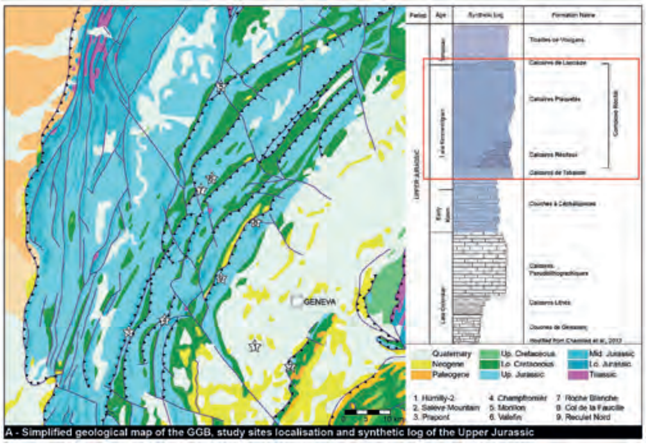

A - Simplified geological map of the GGB, study sites localisation and synthetic log of the Upper Jurassic

Methods

- Samples from outcrops and cores were prepared for thin section analysis. Thin sections, impregnated with epoxy resin dyed by Methylene blue, were used to define the texture, grain type, cement type, and pore-type distribution.
- Sequence of diagenetic events and their mineralogy was constrained using Cathodoluminescence (CL) analysis and Calcite staining.
- S.E.M. images and semi-quantitative analyses and mapping helped further characterization of diagenetic features.

Results

Most of the initial porosity in the different unit studied was filled by the precipitation of several stages of calcite cementations.

Dolomitization precipitated during early diagenesis and overprinted any precedent stages. In most of the case, the dolomitization is mainly represented by planar, replacement dolomite.

Dedolomitization is observed a by either: (1) an almost complete dissolution leading to the creation of secondary pore space or (2) a two-step calcitization driven by the infiltration of Ca-rich water leading to dissolution, formation of microvugs and then precipitation of calcite.

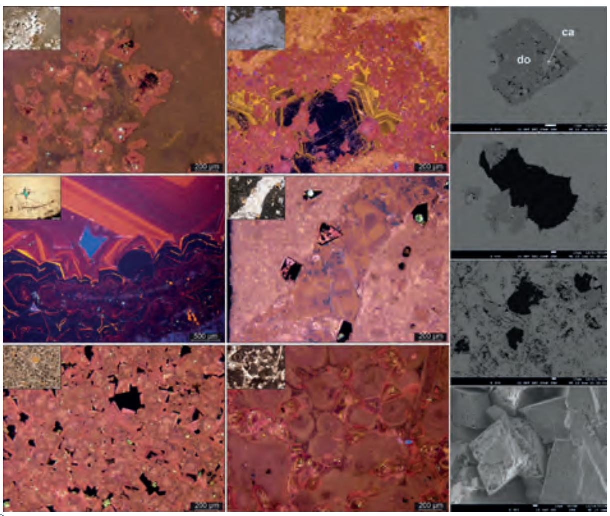

Major Insights

The Upper Jurassic carbonate rocks form a complex carbonate reservoir strongly affected by diagenesis. Based on the petrographic data acquired from sub-surface and outcrops, the following conclusions can be made:

- Dolomitization occurred during early diagenesis and overprinted all precedent stages. The most affected units are the Calcaires de Tabalcon and the Calcaires Récifaux.
- The first stages of dolomitization are interpreted to be induced by a reflux-type model involving mesosaline to hypersaline fluid originating from evaporitic conditions in a lagoonal environment. The third stage of replacive, fabric-destructive dolomite is explained by shallow burial dolomitization producing syntaxial overgrowth dolomite over pre-existing nuclei. **This process is responsible for the highly porous sucrosic dolomite occurring in the Reculet section.**
- Dedolomitization is identified at different order of magnitude by either: (1) an almost complete dissolution leading to the creation of secondary pore space or (2) a two-step calcitization driven by the infiltration of Ca-rich water leading to dissolution, formation of micro-vugs and then precipitation of calcite.
- **The creation of secondary pore space could provide a good connectivity between the intraparticular or matricial microporous network and the interparticular moldic macroporous network. This enhanced connectivity could therefore provide good reservoir properties suitable for geothermal energy exploitation.**

Carbonate heterogeneities remains to be a major issue when assessing the exploitation potential. Understanding of the paragenesis affecting such reservoirs is an important step towards a better exploitation of resources currently available.

Conclusions and Outlooks

- ✓ New insights on the diagenesis that affected the GB and associated fluid migrations.
- ✓ Understanding of how the pore network evolved can be used to explain the reservoir properties observed in the Upper Jurassic carbonate rocks of the GB.

GEOTHERMIE 2020

RÉPUBLIQUE ET CANTON DE GENÈVE

SIG

- **Objectives:** assessment of geothermal potential in the Geneva Basin carbonate rocks
- **Concept:** characterization of diagenetic features, pore network and impact on reservoir properties
- **Main Partners:** Services Industriels Genevois (SIG), Etate de Genève (GESDEC), University of Geneva

SCCER SoE
SWISS COMPETENCE CENTER for ENERGY RESEARCH
SUPPLY of ELECTRICITY

SCCER-SoE Annual Conference 2017

In cooperation with the CTI
Energy
Swiss Competence Centers for Energy Research
Commission for Technology and Innovation CTI

ÉCOLE POLYTECHNIQUE FÉDÉRALE DE LAUSANNE

Investigation of the evolution in physical properties of crustal rocks with different degree of microfracturation.

Lucas Pimienta & Marie Violay
Laboratory of Experimental Rock Mechanics, EPFL, Lausanne, Switzerland

European Commission

Motivation:

Field seismic and electrical resistivity are powerful tools to investigate from the surface geological reservoir rocks at depth.
The two methods are complementary and have been largely used to prospect for oil/gas reservoirs. However, little is still known on the intrinsic dependences of the two properties to the degree of microfracturation (e.g. Pimienta et al., 2017). Moreover, electrical properties have seldom been measured in the high pressure and high temperature range (Violay et al., 2012)
Using thermal treatment at different temperatures, known to induce a variable degree of microfracturation in rocks (e.g. Nasseri et al., 2007), the aim of this work is to investigate how the degree of microfracturation affects the physical properties of rocks.

Project:

- ***PROGRESS:*** *PROspection and PROduction of Geothermal RESservoirS*
- Understand the links between physical properties in geothermal reservoir rocks.

Samples & Methods:

- ➢ Approach: Evolution in properties for varying degree of damage
- ⇒ Thermal treatment in oven for T in the range of [20,1000] °C

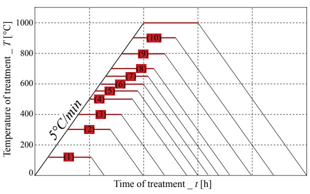

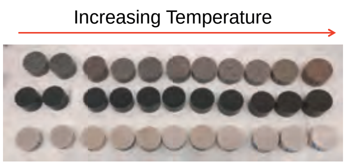

- ➢ Rocks samples: (11 for each rock)
- **Diorite** : ϕ = [0.1;0.3]% // Approx. 30 % quartz
- **Granite** (Westerly) : ϕ = [0.7;1.3]% // Approx. 30 % quartz
- **Sandstone** (Fontainebleau): ϕ = [4.1;6.4]% // Quartz of 100%

- ➢ Petrophysical characterisation:
  - ➢ Porosity
  - ➢ P- & S-wave velocities
  - ➢ Electrical impedance:
    - ➢ Frequency of 1 kHz
    - ➢ Pore fluid : Brine (tap water + 1g/L of NaCl)

Results

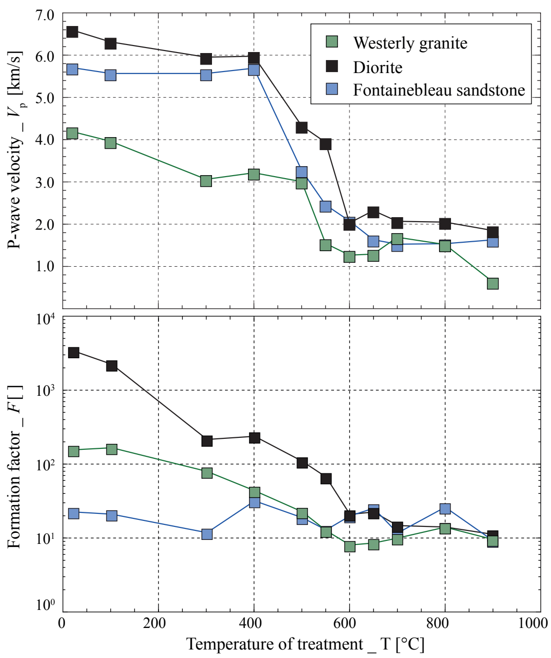

Variable dependence to the temperature for the two properties & the different rock types:

- ➢ Elastic properties: Large decrease in Vp starting from 400°C, for all rocks
- ➢ Electrical properties:
  - ➢ Largest decrease for the **Diorite** (T < 600°C)
  - ➢ Largest decrease for the Granite (T < 600°C)
  - ➢ No variation for **Sandstone**

Interpretation

- ➢ Normalised Vp : Same variations for all rocks. Decrease of up to about 80% of the initial property
  => Very large degree of damage for all three samples.
- ➢ Inverse formation factor F :
  => **Granite** & **Diorite :** Variations for same T as Vp.
  => Sandstone: Large microfracturation but no effect on F or ϕ.

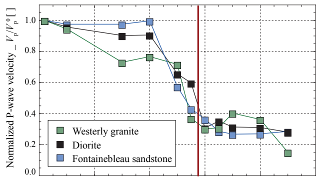

Inverse formation factor F :

- **Granite** & **Diorite** : Direct correlation with Vp & ϕ.
- **Sandstone**: No correlation with Vp => Large microfracturation but no effect on transport properties

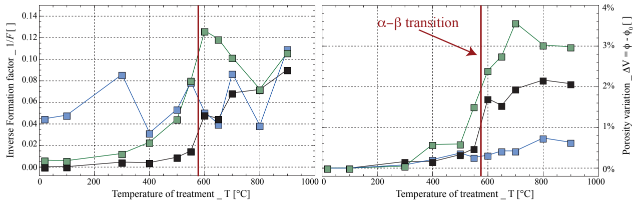

Conclusion

- ➢ Dramatic effects of the temperature in rocks, even though temperature rate is kept low
  ⇔ Role of grains anisotropic thermal expansions.
- ➢ Variable dependence to the temperature for the different properties, and the different rocks.
- ➢ Rather than being the trigger of changes in properties, the α−β transition is the temperature for which the properties reach their asymptotic value.

⇔ The transition may not be the cause for the variations in properties !?

- ➢ Independent of the thermal variation, large effects of the rock type:
  - ➢ **Diorite**: not initially microcracked & not porous => Most dramatic effects on all properties
  - ➢ **Granite**: Initially microcracked & not porous => Less dramatic effects but same variations for all properties
  - ➢ **Sandstone**: not initially microcracked, but porous => Dramatic effects still observed for Vp, but little change in porosity and permeability.

References

- Nasseri, M. H. B., Schubnel, A., & Young, R. P. (2007). Coupled evolutions of fracture toughness and elastic wave velocities at high crack density in thermally treated Westerly granite. *International journal of rock mechanics and mining sciences*, *44*(4), 601-616.
- Pimienta L., Sarout, J., Esteban, L., David, C., & Clennell, B. (2017): Pressure-dependent Elastic, Electric and Hydraulic transport properties of porous and permeable rocks: Insights into the links between transport properties, *Journal of Geophysical Research*, ***major revisions***.
- Violay, M., Gibert, B., Azais, P., Pezard, P. A., & Lods, G., 2012, A new cell for electrical conductivity measurement on saturated samples at upper crust conditions, *Transport in porous media*, **91**(1), 303-318.

SCCER SoE

SWISS COMPETENCE CENTER for ENERGY RESEARCH
SUPPLY of ELECTRICITY

SCCER-SoE Annual Conference 2017

In cooperation with the CTI
Energy
Swiss Competence Centers for Energy Research
Commission for Technology and Innovation CTI

A numerical approach for studying attenuation in interconnected fractures

Beatriz Quintal[1], Eva Caspari[1], Klaus Holliger[1], and Holger Steeb[2]

[1]University of Lausanne, Switzerland; [2]University of Stuttgart, Germany

Introduction

Squirt flow is the main cause of acoustic dissipation in porous rocks fully saturated with a liquid. Classical microscopic models for squirt flow are based on interconnected microcracks (O'Connell and Budiansky, 1977) or on microcracks connected to spherical pores (Murphy et al., 1986). A squirt-type flow may, however, also occur at the mesoscopic scale within hydraulically interconnected fractures. This phenomenon is thus a potential indicator of fracture interconnectivity and was numerically studied by Rubino et al. (2013) using Biot's (1941) equations to describe both fractures and background as porous and permeable media. Vinci et al. (2014) then used a scheme that couples Biot's equations to describe the porous and permeable background with a 1D solution of Navier-Stokes equations for fluid flow within the fractures. Here we propose a simpler approach that couples Hooke's law with the Navier-Stokes (HNS) equations to describe the laminar flow of a viscous compressible fluid in conduits that are embedded in an isotropic, linear elastic solid.

Numerical scheme

The coupled HNS equations reduce to Hooke's law in the subdomains representing an elastic solid and to the linearized, quasi-static Navier-Stokes' equations in the subdomains representing a compressible viscous fluid by simply accordingly setting the values of three material parameters throughout the numerical model: shear viscosity, and bulk and shear moduli (Quintal et al., 2016). The equations are solved in the frequency domain and the results allow for the dissipation caused by fluid flow or, more accurately, by fluid pressure diffusion.

Results compared to those based on Biot's equations

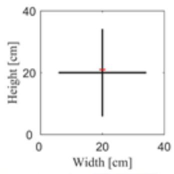

Numerical model for interconnected rectangular fractures saturated with water. The aperture is 1 mm and the length of the fractures is 28 cm.

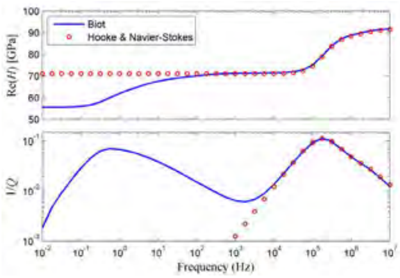

Numerical results for the real part of the P-wave modulus Re(H) and attenuation 1/Q based on the coupled HNS equations and, for comparison, on Biot's (1941) equations.

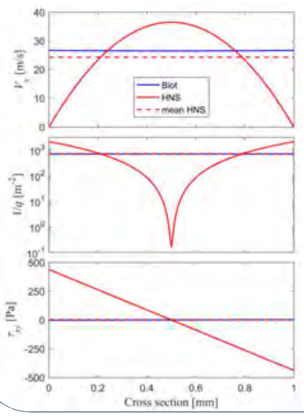

Fluid velocity in the vertical direction V_y, local contribution 1/q to the overall attenuation 1/Q, and shear stress in the fluid τ_{xy}, on a cross section of the vertical fracture at 21 cm (indicated by red line in the model) and at the frequency of the high-frequency attenuation peak. One solution is based on the coupled HNS equations and the other, for comparison, on Biot's equations. The dashed line indicates the mean value of the result based on the HNS solution.

Results compared to an analytical solution for squirt flow

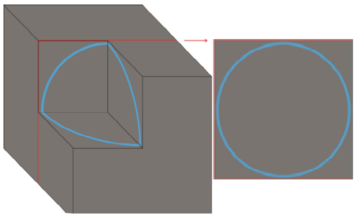

3D model for a spherical shell with radius of 150 μm and thickness of 1 μm that represents a micro-crack. The shell/crack is filled with water and quartz properties describe the background. The cross section defines a 2D model.

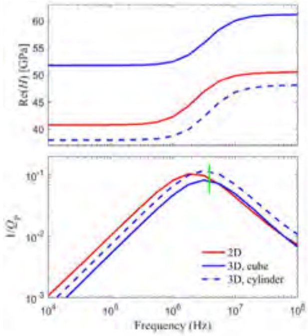

Numerical solution for the P-wave modulus Re(H) and attenuation 1/Q, based on the coupled HNS equations, for the 3D and 2D models above and a 3D model consisting of a cylinder embedding the spherical shell. The green line marks the characteristic frequency based on the analytical solution by O'Connell and Budiansky (1977) for such an spherical crack.

Conclusions and outlook

Numerical results based on the coupled Hooke and Navier-Stokes (HNS) equations were compared with those based on Biot's equations for a scenario involving interconnected fractures. We observed excellent agreement of results for the overall attenuation caused by squirt-type flow, despite differences in the attenuation spatial patterns. At much lower frequencies, the results differ because pressure diffusion in the porous background, described by Biot's equations, is not accounted for by the coupled HNS equations.

Attenuation was also computed based on the coupled HNS equations for a 3D model involving a spherical crack. The frequency of the attenuation peak was successfully compared with that from an analytical solution for squirt flow, which further validates our approach.

Our numerical analyses show that the proposed scheme based on the coupled HNS equations can be readily employed to study flow in interconnected mesoscopic fractures as well as the microscopic squirt flow. In the coming years, we will derive 3D models from micro-tomography images of thermally fractured glass samples to compute frequency-dependent attenuation. The results will then be compared with laboratory measurements of seismic attenuation in those fractured samples. This follow-up research will be co-funded by the Swiss National Science Foundation (SNSF) and the German Research Foundation (DFG) in the context of a recently approved cross-border research project.

References

Biot (1941) General theory of three-dimensional consolidation: Journal of Applied Physics
Murphy, Winkler, and Kleinberg (1986) Acoustic relaxation in sedimentary rocks, dependence on grain contacts and fluid saturation: Geophysics
O'Connell and Budiansky (1977) Viscoelastic properties of fluid-saturated cracked solids: Journal of Geophysical Research - Solid Earth
Quintal, Rubino, Caspari, and Holliger (2016) A simple hydromechanical approach for simulating squirt-type flow: Geophysics
Rubino, Guarracino, Müller, and Holliger (2013) Do seismic waves sense fracture connectivity?: Geophysical Research Letters
Vinci, Renner, and Steeb (2014) On attenuation of seismic waves associated with flow in fractures: Geophysical Research Letters

SCCER SoE
SWISS COMPETENCE CENTER for ENERGY RESEARCH
SUPPLY of ELECTRICITY

SCCER-SoE Annual Conference 2017

In cooperation with the CTI
Energy
Swiss Competence Centers for Energy Research
Schweizerische Eidgenossenschaft
Confédération suisse
Confederazione Svizzera
Confederaziun svizra
Swiss Confederation
Commission for Technology and Innovation CTI

Quantification of the 3D thermal anomaly in the orogenic geothermal system at Grimsel Pass

Christoph Wanner, Larryn W. Diamond, Peter Alt-Epping,
Institute of Geological Sciences, University of Bern (wanner@geo.unibe.ch)

Motivation

Orogenic belts without active igneous activity are recognized as plays for geothermal power production. Owing to lower discharge temperatures than those in volcanic-regions, these systems, which we refer to as "orogenic geothermal systems", are classified as low-enthalpy resources. In the framework of the SCCER-SoE Task 1.1 we are conducting thermal hydraulic (TH) modeling of the orogenic geothermal system at Grimsel Pass to quantify its 3D geothermal anomaly and to evaluate the general potential of such orogenic geothermal systems for geothermal power production.

The Grimsel Pass geothermal system

- Discharge of hydrothermal springs with T≤28 °C into a gas tunnel beneath Grimsel Pass
- They occur over a narrow tunnel section of <100 m, where it intersects the WSW–ENE-striking Grimsel Breccia Fault (GBF)
- Hydrothermal activity is also manifested by the occurrence of a 3 Ma old hydrothermal breccia formed ~3 km below the paleosurface
- Oxygen isotopes and fluid inclusions in quartz and adularia reveal a meteoric fluid origin and a breccia formation temperature of 165 °C
- The Na-K geothermometer applied to the thermal spring waters provides strong evidence that the circulating meteoric water reaches a temperature of at least 214 °C, and more likely ~250°C
- Such temperatures correspond to a remarkable penetration depth of ~10 km, given that the background geothermal gradient of 25 °C/km is the only source of heat in the area.

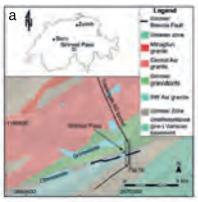

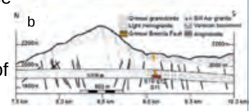

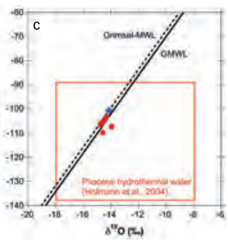

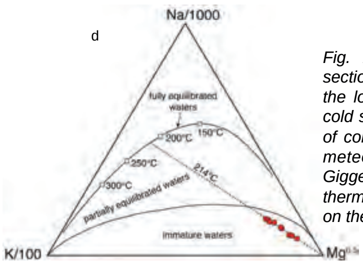

Fig. 1: (a,b) Geological map and cross section of the Grimsel Pass area showing the localities of thermal (red symbols) and cold springs (blue symbol). (c) δ²H vs. δ¹⁸O of cold and thermal springs indicating their meteoric origin. (d) Ternary Na-Kg-Mg Giggenbach diagram demonstrating that all thermal spring samples (filled circles) plot on the 214 °C isotherm.

Model setup

- Simulation of the upflowing segment only
- Large 3D domain to capture the interplay between advective and conductive heat transport
- Constant width of the GBF along the tunnel (100 m)
- Variable extent of the upflow zone parallel to the GBF (50–150 m)
- Initial hydrostatic pressure distribution
- $P > P_{hydrostatic}$ below upflow zone, corresponding to the hydraulic head driving the system (500–800 m)
- Initial conductive temperature distribution

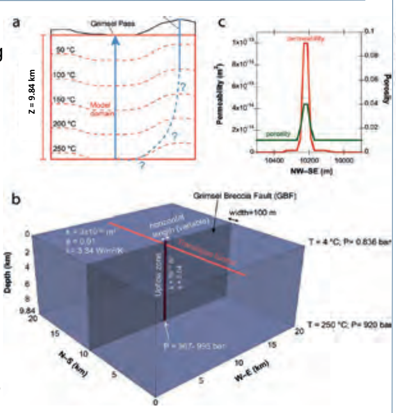

Fig. 2: (a) Schematic meteoric water circulation model. (b) Model setup with specified initial and boundary conditions. (c) Specified permeability and porosity profile along the Transitgas tunnel.

Sensitivity analysis

- Steady-state temperature distribution is approached in less than 5000 a
- Model results demonstrate that the extent of temperature anomalies induced by fracture-flow hydrothermal systems is mainly controlled by
  - the 3D extent of the fault system
  - the upflow velocity, i.e., by the fault zone permeability as well as the hydraulic head gradient driving hydrothermal circulation

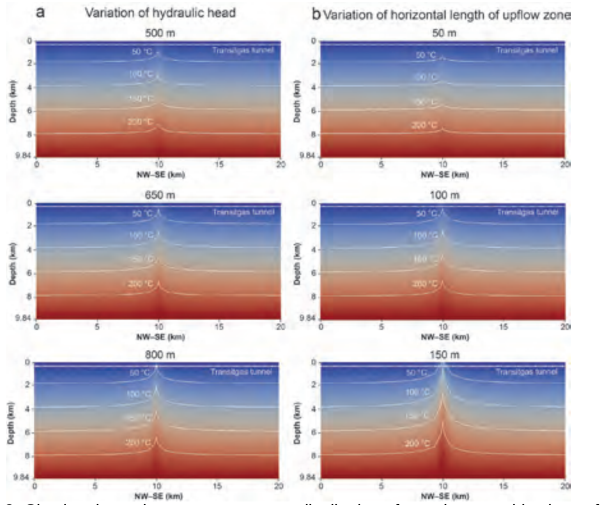

Fig. 3: Simulated steady-state temperature distributions for various combinations of hydraulic head differentials and horizontal length of the upflow zone parallel to the GBF. The panels show the model slice that is perpendicular to the GBF and that includes the Transitgas tunnel.

Quantification of the thermal anomaly

- The model was calibrated against the discharge temperature of thermal springs and the temperature recorded along the tunnel wall
- Breccia formation temperature and $T_{discharge}$ could not be matched with the same parameter set, suggesting that the upflow rate was larger when the hydrothermal breccia was formed 3 Ma ago
- The calibrated model was used to calculate the heat in excess of that provided by the background conductive temperature profile:

$$H = \sum_i C_p \cdot \rho \cdot V_i \cdot \Delta T_i$$

C_p: heat capacity; ρ: bulk rock density; V_i: volume of grid block i; ΔT_i: difference to background T profile

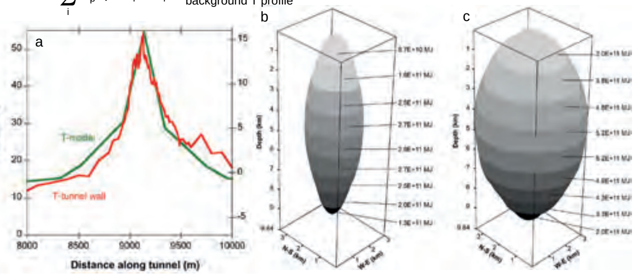

Fig. 4 (a): Comparison between measured and modeled temperatures along the wall of the Transitgas tunnel. (b,c) Anomalous heat per km depth predicted for: (b) the calibrated model simulating the current flow system and (c) the model simulating the temperature of the fossil system (i.e., 165 °C at a depth of ~3 km).

Conclusions

- Converting heat excesses shown in Figures 4a,b to theoretical geothermal power output by dividing by time (20 a) yields values from 10–40 MW per km depth, demonstrating that orogenic geothermal systems are promising plays for geothermal power production
- Based on our modelling, exploration should focus on high topography areas such as those in the Vallais and in surrounding valleys of the Central Alps where hydraulic head gradients and hence upflow rates are at maximum values.

SCCER SoE
SWISS COMPETENCE CENTER for ENERGY RESEARCH
SUPPLY of ELECTRICITY

SCCER-SoE Annual Conference 2017

In cooperation with the CTI
Energy
Swiss Competence Centers for Energy Research
Swiss Confederation
Commission for Technology and Innovation CTI

Causes of abundant calcite scaling in geothermal wells in the Bavarian Molasses Basin, Southern Germany

Christoph Wanner[1], Florian Eichinger[2], Thomas Jahrfeld[3], Larryn W. Diamond[1]
[1]Institute of Geological Sciences, University of Bern (wanner@geo.unibe.ch); [2]Hydroisotop GmbH, Schweitenkirchen, Germany; [3]Renerco Plan Consult, Munich, Germany

Motivation

Over the past 15 years the Bavarian Molasse Basin in southern Germany has become a veritable hotspot for geothermal power. Currently 22 geothermal power plants are being operated. Typical flow rates are between 30 and130 L/s and the production temperatures reach up to 150 °C. Despite these favorable reservoir conditions, the use of many of the wells for heat and power production is highly challenging. The main difficulty, especially in the deep (>3000 m) boreholes with temperatures >120°C, is that substantial calcite scaling is hindering the proper operation of the pumps within the wells and of the heat exchangers at the surface. As a consequence, high maintenance costs (e.g., replacing downhole pumps: ~€500'000) still inhibit the economically sustainable operation of these plants. For this study, we used a combination of analytical and numerical techniques to identify the main processes controlling calcite scaling at the Kirchstockach geothermal plant, located 15 km SE of Munich.

Kirchstockach geothermal power plant

- Binary cycle power plant with an installed capacity of 5.5 MW_{el}
- Downhole pump is installed at 800 m depth
- Scale formation is observed at the pump, the riser pipe and in the plant at the surface
- Scales consist of almost pure calcite with minor corrosion products (magnetite, pyrrhotite, pyrite)
- Scaling thicknesses correspond to a low calcite precipitation rate of about 1.2×10^{-9} mol/s/m²

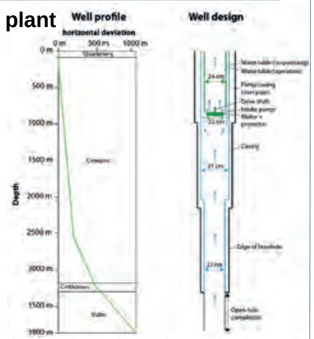

Fig. 1: Schematics of the production well

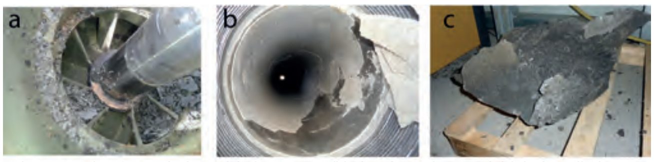

Fig. 2: Scales formed along (a) the pump, (b) the riser pipe, and (c) in installations of the geothermal plant at the surface.

Wellhead water samples

- Weakly mineralized Na-HCO_3- water type (TDS: 430-500 mg/L)
- Constant production temperature of 135°C
- Constant composition with respect to major anions and cations
- Varying composition with respect to dissolved [Ca^{2+}] and [HCO_3-]
  - ➢ reflects varying calcite saturation state
- Calcite and dolomite dissolution rates are rather fast
  - ➢ Chemical equilibrium is likely to prevail under in-situ reservoir conditions
  - ➢ Well head composition does not reflect the composition at reservoir P,T
  - ➢ Variation in TDS and deviation from carbonate equilibrium is an effect of scaling formation
  - ➢ Carbonate equilibrium (SI=0) is obtained by numerically adding CO_2

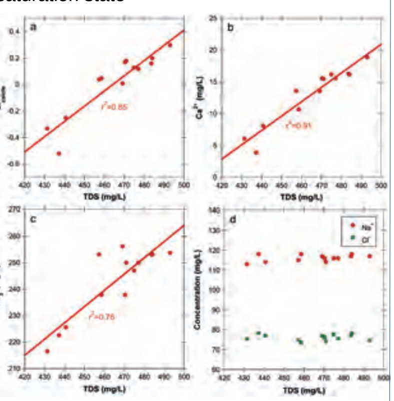

Fig. 3: Variation in compositions of wellhead fluid samples. SI: saturation index. TDS: total dissolved solids.

Fluid inclusions

- Gas (N_2+CO_2) and petroleum inclusions are identified in calcite crystals
  - ➢ Demonstrate the presence of a free gas phase in the upflowing water + petroleum (3-phase system)
- Dissolved gas concentrations of wellhead samples are well below saturation (at T=135°C, 18 bar)
- Homogenization temperature of petroleum inclusions T_h correspond to the production temperature (T_h=128–138 °C; T_{prod}=135°C)
  - ➢ No indication of an unwanted temperature increase in the well

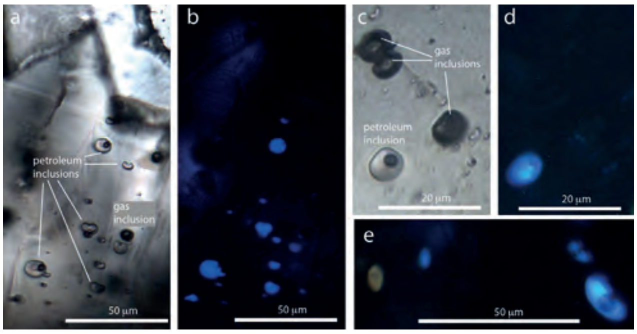

Fig. 4: Examples of primary gas and petroleum inclusions observed in calcite crystals. Microphotographs (a) and (c) taken under normal transmitted light. Microphotographs (b), (d) and (e) taken under UV reflected light.

Preferred scaling formation model

All observations can be explained by the following sequence of processes:

- Carbonate equilibrium is prevailed at reservoir conditions (SI=0)
- Pressure somewhere drops to 4-6 bar within the production well
- Owing to its local pressure minimum, the pump is the most likely location
  - ➢ Effect of the fast rotating centrifugal pump (i.e. cavitation, Fig. 6)
- Boiling of the produced fluid
- N_2 and CO_2 are stripped into gas phase
- Immediate calcite supersaturation ($SI_{calcite}$>>0)
- Gas phase partially persists
- Scaling formation during further upflow and in the power plant
- Trapping of gas (CO_2, N_2) in precipitating calcite crystals

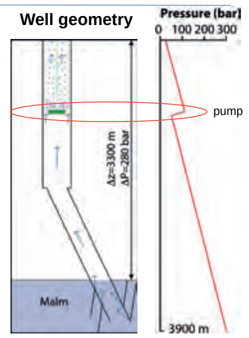

Fig. 5: Boiling scenario and idealized pressure profile along the well.


Fig. 6: Cavitating propeller model in a water tunnel experiment.

	P (bar)	Water composition					Gas composition				
		HCO_3 (mg/L)	CO_2 (mg/L)	N_2 (NmL/kg)	pH	$SI_{calcite}$	Sg (vol%)	H_2O (vol%)	N_2 (vol%)	CO_2 (vol%)	(N_2/CO_2) (vol ratio)
Simulation	4.6	241	132	10.1	6.69	0.35	8.4	73.2	19.4	7.4	2.6
Sample KST-12	-	241	132	8.0	6.67	0.30	-	-	-	-	2.37-6.9

Table 1: Comparison of measured wellhead fluid composition with that predicted from boiling calculations (CHILLER). Also shown is the simulated N_2/CO_2 ratio of the coexisting gas phase in comparison to the ratio measured in gas inclusions.

For more information:


Geothermics

Causes of abundant calcite scaling in geothermal wells in the Bavarian Molasse Basin, Southern Germany

Christoph Wanner, Florian Eichinger, Thomas Jahrfeld, Larryn W. Diamond

70 NRP Energy Turnaround National Research Programme

SCCER-SoE Annual Conference 2017

SCCER SoE
SWISS COMPETENCE CENTER for ENERGY RESEARCH
SUPPLY of ELECTRICITY
In cooperation with the CTI
Energy Swiss Competence Centers for Energy Research
Schweizerische Eidgenossenschaft
Confédération suisse
Confederazione Svizzera
Confederaziun svizra
Swiss Confederation
Commission for Technology and Innovation CTI

Measuring pressure dependent fracture aperture distribution in rough walled fractures using X-ray computed tomography

Quinn C. Wenning and Claudio Madonna – *Department of Earth Sciences, ETH Zurich*
Lisa Joss and Ronny Pini – *Department of Chemical Engineering Imperial College London*

1. Introduction

- Knowledge of fracture (aperture) distribution is paramount for sound description of fluid transport in low-permeability rocks.
- In the context of geothermal energy development, quantifying the transport properties of fractures is needed to quantify the rate of heat transfer and optimize the engineering design of the operation.
- Core-flooding experiments coupled with non-invasive imaging techniques (e.g., X-Ray Computed Tomography – X-Ray CT) represent a powerful tool for making direct observations of these properties under representative geologic conditions.

2. Sample preparation and characterization

- Thermally treated samples (cycles of heating to 400 °C followed by quenching) with slightly enhanced porosity (1.6 % heat treated vs. 0.7 % no treatment) were prepared with a diameter = 5 cm and length = 10 cm.
- A single fracture along the core was induced via a modified Brazilian test with pointed wedged spacers placed along the top and bottom of the sample.

Fig. 1 Left: Brazilian induced fracture and Right: comparison of thermally shocked (left) and not shocked (right) samples.

3. Computed tomography methods

- The method for fracture aperture estimation follows the calibration free missing attenuation method [Huo et al., 2016].
- CT number in the vicinity of a fracture will be reduced due to density deficiency in the gas filled fracture.
- Smearing of the X-ray attenuation due to partial volume effects will cause lower CT numbers adjacent to the fracture.
- Main assumption is that all X-ray attenuation is conserved and that the real CT value of the un-fractured rock can be estimated by neighboring voxels.

$$CT_{MA} = \sum_{i=1}^{N_{vox}} (CT_{r,i} - CT_i)$$

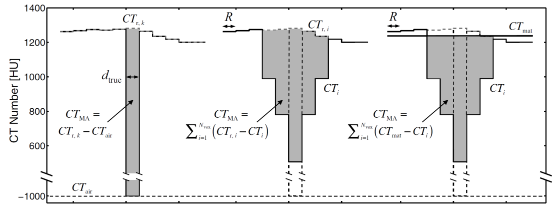

$$d \cdot (CT_{r,k} - CT_{gas}) = R \cdot CT_{MA} \qquad d = \frac{R \cdot \sum_{i=1}^{N_{vox}} (CT_{r,i} - CT_i)}{CT_{r,k} - CT_{gas}} \qquad d = \frac{R \cdot \sum_{i=1}^{N_{vox}} (CT_{mat} - CT_i)}{CT_{mat} - CT_{gas}}$$

Fig. 2 Schematic of true fracture, smeared fracture and known rock matrix CT value, and smeared fracture with estimated matrix CT [Huo et al., 2016].

Fig. 3 The use of He and Kr gases with differing CT number allows us to estimate fracture aperture with two fluids independently.

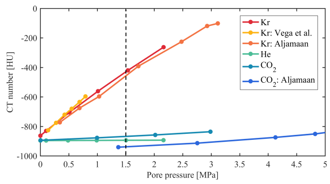

4. Results

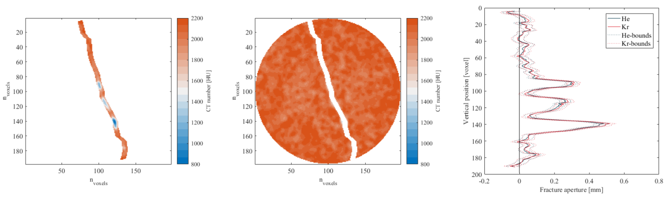

Fig. 4 CT scans of the fracture trace (left) and matrix area (middle), and aperture estimation using He and Kr (right) for a single slice.

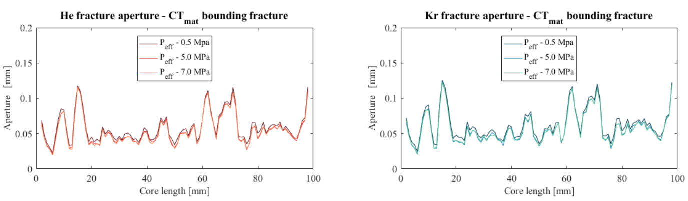

Fig. 5 1D average hydraulic aperture along the length of the core for increasing effective pressure (i.e., average aperture per slice scan).

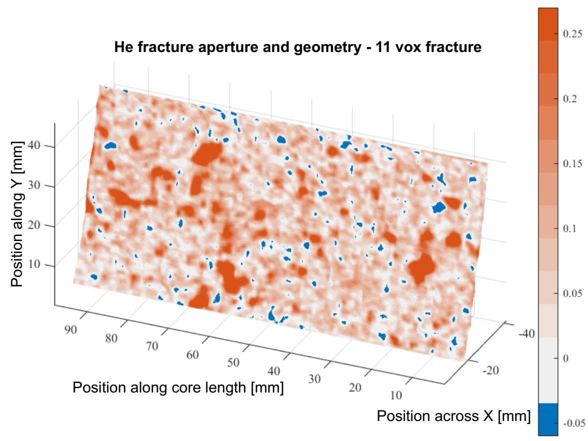

Fig. 6 Fracture aperture heterogeneity for a 5 MPa effective pressure using He as the pore fluid.

5. Discussion

- Application of the calibration free missing attenuation method to rough-walled fractures gives the similar aperture estimations for both He and Kr gases (Fig. 4 and 5).
- Changes in average hydraulic aperture due to confining pressure are consistent with literature (see Fig. 7).
- While the average hydraulic aperture changes are comparable with literature, the CT scan shows heterogeneity of the fracture aperture distribution (Fig. 6), which will influence fluid channelization and, thus, rate of heat transfer and fluid flow in geothermal reservoirs.

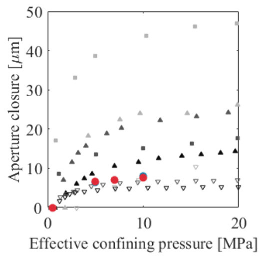

Fig. 7 Comparison of the whole core average hydraulic aperture measured with our CT results and previously published fluid flow experiments.

- He
- Kr
- Granite - Tsang and Witherspoon, 1981
- Marble - Tsang and Witherspoon, 1981
- Granite A - Vogler et al., 2016
- Granite B - Vogler et al., 2016
- Granite C - Vogler et al., 2016

Task 1.2

Title

Reservoir stimulation and engineering

Projects (presented on the following pages)

Scaling spatial distribution of fractures using borehole images: An application to Basel geothermal reservoir
M. J. Afshari, B. Valley, K. Evans

Simultaneous Visualization of Fluid Flow and Mineral Precipitation in Fractured Porous Media
M. Ahkami, X. Kong, M. O. Saar

Acoustic monitoring of laboratory hydraulic fracture growth under stress and pore pressure
T. E. Blum, B. Lecampion

Cross-borehole characterization of permeability enhancement & heat transport in stimulated fractured media: preliminary results from the ISC experiment at the Grimsel Test Site
Alternative: Work Package 5
B. Brixel, M. Klepikova, M. Jalali, F. Amman, S. Loew

Effect of fluid viscosity on fault frictional behavior
C. Cornelio, E. Spagnuolo, G. Di Toro, M. Violay

Injection Protocol and First Results of Hydraulic Fracturing Experiments at the Grimsel Test Site
Alternative: Work Package 5
N. Dutler, B. Valley, L. Villiger, H. Krietsch, M. Jalali, V. Gischig, J. Doetsch, F. Amann

Impact of CO_2 injection on the hydro-mechanical behaviour of a clay-rich caprock
V. Favero, L. Laloui

Visualizing salt tracers using GPR
P. Giertzuch, J. Doetsch, A. Shakas, M. Jalali, A. Kittilä, H. Maurer

A comparison of the seismo-hydro-mechanical observations during two hydraulic stimulations at the Grimsel Test Site
Alternative: Work Package 5
V. Gischig, J. Doetsch, M. Jalali, F. Amann, H. Krietsch, L. Villiger, N. Dutler, B. Valley

Permeability Changes Induced by Hydraulic Stimulation at the Grimsel Test Site
Alternative: Work Package 5
M. Jalali, V. Gischig, J. Doetsch, H. Krietsch, L. Villiger, N. Dutler, B. Valley, K. F. Evans, F. Amann

A matlab package for thermo-hydraulic modeling and fracture stability analysis in fractured reservoirs
G. Jansen, B. Valley, S. A. Miller

A multi-parametric evaluation of the Wallace-Bott hypothesis in the presence of a fluid source
M. Kakurina, Y. Guglielmi, C. Nussbaum, B. Valley

Tracer based characterization of the connected fracture volume in the DUG Lab at the Grimsel Test Site
Alternative: Work Package 5
A. Kittilä, K. Evans, M. Jalali, M. Willmann, M. O. Saar

In situ characterization of groundwater flow and heat transport in stimulated fractured network using DTS
M. Klepikova, B. Brixel, M. Jalali, S. Loew, F. Amann

How much can we interpret mineral surface area with distributions of minerals and pores?
X. Kong, J. Ma, D. Webster, M. O. Saar

Geological characterization and in-situ stress state of the ISC experimental volume
Alternative: Work Package 5
H. Krietsch, V. Gischig, F. Amann, J. Doetsch, M. Jalali, B. Valley

Deformation and tilt measurements during the ISC experiment at the Grimsel Test Site
Alternative: Work Package 5
H. Krietsch, V. Gischig, B. Valley, F. Amann

Core-scale reactive transport modelling of injection of CO_2-charged brine into natural sandstone
J. Ma, X. Kong, M. O. Saar

Mixed finite element method for recovering stress and displacement fields
M. Nejati, T. Driesner

Numerical Modeling of Natural Convection in Fractured Media
J. Patterson, T. Driesner

Enhancing drilling performance by combining conventional and thermal spallation drilling: A feasibility study
E. Rossi, M. A. Kant, C. Madonna, M. O. Saar, P. R. von Rohr

Pico-seismicity during hydraulic stimulation experiments at the Grimsel Test Site
Alternative: Work Package 5
L. Villiger, V. Gischig, J. Doetsch, H. Krietsch, M. Jalali, N. Dutler, B. Valley, K. Evans, F. Amann, S. Wiemer

An Implicit Level Set Scheme to simulate planar 3D hydraulic fracture propagation
H. Zia, B. Lecampion

SCCER SoE
SWISS COMPETENCE CENTER for ENERGY RESEARCH
SUPPLY of ELECTRICITY

SCCER-SoE Annual Conference 2017

In cooperation with the CTI
Energy
Swiss Competence Centers for Energy Research
Commission for Technology and Innovation CTI

Scaling spatial distribution of fractures using borehole images: An application to Basel geothermal reservoir

Mohammad J. Afshari[(1)], *Benoît Valley*[(2)], *and Keith Evans*[(3)]
(1) ETH Zürich, Geological Institute (mohammad.moein@erdw.ethz.ch)
(2) University of Neuchâtel, Center for Hydrogeology and Geothermics
(3) ETH Zürich, Institute of Geophysics

Motivation

Characterization of the natural fractures is key to create a geological model which permits the accurate design and assessment of Enhanced Geothermal System (EGS) development strategies. Our knowledge about the existing fractures in early stages of reservoir creation is restricted to borehole data. Constraining the stochastic fracture network realizations, also referred as Discrete Fracture Networks (DFN), is expected to improve our predictions of seismo-hydromechanical response of a reservoir during hydraulic stimulation.

The primary motivation of this research is to constrain three dimensional *(3-D)* spatial distribution of fractures in a reservoir using borehole observations. First of all, we start with scaling of fracture patterns in a deep borehole such as Basel-1. We base our analysis on the fractures inferred from acoustic televiewer logs in Basel-1 by Ziegler *et al.* (2015). Then, we use synthetic fracture networks to explore the possible extraction of scaling relationships of *2-D* and *3-D* spatial organizations from *1-D* data.

Methodology

1. Characterization of borehole data: The scaling exponent of fracture patterns (in any dimension) can be computed by fitting a power-law to the corresponding correlation function such as equation 1 where,

$$C(r) = \frac{1}{N^2} N_p(r) \sim r^D \qquad (1)$$

N_p is the number of pairs less than *r* apart,
N the total number of fractures and
r is the distance between two fractures.

2. Generate synthetic networks: According to the literature, the only DFN model with established stereological relationships (i.e. relations among the spatial distributions in one, two and three dimensions) is a dual-power law (Davy *et al.*, 1990, Darcel *et al.*, 2003). This research is focused on performing a critical analysis of such stereological relationships in one and two dimensions, and its possible extension to three dimensions. Equation 2 represents DFN model we apply where,

$$n(l, L).dl = c.L^D l^{-a}.dl \qquad (2)$$

$n(l,,L).dl$ is the number of fractures in the length range of $[l, l + dl]$,
L is the domain length,
D is the correlation dimension,
a is the length exponent with c as a constant.

3. Analyze the possible application of stereological relationships to Constrain DFNs: The process of such an analysis is given in the following flowchart.

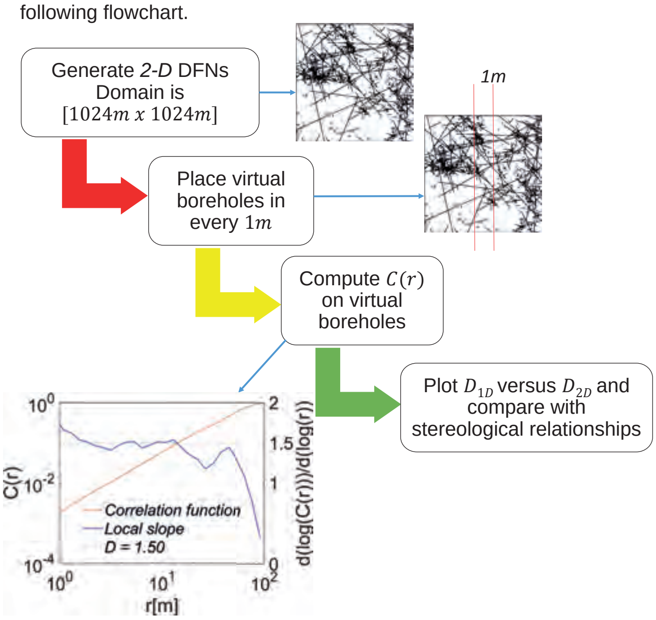

Figure 1. The flowchart of analyzing the application of stereological relationships to Constrain DFNs.

Results

First of all, we present the correlation function of fracture patterns in a deep borehole drilled into crystalline basement (Basel-1). Figure 2 proves the fractal patterns of complete fracture dataset and the dominant fracture set.

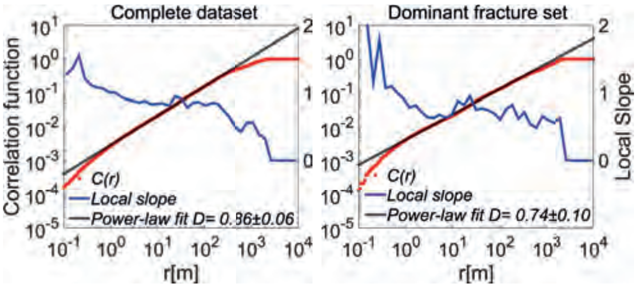

Figure 2. Fractal analysis of the complete fracturing dataset and the dominant fracture set in Basel-1 borehole.

The scale invariance of fracture patterns in Basel-1 might help us to constrain DFNs using available stereological relationships in literature. Figure 3 represents the results of a stereological analysis for two typical length exponents. It is important to note that there is a transition in behaviour of synthetic networks in $a = 2$. Exponents higher than *2,* have a higher frequency of smaller fractures and vice versa.

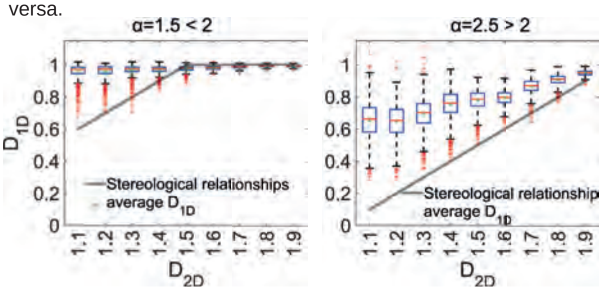

Figure 2. Detailed stereological analysis of synthetic networks in comparison to stereological relationships.

Discussion

- We observed fractal fracture patterns in Basel-1 borehole.
- There is a large discrepancy between the analytical predictions and stereological analysis in synthetic networks.
- The stereological analysis the we performed shows that D_{2D} cannot be reliably estimated from *1-D* data. .
- Estimating *3-D* spatial distribution form one boreholes involves a huge uncertainty associated with estimating D_{2D}. In addition, there is no information about the length distributions of *3-D* fracture planes in the reservoir.

Acknowledgements

The research leading to these results has received funding from the European Community's Seventh Framework Program under grant agreement No. 608553 (Project IMAGE).

References

Ziegler, M., Valley, B., Evans, K. F. (2015). Characterisation of natural fractures and fracture zones of the Basel EGS reservoir inferred from geophysical logging of the Basel-1 well. *World Geothermal Congress Melbourne, Australia*, 19-25.
Davy, P., Sornette, A., Sornette, D. (1990). Some consequences of a proposed fractal nature of continental faulting. *Nature* **348**, 56-58.
Darcel, C., Bour, O., Davy, P. (2003). Stereological analysis of fractal fracture networks. *Journal of Geophysical Research: Solid Earth* **108**.

SCCER SoE
SWISS COMPETENCE CENTER for ENERGY RESEARCH
SUPPLY of ELECTRICITY

In cooperation with the CTI
Energy
Swiss Competence Centers for Energy Research
Schweizerische Eidgenossenschaft
Confédération suisse
Confederazione Svizzera
Confederaziun svizra
Swiss Confederation
Commission for Technology and Innovation CTI

Simultaneous Visualization of Fluid Flow and Mineral Precipitation in Fractured Porous Media

Mehrdad Ahkami, Xiang-Zhao Kong, Martin O. Saar*

Geothermal Energy and Geofluids, Institute of Geophysics, ETH Zurich, Switzerland
** Email: mahkami@ethz.ch*

Background - Motivation

Mineral precipitation during Enhanced Geothermal Systems (EGS) can reduce the efficiency and life time.

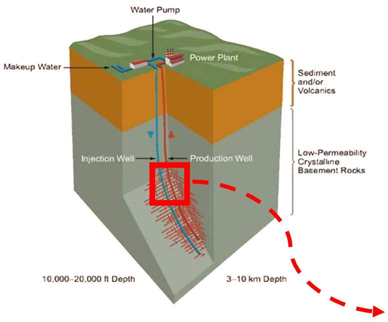

Pore Clogging

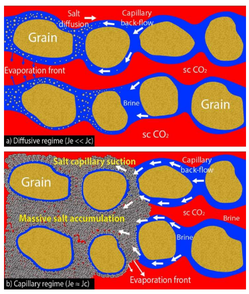

Major causes of mineral precipitation:

- Perturbation of temperature and pressure
- Mixing of two different fluids
- Introducing of a fluid that is out of equilibrium with mineral phase

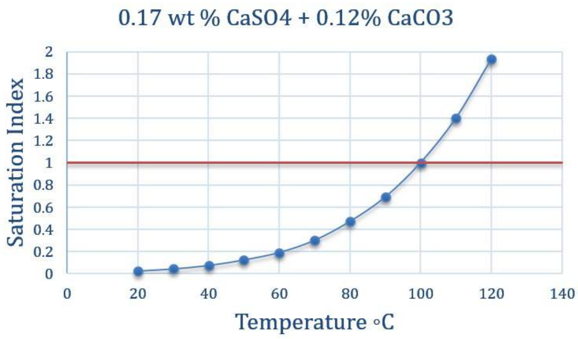

Visualization of Flow by Particle Shadow Velocimetry (PSV)

Fluid is seeded with tracer particles, which are assumed to follow flow dynamics. The motion of seeding particles is illuminated and recorded to determine flow velocity.

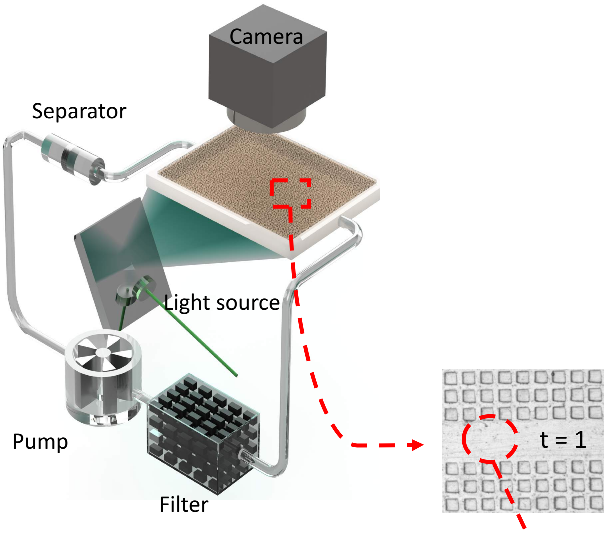

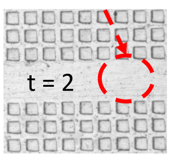

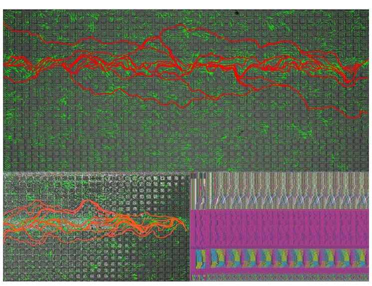

Particle shadow(s) recorded by camera

Lattice Boltzmann simulations, using lbHydra

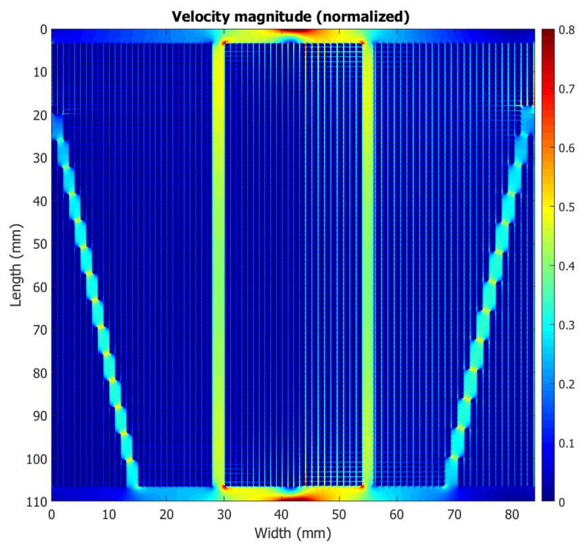

- Lattice Boltzmann method (LBM) was used to calculate the permeability and pressure drop in media to be used in experimental design.
- LBM method was used to design the cell for PSV experiment, to ensure one order of magnitude difference in velocity between fracture and matrix.

Acknowledgement

The project is funded by ETH Research Grant under grant No. ETH-12 15-2.

GEO Geothermal Energy & Geofluids
WSS WERNER SIEMENS-STIFTUNG
ETH Eidgenössische Technische Hochschule Zürich
Swiss Federal Institute of Technology Zurich

References:

- Miri, Rohaldin, and Helge Hellevang. "Salt precipitation during CO 2 storage—A review." *International Journal of Greenhouse Gas Control* 51 (2016): 136-147.
- "3 Renewable Electricity Generation Technologies." National Research Council. *Electricity from renewable resources: Status, prospects, and impediments*. National Academies Press, 2010. Page 93

Acoustic monitoring of laboratory hydraulic fracture growth under stress and pore pressure

Thomas E. Blum[1], and Brice Lecampion[1]

[1]Geo-Energy Laboratory — Gaznat chair on Geo-Energy, EPFL, Lausanne, Switzerland

I - Introduction

- Fluid-driven fracturing present in a wide range of applications
  - oil and gas extraction
  - geothermal energy recovery
  - CO2 sequestration
- Need for models to
  - efficiently fracture the targeted rock formation and quantify fracturing
  - better understand the physics of fluid-driven fracturing
  - get an estimate of fracture size and shape during growth
- Theoretical models
  - analytical or numerical solution
  - based on assumptions on fluid and rock properties, geometry. . .
- Scaled laboratory experiments
  - allow to validate theoretical predictions
  - provide complete datasets of individual experiments performed under controlled conditions
  - include physical limitations
  - history of lab-scale geophysics for geomechanical problems (Hall, 2009)

II - Existing work

- The DelFrac Consortium at TU Delft pioneered this field by building an acoustic monitoring setup inside a triaxial press applying three independent stresses on a cubic specimen (Groenenboom, 1998).
- The CSIRO group in Melbourne also has a triaxial press used for hydraulic fracturing experiments, but mostly uses photometric monitoring methods (Kovalyshen et al., 2014).
- Comparison of existing setups and planned GEL setup

	TU Delft	CSIRO	GEL
Specimen size	300 mm cube	350 mm cube	250 mm cube
Max. stress	30 MPa	25 MPa	20 MPa
Max. injection pressure	50 MPa	75 MPa	50 MPa
Transducers	48	6	64
Frequency	0.5 MHz	1 MHz	1 MHz

- Limitations
  - maximum applicable stress
  - injection rate: controls experiment duration
  - pore pressure? not possible in most setups

III - Laboratory setup

- Planned experimental setup
  - triaxial frame with cubic-shaped specimens of up to 250 mm in length
  - independent stresses on each axis up to 20 MPa
  - pore pressure inside the frame up to 5 MPa
  - high-pressure injection pump with a maximum pressure of 50 MPa
  - flow rate ranging from 1 $\mu L/\text{min}$ to 90 mL/min
  - glued wellbore and notching at the bottom for fracture initiation
- Triaxial cell in testing phase, loaded horizontally

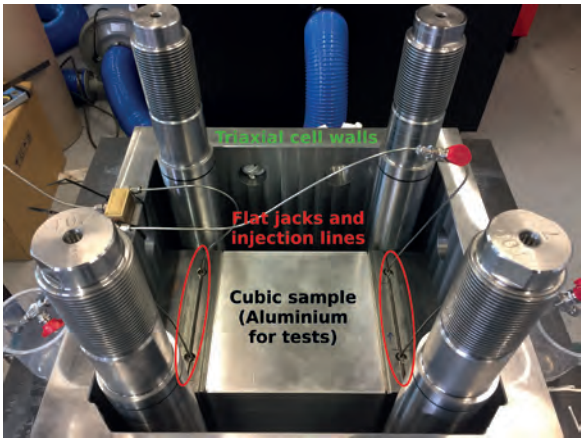

IV - Acoustic monitoring

- Acoustic monitoring setup
  - 54 longitudinal and 10 shear piezoelectric transducers
  - 32 sources swept through a multiplexer
  - function generator and high-power amplifier to create 300 V_{pp} excitation signal
  - 32 receivers connected to high-speed board for simultaneous acquisition at 50 MHz
  - transducers on all sides, most transducers on the sides parallel to the fracture plane
  - full acquisition duration on the order of a few seconds
- Schematic of the triaxial cell with confining stresses, injection line and piezoelectric transducers, simplified propagation modes at bottom right

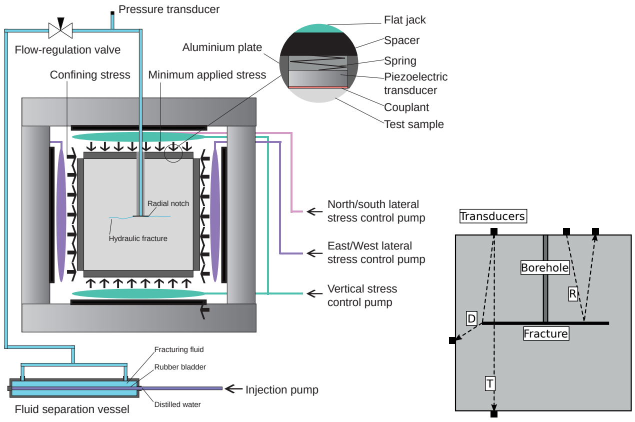

- Wave modes propagating through the sample
  - T: transmitted waves go through the fluid-filled fracture and carry information on the fracture thickness
  - R: waves that are reflected at the fracture interface carry information about the position of the fracture, and also about the occurrence of fluid lag
  - D: waves diffracted from the tip of the fracture carry information about the position of the fracture tip (Groenenboom et al., 2001)
- Thickness estimation (Groenenboom and Fokkema, 1998; Kovalyshen et al., 2014) Transmission coefficient for P-waves:

$$T(\omega, h) = \frac{(1 - r_{ff}^2)\exp(i\alpha)}{1 - r_{ff}^2 \exp(2i\alpha)} \quad (1)$$

- h fluid thickness
- ω wave frequency
- $r_{ff} = \frac{z_r+1}{z_r-1}$
- impedance ratio $z_r = \frac{\rho_f c_f}{\rho_s c_s}$
- ρ_s, ρ_f densities of solid and fracturing fluid
- c_s, c_f P-wave velocities of solid and fracturing fluid
- $\alpha = \frac{\omega h}{c_f}$

V - Preliminary results

- Thickness detection test:
  - two PMMA slabs, 125 mm thick, on top of each other
  - water layer in between
  - thickness varies through tightening of a clamp
  - simple transmission measurement with two opposing transducers

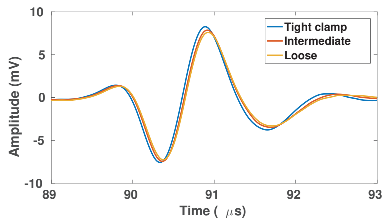

- Thickness changes
  - delayed arrival when fluid thickness increases due to travel through fluid layer
  - but also decreased amplitude: change in transmission coefficient

VI - Future applications

- Investigation of the process zone in quasi-brittle materials
- Fracture propagation in anisotropic or inhomogeneous materials
- Effects of mixed-mode fracturing with fracture reorientation
- Fracture profile for different fluid types: Newtonian, “power-law” . . .

VII - Conclusion

- Unique experimental capabilities with triaxial stresses and pore pressure
- Dense ultrasonic monitoring for improved fracture geometry estimation
- Growing list of applications
- Full operation expected end of 2017!

References

J. Groenenboom. *Acoustic monitoring of hydraulic fracture growth.* PhD thesis, TU Delft, 1998.

J. Groenenboom and J. T. Fokkema. Monitoring the width of hydraulic fractures with acoustic waves. *Geophysics*, 63:139–148, 1998.

J. Groenenboom, D. B. van Dam, and C. J. de Pater. Time-Lapse Ultrasonic Measurements of Laboratory Hydraulic-Fracture Growth: Tip Behavior and Width Profile. *SPE Journal*, 6(01):14–24, Mar. 2001.

S. A. Hall. When geophysics met geomechanics: Imaging of geomechanical properties and processes using elastic waves. In D. Kolymbas and G. Viggiani, editors, *Mechanics of Natural Solids*, pages 147–175. Springer Berlin Heidelberg, 2009.

Y. Kovalyshen, A. P. Bunger, J. Kear, and D. Kasperczyk. Comparison between ultrasonic and photometric methods for hydraulic fracture laboratory monitoring. *International Journal of Rock Mechanics and Mining Sciences*, 70:368–374, Sept. 2014.

http://gel.epfl.ch

thomas.blum@epfl.ch

SCCER-SoE Annual Conference 2017

SCCER SoE
SWISS COMPETENCE CENTER for ENERGY RESEARCH
SUPPLY of ELECTRICITY

In cooperation with the CTI
Energy
Swiss Competence Centers for Energy Research

Cross-borehole characterization of permeability enhancement & heat transport in stimulated fractured media : preliminary results from the ISC experiment at the Grimsel Test Site

Bernard Brixel*, Maria Klepikova*, Mohammadreza Jalali*, Florian Amann*, Simon Loew*
*Institute of Geology, Group of Engineering Geology, NO Building, Sonneggstrasse 5, ETHZ, 8092 Zurich

Motivation

1. Detect and characterize permeability enhancement in response to hydro-shearing
2. Understand the effects of stimulation on fluid flow and heat transport
3. Identify the permeable fractures that contribute to heat transport

Approach & Concepts

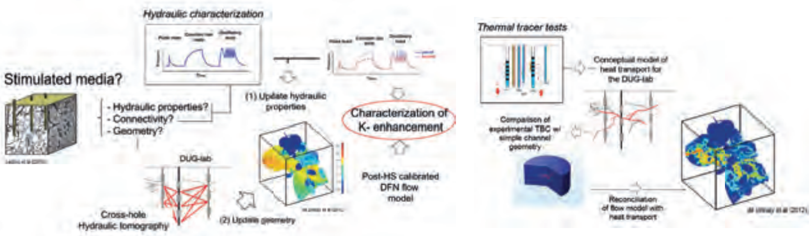

Fig. 1 Proposed in-situ methods and numerical approach

Methods

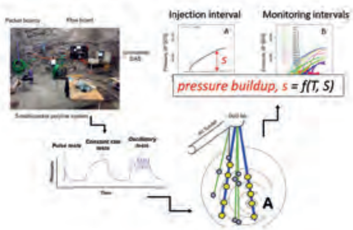

Fig. 3. Injection test procedure & monitoring

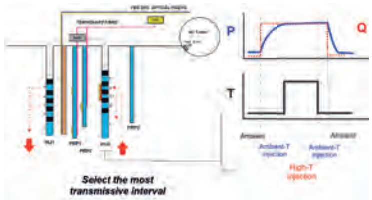

Fig. 4. Heat tracer test procedure & monitoring

Geology & Site layout

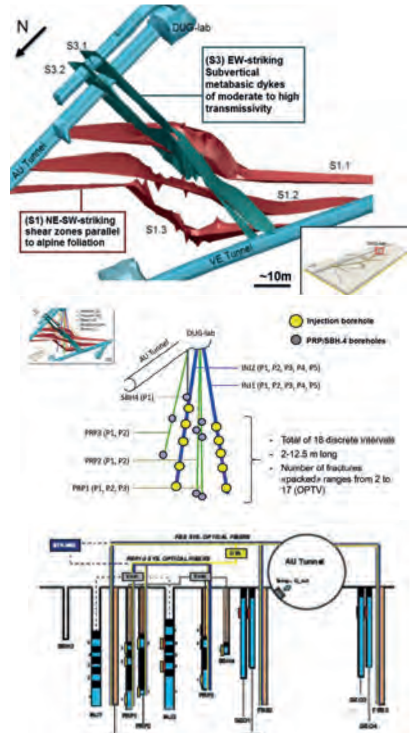

Fig. 2

Preliminary field results

Permeability enhancement

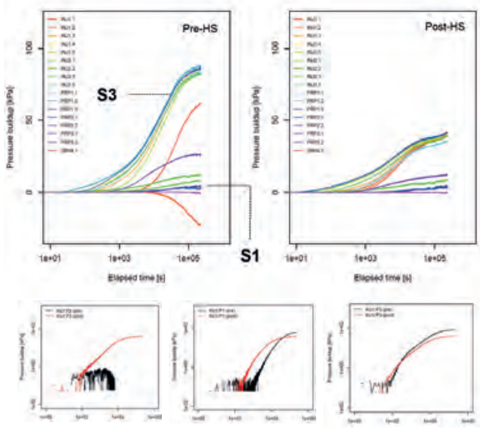

Fig. 5. Pressure transients in response to a constant rate injection test, pre vs. post- hydraulic stimulation

Heat transport

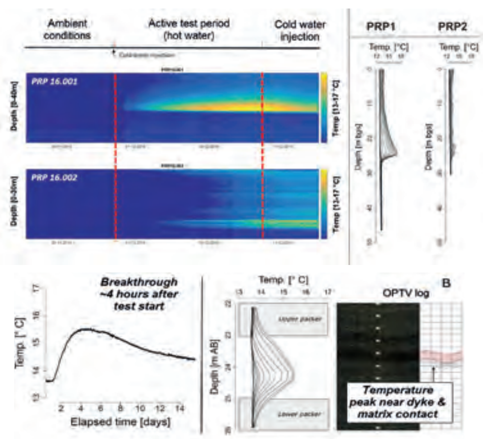

Fig. 6. Thermal breakthroughs and temperature profiles in open boreholes (top) vs packed-off interval (bottom)

Conclusions

1. Pressure transients from hydraulic tests completed following the same procedure, both before and after hydraulic shearing, show that the connectivity of the fracture network increased, at least over a scale of 10 m.
2. Both NEW and ENHANCED connections have been detected through hydraulic testing (see Fig. 5).
3. The propagation of heat during thermal tracer tests is constrained to discrete flow pathways (see Fig. 6), which helps us identifying the permeable fractures that contributing to heat transport.

Effect of fluid viscosity on fault frictional behavior

Chiara Cornelio[1], Elena Spagnuolo[2], Giulio Di Toro[3] and Marie Violay[1]

[1] Laboratory of Experimental Rock Mechanics, EPFL, Lausanne, Switzerland
[2] Istituto Nazionale di Geofisica e Vulcanologia, Rome, Italy
[3] School of Earth, Atmospheric and Environmental Science, University of Manchester

Introduction

Tectonic fault are often lubricated by viscous fluid which can have different nature e.g. gas, water, brine, melt and viscosities varying over 7 order of magnitude (from 10^{-4} for water to 10^{3} $Pa \cdot s^{-1}$ for melt at high temperature). Moreover, understanding fluids viscosity effects on fault dynamics can shed light on the induced seismicity in engineering reservoirs where fluids with viscosity ranking from $1 mPa \cdot s^{-1}$ to $1000 mPa \cdot s^{-1}$ are also injected during hydraulic fracturing process in order to increase the permeability. Here, we examine the mechanisms coming into play in presence of viscous lubricant film between the rock slip surfaces during both earthquake nucleation (slip rate from $\mu m \cdot s^{-1}$ to $mm \cdot s^{-1}$) and propagation ($mm \cdot s^{-1}$ to $m \cdot s^{-1}$) where mixed lubrication and fully lubricated regime might be activated, using rotary shear tests on precut samples of Westerly granite.

SHIVA Set-Up

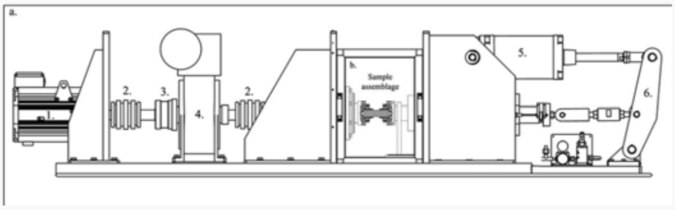

Figure 1: Slow to HIgh Velocity Apparatus. (a) 1. Large electric motor. 2. Bellow couplings. 3. Sprag clutch. 4. Gear box. 5. Air actuator. 6. Steel arm to amplify the axial load. The axial load is imposed by the air actuator and monitored by a computer. The torque is measured using a torque bar.

Table of Experiments

V[mm/s]	H_2O	60%glyc	85%glyc	99%glyc
10^{-2}	s1318	s1312	s1306	\
10^{-1}	s1319	s1313	s1309	\
10^{0}	s1302	\	s1304	\
10^{1}	s1320	s1315	s1308	s1387
10^{2}	s1386	s1317	s1311	s1388
10^{3}	s1303	s1316	s1305	s1389

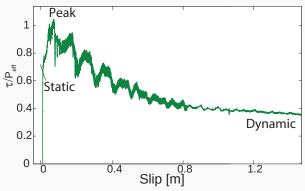

Results

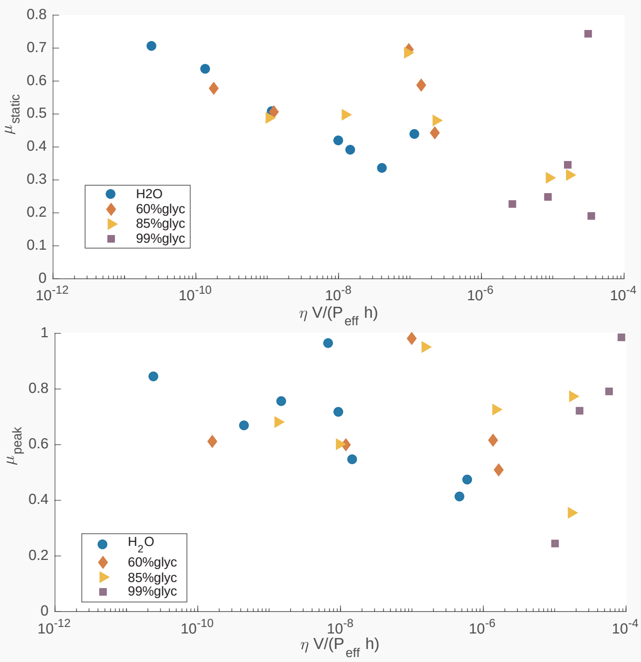

Figure 2: Static and Peak friction coefficient vs Sommerfield number

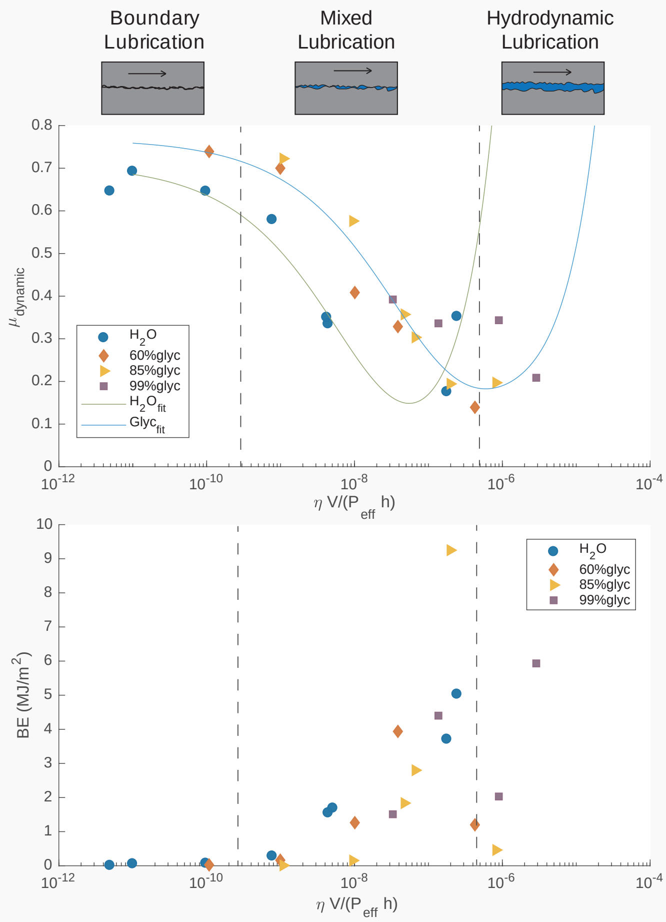

Figure 3: Dynamic friction coefficient and Frictional energy vs Sommerfield number

Conclusion

	μ_{static}	μ_{peak}	$\mu_{dynamic}$	B_E
Presence of fluid	Yes	No	Yes	Yes
Type of fluid	No	No	Yes	No
$\nearrow \eta$	$\searrow$	No	$\searrow$	$\nearrow$
$\nearrow V$	$\searrow$	Slightly	$\searrow$	$\nearrow$

- 30 tests in rotary shear apparatus have been performed, using different viscous fluid and imposing different target slip rate
- Three different lubricated regime have been detected
- Static friction coefficient is strongly dependent on fluid viscosity
- Dynamic friction coefficient is strongly dependent on fluid rheology and viscosity
- Frictional energy does not depend on the nature of the fluid, but it depends on fluid viscosity and velocity
- It increases in boundary and mixed regimes
- It abruptly decreases in fully lubricated regime
- Lubrication $\neq$ Easy EQ Propagation

References

Brodsky, E. E. Kanamori, H. *Elastohydrodynamic lubrication of faults.* J. Geophys. Res. 106, 16,357-16,374 (2001).
Di Toro, G. et al. *Fault lubrication during earthquakes.* Nature 471, 494â498 (2011).
Persson, B. *Sliding Friction. Physical Principles and Applications.* Springer-Verlag Berlin Heidelberg, 2000. doi:10.1007/978-3-662-04283-0

SCCER-SoE Annual Conference 2017

Injection Protocol and First Results of Hydraulic Fracturing Experiments at the Grimsel Test Site

Nathan Dutler*, Benoît Valley*, Linus Villiger**, Hannes Krietsch***, Mohammedreza Jalali***, Valentin Gischig***, Joseph Doetsch*** & Florian Amann***
*Centre for Hydrogeology and Geothermics, University of Neuchâtel, Rue Emile-Argand 11, CH-2000 Neuchâtel
** Swiss Seismological Service, ETH Zurich, Sonneggstrasse 5, CH-8092 Zurich
*** Department of Earth Sciences, ETH Zurich, Sonneggstrasse 5, CH-8092 Zurich

Motivation

Hydraulic fracturing (HF) is a common method to create artificial fractures to create new flow paths and to connect to pre-existing fractures. We aim to study injection parameters, such as injection flow rate and fluid viscosity, and their influence on fracture propagation, fracture geometry and micro-seismicity in crystalline rock.
The HF experiments are part of the in-situ stimulation and circulation project (Amann et al., 2017), which was recently carried out at the Grimsel Test Site.

Propagation mode of hydraulic fractures

- Numerical modelling has been used to study the size and mode (toughness or viscosity dominated) of the growing fractures
- A penny-shaped fracture geometry is assumed due to model calibration with hydraulic fractures during stress characterization phase.
- Definition of fracture toughness value for determining the asymptotes:

$$K = K' \times \left(\frac{t^2}{E'^3 \mu'^5 Q^3}\right)^{\frac{1}{18}}$$

K' fracture toughness value
t time
E' plane-strain modulus
μ' fluid viscosity
Q flow rate

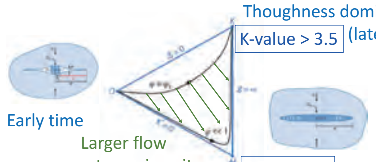

modified from Detournay (2016)

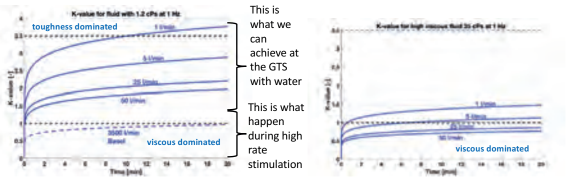

Figure 1: Propagation mode of penny-shaped hydraulic fractures

- To achieve similar behavior than for high rate stimulation, the fluid viscosity was increased using a rheology modifier (i.e. Xanthan Gum Keltro T622 at a 0.025%wt resulting in an expected viscosity of 35-40 cPs at a shear rate of 1 Hz).
- Expected fracture length in ideal isotropic rock is between 25 and 30 m depending on the injection fluid viscosity.

Hydraulic fracture growth in previous experiments (Gischig et al., 2017)

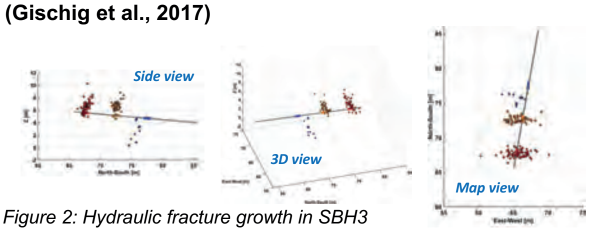

Figure 2: Hydraulic fracture growth in SBH3 borehole observed by micro-seismic monitoring

- Small injection flow rates were used (1-5 lpm)
- Impression packer show an opening along the foliation plane (157/75°)
- Micro-seisimic monitoring show fracture propagation in E-W direction

Injection protocol

- Injection of ~1 m^3 fluid for each injection phase
- The injection protocol includes the following elements:
  1. Initial pulse tested to verify packed interval integrity
  2. A formation breakdown test at relatively low flow rate (i.e. 5 lpm)
  3. A main fracture propagation phase with flow rates up to 100 lpm. Two cycles are used to reach high flow rates due to pump change at 35 lpm. Flushing is added to the high viscous gel injection protocol (Figure 3B).
  4. A pressure rate test to measure the stress normal to the created fracture

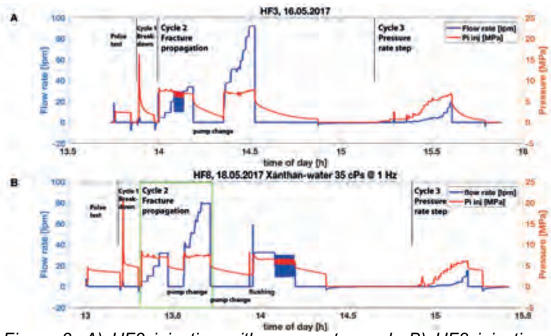

Figure 3: A) HF3 injection with pure water and B) HF8 injection with Xanthan-salt-water-mixture (green window) and additional flushing cycle. The flow rate is indicated by the blue solid line and the corresponding interval pressure is red.

The breakdown pressure for HF3 was at 16.2 MPa. The jacking pressure measured 5.8 MPa and the final injectivity measured 0.88 l/min/MPa. The break down pressure for HF8 was at 21.1 MPa and the jacking pressure measured 5.0 MPa. The final injectivity measures 0.20 l/min/MPa. For all HF-experiments the injectivity increased 100 to 1000 times.

Preliminary Insights

1. HF connects to pre-existing fractures such that the fracture fluid leak-off. Further fracture propagation is leaded by hydraulic shearing due to hitting a pre-existing system. The effect of shearing is depended on the fluid (flow rate and viscosity) and the early stage fracture orientation/geometry.
2. Likelihood to create single flow path rather than flow volume.
3. Evidence for creating a temporary hydraulic connection to the fracture system that closes after stimulation.
4. The injectivities after HF are around 0.1 to 1 l/min/MPa. These are similar to the HS-experiments.
5. The prediction of E-W fracture propagation needs to be validated by the microseismic cloud and the opening along the foliation plane is yet not be validated by acoustic televiewer log.

References

- Amann, F., et al. (2017), The seismo-hydro-mechanical behaviour during deep geothermal reservoir stimulation: open questions tackled in a decameter-scale in-situ stimulation experiment. Solid Earth Discuss., https://doi.org/10.5194/se-2017-79
- Detournay, E. (2016). Mechanics of Hydraulic Fractures. In Davis, SH and Moin, P, (eds), Annual Review of Fluid Mechanics, vol 48, p. 311-339.
- Gischig, V.S., Doetsch, J., Maurer, H., Krietsch H., Amann F., Evans, K.F., Nejati, M., Jalali, M., Valley, B., Obermann, A., Wiemer, S. and Giardini, D. (2017), On the link between stress field and small-scale hydraulic fracture growth in anisotropic rock derived from microseismicity. Solid Earth Discuss., https://doi.org/10.5194/se-2017-78

Email: nathan.dutler@unine.ch

SCCER SoE
SWISS COMPETENCE CENTER for ENERGY RESEARCH
SUPPLY of ELECTRICITY

SCCER-SoE Annual Conference 2017

In cooperation with the CTI
Energy
Swiss Competence Centers for Energy Research
Commission for Technology and Innovation CTI

Impact of CO_2 injection on the hydro-mechanical behaviour of a clay-rich caprock

Valentina Favero and Lyesse Laloui

Introduction

Research of the chair "Gaz Naturel" – Petrosvibri at the EPFL contributes to SCCER-SoE WP1: "DGE and CO_2 sequestration". WP1 research focuses on problems for future realization of CO_2 storage in Switzerland. Proper assessment of carbon dioxide storage procedures allows to significantly reduce its concentration in the atmosphere and thus directly contributes to Swiss energy strategy 2050. The sound characterization of reservoirs and caprocks in Switzerland and the assessment of their potential for CO_2 storage is therefore fundamental.

In order to grant a safe injection of CO_2 into reservoir formations, the overlaying shaly caprock must perform efficiently. This work aims at identifying the relevant processes related to shale-CO_2 interactions and the impact of CO_2 injection on the mechanical properties of the material.

Experimental methodology

Cylindrical specimens of intact Opalinus Clay shale :

- height ≈ 12.5 mm
- diameter = 35 mm

An advanced oedometric system (imposing zero lateral strain) is used (Figure 1).

Procedure for Test 1 and Test 2:

- Saturation in constant volume conditions;
- Pore water pressure increase to 7.3 MPa while maintaining constant vertical effective stress;
- Consolidation in steps to the desired stress state;
- CO_2 injection at liquid state (23°C, pressure up to 12 MPa)
- Mechanical compression up to 90 MPa of vertical total stress.

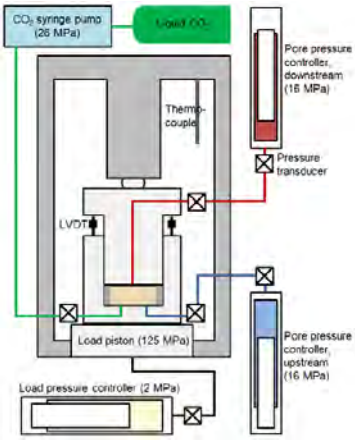

Figure 1: Advanced oedometric system.

The stress paths of the tests are depicted below:

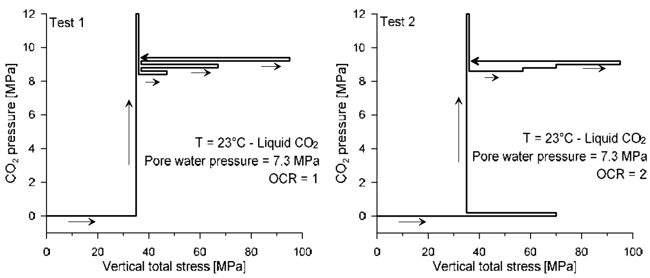

Results

Vertical strain versus vertical effective stress during oedometric loading and during CO_2 injection at constant vertical effective stress.

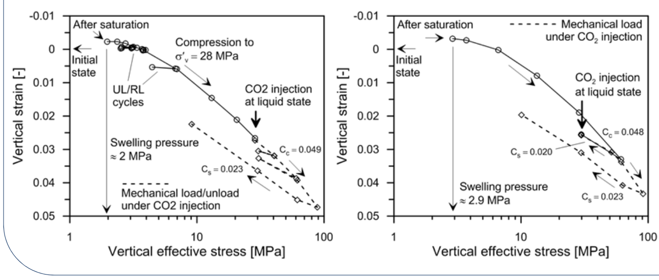

Results and Discussion

Loading (test 1) and unloading (test 2) steps prior to CO_2 injection (black solid line), followed by the CO_2 injection phase (red line)

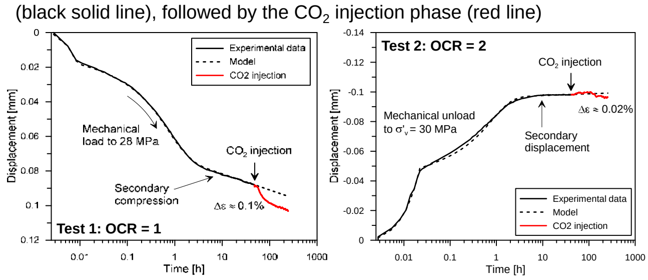

Strain induced by CO_2 injection is relevant at OCR = 1

→ material structure is more prone to collapse when it is found in normally consolidated conditions.

Details of the CO_2 injection phase:

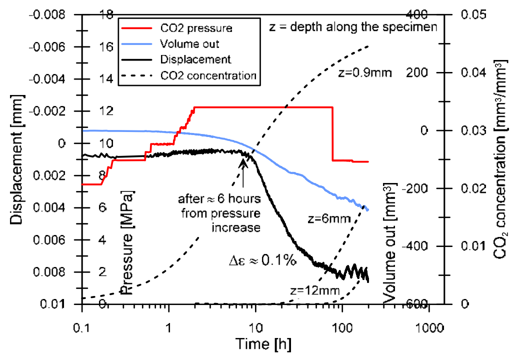

Possible causes of strains induced by CO_2 injection:

→ Desaturation effects (CO_2 / pore water differential pressure)

→ Double layer effects induced by the diffusion of CO_2

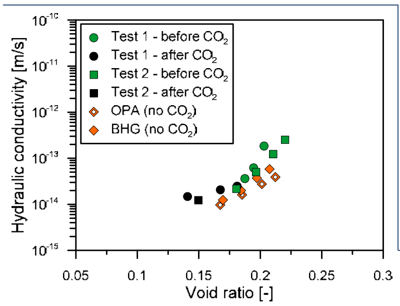

The impact of CO_2 injection on the deformation behaviour of the material appears to be limited compared to the deformation behaviour induced by a mechanical loading.

Diffusion of CO_2 into the shale does not impact significantly the hydro-mechanical properties of the material, since no significant change in oedometric modulus and hydraulic conductivity are highlighted after the injection of CO_2.

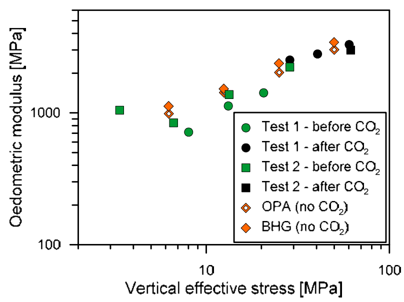

Acknowledgement

V. Favero is an SCCER-SoE postdoctoral researcher. The tested shale is provided by Swisstopo.

SCCER-SoE Annual Conference 2017

Visualizing salt tracers using GPR

Peter-Lasse Giertzuch, Joseph Doetsch*, Alexis Shakas**, Mohammadreza Jalali*, Anniina Kittilä*, Hansruedi Maurer**
* Department of Earth Sciences, ETH Zurich, CH-8092 Zurich; ** Institute of Earth Sciences, University of Lausanne, CH-1015 Lausanne

Motivation

Hydraulic tracer tests are a powerful tool to characterize connections between subsurface locations, but the actual flow path remains unresolved. One potential method to investigate this is presented here and relies on Ground Penetrating Radar (GPR) and salt tracers. The experiments described here were conducted within the ISC project at the the Grimsel Test Site (GTS).

Single-Hole Reflection GPR

The GPR reflection response is sensitive to electrical conductivity and permittivity. At interfaces with changing parameters, a signal reflection occurs. This way structural changes, i.e. shear zones, can be imaged.

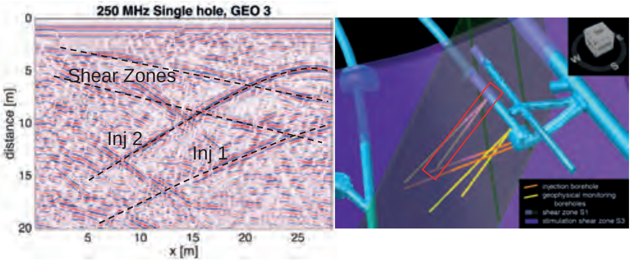

For single-hole reflection GPR the transmitter and the receiver were moved with a fixed distance in the same borehole. Every 5 cm a trace is recorded, which adds up to a reflection image. The acquisition was performed with 250 MHz antennas in borehole GEO 3, indicated in red on the schematics. Amongst other reflections, the structures from the shear zones and the two injection lines are well visible in the data.

Salt Tracer for GPR

Salt water changes the electrical conductivity locally, hence induces a signal change. As salt water has a higher density than tap water, ethanol is added to achieve a neutrally buoyant tracer to achieve comparability with other tracer tests.

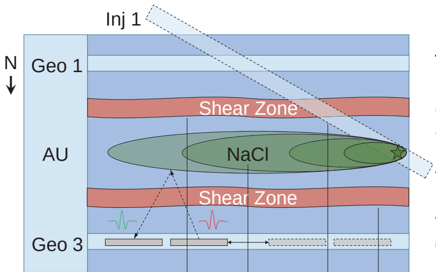

Top view schematics. Note: The shear zones and the boreholes have an inclination and do not lie parallel as drawn in the schematics. The reflection image shows the result from the real geometry.

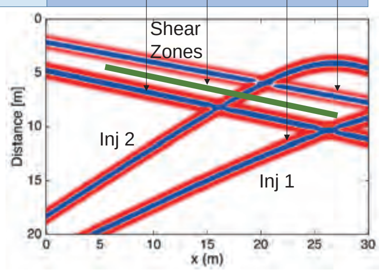

Calculated model. Reflections from the shear zones occur from changes in the permittivity, due to a different water content than the surroundings. The tracer reflection arises from a change of electrical conductivity.

The tracer used here is composed of: 85 kg water, 21 kg ethanol and 4.5 kg of salt, which leads to a conductivity of 31.8 mS/cm. It was injected in injection line 1 of the GTS over a course of 90 min with tap water and two dye tracers injected before and after for later comparison.

Difference Imaging

The salt tracer only induces small changes in the GPR reflection image. To retrieve the tracer information, a reference image is acquired before tracer injection. The difference between the following measurements and the reference should leave only the tracer visible. Small variations in the data, especially time or phase shifts, have a large impact on the differences. The following processing steps were used to correct for these issues:

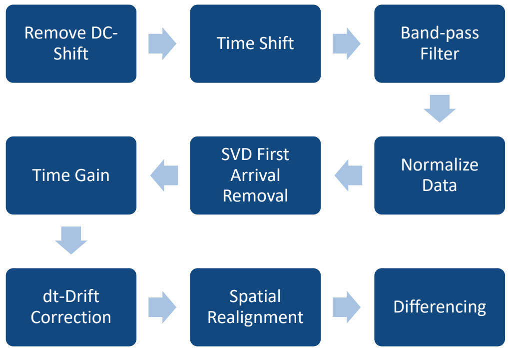

Results

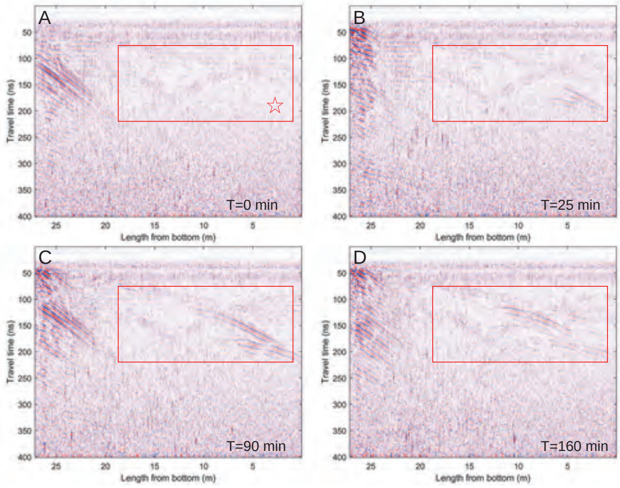

Difference images at increasing time from A to D. The borehole and shear zone reflections are mostly eliminated by the differencing. Artifacts on the top left of the images arise from effects in the tunnel.

A: Tracer not yet visible.
B: Tracer visible at injection point (indicated in A).
C: Tracer propagates.
D: Tracer propagates further and starts to vanish from dilution.

Conclusion & Outlook

The current state of the project proves that salt tracers can be used to monitor tracer movement using GPR. Together with additional information from hydraulic tracer tests, more information on the flow path, the media porosities and tracer velocities can be gained. In the future the GPR data with integration of hydraulic tracer test results will be used to generate a hydraulic model of the ISC project volume.

Email: peter-lasse.giertzuch@erdw.ethz.ch

SCCER-SoE Annual Conference 2017

A comparison of the seismo-hydro-mechanical observations during two hydraulic stimulation at the Grimsel Test Site

Valentin Gischig*, Joseph Doetsch*, Mohammadreza Jalali*, Florian Amann*, Hannes Krietsch*, Linus Villiger**, Nathan Dutler***, Benoît Valley***
* Department of Earth Sciences, ETH Zurich, CH-8092 Zurich; ** Swiss Seismological Service, ETH Zurich, CH-8092 Zurich
***Centre for Hydrogeology and Geothermics, University of Neuchâtel, CH-2000 Neuchâtel

Stimulation interval HS4 at 27.2 - 28.2 m in borehole INJ1, S3 shear zone

Stimulation interval HS1 at 39.75 - 40.75 m in borehole INJ2, S1 shear zone

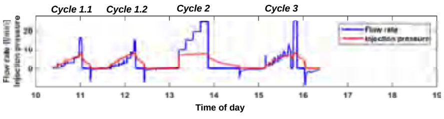

Injection strategy

Cycle 1.1: Pressure –controlled, determination of initial injectivity, breakdown of rock

Cycle 1.2: Pressure –controlled, determination of jacking pressure

Cycle 2: Rate-controlled, actual stimulation

Cycle 3: Pressure –controlled, determination of final injectivity and jacking pressure

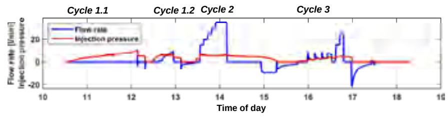

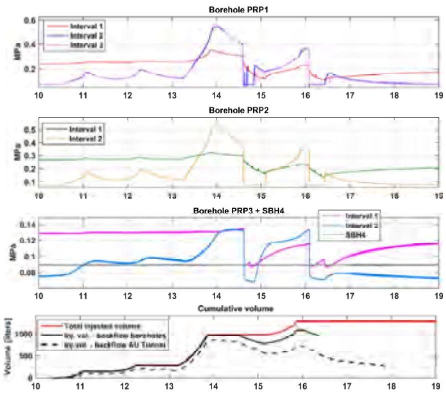

Pressure monitoring

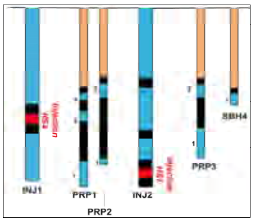

A total of 12 pressure observation intervals to record pressure evolution

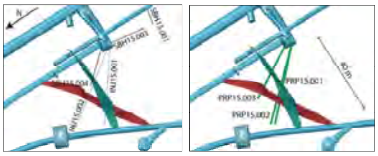

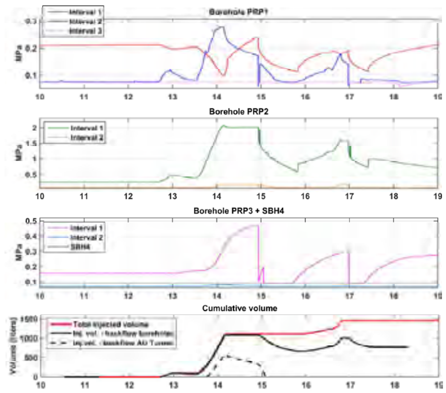

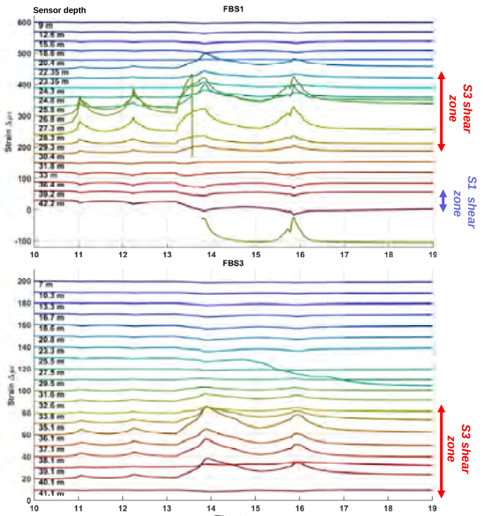

Deformation monitoring

Longitudinal strain with fibre-optics sensors
60 FBG sensors and distributed strain sensing cable in 3 boreholes

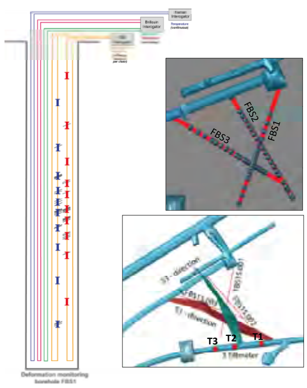

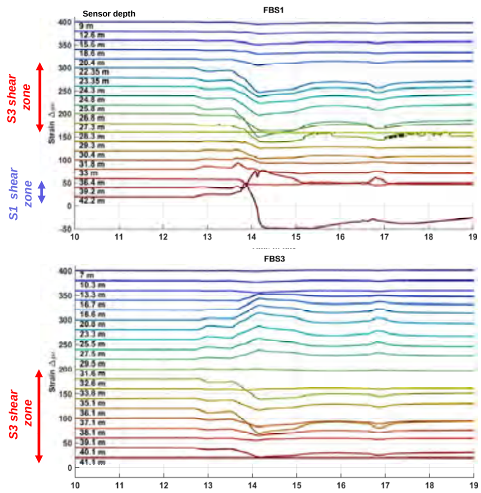

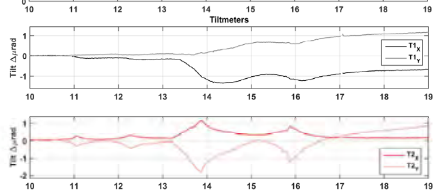

3 horizontal tiltmeters

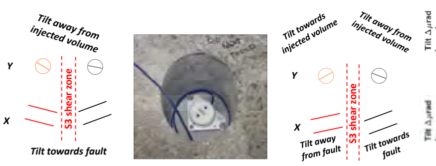

See Krietsch et al. for more details

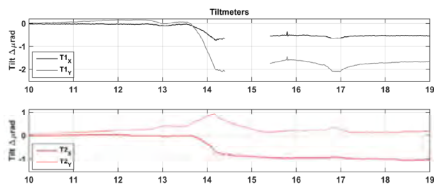

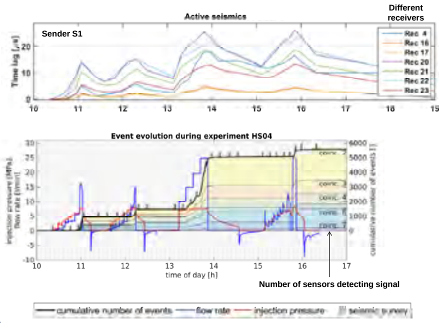

Active + passive seismics

Systematic travel time changes in the stimulated volume
Variable number of seismic events

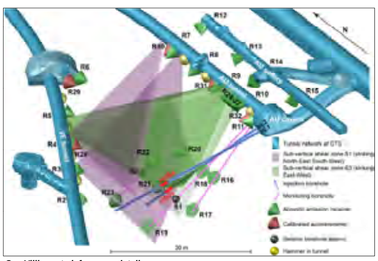

See Villiger et al. for more details

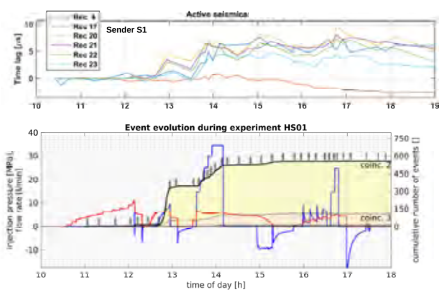

Email: gischig@erdw.ethz.ch

SCCER SoE
SWISS COMPETENCE CENTER for ENERGY RESEARCH
SUPPLY of ELECTRICITY

SCCER-SoE Annual Conference 2017

In cooperation with the CTI
Energy
Swiss Competence Centers for Energy Research
Swiss Confederation
Commission for Technology and Innovation CTI

Permeability Changes Induced by Hydraulic Stimulation at the Grimsel Test Site

Mohammadreza Jalali, Valentin Gischig*, Joseph Doetsch*, Hannes Krietsch*, Linus Villiger**, Nathan Dutler***, Benoît Valley***, Keith F. Evans**, Florian Amann**

* Department of Earth Sciences, ETH Zurich, Sonneggstrasse 5, CH-8092 Zurich
** Swiss Seismological Service, ETH Zurich, Sonneggstrasse 5, CH-8092 Zurich
*** Centre for Hydrogeology and Geothermics, University of Neuchâtel, Rue Emile-Argand 11, CH-2000 Neuchâtel

Introduction

In-situ stimulation and circulation (ISC) experiment is a unique decameter stimulation experiment which was initiated at the Grimsel Test Site (GTS) in August 2015 [Amann et al., 2017]. The main objective of the ISC experiment is improving our understanding of the thermo-hydro-mechanical and seismic (THMS) processes during hydraulic stimulation of crystalline rocks. In particular, we are interested in

- The creation of sustainable heat exchanger via permanent hydraulic conductivity enhancement during high-pressure fluid injection
- Ways to maximize the ability to assess, model and control induced seismic hazard and risk.

A series of hydraulic stimulation tests had been executed as part of the ISC experiment to fulfill the objectives, which are (Figure 1, Table 1):

- Ten mini hydraulic fracturing (MHF) and one hydraulic testing in pre-existing fractures (HTPF) in SBH boreholes (September 2015)
- Six hydraulic shearing (HS) in INJ boreholes (February 2017)
- Six hydraulic fracturing (HF) in INJ boreholes (May 2017)

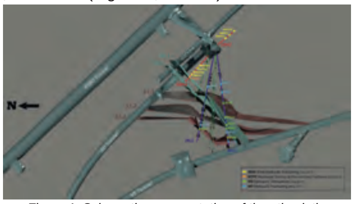

Figure 1. Schematic representation of the stimulation intervals during the ISC experiment.

In this study, the effect of these multi-scale hydraulic stimulation on permeability enhancement and injectivity increment of the rock volume is studied.

Hydraulic Stimulation Mechanisms

Hydraulic stimulation describes two distinct but related mechanisms, which are

(1) initiation and propagation of new fractures (mode I fractures), so-called ***hydraulic fracturing (HF)***, and

(2) shearing of pre-existing fractures (mode II and III), i.e. ***hydraulic shearing (HS)*** (Figure 2).

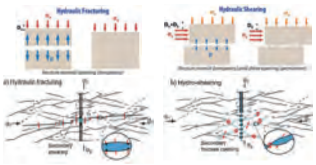

Figure 2. Hydraulic fracturing and hydraulic shearing mechanisms

The occurrence of dominant mechanisms depends on ***rock mass properties*** such as ***rock mass structure***, ***in-situ stress condition***, the ***orientation of existing structures*** such as fractures, faults, and foliation as well as the ***injection properties*** such as ***injection rate*** and ***fluid viscosity***.
In reality, shearing as well as fracture formation and opening may occur concomitantly, and the distinction between them during injection is challenging.
A major difference between HF and HS is the resultant permeability enhancement; it tends to be irreversible for HS but is mostly reversible for HF as the fractures almost fully close after depressurization.

Permeability Changes During Stress Measurement

Ten mini hydraulic fracturing and one HTPF test were performed in three stress measurement boreholes, i.e. SBH1, SBH3, and SBH4 in order to estimate the orientation and magnitude of the principal stresses in the stimulated rock volume [Krietsch et al., 2017]. To determine the impact of these meter-scale hydraulic stimulations in the SBH3 and SBH4 boreholes, permeability, storativity and flow regime of each test were measured before and after the stress measurement using the conventional packer tests [Jalali et al., 2017].

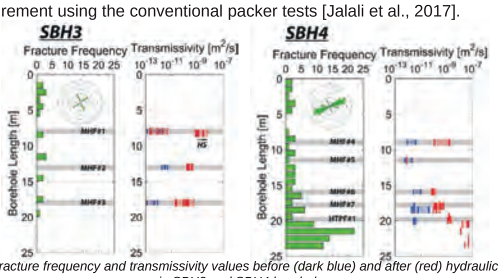

Figure 3. Fracture frequency and transmissivity values before (dark blue) and after (red) hydraulic fracturing in SBH3 and SBH4 boreholes.

Permeability Changes During Hydraulic Shearing and hydraulic Fracturing

Hydraulic stimulation during ISC experiment consists of two parts:

- High-pressure water injection into existing faults and fracture zones within the test volume so that the effective normal stress on the structures is reduced and hydraulic shearing is triggered → Hydraulic Shearing (HS)
- High-pressure water and Xanthan injection into fracture-free borehole intervals so as to initiate and propagate hydraulic fractures → Hydraulic Fracturing (HF)

Permeability and transmissivity changes as a result of hydraulic stimulation were measured using step-pressure tests as well as conventional packer tests (Figure 4 & 5).

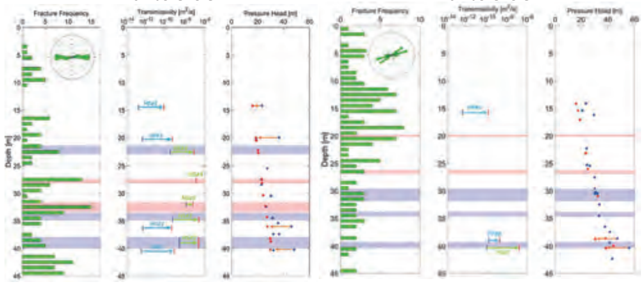

Figure 4. Fracture frequency, transmissivity and pressure head values before (dark blue) and after (red) hydraulic stimulations in two injection boreholes.

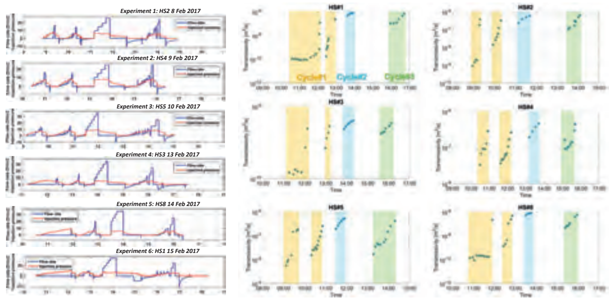

Figure 5. Transient transmissivity changes as a response to injection pressure and flow rate during six hydraulic shearing tests

Table 1. Summary of all the hydraulic stimulation tests conducted during the ISC experiment

Borehole	Test	Structure	Injected Volume [lit]	Initial Trans. [m²/s]	Final Trans. [m²/s]	Change in Trans.	Detected Events
SBH3	MHF#1	---	7.9	3.8E-13	1.5E-10	380	1161
	MHF#2	---	10	3.2E-12	2.1E-10	70	482
	MHF#3	---	10.4	2.2E-12	5.0E-12	2	274
SBH4	MHF#4	---	10.9	1.9E-12	1.1E-10	60	2258
	MHF#5	---	9.7	5.9E-13	8.7E-13	2	1692
	MHF#6	---	9.1	2.2E-12	7.0E-11	30	772
	MHF#7	---	11.5	3.1E-12	2.2E-10	70	406
	HTPF#1	S3.1	28.8	3.8E-12	9.1E-10	240	253
INJ1	HS#2	S1.3	797	2.5E-09	2.2E-07	90	1203
	HS#3	S1.2	831	4.8E-10	2.3E-07	490	314
	HS#4	S3.1	1253	1.2E-07	1.2E-07	1	5606
	HS#5	S3.2	1211	1.2E-08	5.5E-08	5	2452
	HS#8	S1.1	1258	2.8E-10	7.5E-08	270	3703
	HF#1	---	971	2.9E-13	7.5E-10	2550	N/A
	HF#2	---	816	4.2E-13	4.0E-10	950	N/A
	HF#3	---	893	3.8E-13	4.5E-10	1190	N/A
	HF#5	---	1235	1.5E-13	6.1E-11	420	N/A
INJ2	HS#1	S1.3	982	8.3E-11	1.5E-07	1850	560
	HF#6	S1.3	943	4.0E-10	1.7E-09	4	104
	HF#8	---	1501	3.1E-13	1.2E-10	165	362

References

- Amann, F., et al. (2017), The seismo-hydro-mechanical behaviour during deep geothermal reservoir stimulation: open questions tackled in a decameter-scale in-situ stimulation experiment. Solid Earth Discuss., https://doi.org/10.5194/se-2017-79
- Jalali M.R., et al. (2017), Mechanical, hydraulic and seismological behavior of crystalline rock as a response to hydraulic fracturing at the Grimsel Test Site. *51st US Rock Mechanics/Geomechanics Symposium*. American Rock Mechanics Association, 2017.
- Krietsch, H., et al. (2017), Stress measurements in crystalline rock: Comparison of overcoring, hydraulic fracturing and induced seismicity results. *51st US Rock Mechanics/Geomechanics Symposium*. American Rock Mechanics Association, 2017.

SCCER-SoE Annual Conference 2017

A matlab package for thermo-hydraulic modeling and fracture stability analysis in fractured reservoirs

Gunnar Jansen , Benoît Valley and Stephen A. Miller
Centre for Hydrogeology and Geothermics - University of Neuchâtel

Motivation

A large fraction of the world's water and energy resources are located in naturally fractured reservoirs within the earth's crust. Understanding the dynamics of such reservoirs in terms of flow, heat transport and fracture stability is crucial to successful application of engineered geothermal systems (also known as enhanced geothermal systems, EGS) for geothermal energy production in the future. The reservoir development characteristics such as permeability creation and induced seismicity largely depend on the traits of pre-existing fractures such as porosity, permeability and orientation within the local stress field. One of the primary driving mechanisms for permeability creation in EGS involves shear failure induced by fluid injection at high pressures.

Methods

We present and validate an implementation of an embedded discrete fracture model (EDFM) for single phase flow and heat transport with additional capabilities to determine fracture stability in fractured reservoirs.

The conceptual idea of the EDFM is the separation of a fractured reservoir into a fracture and a damaged matrix domain. A transfer function accounts for coupling effects between the two domains (Figure 1).

Fracture and matrix domains are computationally independent except for the transfer function. As the fractures are generally very thin and highly permeable compared to the surrounding matrix rock this allows for a lower dimensional representation of fractures.

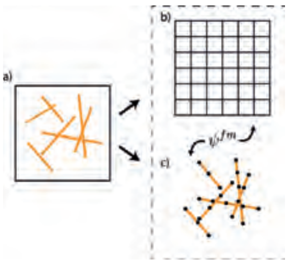

Figure 1: A fractured domain a) is separated in a uniform grid b) and a fracture grid c). The two resulting domains are coupled using the transfer function ψ_{fm}.

Validation on crossing fractures

We compare our solution to a reference solution computed by *COMSOL Multiphysics* which is a widely used finite element package with subsurface flow and transport capabilities. The reference solution is computed on a conforming discrete fracture network were the matrix elements are aligned exactly on the grid with very high resolution.

We evaluate the coupled results of fluid flow and heat transport over 40 years.

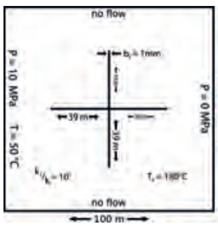

Figure 2: Numerical setup for the initial validation. Incompressible fluids are assumed.

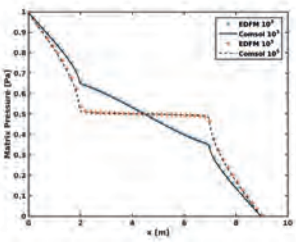

Figure 3: Matrix pressure at y=4.5m. Two permeability contrasts between matrix and fracture are evaluated.

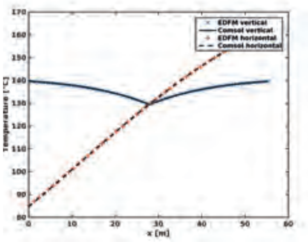

Figure 4: Fracture temperatures through vertical and horizontal fractures after 40 years.

Validation on a complex fracture network

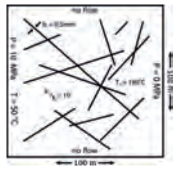

Figure 5: Numerical setup for the validation. Incompressible fluids are assumed.

We evaluate the coupled flow and heat transport on a more complex fracture geometry. The geometry consists of a total of 13 fractures within a square domain.

- Maximum pressure deviations from the reference are below ±5% (NRMSE: 0.35%)
- Maximum temperature deviations from the reference up to 10% (NRMSE: 2.22%)

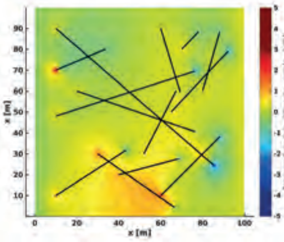

Figure 6: Pressure deviation from reference solution. A region of elevated error is visible in the lower part of the domain. Significant deviations are also visible at some fracture tips.

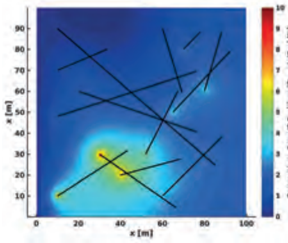

Figure 7: Temperature deviation from the reference solution. The matrix temperatures are generally overestimated compared to the reference.

Fracture stability analysis (FSA)

Fracture slip is likely to occur if the shear stress to effective normal stress ratio equals or exceeds the frictional sliding resistance.

$$T_s = \begin{cases} \frac{\tau}{\sigma_{neff}} < \mu_s & \text{(stable)} \\ \frac{\tau}{\sigma_{neff}} \geq \mu_s & \text{(unstable)} \end{cases}$$

We assume that unstable (sliding) fractures undergo a stepwise change in fracture permeability.

$$k_{fr} = \begin{cases} k_{fr} & \text{if } T_s < \mu_s \\ x \cdot k_{fr} & \text{if } T_s \geq \mu_s \end{cases}$$

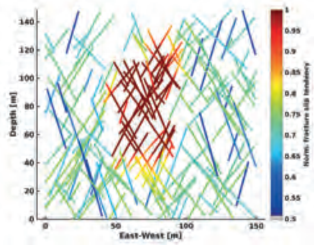

Figure 8: Fracture stability in the reservoir after 10 days of injection. The fracture stability is high with values well below the failure condition (μ = 0.6) in large parts of the reservoir. Stability drastically reduces closer to the injection (red).

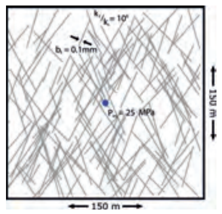

Figure 9: Numerical setup to evaluate the fracture stability. A constant injection pressure of 25 MPa is applied in the borehole (blue circle). On the outer boundaries no-flow boundary condition are assumed.

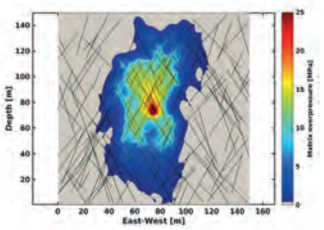

Figure 10: Matrix pressure in the reservoir after 10 days of injection (permeability enhancement factor of x = 10). Due to the constant injection pressure, the extend of the high-pressure zone is enlarged.

Conclusion

We validated a fractured reservoir modelling framework implemented in *matlab* which can be used as a standalone simulation package for TH(M) case studies in geothermal reservoirs or as a blue print for the re-implementation of the method e.g. in a high performance computing (HPC) framework. This package will soon be made available to the scientific community as open source.

SCCER SoE

SWISS COMPETENCE CENTER for ENERGY RESEARCH
SUPPLY of ELECTRICITY

SCCER-SoE Annual Conference 2017

In cooperation with the CTI

Energy
Swiss Competence Centers for Energy Research

Schweizerische Eidgenossenschaft
Confédération suisse
Confederazione Svizzera
Confederaziun svizra

Swiss Confederation

Commission for Technology and Innovation CTI

A multi-parametric evaluation of the Wallace-Bott hypothesis in the presence of a fluid source

Maria Kakurina[1], Yves Guglielmi[2], Christophe Nussbaum[1] and Benoit Valley[1]

(1)University of Neuchâtel, CHYN, Neuchâtel, Switzerland, (2)University of California Berkeley, Berkeley, CA, United States, (3)Swisstopo, Wabern, Switzerland

Introduction

Fault slip data inversion methods to estimate the in-situ stress are generally based on the Wallace-Bott hypothesis, stating that the slip on the fault plane occurs in the direction of the maximum resolved shear stress (Wallace 1951, Bott 1959). In this work we focus on validation of the Wallace-Bott hypothesis in the presence of the fluid point source that may induce slip reorientations. A multi-parametric study covering (i) fault geometry such as planar and non-planar faults, (ii) fault orientation, (iii) friction angle, (iv) dilation angles, (v) joint stiffness was performed to understand the effect of each parameter on the misfit angle between the simulated slip vectors and the resolved shear stresses in the presence of the fluid injection.

Methods

- Analytical solution from Bott (1959)
- Numerical solution using the 3D distinct element method (Figure 1)
  - linearly elastic, homogeneous, isotropic, deformable blocks
  - *Coulomb slip* model joint model
  - Active (fracture) and inactive (rock mass) parts of the joint
  - $\sigma_{xx} = 3$ MPa, $\sigma_{yy} = 5$MPa, $\sigma_{zz} = 6$ MPa; $pp = 0.5$ MPa
  - 8 increasing steps of 0.5MPa, starting with a 1 MPa initial pressure
  - Rake of the slipping vectors are compared to the analytical solution

Block		
Mass density, kg/m³	2450	
Bulk modulus, Pa	5.9e9	
Shear modulus, Pa	2.3e9	
Joint	*Active part*	*Inactive part*
Normal stiffness, GPa/m	5.0e11	5.0e11
Shear stiffness, Pa	2.5e11	2.5e11
Friction angle, Pa	22˚	40˚
Cohesion, Pa	0	1.0e30

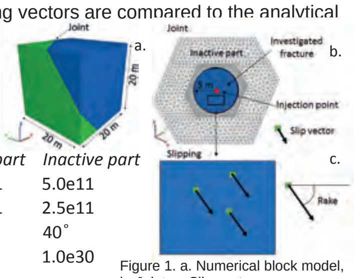

Figure 1. a. Numerical block model, b. Joint, c. Slip vectors

Results

The fluid pressure and shear displacement vectors on the fracture are shown in Figure 2. Increasing fluid pressure decreases the effective normal stress and causes the elastic and subsequent plastic deformation of the model. The perturbation of stress in the vicinity of the fluid source is shown in Figure 3. It can be observed that the stress tensors (cross symbol) is altered by the increasing fluid pressure. After slip occurs, the minimum principal stress is rotating towards the direction perpendicular to the fracture opening due to shear stress release by slip on the fault plane.

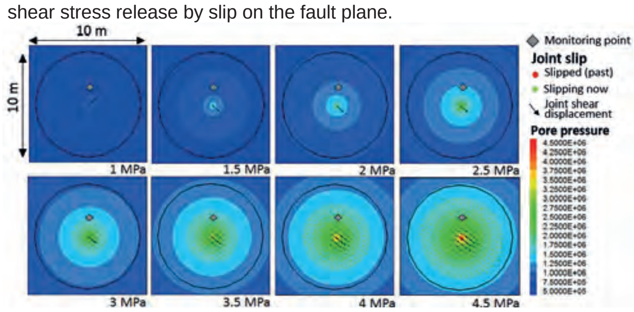

Figure 2. Pore pressure distribution on the fracture during the fluid injection. Normal view on the plane

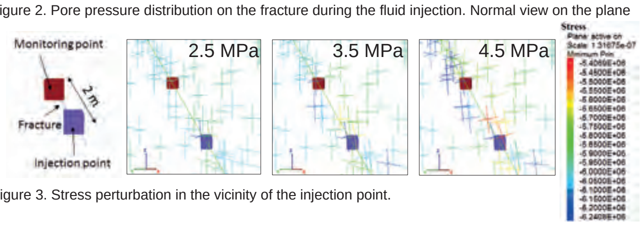

Figure 3. Stress perturbation in the vicinity of the injection point.

Changes in effective stress move the stresses to the joint failure criteria with the fluid pressure increase (Figure 4, left). The numerical result deviates from the analytical solution away from the injection point with increasing fluid pressure and does not exceed 5° (Figure 4, right).

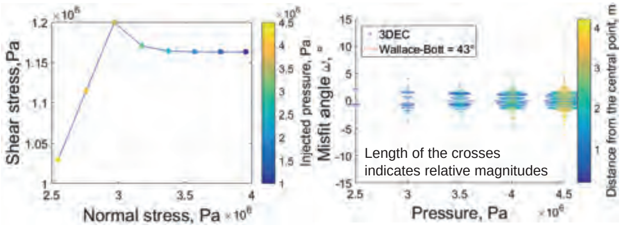

Figure 4. Left-Effect of fluid pressure on sliding condition for the failure envelope. Right - Comparison of the rake computed by 3DEC and by analytical solution on different pressure steps

Sensitivity analysis

The parameters of the model described previously are taken as the reference for this sensitivity study (Figure 5). Therefore, for each model computation, a single parameter is changed from the reference model to address its influence on the results.

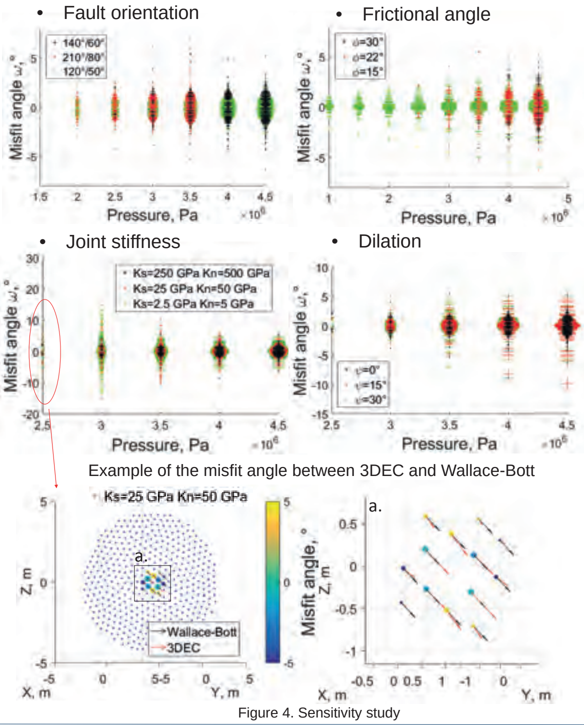

Figure 4. Sensitivity study

Conclusion

- Slip orientation is controlled by the fault geometry and reduced stress tensor
- Fluid injection causes stress perturbation around the injection point
- Generally for a given far-field stress the fluid injection affects the mean misfit angle between the analytical and numerical solutions within the practical threshold (5°).
- Joint stiffness, dilation and friction angle are the key factors influencing the misfit angle. They should be investigated with more details to seek for generalization of the conclusion of this study

References

Bott, M. H. P. (1959). The mechanics of oblique slip faulting. Geological Magazine, 96(02), 109-117.

Wallace, R. E. (1951). Geometry of shearing stress and relation to faulting. The journal of Geology, 59(2), 118-130.

SCCER SoE
SWISS COMPETENCE CENTER for ENERGY RESEARCH
SUPPLY of ELECTRICITY

GEG
Geothermal Energy & Geofluids

SCCER-SoE Annual Conference 2017

Tracer based characterization of the connected fracture volume in the DUG Lab at the Grimsel Test Site

A. Kittilä, K. Evans, M. Jalali, M. Willmann, and M.O. Saar
ETH Zurich

In cooperation with the CTI
Energy
Swiss Competence Centers for Energy Research
Commission for Technology and Innovation CTI

Background

Tracer tests were conducted at the DUG Lab at the Grimsel Test Site (GTS) as part of the ISC experiment (Amann et al. 2017) in order to characterize the connected fracture volume. A total of four tests were conducted, the first two before the hydroshear stimulation program and the second two a month after. Tests 1-3 featured injection into intervals of INJ2 with production from an interval in INJ1, a fracture zone in the AU gallery, and several intervals in PRP observation holes (Tests 2 and 3 only). These tests allow an assessment of changes to flow paths resulting from the stimulations.
Test 4 featured injection into two intervals of INJ1 with production from Interval 4 of INJ2, the AU tunnel and the PRP intervals. In this test (and Test 1), novel DNA nanotracer particles were injected with the standard solute dye tracers. The DNA nanotracers provide additional information of the preferential flow paths and the accessible pore volume due to size exclusion.

Materials and Methods

In all four tracer tests, two distinct intervals in the injection hole were injected with two of four available solute dye tracers. The DNA nanotracers (Paunescu et al. 2013) were produced by the company Haelixa.

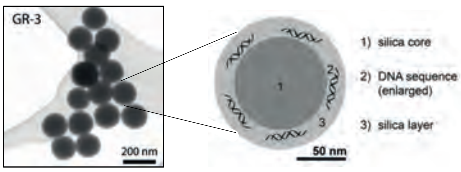

The environmentally friendly DNA-labeled silica particles allow the production of virtually unlimited number of uniquely identifiable tracers exhibiting the same transport properties.

Moment analysis (Shook and Forsmann 2005) was used to determine swept pore volume and flow-storage geometry from the individual recorded tracer concentration histories. First, the concentration histories are normalized to age distribution functions:

$$E(t) = \frac{C(t)\rho q_{\mathrm{out}}}{M_{\mathrm{inj}}},$$

which are used to determine the swept volume:

$$V_p = \frac{m}{M_{\mathrm{inj}}} q_{\mathrm{inj}} \left(\frac{\int_0^\infty tE(t)dt}{\int_0^\infty E(t)dt} - \frac{t_{\mathrm{slug}}}{2} \right).$$

Multi-rate mass transfer (MRMT) model (Haggerty and Gorelick 1995) implemented in **random walk particle tracking (RWPT) method** (Salamon et al. 2006) was applied to characterize the anomalous mass transport. In this approach, the medium is considered to contain overlapping mobile and immobile continua that exchange mass. Immobile zones with different properties can be assigned to account for the different total pore volumes swept by the solute and DNA nanotracers.

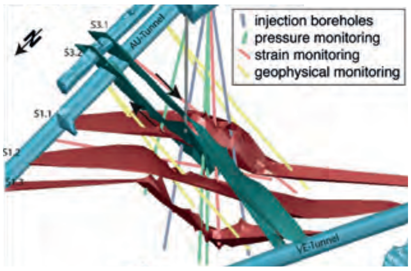

Overview of the DUG Lab (Amann et al. 2017) with two major shear zones S1 and S3, and boreholes. In the tracer tests, only injection (INJ) and pressure monitoring (PRP) boreholes were used.

References

Amann et al. 2017. Solid Earth Discussions, 1-55.
Haggerty and Gorelick 1995. Water Resources Research 31, 2383-2400.
Paunescu et al. 2013. Nature Protocols 8, 2440-2448.
Salamon et al. 2006. Water Resources Research 42, W11417.
Shook and Forsmann 2005. INL/EXT-05-00400, 20 p.

Results

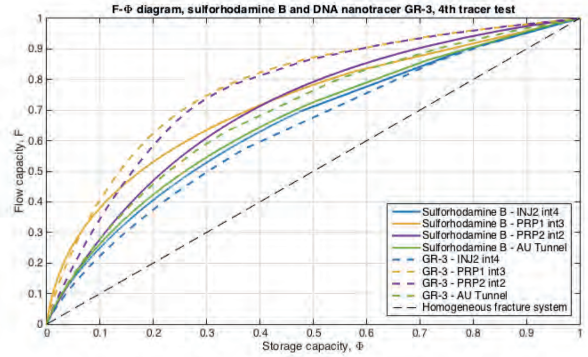

Comparison of flow/storage geometries of solute sulforhodamine B and DNA nanotracer named GR-3. Deviation from the diagonal is a measure of flow path heterogeneity, or channeling. In general, the DNA nanotracers experience more channeling, i.e., smaller pore volumes provide larger fractions of the total flow.

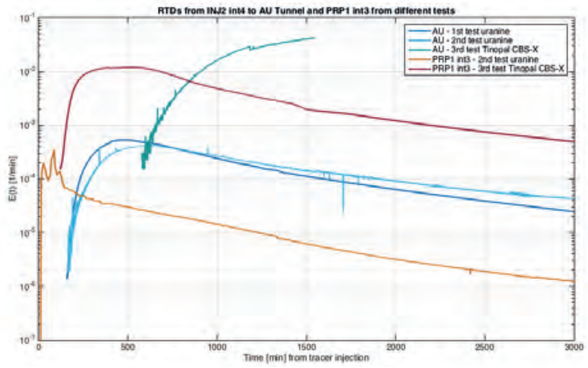

Illustration of tracer signals recorded at the AU Tunnel and PRP1 borehole from Tests 1-3 that all feature injection into Interval 4 of the INJ2 borehole. Test 3 was conducted after the stimulation phase. Stimulation did not directly target either of the structures, but the significant delays in the signals from Test 3 was unexpected. We hypothesize that residual thermal effects from injection of warmer water immediately prior to Test 3 had a larger influence than the stimulation.

The analysis of the anomalous transport with the MRMT model is on-going.

Discussion and Outlook

- The DUG Lab fracture volume was characterized by combining DNA nanotracer particles and solute dye tracers.
- Four tracer tests have been completed, each of which had two separate injections.
- The early termination of Tests 1-3 required undesirable data extrapolation. Future tests should be continued for a longer time.
- The DNA nanotracers arrived invariably earlier than the solutes.
- The results show that the swept volume of the DNA nanotracers is about a tenth of that from the solute tracer for the same injection-production pairs.
- Indications of multiple preferential flow paths are seen in several recorded tracer signals.
- The on-going analysis with the MRMT model will be used to evaluate the interplay between heterogeneous flow field and different mass transfer processes.

In situ characterization of groundwater flow and heat transport in stimulated fractured network using DTS

Maria Klepikova, Bernard Brixel, Reza Jalali, Simon Loew, Florian Amann

ETH Zurich, Geological Institute, Zurich, Switzerland

Objectives

Stimulation and Circulation (ISC) experiment at the Grimsel Test Site is dedicated to study seismo-hydro-mechanical coupled processes relevant for the development of a sustainable heat exchanger in low permeability crystalline rock under controlled conditions. Distributed Temperature Sensing (DTS) technology offers great promise for locating discrete fractures and measuring their hydraulic and heat exchange properties. We use Active - DTS tests and cross-borehole thermal tracer tests to investigate ground water flow and heat transport in fractured media before and after hydraulic stimulation.

Distributed Temperature Sensing at Grimsel Test Site (GTS)

DTS uses the Raman backscatter characteristics of light emitted following a laser pulse into a fiber optic cable to determine the distributed temperature along fiber with a spatial resolution of a few decimeters and temporal resolution of several seconds. At GTS several boreholes were equipped with distributed temperature-sensing optical fibers that are grouted in place.

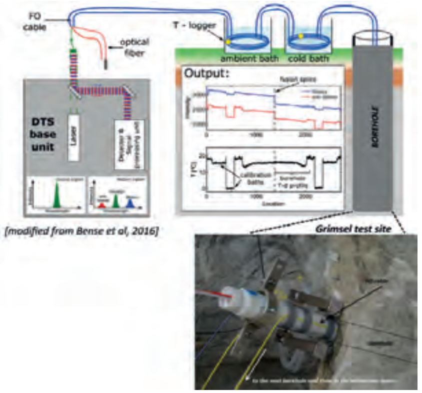

Figure: Schematic of DTS principles based upon Raman backscatter detection. In this cartoon, a fiber-optic cable is deployed in a double-ended setup [1].

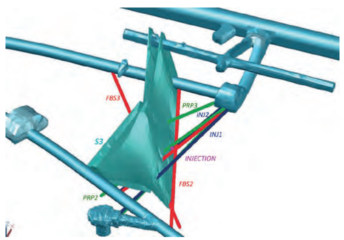

Figure: The boreholes drilled for the ISC experiment. PRP 1-3 and FBS 1-3 boreholes are equipped with DTS FO cables. The S3 shear zone is the target zone for the hydraulic stimulation.

Active-DTS Experiment

In A-DTS, the electrical heating cable [2, 3] or borehole fluid [4, 5] is heated. The temperature response along the FO cable deployed in the middle of the borehole during the heating and subsequent cooling allows:

- In situ determination of rock thermal properties.
- Fracture detection.
- Characterization of fracture inflows.

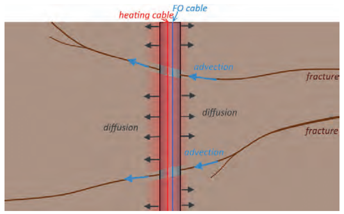

Figure: Schematic of Active-DTS method in a well intersecting two transmissive fractures. Heating- and cooling data can be used to infer thermal properties of the formation as well as groundwater flow.

Figure: Measurement setup for A-DTS tests in INJ 1 and INJ 2 boreholes. The bottom-piece and the connection points of the DTS /injection rod. The cable connection points were isolated towards the injection tube with pieces of foam.

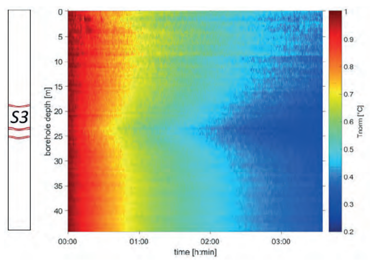

Figure: Normalized FO-DTS data showing relative temperature anomaly from A-DTS test in INJ 2 while INJ 1 was pressurized to 5.5 bar. 1 corresponds to initial temperature anomaly at respective depth, 0 means a full recovery to ambient groundwater temperature. The impact of the cooling inflow at $23.5\ m$ is pronounced. At this depth the S3 shear zone intersects the INJ2 borehole.

Cross-borehole thermal tracer test

A cross-borehole thermal tracer test is analyzed to identify fractures involved in heat transport and to measure thermal breakthrough curves in multiple observation points located at different distances from the injection point. The subsequent analysis of the measured breakthrough curves may provide new insights on flow channeling as well as fracture geometry [6].

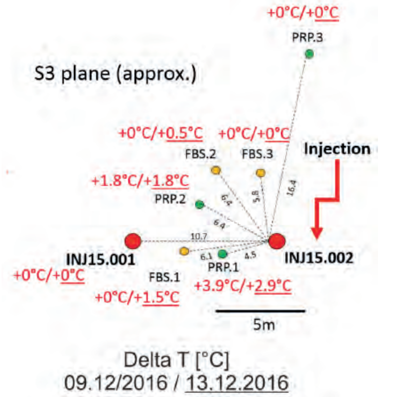

Figure: DTS measurements during the thermal tracer test conducted before the hydraulic stimulation. In-plane view of thermal anomalies measured in observation boreholes 10 and 14 days since the beginning of the heat injection in INJ 2.

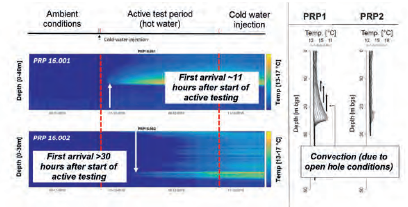

Figure: DTS measurements in PRP 1 and PRP 2 boreholes during the thermal tracer test conducted before the hydraulic stimulation.

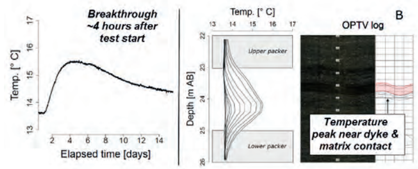

Figure: DTS measurements in PRP 1 borehole during the thermal tracer test conducted after the hydraulic stimulation.

Conduction of tests before and after hydraulic stimulation allows to quantify the effect of hydraulic stimulation on distribution of hydraulic and heat transport properties.

Conclusion

Our study confirms that FO DTS enables investigation of hydrogeological processes with high spatial and temporal resolution. In particularly, DTS monitoring in active mode allows fracture detection and characterization of fracture hydraulic properties similarly to fluid conductivity logs. The advantage of the A-DTS compared to the classical fluid conductivity logging is that

- no salt is added to the system
- measurements are conducted without logging-induced mixing

Cross-borehole heat tracer tests allows to understand heat transport processes in fractured media. Conduction of tests before and after hydraulic stimulation allows to quantify the effect of hydraulic stimulation on heat exchange properties of the media.

References

[1] V. F. Bense, T. Read, and A. Verhoef. Using distributed temperature sensing to monitor field scale dynamics of ground surface temperature and related substrate heat flux. *Agricultural and Forest Meteorology*, 220:207–215, 2016.

[2] T. Read, O. Bour, V. Bense, T. Le Borgne, P. Goderniaux, M.V. Klepikova, R. Hochreutener, N. Lavenant, and V. Boschero. Characterizing groundwater flow and heat transport in fractured rock using fiber-optic distributed temperature sensing. *Geophysical Research Letters*, 40(10):2055–2059, may 2013.

[3] Thomas I. Coleman, Beth L. Parker, Carlos H. Maldaner, and Michael J. Mondanos. Groundwater flow characterization in a fractured bedrock aquifer using active DTS tests in sealed boreholes. *Journal of Hydrology*, 528:449–462, 2015.

[4] T. Read, V. F. Bense, R. Hochreutener, O. Bour, T. Le Borgne, N. Lavenant, and J. S. Selker. Thermal-plume fibre optic tracking (T-POT) test for flow velocity measurement in groundwater boreholes. *Geoscientific Instrumentation, Methods and Data Systems*, 4(2):197–202, 2015.

[5] Andrew T. Leaf, David J. Hart, and Jean M. Bahr. Active Thermal Tracer Tests for Improved Hydrostratigraphic Characterization. *Ground Water*, 50(5):726–735, 2012.

[6] Maria V. Klepikova, Tanguy Le Borgne, Olivier Bour, Marco Dentz, Rebecca Hochreutener, and Nicolas Lavenant. Heat as a tracer for understanding transport processes in fractured media: Theory and field assessment from multiscale thermal push-pull tracer tests. *Water Resources Research*, 52(7):5442–5457, 2016.

Contact Information

- Web: https://sites.google.com/site/klepikovalambert/
- Email: maria.klepikova@erdw.ethz.ch
- Phone: +41 (0)44 633 80 24

How much can we interpret mineral surface area with distributions of minerals and pores ?

Xiang-Zhao Kong[1,*], Jin Ma[1], Duncan Webster[2], Martin O. Saar[1]
[1]Geothermal Energy & Geofluids Group, Department of Earth Sciences, ETH-Zürich, CH-8092, Switzerland (Corresponding Email: xkong@ethz.ch)
[2]SCANCO Medical AG, Fabrikweg 2, CH-8306, Bruettisellen, Switzerland

Introduction

Fluid-rock reactions play an important role in many geo-engineering processes, such as Enhanced Geothermal Systems (EGS) and Carbon Capture, Utilization, and Storage (CCUS). These reactions may change the reservoir permeability dramatically by mineral precipitation and/or dissolution:

- unfavorable reactions can lead to a significant decrease of reservoir productivity/injectivity in EGS and CCUS;
- favorable reactions can lead to a higher heat productivity in EGS or facilitate long-term CO_2 mineral trapping in CCUS.

However, the progress of these reactions depends on individual mineral accessible surface areas that are, in general, poorly constrained for natural geologic samples. In general, reactive surface area is estimated using methods including geometric model, Brunauer–Emmett–Teller (BET) gas absorption method, batch and flow-through experiments, and imaging technologies based on the principle of stereology. In this study, we take the advantages of both BET method and imaging technologies to determine accessible reactive surface areas of individual minerals. These measurements will be later calibrated in future flow-through experiments.

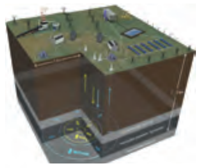

Buscheck, Bielicki, Edmunds, Hao, Sun, Randolph, Saar, Geospheres, 2016

Sample characterization

The rock samples used in this study are sandstones from a depth of 954.6 m from Geothermal well Vydmantai-1, located at the Southeast coast of the Baltic Sea of Lithuania. A thin section microscopy image (Figure 1) indicates an average grain size of 65 μm - 250 μm.

The rock composition (Table 1) was determined using XRF, XRD, and SEM image processing. Chemical formulas of individual minerals were determined by quantitative SEM chemical analysis.

Table 1 Rock composition

Mineral	Average chemical formula	Density g/cm³	XRF+XRD vol.%	SEM vol. %
Quartz (Qtz)	SiO_2	2.62	47.65	45.53
Dolomite (Dol)	$CaMg_{0.77}Fe_{0.23}(CO3)_2$	2.84	12.36	12.22
K-feldspar (Ksp)	$KAlSi_3O_8$	2.56	11.82	9.93
Muscovite (Mu)	$K_{0.85}Na_{0.15}Al_2(AlSi_3O_{10})(OH)_2$	2.82	5.38	4.76
Kaolinite (Kln)	$Al_{1.9}Si_{2.1}O_5(OH)_4$	2.60	0.91	5.64
Ilmenite (Ilm)	$Fe_2Ti_5O_{12}$	4.72	0.23	0.27

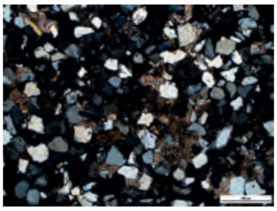

Figure 1 Transmitted light microscopy interference colour image of thin section

Helium gas pycnometry measurements provide a sample porosity of 21.9±0.4%, which agrees well with the estimated porosity of 21.65% from 2D image analyses on the binary image (Figure 2b). The volume fraction of individual minerals calculated from SEM images agrees well with XRD and XRF results (Table 1). This promotes the usage of further image analyses for mineral accessible surface area.

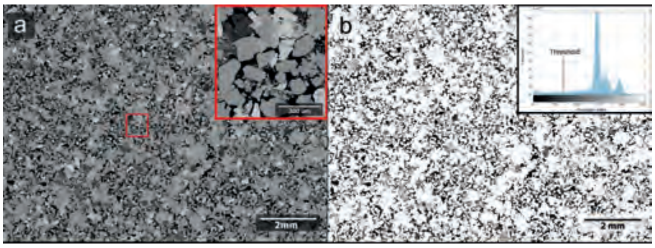

Figure 2 SEM-BSE analysis results: (a) grayscale SEM-BSE image with resolution of 1.2 μm and a x5 zoom-in on the top right, (b) the binary image with black presenting pores and white representing grains. (Inset) grayscale histogram of the SEM-BSE image.

Both SEM-BSE (Figure 2a) and SEM-EDS (Figure 4) images were collected on the same thin section area (11.37mm x 8.34 mm) with pixel resolutions of 1.2 μm and of 2.4 μm, respectively. A binary image (Figure 2b) was converted from the SEM-BSE image, using a threshold of 70, on a scale of 0 to 255 (black to white).

Pore size distribution (PSD)

The pore-size distribution (PSD) (Figure 3) was analyzed using three methods, including mercury (Hg) intrusion porosimetry, analyses of SEM-BSE (1.2 μm), and 3D CT (19.5 μm) images. In general, all measurements agree well with each other. The discrepancies are very likely introduced by the difference in measuring principles (pore throat size during mercury injection methods and pore size during image processing). In 3D CT analysis, due to limited resolution, most pores have been filtered out and only ~16% pores (relatively large) remain 'visible'. However, there is still a good match between results for the 2D and 3D image analyses. This provides a positive validation for the stereological method used in this study.

Figure 3 Pore size measured using porosimetry, SEM image analysis (Figure 2b) and 3D micro-CT analysis.

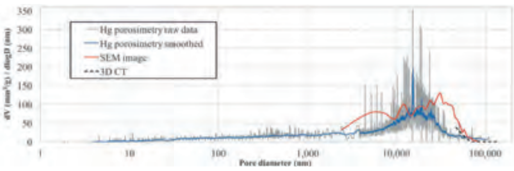

Reactive surface area analysis

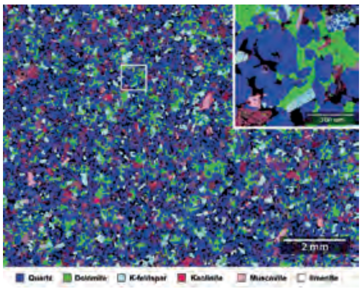

Figure 4 Mineral distribution on the SEM-EDS image (2.4 μm resolution).

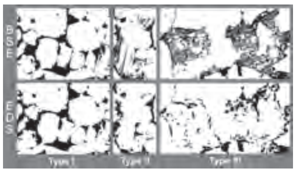

Figure 5 Comparison of the binary images of SEM-BSE (top) and SEM-EDS (bottom). In mineral fraction and surface area analyses, minerals were classified into 3 groups: (I) minerals with fully filled grains, such as quartz, dolomite, K-feldspar, and ilmenite; (II) minerals with partially filled grains, such as muscovite; (III) minerals with poorly filled grains, such as Kaolinite. To minimize the differences between BSE and EDS images, different corrections are applied to different groups (type) of minerals.

	Pore	Qtz	Dol	Ksp	Mu	Kln	Ilm	Total
EDS Area Fraction (AF) (%)	21.64	44.82	12.03	9.77	4.88	6.29	0.27	99.7
EDS PD (m/m²) of mineral grains		63003.3	64049.7	60724.7	102063.2	196802.0	147541.4	
Accessible EDS PD (m/m²)		18382.6	1605.5	2181	1767.8	6875.4	242.1	31054.5
Correction due to resolution difference between BSE and EDS images (perimeter density (PD) obtained from BSE image: 51567.3 m/m²)								
Correction factor for EDS AF		1.02^{I}	1.02^{I}	1.02^{I}	0.98^{II}	0.9^{III}	1.02^{I}	
Corrected EDS AF (%)	21.65	45.53	12.22	9.93	4.76	5.64	0.27	100
Correction factor for EDS PD		1.3^{I}	1.3^{I}	1.3^{I}	1.94^{II}	2.98^{III}	1.3^{I}	
Corrected accessible EDS PD (m/m²)		23897.4	2087.2	2835.3	3429.5	20488.8	314.7	53052.9
Roughness correction based on literature BET SSA of pure mineral grains and later calibrated to measured bulk BET SSA: 1.447 m²/g)								
Accessible mass-SSA (m²/g) calculated from corrected EDS PD		0.0144	0.0013	0.0017	0.0021	0.0124	0.0002	0.032
Accessible SSA fraction (%)		45.05	3.93	5.34	6.47	38.62	0.59	
Mass-SSA (m²/g) of mineral grains calculated from corrected EDS PD		0.04	0.037	0.039	0.089	0.230	0.052	
Typical literature BET mass-SSA (m²/g)		0.02-0.55	0.07-1.96	0.08-0.25	0.66-5.53	13.2-78.0	n.a.	
Correction factor for calculated mass-SSA		5	50	5	50	100	25	
Corrected mass-SSA (m²/g) of mineral grains		0.20	1.87	0.19	4.47	23.04	1.29	
Corrected accessible mass-SSA (m²/g)		0.07	0.06	0.01	0.06	1.24	0.005	1.441
Accessible mass-SSA fraction (%)		5.00	4.37	0.59	3.59	85.79	0.66	

Table 2 Various corrections for mineral area fractions (AF), perimeter density (PD) and specific surface areas (SSA) based on SEM-BSE image and BET values from literatures. Superscripts I, II, and III represent the three types of minerals in Figure 5.

To minimize the resolution mismatch between the SEM-BSE and the SEM-EDS images, minerals are grouped into 3 different types (Figure 5). Then corrections for each group were applied to reduce the relative difference of the perimeter density from 40.0% to 2.9%.

Mass-specific surface area (SSA) of whole rock samples was measured by the BET method with nitrogen as the adsorption gas at a temperature of 77.3 K. A bulk mass-SSA = 1.447 m^2/g was obtained using a 5-point method with a correlation coefficient of R^2=0.99995.

Perimeter density (m/m^2), *i.e.*, the ratio between solid perimeter and solid area, was first calculated using the SEM-BSE binary image (Figure 2b). Based on the principle of stereology (Weibel, 1969), mass-SSA (m^2/g) was then the product of a bias correction factor of $4/\pi$, the reciprocal of bulk rock density that is measured to be 2.11 g/cm^3, and the perimeter density. The stereological analyses on both the SEM-BSE image (Figure 2b) and the SEM-EDS image (corrected) yield mass-SSA values of 0.031 m^2/g and 0.032 m^2/g, respectively.

Roughness correction was also applied to individual minerals such that a good match to the BET measurements of the sample SSA can be achieved. Table 2 shows the BET literature values for pure individual minerals, accessible surface areas and their fractions before and after the corrections with different correction factors listed in Table 2. Compared to literature values, our SSA values for individual minerals are reasonable. The bulk SSA, i.e., the overall accessible SSA of all minerals, is then calculated to be 1.441 m^2/g, i.e., close to the bulk BET measurement (1.447 m^2/g).

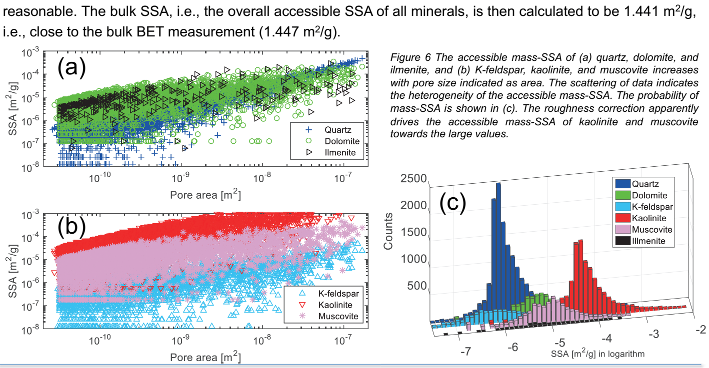

Figure 6 The accessible mass-SSA of (a) quartz, dolomite, and ilmenite, and (b) K-feldspar, kaolinite, and muscovite increases with pore size indicated as area. The scattering of data indicates the heterogeneity of the accessible mass-SSA. The probability of mass-SSA is shown in (c). The roughness correction apparently drives the accessible mass-SSA of kaolinite and muscovite towards the large values.

Conclusions

We have quantified porosity and pore-size distribution (PSD) of rock samples, using a Helium gas pycnometer and Hg porosimetry, respectively. Rock compositions are determined by a combination of XRF, XRD, and SEM-EDS, which are later geometrically mapped onto 2D images derived from SEM-BSE. The stereological method used in this study is validated through comparisons of mineral volume fraction, porosity, and PSD results from image processing and laboratory measurements. Normalization of stereological SSA to BET measurements yields roughness corrections of individual minerals. Due to the computational expensive of 3D micro-CT analysis, 3D reactive surface area analysis is still on-going and will be presented in our peer-review paper.

Acknowledgements

This work is supported by an European project, entitled "Demonstration of soft stimulation treatments of geothermal reservoirs project" (DESTRESS), funded by European Union's Horizon 2020 research and innovation program under the grant agreement No.691728. The rock sample is provided by Geoterma, a Lithuanian geothermal energy company. The 3D micro-CT analysis was performed by Dr. Duncan Webster at SCANCO Medical AG, Zurich, Switzerland.
The Geothermal Energy & Geofluids (GEG) group is endowed by the Werner Siemens Foundation, which is hereby gratefully acknowledge. The GEG group is also a research partner of SCCER-SoE, Switzerland.

SCCER SoE
SWISS COMPETENCE CENTER for ENERGY RESEARCH
SUPPLY of ELECTRICITY

SCCER-SoE Annual Conference 2017

In cooperation with the CTI
Energy
Swiss Competence Centers for Energy Research
Swiss Confederation
Commission for Technology and Innovation CTI

Geological characterization and in-situ stress state of the ISC experimental volume

H. Krietsch, V. Gischig, F. Amann, J. Doetsch, M.R. Jalali, B. Valley

Motivation

The In-Situ Stimulation and Circulation (ISC) experiment has recently been carried out at the Grimsel Test Site (Amann et al., 2017). It includes **six hydro-shearing** and **six hydraulic fracturing** experiments. A precise geological model and detailed knowledge of the in-situ stress state is crucial for the analysis and interpretation of the hydromechanical response of the experimental volume to high-pressure fluid injection. For this purpose an extensive geological characterization combining tunnel-mapping, core- and geophysical borehole logging (OPTV, ATV, FWS) was conducted, in combination with detailed geophysical surveys (i.e. GPR and seismic tomography). Additionally, a comprehensive stress measurement campaign, including overcoring (USBM & CSIRO HI) and hydraulic fracturing was carried out (Gischig et al., 2017, Krietsch et al., 2017).

Geological Model

The precise locations and orientations of shear zones and fractures were mapped using geophysical borehole and core logs. In total five shear zones are identified: three S1 (strike N52°E) and two S3 (strike N93°E) shear zones. The three S1 shear zone are characterized by an increase in foliation intensity. The two S3 shear zones are localized in one metabasic dyke, each, and separated by 2.5 m. Additionally, information about fracture density are gathered. As the boreholes approach the shear zones, the fracture density increases from 0-3 frac/m (host rock) to 14-22 frac/m.

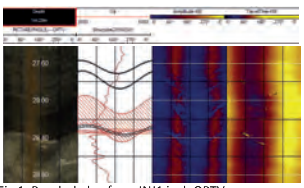
Fig 1. Borehole log from INJ1 incl: OPTV FWS and ATV

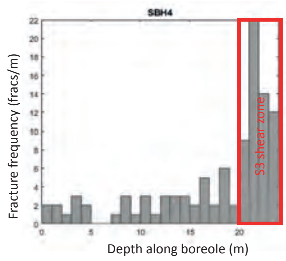

Fig 2. Fracture density along SBH4 with increase fracture density towards the shear zone

To build a geological model, geological observations are combined with geophysical surveys. The combination of geological mapping and seismic tomography revealed a highly fragmented zone between the two S3 shear zones that correlates with a drop in P-wave velocity. A dextral shear sense along the S3 shear zone was determined from mapping of S1 shear zones and GPR.

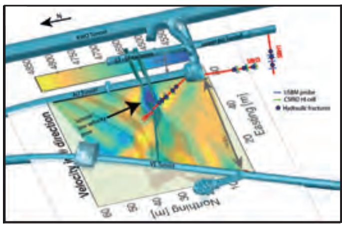
Fig 3. Seismic tomography combined with geological model. Highly fractured zone visible as low p-wave-velocity zone. Stress measurement locations are indicted, too.

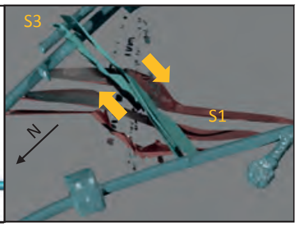

Fig 4. Three S1-orientated shear zones (red) and two S3-orientated shear zones are shown with fractures along PRP and INJ boreholes are shown, and shear sense of the S3-shear zone.

Stress measurements

Two stress field solutions were found : one for the 'far-field' and one close to the shear-zone. The orientations obtained from USBM, CSIRO-HI and HF are consistent for each tensor.

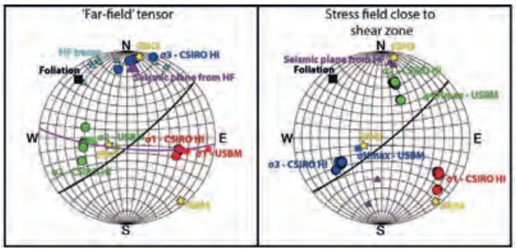

Fig 5. Final orientations of the stress tensors. Circles: CSIRO HI results; Small stars: USBM results; Yellow star: boreholes; Triangle: HF results; Half-circles: foliation plane (black), seismic plane (purple).

The magnitudes for the 'far-field'-tensor range from 13.1 to 14.4 MPa for σ_1, 9.2 to 10.2 MPa for σ_2, and 8.6 to 9.7 MPa for σ_3. A drop in principal stress magnitudes was observed, as the measurements approached the shear zones.

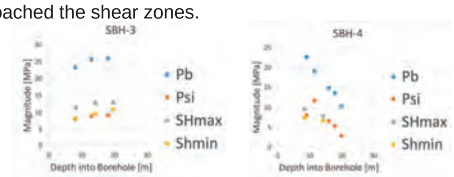

Fig 6. Stress magnitudes for SBH3 and SBH4. SBH3 measures the 'far-field' and SBH4 the stress drop as it approaches the shear zone.

Combination of geology and stress field

Based on the 'far-field' tensor the slip and dilation tendencies of all mapped geological structures were calculated. S1 shear zones have the highest slip tendencies, and S3 shear zones the highest dilation tendencies.

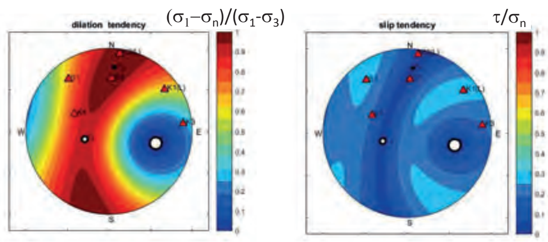

Fig 7. Dilation and slip tendency based on 'far-field' tensor correlated with mapped geological structures.

ATV logs conducted after hydroshearing experiment of an S1 parallel fracture indicate shear dislocation along stimulated structure. The offset can be quantified.

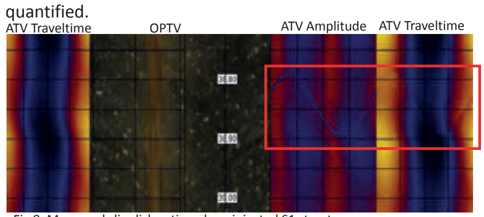

Fig 8. Measured slip dislocation along injected S1 structure.

References

Amann, F., et al. (2017), The seismo-hydro-mechanical behaviour during deep geothermal reservoir stimulation: open questions tackled in a decameter-scale in-situ stimulation experiment. Solid Earth Discuss., https://doi.org/10.5194/se-2017-79
Gischig, V., et al. (2017), On the link between stress field and small-scale hydraulic fracture growth in anisotropic rock derived from microseismicity. Solid Earth Discuss., https://doi.org/10.5194/se-2017-78
Krietsch, H., et al. (2017), Stress measurements in crystalline rock: Comparison of overcoring, hydraulic fracturing and induced seismicity results. *51st US Rock Mechanics/Geomechanics Symposium*. American Rock Mechanics Association, 2017.

SCCER SoE
SWISS COMPETENCE CENTER for ENERGY RESEARCH
SUPPLY of ELECTRICITY

SCCER-SoE Annual Conference 2017

In cooperation with the CTI
Energy
Swiss Competence Centers for Energy Research
Swiss Confederation
Commission for Technology and Innovation CTI

Deformation and tilt measurements during the ISC experiment at the Grimsel Test Site

H. Krietsch, V. Gischig, B. Valley, F. Amann

Motivation

A decameter scale stimulation experiment, including six hydraulic shearing (HS) and six hydraulic fracturing (HF) experiments, has recently been conducted at the Grimsel Test Site. One aim was the quantification of the spatial mechanical response during high pressure fluid injections into a pre-existing fracture network and intact rock mass. Multiple Fibre Bragg-Grating (FBG) sensors, distributed fibre optics strain systems (DBS) and tiltmeters were installed to monitor the deformations. In this contribution we present exemplary results from HS and HF experiments.

Sensors

A total of 60 FBG sensors were distributed in three differently oriented boreholes, covering intact rock and various fractures. The sensors average the strain over a 1 m baselength, and have a resolution of 0.1 µstrain and accuracy of 1 µstrain. Additionally, two DBS chains with a resolution of 1 µstrain and accuracy of 10 µstrain, covering three boreholes, each, were installed. At the tunnel west of the experiment, three tiltmeters were installed measuring the deviation from horizontal in two axes with a sensitivity of 0.1 µradians.

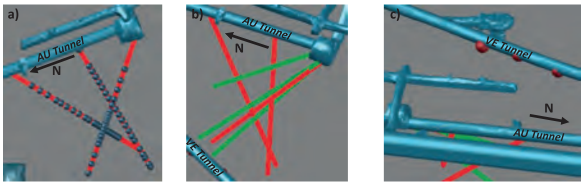

Figure 1. Sensor locations in the test volume: a) 20 FBG-sensors per borehole, b) FBS (red) and PRP Boreholes (green) with one loop per group, c) Position of three tiltmeters in VE-tunnel west of volume.

FBG strain measurements

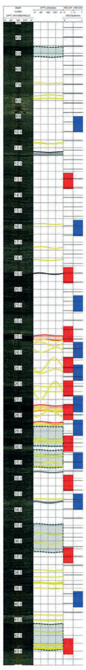

Depending on their position within the boreholes, the FBG sensors show different behaviour during the fluid injection. The magnitude of the recorded strain depends on the distance between sensor and injection interval, and whether the sensor covers a fracture or not. For the stimulation experiment HS1 (injection into S1 shear zone) the recorded strains in FBS3 may indicate a dextral shearing of the S1 shear zone. This may be interpreted from the tensional behaviour in the upper half of the borehole and the compressional behaviour at the lower part.

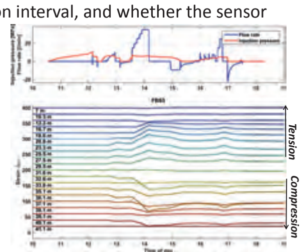

Figure 3. Transient strain signals in FBS3 during HS1 correlated with the injection flow rate and pressure

Figure 2. Exemplary borehole design for FBS1-borehole.

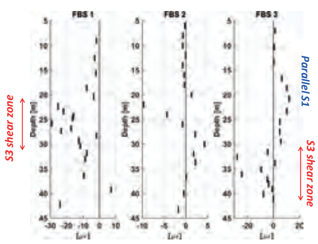

Figure 4. Maximum recorded strains during HS1 experiment. The strain signals indicate different behaviour depending on borehole orientation and sensor locations.

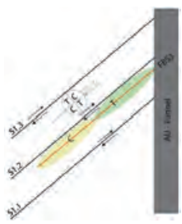

Figure 5. Schematic interpretation of the HS1 experiment, with indicated shear sense along S1 shear zones.

DBS strain measurements

Compared to the FBG sensors, the DBS have a resolution too low to precisely monitor the deformation due to the stimulations. In each borehole, one leg was packed (i.e. distinct base length of 0.6 m) and one leg was bare. The measurements indicated that the packed leg is more accurate than the bare one, but still of lower quality than the FBG recordings. For the description of the spatial mechanical response during the stimulation, the DBS is used in a qualitative way. In the PRP boreholes the movement of the packer due to an increase in interval pressure is visible in the strain data. During HF8 the hydrofrac propagated through the resin (yellow) above interval 1 in PRP2, which can be seen in the DBS.

.

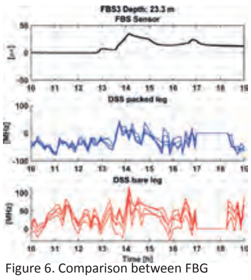

Figure 6. Comparison between FBG sensors, packed and bare leg DBS measurements in FBS3. Data represent strain at specific point over time.

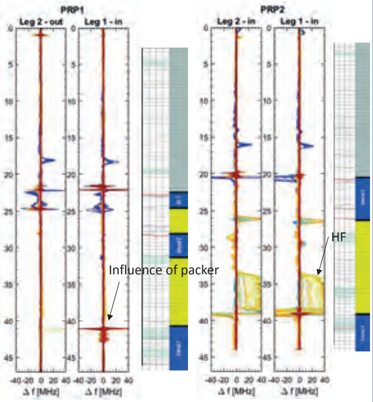

Figure 7. Distributed strain signals in PRP boreholes. Strong influence of packer movement can be observed. Above interval 1 in PRP2 a hydrofrac propagated through the resin.

Tilt measurements

Tilt measurements are as additional constrain for the orientation of stimulated shear zone. The tilt signals need to be corrected for the tunnel free surface effects with help of numerical modeling .

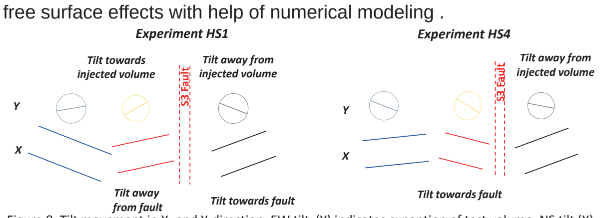

Figure 8. Tilt movement in X- and Y-direction. EW tilt (Y) indicates expantion of test volume. NS tilt (X), is sensitive to shear zone orientation and injection location. HS1 and HS4 indicate different behaviour in X-tilt, due to different orienation of shear zone, and different location of injection interval.

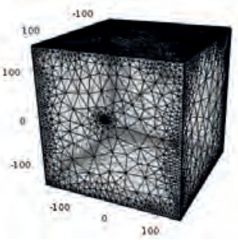

Figure 9. Geometry of tilt model. Normal opening of penny-shaped fractur with different orientations.

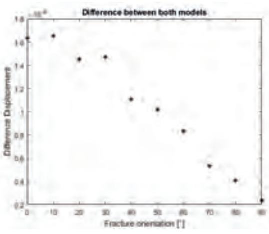

Figure 10. Modelled influence of the tunnel on the tilt-field. Difference displacement represents ratio tunnel/rock mass displacement.

Figure 11. Displacement field around the opening fracture

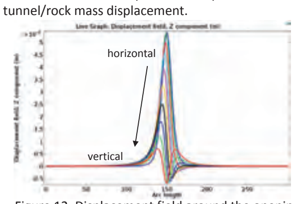

Figure 12. Displacement field around the opening fracture

SCCER SoE
SWISS COMPETENCE CENTER for ENERGY RESEARCH
SUPPLY of ELECTRICITY

SCCER-SoE Annual Conference 2017

In cooperation with the CTI
Energy
Swiss Competence Centers for Energy Research
Swiss Confederation
Commission for Technology and Innovation CTI

Core-scale reactive transport modelling of injection of CO_2-charged brine into natural sandstone

Jin Ma, Xiang-Zhao Kong, Martin O. Saar*

Geothermal Energy and Geofluids, Institute of Geophysics, ETH Zurich, Switzerland
** Email: jin.ma@erdw.ethz.ch*

Introduction

Fluid-rock reaction is an important process involved in many geological and geo-engineering systems such as chemical stimulation of enhanced geothermal systems (EGS) (Potier et al., 2009) and carbon capture, utilization, and storage (CCUS) (Guas, 2010; Xu et al., 2003). These reactions lead to mineral dissolution and precipitation which may cause changes of reservoir porosity and permeability (Cai et al., 2009; Nogues et al., 2013). Due to the complexity of coupled fluid flow and fluid-rock reactions in heterogeneous porous media, it is challenging to predict long-term operation performance of geothermal reservoirs.

Geochemical transport modelling is well recognized as a powerful approach to probe the physical and chemical evolution of subsurface systems (Beckingham et al., 2016). In this study, a 1D core-scale reactive transport model is developed to simulate the injection of CO_2-charged brine into a natural sandstone core. We present the simulation results using calculated ion concentrations to interpret mineral dissolution/precipitation reactions in a multi-mineral system.

Model description

We employed PFLOTRAN to perform a 1D core-scale reactive transport simulations at an outlet pressure of 10 MPa and a temperature of 40 ℃. We modelled an injection of CO_2-rich brine at a constant volumetric flow rate of 2 ml/min into a cylindrical sandstone specimen with a length of 3.9 cm and a cross section area of 5.29 cm^2 as shown in Figure 1. The NaCl concentration of the injected fluid is 1 mol/l, and 0.8 mol/l CO_2(aq) was dissolved into it to reach 80% of CO_2 solubility at such simulation conditions.

Fig.1 Sketch of the model with constant flow rate at the inlet and constant pressure at the outlet.

The rock properties in this model follow a sandstone sample from the geothermal reservoir, Vydmantai (954.6 m deep), Lithuania. Its porosity is measured to be 0.22 using He pycnometer and permeability 300 mD using flow-through experiments. The sandstone composition is listed in Table 1. Other parameters, such as mineral volume fraction and reactive surface area, take the results from analyse of SEM-EDS image (Figure 2). Mineral reaction rate constants are taken from Palandri et al. (2004).

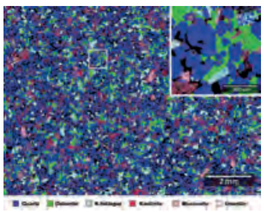

Fig.2 Mineral distribution of the SEM-EDS image with a resolution of 2.4 µm.

Table 1 Mineral system of the rock sample used in the model

Mineral	Formula	Volume fraction (%)	Reactive surface area (cm^2/cm^3)	Rate constant ($mol/cm^2/s$)
Quartz	SiO_2	46.0	1521.4	1.0 x 10^{-17}
Dolomite	$CaMg(CO_3)_2$	12.0	1328.7	3.0 x 10^{-8}
K-feldspar	$KAlSi_3O_8$	10.0	180.5	1.0 x 10^{-12}
Muscovite	$KAl_3Si_3O_{10}(OH)_2$	5.0	1310.0	1.0 x 10^{-16}
Kaolinite	$Al_2Si_2O_5(OH)_4$	5.0	26087.2	5.0 x 10^{-16}
Ilmenite	$FeTiO_3$	0.3	100.2	4.5 x 10^{-13}

Results and discussion

In the following, we only show the concentration of Ca++, because Ca++ and Mg++ only exists in dolomite with a mole ratio of 1:1. Figure 3 shows major ion concentrations at PV=0.53 and PV=793. Concentration of Na+ does not change much during the whole simulation. The simulation results show that when the volume of the injected fluid is less than one total pore volume (PV) of the core, ion concentrations clearly indicate a diffusion-controlled reaction front from 12 mm to 24 mm. At PV=0.53, compared to other cation (K+, Fe++, Al+++, and SiO_2(aq)) concentrations, Ca++ concentration is not affected by the dilation (mixing) at the inlet because of relatively high reaction rate of dolomite. When the injection volume of fluid is more than one pore volume (PV>1), a sharp concentration front is developed due to depletion of minerals, in particular for dolomite. This concentration front is migrating towards the outlet with a speed of 0.0174 mm/PV. Figure 3 shows a typical front pattern at PV=793 where Ca++ concentration is nearly zero from the inlet to the front, followed by a dramatic increment after the front.

Figure 4 shows the saturation index (SI) and the relative change of volume fractions of 5 major minerals in the system at both PV = 0.53 and PV = 793. When PV<1, volume fraction of most minerals do not change, except dolomite due to its high reactivity. The SI profiles indicate a potential dissolution of K-feldspar and a potential precipitation of kaolinite. When PV >1, similar to the concentration profiles, a sharp front is formed at the reaction front. Behind the front, all major minerals stay under-saturated, except for quartz which is closed to equilibrium. At the reaction front, muscovite and kaolinite quickly reach over-saturation but then are back to the equilibrium vicinity. Dissolution of K-feldspar and precipitation of kaolinite along the whole core is suggested.

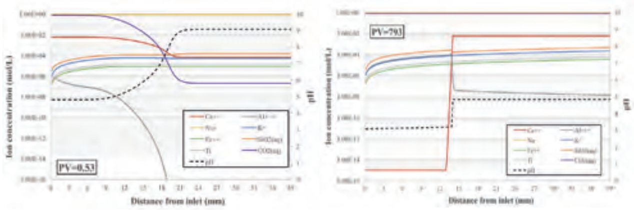

Fig.3 Ion concentrations (mol/L) and pH profiles at injection volumes of PV=0.53 and PV=793.

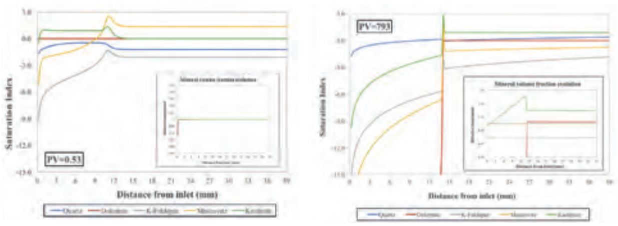

Fig.3 Saturation index (SI) and volume fraction relative change of minerals at injection volumes of (left) PV=0.53 and (right) PV=793.

Acknowledgement

The project is funded by the European Union's Horizon 2020, "DESTRESS" under grant No. 691728.

DESTRESS
GEG
ETH
Eidgenössische Technische Hochschule Zürich
Swiss Federal Institute of Technology Zurich

SCCER SoE
SWISS COMPETENCE CENTER for ENERGY RESEARCH
SUPPLY of ELECTRICITY

SCCER-SoE Annual Conference 2017

In cooperation with the CTI
Energy
Swiss Competence Centers for Energy Research
Swiss Confederation
Commission for Technology and Innovation CTI

Mixed finite element method for recovering stress and displacement fields

Morteza Nejati, Thomas Driesner
SCCER-SoE, ETH Zurich, Switzerland

Introduction

Stresses and displacements computed directly from the finite element solution of geomechanical problems can be extremely inaccurate when using low order finite elements such as two-noded line element, three-noded triangular element, and four-noded tetrahedral element. These elements are extremely efficient in terms of computation cost, and therefore their use in large geomechanical models is of interest. Stress and displacement recovery methods are designed to improve the accuracy of low order elements for two main reasons: (i) To obtain better estimates of the stress and displacement throughout the domain, and (ii) To provide a benchmark for discretization error estimation which is useful for efficient mesh generation and mesh adaptivity. Previous methods solely focus on stress recovery and are based on polynomial choices outside the ones provided from finite element shape functions. Recovery by equilibrium in patches [1], recovery by compatibility in patches [2], and recovery by enhanced equilibrium in patches [3] are examples of these methods. In this research, a new method called recovery by enhanced compatibility and equilibrium is proposed, which is able to recover displacements as well as stresses, and it only uses the polynomials available from isoparametric element types to enhance the accuracy of the field variables.

Methodology

The two main variational theorems in the theory of elasticity are principle of minimum potential energy, and principle of minimum complementary energy. Minimum potential energy is based of a functional of displacement, where compatibility conditions are satisfied as priori by assuming a continuous displacement over the entire domain and permitted variation of displacement which satisfies the prescribed displacement boundary conditions. This variational equation gives the equilibrium equations. Minimum potential of complementary energy is a functional of stresses, where equilibrium condition is satisfied as priori by assuming equilibrated stresses with body forces and permitted variation of stresses. This variational equation is equivalent to the compatibility of displacements. In these two principles, one of equilibrium or comparability is assumed over the domain, while the other condition is satisfied by the variational equation. Reissner [4] defined a variation theorem in which neither compatibility nor equilibrium is assumed as priori, whereby both equilibrium and comparability are outcomes of the variational equation. This mixed variational theorem does not favor equilibrium over compatability or vise versa, and permits simultaneous use of an assumed stress field and an assumed displacement field.

Let σ_{ij} and u_i be the components of the assumed stresses and displacements, respectively. The Reissner functional π_R is defined in terms of assumed independent stresses and displacements as:

$$\pi_R = \int_\Omega \left(\sigma_{ij} u_{i,j} - \frac{1}{2}\sigma_{ij} S_{ijkl} \sigma_{kl} - F_i u_i\right) \mathrm{d}\Omega - \int_{\Gamma_T} \bar{T}_i u_i \, \mathrm{d}\Gamma - \int_{\Gamma_u} (u_i - \bar{u}_i) T_i \, \mathrm{d}\Gamma \quad (1)$$

Here S_{ijkl} denotes the components of the fourth-order elasticity matrix, F_i is the body force component, Ω is the domain of interest, and $\bar{T}_i$ and $\bar{u}_i$ are the traction and displacement boundary conditions applied along Γ_T and Γ_u. After the finite element solution with low order elements is performed, the displacements are obtained and can be used as the boundary values for single or a patch of elements to solve for more accurate stresses and displacements using the mixed finite element.
Let us assume that $T_i = \bar{T}_i$ on Γ_T. The variation of the functional in Eq. (1) with respect to displacement and stress gives:

$$\begin{aligned} &\int_\Omega \delta u_i (\sigma_{ij,j} + F_i) \, \mathrm{d}\Omega = 0 \\ &\int_\Omega \delta\sigma_{ij} (u_{i,j} - S_{ijkl}\sigma_{kl}) \, \mathrm{d}\Omega + \int_{\Gamma_u} \delta T_i (\bar{u}_i - u_i) \, \mathrm{d}\Gamma = 0 \end{aligned} \quad (2)$$

By simultaneously solving these two equations for the displacement and stress, highly accurate recovered fields can be obtained.

Results and discussion

Figure 1 compares recovered values against the directly calculated ones as well as the exact values for a one-dimensional model. Figure 2 also shows how the order of convergence increases by using different orders of polynomials for the recovered estimates. These result show that the proposed method is highly efficient in recovering FE values with low accuracy. This is in particular important for efficiently modeling large thermo-hydro-mechanical systems with low-order elements.

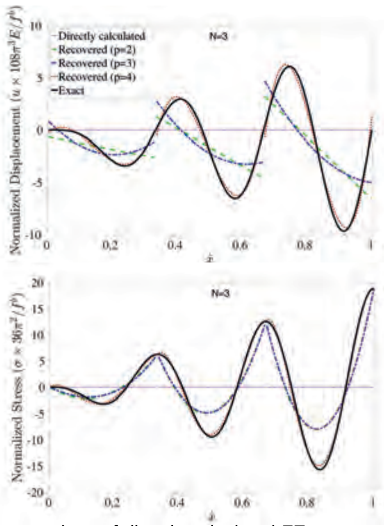

Fig 1. The comparison of directly calculated FE stress and displacement using three elements with the recovered ones and the exact solutions for the 1D problem which is subjected to $F^b = f^b \bar{x} \sin(6\pi\bar{x})$ and fixed at two ends. The recovered values are obtained using stress polynomials of order p and displacement polynomial of order q=p-1 for each individual element.

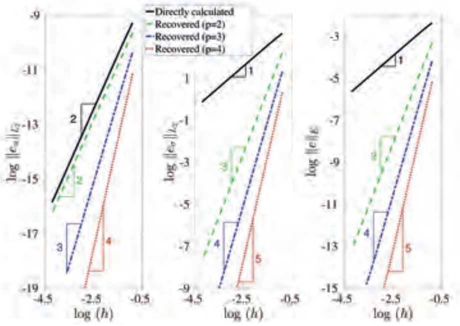

Fig 2. The convergence rate of displacement, stress and energy error estimates by using the proposed approach with polynomials of order p for stress, and q=p-1 for displacement for a one-dimensional problem.

References

[1] Boroomand, B., Zienkiewicz, O. C., 1997. Recovery by equilibrium in patches (REP). International Journal for Numerical Methods in Engineering 164, 137–164.
[2] Ubertini, F., 2004. Patch recovery based on complementary energy. International Journal for Numerical Methods in Engineering 59 (11), 1501–1538.
[3] Payen, D. J., Bathe, K.-J., 2012. A stress improvement procedure. Computers and Structures 112-113, 311–326.
[4] Reissner, E., 1950. On a variational theorem in elasticity. Journal of Mathematics and Physics 29, 90-95.

SCCER-SoE Annual Conference 2017

Numerical Modeling of Natural Convection in Fractured Media

James Patterson, Thomas Driesner
Institute of Geochemistry and Petrology, ETH Zurich, Switzerland

Before EGS: In-situ Geothermal Gradient

Geothermal gradient is a key reservoir characteristic in determining how deep a well must be drilled to reach a certain temperature. However, faults and fractures in these rocks may facilitate natural convection: the process by which thermally-induced density differences of water cause cold, dense water to cycle deeper into the basement while hot, light water moves towards the surface. This can result in spatially varying temperatures around the upward/downward flowing plumes and can dramatically influence produced fluid temperature. This research seeks to better understand the role of natural convection in fractures on temperature variations in the subsurface and its implications for geothermal energy. We use the Complex Systems Modeling Platform (CSMP++), a reservoir modeling platform developed in part at ETH Zurich.

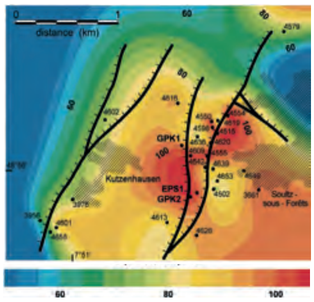

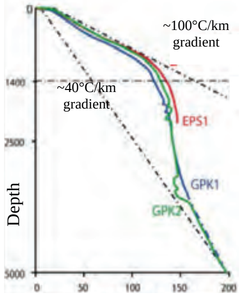

Fig. 1 (left): Measured and interpolated temperature at 800m depth; irregular shape distribution indicates convective plumes.[1]
Fig. 2 (right): Temperature profile to 5000m depth in 3 wells featured in Fig. 1. Sharp drop in gradient around 1400m due to impermeable layer blocking convection.[2]

Thermal Perturbation from Convection in a Single Fracture

As fluid at the bottom of a fracture is heated, it rises through the highly permeable fracture, carrying heat to the top of up-flow zones, while cold fluid sinks and cools the rock at the bottom of down-flow zones. The spacing and strength of these up- and down-flow zones are primarily a function of fracture aperture/permeability. Complex 3-dimensional thermal perturbations form around the fracture. Heating patterns above the fracture may be indicative of individual, wide convection cells or multiple narrow cells along a fracture in the subsurface.

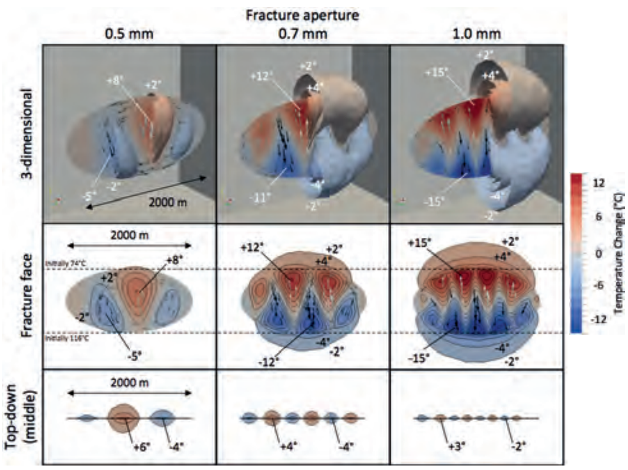

Fig. 3: Change in temperature around a fracture with aperture 0.5 mm, 0.7 mm, and 1.0 mm. Larger apertures result in narrower convection cells and stronger heating/cooling of host rock.

References

[1] Clauser, C., Griesshaber, E., Neugebauer, H.J. (2002) Decoupled thermal and mantle helium anomalies: Implications for the transport regime in continental rift zones. Journal of Geophysical Research, Vol. 107.
[2] Siffert, D., Haffen, S., Garcia, M.H., Geraud, Y. (2013) Phenomenological study of temperature gradient anomalies in the Buntsandstein formation, above the Soultz geothermal reservoir, using TOUGH2 simulations. 38th Stanford Workshop on Geothermal Reservoir Engineering.

Flow Patterns Around a Single Fracture

Convection within a fracture also induces fluid flow in permeable host rocks. Two forces drive fluid flow around the fracture:

- Circulation of fluid in the fracture drives fluid inflow/outflow through the fracture walls
- The convection-driven thermal perturbation heats/cools fluid near the fracture, inducing buoyancy-driven fluid flow in the host

The combination of inflow/outflow (flow perpendicular to fracture face) and buoyant forces (vertical flow) creates secondary convection cells that circulate parallel to fracture strike (in the 0.7 and 1.0 mm cases).

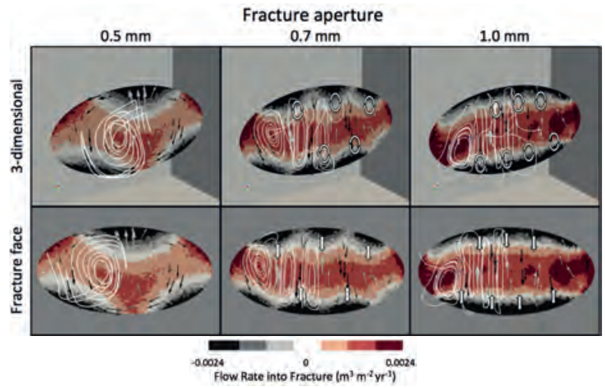

Fig. 4: Inflow (red) and outflow (black) patterns in a fracture with 0.5 mm, 0.7 mm, and 1.0 mm aperture. Fluid flow streamlines show complex patterns surrounding fracture, including secondary convection cells forming in the 0.7 and 1.0 mm cases.

Multiple Heterogeneous Fractures

Real fractures have heterogeneous aperture distributions, creating regions of high or low permeability. This influences the location and strength of natural convection cells. Additionally, fractures typically occur in sets of multiple fractures with similar orientations. The thermal perturbation caused by natural convection affects convection patterns in neighboring fractures, creating a "synchronization" effect – up-flow and down-flow regions will self-organize and create convection "rolls" across multiple fractures.

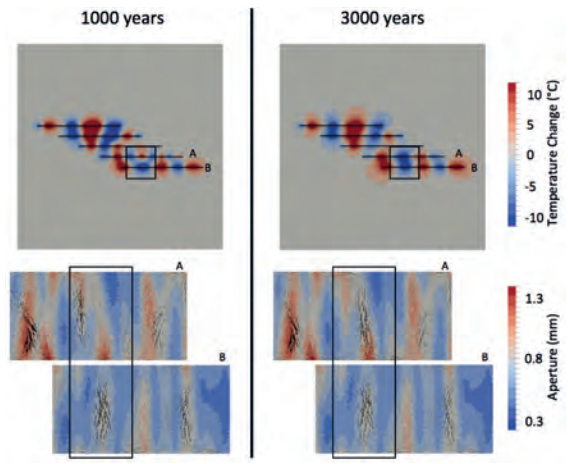

Fig. 5: Bird's-eye view of slice at 2500 m depth; two intersecting fracture sets. Colored by temperature difference. Convection tubes form across fractures, regardless of fracture length.

Conclusions and Future Work

Fundamental understanding of thermal perturbations created by convection within a fracture aids us in understanding subsurface fracture and flow networks. Additionally, further insight may be gained by accounting for more complicated physical processes (e.g. thermo-mechanics), modeling site-specific geometries, and by investigating optimal well placement in such a setting.

SCCER SoE
SWISS COMPETENCE CENTER for ENERGY RESEARCH
SUPPLY of ELECTRICITY

SCCER-SoE Annual Conference 2017

In cooperation with the CTI
Energy
Swiss Competence Centers for Energy Research
Commission for Technology and Innovation CTI

Enhancing drilling performance by combining conventional and thermal spallation drilling: A feasibility study

Edoardo Rossi[a,b], Michael A. Kant[b], Claudio Madonna[a], Martin O. Saar[a], Philipp Rudolf von Rohr[b]

[a]ETH Zürich, Department of Earth Sciences, Sonneggstrasse 5, 8092 Zürich
[b]ETH Zürich, Institute of Process Engineering, Sonneggstrasse 3, 8092 Zürich

Motivation

The utilization of deep geothermal energy is impeded by the high drilling costs, which account for more than 40% of the total investment for a geothermal power plant [1]. Currently employed drilling methods are based on mechanical abrasion and exportation of the rock, resulting in substantial drill bit wearing and low rates of penetration (ROP) in hard rocks.

A novel approach is to implement a thermal assistance at the front face of the drill bit to enhance the performance of conventional rotary drilling and reduce the overall costs.

Concept

A hot-jet is used to thermally assist the conventional drilling by inducing shock heating and therefore thermally weakening the rock material. The material exportation would therewith require lower forces on the drill bits which also implies reduced drill bit wearing.

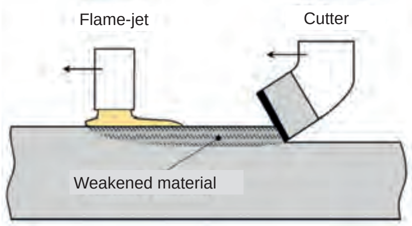

Figure 1: Concept of combined thermo-mechanical drilling [2]

Combined thermo-mechanical drilling

The combined drill head features:

- Fuel (methane) and oxidizer (air) used as reaction fluids
- A combustion chamber where the fluids are combusted
- The drilling mud is also used to cool down the combustion chamber
- At the bit face a flame slot is prescribed
- Conventional cutters are placed next to flame-jets

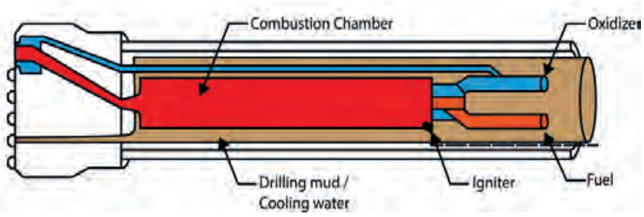

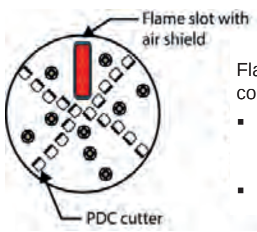

Flame nozzles include an ***air-shielding*** concept:

- Constrain and maximize flame heat transfer to the rock
- Guarantee low temperatures at the cutters

Figure 2: Potential implementation of combined thermo-mechanical method [3]

Preliminary experiments

In order to evaluate the weakening effects of high heating rates-flame treatments, the strength after heating of Rorschach sandstone and Central Aare granite are analyzed. Different heating rates are studied to highlight the different behavior of the rocks after oven and flame heating.

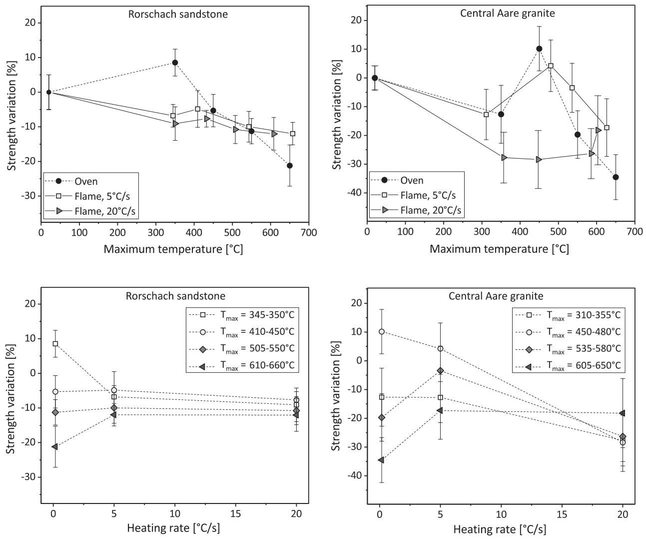

Figure 3: Rock strength variation for different treatment temperatures and heating rates

- → No hardening behavior after flame heating for sandstone and granite
- → Sandstone material is weakened for any temperature when flame-treated
- → 30% strength decrease of granite when treated at high heating rates
- → Low heating rates: thermal cracking due to thermal expansion stresses
- → High heating rates: thermal cracking due to high thermal gradients

Conclusions

The feasibility of the combined drilling method was demonstrated by means of the strength reduction after treating the rock with a flame-jet. Thus, local and high heating rate flame treatments can be implemented to weaken the rock material yielding lower forces on the drill bits and therefore increased performance and reduced drilling costs.

Additionally, the shielding of the flame is fundamental to allow this method to be effectively applicable and to be used in the field as an alternative drilling approach.

As a final step, the technology shall be implemented in order to finally prove the applicability and the related improvements in terms of drilling performances.

References

[1] Tester J.W. et al. (2006). The future of geothermal energy: Impact of enhanced geothermal systems (EGS) on the United States in the 21st century, *Massachusetts Institute of Technology*

[2] Rossi E. et al. (2017). The effects of flame-heating on rock strength: Towards a new drilling technology. *51st US Rock Mechanics/Geomechanics Symposium 25-28 June 2017, San Francisco, USA.*

[3] Kant M.A. et al. (2017) Enhancing the drilling process for geothermal resources by combining conventional drilling and the spallation technology. *Proceedings, 42nd Workshop on Geothermal Reservoir Engineering, Stanford: Stanford University, 2017*

IPE Institute of Process Engineering
DERDW EARTH SCIENCES
Bundesamt für Energie BFE
Swiss Federal Office of Energy SFOE
INTERNATIONALES GEOTHERMIEZENTRUM
INTERNATIONAL GEOTHERMAL CENTRE

SCCER-SoE Annual Conference 2017

Pico-seismicity during hydraulic stimulation experiments at the Grimsel Test Site

Linus Villiger*, Valentin Gischig**, Joseph Doetsch**, Hannes Krietsch**, Mohammadreza Jalali**, Nathan Dutler ***, Benoît Valley ***, Keith Evans**, Florian Amann** & Stefan Wiemer*

* Swiss Seismological Service, ETH Zurich, CH-8092 Zurich; ** Department of Earth Sciences, ETH Zurich, CH-8092 Zurich; ***Centre for Hydrogeology and Geothermics, University of Neuchâtel, CH-2000 Neuchâtel

Introduction

The In-situ Stimulation and Circulation (ISC) experiment at the Grimsel Test Site (GTS) is an ongoing interdisciplinary project to study the pressure, temperature and stress changes in the rock mass due to hydraulic stimulation (Amann et al., 2017; Gischig et al., 2017). In early 2017, the project entered the second phase, which included the main stimulation experiments. It involved high-pressure fluid injections into two shear zones (S1, S3) along which slip was induced (i.e. hydraulic-shearing). In May 2017 the second series of experiments followed. These experiments involved injection at even higher pressures and larger flow rates which induced tensile-dominant fracturing (i.e. hydraulic fracturing). The entire experiment series was established to support research related to deep geothermal energy which should play a significant role in the Swiss energy mix by 2050 (Swiss Energy Strategy 2050).

Six sections (HS02, 04, 05, 03, 08, 01) of 1 to 2 m length distributed over the two injection boreholes were stimulated during the hydraulic shearing experiments (HS). Six different sections in intact rock within the same boreholes were stimulated during the hydraulic fracturing experiments (HF). During the experiments a multi-sensor monitoring system was in place:

Hydraulic monitoring
- injection pressure, flow rate
- pressure monitoring boreholes

Deformation monitoring
- fiber-optics (FBG's, distributed) in deformation monitoring boreholes
- 3 tilt meters in VE tunnel
- 4 extensometers in AU tunnel

Seismic monitoring
- continuous acquisition at 200 kHz
- 26 Acoustic emission sensors in tunnels and seismic monitoring boreholes
- 5 accelerometer in tunnels
- 2 seismic sources in boreholes, 8 hammers in tunnels

Seismic monitoring network at GTS

The figure below shows an overview of the seismic monitoring network installed during the performed experiments at GTS. The intervals stimulated during experiment HS01 and HS04 are highlighted in red.

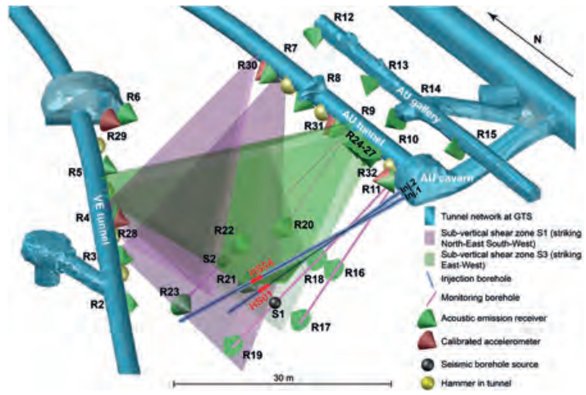

Overview hydraulic-shearing experiments

Only the HS experiments are considered in this poster. In the following, injectivity increase of all HS experiments estimated from the slope of injection pressure vs. flow rate at low pressure during step-pressure tests are stated. Experiments show a high variety in seismic response as well as in injectivity gain even though the injection protocol as well as the amount of injected volume was similar for all experiments. The stimulation of shear zone S3 generates a much higher seismic response compared to injections into shear zone S1.

Experiment	Injection in, interval [m]	Structure	Initial injectivity, final injectivity [l/min/MPa]	Change in injectivity [ ]	Inj. Volume [liter]	Total events [ ]
HS02	Inj1, 38.0 - 40.0	S1	0.018, 1.62	89	797	1203
HS04	Inj1, 27.2 - 28.2	S3	0.9, 0.9	1	1253	5606
HS05	Inj1, 31.5 -32.5	S3	0.086, 0.4	5	1211	2452
HS03	Inj1, 34.3 - 35.3	S1	0.0035, 1.7	486	831	314
HS08	Inj1, 22.0 - 23.0	S1 (S3)	0.002, 0.54	270	1258	3703
HS01	Inj2, 39.8 - 40.8	S1	0.0006, 1.11	1850	982	560

Event evolution during hydraulic shearing experiments

This section shows, flow rate, injection pressure and cumulative number of seismic events for experiment HS01 and HS04. During HS01 shear zone S1 and during HS04 shear zone S3 was stimulated. Events which are detected at all 8 borehole stations (R16 - R23) and more stations in the surrounding tunnels contribute to the cumulative number of events of coinc. 8. Events which are detected at 7 borehole stations and other surrounding stations contribute to coinc. 7 and so forth. The vertical stripes on top of the "cumulative number of events" line indicate performed seismic surveys during which the search for induced seismic events was suspended.

All experiments show, after breakdown of the respective interval, a threshold pressure which has to be reached to initiate seismicity. Some seismic events are initiated after shut-in. Also the subsequent venting phase initiates seismic events.

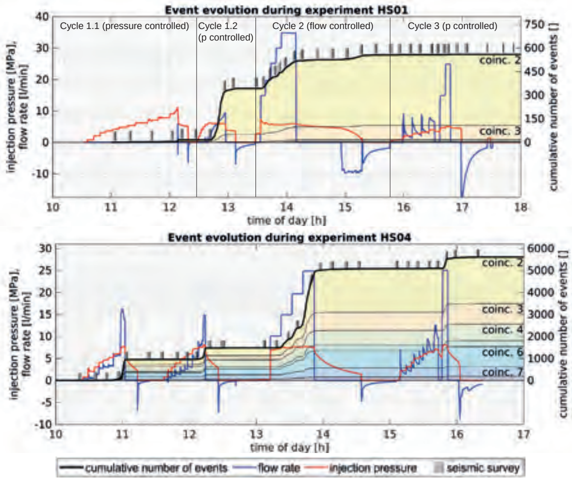

Location of seismicity during experiment HS04

The figure below shows the absolute location of 1000 events of experiment HS04 in a view towards North (A), a view towards West (B) and in top view (C). The highest accuracy in location is thereby achieved by locating the events of coincidence level 8. The error in location increases with decreasing coincidence level (i.e. with decreasing detection quality). The location of the presented events was performed using manually picked P-wave arrivals in a homogeneous and isotropic velocity model having a P-wave velocity of 5150 m/s. The relative magnitude (Mr) stated was determined from recorded peak amplitudes of the respective event.

Already, the location using this simple velocity model shows a clustering of events, as well as a clustering of high magnitude events.

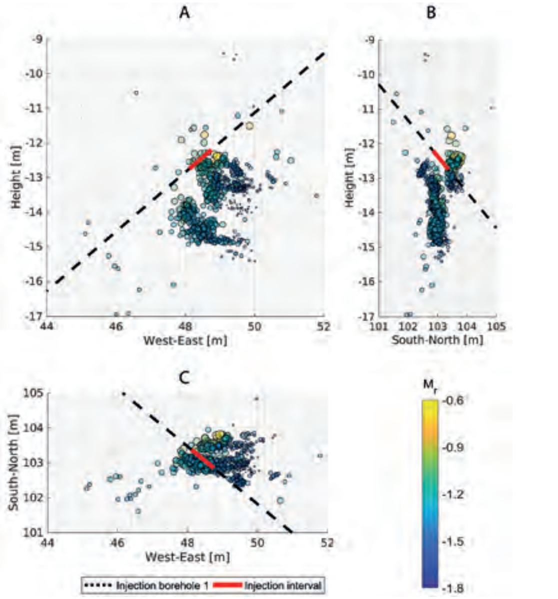

Conclusion and Outlook

- The performed hydraulic-shearing experiments show high variability in injectivity gain as well as in seismic response. Exceeding a specific injection pressure onsets seismicity. Induced seismic events tend to form cluster in both spatial distribution and magnitude.
- In a next step, event location will be performed for all 12 experiments with more advanced location techniques (e.g. joint hypocenter determination), additionally location accuracy will be quantified.

Reference

- Amann, F., et al. (2017), The seismo-hydro-mechanical behaviour during deep geothermal reservoir stimulation: open questions tackled in a decameter-scale in-situ stimulation experiment. Solid Earth Discuss., https://doi.org/10.5194/se-2017-79
- Gischig, V.S., Doetsch, J., Maurer, H., Krietsch H., Amann F., Evans, K.F., Nejati, M., Jalali, M., Valley, B., Obermann, A., Wiemer, S. and Giardini, D. (2017), On the link between stress field and small-scale hydraulic fracture growth in anisotropic rock derived from microseismicity. Solid Earth Discuss., https://doi.org/10.5194/se-2017-78

Email: linus.villiger@sed.ethz.ch

SWISS COMPETENCE CENTER for ENERGY RESEARCH
SUPPLY of ELECTRICITY

SCCER-SoE Annual Conference 2017

In cooperation with the CTI
Energy
Swiss Competence Centers for Energy Research
Commission for Technology and Innovation CTI

An Implicit Level Set Scheme to simulate planar 3D hydraulic fracture propagation

GeoEnergyLab

Haseeb Zia, Brice Lecampion

Swiss National Science Foundation

Motivation

Hydraulic fractures are tensile fractures that propagate in an initially stressed rock due to the injection of fluid at a given rate. Simulating the propagation of such fractures is a challenge as there are multiple processes involved that are operating at multiple scales. Numerically capturing these processes on the full range of both temporal and spatial scales is challenging and has been the subject of many studies in the last few decades. The Implicit Level Set Algorithm (ILSA) [Peirce & Detournay 2008] is one such numerical scheme that aims at resolving these multiscale processes with relatively low computational cost. We present here an open-source Python implementation of this scheme.

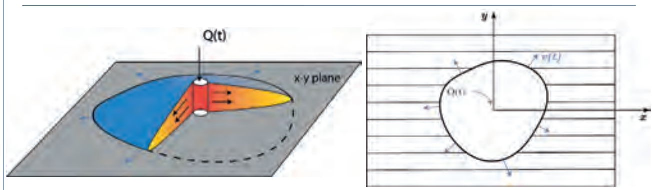

Fig 1: The fracture is assumed to be planar (propagating in x-y plane)

ILSA Scheme

The Implicit Level Set Algorithm (ILSA) simulates the propagation of planar 3-dimensional hydraulic fractures. The solution of elasticity and the fluid flow is obtained in a fully coupled manner. The propagation is tackled combining a level set scheme and the hydraulic fracture tip solution [Garagash et al. 2011]. The following numerical techniques are used to solve the coupled problem.

- Finite Volume method for the fluid flow.
- Displacement discontinuity method for elasticity.
- Level set method to track the fracture front.

The scheme uses a Cartesian grid. The main strength of the scheme is its utilization of the plane-strain semi-infinite hydraulic fracture solutions to capture the near-tip behaviour. This allows it to compute the solution on a relatively coarse grid, making it both accurate and computationally efficient.

Governing Equations

The following equations describe the process of hydraulic fracture propagation.

- Elasticity for planar mode I fracture can be re-written as the following boundary integral equation

$$p = p_f - \sigma = -\frac{E'}{8\pi}\int_{A(t)} \frac{w(x',y',t)\,dA(x',y')}{[(x'-x)^2+(y'-y)^2]^{3/2}}$$

[Hills et al. 1996]

- Fluid continuity:

$$\frac{\partial w}{\partial t} + \nabla\cdot q + g_L = Q(x,y)\delta(x,y),$$

with Poiseuille law and Carter leak-off:

$$q = -\frac{w^3}{\mu'}\nabla p_f, \quad g_L = \frac{C' H(t-t_0(x,y))}{\sqrt{t-t_0(x,y)}}$$

Tip Asymptotics

It can be shown that the equations governing the near tip behaviour of the fracture are identical to the governing equations for the problem of a steadily propagating semi-infinite fluid driven fracture [Desroches et al. 1994, Garagash & Detournay 2000, Garagash et al. 2011]. In the near-tip region, these equations provide the exact relations between the fracture parameters such as width and pressure, and the distance from the front.

For example, in the limiting toughness (Eq. a) and viscosity (Eq. b) dominated cases, the fracture width in the tip region is given by

$$\hat{w} = \frac{K'}{E'}\hat{x}^{1/2} \quad \text{(a)}$$

[J.R. Rice 1968]

$$\hat{w} = (18\sqrt{3}V\frac{\mu'}{E'})^{1/3}\hat{x}^{2/3} \quad \text{(b)}$$

[Garagash et al. 2000].

The complete solution capturing the transition between different propagation regimes has been obtained numerically [Garagash et al. JFM 2011]. Here, we are using the approximation provided by Dontsov and Peirce [2015]. The ILSA scheme couples these tip solutions with the finite fracture discretization to resolve the tip behaviour at the sub-grid scale.

Validation

The scheme has been validated with a number of test cases. The figures below show the comparison of the solution computed by the ILSA scheme against the analytical solution for the case of viscosity dominated propagation.

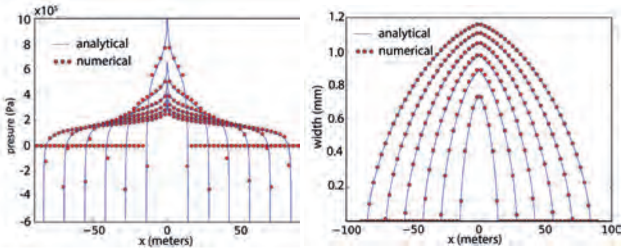

Fig 2: Time evolution of fracture width and pressure at the x-axis line.

Further test cases

- Confined propagation

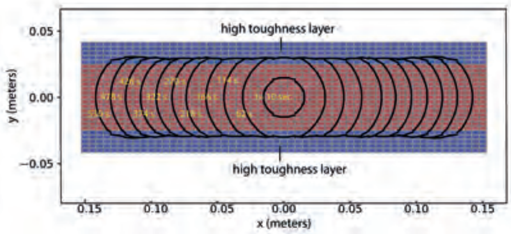

Fig 3: Footprint of a fracture propagating in a layer confined by high toughness layers

- Asymmetric Stress contrast

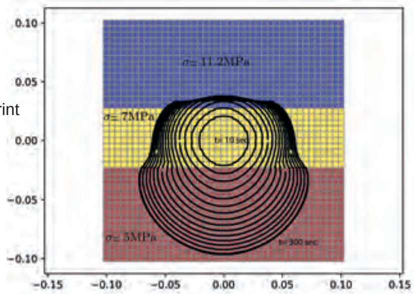

Fig 4: Time evolution of footprint of a fracture propagating in a layer bounded by layers with different confining stresses.

References

- Peirce, A., & Detournay, E. (2008). An implicit level set method for modeling hydraulically driven fractures. Computer Methods in Applied Mechanics and Engineering, 197(33), 2858-2885.
- Hills, D. A., Kelly, P. A., Dai, D. N., & Korsunsky, A. M. (2013). Solution of crack problems: the distributed dislocation technique (Vol. 44). Springer Science & Business Media.
- Rice, J. R. (1968). Mathematical analysis in the mechanics of fracture. Fracture: an advanced treatise, 2, 191-311.
- Garagash, D., & Detournay, E. (2000). The tip region of a fluid-driven fracture in an elastic medium. Transactions-American Society of Mechanical Engineers, Journal of Applied Mechanics, 67(1), 183-192.
- Desroches, J., et al. "The crack tip region in hydraulic fracturing." Proceedings of the Royal Society of London A: Mathematical, Physical and Engineering Sciences. Vol. 447. No. 1929. The Royal Society, 1994.
- Garagash, D. I., Detournay, E., & Adachi, J. I. (2011). Multiscale tip asymptotics in hydraulic fracture with leak-off. Journal of Fluid Mechanics, 669, 260-297.

Task 1.3

Title

Hydrothermal heat exploitation and storage

Projects (presented on the following pages)

Deep Borehole Heat Exchanger for non-productive geothermal and hydrocarbon wells
L. Guglielmetti, A. Moscariello

Two pathways of SiO2 scaling inside a high-enthalpy geothermal power plant
D. B. van den Heuvel, E. Gunnlaugsson ,I. Gunnarsson, L. W. Diamond, L. G. Benning

SCCER SoE
SWISS COMPETENCE CENTER for ENERGY RESEARCH
SUPPLY of ELECTRICITY

SCCER-SoE Annual Conference 2017

In cooperation with the CTI
Energy
Swiss Competence Centers for Energy Research
Swiss Confederation
Commission for Technology and Innovation CTI

Deep Borehole Heat Exchanger for non-productive geothermal and hydrocarbon wells

Luca Guglielmetti and Andrea Moscariello
Earth Science Department, University of Geneva

ABSTRACT: Hydrocarbon and geothermal wells that ceased to produce or never produced might be retrofitted with heat extraction systems to either generate electricity or to produce heat for local mini-grid distribution.

The goal of this very preliminary study is to evaluate the approaches published in recent literature in order to figure out how a co-axial deep wellbore heat exchanger where an organic working fluids extract heat from the host rock, vaporizes while descending and then flow towards the surface. Three case studies are considered in this study:

- Larderello (Tuscany, Italy) where, despite the high temperatures, several wells are non productive due to the presence of non-condensable gases
- Po Plain & Emilian Apennines (Northern Italy) wells which reached temperature up to 180˚C
- St. Gallen geothermal well which reached temperatures above 140˚C at 4250m in depth and was abandoned due to the presence of hydrocarbons.

In the three cases, a comparison between different working fluids including water and organic fluids is presented to provide the optimal solution to increase the economic value of accessible end-of-lifewells producing heat or power using closed-loop and zero-emission small ORC power plants.

APPROACH: The general consensus is that coaxial heat exchanger (HE) may have some advantages over U-tube geometry in reducing resistance between the circulating fluid and the bore-hole wall. The main parameters that influence the performances of the heat exchanger are: **flow rate**, **geothermal gradient**, **bottom-hole temperature**, **inlet fluid temperature,** injection pressure, **fluid velocity**, and **insulation on the inner pipe**. Working fluids such as R125, R134a, R236a and **R245fa** are the most efficients for the geothermal power generation using abandoned wells. To produce electricity **Organic Rankine Cycle ORC** power plants have proven higher efficiency than Flash systems, for low temperature conditions. The techniques of heat extraction consists in a concentric double-pipe HE where a working organic fluid circulates in order to produce acceptable amount of thermal energy suitable for power production. The fluid circulates in the coaxial double-pipe HE, and heat transfer occurs without mass transfer. The fluid circulates in the well by means of a concentric double pipe. Cold fluid is injected into the well through the outer pipe, and the heat transfers from the hot rock to the fluid during injection. The hot fluid rises up through the inner pipe and is extracted at the wellhead. To avoid heat transfer between the inner and outer pipes, extruded thermal insulation surrounds the inner pipe. The computational models proposed in litterature take into account a transient model based on mass, energy, and momentum conservation equations for the well flow, and the simulation helps to determine the state of the fluid from injection to retrieval.

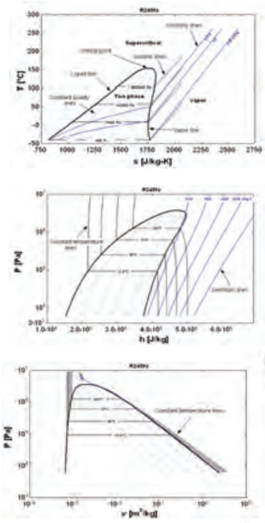

A: Ts Thermodynamic diagram for R245fa
B: Ph Thermodynamic diagram for R245fa
C: PV Thermodynamic diagram for R245f

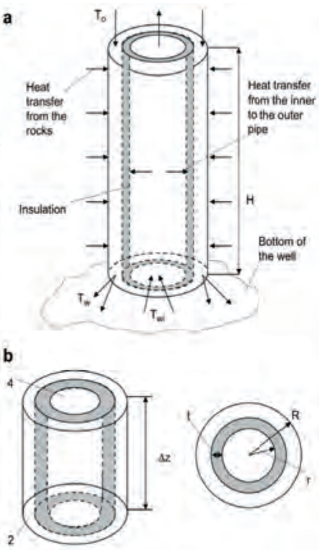

(a) Schematic representation of the heat transfer in the well. (b) The scheme for direction of the flow and the top view of the pipes in the well. (from Davis, Michaelides, 2009)

Power output and commercial analysis: The three case studies show potentially favourable conditions for the installation of a BHE and the equipment of a ORC power plant for power production. The most favourable conditions are in Larderello thanks to the high temperature at rather shallow depth. The installed power capacity can range between 100 to 500 kw_{el} (assuming an natural upflow of the working fluid). The investment costs can range between 2 and 3.5 M$ depending on the depth of the well and the size of the ORC. These conditions can lead to the economic feasibility of the installations.

	Reservoir temperature (°C)	Reservoir Depth (m)	Gross Power Output (kWel)	Net Power Output (kWel)	Investment ($)	Incentives ($/MWel)	Break-even point (years)
Larderello	180	500	2410	500	$ 3,500,000	$ 275	5
Po Plane	184	6642	890	120	$ 2,500,000	$ 275	12
St. Gallen	145	4250	735	100	$ 2,000,000	$ 300	7

CONCLUSIONS: In this screening study, a geothermal power generation model based on transient formation heat transfer is presented for different areas accounting for accessible and abandoned geothermal wells in high and low enthalpy systems, and for closed-in oil wells with different ranges of well depths and geothermal gradients. The electricity generation using various organic fluids as working fluids is simulated. The electricity produced is little compared to standard geothermal power production mostly because of low heat transfer rates through the rock and reduced velocity and flow rate. However, if clusters of disused wells in old hydrocarbon fields could be connected together the geothermal power output could be realised with attractive economic screening values. A more detailed study, including different types of fluid and 3D well modelling can provide stronger results to support the development of this kind of system and will help optimizing the design of effective ORC power plants for this kind of projects.

REFERENCES:

Bu, X., Ma, W., & Li, H. (2012). Geothermal energy production utilizing abandoned oil and gas wells. Renewable Energy, 41,80–85.

Cheng, W. L., Li, T. T., Nian, Y. L., & Wang, C. L. (2013). *Studies on geothermal power generation using abandoned oil wells*. Energy, 59, 248–254.

Cheng, W. L., Li, T. T., Nian, Y. L., & Xie, K., (2014). *Evaluation of working fluids for geothermal power generation from abandoned oil wells*. Applied Energy, 118, 238-245

Davis, A. P., & Michaelides, E. E. (2009). *Geothermal power production from abandoned oil wells*. Energy, 34, 866–872.

Templeton, J. D., Ghoreishi-Madiseh, S. A., Hassani, F., & Al-Khawaja, M. J. (2014). *Abandoned petroleum wells as sustainable sources of geothermal energy*. Energy, 70, 366–373.

Wei, D., Lu, X., Lu, Z., & Gu, J. (2007). *Performance analysis and optimization of organic Rankine cycle (ORC) for waste heat recovery*. Energy Conversion and Management, 48, 1113–1119.

SCCER SoE

SWISS COMPETENCE CENTER for ENERGY RESEARCH
SUPPLY of ELECTRICITY

SCCER-SoE Annual Conference 2017

In cooperation with the CTI
Energy
Swiss Competence Centers for Energy Research
Swiss Confederation
Commission for Technology and Innovation CTI

Two pathways of SiO_2 scaling inside a high-enthalpy geothermal power plant

DB van den Heuvel[1,2], E Gunnlaugsson[3], I Gunnarsson[3], LW Diamond[1], LG Benning[2,4]

[1]Institut für Geologie, Universität Bern, [2]School of Earth and Environment, University of Leeds, [3]Reykjavik Energy, [4]Interface Geochemistry, GFZ Potsdam

1. Background

Precipitation (or scaling) of amorphous silica (SiO_2) is one of the biggest issues in high-enthalpy geothermal power plants worldwide, strongly reducing the amount of energy produced. While the precipitation in laboratory experiments is relatively well understood[1,2], the findings cannot be transferred directly to processes occurring inside geothermal pipelines due to the more complex fluid compositions, higher flow rates and rapid changes in physico-chemical conditions (e.g. cooling in the heat exchanger). However, a better understanding of SiO_2 precipitation inside geothermal power plants is needed to develop more successful mitigation approaches in the future.

2. Approach - Hellisheiði power plant (SW-Iceland)[3]

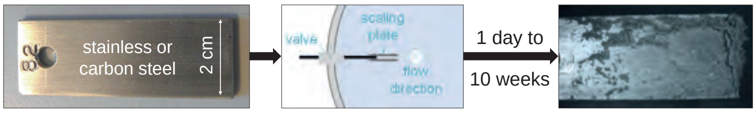

Fluid: Temperature & flow rate + Chemistry (ICP, IC)
Precipitates: Composition (XRD, EDS) + Scale microtexture (binocular, SEM, TEM)
Rates (Δthickness of precipitates and m(SiO_2) deposited)

3. Fluid chemistry

Temperature: 60 – 120 °C Flow rate: 220 – 430 L/s
Salinity: 0.9 – 2.6 %

Silica in the fluid
Dissolved SiO_2: 550 – 800 mg/L
(thereof monomeric silica: 75 – 85 %)
Particulate SiO_2: 0.2 to 0.3 mg/L (< 0.03 % of $SiO_{2(tot)}$)

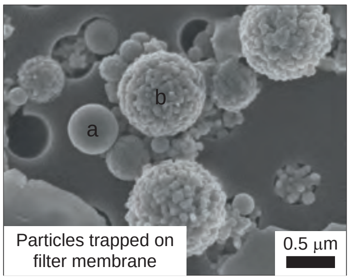

(a) Smooth SiO_2 microspheres

(b) Aggregates consisting of numerous smaller particles

4. Description of precipitates

Composition: amorphous SiO_2 containing Na, Cl, S, Al, Fe etc. (quantification currently underway)

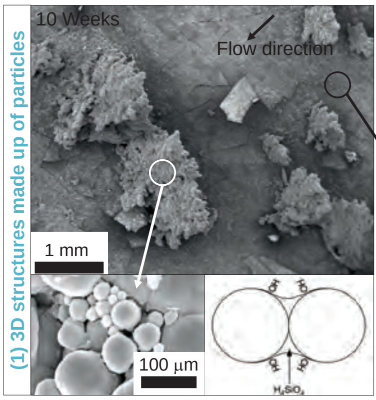

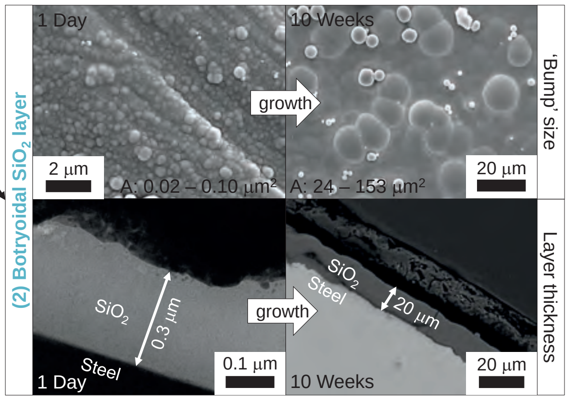

Particle growth
- High c($SiO_{2\,(aq)}$)
- Elevated temperature
- Alkaline pH

Particle deposition
- Large particle size
- Hydrodynamics[4]

Layer nucleation
- Surface roughness[5]

Layer growth
- High c($SiO_{2\,(aq)}$)
- Elevated temperature
- Alkaline pH

CONTROLLING FACTORS

6. Precipitation mechanism and rates

Two types of precipitates occurring within the Hellisheiði power plant:

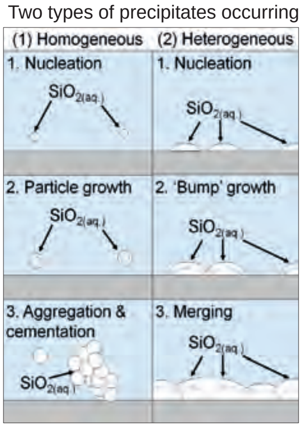

→ Two different mechanisms of precipitation (homogeneous vs. heterogeneous nucleation)

→ Different precipitation rates*

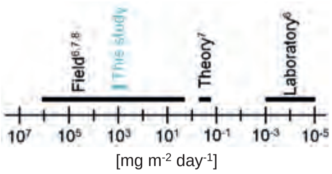

* Precipitation rates could only be quantified for the heterogeneous pathway in this study but observations show that the homogeneous pathway is faster

7. Implications for geothermal energy production

- To mitigate SiO_2 scaling completely, both pathways need to be inhibited/slowed down ⇨ development of novel additives
- Different textures affect hydrodynamics differently: 3D structures = turbulent flow
- Universal process? ⇨ more *in-situ* studies

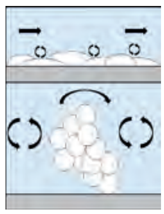

8. Effect of salinity?

High salinity enhances precipitation via homogeneous pathway (aides aggregation of particles)
- Faster scaling rates (up to 8.5·10⁵ mg m⁻² day⁻¹ at 5 % salinity)
- Turbulent flow ⇨ friction ⇨ reduced fow rate ⇨ less energy

⇒ High-enthalpy systems in sedimentary basins (e.g. the Molasse Basin) are at greater risk of extensive and detrimental SiO_2 scaling

Acknowledgement

The authors are grateful to the staff at Hellisheiði involved in the sampling and analyses conducted as part of this study and the following people for technical support: R. Walshaw (SEM) and L. Neave (XRD), both University of Leeds, R. Wirth (TEM) and A. Schreiber (FIB), both GFZ Potsdam and A. Berger (SEM), Universität Bern. This research was made possible by a Marie Curie grant from the European Commission (MINSC ITN 290040) and the 2014 IGA PhD Student Research Grant.

References:

[1] Icopini et al., *GCA*. **2005**, 69. [2] Tobler et al., *GCA.* **2009**, 73. [3] Meier (now van den Heuvel) et al., *Min. Mag.* **2014**, 78. [4] Hawkins et al., *Europhys. Let.* **2013**, 102. [5] van den Heuvel et al., in prep. for *Geothermica*. [6] Carroll et al., *GCA.* **1998**, 62. [7] Tobler et al., *Geobiol.* **2008**, 6. [8] Okazaki et al., *Sci. Rep.* **2017**, 7. [8] Rimstidt & Barnes, *GCA.* **1980**, 44.

The results presented here are in the final stages of preparation for submission to *Chemical Geology* as van den Heuvel et al., Geothermal pipelines as a well-constrained system for the study of amorphous silica precipitation mechanisms and rates.

Task 1.4

Title

Geo-data infrastructure and analysis

Project (presented on the following page)

GeoTherm: The Federal Data Infrastructure for Deep Geothermal Energy
M. Faubert, M. Manzini, L. Boulicault, L. Glaus, C. Minnig, S. Brodhag, R. Baumberger

SCCER SoE
SWISS COMPETENCE CENTER for ENERGY RESEARCH
SUPPLY of ELECTRICITY

SCCER-SoE Annual Conference 2017

In cooperation with the CTI
Energy
Swiss Competence Centers for Energy Research
Swiss Confederation
Commission for Technology and Innovation CTI

GeoTherm
The Federal Data Infrastructure for Deep Geothermal Energy

M.Faubert, M.Manzini*, L.Boulicault*, L.Glaus**, C.Minnig*, S.Brodhag*, R.Baumberger**

**Federal Office of Topography swisstopo, Swiss Geological Survey, Seftigenstrasse 264, CH-3084 Wabern*
***SCCER-SoE, ETH Zürich, Sonnegstrasse 5, CH-8092 Zürich*

GeoTherm is the public federal database for deep geothermal energy. It provides a data infrastructure for all existing and future data. It facilitates their access and usability.

Challenges for geothermal projects

- Having an updated national overview of relevant data
- Difficult access to data limits our understanding of swiss deep geology
- Limited understanding of subsurface increases risks for geothermal projects
- Data acquisition and inventorization is expensive and time consuming

Advantages of GeoTherm

✓ Harmonized data in Switzerland
✓ Perennial data storage
✓ Easy access to free data
✓ Overview of existing data

Context

Energy strategy 2050
Legal: GeoIA[1], OGN[2], OGéo[3] and EnA[4]
Motions: 11.3563 (Gutzwiler) [5]
11.4027 (Riklin) [5]

*Geo Information and Production System

Data Collection

We collect geological data of national interest[2] that are relevant for developing deep geothermal projects. The motivation is the decided phase out of nuclear power and the necessary promotion of renewable energy in Switzerland.

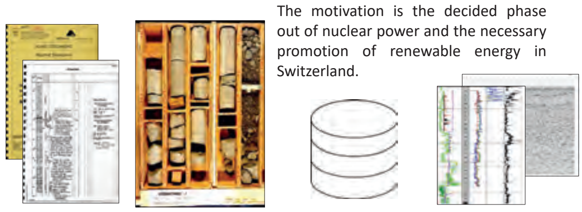

Literature data | Samples | External databases (CREGE, SAPHYR) | Raw/Interpreted data

Data model[6]

Data model → Implementation

- Definition and harmonization of standards (data format, metadata)
- Selection and organization of relevant data
- Quality checks

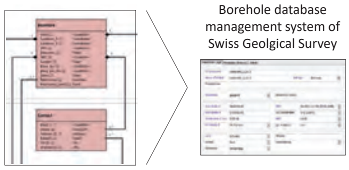

Borehole database management system of Swiss Geolgical Survey

Data web-publication

In order to make the existing data visible, we always publish the metadata of existing datasets.

Metadata[8]: Data describing data. Allows to find the data and to assess their relevance. E.g. Location coordinate, owner, content, etc.
Data[8]: Findings gained through obervations, measurements, statistical surveys. Data can be stored in analog, digital or physical form.

The use and publication of all collected data are agreed upon by a contract between the data owner and swisstopo.
Data from projects which were partially or fully financed by the state will be published according to the EnA[4] law and the legal framework of geological data[7] (geologyportal.ch).

Metadata	Non confidential
Data	Non confidential or confidential → According contract → OGéo[3]

Products: 3 layers

1. Deep geothermal projects (now available on map.geo.admin.ch)
2. Geothermal potential studies (in prep.)
3. Wells >500m MD (in prep.)

1.

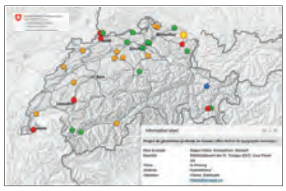

2.

3.

Perspective

- Integration of cantons data
- Layer of Reflexion Seismic
- Layer of Seismic Monitoring (in coll. With SED)
- Layer of temperature

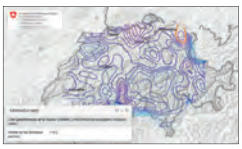

Update of the heat flow map
(in coll. with SGPK)

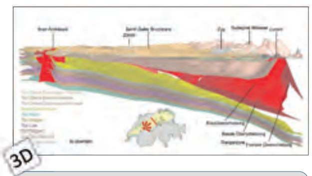

Parametrizing GeoMol 3D model[9] with temperature data

Take Home Message

GeoTherm will facilitate the development of new deep geothermal projects by **enhancing geological data exchanges**. This project highly contributes to the Federal Energy Strategy 2050.

Only an **active collaboration** and **transparent sharing** of data between all the involved stakeholders will help us to apply the new prescriptions for energy in Switzerland.

[1] Federal act on Geoinformation (GeoIA) 510.62, 2007.10.05
[2] Ordonnance sur la géologie nationale (OGN) 510.624, 2008.05.21
[3] Ordonnance sur la géoinformation (Ogéo) 510.620, 2008.05.21
[4] Energy Act (EnA) 30.09.2016
[5] Motions: Gutzwiller F., 11.3562 et 11.3563, 15.06.2011. Riklin K., 11.4027, 30.09.2011.
[6] Brodhag S. & Oesterling N. (2014): Datenmodell Bohrdaten. Beschreibung des Kernmodels mit Objektkatalog und UML-Model. Version 2.0, Bundesamt für Landestopographie swisstopo
[7] Kettiger, D. (2017): Rechtlicher Rahmen für das Erheben, Nachführen und Verwalten von geologischen Daten. Landesgeologie, No.9, Bundesamt für Landestopographie swisstopo
[8] Landesgeologie (in prep.): Datenaustausch und Datenfreigabe: Minimalanforderungen an Datenaustausch unter (Bundes-)Behörden, Ämtern und Privaten. Version 2.0, Bundesamt für Landestopographie swisstopo
[9] Landesgeologie (in prep.): GeoMol – Geologisches 3D-Modell des Schweizer Molassebeckens. – Ber. Landesgeol. *10*.

Acknowledgments

We would like to thank every person that supports us and without whom this project would not have taken place :
BFE collaborators, swisstopo collaborators, swisstopo KOGIS
Everyone that contributed to the project in Cantonal and Federal administrations
Universities and ETHZ (UniNe, UniGe, UniBe)
Regina Reber, Serge Zacharias, Emilie Sammali

Work Package 2: Hydropower

According to the Energy Strategy 2050, the mean annual hydropower production has to be increased under present framework conditions by 1.53 TWh/a and by 3.16 TWh/a under optimized conditions (see roadmap on next page). In view of environmental and socio-economical constraints, this foreseen increase is extremely challenging and can be reached only by innovative and sustainable solutions for new hydropower plants and by the extension and optimization of existing schemes. The expected increase in power production from small hydropower plants (SHPP) requires the development of criteria for a careful site selection as well as strategies to optimize power production within a river network while at the same time minimizing the negative impacts on stream ecology. The effect of climate change will not only impact the availability of water resources in time but also the behavior of the catchment areas by an increased sediment yield and more frequent natural hazards, and thus considerably endanger waterpower production in the near future. The critical period of energy supply in Switzerland is still the winter half year, where 4 TWh had to be imported in average over the past 10 years. Therefore, Switzerland has to increase its storage capacity by new reservoirs where possible and to increase the volumes of existing ones.

After discussions with industry the road map developed in Phase I addressed the following challenges for reaching the technical and political goals of Energy Strategy 2050:

- The change of production potential due to effects of future climate forcing, which are expected to impact water availability (glacier retreat, snow accumulation and melt, streamflow regimes, and sediment production and transport) as well as the operation safety of structures in view of new natural hazards (floods, slope instabilities, etc.);
- The efficiency improvement of existing HPPs, which can be achieved by their expansion to allow a more flexible operation to accommodate new and highly fluctuating demands;
- The contribution of new technological solutions to adapt existing infrastructures to increase efficiency of production and operation flexibility during seasonal and daily peak demands, while maintaining the same level of (infra)structural safety and supply security;
- The assessment of the effects of HPPs new and harsher operation regimes and increased numbers of SHPs on aquatic ecosystems and the development of strategies to reduce these impacts (e.g. by developing innovative strategies of environmental flow releases);
- The definition of future boundary conditions for the operation of HPPs based on the development of electricity demand and market dynamics under uncertain social, economic and political forcings;
- The assessment of multi-objective operation strategies of HP systems, which maximize power production, reliability and flexibility of supply, profitability of operation and ecosystem conservation, under the constraints of a more fluctuating demand – due to higher fraction of renewable production – and an uncertain market.

In Phase II, based on the feedback from the hydropower industry as well as recent energy-political developments in Switzerland and Europe, WP2 focuses on five key research directions including three demonstrators for large hydropower (FLEXSTOR), small hydropower, and the problemc of reservoir sedimentation (SEDMIX):

KD I: Increase of flexibility in hydropower operation – structural and operation requirements
KD II: Update of climate change impacts on HP production and required adaptation strategies
KD III: Extreme natural events, hazards and risk of HP operation
KD IV: Design of new projects under uncertainties
KD V: Reservoir sedimentation and sustainable use of storage HP

Highlights 2017

New stochastic space-time explicit weather generator

In order to explore the impacts of climate change a weather generator was developed. The model is able to reproduce present key climate variables as demonstrated for three catchments in Switzerland. The reparameterisation scheme to enable the generation of high resolution climate variables for the future will be completed by the end of 2017. The value of such model spans beyond the SoE: the Joint Activity Scenarios & Modelling will use results for the assessment of (i) the climatic hydro power potential in the coming decades, and (ii) the main climatic drivers for energy consumption and generation (mean temperatures, solar irradiation, wind speed).

Improved understanding of reservoir sedimentation and its impact on turbine runners

The BASEMENT software is currently developed further to model long-term reservoir sedimentation processes. First calculations show promising results regarding the evolution of Gilbert-type deltas, i.e. steep coarse-grained deltas, and the deposition for non-stratified suspended sediment transport. The models will be run based on climate change scenarios for a time frame up to 2100. In an extensive field study at HPP Fieschertal the link between sediment parameters and turbine abrasion was investigated. An analytical model for turbine erosion was adapted for coated runners of Pelton turbines. It allows to estimate the erosion depth over time for a given suspended sediment concentration, particle properties, and turbine configuration. In addition, the abrasion resistance of different tunnel invert materials was experimentally investigated in three Swiss sediment bypass tunnels. New criteria have been developed for the use of bottom outlet for turbidity current venting at dams, in view of extending the lifetime of live storage. The dynamics of fine sediment deposition in reservoirs is currently being investigated and will provide further insights on key physical processes for later integration in computational modelling tools.

Environmental impacts: experiments & modelling

A controlled experimental flood was released on the Sarine River (KD I). The aim was to restore dynamic ecological conditions that are as natural as possible, whilst maintaining storage hydropower generation. In addition, an extensive field campaign was launched in summer 2017 to investigate the effects of small-scale run-of-river hydropower plants on habitat conditions and ecosystem functioning in mountain streams. A tool for a system scale approach to small-scale hydropower planning was extended to allow for a qualitative assessment of biodiversity loss in larger river systems. The Engadin region was identified as a suitable case study.

Integrated modelling framework for hydrological processes and hydropower systems

The framework allows to simulate the feedbacks between the operation of hydropower systems and the natural hydrological processes leading to streamflow generation and inflow to reservoirs. It can be used to assess how hydropower infrastructure operation responds to different drivers, such as changes of climate, electricity price and demand. The model is currently applied to two hydro-power system configurations representing different typical Alpine hydroclimatic regimes (ice/snow & rain/snow dominated) and hydropower schemes (storage and pump-storage plants).

Hydropower design under uncertainties

The construction of hydropower plants, especially in the case of large schemes, requires high investments with long payback periods. Thus, future uncertainties have to be considered in early design stages in order to obtain robust and flexible projects with high resilience. In the framework of a PhD research project a novel contribution for the engineering practice was presented with a new framework which allows a straightforward selection of the design objective and the required design method in order to consider uncertainties in early design stages of hydropower projects. I could be shown how the methods of Robust Decision Making, Info-Gap Decision Theory and Flexible Design have to be formulated and applied to a real hydropower project.

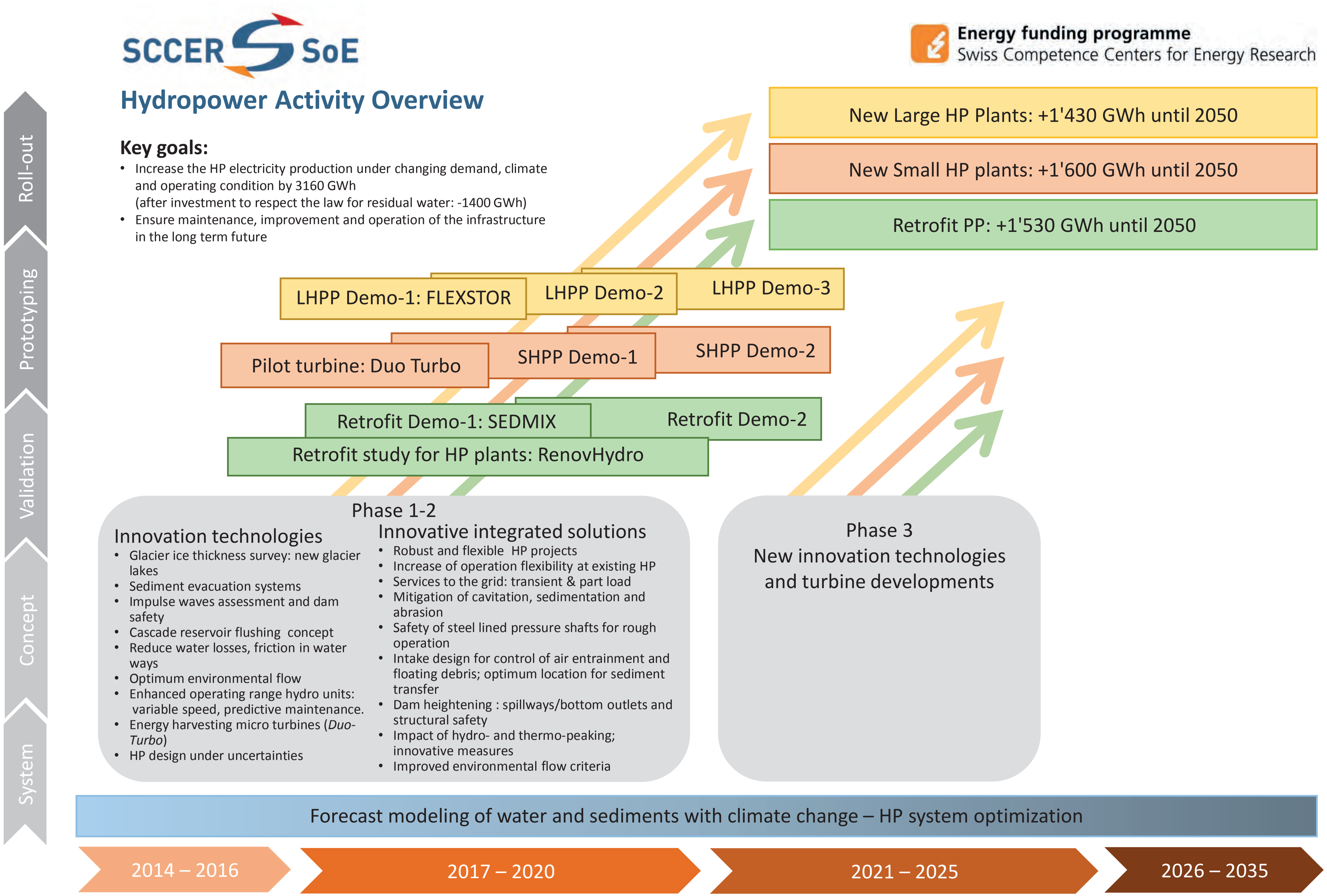
SCCER SoE
Energy funding programme
Swiss Competence Centers for Energy Research
Hydropower Activity Overview
Key goals:
• Increase the HP electricity production under changing demand, climate and operating condition by 3160 GWh (after investment to respect the law for residual water: -1400 GWh)
• Ensure maintenance, improvement and operation of the infrastructure in the long term future
New Large HP Plants: +1'430 GWh until 2050
New Small HP plants: +1'600 GWh until 2050
Retrofit PP: +1'530 GWh until 2050
LHPP Demo-1: FLEXSTOR
LHPP Demo-2
LHPP Demo-3
Pilot turbine: Duo Turbo
SHPP Demo-1
SHPP Demo-2
Retrofit Demo-1: SEDMIX
Retrofit Demo-2
Retrofit study for HP plants: RenovHydro
Phase 1-2
Innovation technologies
• Glacier ice thickness survey: new glacier lakes
• Sediment evacuation systems
• Impulse waves assessment and dam safety
• Cascade reservoir flushing concept
• Reduce water losses, friction in water ways
• Optimum environmental flow
• Enhanced operating range hydro units: variable speed, predictive maintenance.
• Energy harvesting micro turbines (Duo-Turbo)
• HP design under uncertainties
Innovative integrated solutions
• Robust and flexible HP projects
• Increase of operation flexibility at existing HP
• Services to the grid: transient & part load
• Mitigation of cavitation, sedimentation and abrasion
• Safety of steel lined pressure shafts for rough operation
• Intake design for control of air entrainment and floating debris; optimum location for sediment transfer
• Dam heightening : spillways/bottom outlets and structural safety
• Impact of hydro- and thermo-peaking; innovative measures
• Improved environmental flow criteria
Phase 3
New innovation technologies and turbine developments
Forecast modeling of water and sediments with climate change – HP system optimization
Roll-out
Prototyping
Validation
Concept
System
2014 – 2016
2017 – 2020
2021 – 2025
2026 – 2035

Task 2.1

Title

Morpho-climatic controls

Projects (presented on the following pages)

Machine learning methods for predicting hourly to monthly energy demand based on hydro-meteorological measurements and forecasts
K. Bogner, M. Zappa

Spatial precipitation interpolation over an alpine catchment
A. Foehn, J. Garcia Hernandez, G. De Cesare, B. Schaefli A. J. Schleiss

Skill transfer from weather to runoff forecasts in high mountain catchments
S. Gindraux, D. Farinotti

Helicopter-borne ice penetrating radar surveys on the glaciers in the Swiss Alps
M. Grab, A. Bauder, L. Schmid, F. Ammann, L. Langhammer, P. Lathion, H. Maurer

Pre- and Post-processing of an Extended-range Hydrometeorological Ensemble Prediction System
S. Monhart, C. Spirig, J. Bhend, K. Bogner, M. A. Liniger, C. Schär, M. Zappa

Generation of high resolution climate variables for hydropower studies: preliminary model simulations
N. Peleg, S. Fatichi, P. Burlando

High spatio-temporal resolution climate scenarios for snowmelt modelling in small alpine catchments
M. Schirmer, N. Peleg, P. Burlando, T. Jonas

Climate change impacts on HP production and required adaptation strategies - a synthesis
M. Stähli + all partners related to task 2.1

SCCER SoE
SWISS COMPETENCE CENTER for ENERGY RESEARCH
SUPPLY of ELECTRICITY

SCCER-SoE Annual Conference 2017

In cooperation with the CTI
Energy
Swiss Competence Centers for Energy Research
Swiss Confederation
Commission for Technology and Innovation CTI

Machine learning methods for predicting hourly to monthly energy demand based on hydro-meteorological measurements and forecasts

K. Bogner and M. Zappa

Motivation

Prediction of the energy demand could be of interest for the hydro-power production. Especially in periods of water deficits or surplus this information could be beneficial for the planning of optimal strategies for the upcoming weeks and months. Thus different machine learning methodologies have been tested for predicting possible future demands. First tests have been applied based on the information of hydro-meteorological data and the energy consumption of the Canton Tessin given by SWISSGRID (https://www.swissgrid.ch/swissgrid/de/home/reliability/griddata/data_downloads.html)

Methods

Three different machine learning techniques have been applied:

- **Multivariate Adaptive Regression Splines (MARS)**
  MARS build linear relationships between predictors and a target by segmenting predictor variables. Possible non-linear relationships can be identified by integrating all segments.
- **Support Vector Machines (SVM)**
  Kernel-based learning method uses an implicit mapping of the input data into a high dimensional feature space defined by a kernel function
- **Random Forest**:
  Random forest is a tree-based algorithm which involves building several trees (decision trees), then combining their output to improve generalization ability of the model. The method of combining trees is known as an ensemble method.

Since the demand shows strong periodicity components, intra-day and weekly fluctuation, additionally a **VectorAutoregressiveRegression** model with eXogeneous Input (**VARX**) in the wavelet domain has been applied

Data

Simplified assumptions: Region of Lugano used as a proxy for the consumption/demand; thus the meteorological data of Lugano are used as main **Predictors**

- hourly measurements of Temperature, Precipitation, Global Radiation, Windspeed, Winddirection, Pressure
- Additionally it is assumed that the hydropower plant from Verzasca is the most important producer of energy for the Tessin, thus the inflow to the plant is taken as predictor also
- Further periodicity aspects (intra-daily as Sin and Cos), information of weekday and holidays are included

Target:
The total consumption/demand of the Canton Tessin

Results

Coefficients of determination (R^2, which corresponds to the Nash-Sutcliffe coefficient) of the different models for the training (calibration) period (2015-2016) and the testing (validation) period 2017

Model	Training	Testing
MARS	0.70	0.64
SVM	0.80	0.61
Regression Forest	0.90	0.60
Combination	0.84	0.66

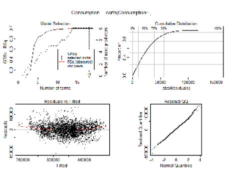

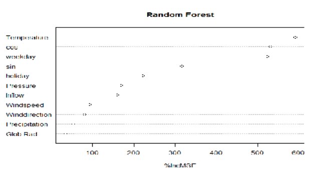

Results of the MARS model for the training period:

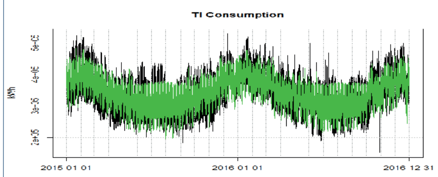

and for the testing period:

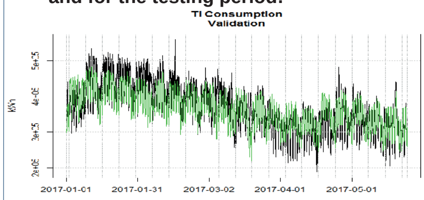

coefficients

(Intercept)	420357.98
holiday	-39027.83
h(0.5-sin)	7342.88
h(sin-0.5)	-80454.02
h(-0.258819-cos)	9140.52
h(cos- -0.258819)	-69146.05
h(weekday-2)	-35906.66
h(weekday-3)	52533.69
h(weekday-5)	-12798.74
h(6.894-Inflow)	1880.64
h(Inflow-6.894)	246.90
h(6.5-Temperature)	4792.46
h(Temperature-6.5)	-7478.59
h(Temperature-17.3)	7433.11
h(138-Glob.Rad.)	-30.59
h(Glob.Rad.-138)	17.28
h(194-Winddirection)	55.37
h(Winddirection-194)	30.00

Selected 18 of 19 terms, and 8 of 11 predictors
Termination condition: Reached nk 23
Importance: cos, Temperature, sin, weekday, holiday, Inflow, Glob.Rad., Winddirection,
GCV 1142795537 RSS 1.9959e+13
GRSq 0.699253 RSq 0.7004182

Prediction of the May of the consumption/demand plus uncertainty bands (50% and 90%)

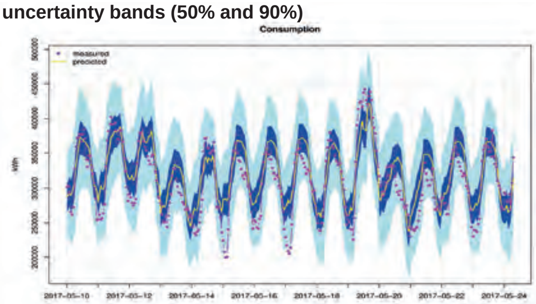

Results of the VARX model

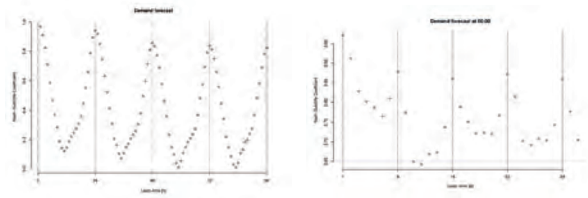

The Autoregressive model clearly identifies the intra-daily (left) and the weekly fluctuations (right). Around midnight the VARX model gives better results as the MARS (R^2 indicated as horizontal line). The Figure on the right side shows the forecasts at midnight only for one month highlighting the weekly periodicity and the good performance of the VARX at the weekend.

Outlook

Coupling of monthly weather forecasts and the MARS, VARX models and estimation of the predictive uncertainty

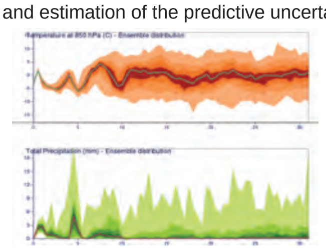

Example of a monthly Ensemble forecast, which could be used for demand forecasting

Open Question:

How useful is this for the hydropower industry as additional information for optimizing the production? Any comments are very much appreciated: konrad.bogner@wsl.ch

SCCER SoE
SWISS COMPETENCE CENTER for ENERGY RESEARCH
SUPPLY of ELECTRICITY

SCCER-SoE Annual Conference 2017

In cooperation with the CTI
Energy
Swiss Competence Centers for Energy Research
Schweizerische Eidgenossenschaft
Confédération suisse
Confederazione Svizzera
Confederaziun svizra
Swiss Confederation
Commission for Technology and Innovation CTI

Spatial precipitation interpolation over an alpine catchment

Alain FOEHN[1], Javier GARCÍA HERNÁNDEZ[2] , Giovanni DE CESARE[1], Bettina SCHAEFLI[3], Anton J. SCHLEISS[1]
Contact : alain.foehn@epfl.ch
[1]Laboratoire de Constructions Hydrauliques (LCH-EPFL), [2]Centre de Recherche sur l'Environnement Alpin (CREALP), [3]Institut des Dynamiques de la Surface Terrestre (IDYST-UNIL)

Motivation

Estimating with good accuracy the precipitation causing floods is crucial for the security of the population and infrastructures. Optimal exploitation of the available data is therefore desired. Combination of available **rain-gauge networks** and **weather radar** data (Sideris 2014) over the Upper Rhone River basin upstream of Lake Geneva in Switzerland is therefore explored in this study (Fig. 1).
The project aims at evaluating and compare the respective performances of the interpolation methods based on the combination of the available data.

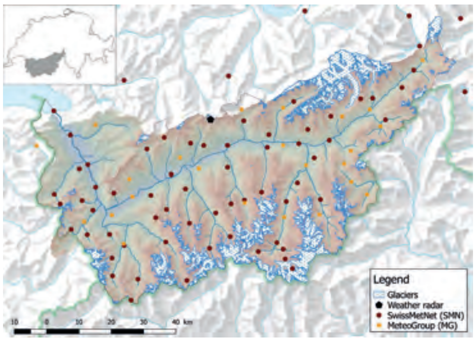

Fig. 1 : Upper Rhone River basin (case study) with location of the meteorological stations and the weather radar of Pointe de la Plaine Morte.

Case study and methodology

Two independent networks of rain-gauges are used for the study, the SwissMetNet (SMN) network of the Swiss Federal Office of Meteorology and Climatology (MeteoSwiss) and the data of the private company MeteoGroup Schweiz AG (MG).

Three different methods are applied and investigated :

- **Raw radar data**: the hourly raw radar composite precipitation estimate is used as precipitation estimate over the basin.
- **Inverse distance weighting (IDW)**: inverse distance weighting is applied to the SMN stations, with a power coefficient of 2.
- **Regression co-kriging (RCK)**: a linear regression is first applied to the radar precipitation estimates to define a multiplying coefficient for both the primary (SMN) and secondary (MG) variables. Application of these coefficients to the radar raster provides the trend. Residuals are then computed at all stations, given by the difference between the rain-gauge values and the values of the corresponding trend pixels. To obtain interpolated residuals, co-kriging (Myers, 1982) is applied to the residuals. This raster of interpolated residuals is then added as a local correction to the trend to obtain the final estimation.

The performance of the methods is evaluated based on the leave-one-out cross-validation approach using five performance indicators:

$$\mathbf{Bias} = 10\log_{10}\frac{\sum_{i=1}^{N}\hat{g}_i}{\sum_{i=1}^{N}g_i} \qquad \mathbf{MAD} = \mathrm{median}(|\hat{g}_i - g_i|) \qquad \mathbf{RMSE} = \sqrt{\frac{\sum_{i=1}^{N}(\hat{g}_i - g_i)^2}{N}}$$

$$\mathbf{MRTE} = \frac{1}{N}\sum_{i=1}^{N}(\sqrt{\hat{g}_i} - \sqrt{g_i})^2 \qquad \mathbf{Scatter} = \frac{1}{2}(\mathrm{CEDF}_{84} - \mathrm{CEDF}_{16})$$

where g_i is the observed value at a station, $\hat{g}_i$ the cross-validation estimation, N the number of rain-gauges and CEDF the cumulative error distribution function of the ratios between estimated and observed values, expressed in decibel. The four analysed events are described in Table 1.

Table. 1 : Events considered for the analysis.

Event	1	2	3	4
Occurrence	Nov. 14	May 15	Jan. 16	Mar. 17
Duration [h]	44	84	69	46
Median cumulative rain at gauges [mm]	37.5	96.2	41.2	34.2
Maximum cumulative rain at gauges [mm]	179.5	375.7	158	68.3

Results

The obtained performance indicators, aggregated per event, and the total precipitated volume over the basin, are presented in Fig 2. Detailed results on an hourly basis are provided for the second event in Fig. 3.

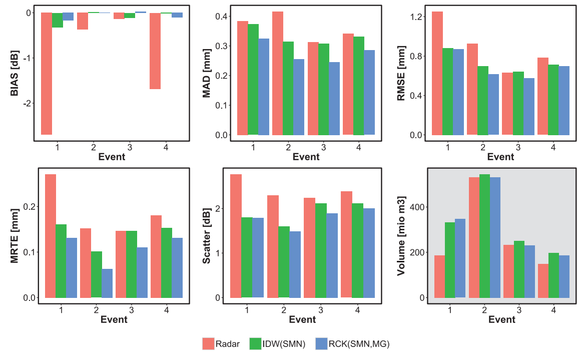

Fig. 2 : Event-average performance indicators and total precipitated volume (gray background) for the four events.

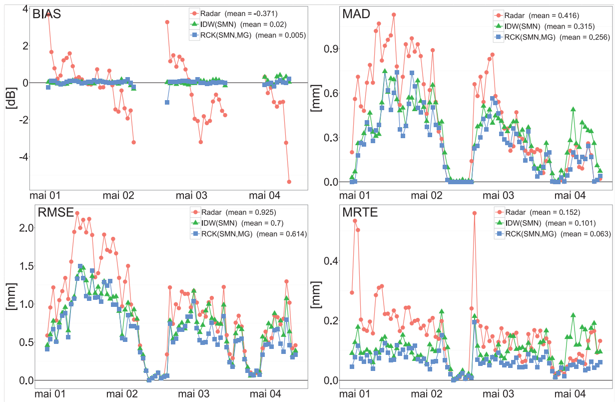

Fig. 3 : Hourly performance indicator values for the event 2 (May 2015). The scatter indicator is not shown as it is computed only over the event.

Discussion and conclusion

The **RCK method using both SMN and MG provides the best results** (Fig. 2), whereas using raw radar data leads to the lowest performance, in particular in terms of bias. **The difference between IDW and RCK is higher when the precipitation fields are characterized by strong spatial gradients**. This is well visible in Fig. 3 over the last ten hours of event 2 (MAD and MRTE), during which a clear south-west to north-east precipitation limit was visible over the studied basin.

Future improvements of the methodology could include pre-treatment of the radar data, to account for shielding of the radar beam by mountains, and integration of additional covariates in the RCK regression step.

References

Foehn, A., García Hernández, J., Schaefli, B., De Cesare, G. and Schleiss, A. J. (2016). *Spatialization of precipitation data for flood forecasting applied to the Upper Rhone River basin*, International Conference Hydro 2016, Montreux.

Myers, D. E. (1982). *Matrix formulation of co-kriging*. Journal of the International Association for Mathematical Geology, 14(3). 249–257. ISSN 0020-5958, 1573-8868. doi: 10.1007/BF01032887.

Sideris, I. V., Gabella, M., Erdin, R. and Germann, U. (2014). *Real-time radar-rain-gauge merging using spatio-temporal co-kriging with external drift in the alpine terrain of Switzerland: Real-time radar-rain-gauge merging*. Quarterly Journal of the Royal Meteorological Society, 140(680). 1097–1111. ISSN 00359009. doi: 10.1002/qj.2188.

SCCER SoE
SWISS COMPETENCE CENTER for ENERGY RESEARCH
SUPPLY of ELECTRICITY

SCCER-SoE Annual Conference 2017

WSL Eidg. Forschungsanstalt für Wald, Schnee und Landschaft WSL
ETH Eidgenössische Technische Hochschule Zürich Swiss Federal Institute of Technology Zurich
VAW Versuchsanstalt für Wasserbau, Hydrologie und Glaziologie

In cooperation with the CTI
Energy Swiss Competence Centers for Energy Research

Skill transfer from weather to runoff forecasts in high mountain catchments

Gindraux Saskia, Farinotti Daniel

Contact: saskia.gindraux@wsl.ch

Context and objectives

Aim of the study:
1. Investigate the propagation of forecast skills from weather to runoff predictions in high mountain catchments.
2. Examine if the skill transfer is affected by the morphological characteristics of a given catchment or/and by the hydrological model used.

⇨ The overall objective is to improve runoff forecasts which in turn will help increasing the electricity production in the hydropower sector.

Research question: How does a given skill in meteorological input variables translates into the skill of the corresponding hydrological forecasts?

Main steps followed:
1. Weather prediction were produced in a modeling framework and their forecast skill was quantified.
2. The weather forecasts were used to a force hydro-glaciological model in order to generate runoff predictions.
3. The transfer of the skill is evaluated (ongoing study).

Methods

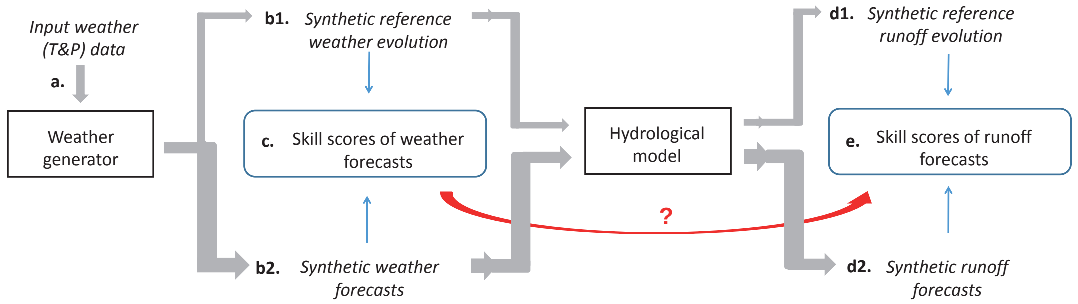

Figure 1: Methodological workflow of the study

a: An observed temperature and precipitation time was used as input in an in-house weather generator (Farinotti 2013).
b1: A time series that is statistically equivalent to the input data was generated and used as synthetic reference weather evolution.
b2: The synthetic weather forecasts were generated by modifying the reference weather evolution (i.e. addition of a trend, a bias, noise, etc.).
c: Skill scores of the weather forecasts were calculated based on the reference forecast.
d1: The reference weather evolution was fed into a hydrological model to generate the reference runoff evolution.
d2: Each weather forecast were fed into the same hydrological model to produce its corresponding runoff forecast.
e: The skill scores for the runoff forecasts were calculated.

Preliminary results

Example of synthetic weather forecasts (from step b1+b2)

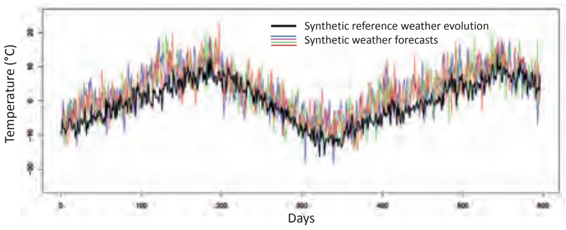

Daily forecasts generated with a trend of 4°C, a bias of 2°C, a long-term oscillation, changes in daily, monthly and yearly variability as well as random noise.

Example of runoff forecasts (from step d1+d2)

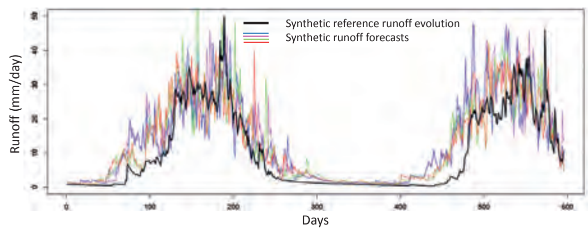

Daily synthetic runoff forecasts generated with the Glacier Evolution Runoff Model. The synthetic weather forecasts were used as input data.

Skill scores of the synthetic weather forecast (from step c)

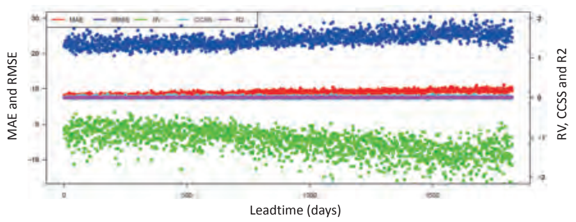

Skill scores of the runoff forecast (from step e)

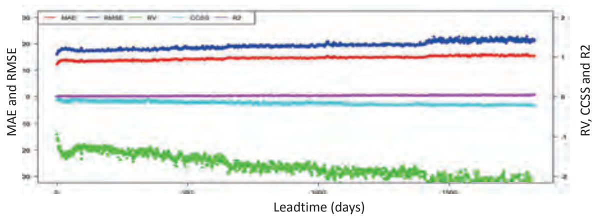

Mean Absolute Error (MAE) / Root Mean Square Error (RMSE) / Reduction of Variance (RV) / Correlation Coefficient Skill Score (CCSS) / Correlation coefficient (R2)

Next steps

The next step is to analyze the transfer of forecast skills. For this, the skill scores calculated from the weather forecasts (temperature and precipitation) will be evaluated against the corresponding scores calculated from the runoff forecasts, over different leadtimes. A similar analysis will be conducted on a glacier-free catchment to observe if the forecast skill transfers differently.

Reference: Farinotti, D. (2013). On the effect of short-term climate variability on mountain glaciers: insights from a case study. *Journal of Glaciology*, *59*(217), 992-1006

SCCER-SoE Annual Conference 2017

Helicopter-borne ice penetrating radar surveys on the glaciers in the Swiss Alps

Melchior Grab, Andreas Bauder, Lino Schmid, Fabian Ammann, Lisbeth Langhammer, Patrick Lathion, Hansruedi Maurer

1. Introduction

Electricity production from hydropower plants in Switzerland is dependent on the water resources existing in the alpine area and on the annual river run-off from these regions. With the ongoing retreat of the glaciers in the Swiss Alps, these factors will change strongly in the near future. Thus, to adapt the strategies for the hydropower production under consideration of these changing environmental conditions, better knowledge is required about the present volume and geometry of alpine glaciers and of the topography of the glacier beds.

2. Project – Overview and Current State

The goal of this project is to estimate the total ice volume in the Swiss Alps and to deliver information about the glacier bed topography. During the first phase of SCCER-SoE, the three "pillars", needed to reach this project goal, were obtained. This includes (see Fig. 1) the helicopter-borne ground penetrating radar (GPR) instrument (surveying capabilities), the MATLAB®-based software libraries to derive the glacier bed from the radar data (processing capabilities), and a GIS database through which the 2D Images through the glaciers showing the ice-thickness can be organized (Database capabilities).

Based on these pillars, the focus was set during the past year on the radar data acquisition and the data processing in order to obtain the ice thickness maps ("roof" of the project, Fig. 1)

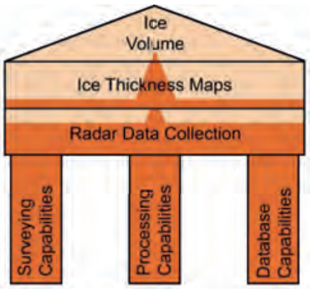

***Figure 1:** Project sketch. Three "pillars" of capabilities were needed before the "roof", i.e. the ice thickness data, can be gathered. Dark shaded colors are the completed sections and light shaded colors are the planned sections.*

3. GPR Instrument and Data Acquisition

The data is acquired with two pairs (Tx & Rx) of 25 MHz GPR antennas, mounted orthogonal to each other on a wooden frame, which is carried by a helicopter (Fig. 2). After the GPR-system was lost during a campaign in October 2016, a new system has been built with the newest available hardware and with an optimized assemblage and cabling. The new system was successfully tested in February 2017 and then used for acquiring data until early Summer 2017. A data example is shown in Fig. 3.

4. GPR Data-Processing

The GPR data is processed using the processing capabilities, built during the first phase of the SCCER-SoE project. Parts of it were recently optimized in the frame work of a Master thesis. This includes an optimized removal of signal ringing due to the interference with reflections from the helicopter (see Fig. 3, top), and a more powerful migration algorithm, which enables to image reflections effectively at their presumably true position also in presence of steep reflectors and strong lateral inhomogeneities, e.g. due to a rough glacier surface. The updated processing flow looks as follows:

- `Set time zero`
- `Time window cut`
- `Optimized SVD-filter for ringing removal`
- `Bandpass filtering`
- `Determination of surface reflections`
- `Deconvolution`
- `Reverse time migration (RTM)`
- `Glacier bed picking`

A data example, processed using the newest processing features, is shown in Fig. 3. Bed rock reflections are easily identifiable and are also visible in shallow parts which are more affected by signal ringing.

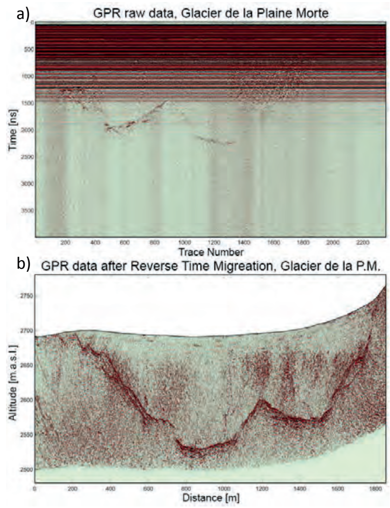

***Figure 3:** a): Raw data. Ringing (interference with helicopter) superimposes bed rock reflections. b): Final reflection profile, processed using the updated processing flow.*

5. Glacier Beds and Ice Thickness Maps

From the processed GPR-reflection profiles, the glacier bed is identified, whereas reflections from other rock faces and off-plane objects are excluded from the interpretation (example shown in Fig. 4 b). Continuous ice thickness maps are then obtained from glaciological ice thickness estimation modelling, which uses the discrete GPR profiles as input parameters. Exemplarily, such an Ice thickness map, obtained for the Glacier de Zinal, is shown in Fig. 4 c.

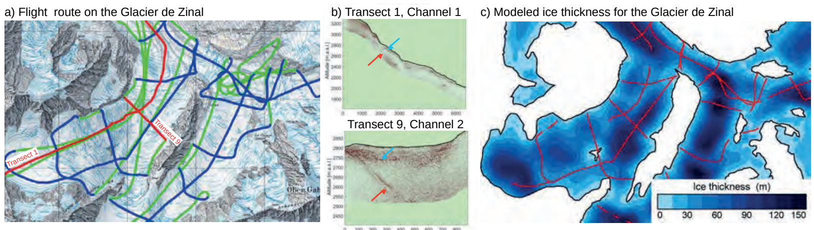

***Figure 4:** a) GPR survey flown on the Glacier de Zinal, transects are marked blue, number 1 and 9 are highlighted red. b) GPR profiles of transect 1 and 9, with glacier bed indicated with the blue arrow. Red arrows show reflections from a rock face. c) Ice thickness based on GPR data, red lines show the transects where the glacier bed was identified in the GPR data*

6. Outlook

Currently, our focus is on the processing of the data, recorded during the winter season 2016/2017 in Graubünden and in the Bernese and Valais alps (blue areas in Fig. 5). For the upcoming winter season, data acquisition in central Switzerland and in the Lauterbrunnen/ Grindelwald region is planned (encircled areas in Fig. 5).

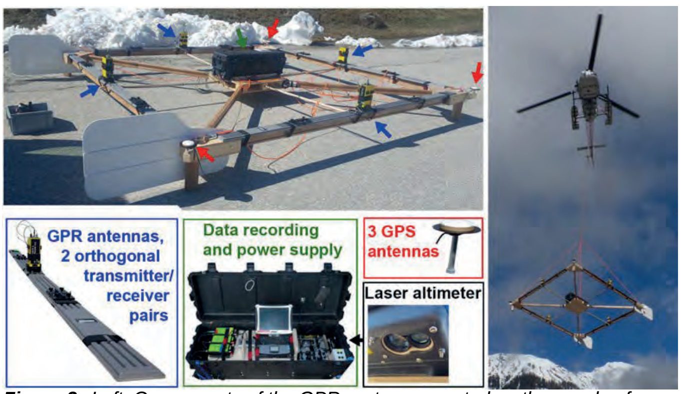

***Figure 2:** Left: Components of the GPR system, mounted on the wooden frame. Right: GPR system attached to a helicopter.*

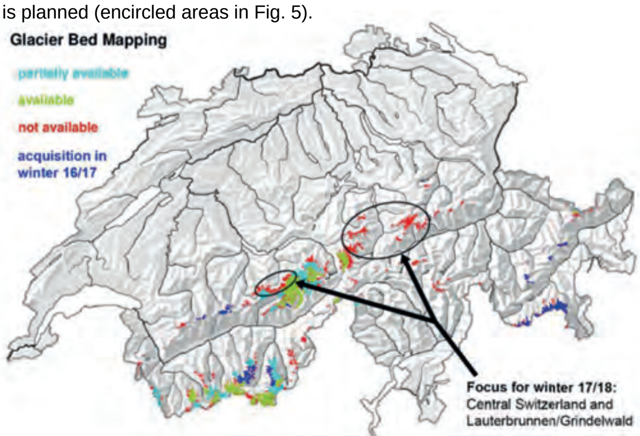

***Figure 5:** Current (September 2017) status of the glacier bed mapping*

SCCER SoE

SWISS COMPETENCE CENTER for ENERGY RESEARCH
SUPPLY of ELECTRICITY

SCCER-SoE Annual Conference 2017

In cooperation with the CTI

Energy
Swiss Competence Centers for Energy Research

Commission for Technology and Innovation CTI

70 NRP Energy Turnaround
National Research Programme

Pre- and Post-processing of an Extended-range Hydrometeorological Ensemble Prediction System

Samuel Monhart[1,2,3], Christoph Spirig[2], Jonas Bhend[2], Mark A. Liniger[2], Konrad Bogner[1], Christoph Schär[3] and Massimiliano Zappa[1]

[1] Swiss Federal Research Institute, WSL
[2] Federal Office of Meteorology and Climatology, MeteoSwiss
[3] ETH Zurich, Institute for Atmospheric and Climate Science

Motivation

We aim at highlighting potential benefits from probabilistic hydro-meteorological forecasts based on Ensemble Prediction Systems in order to provide planning basis for Alpine catchments with installed hydropower capabilities.
Test case: In quasi-operational model the hydrological model PREVAH is driven by extended-range weather forecasts provided by ECMWF (from April 2014 to April 2015). These forecasts consist of 51 members and cover lead times up to 32 days. First results and the verifications of the statistical correction of meteorological input data (pre-processing) and hydrological outputs (post-processing) will be presented here.

Pre-processing

Problem: Gap between meteorological (50 km) and hydrological (500 m) model resolutions and inherent biases of the meteorological forecasts
Method: A mean debiasing and a Quantile Mapping (QM) technique have been applied to correct the forecasts. We use temperature and precipitation for 1637 stations across Europe to evaluate the meteorological forecasts used as input to the hydrological model.
Verification: Continuous Ranked Probability Skill Score (CRPSS), a measure considering both the sharpness and the reliability of the forecast. Reference: Climatology.

Pre-processing: Results

The skill of the forecasts depends on the lead time, the season and the location. In terms of reliability and resolution (CRPSS) the forecast show skill for about two weeks. The QM approach outperforms the simple mean debiasing. Forecasts for stations in complex terrain show less skill but the relative effect of the bias correction is larger.

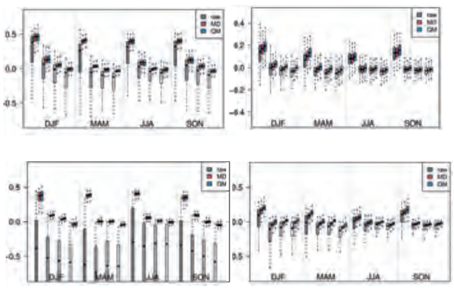

Results: Quality of the hydrological Forecasts

For the hydrological processing, the meteorological forecasts are corrected following the procedure described above but using a 2km grid for a small catchment in the southern part of the Alps (Verzasca). Results indicate that pre-processing enhances the CRPSS for all lead times. In spring and autumn, the benefit is largest, whereas during summer and winter there is no clear benefit.

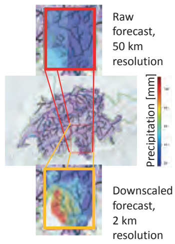

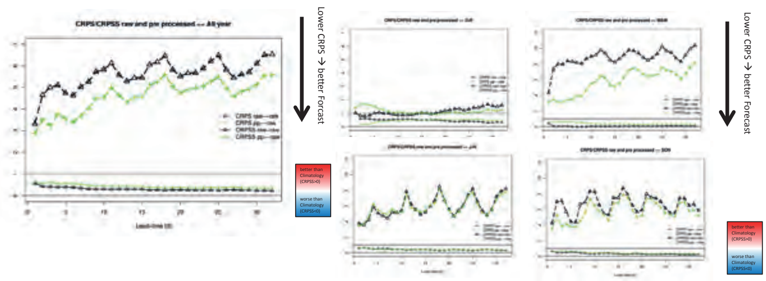

Post-processing

Problem: hydrological predictions exhibit biases.
Method: different methods have been applied with varying complexity combining wavelet transformations and Quantile Regression Neural Networks (QRNN) and including the derivation of predictive uncertainties (Bogner et al., 2016)
Verification: Continuous Ranked Probability Skill Score (CRPSS). Reference: Climatology

Post-processing: Preliminary results

For the verification of the quality of the hydrological forecasts the CRPSS for the uncorrected and the corrected ensemble is shown for streamflow predictions in the Verzasca catchment (VAG). Depending on the correction method the forecasts from this particular year are improved up to day 7 and 14 respectively. Seasonal differences are even more pronounced.

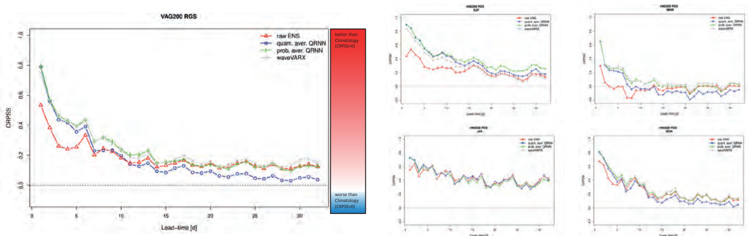

References and Partners:

- *MeteoSwiss* for the verification and processing of the meteorological forecasts
- Scientific collaboration with the *Institute of Environmental Engineering, ETHZ*, hydropower optimization, (see poster by Anghileri et al.)
- Private partner *Hydrique Ingenieurs* for the operational setup of the prediction system including hydropower optimization

K. Bogner, K. Liechti, and M. Zappa. Post-Processing of Stream Flows in Switzerland with an Emphasis on Low Flows and Floods. *Water*, 8(4):115, 2016.

Combination of Pre- and Post-processing: Preliminary results

For the verification of the quality of the hydrological forecasts the CRPSS for the uncorrected and the corrected ensemble is shown for streamflow predictions in the Verzasca catchment (VAG). Depending on the correction method the forecasts from this particular year are improved up to day 7 and 14 respectively. Seasonal differences are not yet analysed.

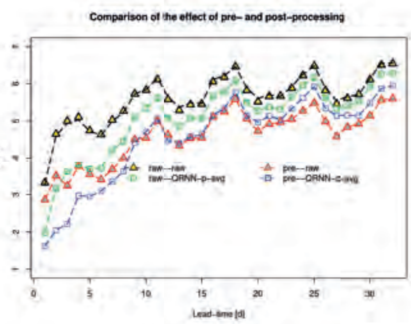

SCCER SoE
SWISS COMPETENCE CENTER for ENERGY RESEARCH
SUPPLY of ELECTRICITY

SCCER-SoE Annual Conference 2017

In cooperation with the CTI
Energy
Swiss Competence Centers for Energy Research
Swiss Confederation
Commission for Technology and Innovation CTI

Generation of high resolution climate variables for hydropower studies: preliminary model simulations

Nadav Peleg, Simone Fatichi, Paolo Burlando

Summary

The main objective of this study is to generate very high-resolution climate scenarios to assess the impact on hydropower production and operation along the 21st century using the state of the art regional climate models (RCMs) from the Euro-CORDEX initiative.

The climate variables are simulated using a new stochastic weather generator, **A**dvanced **WE**ather **GEN**erator for **2-d**imension grid (AWE-GEN-2d), that was recently developed. A re-parameterization scheme has been suggested in order to simulate climate variables for future climate, but has yet to be peer-reviewed.

Here, we demonstrate the ability of AWE-GEN-2d to simulate high-resolution climate variables for a future climate by simulating a single realization driven by a single RCM for the years 2020-2100. The Engelberger catchment, representing a complex orography terrain in the Alps, was chosen as a case study.

AWE-GEN-2d products will be available for the SCCER members upon demand. An example for an ongoing collaboration (Gletsch Glacier) is presented in the poster by Schirmer et al.

AWE-GEN-2d re-parameterization

The method for generating future climate projections consists in re-evaluating some of the parameters of AWE-GEN-2d, as compared to the parameter values obtained from observations, using inferences from climate model outputs. Factors of change (FC) are used to quantify the projected change for several statistics of climatic variables by comparing a specific control scenario (a period of time when both observations and climate model simulations are available) with a specific future scenario (only model simulations are available).

FC is estimated only for precipitation (considering the future changes in spatial occurrence and precipitation intensity), cloud cover (during intra-storm period) and near-surface air temperature (delta change approach is applied). Other simulated climate variables (e.g. incoming shortwave radiation or relative humidity) will be affected as a result of linkages with the modified climate variables. The FC is determined from a set of 14 daily regional climate models (from Euro-CORDEX project).

AWE-GEN-2d is used to simulate the climate variables for the 21st century period (2020—2100). This is done by applying a decadal moving window for which the statistics from the climate models are estimated on a 30-year period basis.

AWE-GEN-2d will be used to generate 280 simulations (14 climate models x 2 emission scenarios x 10 realizations) of 80-year period for each location of interest, to account for the uncertainties emerges from the emission scenario, climate models and the internal (stochastic) climate variability.

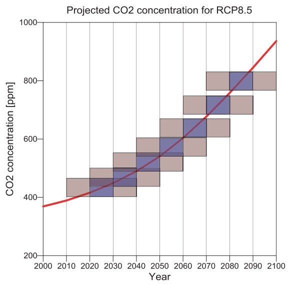

Case study

AWE-GEN-2d was calibrated and validated for the Engelberger catchment (see Peleg et al., 2017). Precipitation is simulated for 5-min and 2-km resolution, while the other climate variables (e.g. temperature, radiation, relative humidity, near-surface wind speed) are simulated for hourly and 100-m resolution.

FC were calculated for one climate model chain for this demonstration: the SMHI-RCA4 regional climate model that is driven by the CNRM-CERFACS-CNRM-CM5 global circulation model. FC are calculated for the extreme GHG emission scenario (RCP85). Results from a single realization simulating the period 2020—2100 are presented.

Cloud cover

The projected annual mean cloud cover over Engelberger catchments for the period lasting to the end of the century is presented. The future projected cloud cover is very similar to the present cloud cover, as the FC for this region is relatively small (~5%), and fall within the expected range of the natural annual variability (~8%), i.e. the signal of the climate change is not pronounced.

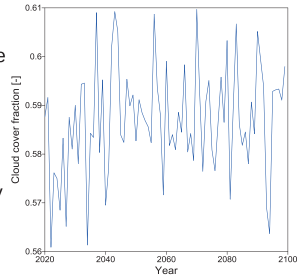

Precipitation

The projected annual mean precipitation over Engelberg station for the 21th century is presented (right figure). As for the cloud cover, the climate change signal is weak and is in the same order as of the natural annual variability of precipitation (~10%). Large variability is expected in space due to the precipitation stochastic nature, and is indeed captured by AWE-GEN-2d. The mean precipitation difference between two decades representing the end of the century (2081—2090) and near-future climate (2021—2030) is presented in the left figure.

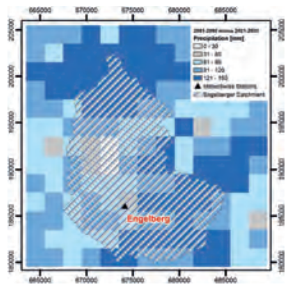

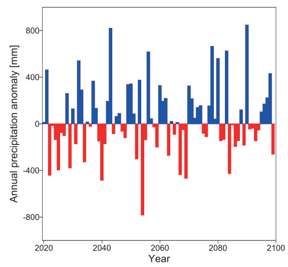

Temperature

A significant climate change signal in temperature is projected (>3°C), as demonstrated for the Engelberg station (right figure).

AWE-GEN-2d ability to simulate the projected temperatures on a fine grid scale is shown in the figures below, comparing mean decadal temperatures between near-future (left) and end of the century (right).

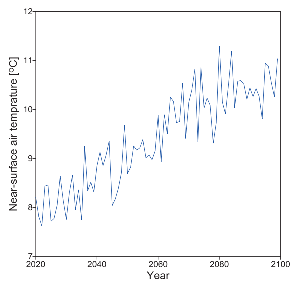

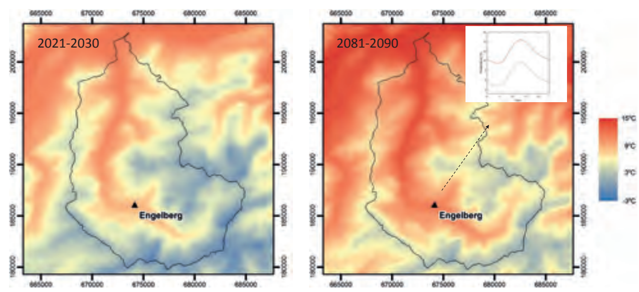

Peleg, N., S. Fatichi, A. Paschalis, P. Molnar, and P. Burlando (2017), An advanced stochastic weather generator for simulating 2-D highresolution climate variables, J. Adv. Model. Earth Syst., 9, 1595–1627.

SCCER SoE
SWISS COMPETENCE CENTER for ENERGY RESEARCH
SUPPLY of ELECTRICITY

SCCER-SoE Annual Conference 2017

In cooperation with the CTI
Energy
Swiss Competence Centers for Energy Research
Swiss Confederation
Commission for Technology and Innovation CTI

High spatio-temporal resolution climate scenarios for snowmelt modelling in small alpine catchments

Michael Schirmer, Nadav Peleg, Paolo Burlando, Tobias Jonas

Motivation

The aim of this project is to support economic risk assessments of long-term investments by small hydropower plant (SHP) operations due to a changing climate. We will estimate the impact of climate change on distribution and frequency of the inflow in a snowmelt dominated tributary of a SHP using an innovative combination of novel components: a stochastic 2-dimensional weather generator, and a high-resolution energy balance snow cover model. Preliminary results for the present climate are presented.

Methods

The weather generator (AWE-GEN-2d, see poster by Peleg et al.) produces a physically-consistent set of climate variables in a high temporal and spatial resolution, satisfying the fine-resolution that is required for energy balance modelling of snowcover accumulation and melt.

The energy balance snow model (JIM/FSM) allows applications at very high spatial resolution by specifically accounting for small-scale processes relevant in mountainous environments. This model upgrade integrates developments such as a subgrid-paramerization of snow covered area based (SCA) on terrain variables to implicitly account for snow redistribution.

40-year of monitoring data for snow water equivalent (SWE) was used to verify snow distribution patterns at coarser spatial scale.

Location – Demonstrator project for SHPs

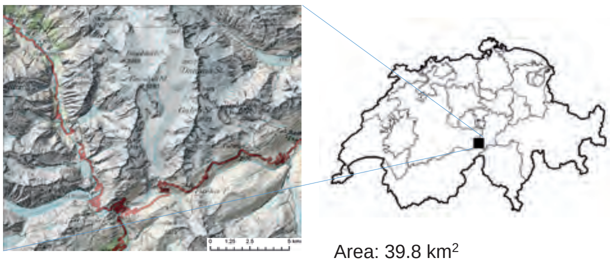

Area: 39.8 km^2
Glaciation: 52%
Mean elevation: 2719 m a.s.l.

Comparison with SWE climatology

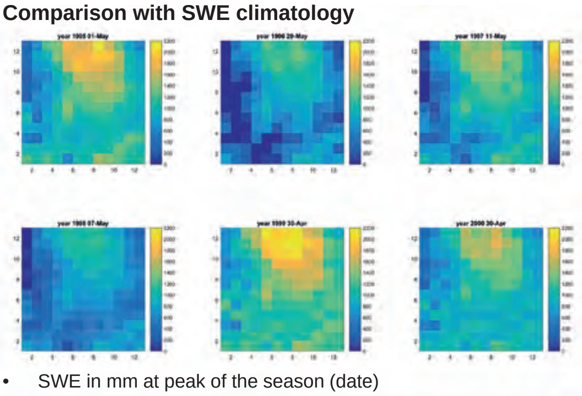

- SWE in mm at peak of the season (date)
- 40 years available
- 1 km resolution based on observations, temperature index modelling and data assimilation techniques.

Preliminary results

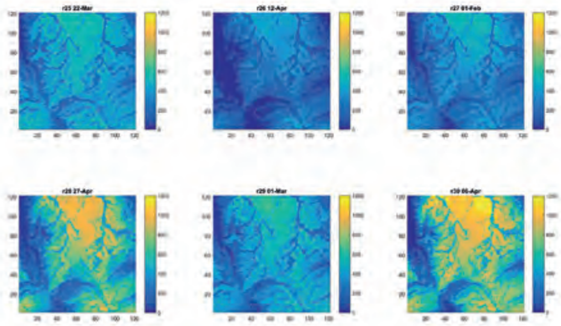

- SWE in mm at peak of the season (date) of six realizations
- Weather generator (WG) delivers 30 realisations representing the natural climate variability
- WG provides hourly data in a spatial resolution of 100 m by 100 m
- Energy balance (EB) model integrates terrain based precipitation and SCA parameterisations (e.g. less snow in steep locations)

SWE development

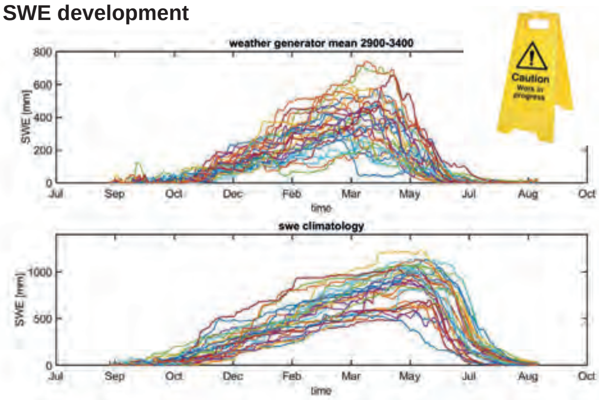

- Average SWE of 30 years/realizations in an elevation band of 2900 to 3400 m
- Preliminary results of WG/EB model has certain differences to a current climatology, e.g. related to SWE amounts, mid winter melt conditions, earlier melt out

Outlook

- Account for differences between SWE climatology and the results of the weather generator/energy balance model combination
- Couple results with a gridded hydrological model and compare results with 30 years of runoff observations
- Generate time series climate scenarios based on the output of regional climate models
- Estimate the impact of climate change on distribution and frequency of the inflow at the intake of the SHP in Gletsch and other small mountain catchments (e.g. Adont, Grisons)
- **This is the first time that such an innovative combination of methods is applied enabling a realistic representation of small-scale processes in alpine terrain. Accounting for spatial variability is key to accurately assess changes in the distribution and frequency of runoff in small mountain catchments.**

SCCER SoE
SWISS COMPETENCE CENTER for ENERGY RESEARCH
SUPPLY of ELECTRICITY

SCCER-SoE Annual Conference 2017

In cooperation with the CTI
Energy
Swiss Competence Centers for Energy Research
Swiss Confederation
Commission for Technology and Innovation CTI

Climate change impacts on HP production and required adaptation strategies – a synthesis

All partners related to Task 2.1 (Lead: Manfred Stähli, WSL)

Background

Climate change will considerably alter the timing and the amount of water available for HP production, and it will change the supply and transport of sediments to HP dams and infrastructure. In addition to these natural controls, climate change will also have indirect impacts on future HP production: for example, the demand for electricity – and thus the market price – will change with a warming climate, and climate change will also control the production of alternative renewables.

HP industry needs to know what that finally means for the hydropower production in the future and how they can adapt in an optimal way.

Recognizing that is one of the most pressing issues for HP industry, SCCER SoE decided to compile a specific synthesis on this issue by the end of phase II.

Previous syntheses of climate change impacts on HP production in Switzerland

This will not be the first comprehensive study of climate change impacts on HP production in Switzerland. One of the first such assessments was published by Westaway (2000) for the Grande Dixence hydro-electricity scheme. A first synthesis for the Swiss alpine HP production was compiled by Schaefli et al. (2007). The most recent comprehensive synthesis was issued by SwisselectricResearch, BfE, Canton Valais and FMV and published in 2011.

Why yet another synthesis on climate-change impact on HP production?

- Climate change scenarios for Switzerland will be updated in 2018 (based on most recent emission scenarios)
- A lot of new research results have been gained since 2011, and numerical models have been improved and applied in a more integrated way.
- Adaptation measures were not considered in previous studies.

Preliminary concept of the upcoming synthesis

The synthesis report will consist of two parts:

- one summarizing **the (quantitative) changes** in water availability, sediment yield and HP production accounting for climate-change induced effects on electricity demand and other renewables.
- one proposing **adaptation measures** for the HP industry.

The synthesis report shall be guided by specific questions of operators, decision makers and administrators of HP production in Switzerland (see below).

Timeline:
Nov 2017: Synthesis concept is approved (Site visit KTI) and list of guiding research questions is consolidated.
Dec 2017: New climate-change scenarios CH2018 available
Dec 2018: First preliminary draft of the synthesis available

Specific questions to be answered in this synthesis

Operators, decision makers and administrators of HP production in Switzerland have very clear specific questions when it comes to the future impact of climate change. Our synthesis shall be guided by such questions and answer them explicitly.

Here is a selection of potential questions that could be addressed:

- How will HP production change in winter (in relation to the expected overall winter-time demand)?
- Where (in Switzerland) will sediment delivery to HP intakes increase/ decrease in future?
- What consequences would changes in general weather patterns (e.g. jet stream) have for HP production?
- Worste-case scenario – what are the perspectives for HP if the international climate politics fails?

Task 2.2

Title

Infrastructure adaption

Projects (presented on the following pages)

Assessment of the cavitation risk for throttled surge tanks
N. J. Adam, G. De Cesare, A. J. Schleiss

Menacing Waves: Enhancing the Risk Assessment for Impulse Waves in Reservoirs
C. Beck, L. Schmocker, H. Fuchs, F. Evers, R. Boes

Kraftwerk Juchli - Exploitation of Juchli waterfall with a small hydropower plant
M. Bienz, S. Stähly, G. De Cesare, A. J. Schleiss

Impacts of Future Market Conditions on Hydropower Storage Operations
Alternative: Work Package 5
L. Chambovey, J. P. Matos, P. Manso, A. J. Schleiss, H. Weigt, I. Schlecht, F. Jordan

Fine sediment release from reservoirs through venting of turbidity currents
S. Chamoun, G. De Cesare, A. J. Schleiss

Rehabilitation of Isola arch-gravity dam facing an internal swelling reaction
F. del Drago, P. Manso, A. Schleiss

Potential for future hydropower plants (HPPs) in Switzerland
D. Ehrbar, L. Schmocker, D. Farinotti, R. M. Boes

Fine sediment management at hydropower schemes considering turbine erosion
D. Felix, I. Albayrak, R. Boes

Blocking probability at spillway inlets under driftwood impact
P. Furlan, M. Pfister, J. Matos, A. J. Schleiss

Exploitation optimale de la force hydraulique de la Plessur dans les Grisons (CH)
T. Glassey, A. J. Schleiss, G. De Cesare, S. Schwindt

Air demand of bottom outlets
B. Hohermuth, L. Schmocker, R. M. Boes

Hydropower potential at Rhône Glacier
V. Hutter, D. Ehrbar, L. Schmocker, D. Farinotti, R. M. Boes

Utilisation optimale du potentiel hydroélectrique d’un bassin versant alpin: le barrage de Khudoni en Géorgie
M. Jordan, S. Venuleo, P. Manso, A. Schleiss

Online prediction tool for hydropower energy (Opt-HE)
F. Jordan, G. Artigue, K. Cros, C. Loetscher, O. Etter, A. Schleiss

SCCER SoE
SWISS COMPETENCE CENTER for ENERGY RESEARCH
SUPPLY of ELECTRICITY

SCCER-SoE Annual Conference 2017

In cooperation with the CTI
Energy
Swiss Competence Centers for Energy Research
Commission for Technology and Innovation CTI

Assessment of the cavitation risk for throttled surge tanks

Nicolas J. Adam, Giovanni De Cesare & Anton J. Schleiss
Laboratoire de Constructions Hydrauliques (LCH), Ecole Polytechnique Fédérale de Lausanne (EPFL)

Introduction

The Swiss confederation aims to phase out nuclear power production with the Energy Strategy 2050. Hydroelectricity has supplied approximatively 60% of the domestic electricity production for 40 years (SFOE, 2016). High head power plants (Figure 1), which represents 60% of Swiss hydroelectricity, may be refurbished in order to increase their flexibility or their peak-hours generation to supply the versatility of the new means of generation, e.g. wind or solar generation.

Surge tanks (Figure 1) are hydraulic devices, part of a high head power plant. They protect the pressure tunnel from the water hammer, which are produced by the change of discharge in the waterway system, and damp the mass oscillations. An increase of the generation capacity, either by heighten the dam or increase the discharge capacity, leads generally to a worsening of the mass oscillations. Throttled surge tanks improve the damping of mass oscillations. It allows optimizing the behavior of an existing surge tank. There are different types of throttle such as orifice, rack or bar screen and vortex throttle. This study focuses on chamfered orifices as shown in Figure 2.

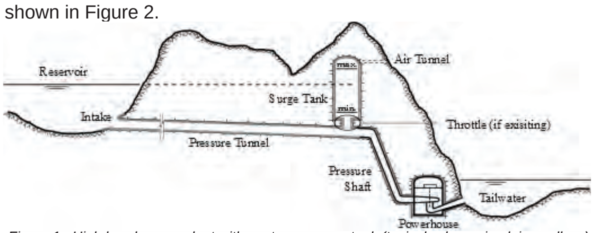

Figure 1 : High head power plant with upstream surge tank (typical scheme in alpine valleys)

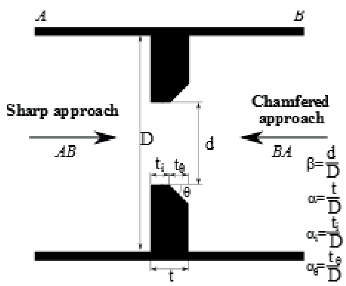

Figure 2 : Chamfered orifices and main geometrical parameters

Cavitation risk with incipient cavitation number σ_i

The incipient cavitation number σ_i, given by Eq. (1),characterizes the cavitation within the throttle. In this cavitation stage, there is no damage to the structures and the influence of the cavitation is very low on the flow characteristics, e.g. head losses produced by the throttle.

$$\sigma_i = \frac{p_u - p_{vg}}{p_u - p_d} \tag{1}$$

Ferrarese et al. (2015) proposed a new method for predicting σ_i. The pressures involved in the evaluation of σ_i are based on single phase CFD simulations. They showed that the value of σ_i is well predicted when the minimum pressure p_{min} in the pipe is equal to the vapour pressure p_{vg} as given by Eq.(2).

$$\sigma_i = \frac{p_u - p_{\min}}{p_u - p_d} \tag{2}$$

Figure 3 gives the predicted values of for an orifice as a function of the contraction ratio β and the inner thickness ratio α_i for the sharp approach flow.

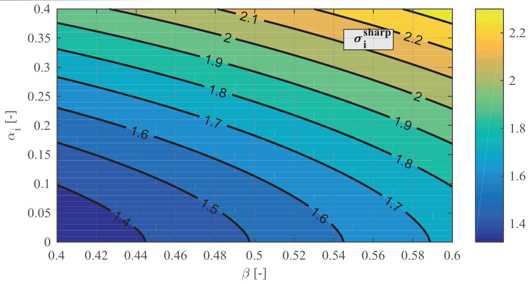

Figure 3 : Incipient cavitation number for the sharp approach flow as a function of β and α_i

Cavitation risk in surge tank orifices

By assuming a quasi-steady flow in the mass oscillations between the surge tank and the reservoir and that cavitation does not influence the head losses and the other flow characteristics, the limit between the zone without and with a risk of cavitation for down-surge (Eq.(3)) and for up-surge (Eq.(4)) as:

$$H_{ST} = \sigma_i \left[\frac{8\beta^4}{g\pi^2 d^4} k - \kappa_Q \right] Q^2 + p_{vg} \tag{3}$$

$$H_{ST} = (\sigma_i - 1) \left[\frac{8\beta^4}{g\pi^2 d^4} k - \kappa_Q \right] Q^2 + p_{vg} \tag{4}$$

Where k is the head loss coefficient, d the inner thickness ratio, κ_Q is a correction factor due to the difference of kinetic energy between the pressure tunnel and the surge tank and Q the discharge flowing into or out of the surge tank.

These two limits of the cavitation risk are applied to an existing throttled surge tank (Adam et al.,2017) subjected to an emergency closure (Figure 4). Two cavitation risks are highlighted but with relative small durations (17s for the up-surge and 80 s for the down-surge). However, this cavitation is still limited.

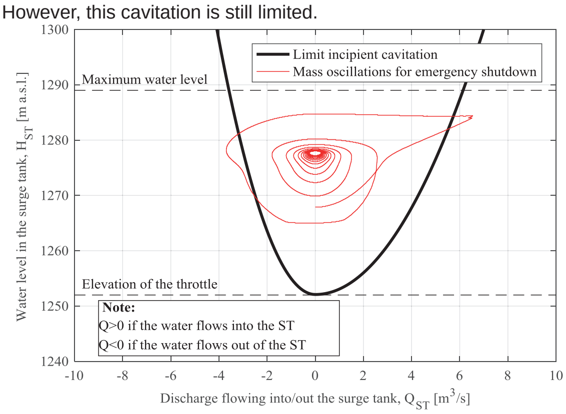

Figure 4 : The cavitation risk (water at 5°C) for the Gondo surge tank (Adam et al.2017) subjected to an emergency shutdown leading to converging mass oscillations

References

Adam, N.J., De Cesare, G., Nicolet, C., Billeter, P., Angermayr, A., Valluy, B. & Schleiss, A.J. (accepted for publication). Design of a throttled surge tank for the refurbishment by power increase of a high head power plant. Journal of Hydraulic Engineering.

Ferrarese, G., Messa, G. V., Rossi, M. M., & Malavasi, S. (2015). New method for predicting the incipient cavitation index by means of single-phase computational fluid dynamics model. Advances in Mechanical Engineering, 7(3), 1687814015575974.

SFOE (2017). Statistique suisse de l'électricité 2016. Technical report, Swiss Federal Office of Energy.

SWISS COMPETENCE CENTER for ENERGY RESEARCH
SUPPLY of ELECTRICITY

SCCER-SoE Annual Conference 2017

FlexSTOR

In cooperation with the CTI
Energy
Swiss Competence Centers for Energy Research
Commission for Technology and Innovation CTI

Menacing Waves: Enhancing the Risk Assessment for Impulse Waves in Reservoirs

Claudia Beck, Lukas Schmocker, Helge Fuchs, Frederic Evers, Robert Boes - VAW, ETHZ; Axel Volkwein - WSL

Motivation

Impulse waves, generated by avalanches, ice- or rockfalls, may seriously impair the reservoir of a hydropower plant. In some cases they even overtop or damage the dam and trigger hazardous flood waves (Fig. 1). Examining their potential impact is therefore an inevitable part of a comprehensive hazard assessment for hydropower reservoirs in alpine areas.

Fig 1: Impulse wave generation at Grindelwald Glacier Lake (Photo: Hans-Ruedi Burgener)

The impulse wave features in reservoirs and the possibility of dam overtopping can be evaluated by a computational procedure established at VAW (Heller et al. 2009). Recent research on spatial wave propagation (Evers and Hager 2016)will complete this hazard assessment tool. For a proper validation of the procedures based on analytical and semi-empirical data from small-scale models, reliable field data on impulse waves or large-scale experiments are still missing. New field data shall therefore be collected by means of a large-scale field test. An innovative test-setup is planned at Grimselsee, where artificially generated impulse waves will be studied in prototype. For the impulse waves generation, a rail wagon will slide on guiding rails at high speed into the reservoir.

Laboratory tests

Within the CTI project FlexSTOR, both laboratory tests at VAW and prototype field tests at Grimselsee are carried out to investigate the impulse wave generation and propagation. A rail wagon will be used to represent gravitationally-driven landslides. The small-scale model tests were carried out with a model scale of 1:50 (Fig. 2). A rail wagon was manually accelerated on an inclined ramp. The wave heights were measured at three locations along the wave propagation path using ultrasonic distance sensors. The tests showed that for a targeted slide mass of 10 tons and an impact velocity of around 25 m/s, the maximum resulting wave height in prototype is ≈1 m.

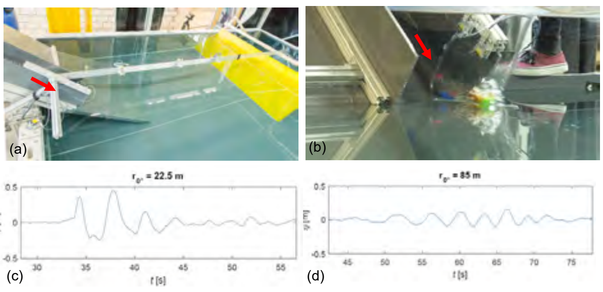

Fig 2: (a) Part of Grimselsee in VAW Laboratory at 1:50 scale; (b) Impact of railway wagon and wave generation in laboratory; Water surface displacement η at a propagation distance of (c) 22.5 m and (d) 85 m.

Field tests

The prototype tests planned at the KWO reservoir Grimselsee offer a unique chance to collect rare and valuable field data on impulse wave generation and propagation under systematic and controlled conditions. An optimum location for the field test is Grimselsee, as there is already a gate rail available where a rail wagon can be slid into the reservoir (Figure 3 and 4). The rail has an inclination of 48° and the load capacity of the rail wagon is around 5-10 tons. The field tests are scheduled for summer 2018, when the reservoir will be at a low level and the rail wagon may be accelerated to about 25 m/s before impact.

Fig 3: Lowered Grimselsee in 2006 with Spitallamm dam on the left and existing railway. (Photo: KWO)

Fig 4: Rail wagon with a weight of approx. 6 tons. Additional weight will be added with steel plates and water tanks. The wagon front will be equipped with a vertical steel plate to increase momentum transfer.

Acknowledgement

This project is financially supported by the Swiss Commission for Technology and Innovation (CTI) with the industrial partner Kraftwerke Oberhasli (KWO). It is part of the FlexSTOR project which stands for “Solutions for flexible operation of storage hydropower plants in changing environment and market conditions” and is embedded in the Swiss Competence Centre for Energy Research - Supply of Energy (SCCER-SoE) framework. .

References

Evers, F.M., Hager, W.H. (2016). Spatial impulse waves: wave height decay experiments at laboratory scale. Landslides, 13(6), 1395-1403. DOI:10.1007/s10346-016-0719-1

Heller, V., Hager, W.H., Minor, H.-E. (2009). Landslide generated impulse waves in reservoirs - basics and computation. VAW *Mitteilung* 211, Boes, R., ed., ETH Zürich, Switzerland.

SCCER-SoE Annual Conference 2017

SCCER SoE SWISS COMPETENCE CENTER for ENERGY RESEARCH SUPPLY of ELECTRICITY

In cooperation with the CTI

Energy Swiss Competence Centers for Energy Research

Commission for Technology and Innovation CTI

Kraftwerk Juchli
Exploitation of Juchli waterfall with a small hydropower plant

Maxime BIENZ[1], Severin STÄHLY[1], Giovanni DE CESARE[1], Anton J. SCHLEISS[1]

[1]Laboratoire de constructions hydrauliques (LCH), Ecole Polytechnique Fédérale de Lausanne (EPFL)

Introduction

The small hydropower plant project Kraftwerk Juchli, proposed by Kraftwerke Oberhasli AG (KWO), would allow using the potential created by the construction in the 1950's of the underground gallery to transfer the water collected from the river Bächlibach to the lake of Grimsel.

The project is situated on the territory of the municipality of Guttannen in the canton of Bern, near the pass of Grimsel (see Figure 1).

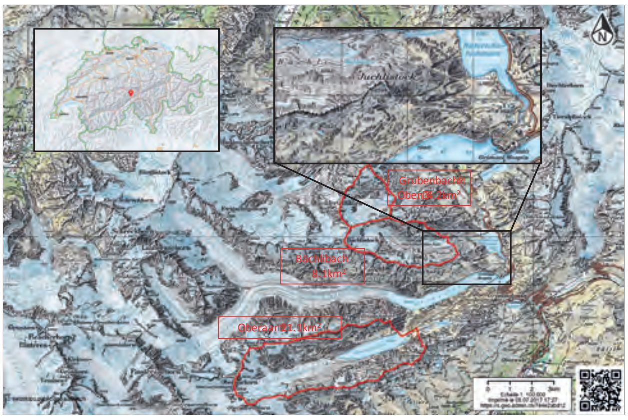

Figure 1. Geographical situation of the Kraftwerk Juchli project and the watersheds studied with the RS Minerve software (geodata © swisstopo).

The adduction gallery concerned by this project is represented in Figure 1. It allows connecting the Bächli lake with the Aar valley at the level of the Grimsel lake by passing under Juchlistock. The tunnel has a total length of 1'348 meters and a slope of 0.75%.

The existing facilities located in the Bächli valley are represented in Figure 2. The area located upstream of the Bächlibach dam is a protected alluvial zone with a national level of importance, forbidding any modification of the environment.

Figure 2. The Bächlibach dam which diverts the water into the Bächli gallery. The water intake is equipped with a trashrack to avoid big stones to enter the gallery. The capacity of the water intake is 7.5 m³/s.

In addition, the former artillery fortress of Grimsel as well as the project of replacing the Spitallamm dam could bring some synergies to the project. Scenarios with or without the extra height of the level of Grimsel lake are to be taken into consideration.

Methods

1. Modelling of the Bächlibach and Grubenbach Oben watersheds on the software RS Minerve. The results of the modeling will supply the discharge data at the exit of the watershed.
2. Study of various alternatives of exploitation of the waters from the Bächli river.
3. The most interesting alternative is chosen for a more thorough study which contains the dimensioning of the hydraulic elements.
4. Study of the project's impact on the environment.
5. Estimation of the cost for the construction of the small hydropower plant.

Concepts of exploitation and alternatives

- Concept of exploitation : Run-of-river.
- Storage and turbine-and-pump are not practicable because of their impact on the environment.

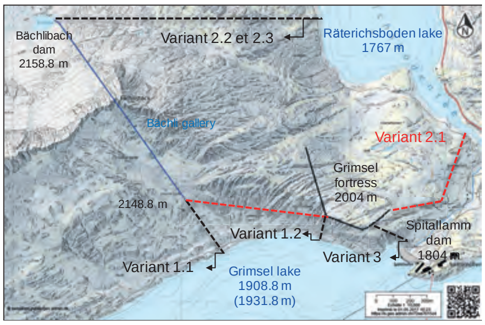

Figure 3. The variants of exploitation for the project Kraftwerk Juchli. The solid lines represent the existent galleries (geodata © swisstopo). Representation of the different existing facilities and their altitude. The maximum elevation of the level of the Grimsel lake is 1908.8 m a.s.l. but a project is in study to raise the level to 1931.8 m a.s.l. The Spitallamm dam is one of the two dams which were built to create the Grimsel reservoir. The Grimsel fortress could be used to install a part of the penstock pipe.

Alternatives

1. Bächlibach – Grimsel lake	Head : 250 m (227 m)
2. Bächlibach – Räterichsboden lake	Head : 390 m
3. Bächlibach – Spitallamm dam	Head : 353 m

From the 6 variants proposed, variant 2.1 (see Figure 3) is chosen as the best one for which all works have been designed.

Pre-project of the small hydropower plant

With a designed discharge of 1.7 m³/s, 19.1 GWh/year of net power can be produced by means of one Pelton turbine.

Hydraulic structures :

- Efficiency of the sandtrap : 0.2 mm
- Length of the penstock pipe : 1'830 m
  - 1'355 m : polystyrene reinforced with fiberglass (PRV)
  - 475 m : stainless steel
- Turbine Pelton : 2 injectors and a vertical axe of rotation (see Figure 4)

Figure 4. Picture of a Pelton turbine with two injectors from the power plant Le Lauzet in France (Cerec Engineering):

The engine room is installed in the assembly cave of the Grimsel 1 hydropower plant.

Conclusion

- Installed capacity : 5.8 MW
- Investment cost : 12.2 million CHF

Civil works :	8 million CHF
Hydromechanical equipment :	1 million CHF
Other costs (engineer, capital cost, etc.) :	3.2 million CHF

Economic evaluation

Return period : 25 years, till the end of the actual concession.

Interest rate: 3 %

- **Generation cost** : 4.4 cts/kWh

The profitability of the project is guaranteed if it benefits from the compensatory feed-in remuneration (RPC). Without the RPC, the project can be profitable if the electricity selling price is a bit higher than the actual market price. A renewable energy label could ensure a bonus of 1 ct/kWh.

SCCER SoE
SWISS COMPETENCE CENTER for ENERGY RESEARCH
SUPPLY of ELECTRICITY

SCCER-SoE Annual Conference 2017

FlexSTOR

In cooperation with the CTI
Energy Swiss Competence Centers for Energy Research
Swiss Confederation
Commission for Technology and Innovation CTI

Impacts of Future Market Conditions on Hydropower Storage Operations

Loïc Chambovey[1], J.P. Matos[1], P. Manso[1], A.J. Schleiss[1], H. Weigt[2], I. Schlecht[2], F.Jordan[3]
[1] EPFL-LCH, [2] FoNEW, [3] Hydrique
Corresponding author's email address : jose.matos@epfl.ch

Introduction

In this work developed within the Energy Strategy 2050 frame, we want to assess future hydropower production constraints using numerical simulation tools and several scenarios, both climatic and economic, prepared by partners. Through the specific case study of the KWO system, several alternatives will be explored, including benefits from storage vs run-off-based production.

Case Study : KWO System, Upper Aar river basin

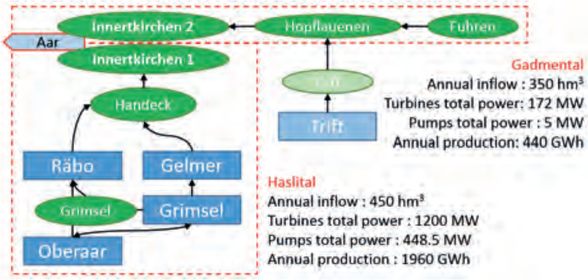

Figure 1 : Simplified KWO Scheme with main reservoirs (blue) and power stations (green). Light green and blue show future Trift infrastructures.

Numerical Modelling

Routing System 3, developed by Hydrique Ltd. in Lausanne, is a tool that allows building semi-distributed hydrological models using modules representing different elements and functions of catchments and hydraulic infrastructures. Figure 2 illustrates the global KWO model.

The hydraulic part uses the *Optiprod* module of RS3, to simulate an optimised production based on target curves day-ahead prices, base operation prices, and elasticity coefficients (Figure 3).

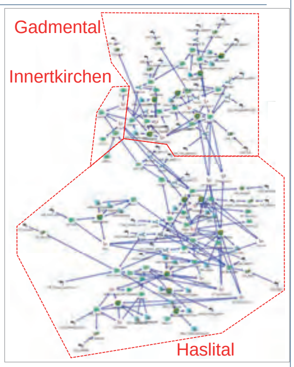

Figure 2 : RS3 full KWO model

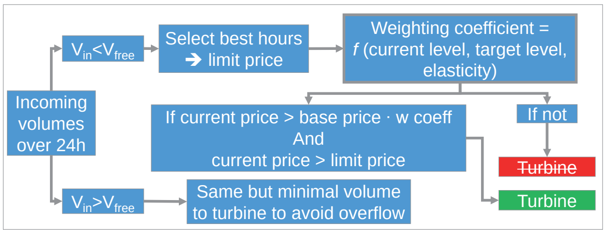

Figure 3 : 'Optiprod' decision'algorithm (simplified)

Limits :

- Operation constraints (maintenance, long-term contracts, grid balancing) can not be reproduced
- Simulated facilities are not coordinated with each other.

Despite existing limitation, adjusting coefficients allows the simulation of coherent behaviours, leading to an annual production close to reality (according to historical daily flows given by KWO).

Aknowledgments

Thanks are owed to Jan Baumgartner, Marcel Schläppi and the rest of the KWO team. Likewise, we are thankful to Massimiliano Zappa from WSL for his contributions.

Available scenarios

Economic scenarios by FoNEW (*Forschungstelle fur Nachaltige Wasser- und Energieversorgung*), from the *Swissmod* electricity market model. They include a base scenario and variations over three main hypothesis : carbon prices, fuel prices and (non-hydraulic) renewable part in total production. Data provided from 2020 to 2030.

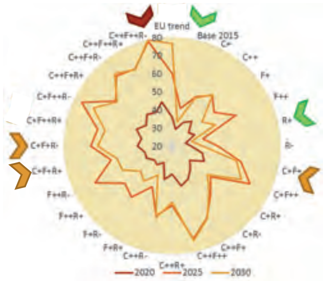

Figure 3 : Economic scenarios (mean prices €/MWh)

Results – economic impacts

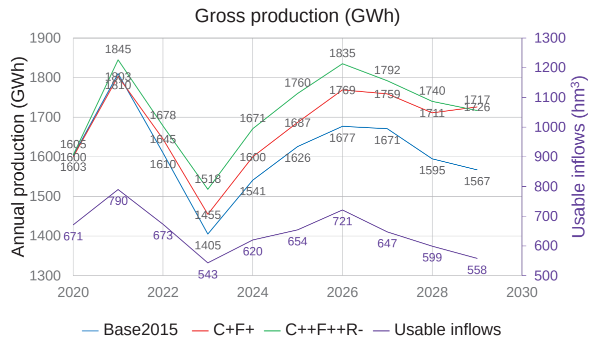

Figure 4 : Simulated annual production and usable inflows predicted by A1B climate scenario (WSL). Simulations for the hydrological year 2015-16 lead to 2050 GWh produced from 841 hm³ available inflows.

Simulated annual production (Figure 4) logically follows variations of inflows (purple). The difference between economic scenarios (only three represented above) comes from the pump-storage station, which activity depends mainly on peak energy prices.

Discussion – improvement opportunities

Benefits of the new Trift dam (collecting and storing about 60% of Gadmental inflows) include 8-10% increase in total production (from the new power station) and a 13-15% rise in revenues (production increase and better operation time thanks to annual storage).

Other ways of improvement :

- Enlarging lake Grimsel (currently too small compared to its inflows, and higher flexibility for future pump-storage operations).
- Turbining water from Mattenalpsee to Räterichsbodensee (currently transferred without production).
- Exploiting unused parts of the watershed (Urbachtal, lower Haslital).

Options with less potential benefits :

- Increasing the capacity of diversions (already capturing more than 95% of total inflows and more than 90% in the future).
- Turbining from small lakes (only small volumes available).

Conclusion

Using Routing System 3 modelling tools and several climatic and economic scenarios, future constraints were simulated and a set of possible improvements explored. In particular, the benefits from annual storage vs run-off operations were shown.

The complexity of the KWO case study renders precise simulation difficult and a deeper analysis may require the development of new tools. However, the method can easily be applied to other infrastructures, existing or planned, or even to a generic installation, representative on a larger regional or national scale.

SCCER-SoE Annual Conference 2017

SCCER SoE
SWISS COMPETENCE CENTER for ENERGY RESEARCH
SUPPLY of ELECTRICITY

In cooperation with the CTI
Energy
Swiss Competence Centers for Energy Research
Commission for Technology and Innovation CTI

Fine sediment release from reservoirs through venting of turbidity currents

Sabine Chamoun, Giovanni De Cesare, Anton J. Schleiss

swisselectric research

Introduction

Dams are essential structures in modern societies. The reservoirs created by such structures provide crucial services such as irrigation, hydropower, flood control, and water supply. Nevertheless, processes such as sedimentation are hindering the sustainability of reservoirs, shortening their lifetime and reducing their efficiency. One of the main sources of fine sediments in reservoirs are turbidity currents, created by density differences due to their high sediment concentrations. Turbidity currents can flow along the reservoir and reach the dam site. Therefore, the sediments they suspend can block low-level outlets/intakes and reduce the capacity of the reservoir. Dealing with such currents can be done by venting it through low-level hydraulic structures. In the present work, different parameters related to venting were investigated. Their effect on the sediment release efficiency were studied using experimental and numerical approaches. The influence of outflow discharge using the horizontal bed is presented hereafter. Both experimental and numerical results are shown and compared.

Methods

The approach used in this research was mainly experimental. A long and narrow flume was used at the Laboratory of Hydraulic Constructions (LCH). It simulates the reservoir in which turbidity currents were triggered. The latter flew along the reservoir until reaching a wall simulating the dam and into which a rectangular orifice, representing the bottom outlet, was placed. An outflow discharge was applied at the outlet when the current reached it. The turbidity current was then vented and evacuated into a downstream basin. Inflow and outflow discharges and concentrations were amongst the main parameters tested. Deposition was also measured in space and time and allowed to reach realistic efficiency values by subtracting deposited sediment masses from inflowing mass when comparing the latter to the outflowing sediment masses. This is done since no retrogressive erosion is involved during venting. These parameters allowed the calculation of the venting efficiency in time, which is used as the main criterion to compare the different scenarios tested using different outflow discharges among others.
Moreover, a numerical model was built based on the geometry of the experimental model. The software ANSYS Inc. was used with the CFX solver. In order to simulate the complex dynamics of turbidity currents including deposition, drag and the sediment's settling velocities, several equations were added to the solver as CEL expressions. The expressions' parameters were then calibrated and the results were validated based on the experimental data. The numerical results served as an extension to the experimental data.

Experimental results and discussion

Numerous reported cases of reservoirs where turbidity currents occur showed that the bed in the close vicinity of the outlet/dam approaches horizontal. In fact, when a turbidity current reaches the dam, unless it is evacuated, it reflects at the dam forming a muddy lake which eventually settles, thus flattening the slope of the thalweg. For this reason, one of the slopes tested is horizontal.

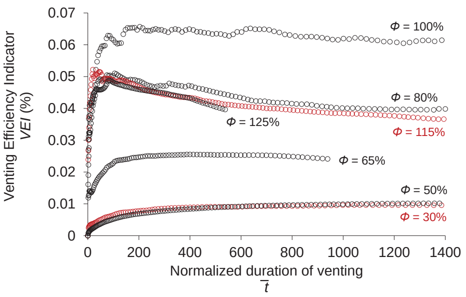

Fig.1: Venting efficiency indicator as a function of the normalized venting duration for different venting degrees tested using the horizontal bed

Seven different venting degrees ϕ, defined as the ratio between the outflow discharge and the turbidity current inflow discharge, were tested starting from 30% up to 125%. The criterion shown in Fig. 1 is the venting efficiency indicator (*VEI*) which considers not only sediment fluxes in and out of the flume during venting, but also the clear water losses induced by venting. Water loss is a particularly important aspect regarding reservoirs used for hydropower generation. It was shown that the venting degree ϕ = 100% induced the least water losses and the highest sediment release. For higher venting degrees, the clear water loss increased thus decreasing the efficiency of venting. More details on the presented experimental results can be found in Chamoun et al. (2017).

Numerical results and discussion

The geometry of the numerical model was based on the experimental model. In order to validate the model, criteria such as the front velocity (Fig. 2), the outflow concentration (and thus the venting efficiency) and velocity profiles from the body of the current were considered.

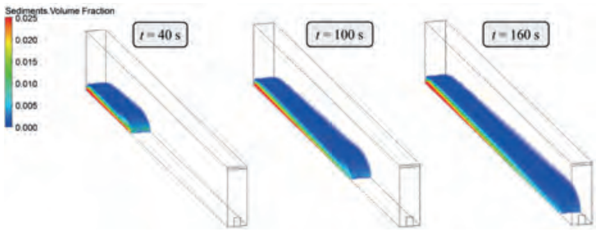

Fig.2: The progress of the turbidity current simulated numerically at different time steps "t" of the simulation.

The Representative venting efficiency *RVE*, which computes the average value of the efficiency calculated once outflow concentrations reach a steady value, is shown in Fig. 2 as a function of venting degree. Contrarily to the *VEI*, the *RVE* only accounts for inflow and outflow sediment masses and does not consider clear water losses. The numerical model allowed testing higher venting degrees than the experimental tests reaching ϕ = 200%. As concluded experimentally, the *RVE* values show that starting ϕ = 100%, there exists a change of trend. The rate of increase of efficiencies is reduced. Therefore, the water losses start increasing when ϕ > 100%. Hence, the venting degree leading to the highest venting efficiencies in the presence of a horizontal bed in the vicinity of the outlet is of 100%.

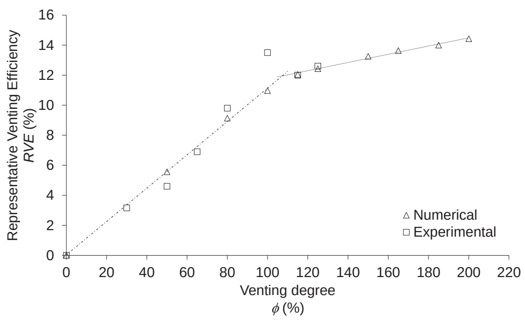

Fig.3: Representative venting efficiency RVE as a function of the venting degree ϕ for a horizontal bed. The trend lines correspond to the numerical data.

References

Chamoun, S., De Cesare, G., & Schleiss, A. J. (2017a). Venting of turbidity currents approaching a rectangular opening on a horizontal bed. *Journal of Hydraulic Research* (Accepted for publication, available online).

Acknowledgments: This research is funded by Swisselectric Research and the Swiss Committee on Dams.

SCCER SoE
SWISS COMPETENCE CENTER for ENERGY RESEARCH
SUPPLY of ELECTRICITY

SCCER-SoE Annual Conference 2017

In cooperation with the CTI
Energy
Swiss Competence Centers for Energy Research
Swiss Confederation
Commission for Technology and Innovation CTI

Rehabilitation of Isola arch-gravity dam facing an internal swelling reaction

Filippo del Drago[1], Dr. Pedro Manso[1], Prof. Anton Schleiss[1]
[1]Laboratoire de Constructions Hydrauliques- EPFL, Lausanne

Motivation of the project

As many other aging Swiss dams, the Isola arch-gravity dam, built in 1960, is facing an internal swelling reaction inducing an adverse stress and strain state. In order to avoid structural issues linked to diffused and uncontrolled cracking, solutions for reducing the effects of concrete swelling on the structure are studied.

Current state of the structure

1. Downstream face of the dam

2. Gated Spillway with cracking and brown colouring of concrete due to internal swelling reaction

3. Upstream face of the dam with watertight membrane band

Crown cantilever height	45	m
Arch crown height (Bloc 10)	35	m
Concrete volume	71'000	m3
Maximum base width	22	m
Crest width	5.5	m
Crest length	290	m
Reservoir volume	6.2e6	m3
Lombardi coefficient	11	

Table 1. Dam characteristics

4. Dam location: San Bernardino

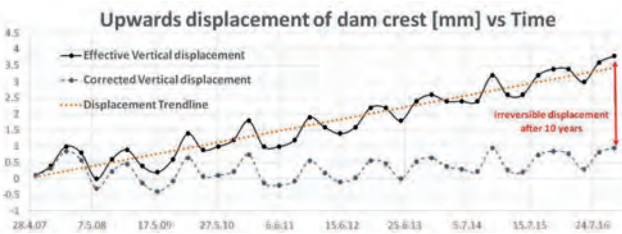

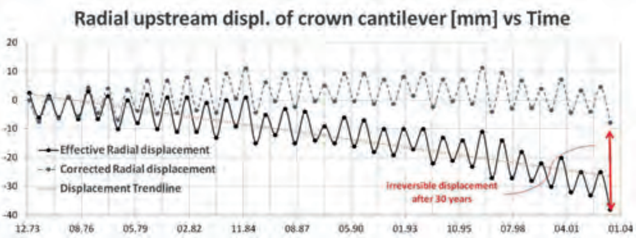

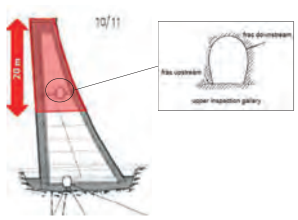

5. Active swelling zone and upper inspection gallery sub-horizontal crack (30°)

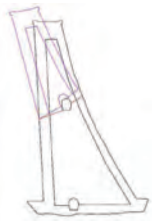

6. Possible displacement mechanism deduced from observed cracking

Multiple criteria decision analysis

If no action is taken:
- Cracking will increase
- Local stability may be put at risk
- Water penetration in the dam body may occur.
- Concrete resistance and stiffness will decrease

The selected solution is the **diamond wire slot cutting** for it is:
- Economical
- Fast
- Sustainable

Parameters to be determined for such an intervention are:
- Number of slots
- Length of slots
- Position of slots
- Width of slots

Designing the diamond wire slot cutting intervention

Objective of intervention: elastic recovery of accumulated strain by allowing concrete to expand at slots. A FEA is used to forecast slot closure in order to design intervention.

Main assumptions:
-swelling is homogeneous across affected areas
- chemical expansion modelled by an equivalent thermal expansion

Crest length	300	m
Average strain	0.02%	
Elasticly recoverable strain	0.01%	
Expected strain recovery	30	mm
Slot length	10	m
Expected slot closure	8	mm
Minimum required slots	4	

Table 2. Intervention characteristics

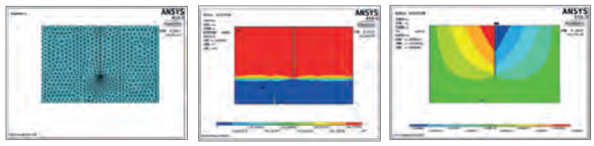

7. 2D FE model of concrete plate with slot: (a) mesh; (b) equivalent thermal load; (c) horizontal strain

Intervention proposal

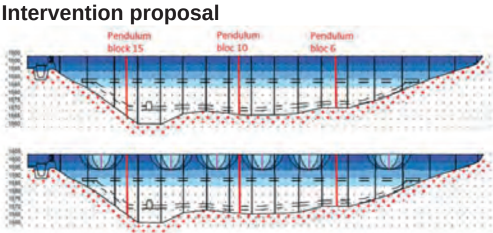

8. Qualitative arch stresses before and after intervention of 6 slots scheme.

Conclusion

Diamond wire slot cutting is a promising technique for the many dams facing internal swelling. Many improvements can still be made in the understanding of the swelling behavior. For better surveillance, an update of the current legislation on dam safety requirements should contain some limit values for expanding concrete.

Acknowledgements

Ing. M. Cuska of *Axpo dam safety department* and Ing. F. Amberg of *Lombardi* for providing the information about the case study.

References

Axpo Dam Safety Department; Caron, P. et al. 2003. «Slot Cutting of Concrete Dams: Field Observations and Complementary Experimental Studies.» *ACI Structural Journal* 430-439.;
Amberg, Francesco. 2011. «Performance of Dams affected by Expanding Concrete.»

SCCER SoE
SWISS COMPETENCE CENTER for ENERGY RESEARCH
SUPPLY of ELECTRICITY

SCCER-SoE Annual Conference 2017

70 NRP Energy Turnaround
National Research Programme

In cooperation with the CTI
Energy
Swiss Competence Centers for Energy Research
Swiss Confederation
Commission for Technology and Innovation CTI

Potential for future hydropower plants (HPPs) in Switzerland

Daniel Ehrbar, Lukas Schmocker, Daniel Farinotti, Robert Boes – VAW ETH Zurich

Introduction

Climate change leads to glacier retreat in the Swiss Alps (Fig. 1). This has a twofold impact on hydropower in the periglacial environment:
(a) new potential locations for HPP reservoirs become ice-free
(b) additional meltwater from glaciers may be available for production

Fig. 1: Retreat of Trift Glacier from 30 June 2004 (left) to 3 July 2014 [© VAW]

The Swiss Energy Strategy 2050 anticipates 37'400 GWh annual electricity production from hydropower in 2035. In 2016, the annual production reached 36'264 GWh. Therefore, a further annual potential of about 1'136 GWh needs to be exploited. This project investigates hydropower potential in Switzerland arising from glacier retreat.

Methods

Glacier runoff projections from Huss & Hock (2015) were used. Three different representative concentration pathways (RCP) and ten global circulation models (GCM) were applied to 1'576 Swiss glaciers.

Site selection was based on expected glacier runoff volumes. Fig. 2 shows annual runoff volumes in 2035 for RCP 4.5, which range up to 283 hm³ in the Aletsch Glaciers catchment. Ice-free sites with high runoff volumes were investigated further.

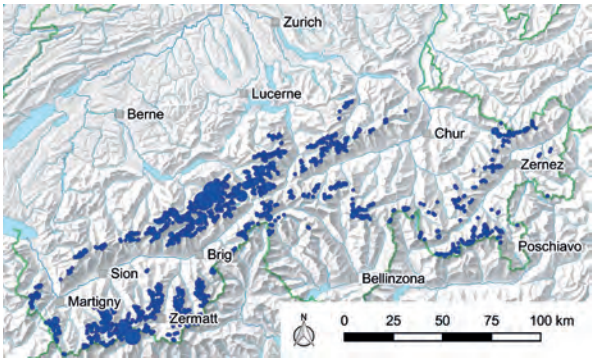

Fig. 2: Relative glacier runoff volumes in 2035 for RCP 4.5, with data from Farinotti *et al.* (2016) (largest dot represents 283 hm³ annual discharge volume)

Site rating depended on a rating matrix where economy was weighted with 60%, environment with 25%, and society with 15%. Production, installed capacity, storage capacity, investment costs, and sediment continuity were the most important factors, each weighted with 10 or 11%. Reservoir sedimentation, vulnerability to natural hazards, impacts on land use and tourism, intrusion into protected areas, use for flood protection etc. were less important factors.

Results

Technical potential of eight future HPPs is given in Tab. 1. The calculations were conducted by Gauye *et al.* (2017) and Helfenberger *et al.* (2017), except for Trift Glacier. An annual technical potential of 1'171 GWh (from natural runoff, without pumped storage operation) is identified.

Tab. 1: Selected potential future hydropower plants

location [name of nearest glacier]	**annual production** [GWh]	**reservoir volume** [hm³]
Aletsch Glaciers (all)	180	106
Baltschieder Glacier	74	27
Gorner Glacier	119	34
Grindelwald Glacier	130	92
Hüfi Glacier (Maderan valley)	171	60
Rhone Glacier	98	23
Roseg Glacier	253	89
Trift Glacier	146*	85*
total	**1'171**	**516**

* www.grimselstrom.ch/ausbauvorhaben/projekt-speichersee-und-kraftwerk-trift

Feasibility is given in general. Narrow gorges and steep rocky slopes provide favourable technical conditions (Fig. 3). The adoption of the Energy Strategy 2050 is an indication of social acceptance of hydropower, and it improves economical constraints. Nevertheless, building site preparation will be costly, and the integration into the existing dense hydropower network will be a major challenge.

Fig. 3: Visualisation of a potential hydropower reservoir at Gorner Glacier, from Farinotti *et al.* (2016)

Conclusions

The goals of the Energy Strategy 2050 concerning electricity supply from hydropower could be achieved with eight new large-scale storage reservoirs in the periglacial environment by 2035.

Acknowledgements

This project is financially supported by the Swiss National Science Foundation (SNSF) within the National Research Programme 70 "Energy Turnaround" Project No. 153927.

References

Farinotti, D., Pistocchi, A. & Huss, M. (2016). From dwindling ice to headwater lakes: could dams replace glaciers in the European Alps? *Environmental Research Letters* 11(5) doi: 10.1088/1748-9326/11/5/054022
Gauye, F., Sartori, F. & Wydler, J. (2017). Wasserkraftpotential in der Schweiz aufgrund des Gletscherrückzugs. *Project Thesis*, VAW, ETH Zurich [in German; unpublished]
Helfenberger, M., Kannanmannil, R. & Klar, S. (2017). Wasserkraftpotential im Kanton Wallis aufgrund des Gletscherrückzugs. *Project Thesis*, VAW, ETH Zurich [in German; unpublished]
Huss, M. & Hock, R. (2015). A new model for global glacier change and sea-level rise. *Frontiers in Earth Science* 3. doi: 10.3389/feart.2015.00054

SWISS COMPETENCE CENTER for ENERGY RESEARCH
SUPPLY of ELECTRICITY

SCCER-SoE Annual Conference 2017

FlexSTOR

In cooperation with the CTI

Energy
Swiss Competence Centers for Energy Research

Commission for Technology and Innovation CTI

Fine sediment management at hydropower schemes considering turbine erosion

D. Felix, I. Albayrak, R. Boes – VAW, ETH Zürich

Introduction

Rivers transport sediment particles of various sizes depending on the catchment properties, the season and the weather (Fig. 1). This is a challenge in the design and operation of hydropower plants (HPPs). Sediment deposits reduce the active storage of reservoirs (Fig. 2) and may compromise the operational safety of dams. High concentration of hard sediment particles in the turbine water cause turbine erosion mainly in medium- and high-head HPPs (Fig. 3). This has negative effects on the energy- and cost-efficiency, and eventually on the availability and safety of HPPs.
To mitigate these negative effects, strategies for the sediment management at reservoirs and HPPs are of prime importance.

Fig. 1: Mountain stream transporting sediment (Wysswasser downstream of the Fieschergletscher, Valais; picture: VAW 2013) with microscope image of suspended sediment particles (IGT, ETH Zürich; Felix 2017).

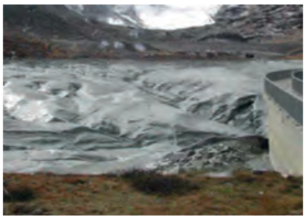

Fig. 2: Fine sediment deposits in a HPP reservoir (Reservoir Turtman, Valais; Schleiss 2005).

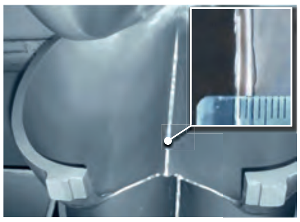

Fig. 3: Hydro-abrasive erosion on a Pelton turbine runner (HPP Fieschertal, Gommerkraftwerke AG; Felix 2017).

Reducing the sediment load in the turbine water of run-of-river HPPs by temporary shutdowns

During and after heavy precipitations (summer thunderstorms) the river discharge increases and the suspended sediment concentration (SSC) may rise by a factor of 100 compared to normal summer conditions. Moreover, coarser sediment particles are transported.
In such conditions, turbine erosion progresses faster than usual and the erosion-induced costs per kWh may exceed the electricity price.
If permitted by the regulatory framework and production obligations, it is therefore beneficial to close water intakes and to pause turbine operation in periods of high sediment load. Figure 4 shows an example of a shutdown scenario, which would have prevented consequential costs corresponding to almost 3% of the usual annual revenue.

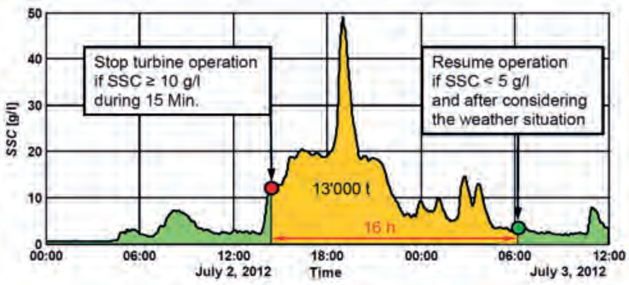

Fig. 4: Time series of suspended sediment concentration (SSC) in the power waterway of HPP Fieschertal during a major flood event with shutdown scenario. The orange area shows the sediment load which would have been prevented from passing the turbines (Felix 2017).

Increasing the fine sediment load in the turbine water of storage HPPs to reduce reservoir sedimentation

In reservoir lakes serving for seasonal storage, a large part of the incoming sediment particles settle. Hence, reservoir sedimentation is becoming a problem in the medium and long term.
There are various countermeasures to reduce the sediment input and to increase the sediment output from a reservoir. Occasional sediment release at the dam toe, as typically in flushing operations, causes temporarily high SSC which may have negative ecological effects. Another option to reduce reservoir sedimentation and avoiding such high downstream SSC, is to increase the fine sediment transport through the power waterway (Fig. 5). As a consequence, the sediment-induced costs due to erosion of hydraulic machinery increase. The target SSC in the turbine water results from an economic trade-off between these costs and the value of avoided or restored active storage.

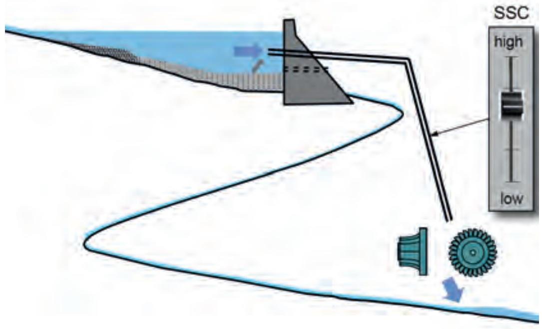

Fig. 5: Schematic of a storage HPP showing the option of increasing the suspended sediment concentration (SSC) in the turbine water to reduce reservoir sedimentation (Felix *et al.* 2017).

The SSC in the turbine water can be increased by reducing the sedimentation of particles inside the reservoir (e.g. by venting of turbidity currents or injection of water/air) or by hydraulic transport of fine sediment from the reservoir bottom in front of the power water intake (by hydro-suction or air-lift).

Conclusion and Outlook

Techniques to monitor the sediment situation (in real-time), turbine erosion and efficiency changes are available. Sediment and erosion data from field studies allow to calibrate and validate analytical models for turbine erosion prediction (e.g. IEC 62364 2013, Felix 2017).
In combination with economic analyses, such data and models serve as a basis to improve the operation of HPPs. Depending on the HPP layout, the natural conditions, and the time horizon for optimization, it is economically favourable to reduce or to increase the sediment concentration in the turbine water.

References

Felix D. (2017). Experimental investigation on suspended sediment, hydro-abrasive erosion and efficiency reductions of coated Pelton turbines. *Diss.* 24145 and *VAW-Mitteilungen* 238 (R. M. Boes, ed.), ETH Zürich.

Felix D., Albayrak I., Boes R. (2017). Weiterleitung von Feinsedimenten via Triebwasser als Massnahme gegen die Stauraumverlandung. *Wasser Energie Luft* 109(2): 85-90.

IEC 62364 (2013). Hydraulic machines - Guide for dealing with hydro-abrasive erosion in Kaplan, Francis and Pelton turbines. *International Electrotechnical Commission*, Geneva.

Schleiss A.J. (2005, ed.) INTERREG IIIB - Projet ALPRESERV. Conférence sur la problématique de la sédimentation dans les réservoirs - Gestion durable des sédiments dans les réservoirs alpins, *Communication* 22, LCH, EPFL.

SCCER SoE
SWISS COMPETENCE CENTER for ENERGY RESEARCH
SUPPLY of ELECTRICITY

SCCER-SoE Annual Conference 2017

In cooperation with the CTI
Energy
Swiss Competence Centers for Energy Research
Swiss Confederation
Commission for Technology and Innovation CTI

Blocking probability at spillway inlets under driftwood impact

Paloma Furlan, M. Pfister, J. Matos and A.J. Schleiss*
**corresponding author: paloma.furlan@epfl.ch*

Introduction

Large Woody Debris (LWD) have a great influence in the ecosystem and geomorphology of a river, but it can also be considered dangerous when entering in contact with hydraulic constructions (Fig 1).

Figure 1: Picture from downstream of San Clemente Dam, USA. (NOAA)

Accumulation and blockage of floating material at spillway inlets can lead to significant problems as it might interfere with the normal functioning of the structure and avoid the safe pass of a flood. If it continues to accumulate, effects of floods, scouring or sediment deposition will be intensified. Knowledge of LWD blockage process is vital regarding safety evaluation of dams.

The present research project aims to describe and quantify systematically the influence of LWD characteristics on the blocking process and the effects a blockage can have on the rating curve of an ogee crested spillway with piers.

Methodology and experiments

A physical model was designed and constructed in the facilities of LCH (Fig 2). An ogee crested spillway with round nose piers was chosen as it is a widely used structure and has a great ability to pass floods.

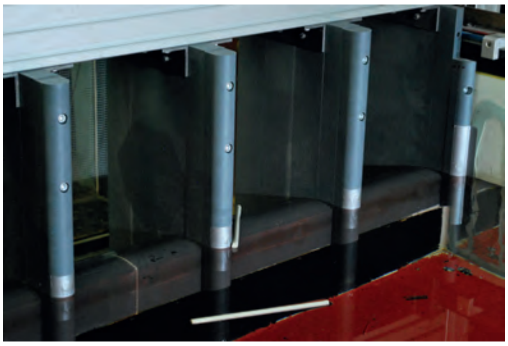

Figure 2: Picture from upstream of the experimental facility at LCH

Different configurations of experiments are being tested, always having a reservoir approach. In Fig 3, a single stem experiment can be seen.

Figure 3: Picture from above the experimental facility at LCH

Parameters

The aim is estimating blocking probabilities in relation to:

- **Number of experimental repetitions**;
- **Density** of floating material;
- **Length and diameter** of LWD;
- **Group influence** and interactions between LWD;
- Amount of functioning **bays**;
- **Volume** of LWD blocked and **head increase**;

Preliminary results

“How many times should an experiment be repeated until it gives reliable results?” It is a commonly asked question among researchers involved with LWD studies. Different mathematical tools can give a good overview of the accuracy achieved from an experiment by means of confidence intervals.

This question was approached with individual stem experiments where different hydraulic conditions were established and systematically tested. The results were considered binomial as a stem could pass or block and the blocking probability was computed as follows:

$$\Pi(i) = \frac{\sum blocked\ stems}{\sum provided\ stems}$$

To understand the influence of density for blocking probabilities different stem densities were tested with constant initial conditions. Fig 4 shows the blocking probabilities obtained for one stem in function of its density (normalized with the density of water) after 30 repetitions of the experiment.

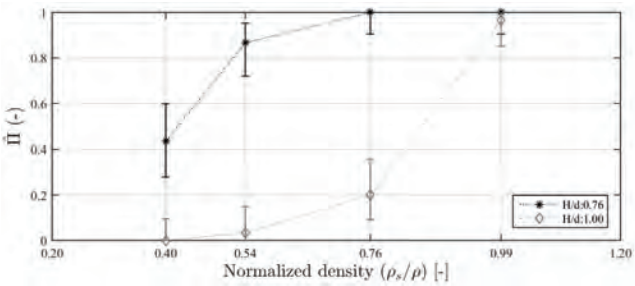

Figure 4: Blocking probability estimation in function of density

The different lines represent two different hydraulic conditions. It can be seen how an increment of density increases the blocking probability under the tested conditions for one size of stem.

Conclusions

Blocking probabilities of large woody debris is a random process, nevertheless with a statistical approach some open questions can be clarified. A wide spectrum of combinations has been tested to analyze the **replications** and its influence. For blockage experiments of individual stems, results can be considered statistically reliable at 30 repetitions (error in the estimation of blocking probability smaller than 0.09 with 90% confidence).

Systematic experiments to quantify the influence of **density** in blocking probabilities have been made and are being analysed. Different sizes of stems were tested with different transport regimes. In the next phase of work, analysis of **head increments** due to a blocked volume of large woody debris will be made.

Acknowledgments
This research project is developed in the scope of the Ph.D. Thesis by Paloma Furlan under the joint IST-EPFL doctoral program H2Doc. It is funded by the Portuguese Foundation for Science and Technology, LCH-EPFL and EDF.

SCCER SoE
SWISS COMPETENCE CENTER for ENERGY RESEARCH
SUPPLY of ELECTRICITY

SCCER-SoE Annual Conference 2017

In cooperation with the CTI
Energy
Swiss Competence Centers for Energy Research
Swiss Confederation
Commission for Technology and Innovation CTI

Exploitation optimale de la force hydraulique de la Plessur dans les Grisons (CH)

Thomas GLASSEY, Prof. Dr. A. J. SCHLEISS, Dr. G. DE CESARE, S. SCHWINDT
thomas.glassey@epfl.ch

Introduction

La Plessur s'écoule dans la vallée du Schanfigg d'Arosa à Coire dans le canton des Grisons. Actuellement, trois aménagements en cascade utilisent la force hydraulique de cette rivière. Les paliers supérieur (KW Litzirüti) et inférieur (KW Chur - Sand) ont été récemment rénovés. Les installations du niveau intermédiaire (KW Lüen) ont déjà plus de 100 ans et méritent une réhabilitation. De plus, une chute de 400 m entre les aménagements supérieur et inférieur reste inexploitée. Le but de ce projet est donc de proposer une variante permettant d'utiliser idéalement ce tronçon médian en tenant compte des contraintes extérieures et des aménagements existants.

Méthodologie

Après une étude du contexte, de l'environnement et des installations existantes, une analyse multicritère a été menée dans le but de définir le tracé optimal. Les aspects techniques, fonctionnels, économiques et environnementaux ont été pris en compte pour cet examen. Un pré-dimensionnement de neuf variantes a été réalisé sur la base d'hypothèses simplificatrices. Le passage en rive droite ou en rive gauche, l'utilisation d'affluents latéraux ou encore l'intégration de l'aménagement intermédiaire définissent les différents tracés.
La variante retenue a ensuite été dimensionnée jusqu'au stade d'avant projet.

Variante retenue

Galerie d'amenée principale		
Longueur	6752	m
Pente	4.00	‰
Diamètre d'excavation	3.40	m
Diamètre intérieur	≈ 2.85	m

Cheminée d'équilibre		
Niveau supérieur	1493.3	m
Niveau inférieur	1346.3	m
Oscillation maximale	1443.9	m
Oscillation minimale	1355.7	m
Diamètre de la cheminée	1.6	m
Diamètre de l'épanouissement	5.0	m
Hauteur de l'épanouissement	20.0	m

Site de Litzirüti - Plessur		
Rejet maximal de la centrale	3.0	m^3/s
Débit de la prise d'eau	5.0	m^3/s
Niveau de la prise d'eau	1390.0	msm
Capacité du dessableur Bieri	5.0	m^3/s

Bassin de compensation		
Volume total	67'000	m^3
Niveau maximal	1388.0	msm
Niveau minimal	1374.0	msm
Niveau de la prise d'eau	1371.8	msm

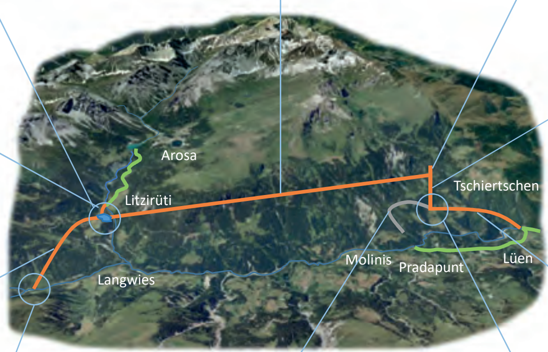

Puits vertical		
Hauteur du puits	554.6	m
Diamètre intérieur	1.6	m
Épaisseur du revêtement béton	40	cm
Diamètre de l'armature	16	mm
Espacement de l'armature	15	cm

Galerie d'amenée		
Longueur	2452	m
Pente	3.00	‰
Diamètre d'excavation	3.40	m
Diamètre intérieur	≈ 2.85	m

Galerie de fuite		
Longueur	2540	m
Pente	3.00	‰
Diamètre d'excavation	3.40	m
Diamètre intérieur	≈ 2.85	m

Site sur le Sapünerbach et Fondeierbach		
Débit de la prise d'eau	3.5	m^3/s
Niveau de la prise d'eau	1400.0	msm
Capacité du dessableur Bieri	3.5	m^3/s

Galerie d'accès à la centrale		
Longueur	3489	m
Pente	10.0	%
Diamètre d'excavation	6.20	m

Centrale souterraine		
Débit équipé	2 x 4.25	m^3/s
Puissance installée	44.57	MW
Axe des turbines	785.0	msm
Diamètre des turbines Pelton	2.21	m
Nombre d'augets	26	-
Épaisseur du blindage	54	mm

Fig. 1: Présentation de la variante retenue

Production et aspects économiques

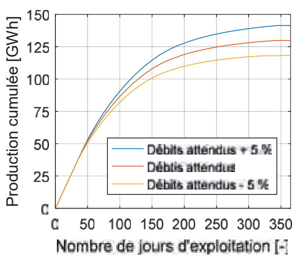

Fig. 2: Production annuelle attendue

Aspects économiques		
Coûts de construction	244.0	Mio CHF
Durée des travaux	env. 2	ans
Volume des excavations	330'000	m^3
Chute brute maximale	603.0	m
Chute nette maximale	592.1	m
Production annuelle	129.9	GWh/an
Pertes pour KW Lüen	20.5	GWh/an
Prix de revient par kWh	15.92	Ct./kWh
Investissement par KW	5475	CHF/kW

Tab. 1: Aspects économiques de la variante retenue

Conclusion

La variante retenue demande la mise en place de moyens de construction lourds. De plus, l'investissement initial est conséquent. Ceci induit un risque financier accru pour la réalisation du projet. Le prix de revient est lui aussi relativement élevé.

Malgré ces incertitudes économiques, la variante retenue exploite de manière optimale le grand potentiel de la vallée du Schanfigg et permet d'accroître de manière significative la production hydroélectrique locale et indigène. Le bénéfice escompté tend donc à dominer le risque financier.

SCCER SoE
SWISS COMPETENCE CENTER for ENERGY RESEARCH
SUPPLY of ELECTRICITY

SCCER-SoE Annual Conference 2017

In cooperation with the CTI
Energy
Swiss Competence Centers for Energy Research
Schweizerische Eidgenossenschaft
Confédération suisse
Confederazione Svizzera
Confederaziun svizra
Swiss Confederation
Commission for Technology and Innovation CTI

Air demand of bottom outlets

Benjamin Hohermuth, Lukas Schmocker, Robert Boes – VAW, ETHZ

Motivation and Objectives

Bottom outlets are a key safety feature of large dams. Future demands on bottom outlets will likely increase due to (i) dam heightening as promoted by the Swiss energy strategy 2050 and (ii) more frequent sediment flushing due to increasing reservoir sedimentation rates. Bottom outlets frequently encounter problems with cavitation damage, gate vibration and flow chocking. These problems can be mitigated by sufficient aeration. However, current knowledge does not allow for a coherent design of the air vent. This project aims to improve air demand design equations by including the effects of

- Energy Head H_E
- Relative gate opening a/a_{max}
- Air vent loss coefficient ζ
- Tunnel length L
- Tunnel slope S_o

Hydraulic model tests

The hydraulic Froude scale model has an approximate scale of 1:5 to 1:10, thereby representing a typical bottom outlet in Switzerland. It features a rectangular tunnel cross-section with a maximum length of 20.7 m (Fig. 1). Two high-head pumps deliver a discharge Q_w up to 600 l/s at an energy head H_E of 30 m w.c. at the gate. The investigated parameter range is shown in Figure 2.

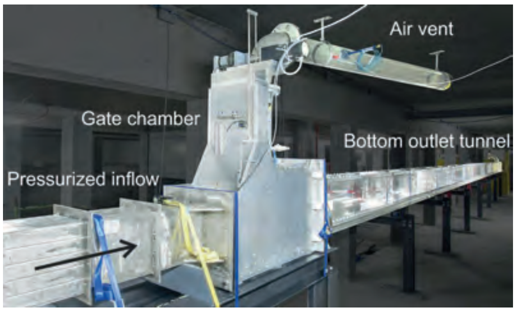

Fig. 1: Hydraulic scale model at Laboratory of Hydraulics, Hydrology and Glaciology (VAW)

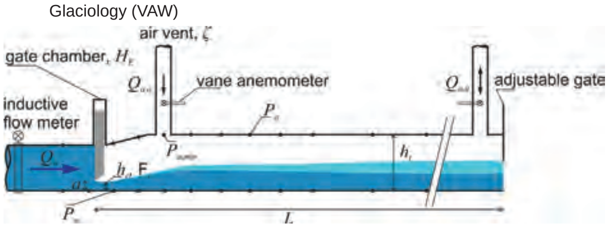

Fig. 2: Model setup and notation

Tunnel width	W = 0.2 m	Relative gate opening	a/a_{max}= 0.1 - 0.8
Tunnel height	h_t = 0.3 m	Water discharge	Q_w = 60 - 600 l/s
Tunnel length	L = 20.6, 12.6, 6.6 m	Air vent loss coefficient	ζ = 0.7 - 37
Energy head	H_E = 5 - 30 m w.c.	Tunnel slope	S_o = 0 - 0.03

Results

Air discharge through the air vent $Q_{a,o}$ increases with increasing H_E (Fig. 3a, c). An increase in $Q_{a,o}$ is observed for small a/a_{max} due to the formation of spray flow (Fig. 3a). $Q_{a,o}$ increases with increasing a/a_{max} for free surface flow conditions at moderate gate openings. For large a/a_{max} and high H_E, $Q_{a,o}$ drops considerably due to the formation of foamy flow (full flowing tunnel, Fig. 3a).

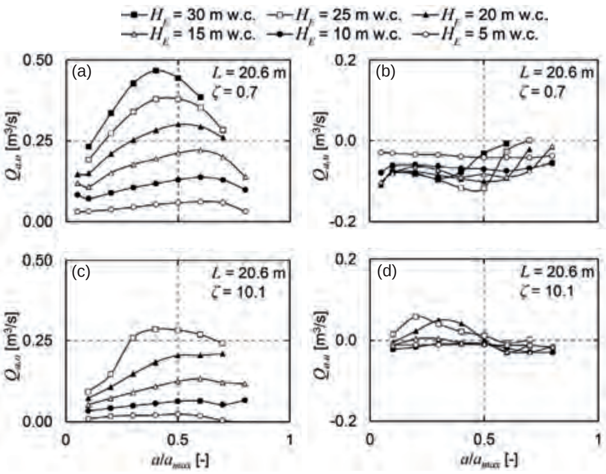

Fig. 3: Air discharge through air vent (a), (c) and from tunnel end (b), (d) as a function of relative gate opening for different energy heads and air vent loss coefficients.

The air discharge from the tunnel end $Q_{a,u}$ is always negative, indicating that air is flowing out of the tunnel for the given tunnel configuration (Fig. 3b). An increase in ζ leads on the one hand to an overall decrease in $Q_{a,o}$ (Fig. 3c). On the other hand $Q_{a,u}$ increases and the positive values indicate air flowing into the tunnel, leading to a counter-current air flow (Fig. 3d). A similar effect is observed if the tunnel length is reduced. Strong counter-current air flows, especially in long tunnels, can lead to intermittent flow chocking.

Discussion and Outlook

Air demand is usually defined as the ratio between the air and the water discharge $\beta = Q_a/Q_w$. For a given tunnel and air vent geometry, β is mainly a function of the Froude number at the vena contracta F_c (Fig. 4). However, the fits are shifted downwards with increasing ζ (Fig. 4a) and decreasing L, respectively (Fig. 4b).

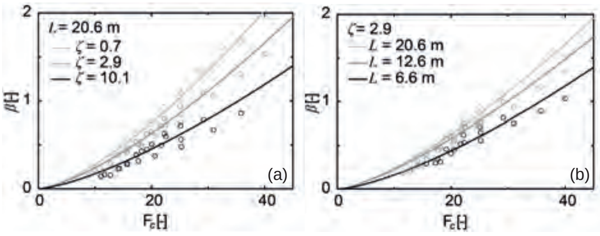

Fig. 4: Air demand β as a function of F_c for (a) increasing air vent loss ζ and (b) decreasing tunnel length L.

These preliminary results show that hydraulic model tests can be used to investigate the effect of different – previously not considered – parameters on the air demand. Thus, the design and the operational safety of bottom outlets can be improved with systematic experimental modelling techniques.

Acknowledgement

This project is financed by the Swiss National Science Foundation (Grant Nr. 163415) and is embedded in the Swiss Competence Centre for Energy Research - Supply of Energy (SCCER-SoE) framework.

SCCER SoE
SWISS COMPETENCE CENTER for ENERGY RESEARCH
SUPPLY of ELECTRICITY

SCCER-SoE Annual Conference 2017

70 NRP Energy Turnaround
National Research Programme

In cooperation with the CTI
Energy
Swiss Competence Centers for Energy Research
Swiss Confederation
Commission for Technology and Innovation CTI

Hydropower potential at *Rhône Glacier*

Valeria Hutter, Daniel Ehrbar, Lukas Schmocker, Daniel Farinotti, Robert Boes – VAW ETH Zurich

Introduction

Climate change causes glacier retreat, and recently glaciated locations become ice-free. These sites may be used for hydropower production. The Swiss Energy Strategy 2050 supports additional production within the periglacial environment. *Rhône Glacier* is a potential site for a future hydropower plant, as a new lake – *Rottensee* – starts forming.

Boundary conditions

On 21 May 2017, the first package of measures of Energy Strategy 2050 was accepted by popular vote. Large-scale hydropower shall become more competitive again by means of investment subsidies, market premium or status of national interest.

Important boundary conditions that need to be taken into account within the project perimeter are:
- pasture landscape,
- BLN object 1710 "*Rhône Glacier* with forefield",
- the already existing hydropower network,
- tourism at *Rhône Glacier*, and
- the future runoff evolution due to climate change

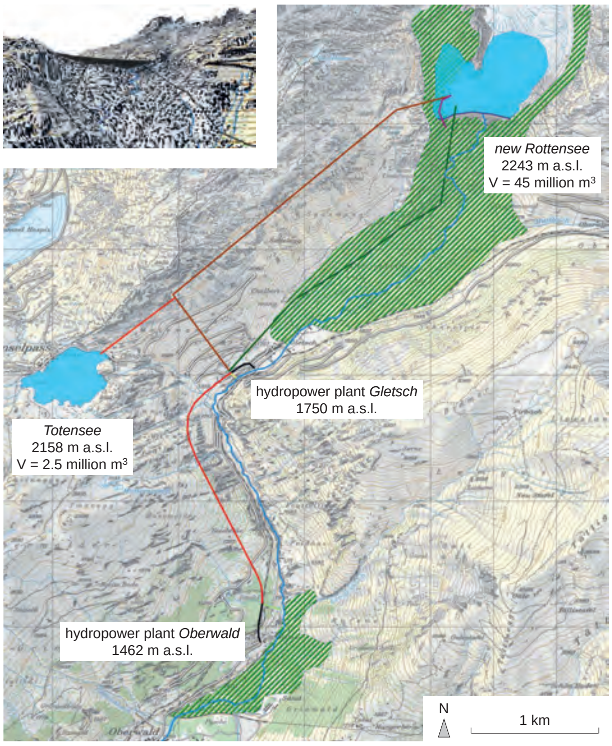

Fig. 1: Topographical map of the project perimeter with the different parts of the project and the most relevant boundary conditions (in red: power waterways, in green: floodplain / meadow) [© swisstopo]
inset: Visualisation of the dam as seen from *Furka* pass [© swisstopo]

Concepts

Different concepts were developed and compared to each other by applying a rating matrix, accounting for economy, environment, and society. The selected concept is sketched in Fig. 1, integrating the new *Rottensee* into the existing hydropower network.

Layouts and dimensions

4 different layouts were investigated for the best concept. Governing factors are:
- design discharge and number of turbines,
- ratio of reservoir volume to annual inflow,
- hydraulic head, and
- location of waterways (surface or underground).

Reservoir
The reservoir will have a volume of circa 45 million m³ in 2065; the dam height will be 38 m (Schleiss 2017). Due to earthquake risks and topographical constraints, a gravity dam is recommended.

Discharge
A semi-baseload power station with more than 4'000 production hours per year will result in a design discharge of circa 3.1 m³/s at *Rottensee* and 0.25 m³/s at *Totensee*.

Head
Maximum head is 493 m at *Rottensee* and 408 m at *Totensee*.

Cost estimate
Costs vary between circa 150 and 160 million CHF, depending on the chosen layout (Fig. 2).

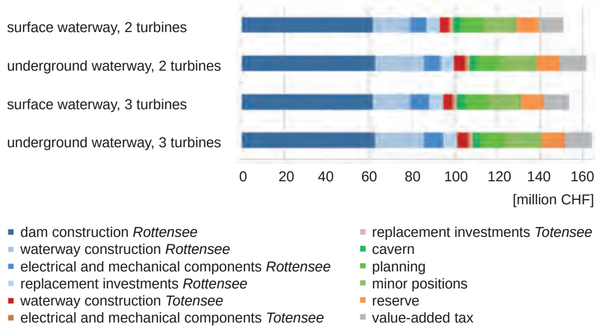

Fig. 2: Cost estimates for four layouts, based on Steiner & Vetsch (2010), Alvarado-Ancieta (2012), and VAW (2015)

Conclusions

A new reservoir for hydropower production could be built at *Rhône Glacier*. It would result in a production of ca. 55 GWh/a. Production costs would be 0.12–0.18 CHF/kWh, depending on the layout.

Acknowledgements

This project is financially supported by the Swiss National Science Foundation (SNSF) within the National Research Programme 70 "Energy Turnaround" Project No. 153927. The collaboration of Forces Motrices Valaisannes (FMV) is gratefully acknowledged.

References

Alvarado-Ancieta, C. (2012). Kostenschätzung 2012 für die elektrische und mechanische Ausrüstung des Krafthauses in Wasserkraft- und Pumpspeicher-Projekten. *Wasserkraft & Energie* Heft 3: 12-35
Boes, R. M. (2015). Wasserbau II. *Skript*, ETH Zürich
Schleiss, A. (2017). Die Bedeutung des Ausbaus alpiner Speicherseen für eine sichere und konkurrenzfähige Stromversorgung. *Energie-Apéros 2017*, Brig
Steiner, M. & Vetsch, H. (2010). Druckleitungen für Wasserkraftanlagen. *Bachelorarbeit*, VAW, ETH Zürich
VAW (2015): Kostengrundlage studentische Arbeiten. *VAW*, ETH Zürich

SCCER SoE
SWISS COMPETENCE CENTER for ENERGY RESEARCH
SUPPLY of ELECTRICITY

SCCER-SoE Annual Conference 2017

In cooperation with the CTI
Energy
Swiss Competence Centers for Energy Research
Commission for Technology and Innovation CTI

Online prediction tool for hydropower energy (Opt-HE)

Dr F. Jordan, Dr G. Artigue (Hydrique Engineers)
K. Cros, C.-A. Loetscher, O. Etter, Prof. Dr A. Schleiss (LCH-EPFL)
fred.jordan@hydrique.ch

hydrique.

ETH zürich

EPFL

The OPT-HE project

OPT-HE : Optimal Prediction Tool for HydroElectricity

Hydrological prediction is a key factor in the optimization of hydropower production, by limiting the water spillings and increasing the water value. These objectives are perfectly in line with the *Energy Strategy 2050,* allowing an increase of the total electricity production with no new impact on the environment.
The partners of the project are five hydropower suppliers, MeteoSwiss and Hydrique Engineers.
The research is realized by Hydrique Engineers, the Laboratory of Hydraulic Constructions (EPFL) and the Institute for Climate and Atmosphere (ETHZ).

Structure of the project

The existing forecasting system at Hydrique Engineers is based on rainfall-runoff simulation, combining the assimilation of discharge gauging stations and human expertise. All these single processes are to be optimized within this project. Four workpackages are completed: general methodology, weather forecast, hydrological processes, operation.

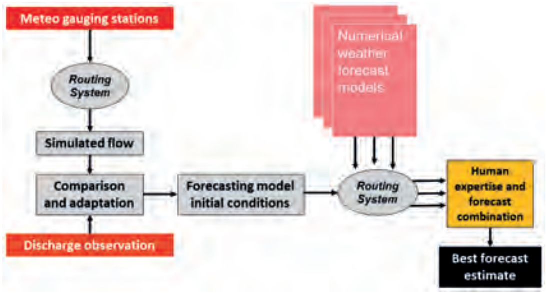

Outcomes

For this project, various tests have been realized, focusing on the specific characteristics of the catchment areas. As the existing system already had a satisfying performance, it was difficult to highlight improvements in the different methods showing a high performance. Out of the 18 different methods tested within the simulation and operation processes, 5 methods have been directly implemented. 3 additional methods, with less impact, have also been applied in the operational forecasting system at Hydrique.

Type of catchment area	Glacier	Prealpine	Jura-region	Added value
Temperature forecast bias	In operation			Very good
Analysis of the sources of forecast error		In operation	In operation	Very good
Influence of new precipitation stations			Rejected	Poor
Glacier model postprocessing with spline correction	In operation			Very good
Discharge assimilation in automatic correction	In operation	In operation	In operation	Very good
Uncertainty quantification and forecast	In operation	In operation	In operation	Very good
Combined glacier model with simulation and machine learning	In operation			Good
Assimilation of CombiPrecip data		Rejected	Rejected	Poor
Precipitation forecast quality assessement		In operation	In operation	Good
Pre-processing of stochastic weather forecast (COSMO-E)	In operation	In operation	In operation	Good
Seasonal forecasting	Rejected	In operation		Good
Precipitation forecast bias		Rejected	Rejected	Poor
Assimilation of COSMO-1 high-resolution forecast		In operation	In operation	Good
Use of COSMO-E instead of sensitivity method for the uncertainty prediction	Rejected	Rejected	Rejected	Poor
Short-term precipitation forecast by combination of observation and numerical weather forecast	Rejected	Rejected	Rejected	Poor
Post-processing of runoff forecasts using previous runs	Rejected	Rejected		Poor
Validation tests of the combined new methods	In operation	In operation	In operation	Very good
Inflow forecast by neural networks	Rejected	Rejected	Rejected	Poor
Influence of vegetation cover interception	Rejected	Rejected	Rejected	Poor

Correction of temperature biases

One of the major source of uncertainty in the inflow prediction for glacier catchments is due to the air temperature forecast. The direct model outputs (light blue) cannot be used. The choice of selected model outputs at locations different from the station, including a systematic bias correction, provide better results (blue and orange lines).
The figure below shows the multiannual bias for the Zermatt station for the COSMO7 model, over 7 years of analysis.

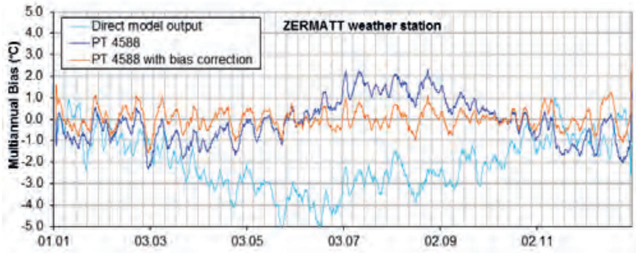

Assimilation of COSMO1 precipitation forecast

The increasing resolution of meteorological models requires an improved integration of the direct model output into the rainfall-runoff model. Indeed, the new assimilation method (*bandes*) attributes model grid points according to the real geometry of the catchment area. In some cases, it provides slightly better outcomes.
The figure below shows the improvements obtained by this method. Both the HIT (proportion above a threshold) and FAR (proportion below a threshold) indicators could be improved at the Montsalvens catchment area in the Sarine river.

HIT and FAR indicators for COSMO2 forecasts at Monsalvens (Sarine river)

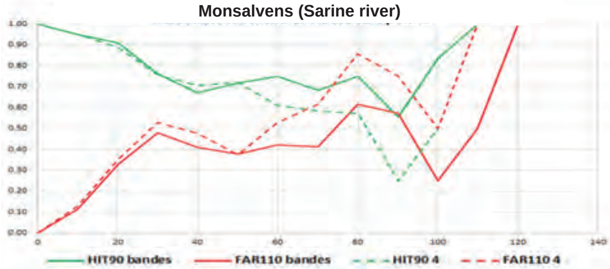

New method for the uncertainty range forecast

Three different models were tested to produce an uncertainty range for the prediction (CI), like statistical confidence interval, quantiles out of probabilistic weather models (COSMOE quantiles) and preliminary meteorological forcing (± 2°C and ± 20% precipitation). The preliminary meteorological forcing of precipitation and temperature results in thinner uncertainty range than the two other methods, for a similar success rate.

Uncertainty range at the Massa river catchment

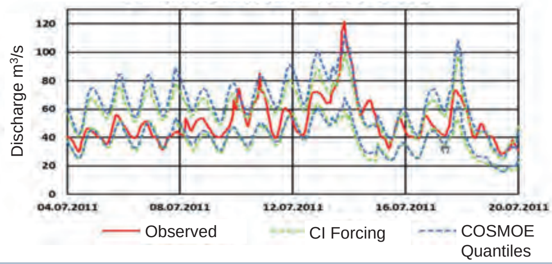

SCCER-SoE Annual Conference 2017

In cooperation with the CTI

Energy
Swiss Competence Centers for Energy Research

Swiss Confederation
Commission for Technology and Innovation CTI

SWISS COMPETENCE CENTER for ENERGY RESEARCH
SUPPLY of ELECTRICITY

Utilisation optimale du potentiel hydroélectrique d'un bassin versant alpin: le barrage de Khudoni en Géorgie

Jordan M. [(1)(2)], *Venuleo S.* [(1)], *Manso P. A.* [(1)], *Schleiss A. J.* [(1)]

[(1)] Ecole Polytechnique Fédérale de Lausanne (EPFL), Laboratoire de Constructions Hydrauliques(LCH); [(2)] KBM SA, Sion; corresponding author: sara.venuleo@epfl.ch

Objectifs

Contexte local	
Pays	Géorgie
Province	Svanétie
Apports moyens annuels (réf. Site 1)	3847 hm³
Bassin versant	Enguri (2780 km²)
Production de sédiments	97 kg/sec. En 1976
Magnitude (Richter)	M=9
Début du projet/Arrêt	1979/1989
Avancement de la réalisation en 1989	25% des travaux
Restauration du projet	2005

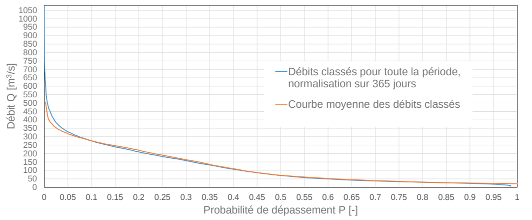

- Les constructions existantes (25%) ont biaisé le choix du site du barrage.
- Les impacts socio-environnementaux liés à l'inondation de Khaishi sont inacceptables.

Etude de variantes

- Pour l'étude de variantes, **trois sites** différents de barrage, avec des concepts d'exploitation de stockage et au fil de l'eau sont évalués, en faisant varier à la fois la hauteur de la retenue et la typologie de la centrale.

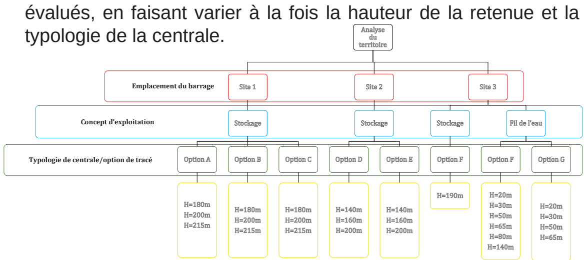

Analyse multicritères

- Après un tri préliminaire, les variantes sont évaluées à partir de critères quantitatifs avant d'utiliser une même échelle de notation de 0 à 100 points pour chaque critère.
- Le **site 1** en amont de Khaishi et en aval de la confluence avec la rivière de Nenskra est retenu et représente une alternative au concept soviétique initial.

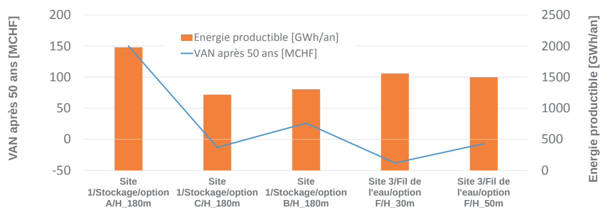

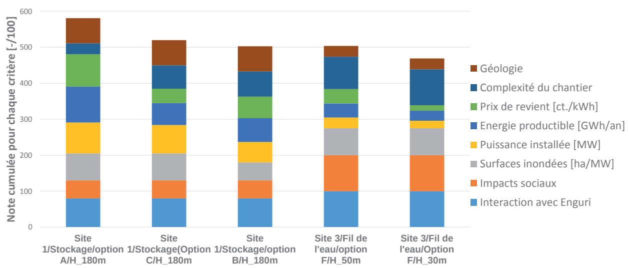

Concept et variante retenue

- Une variante avec **concept d'exploitation de stockage** avec une **gestion intra-annuelle au fil de l'eau en été** est choisie.
- L'énergie de pointe est fournie en été, avec des exportations vers la Turquie, l'Arménie, la Russie, et l'Azerbaïdjan.

Variante retenue	
Hauteur du barrage	182m
Volume utile de la retenue	96 hm³
Hauteur tranche morte/durée de vie utile	56m/93 ans
Puissance installée	551 MW (3 groupes Francis de 184 MW)
Débit équipé	310 m³/s
Energie productible annuelle	2008 GWh/an
Coût total/Coût du barrage	1.08 GCHF/434 MCHF
Gains annuels	100 MCHF
Prix de revient après 50 ans (i=8%)	4.1 ct./kWh
Zones inondées	445 ha/MW
Déplacement de population	Village de Lukhi/Env. 40 personnes
Durée des travaux	7 ans
Nouvelles infrastructures d'accès	2 ponts/1 tunnel/env. 10km de nouvelles routes

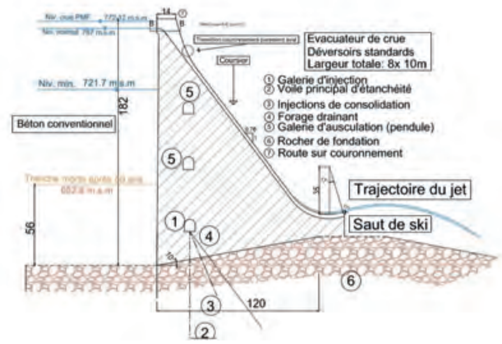

Discussion

- La retenue peut être remplie **40 fois durant une année.**
- Le nouveau concept de Khudoni permet une puissance installée de 551 MW.
- Une puissance moyenne annuelle de 228 MW pour un **marnage faible de 40m.** Puissance moyenne en février: 46 MW
- La variante grand barrage pour maximiser la chute et la puissance installée.
- Cascade de la rivière d'Enguri avec les aménagements d'Enguri (1300 MW) et de Vardnili (340 MW) à l'aval de Khudoni.
- Projet compatible avec une extension future sur le site 3, à l'aval
- **Stratégie 1**: Maximiser la puissance installée
- **Stratégie 2**: Maximiser l'énergie annuelle productible
- **Stratégie 3**: Minimiser les investissements
- Un plan opérationnel de gestion de sédiments avec un tunnel de by-pass est nécessaire.

Remerciements

Un grand merci au bureau ***Stucky SA*** de Renens pour les données de base hydrologiques qui ont permis la réalisation de cette étude et en particulier au chef de projet Juliano Ribeiro pour son aide.

SCCER SoE
SWISS COMPETENCE CENTER for ENERGY RESEARCH
SUPPLY of ELECTRICITY

SCCER-SoE Annual Conference 2017

FlexSTOR

In cooperation with the CTI
Energy
Swiss Competence Centers for Energy Research
Swiss Confederation
Commission for Technology and Innovation CTI

Operation changes of a complex hydropower system over decades

J. P. Matos [(1)], P. A. Manso[(1)], B. Schaefli[(2)] and A.J. Schleiss[(1)]

(1) Laboratoire de Constructions Hydrauliques, Ecole Polytechnique Fédérale de Lausanne (LCH-EPFL)
(2) Institut des Dynamiques de la Surface Terrestre (IDYST-UNIL)
Contact person: jose.matos@epfl.ch

Motivation

Both the production and consumption of electricity are undergoing profound changes. If the disruption caused by new technologies and the political shift towards renewable sources, as well as societal awareness of climate change, have modified the energy market and will likely to continue to do so, the changing climate has the potential to affect hydrology, both directly the precipitation [1] and, even more so, snow and ice melt. It is important to understand the past to understand how complex hydropower systems may adapt to a quickly changing world.

Case study

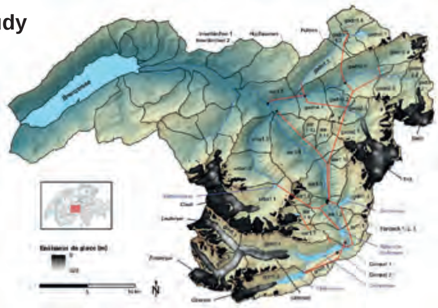

Fig 1. The KWO system and estimated glacier cover in 1993 [2].

Here, the Kraftwerke Oberhasli AG (KWO) hydropower system (Fig. 1) is viewed from production and market perspectives.

- 10 power plants,
- 29 turbines,
- 1368 MW.
- 4 main reservoirs.

Energy market

Since its inception, the SPOT energy price has decreased. It evidences clear seasonal (Fig. 2), weekly, and daily trends that can be exploited by hydropower schemes with storage and pump-storage capabilities.

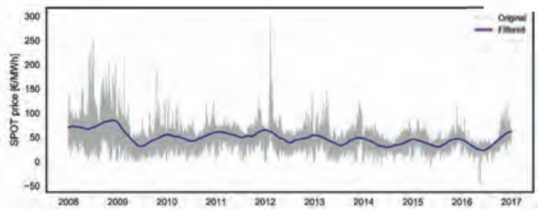

Fig 2. SPOT energy prices in Switzerland (day-ahead, www.epexspot.com).

Hydrology

The overall water available to the system did not undergo dramatic changes over the last decades (Fig. 3).

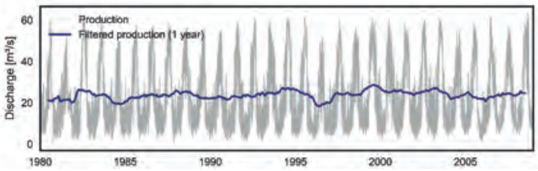

Fig 3. Historical KWO outflows (Innertkirchen 1 plus 2).

Acknowledgements

We are thankful for the support provided by KWO and the Swiss Commission for Technology and Innovation (CTI), which provided the bulk of the funding through project 17902.3 PFIW-IW.

But part of the inflows are due to glacier melting (Fig.4), which will eventually run out as the snow and ice cover reaches an equilibrium [3] .

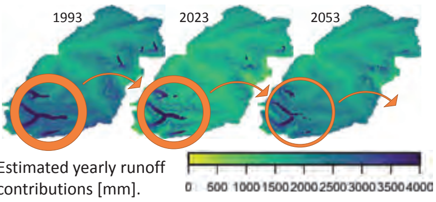

Fig 4. Estimated yearly runoff contributions [mm].

The system: results and conclusions.

Looking at the fluxes of the system (Sankey plot, Fig. 5) and clustering techniques (K-means, Fig. 6), one can isolate the main modes of operation. Insight is gained into daily, seasonal, and long term operations (Fig. 7). According from Fig. 7, pump-storage operations (e.g. Oberaar-Grimsel) have changed more significantly than the lower part of the cascade.

Since 1980, the system has responded much more to energy demand and market than to hydrology. Increasingly, the system adapts to seize intra-weekly and intra-daily opportunities.

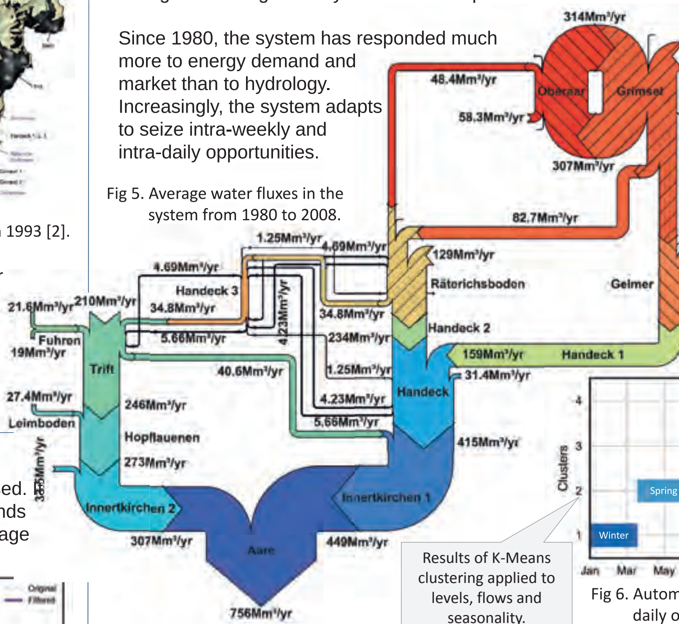

Fig 5. Average water fluxes in the system from 1980 to 2008.

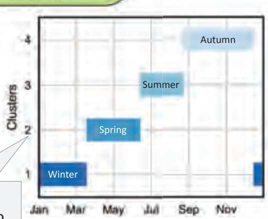

Results of K-Means clustering applied to levels, flows and seasonality.

Fig 6. Automatic clustering of daily operations.

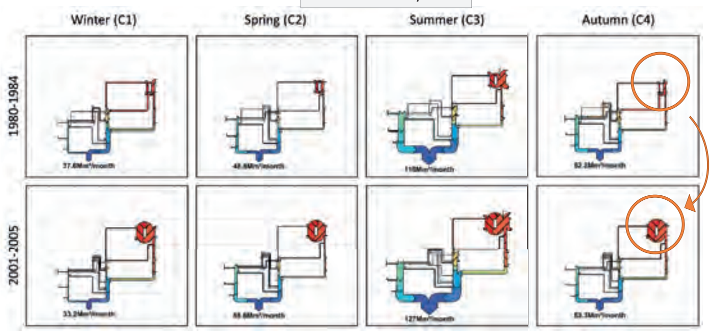

Fig 7. Evolution of the system through time; early 1980's vs early 2000's.

References

[1] G. Blöschl et al., Changing climate shifts timing of European floods. Science, 357 (6351), 2017.
[2] M. P. Bieri, Operation of Complex Hydropower Schemes and its Impact on the Flow Regime in the Downstream River System under Changing Scenarios. Thèse EPFL, n° 5433, 2012.
[3] S. Terrier et al., Impact du retrait glaciaire et adaptation du potentiel hydroélectrique dans les Alpes suisses, La Houille Blanche, 2015 (1).
[4] Matos et al., The operation of a complex Alpine hydropower scheme across four decades (working title), in preparation.

SCCER-SoE Annual Conference 2017

SCCER SoE
SWISS COMPETENCE CENTER for ENERGY RESEARCH
SUPPLY of ELECTRICITY

In cooperation with the CTI
Energy
Swiss Competence Centers for Energy Research
Swiss Confederation
Commission for Technology and Innovation CTI

Evaluation du potentiel d'augmentation du stockage saisonnier d'énergie en Suisse en vue des changements climatiques

Monay Blaise, Dr. Manso Pedro, Dujardin Jérôme, Dr. Massimiliano Zappa, Prof. Schleiss Anton
Laboratoire de Constructions Hydrauliques, EPFL, Station 18, CH-1015 Lausanne

Approche

L'énergie d'origine hydraulique en Suisse représente plus de 60% de la production totale d'énergie pour un réseau hydrographique quasiment exploité à son maximum. La capacité des lacs d'accumulation ne représente que 42% de leur production totale annuelle, ce qui conduit les centrales à accumulation, à la fin du semestre d'été, à devoir turbiner les apports au fil de l'eau. Une partie de la production d'énergie ne peut, par conséquent, pas être concentrée sur le semestre d'hiver, ce qui conduit la Suisse à devoir importer massivement de l'électricité. La capacité de stockage d'énergie doit par conséquent être augmentée, elle permettra également de soutenir le développement des énergie renouvelables et l'abandon du nucléaire dans le cadre de la Stratégie Energétique 2050.

Evaluation du potentiel d'augmentation du stockage saisonnier

La capacité de stockage saisonnière d'un aménagement est définie comme suit:

$$CSS = CE * V_{Utile}$$

CSS : Capacité de stockage saisonnière [GWh]
CE : Coefficient énergétique [kWh/m³]
V_{Utile} : Volume utile [hm³]

L'évaluation du potentiel d'augmentation de la capacité de stockage saisonnière (CSS') est effectuée par la mesure des surfaces entre les courbes de niveaux des bassins versants des retenues.

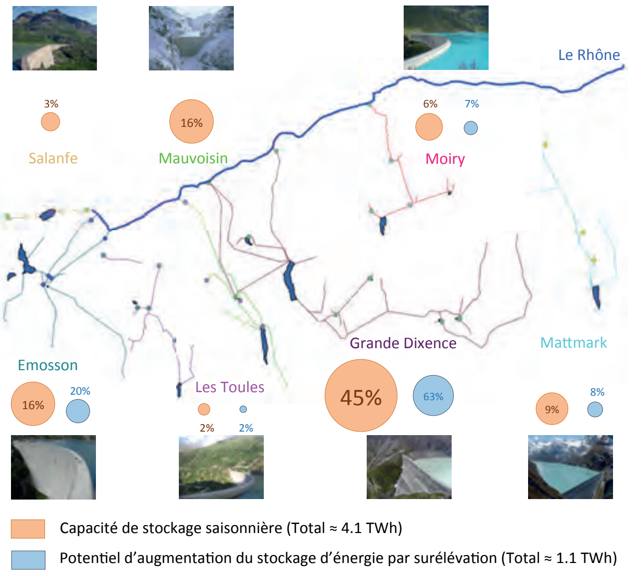

Le modèle hydrologique PREVAH et scénarios d'écoulements futurs

Le modèle hydrologique PREVAH permet d'évaluer les apports en eaux des retenues. Des coefficients de correction mensuels aux prises d'eau sont appliqués en comparant les données de PREVAH aux données de pompage afin de corriger les imprécisions du modèle, principalement dues aux débits résiduels des rivières, à la capacité limitée des prises d'eau et aux périodes de crues.

$$Apports\ totaux = \int_a^A \sum_{i=1}^{12} \left[\sum_{j=1}^{n} Q_{i,j} \cdot S_j + \sum_{j=1}^{p} \psi_{i,j} \sum_{k=1}^{t} Q_{i,j,k} \cdot S_k \right]$$

a & A: Première et dernière année de la période
n,p & t: Nombre de sous-bassins versants naturels, prises d'eau, sous-bassins versants de la prise d'eau
Q: Débit de ruissellement du sous-bassin versant natuel [hm³/km²]
S: Surface du sous-bassin versant [km²]
ψ : Coefficient de captage de la prise d'eau, $\psi \in [0; 1]$

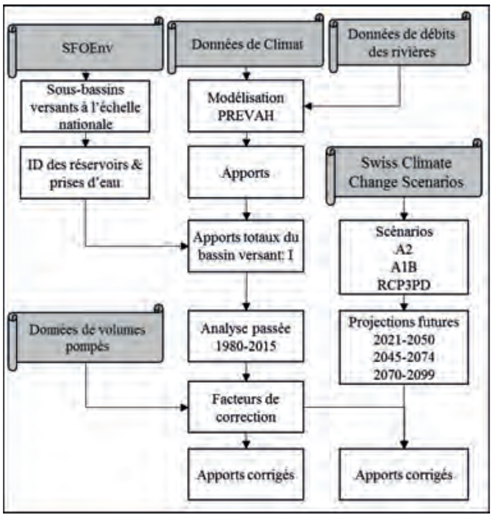

Les volumes d'apports annuels des aménagements de Grande Dixence, Mauvoisin, Mattmark et Moiry à l'horizon 2100 sont présentés ci-dessous (les lignes horizontales représentent le volume utile des aménagements) :

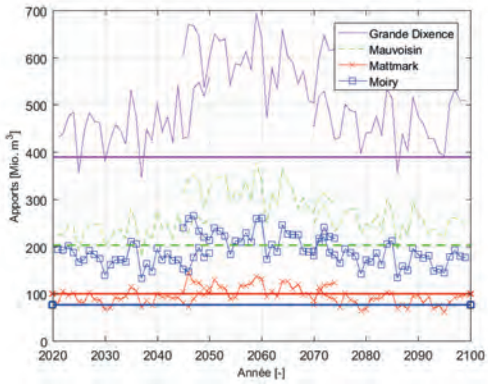

Conclusions et perspectives

- La rive gauche du Rhône présente une capacité de stockage saisonnière de **4.2 TWh**, avec un potentiel d'augmentation de plus de **1 TWh** d'énergie.
- Davantage de volume utile est nécessaire afin de minimiser le turbinage au fil de l'eau des centrales à accumulation, en particulier pour la **période 2045-2074**.
- La retenue du **lac des Dix** est la plus favorable au stockage saisonnier, son coefficient énergétique est le plus élevé de la rive gauche du Rhône.
- L'**aménagement de la Grande Dixence** présente la plus importante augmentation de stockage saisonnier. Pour exploiter pleinement ce potentiel, des projets de pompage s'avèrent nécessaires.

SCCER-SoE Annual Conference 2017

SCCER SoE
SWISS COMPETENCE CENTER for ENERGY RESEARCH
SUPPLY of ELECTRICITY

In cooperation with the CTI
Energy
Swiss Competence Centers for Energy Research
Commission for Technology and Innovation CTI

Confortement d'un barrage poids en maçonnerie présentant une légère courbure en plan : Le barrage de Cenne-Monestiés

A.Nicolle, S. Chamoun, P. A. Manso, A.J. Schleiss
Ecole Polytechnique Fédérale de Lausanne, Laboratoire de Constructions Hydrauliques (LCH), armelle.nicolle@epfl.ch

Objectifs

En raison d'une revue à la hausse de l'hydrologie et malgré un confortement ultérieur à l'aide de tirants précontraints appliqué en 1966, le barrage de Cenne-Monestiés (France) ne respecte plus les critères de stabilité et de sécurité actuels et nécessite un confortement.

Contexte

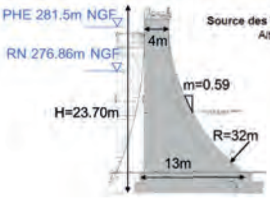

Coupe type

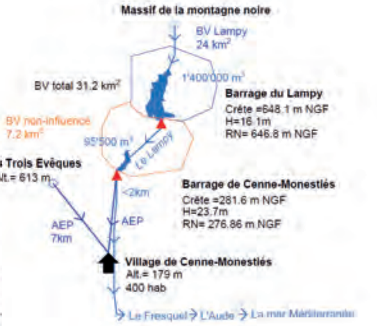

Schéma du système

Caractéristiques	
Type	Barrage poids en maçonnerie, courbure en plan
Date de construction	1883
Rivière	Le Lampy
Usage	Alimentation en eau potable (AEP)
Hauteur sur fondation	23,7m
Longueur en crête	95m
Rayon de courbure en plan	250m
Surface du bassin versant	31.2km²
Capacité utile du réservoir	95 500m³
Organes hydrauliques	Déversoir à seuil libre, 4 pertuis de vidange, 1 prise d'eau

Etude des variantes de confortement

Variante 1: Tirants post-contraints

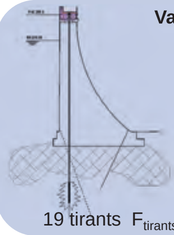

- L'accès au site est difficile et les tirants nécessitent une mise en œuvre légère.
- Les tirants existants limitent les possibilités de disposition.
- Ils exigent un entretien et suivi particuliers et sont sensibles aux infiltrations.

19 tirants $F_{tirants}$=3,6 - 6MN **Co*= 0,8 MCHF**

Variante 2: Epaulement aval

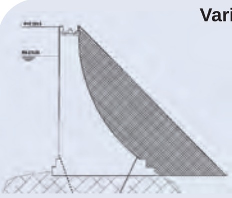

- La solution en béton apporte plus de sécurité en cas de surverses que des matériaux meubles.
- L'épaulement permet l'intégration de galeries et réadaptation des organes hydrauliques.
- Le volume de matériaux à mobiliser est important.

Vol. béton= 7900m³ **Co= 2 MCHF**

Variante 3: Inclinaison amont

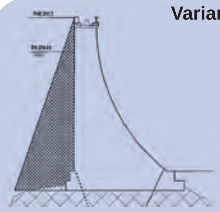

- L'étanchéité du mur amont est réhabilitée.
- Offre la possibilité d'intégrer une galerie au pied amont pour mieux contrôler la fondation.
- Les travaux à l'amont perturberont l'AEP du barrage qui est l'unique captage (la source étant polluée).

Vol. béton= 4000m³ **Co= 1,2 MCHF**

**Co = coûts de construction brut*

Avant-projet

La variante 2 est améliorée avec une surélévation de l'ouvrage de 4m permettant le passage des crues en crête sur un déversoir en marches d'escalier.

	Avant	Après
Hauteur sur fondation	23,7m	27,6m
Niveau de la retenue normale	276.86m NGF	281.0m NGF
Niveau de crue de projet	281.50m NGF	282.93m NGF
Capacité utile du réservoir	95 500m³	187 200m³
Evacuateur de crues (non-vanné)	Rive gauche, 2 arches de 4m	Zone centrale, 3 passes de 11m
Vidanges de fond	4 pertuis contrôlés par 1 vanne	2 pertuis contrôlés par 2 vannes
Système de drainage	Aucun	Interface et épaulement

Economie	
Coût de construction confortement	2 MCHF
Coût de construction de la surélévation	1.3 MCHF
Prix de vente de l'eau (85 000m³/an)	1.06 CHF/m³

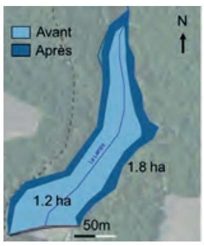

Vue en plan de la retenue

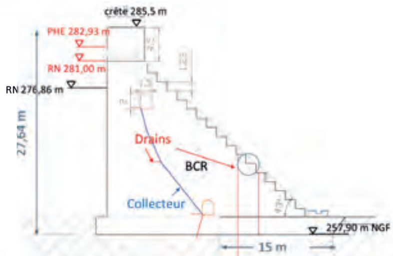

Coupe du barrage surélevé

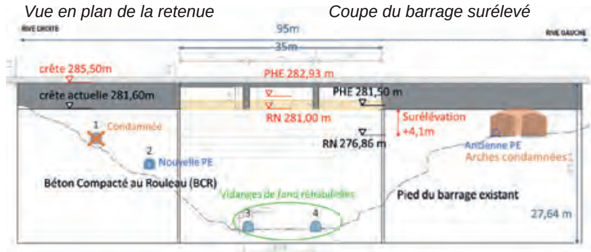

Elévation aval

Conclusions

- La problématique de l'AEP est déterminante, le confortement à l'aval assure la stabilité du barrage sans perturber l'exploitation.
- À court terme la variante 1 (tirants) implique les coûts les plus faibles mais elle doit être intégrer la remise en état de l'évacuateur de crues. La variante retenue est une réponse à long terme qui valorise le réservoir avec un nouveau modèle économique.
- La méthodologie de réalisation de l'épaulement doit faire l'objet d'études de stabilité détaillée. La géométrie (fruit, crête etc.) doit être optimisée.

Références

CFBR, Recommandations pour la justification de la stabilité des barrages-poids, Octobre 2012.
CFBR, Recommandations pour le dimensionnement des évacuateurs de crues de barrages, Juin 2013.

Remerciements GEOS Ingénieurs Conseils SA, Genève

SCCER SoE
SWISS COMPETENCE CENTER for ENERGY RESEARCH
SUPPLY of ELECTRICITY

SCCER-SoE Annual Conference 2017

In cooperation with the CTI
Energy
Swiss Competence Centers for Energy Research
Schweizerische Eidgenossenschaft
Confédération suisse
Confederazione Svizzera
Confederaziun svizra
Swiss Confederation
Commission for Technology and Innovation CTI

Upstream erosion at Piano Key Weirs

Mattia Noseda[1], Prof. Dr. Anton J. Schleiss[1], Prof. Dr. Michael Pfister[1], Ivan Stojnic[1]
[1]Laboratoire de constructions hydrauliques (LCH), Ecole Polytechnique Fédérale de Lausanne (EPFL)

Introduction

Piano Key Weirs (PKWs) are an inlet structure with high hydraulic performance under low heads. The utilization in rivers without a gated weirs next to the structure highlight the challenge about the sediment transport. This study focuses on the upstream erosion at PKWs.

Figure 1: Van Phong Dam, Vietnam

Experimental setup

- Systematic tests were performed in the LCH – Epfl laboratory in a channel of 4.5 meters length with a width of 0.65 and 0.63 meters following the PKW configurations (Figure 2).
- In total 23 tests were performed varying systematically 3 PKWs configurations (Figure 2), 2 sediments type (d_{50} = 1.80 and 6.90 mm) and 4 - 6 discharges (from 0.015 m^3/s to 0.090 m^3/s).
- The river bed was inserted horizontally upstream PKW up to the crest including inlet keys. Only free overfall conditions were considered and all tests were performed in clear water erosion conditions.

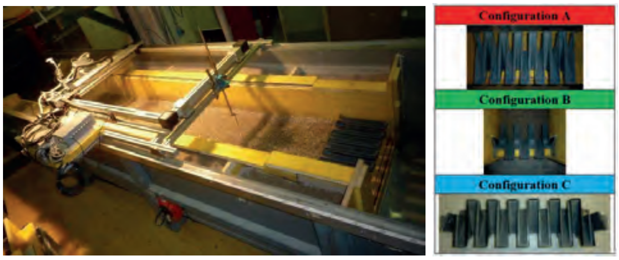

Figure 2: Experimental setup (left) and PKW configurations

Tests

The 23 tests were divided into 7 series (Equilibrium tests + Serie 1,2,3,4,5 and 6). Different photos were taken from different perspectives.

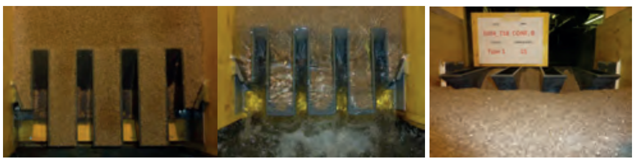

Figure 3: Test 18 - Starting conditions (left), during test (middle) and final conditions (right)

Rating curves tests

The rating curves for configurations A and B were measured at three different upstream fixed depth as $\mathbf{P}$, $\mathbf{P/2}$ and at the crest.

Figure 4: Rating curves tests: fixed level at P (left), at P/2 (middle) and at the crest (right)

Tests Results

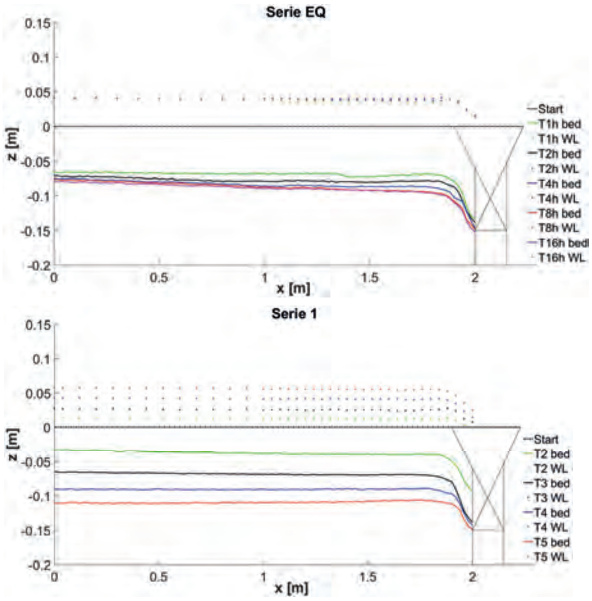

Figure 5: Bed topography (bed) and water level (WL) at the end of tests – Equilibrium tests and Serie 1

With the fine sediment the bed topography and the water surface at the end of the test were almost flat. For the coarse sediment with the discharge of 0.015 m^3/s and 0.030 m^3/s no completely erosion was observed.

Rating curves results

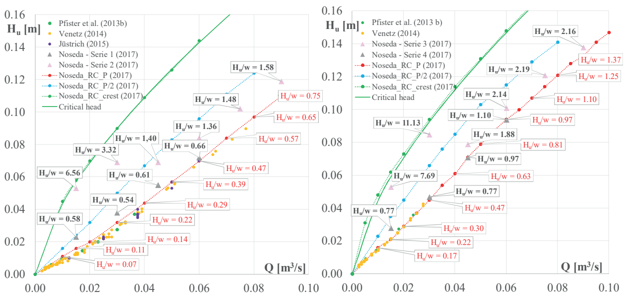

Figure 6: Rating curves results configuration A (left) and B (right): fixed level at P (red dotted line), at P/2 (blue dotted line) and at the crest (green dotted line)

Conclusions

- The ratio between the upstream head and the mean erosion $\mathbf{H_u/w}$ dominates the behavior of the rating curve and determines the increase of $\mathbf{H_u}$.
- The parapet wall plays a role of retention of sediments thus increasing $\mathbf{H_u}$.
- This study allowed highlighting the capacity of PKWs to flushing out the sediments from the inlet keys and that no deposition occurs upstream the structure. In addition, the rating curve of the PKW configuration was an important parameter that dominates the upstream hydraulic conditions.
- **In conclusion, the construction of this type of structure in rivers without a gated weir next to the structure could be considered as feasible.**

Versuchsanstalt für Wasserbau, Hydrologie und Glaziologie

Supervisors: Prof. Dr. Robert M. Boes
Dr. Sameh A. Kantoush

Student: Eliott Odermatt

Networking of Reservoir Sediment Management Groups for Sustainable Water Resources in the River Basin Scale

Introduction

Although all rivers continuously transport sediment, only a small portion of the existing dam perform sustainable sediment management [Figure 1]. The consequence is a lost of storage capacity called sedimentation, along with a lost of benefits, e.g. supply for irrigation and freshwater, hydropower and flood protection.

Objectives

The main objective is to prepare the structure for a new database. Its objectives: *“Collect, share and provide information, principally in the form of datasets, about sediment management, reservoir sedimentation, their impacts, costs, and benefits for modellers, designers, and decision-makers to improve the sustainable management of water resources integrated on the basin scale.”*

Review of Existing Efforts

Fifteen existing efforts on dam and reservoir worldwide were reviewed [Table 1]. They differ in the information they provide [Figure 2], as well as on their type, dimension, access-limitation, and initiator entity. Not a single database actually provides information about sediment management, thus showing the need for a new database.

Name
World Register of Dams
Global Water Information System (dams)
Global Reservoir and Dam Database
National Performance of Dams Program
Reservoir Sedimentation Survey Database
Reservoir Sedimentation Information System
U.S. Geological Survey Sediment Data Portal
Global Data of Erosion and Sedimentation
Global Water Information System (rivers)
Hydrological data and maps (HydroSHEDS)
Dam Impacts on Rivers, Ecosystems and People
International Sediment Initiative
European Sediment Network
Sediment Management Network Group
Regional Sediment Management Program

Table 1: Reviewed efforts

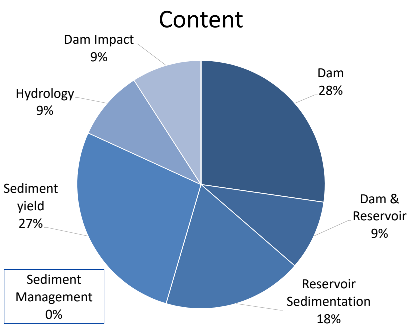

Figure 2: Content of reviewed existing databases

SDMNet Database Development

The developed Sediment and Dam Management Network (SDMNet) database uses the river basin as a key point. Eight zones were identified within the river basin, groups in each zones [Figure 3] and attributes in each group. In total, over 600 attributes were selected to fully describe the river basin, the sediment management and the impact on the environment.

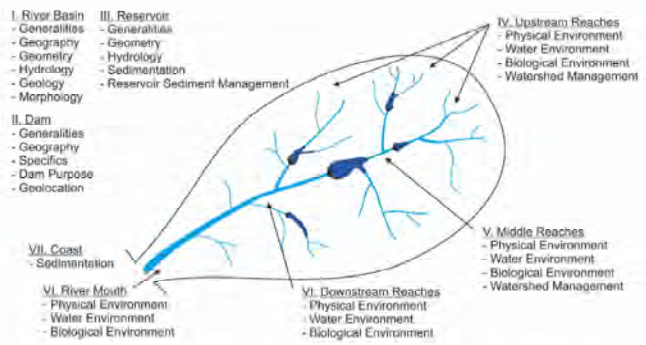

Figure 3: Zonation of the river basin and groups of attributes

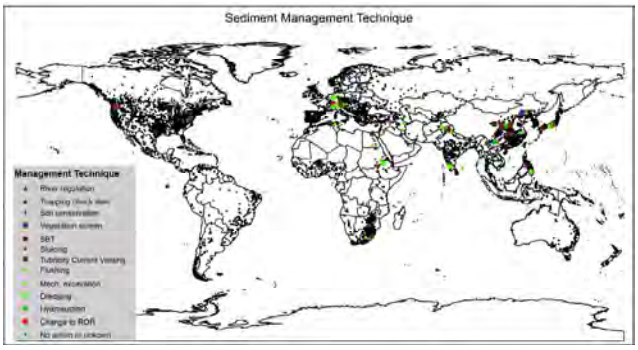

Figure 1: Sediment Management in the world [Data source: GRanD, GDAM]

Case Study: Kurobe River, Japan

The case study of Kurobe River, Japan, is studied to review the developed database structure and to provide a first content for the database. The scope of this case study is to provide a successful example of sediment management on the basin scale. There are 6 dams in the Kurobe river-basin. Dashidaira and Unazuki perform coordinated flushing and sluicing. The operation modus of the two small cascade dams Sennindani and Koyadaira was changed to run-of-river after they suffered severe sedimentation. Kurobe Dam is not managed from a sediment point of view, and no information could be found for Kitamata Dam [Figure 4].

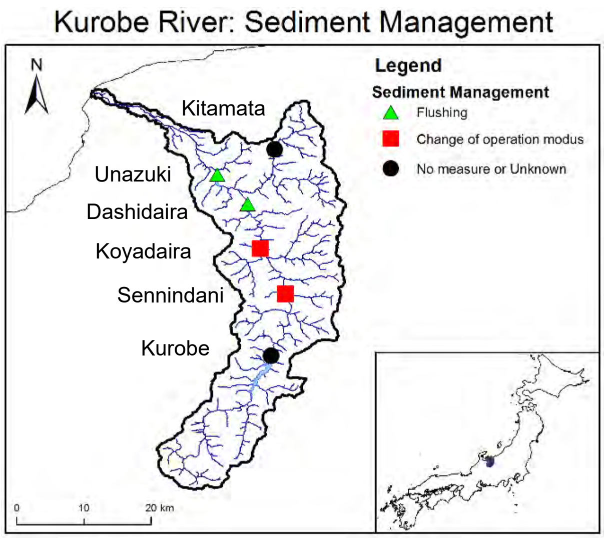

Figure 4: Dams and sediment management [data source: GRanD, NPDP, GDAM, ASTER]

Conclusion and Outlook

Within this project, the structure for the new SDMNet Database was prepared. The database will now be constructed by external consultants. Further, contributions from all over the world will be required to fill the database. To motivate SDMNet members to share this effort, it will be necessary to show them the possible benefits of both sediment management and the database.

ETH Eidgenössische Technische Hochschule Zürich
Swiss Federal Institute of Technology Zurich

Departement Bau, Umwelt und Geomatik
Master Thesis Spring 2017

SCCER SoE
SWISS COMPETENCE CENTER for ENERGY RESEARCH
SUPPLY of ELECTRICITY

SCCER-SoE Annual Conference 2017

In cooperation with the CTI
Energy
Swiss Competence Centers for Energy Research
Commission for Technology and Innovation CTI

Exploring the hydropower potential of future ice-free glacier basins

Vanessa Round[1,2], Matthias Huss[2,3], Daniel Farinotti[2,1]
(1) Swiss Federal Institute for Forest, Snow and Landscape Research WSL, (2) Laboratory of Hydraulics, Hydrology and Glaciology VAW, ETH Zurich
(3)Department of Geosciences, University of Fribourg

Context and motivation

Glacier retreat is exposing **new landscapes** and **changing runoff** regimes in glaciated regions around the world. Newly exposed ice-free basins may provide **new locations for hydropower development**.

Increasing hydropower capacity is in line with global efforts to curb CO_2 emissions, and with the newly approved **Swiss Energy Strategy 2050**. New dams could also mitigate shifts in seasonal **water availability** [1] or potentially **hazardous new glacier lakes** [2].

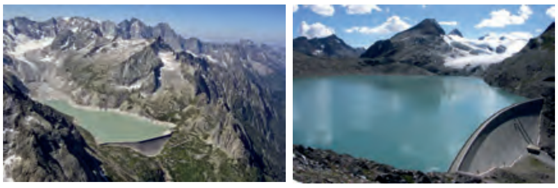

Fig. 1 Switzerland has a long tradition of pioneering Hydropower development in high alpine, glaciated catchments (left: Abigna Dam, right: Griessee).

We develop a method to assess potential dam **storage volume, electricity production** and **feasibility** for each individual glacier location. We apply this to the European Alpine region as a validation before moving the analysis to glaciated regions globally.

Simulation of potential dams

Dam walls are simulated at the current terminus of each glacier
- Subglacial topography from global ice thickness model [3]
- Geometry optimized to minimize “dam-wall area / lake volume”
- Wall dimensions limited to 280 m height, 800 m length

Fig. 2 Dams simulated in European Alps, the Caucasus, New Zealand and Peru

Potential energy production

Potential annual energy production for each site is calculated from projected catchment runoff and hydraulic head.
- Catchment runoff until 2100 from Global Glacier Evolution Model (GloGEM, [4]).
- Available hydraulic head generated from ASTER global elevation model (10% slope limit, 8km distance limit)

Site feasibility assessment

Technical factors
- Average catchment slope (potential for rock fall), global lithology.
- Reservoir fill time
- GloGEM modelled ice retreat: when will the basin be ice free?

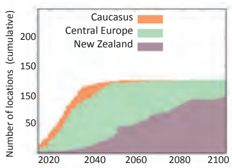

Fig. 3 When will the potential basins become ice-free?
The cumulative number of locations becoming ice-free are shown, for reservoir volumes larger than 10 mio. m^3, in three different regions.

Social and environmental factors
- Demand for electricity: population density, national statistics
- Density of endangered species
- UNESCO protected areas

Economic factors
- Weighted cost to benefit ratio
- Proximity to existing infrastructure

Potential in the European Alps

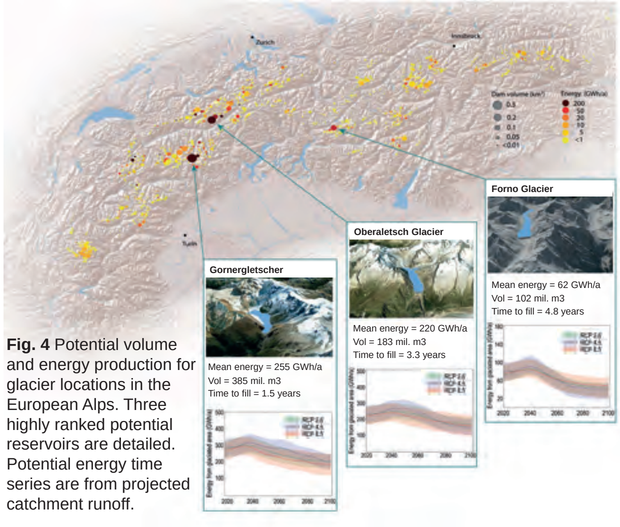

Fig. 4 Potential volume and energy production for glacier locations in the European Alps. Three highly ranked potential reservoirs are detailed. Potential energy time series are from projected catchment runoff.

Our automated methods for assessing potential reservoir volume and energy production for each glacier location reveal significant potential in the European Alpine region.
- >1000 GWh/a could be generated from the five largest potential locations (considering only immediate catchment runoff)
- The largest simulated dam volume exceeds 380 million m^3 (Gornergletscher), approaching the size of Grand Dixence.
- Many of the identified high potential sites correspond with previously recognized or existing dam locations.

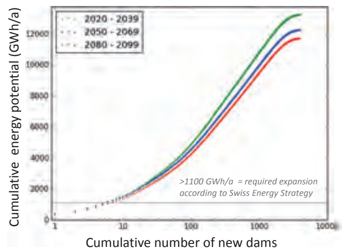

Fig. 5 Cumulative annual energy generation from new dams in projected ice-free basins in the European Alps, over three time periods.
The 1100 GWh/a level indicates the additional production required to meet the Swiss Energy Strategy goals.

Outlook

The potential storage volume and energy production from future ice-free basins in the European Alps is significant. This study is being expanded to investigate the potential in glaciated regions globally. Aside from the physically possible reservoir volumes and energy production, feasibility depends highly on factors such demand for electricity, population density, site accessibility, cost-benefit ratio and technical, environmental and social risks. These are taken into account in the development of a feasibility framework.

References

[1] Farinotti D, Pistocchi A and Huss M (2016) From dwindling ice to headwater lakes: could dams replace glaciers in the European Alps? *Environ. Res. Lett.* 11(5)
[2] Haeberli W, Buetler M, Huggel C, Friedli T L, Schaub Y and Schleiss A J (2016) New lakes in deglaciating high-mountain regions - opportunities and risks, *Clim. Chang.*, 139, 201-214
[3] Huss M and Farinotti D (2012) Distributed ice thickness and volume of all glaciers around the globe, J. Geophys. Res. Earth Surf., 117, F4
[4] Huss M and Hock R (2015) A new model for global glacier change and sea-level rise, *Front. Earth Sci.*, 3:54

SCCER SoE
SWISS COMPETENCE CENTER for ENERGY RESEARCH
SUPPLY of ELECTRICITY

SCCER-SoE Annual Conference 2017

70 NRP Energy Turnaround
National Research Programme

In cooperation with the CTI
Energy
Swiss Competence Centers for Energy Research
Swiss Confederation
Commission for Technology and Innovation CTI

Hydropower potential at *Oberaletsch Glacier*

Romina Rulli, Daniel Ehrbar, Lukas Schmocker, Daniel Farinotti, Robert Boes – VAW ETH Zurich

Introduction

Hydropower shall be further exploited according to the new Swiss Energy Strategy 2050. The goal for 2035 is to achieve an annual domestic electricity production of 37'400 GWh . Due to glacier retreat, *Oberaletsch Glacier* might become a potential future site and a reservoir for hydropower production.

Current situation

Oberaletsch Glacier is located about 10 km north of the city of *Brig*, upstream of *Gibidum* reservoir (Fig. 1). On the one hand, geological boundary conditions are suitable for dam construction, as there is predominantly Aare granite present. On the other hand, the *Valais* is prone to earthquakes, which must be considered when assessing the dam type. A mean annual runoff volume of circa 60 hm³ is estimated from 2020 to 2100 based on climate models.

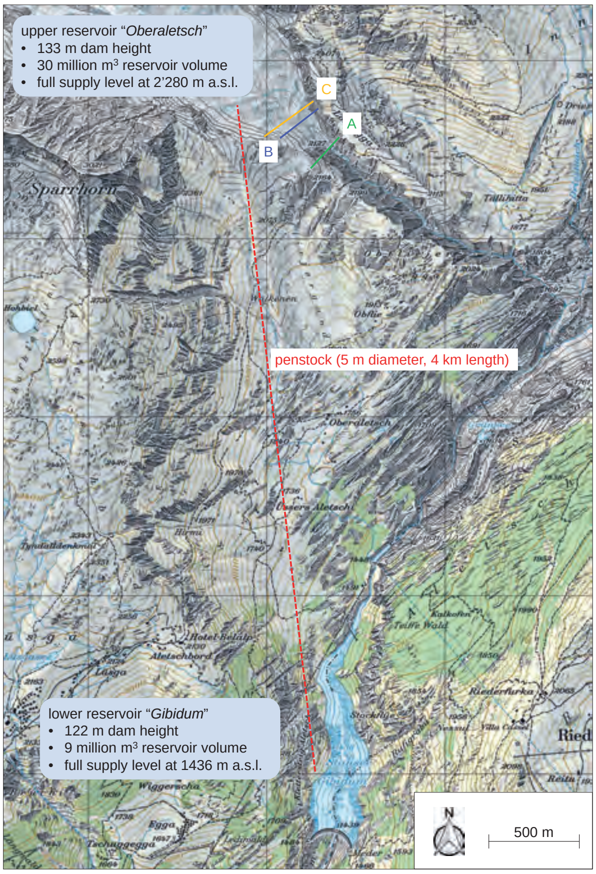

Fig. 1: Situation with potential dam locations and layout of the penstock [map: © swisstopo]

Oberaletsch Glacier is within the UNESCO World Heritage "Swiss Alps Jungfrau-Aletsch" and is well protected by the Federal Inventory of Landscapes and Natural Monuments of National Importance (BLN) 1706 "Bernese High Alps and Aletsch-Bietschhorn region". The new Energy Law is game-changing for this project, because large-scale hydropower is of national interest. Protection of nature and use for the production of renewable energy will have an equal value, so it is no longer impossible to build a reservoir in a protected area.

Results

In a concept study, various types of hydropower plants – run-of-river, storage, and pumped storage – were examined. A pumped storage plant was finally chosen, due to its large technical potential and flexibility and the existence of a lower reservoir, i.e. the *Gibidum* reservoir. In a variation study, three dam locations (Fig. 1) were investigated. Furthermore, three dam types – rockfill dam, arch dam, and gravity dam – were analysed. It turned out that location "C" and an arch dam fit best to the given situation and geological boundary conditions.

Preliminary design study

The full supply level is at 2'280 m a.s.l. The arch dam is 133 m high (Fig. 2) and the reservoir volume is 30 million m³. Four 2-nozzle Pelton turbines are installed 830 m below the full supply level, nearby *Gibidum* reservoir. Due to topographical constraints, a single headrace tunnel with a diameter of 5 m is planned, without surge chamber (Fig. 1). A chute with ski-jump serves as spillway. Given a design discharge of 69 m³/s, an installed capacity of 470 MW can be achieved. Despite the glaciated catchment and highly erodible sediments, infill time (time, until the reservoir is completely filled with sediment) is circa 700 years. The costs of this project have been estimated to 580 Million CHF.

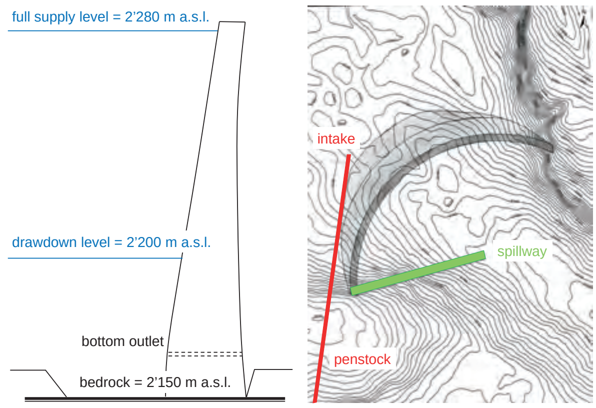

Fig. 2: (left) cross section of the arch dam; (right) situation with arch dam, spillway, and penstock

Conclusions

A reservoir at *Oberaletsch Glacier* with an annual electricity production of up to 1'400 GWh (including pumped storage operation) would contribute substantially to Energy Strategy 2050. Together with *Gibidum* reservoir, a pumped storage plant could be realized. Next planning steps require detailed geological surveys at the dam location.

Acknowledgements

This project is financially supported by the Swiss National Science Foundation (SNSF) within the National Research Programme 70 "Energy Turnaround" Project No. 153927. The close collaboration of Alpiq is gratefully acknowledged.

SCCER-SoE Annual Conference 2017

SCCER SoE
SWISS COMPETENCE CENTER for ENERGY RESEARCH
SUPPLY of ELECTRICITY

In cooperation with the CTI
Energy
Swiss Competence Centers for Energy Research
Swiss Confederation
Commission for Technology and Innovation CTI

Multipurpose Hydropower Plant on Alpine Rhine River

Katharina Sperger, Julian Meister, Robert Boes – VAW, ETHZ

Motivation and Objectives

Ever since storage power plants have started operation in the Alpine Rhine catchment, large and fast water level fluctuations (hydropeaking) occur in the Alpine Rhine. Furthermore, there is a flood protection deficit starting from a 100-year flood along the international river section (Michor et al., 2005). In this work, the construction of a river power plant was investigated, which offers a damping possibility for both hydropeaking and flood discharge at the Alpine Rhine and in addition exploits the hydropower potential of the region.

Concept study

By means of a qualitative cost-benefit analysis, a diversion river power plant in Maienfeld / Bad Ragaz was defined as the best concept. For the best variant, the water level is impounded with a weir to 513 m a.s.l.. A frontal intake and an open headrace channel guide the water to the power house (Fig. 1). Two bulb turbines with a design discharge of 100 m³/s each produce around 110 GWh of electricity per year, resulting in production costs of 9.7 Rp / kWh.

The retention basin located downstream of the power house dampens hydropeaking during the winter months, resulting in water level fluctuations of up to 6 m in the retention basin. In summer, the basin is kept at a minimum water level and the power plant can be operated at full head (15.25 m). During flood events, the basin can be drawn down in advance and then exhibits 1.2 million m³ of flood retention volume.

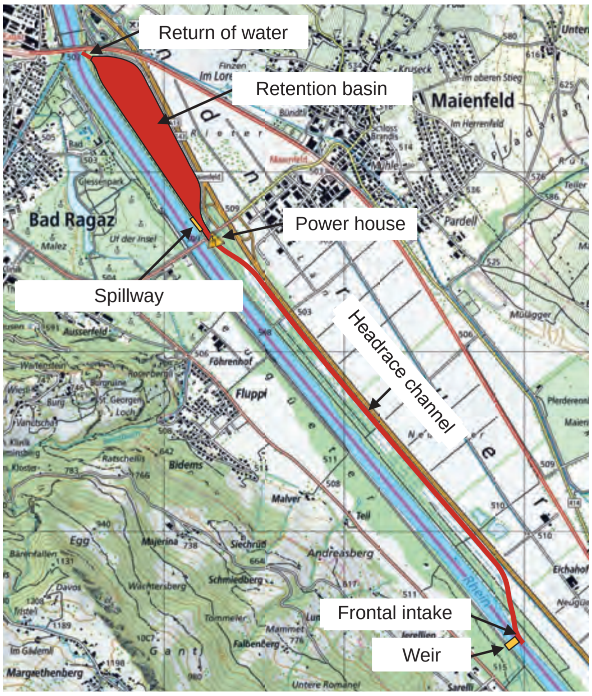

Fig. 1: Situation of the planned power plant (swisstopo, 2017)

Hydropeaking mitigation

The retention capacity of the basin was examined in a hydraulic model with the software *HEC-RAS* (Fig. 2). In the best variant, the ratio of the discharges between down- and upsurge can be reduced to below 1:2.

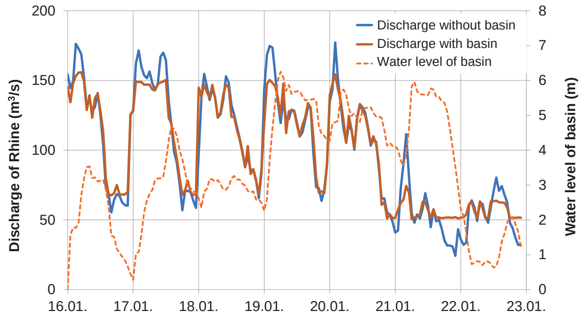

Fig. 2: Discharge of Rhine with and without (BAFU, 2017) retention basin and water level in the retention basin during a characteristic winter week in 2017

The retention basin guarantees that the requirements regarding hydropeaking for the assessment profile AP1 are met (Schälchli et al., 2012). This results in a significant improvement for ecology and bed load equilibrium (Table 1). In combination with further measures, the severe impairment can be minimized and an important contribution to a more near-natural Alpine Rhine River can be achieved.

Table 1: Requirement profiles AP1 to AP4 at the Alpine Rhine between the two tributaries Landquart and Ill River (Schälchli et al., 2012). The damping effect achieved by the retention basin is marked in green.

	Upsurge	Downsurge	Amplitude	Surge increase	Surge decrease	Down- / up-surge ratio
	[m³/s]	[m³/s]	[m³/s]	[m³/s/min]	[m³/s/min]	[-]
Actual state	160 - 200	60 - 70	90 - 130	max. 0.7	max. 0.8	1:2.3 – 1:3.3
AP1	160	79	81	0.7	0.25	1 : 2.0
AP2	140	95	45	0.5	0.2	1 : 1.5
AP3	125	106	19	0.3	0.15	1 : 1.2
AP4	116	116	0	0.2	0.1	1 : 1

Conclusion

The projected river power plant contribute significantly to the exploitation of the hydropower potential (Fig. 3) as well as the mitigation of hydropeaking on the Alpine Rhine.
In addition, the flood safety for downstream regions can be improved by an optimum regulation of the retention basin.

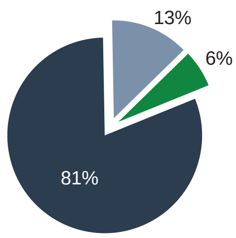

Fig. 3: Exploited hydropower potential of the power plant (green). Light blue: Installed potential at alpine rhine; Dark blue: unexploited potential (Böhl et al., 2003)

References

BAFU (2017). *Hydrologische Daten* der Stationen Domat/Ems (Rhein), Felsenbach (Landquart), Chur (Plessur)
Böhi, W., Bärtsch, J., Fecker, I., Pürer, E., Sele, E. (2003). *Energiehaushalt am Alpenrhein*. Projektgruppe Energie, Internationale Regierungskommission Alpenrhein (IRKA).
Michor K. et al. (2005). *Entwicklungskonzept Alpenrhein*. Im Auftrag der IRKA.
Schälchli, U., Wyrsch, F., Schumacher, A. (2012). *Quantitative Analyse von Schwall-/ Sunk Ganglinien für unterschiedliche Anforderungsprofile*, Arbeitspaket 1. Im Auftrag der IRKA.

SCCER-SoE Annual Conference 2017

Stilling basin performance downstream of stepped spillways

Ivan Stojnić[1], M. Pfister [1,3], J. Matos[2] and A.J. Schleiss[1]
1)Ecole Polytechnique Fédérale de Lausanne (EPFL), Laboratoire de Constructions Hydrauliques (LCH):
2)Instituto Superior Técnico (IST), Lisbon University;
3)University of Applied Sciences and Arts of Western Switzerland (HES-SO, Fribourg)
Corresponding author: ivan.stojnic@epfl.ch

Introduction

In the last three decades, stepped spillways have gained a significant popularity due to the advancements in roller compacted concrete (RCC) construction technique. A key feature of a stepped spillway, when compared to the classical (smooth) spillway, is the significant energy dissipation along the chute. As a result, energy dissipators can be reduced in size. Stilling basins are typically applied as outlet dissipators for stepped chutes.

Figure 1: Pedrógão dam, Portugal (Photo: Ivan Stojnić)

During the 1960's and the 1970's, based on model and prototype studies, several standard stilling basin designs have been developed (USBR, SAF, PWD, WEC etc.). All these standardized basin types have been developed for smooth invert chutes.
The hydraulic behaviour of standard stilling basins (in particular USBR type) in combination with stepped spillways have been tested in some experimental studies (Cardoso el al. 2007, Frizell et al. 2009, 2016, Meireles et al. 2010, Bung el al. 2012, Frizell and Svoboda 2012). However, no systematic studies have been conducted so far providing general design guidelines for stilling basins downstream of stepped chutes.

Objectives

The aim of this study is to systematically investigate the flow features and the overall performance of stilling basins downstream of stepped spillways. The main research questions can be summarized as:

- What is the effect of the self-aerated or non-aerated stepped/smooth chute inflow on the efficiency of the adjacent stilling basin?
- What is the effect of the self-aerated or non-aerated stepped/smooth chute inflow on the dynamic bottom pressures of the stilling basin?
- What are the dimensions (length, baffle block size, etc.) necessary to achieve an efficient operation mode of stilling basins downstream of a stepped chute? Do these differ from the standard types as proposed by USBR?

Research methodology

For this study, a physical model will be used to investigate stilling basin performance downstream of stepped spillways. The facility that was designed and constructed in the facilities of LCH consists of (Figure 2, 3): jet-box, 0.5 m wide and 6.0 m long chute with adjustable slope and 0.5 m wide, 6.0 m long stilling basin.

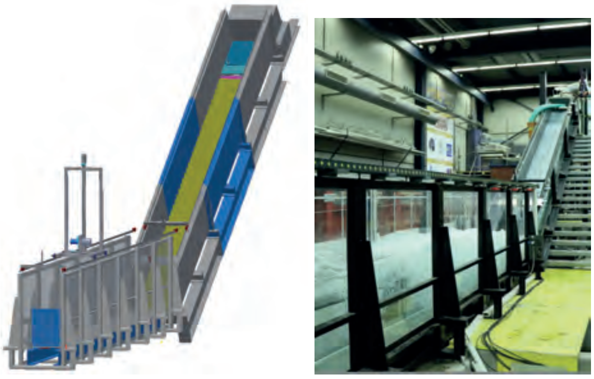

Figure 2: Schematic representation (left) and downstream view of experimental facility(right) at LCH

Parameters and measurements

In order to thoroughly investigate its performance, the following parameters will be systematically varied:

- Chute slope
- Step height (including a smooth chute)
- Discharge
- Stilling basin geometry (basin length, appurtenances geometry - chute blocks, baffle blocks, end sill etc.)
- Tailwater depth

In each test scenario detailed flow measurements will be conducted throughout the spillway. Measurements will be mainly focused on:

- Flow properties at the toe of the chute – air concentration, velocity, flow depths
- Air concentration and velocity distribution in the hydraulic jump
- Flow depths along hydraulic jump
- Roller and jump length
- Dynamic pressures along the stilling basin invert

Figure 3: Side view of experimental facility in operation.

Output

This research is expected to provide a deeper understanding of stilling basin performance under aerated and turbulent inflows as typically produced on stepped chutes. The most important output will be new design recommendations for stilling basins downstream of stepped chutes.

Acknowledgments

This research project is developed in the scope of the Ph.D. Thesis by Ivan Stojnić under the joint IST-EPFL doctoral program H2Doc. It is funded by the Portuguese Foundation for Science and Technology and LCH-EPFL.

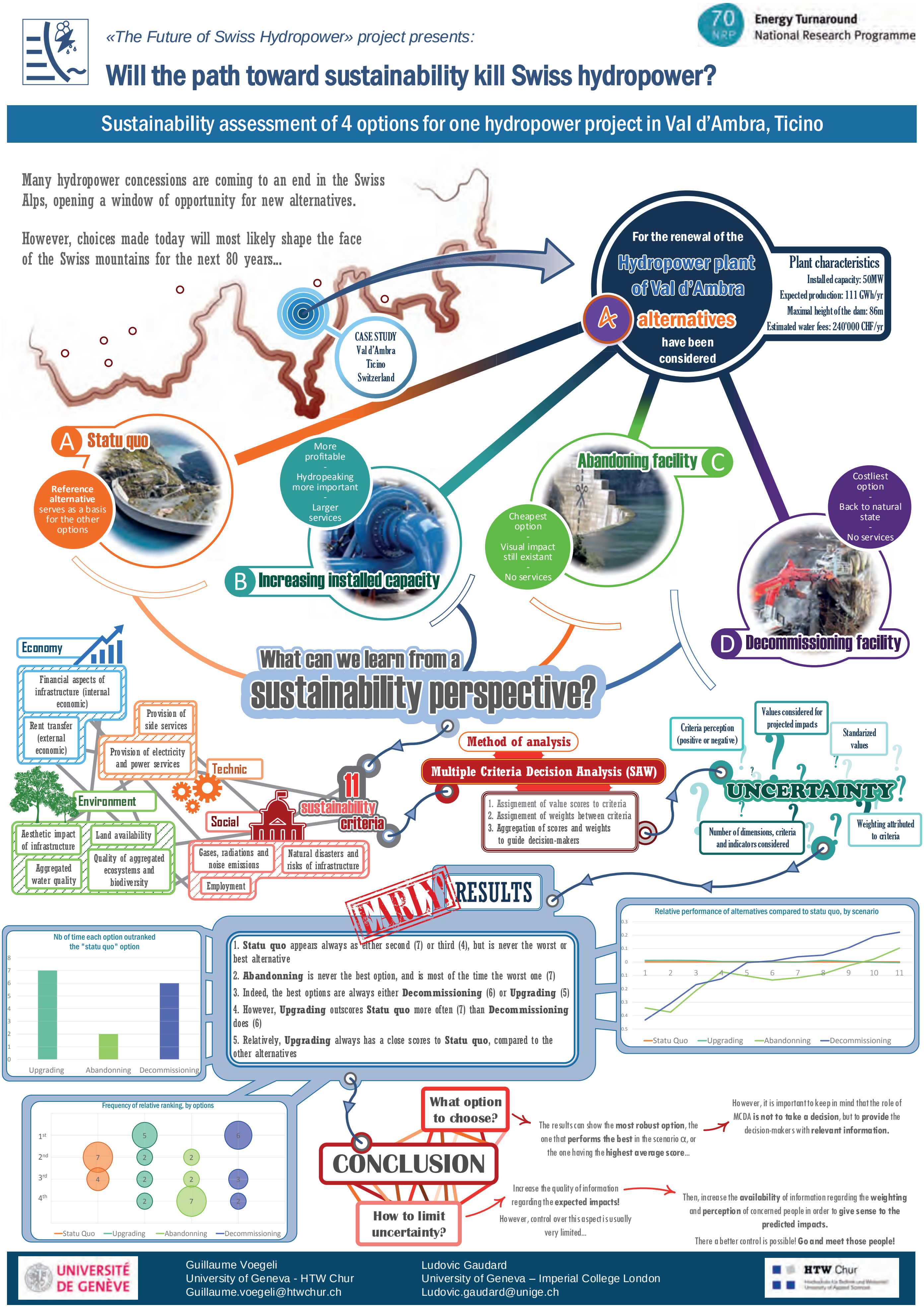
«The Future of Swiss Hydropower» project presents:
Will the path toward sustainability kill Swiss hydropower?
70 NRP Energy Turnaround National Research Programme
Sustainability assessment of 4 options for one hydropower project in Val d'Ambra, Ticino
Many hydropower concessions are coming to an end in the Swiss Alps, opening a window of opportunity for new alternatives.
However, choices made today will most likely shape the face of the Swiss mountains for the next 80 years...
CASE STUDY Val d'Ambra Ticino Switzerland
For the renewal of the Hydropower plant of Val d'Ambra 4 alternatives have been considered
Plant characteristics
Installed capacity: 50MW
Expected production: 111 GWh/yr
Maximal height of the dam: 86m
Estimated water fees: 240'000 CHF/yr
A Statu quo
Reference alternative serves as a basis for the other options
More profitable - Hydropeaking more important - Larger services
B Increasing installed capacity
Abandoning facility C
Cheapest option - Visual impact still existant - No services
Costliest option - Back to natural state - No services
D Decommissioning facility
What can we learn from a sustainability perspective?
Economy
Financial aspects of infrastructure (internal economic)
Rent transfer (external economic)
Provision of side services
Provision of electricity and power services
Technic
Environment
Aesthetic impact of infrastructure
Land availability
Aggregated water quality
Quality of aggregated ecosystems and biodiversity
Social
Gases, radiations and noise emissions
Natural disasters and risks of infrastructure
Employment
11 sustainability criteria
Method of analysis
Multiple Criteria Decision Analysis (SAW)
1. Assignement of value scores to criteria
2. Assignement of weights between criteria
3. Aggregation of scores and weights to guide decision-makers
Criteria perception (positive or negative)
Values considered for projected impacts
Standarized values
UNCERTAINTY
Number of dimensions, criteria and indicators considered
Weighting attributed to criteria
EARLY! RESULTS
Nb of time each option outranked the "statu quo" option
Upgrading Abandonning Decommissioning
1. Statu quo appears always as either second (7) or third (4), but is never the worst or best alternative
2. Abandonning is never the best option, and is most of the time the worst one (7)
3. Indeed, the best options are always either Decommissioning (6) or Upgrading (5)
4. However, Upgrading outscores Statu quo more often (7) than Decommissioning does (6)
5. Relatively, Upgrading always has a close scores to Statu quo, compared to the other alternatives
Relative performance of alternatives compared to statu quo, by scenario
Statu Quo Upgrading Abandonning Decommissioning
Frequency of relative ranking, by options
1st 2nd 3rd 4th
Statu Quo Upgrading Abandonning Decommissioning
What option to choose?
The results can show the most robust option, the one that performs the best in the scenario α, or the one having the highest average score...
However, it is important to keep in mind that the role of MCDA is not to take a decision, but to provide the decision-makers with relevant information.
CONCLUSION
How to limit uncertainty?
Increase the quality of information regarding the expected impacts!
However, control over this aspect is usually very limited...
Then, increase the availability of information regarding the weighting and perception of concerned people in order to give sense to the predicted impacts.
There a better control is possible! Go and meet those people!
UNIVERSITÉ DE GENÈVE
Guillaume Voegeli
University of Geneva - HTW Chur
Guillaume.voegeli@htwchur.ch
Ludovic Gaudard
University of Geneva – Imperial College London
Ludovic.gaudard@unige.ch
HTW Chur

SCCER SoE
SWISS COMPETENCE CENTER for ENERGY RESEARCH
SUPPLY of ELECTRICITY

SCCER-SoE Annual Conference 2017

In cooperation with the CTI
Energy
Swiss Competence Centers for Energy Research
Schweizerische Eidgenossenschaft
Confédération suisse
Confederazione Svizzera
Confederaziun svizra
Swiss Confederation
Commission for Technology and Innovation CTI

Floating Debris at Dam Spillways: Hazard assessment and Engineering Measures

Working Group - Swiss Committee on Dams

Motivation

Flood events in mountainous areas may entrain and transport large amounts of floating debris or large wood (LW). LW may endanger the save operation of dam spillways, as it can result in blocking of the spillway cross section. Already partial blocking of the spillway can decrease the discharge capacity considerably. Due to the resulting backwater rise, the freeboard requirement may not be guaranteed and in an extreme case, uncontrolled overtopping of the dam may occur. The blocking of the Palagnedra spillway, Switzerland, during the flood event in 1978 (Fig. 1) is a prime example demonstrating the hazard potential of transported LW.

Fig 1: Blocking of spillway at Palagnedra Dam in 1978 (Photo: Ofima SA).

Swiss Survey

Although LW transport during flood events is a major threat, limited knowledge is currently available on the interaction between LW and the spillway and the magnitude of a possible backwater rise. No general guidelines on LW management at spillways is currently available. Therefore, the Swiss Committee on Dams established a working group to summarize international guidelines and best practice on LW and floating debris at dam spillways.

A questionnaire was distributed to 60 Swiss hydropower plant (HPP) owners to collect information regarding LW occurrence and problems at spillways. The results demonstrate that LW occurs at approx. 90% of the HPPs and 17% of the HPPs already experienced problems or damages due to LW (Fig.2) .

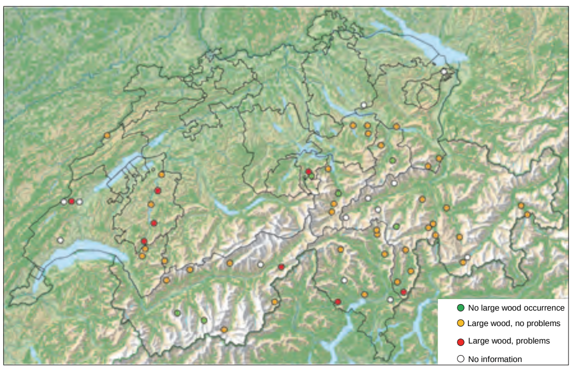

Fig 2: Results of Swiss survey on occurrence and problems regarding large wood at dam spillways.

Hazard assessment

The hazard assessment was summarized in a diagram (Fig. 3) that includes the following main steps:

1. Determination of external loads (e.g. flood discharges, LW potential) and both spillway and dam design (e.g. type, dimensions, freebord, hydraulics)
2. Check guidelines regarding minimal required dimensions of spillway and determine blocking probability
3. Assessment of hazard potential due to spillway blocking
4. Decision if hazard due to floating debris is low or high
5. Develop measures to minimize the potential hazard

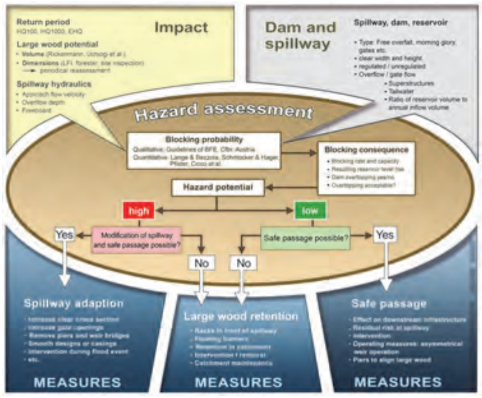

Fig 3: Hazard assessment diagram for floating debris and LW at dam spillways.

Engineering Measures

If the hazard potential and especially the blocking probability are small, large wood may be conveyed through the spillway. If the hazard potential is high, two main measures may be applied to decrease it:

1. Guarantee safe spillway passage of the large wood with spillway adaptations: Increase clear cross section or gate openings, remove piers and weir bridges, use smooth designs or casings, etc.
2. Retain large wood upstream: Check dams and racks in the catchment, floating barriers in calm water sections of the reservoir, racks in front of the spillway, etc.

Some examples are given in Figure 4.

Fig 4: (a) New clear spillway with displaced weir bridge at Palagnedra Dam, Switzerland (Photo: polier.ch), (b) Floating debris barriers at Lake Brienz, Switzerland (Photo: Swiss Airforce), (c) Rack in front of spillway of Thurnberg Reservoir, Austria (Photo: bmlfuw)

Working Group Members

Robert Boes (President, VAW, ETH Zürich), Marius Bühlmann (VAW, ETH Zürich), Heinz Hochstrasser (on behalf of AWEL Canton Zürich), Jean-Claude Kolly (Groupe E), Guido Lauber (Emch + Berger AG), Judith Monney-Ueberl (AWA, Canton Bern), Michael Pfister (LCH, EPFL / HEIA Fribourg), Riccardo Radogna (Ofima SA), Lukas Schmocker (VAW, ETH Zürich / Basler & Hofmann AG), Adrian Stucki (AF-Consult Switzerland AG), Fathen Urso (Holinger AG)

Task 2.3

Title

Environmental impacts of future operating conditions

Projects (presented on the following pages)

Hydro-economic Consequences of Hydro-peaking Removal
Alternative: Work Package 5
L. E. Adams, P. Meier, J. Lund

Disentangling the effects of hydrology and predation on macroinvertebrate community assembly: a field experiment
P. Chanut, F. J. Burdon, T. Datry, C. T. Robinson

Evolution of a gravel-bed river subject to SBT operations
M. Facchini, A. Siviglia, R. M. Boes

Streams impacted by hydropower production through water intakes: do we need sediment flows more than minimum flows?
C. Gabbud, C. Robinson, S. Lane

Impacts of altered pumped-storage operation on water quality
U. G. Kobler, M. Schmid

Trading off energy production from small hydropower with biodiversity conservation
K. Lange, P. Meier, C. Trautwein, M. Schmid, C. T. Robinson, C. Weber, J. Brodersen

System modelling for hydro-peaking mitigation
P. Meier, M. Bieri, P. Manso, F. Zeimetz, C. Gerber, A. Mark, S. Schweizer, A. Fankhauser, B. Schwegler

Modeling macroroughness contribution to riverine ecosystem
A. Niayifar, P. Perona, J. Oldroyd, S. N. Lance, T. J. Battin

In cooperation with the CTI
Energy
Swiss Competence Centers for Energy Research
Schweizerische Eidgenossenschaft
Confédération suisse
Confederazione Svizzera
Confederaziun svizra
Swiss Confederation
Commission for Technology and Innovation CTI

UCDAVIS
CENTER FOR WATERSHED SCIENCES

Hydro-economic Consequences of Hydro-peaking Removal

L.E. Adams[1,2*] P. Meier[2] J. Lund[1]
[1]University of California- Davis, Department of Civil and Environmental Engineering, [2]Eawag, Swiss Federal Institute of Aquatic Science and Technology

1. Introduction

- The Swiss Water Protection Act requires that Swiss hydropower plants must mitigate any serious environmental harms of hydro-electricity by 2030 (e.g., remove hydro-peaking, or sub-daily discharge variability from peak electricity production).
- Building an after-bay or re-operating the hydropower plant system are primary options for attenuating hydro-peaking.
- Our goal is to develop a method for comparing the financial and ecological tradeoffs and required operational changes for choosing different after-bay sizes for removing hydro-peaking.

2. Methods

Two-stage linear programming **maximizes system flexibility for each of several planned after-bay sizes** and **maximizes operational benefits** for the operational changes required to compensate for any hydro-peaking not managed by the after-bay.

$$\min_{x}(\mathbf{z}) =$$

$$\sum_{n}\sum_{T}\sum_{t}\left(\frac{x_T - V_T^{target}}{V_T^{max}}\right)^2 + f^{-}(\mathrm{J},\mathrm{t})f^{lowflow}(\mathrm{J},\mathrm{t}) + f^{+}(\mathrm{J},\mathrm{t})$$

$$-\, B_n(C, e_x, h)$$

n = release points (e.g., each facility and river inflow)
x = outflow to river from each n (m^3/s);
t = operational time step (e.g., 15 min)
T = planning time step (e.g., 30 or 45 min)
V = water volume in after-bay (m^3);
J = ramping rate (positive and negative) (m^3/min);
target = time required between $\int_{t\_empty}^{t\_full} V$ (min);
B = benefits (€ / (kNm/min))
C = turbine flow capacity ($kN\ m\ /\ min$)
h = hydraulic head (m)
e = possible energy production (min)

3. Case Study

The Kraftwerke Oberhasli hydropower system releases to the Aare River in Canton Bern after generating electricity along a cascade of reservoirs and power plants from Innertkirchen 1, the most downstream power house, and Innertkirchen 2, the last of several run-of-river power plants. For KWO and others, **the goal of hydropeaking is to smooth ramping rates at least cost.**

3. Operational Benefits

Operational benefits minimize revenue losses.

$$\mathbf{B}_{(n,T,t)} = E\sum_{t}^{T}\overline{P(e_x)}_t =$$

$$\gamma\,(\varepsilon\, h)_n N_{n,T}\frac{\|(Q-V)_{n,T}\|}{C_n}\Delta t\sum_{t}^{T} P_{t,T}\left(\frac{(Q/C)_n}{\Delta T} * 100\right)_t$$

E = electricity production (kN); P = electricity price (€/min);
Q = inflow (m^3/min); γ= specific weight of water (kN/m^3);
ε = generation efficiency (%); N = time at full capacity (min)

Model Formulation references: Pereira and Pinto (1985), Olivares (2008), and Loucks (1983)

4. Preliminary Results

Releases and revenue losses from hydropower re-operation with no after-bay (baseline conditions).

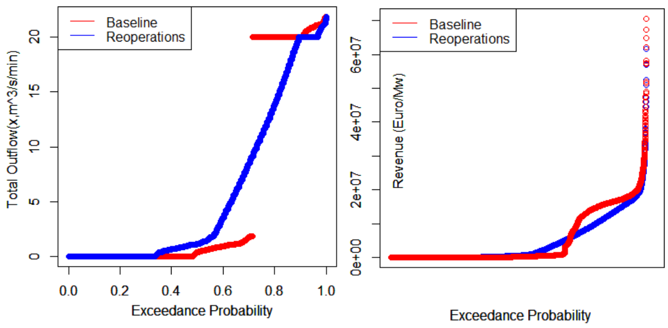

Left: Frequency of Operational Changes to Mitigate Hydro-peaking

Right: Revenue Gains and Losses from Re-operations to avoid hydro-peaking

Operational changes require production during off-peak hours, which on net results in revenue losses equivalent to about 10.6% of average winter revenues, the season in which hydro-peaking is most notable.

5. Future Work

Future work will compare revenue losses from meeting hydro-peaking requirements for different size after-bays with 30- and 40- minute lead time for operations decisions made at 15-minute intervals. Expected final results will form a Pareto Front like this:

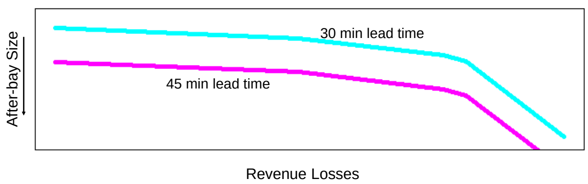

UCDAVIS
UNIVERSITY OF CALIFORNIA

Thanks to the Climate Change, Water and Society IGERT NSF DGE #1069333

*For more information, contact L.E. Adams at leadams@ucdavis.edu

Disentangling the effects of hydrology and predation on macroinvertebrate community assembly: a field experiment

Pierre Chanut[1], Francis John Burdon[1], Thibault Datry[2], Christopher T. Robinson[1]

[1]EAWAG, Dübendorf, Switzerland. Email: pierre.chanut@eawag.ch

[2] IRSTEA, Villeurbanne, France

1. Objectives

- Assessing the effect of floodplain hydrology (connectivity) on aquatic habitat characteristics
- Jointly quantifying the relative effects of floodplain hydrology (connectivity) and fish predation on macroinvertebrate community composition
- Identifying the key ecological processes at play
- Assessing how community assembly rules vary with hydrology (connectivity) and fish predation

2. Experimental setup and analyses

We excavated 24 ponds (~ 9 m^3) in a gravel bar, with homogeneous substrate and distributed them in 8 spatial blocks along a hydrological gradient

Within each block, we assigned a juvenile brown trout treatment: 0 or 2 or 6 fish

We sampled every 15 days for 2 months (invertebrates, periphyton, phys-chem)

Analyses:
- Effects on Community composition: **forward selection & dbRDA**
- Effects on biological traits (Tachet)**: RLQ + Fourth-corner analysis**
- Investigation of assembly rules: **Functional diversity (Null model deviation)**

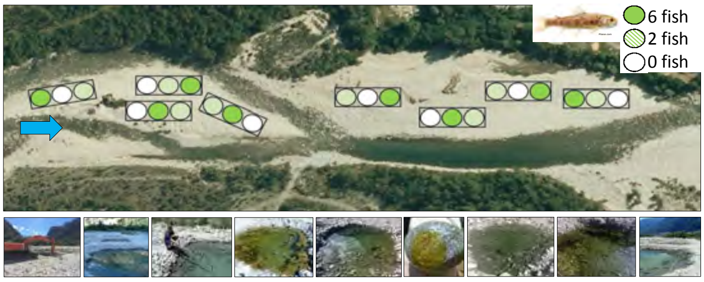

3. Results

3.1 Hydrological gradient

PC1 is structured by alkalinity, conductivity, chlorophyll a and water temperature.

High alkalinity and conductivity results from high concentration of dissolved cations, reflecting longer interaction time between water and rock.

PC 1 is interpreted as the gradient of **connectivity**, used in the rest of the study.

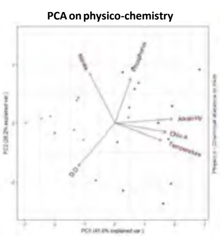

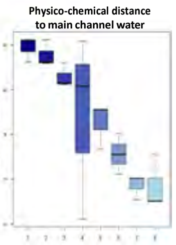

3.2 Community composition

At week 2 The gradient of connectivity constrains community composition

At week 8 The gradient of connectivity remains the main environmental constraint on community composition but the effect of primary productivity has increased.

No effect of fish density on community composition were found

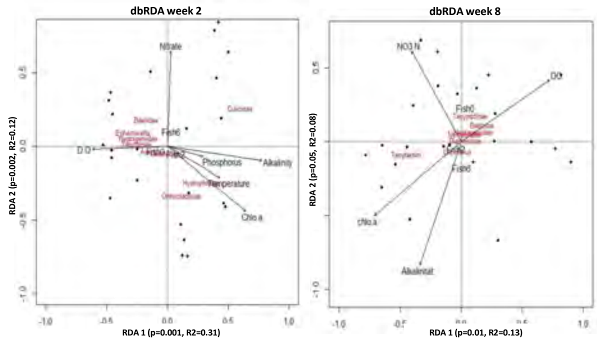

3.3 Trait selection

Traits :
Dispersal :Aquatic / Aerial
Respiration: Aerial / with gills
Locomotion: surface swimmer / open water swimmer / crawler
Feeding habit: Predator

At week 2, *aerial respiration* and *surface swimming* are advantageous traits in the less connected sites. More connected sites are colonized primarily by *aquatic dispersers* and species using *gills* to breathe. A similar pattern is found at week 8

The fish treatment was not found to have significant effect on the traits we investigated.

Dispersal mode affects colonization patterns with active aerial dispersers better able to colonize isolated sites. And the difference in DO among connected and less connected sites appears to be the most important factor constraining community assembly.

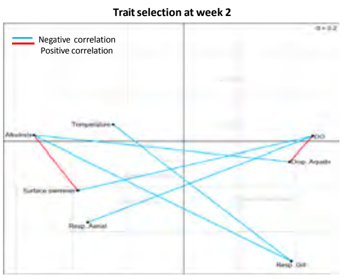

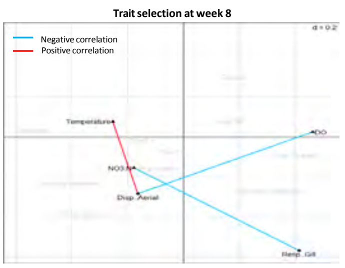

3.4 Assembly rules

At week 2, the less connected sites are functionally over-dispersed compared to the null expectation. This suggests that increased competition in the less connected sites limits niche similarity within each community.

At week 8, functional diversity is no different from the random expectation. No effect of fish density on functional diversity was found.

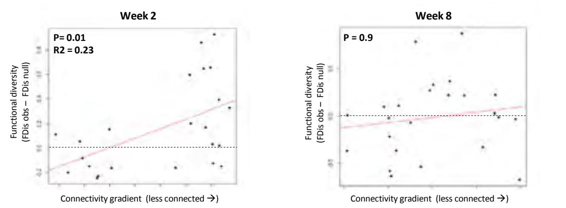

4. Conclusion

- Hydrological connectivity affects primary productivity and constrains invertebrate community assembly through indirect biotic processes (functional over-dispersion).
- Fish density was not found to have a significant effect on community composition neither functional diversity (in a separate analysis, fish presence was found to homogenize community compositions across environmental gradients).
- Based on these results, preserving habitats with various levels of hydrological connectivity is key to conserving biodiversity and ecosystem resilience.
- Both the flooding regime and the low flow conditions have to be adapted to preserve habitat diversity and hydrological connectivity at the floodplain scale.

eawag aquatic research

FNSNF Fonds national suisse Schweizerischer Nationalfonds Fondo nazionale svizzero Swiss National Science Foundation

Acknowledgements
Dr. Eric Harvey; Dr. Amael Paillex; Dr. Dirk Radny

ti Repubblica e Cantone Ticino Dipartimento del territorio

ETH Eidgenössische Technische Hochschule Zürich Swiss Federal Institute of Technology Zurich

SCCER-SoE Annual Conference 2017

SWISS COMPETENCE CENTER for ENERGY RESEARCH
SUPPLY of ELECTRICITY

In cooperation with the CTI
Energy
Swiss Competence Centers for Energy Research
Schweizerische Eidgenossenschaft
Confédération suisse
Confederazione Svizzera
Confederaziun svizra
Swiss Confederation
Commission for Technology and Innovation CTI

Evolution of a gravel-bed river subject to SBT operations

Facchini, M.[1], Siviglia, A., Boes, R.M. – VAW, ETHZ
[1] *facchini@vaw.baug.ethz.ch*

Introduction

Sediment Bypass Tunnels (SBTs) (Fig. 1(a)) have been proven to been an effective countermeasure to reservoir sedimentation (Sumi et al., 2004), but their morphological effects on the downstream reach are still poorly investigated. During flood events, they divert sediment from upstream to downstream around or through the dam (Fig. 1(b)). Therefore, the downstream reach is subject to repeated releases of water and sediment in form of hydrographs (Q_w) and sedimentographs (Q_b) (Fig.1(c)). The overarching goal of this work is to quantify the morphological changes in terms of riverbed slope and grain size distribution (GSD) induced by realistic SBT operations.

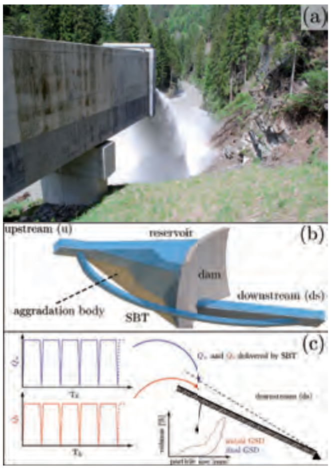

Fig. 1: (a) Solis SBT(Canton Grisons, Switzerland) in operation, (b) sketch of SBT-dam system, (c) 1D numerical study setup.

Conceptual framework for SBT-release scenarios

To properly work, a SBT must have a higher sediment transport capacity than the river flowing in the reservoir. Therefore, given the slope and the GSD of the upstream river reach, the relationship between the water Q_w and the bedload discharge Q_b (bedload rating curve, BRC) can be calculated for the upstream river reach (BRC_u) and the SBT (BRC_{SBT}) (solid red and blue lines in Fig. 2).

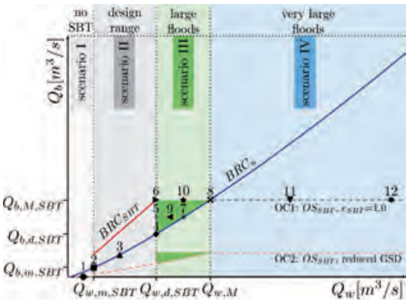

Fig. 2: SBT release scenarios with Bedload Rating Curves (BRC), Operational Conditions (OC), and numbers of numerical runs.

SBTs are usually designed according to a given water discharge value $Q_{w,d,SBT}$. Then, we identify four possible SBT release scenarios (see Fig. 2):

- scenario I (no SBT operation): the SBT is not operated, sediments are stored in the reservoir and water might be conveyed through the dam;
- scenario II (design range): sediment coming from upstream is diverted downstream by the SBT;
- scenario III (large floods): Q_w flowing through the SBT is $Q_{w,d,SBT}$ and the surplus (Q_w>$Q_{w,\,d,SBT}$) can be either stored in the reservoir or conveyed through dam outlets; Q_b is smaller or equal to maximum $Q_{b,M,SBT}$ that can be carried by the SBT releases;
- scenario IV (very large floods): $Q_b = Q_{b,M,SBT}$ and extra water (Q_w>$Q_{w,M}$, where $Q_{w,M}$ is the Q_w needed for carrying $Q_{b,M,SBT}$ in the upstream reach) is released from the dam.

OC1 and OC2 refer to two different Operational Conditions, namely:

- OC1: the bypassing efficiency of the SBT e_{SBT} = 1.0, i.e. all sediments from the upstream reach enter the SBT and are conveyed downstream;
- OC2: the coarsest part (i.e. coarser than fine pebbles) of the sediments from upstream is mined before entering the SBT.

Methods

To quantify the downstream changes in riverbed slope and GSD, we run 1D numerical simulations with BASEMENT (www.basement.ethz.ch). The model describe the hydro-dynamics by the Saint-Venant equations. Friction exerted by flow over a cohesionless bottom composed of mixed sediment induces sediment transport, which is assumed to occur only as bedload. The GSD of the riverbed surface and the development of size stratification are described by using the active-layer approach of Hirano (Hirano 1971, 1972).

Numerical model setup

The specific quantification of the inputs to the numerical runs takes as a reference the reach of the Albula River downstream of the Solis Dam and the Solis SBT (Canton Grisons, Switzerland). The cross-sectional geometry has been simplified to a rectangular channel with a length of 10 km and a constant width of 15 m. We discretize the channel with 100 cross-sections, 100 m apart from one another. Q_w and Q_b are fed at the upstream end of the domain in form of repeated trapezoidal hydrographs and sedimentographs varying sympathetically in time as represented in Fig. 1(c). Each release lasts 12 hours and Q_w and Q_b reach the peak after one hour from the beginning. A quantification of the peak-magnitudes under both OCs is given in Table 1 (values relative to OC1 refer to numbered symbols of Fig. 2).

	run	1	2	3	4	5	6	7	8	9	10	11	12
$Q_w\,[m^3/s]$		30	50	100	170	170	170	223	275	197	222	428	623
$Q_b\,[m^3/s]$	OC1	0	0.23	0.55	1.06	1.49	1.92	1.49	1.92	1.49	1.92	1.92	1.92
	OC2	0	0.07	0.17	0.33	0.46	0.6	0.46	0.6	0.46	0.6	0.6	0.6

Table 1: Summary of input Q_w and Q_b for numerical simulations under different OCs.

Results

Results at mobile-bed equilibrium (after thousands of SBTs operations) are given in Fig. 3 and are presented in terms of a non-dimensional riverbed slope S^* and mean geometric size d_g^*. The reference values S_{ref} and $d_{g,f}$ are relative to the upstream reach and to the feeding, respectively. We chose these references to evaluate the effectiveness of SBTs as a mean for river restoration, i.e. their efficacy in restoring almost natural water and sediment fluxes. Results at mobile-bed equilibrium show that:

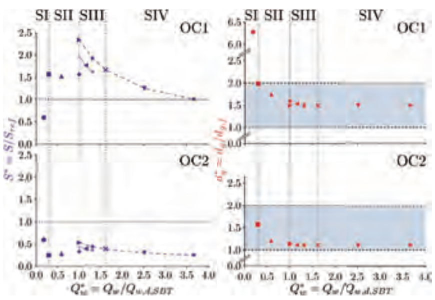

Fig. 3: Results at mobile-bed equilibrium.

1) For a given Q_b, the more water is released the lower the resulting equilibrium slope will be (dashed blue lines in Fig.3);
2) if the feeding is deprived of its coarsest part then $S<S_{ref}$;
3) the riverbed tends to unarmored conditions, i.e. $d_g^*<2$ under almost all circumstances.

On a shorter time-scale, i.e. after 50 SBT-operations, results show that:

1) the riverbed GSD is already close to the equilibrium after a few SBT operations under OC1;
2) under OC2, the rework of the riverbed takes more time since the initial conditions are more apart from the equilibrium than under OC1;
3) both under OC1 and OC2 the riverbed level approaches the equilibrium configuration at the same pace, which is much slower than the one relative to the riverbed GSD.

Conclusions

SBTs operated with e_{SBT} = 1 are able to increase the downstream riverbed slope and reduce the armoring degree of the riverbed surface, while they are causing erosion in the domain if they transport only fines. However, the equilibrium GSDs under OC2 for each run are the one of a sand-bed river, since the feeding is composed mostly by sand. On a shorter time-scale (i.e. tens of events), the GSD converges to the equilibrium faster than the riverbed level. By re-establishing sediment and water fluxes at dams, SBTs might have the power to increase the riverbed slope and break riverbed armoring.

References

Sumi, T., M. Okano, and Y. Takata (2004), Reservoir sedimentation management with bypass tunnels in Japan, *in Ninth International Symposium on River Sedimentation,* pp. 1036–1043.

Hirano, M. (1971), River bed degradation with armoring, Transactions of the Japan Society of Civil Engineers, 3(2), 194–195.

Hirano, M. (1972), Studies on variation and equilibrium state of a river bed composed of nonuniform material, Transactions of the Japan Society of Civil Engineers, 4, 128–129.

ETH zürich
Laboratory of Hydraulics, Hydrology and Glaciology

SCCER-SoE Annual Conference 2017

Streams impacted by hydropower production through water intakes: do we need sediment flows more than minimum flows?

Part of the NRP70 HydroEnv project

Gabbud Chrystelle[1], Robinson Christopher[2] and Lane Stuart[1]

[1]Institute of Earth Surface Dynamics (IDYST), University of Lausanne / [2]Department of Aquatic Ecology, EAWAG, Dübendorf

1. Context - Alpine water intakes

While ecosystem impacts downstream of dams can be managed by a properly designed compensation release like environmental flows or e-flows, they could be insufficient to insure the viability of aquatic life in **the case of water intakes**.

Indeed, the latter are much smaller than dams. **Sediment is trapped in one or two basins before water is abstracted for transfer to storage or at altitude for eventual electricity production** (Fig. 1).

Given their small storage capacity, **these basins have to be flushed/purged of sediment regularly**, through short duration floods with exceptionally high sediment loads. Thus, these intakes do not eliminate sediment connectivity from upstream to downstream (as in dams) but maintain it, whilst potential downstream sediment transport capacity is substantially reduced.

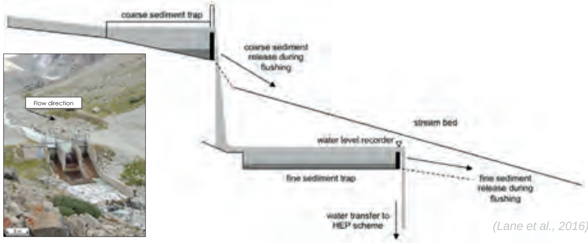

Figure 1: Water intake (here – Bertol Inférieur) and its typical scheme of sediment management through basins

Figure 2: a) High altitude glacial catchment with water intake; b) Channel before and during a (small) purge

The question of sediment in river management is rarely considered. However, in the context of high altitude water abstraction, the **proximity of plants with glaciers induces a high sediment delivery rate to intakes** (Fig. 2a) meaning that flushing can be frequent. Frequent **flushing** (Fig. 2b) may induce deposition and erosion downstream that drastically modifies the geomorphological conditions that determine stream habitat, which can **impact plant and animal communities**.

The aim of this study is to address the management of sediment in intake-controlled Alpine streams and to define **whether we need sediment flows as well as, even instead of, minimum flows**.

2. Study site and Methods

Borgne d'Arolla (Hérens, VS)

- stream fed by a series of both glacial and nival tributaries (Fig. 3)
- regulated by a series of water intakes part of the Grande Dixence scheme
- Sediment trapping and purging

Figure 3: Borgne d'Arolla catchment

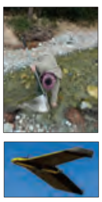

Main methods are (Fig. 4):

- Fluvial geomorphology, river processes, habitat studies
- Drone imagery and DEM production, hydraulic modelling
- Macroinvertebrate sampling

Figure 4: a) Macroinvertebrates ampling; b) Ebee drone

3. Results - Purge modify river morphology and prevent fauna to establish

Figure 5: Vertically, measuring station in both the Borgne [red dotted line] and in the tributaries (T); horizontally, macroinvertebrate abundance (length) and taxa (colours)

1. In June, no purges, macroinvertebrate appear and are numerous and diverse, in both the tributaries and the Borgne
2. In **August, the Borgne is almost void of life**; channel morphology changes daily, no organic matter; sediment load passes from **100mg/l to 6500mg/l during a purge** (Gurnell, 1983); purges occur several times a day in summer
3. In October, they are less purges, pioneers are able to quickly recolonise the Borgne.

→ The tributaries can feed the Borgne (Fig. 5) with macro-invertebrates, but:

- As the tributary habitats are extremely different (OM, temperature, turbidity, etc.), it **is very difficult for the fauna to colonise**
- The constant instability of the channel - **purges - modifies the habitat and drift and kills** the prospective animals.

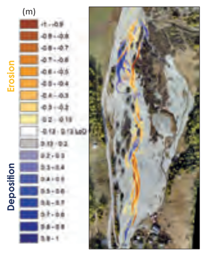

4.5 km downstream from the water intake, sediment **deposition / erosion can be up to 1 m in 4 months** (June – October) (Fig. 6).

Figure 6: Digital Elevation Model of difference between June 2016 and October 2016 to see erosion and deposition areas and amount

Water intakes strongly impact aquatic ecosystems and destroy macroinvertebrate populations during periods of frequent purges.

4. Discussion and perspectives

In this system, the problem is less the water abstraction. Groundwater recharge rapidly leads to minimum flows greater that the Q_{347} defined at the intakes. The problem is sediment purges which induce short duration floods with exceptionally high sediment loads, causing substantial erosion and deposition downstream.

Thus introducing a **minimum flow will not be sufficient and perhaps not even needed**. It is now necessary to identify a suitable sediment management regime as an integral part of designing ecologically sustainable flows in abstraction systems.

This is why not only flow manipulation but also sediment management have to be considered.

One suggestion would be to **stock sediments upstream** the water intake in order to decrease the purges frequency (landscape issues).

Policies should **distinguish between dams and water intakes in the water law** in order to find a win-win solution instead of the **current likely lose-lose solution**, as minimum flows in this kind of system will reduce water available for hydropower production and ecology will not be improved as long as sediment load is not considered.

References

Lane et al. (2016). Sediment export, transient landscape response and catchment-scale connectivity following rapid climate warming and Alpine glacier recession. *Geomorphology*, 210-227.

Gurnell AM (1983). Downstream channel adjustments in response to water abstraction for hydro-electric power generation from Alpine Glacial melt-water streams. *The Geographical Journal*, 149, 342-354.

Acknowledgements

Many thanks to the SNF – NRP70 project "*HydroEnv - Optimizing environmental flow releases under future hydropower operation*" and to the University of Lausanne.

Publication

Gabbud C and Lane SN (2016). Ecosystem impacts of Alpine water intakes for hydropower: the challenge of sediment management. *WIREs Water*, 3(1), 41-61.

SCCER SoE
SWISS COMPETENCE CENTER for ENERGY RESEARCH
SUPPLY of ELECTRICITY

SCCER-SoE Annual Conference 2017

EPFL eawag SBB CFF FFS

In cooperation with the CTI
Energy
Swiss Competence Centers for Energy Research
Commission for Technology and Innovation CTI

Impacts of altered pumped-storage operation on water quality

Ulrike Kobler, Martin Schmid

Eawag, Department of Surface Waters - Research and Management, Kastanienbaum, Switzerland
ulrike.kobler@eawag.ch

FORCING SIHLSEE (1998-2015)

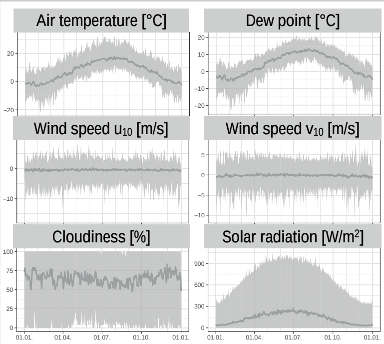

Meteorological Forcing

Bathymetry

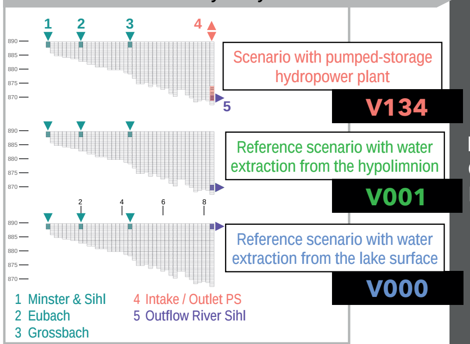

Water Quality Forcing

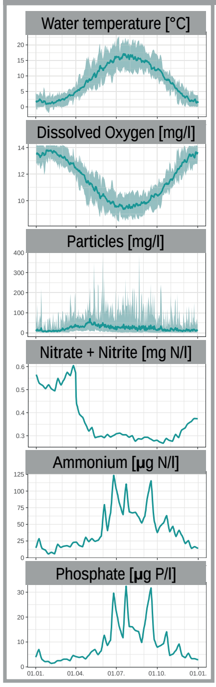

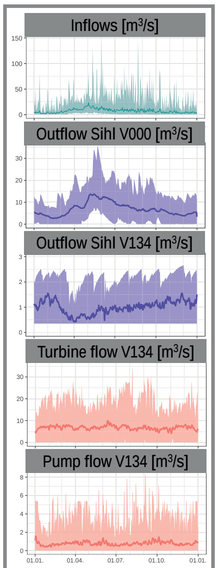

Hydrological Forcing

INTRODUCTION

PS operations are an efficient technology for storing electric energy. This storage capacity addresses main drawbacks of intensified "new renewable" electricity production resulting from changing energy policies. These drawbacks include highly variable production and network load stability problems. However, these PS operations affect physical, biogeochemical as well as ecological properties of the linked water bodies. Especially the impacts on natural lakes need to be limited to keep lake ecology intact.

In this study, we use a two-dimensional model to project the impacts of a PS hydro-power plant between Sihlsee and Upper Lake Zurich on temperature, stratification, oxygen concentrations as well as suspended solid dynamics for 1998-2015. Three different scenarios are discussed in detail for Sihlsee: V134, representing the current situation with the existing PS and two reference scenarios, where a *quasi*-natural outflow is feed into River Sihl either from the lake surface (V000) or from the current intake of the hydropower plant (V001).

STUDY SITE

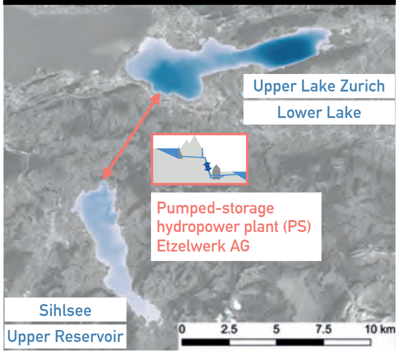

METHODOLOGY

Model Parameters

Observations (OBS)

MODEL

Simulation V134

Simulation V001

Simulation V0

Model Calibration

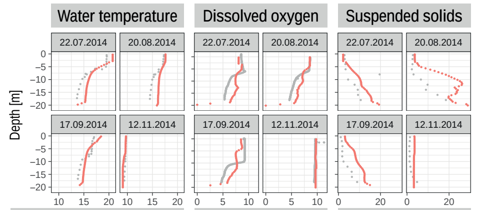

	RMSE [°C]	RMSE [mg/l]	RMSE [mg/l]
Total:	1.15	1.19	4.80
Epilimnion:	1.12	1.08	1.46
Hypolimnion:	1.23	1.44	6.03
Bruce et al. (2017):	1.37		

RESULTS

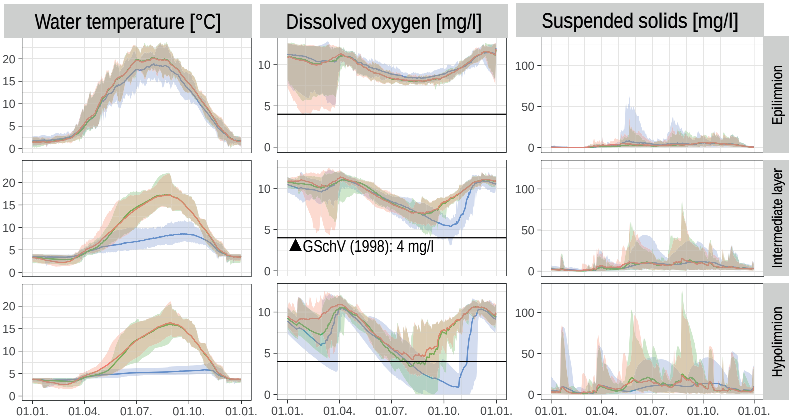

CONCLUSIONS

Water temperature
Sihlsee experiences a warming of its hypolimnion, when water is extracted at the current intake of the hydro-power plant (scenarios V134 and V001). As a result summer stratification is weakened and mixing occurs one or two months earlier than for the reference scenario V000.

Dissolved oxygen
For the scenarios V001 and V134 (water extracted from the hypo-limnion) the shorter and weakened stratification results in less and shorter oxygen depletion in the hypolimnion of Sihlsee. However, all scenarios show DO concentrations less than the legally required 4 mg/l (GSchV, 1998), which is most likely due to unfavourable bathymetry.

Suspended solids
The impacts on stratification also affect the dynamics of suspended solids in Sihlsee. For the reference scenario V000 the suspended solids are likely to remain closer to the lake surface, which also explains the lower concentrations in the hypo-limnion. Yet, limited forcing information must be kept in mind.

References
Bruce, L. et al. (2017). *A multi-lake comparative analysis of the General Lake Model: Stress-testing across a global observatory network.* Environmental Modelling & Software (submitted).
GSchV (1998). *Gewässerschutzverordnung* (SR 814.201).

Acknowledgements
We thank A. Wüest and P. Meier for their overall advice, P. Kathriner, M. Schurter, M. Plüss and the staff at Etzelwerk for assistance with lab and field work, SBB AG for funding and MeteoSwiss, SC Sihlsee, FOEN, cantonal agencies (St.Gallen, Schwyz), WSL and WVZ for providing data.

Trading off energy production from small hydropower with biodiversity conservation

Katharina Lange, Philipp Meier, Clemens Trautwein, Martin Schmid, Christopher Robinson, Christine Weber & Jakob Brodersen*
**katharina.lange@eawag.ch; Eawag, Department of Surface Waters, Kastanienbaum, Switzerland*

Hydropower boom threatenes unique freshwater biodiversity

The construction of small hydropower plants is booming. This exacerbates ongoing habitat fragmentation and degradation, further fueling biodiversity loss. A systematic approach for selecting hydropower sites within river networks may help minimize detrimental effects on biodiversity. Key for designing planning tools is knowledge on reach-scale and basin-scale impacts.

Reach-scale

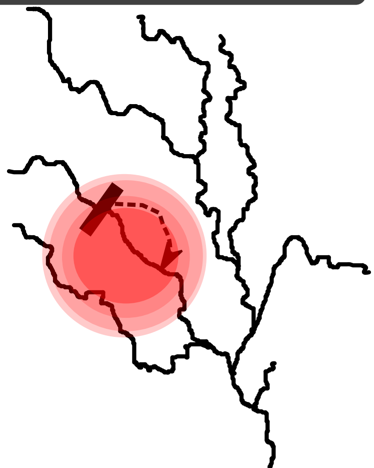

Altered discharge, sediment and temperature regimes

>> impairing ecosystem functioning,
>> negatively affecting fish populations

Basin-scale

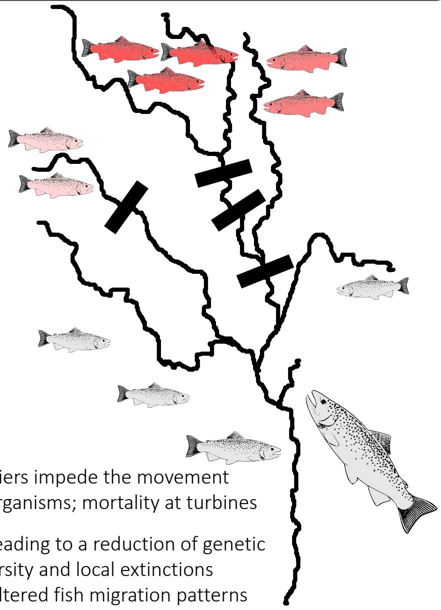

Barriers impede the movement of organisms; mortality at turbines

>> leading to a reduction of genetic diversity and local extinctions
>> altered fish migration patterns

Multiple stressors

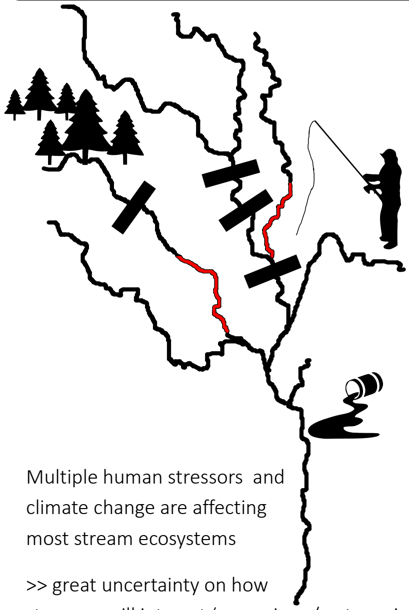

Multiple human stressors and climate change are affecting most stream ecosystems

>> great uncertainty on how stressors will interact (synergisms/ antagonisms)

What we need to know

Downstream propagation of effects – important for cumulative effects of multiple hydropower plants?

Impacts on algal and invertebrate communities which are important for provisioning of ecosystem services ?

Loss of locally adapted genotypes which would lead to a reduction intraspecific biodiversity?

How do river fragment size and the position of dams within the river network drive genetic diversity and the persistance of species within river networks?

How important are cumulative effects of multiple dams for genetic diversity and the persistance of species within river networks?

Do different fish species respond in similar ways?

How will hydropower production and other anthropogenic stressors interact in affecting habitat availability, organisms and ecosystem functions?

Climate change, causing alterations of discharge and temperature regimes, may further affect organism life-histories and ecosystem functioning.

Spatial planning tools

The position of each hydropower plant within the river basin should therefore be compared with alternative sites based on multiple objectives, such as economic gains and low ecological impacts. In multi-objective optimization, the solutions form the so-called Pareto-optimal set where the improvement of one objective can only be achieved at the expense of one or other multiple objectives

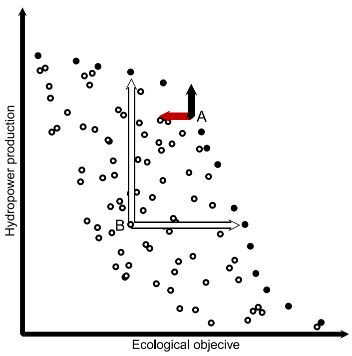

Conclusions

Multiple drivers of biodiversity need to be considered and expressed as indicators, e.g.

- % of unique habitats/populations
- Species-specific habitat-size requirements
- Importance of specific river reaches for spawning/rearing

> Interactions with other stressors may modify the habitat template

➔ Invaluable for policy makers and resource managers
➔ Assist stakeholders and decision makers to develop a shared view and negotiate policies

Manuscript under review with *Frontiers in Ecology and the Environment*

SCCER SoE
SWISS COMPETENCE CENTER for ENERGY RESEARCH
SUPPLY of ELECTRICITY

SCCER-SoE Annual Conference 2017

FlexSTOR

In cooperation with the CTI
Energy
Swiss Competence Centers for Energy Research
Schweizerische Eidgenossenschaft
Confédération suisse
Confederazione Svizzera
Confederaziun svizra
Swiss Confederation
Commission for Technology and Innovation CTI

System modelling for hydro-peaking mitigation

Philipp Meier[1], Martin Bieri[2], Pedro Manso[2], Fränz Zeimetz[2], Christoph Gerber[1], Angela Mark[2], Steffen Schweizer[3], Andres Fankhauser[3], and Benno Schwegler[3]

[1]Eawag, Department of Surface Waters – Research and Management, Kastanienbaum; [2] EPFL, Laboratory of Hydraulic Constructions (EPFL-LCH), Lausanne; [3] Kraftwerke Oberhasli AG (KWO), Innertkirchen

Introduction

Designing efficient measures to mitigate hydro-peaking is a task many hydropower operators in Switzerland face. Constructing a retention basinwhich allows to sufficiently attenuate up- and down-surges in the river, while maintaining the operational flexibility of the powerplant. Such a retention basin needs to be designed carefully by including the entire hydropower system into a detailed analysis.

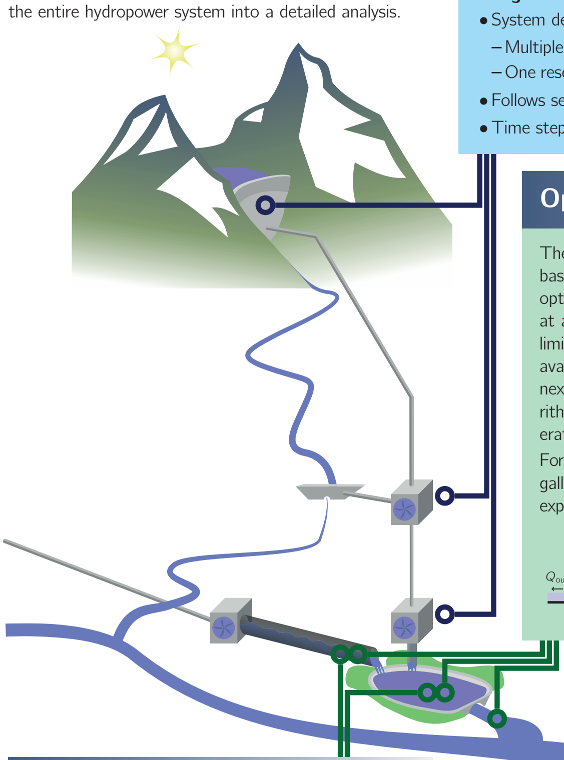

Scenario generator for future hydropower operation

For complex hydropower systems it is not desirable to model the whole system. Therefore, a simple **scenario generator** is developed to reproduce potential future turbine **discharge variability**.

- System defined as network
  - Multiple inflows (water intakes)
  - One reservoir and one power plant
- Follows seasonal cycle
- Time step of 15 minutes

Input data

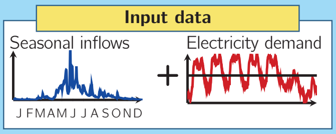

Different discharge scenarios

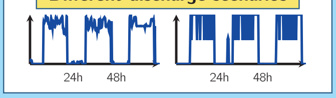

An arbitrary network can be specified:

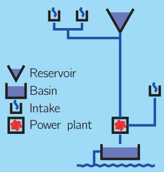

Optimal operation of the retention basin

The performance of a compensation basin is be assessed using a simulation-optimisation model. The model operates at a rolling horizon. This means that only limited information about future inflows is available, inflows are only known for the next 30 minutes. An optimisation algorithm is used to find the best possible operation of the retention volume.

For the KWO case, the two volumes, the gallery and the open-air basin, are included explicitly.

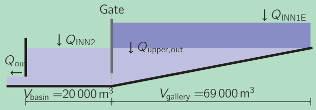

Basin operation model

At each time step a target volume is defined that maximises future operational flexibility.

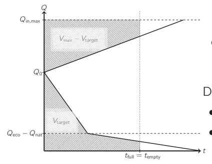

$$\min_{Q_{out}(t)} \left(\frac{V_{lower}(t_{end}) + V_{upper}(t_{end}) - V_{target}}{V_{lower,max} + V_{upper,max}} \right)^2 + \sum_t \left(f_{neg}(J, Q, t) + f_{pos}(J, t) \right)$$

Discharge **gradient** restrictions

- $\frac{dQ}{dt} < 0.7\,\mathrm{m^3\,s^{-1}\,min^{-1}}$
- if $3\,\mathrm{m^3\,s^{-1}} < Q < 8\,\mathrm{m^3\,s^{-1}}$: $\frac{dQ}{dt} > -0.14\,\mathrm{m^3\,s^{-1}\,min^{-1}}$

Reduced discharge gradients

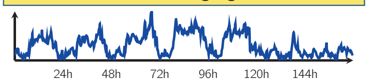

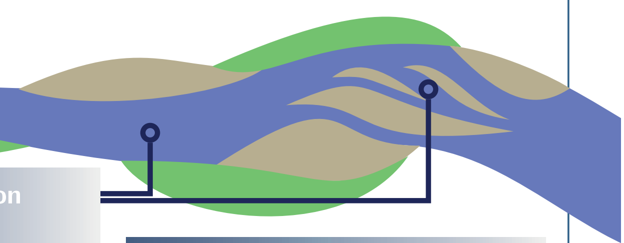

Hydraulic stability of retention basin operation

The operation of the retention volume can be compromised by hydraulic instabilities. Based on extensive data from commissioning tests, the interdependency between water levels, gate openings and power plant discharge is analysed.

Results from commissioning tests

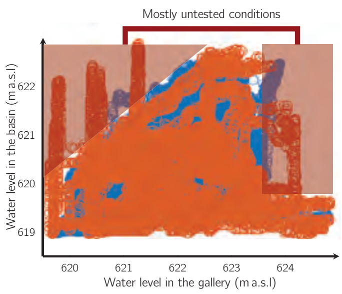

➜ Need to quantify risk of critical combinations

Influence of morphology on hydro-peaking mitigation

The local morphology of the river plays a complimentary role in attenuating hydro-peaking. Morphology not only impacts the propagation of waves, but also the extent of disturbance of fish and macroinvertebrate populations during hydro-peaking events.

Characterising the contribution of river bank morphology to surge gradient attenuation.

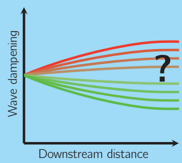

Attenuation from river morphology

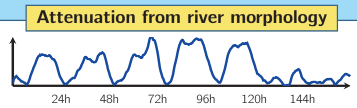

Conclusions

System extensions and upgrades, as well as an increased availability of new renewable energy sources, will significantly impact the operation of hydropower plants. Hydro-peaking might affect the aquatic ecosystem of many rivers.

Using models of relevant infrastructure elements and processes, the most effective mitigation measures can be selected and implemented. The tools developed within this case study will help to design and plan mitigation measures for hydro-peaking in other hydropower schemes and river systems.

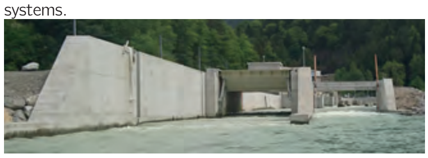

LaTeX TikZposter

SCCER SoE
SWISS COMPETENCE CENTER for ENERGY RESEARCH
SUPPLY of ELECTRICITY

SCCER-SoE Annual Conference 2017

In cooperation with the CTI
Energy
Swiss Competence Centers for Energy Research
Commission for Technology and Innovation CTI

Modeling macroroughness contribution to riverine ecosystem

Amin Niayifar[1] (amin.niayifar@epfl.ch), Paolo Perona[2], Holly J. Oldroyd[3], Stuart N. Lane[4] and Tom J. Battin[1]

Motivation

Changing the natural flow regime, e.g., due to anthropic uses or climate change, causes an environmental degradation in alpine streams

Good understanding of this environmental degradation is of vital importance to minimize such effects

Defining environmental indicators based on macroroughness contribution to riverine ecosystem:

- Creating a wake region where the incoming flow velocity decreases. Fishes minimize energy expenditure by resting in these refuge zones and can easily move to adjacent patches for foraging
- Enhancement of the level of turbulence intensity that results in the increase of reach-scale oxygenation rate

Methodology

A straight river reach of width, w, slope, s, and general bed roughness given by a Manning coefficient, n is considered. The following shows the scheme of the wake and related variables:

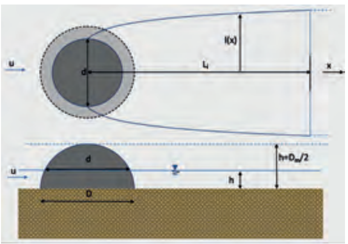

Using the Manning-Strickler relationship and also the streamwise and spanwise length scales of the wake proposed by Negretti et al. (2006), the wake area behind a macroroughness can be calculated as:

$$A_w = \int_0^L l(x)dx = \sqrt{D\sqrt{1-\frac{4\left(\frac{nQ}{\sqrt{Sw}}\right)^{\frac{5}{6}}}{D^2}}\,\frac{\left(\frac{nQ}{\sqrt{Sw}}\right)^{\frac{12}{5}}}{4g^3n^6}}\,B$$

Supposing macroroughnesses with a size density distribution, $p_s(D)$, the density function of the wakes areas can be calculated using the derived distribution approach as follows:

$$p_w(A_w,Q) = p_s(D(A_w,Q))\left\|\frac{dD(A_w,Q)}{dA_w}\right\|$$

The usable area provided by stones for a given flow rate is thus:

$$UA(Q) = \int_{A_{w1}(Q)}^{A_{w2}(Q)} w_w p_w(w_w,Q)dw_w$$

where this equation can be plotted for varying flowrate conditions to build up the usable area curve.

The **environmental threshold** can be defined as the stream flow rate where the derivative of the usable area curve becomes zero

In a case where all the stones have the same diameter:

$$Q_{threshold} = \frac{s^{0.5}wD^{0.33}}{n}$$

Results

Four case studies with different stones diameter are considered:

Delta distribution

Uniform distribution

Truncated exponential distribution

Truncated gamma distribution

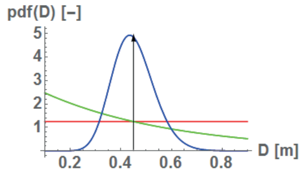

Large stones have a substantial contribution in creating the total wake area in the streams

Environmental threshold at the peak as the usable area decreases significantly

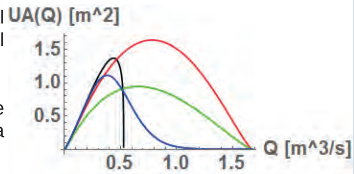

Application of the new model in optimization of a reservoir flow release policies

A simple and robust way of evaluating the environmental friendliness of flow release policies

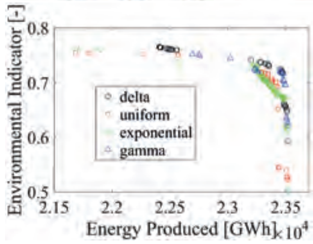

Ongoing Work

Application to a case study (Aare river in the center of Switzerland)

- Characterizing the statistical distribution of stones diameter by taking orthorectified aerial photographs with drones and analysing them with image processing techniques

Measuring the gas exchange coefficient as a function of the stream blockage ratio

- Using the gas (Argon) tracer technique; releasing a gas into a reach and measuring its loss downstream

References

Niayifar, A., & Perona, P. (2017). Dynamic water allocation policies improve the global efficiency of storage systems. *Advances in Water Resources*, *104*, 55-64.

Negretti, M. E., Vignoli, G., Tubino, M., & Brocchini, M. (2006). On shallow-water wakes: an analytical study. *Journal of Fluid Mechanics*, *567*, 457-475.

Appendix

$$B = -2\left(1-\frac{1}{e}\right)^{0.5} + \mathrm{Ln}\left[1+\left(1-\frac{1}{e}\right)^{0.5}\right] - \mathrm{Ln}[1-\left(1-\frac{1}{e}\right)^{0.5}]$$

Task 2.4

Title

Integrated simulation of systems operation

Projects (presented on the following pages)

The role of pumped storage under current and future water availability and electricity prices
D. Anghileri, E. Weber, A. Castelletti, P. Burlando

Using streamflow forecasts to improve hydropower reservoir operations
D. Anghileri, S. Monhart, Z. Chuanyun, K. Bogner, A. Castelletti, P. Burlando, M. Zappa

Evaluation de l'effet d'une crue artificielle et de l'augmentation de sédiments sur la morphologie dans une rivière avec débit résiduel
A. Maître, S. Stähly, M. J. Franca, A. J. Schleiss

How does the HMID behave using numerical data?
S. Stähly, P. Bourqui, C. T. Robinson, A. J. Schleiss

SCCER-SoE Annual Conference 2017

SCCER SoE
SWISS COMPETENCE CENTER for ENERGY RESEARCH
SUPPLY of ELECTRICITY

In cooperation with the CTI
Energy
Swiss Competence Centers for Energy Research
Commission for Technology and Innovation CTI

The role of pumped storage under current and future water availability and electricity prices

D. Anghileri[1], E. Weber[1], A. Castelletti[1], and P. Burlando[1]

1) Institute of Environmental Engineering ETH Zurich. ETH

Motivation

- European energy markets have experienced dramatic changes in the last years because of the massive introduction of Variable Renewable Sources (VRSs), such as wind and solar power sources, in the generation portfolios in many countries.
- This has resulted in lower electricity prices, but, at the same time, in increased price volatility, and in network stability issues.
- Storage hydropower systems play an important role in compensating production peaks, both in term of excess and shortage of energy.
- Hydropower systems are called to a more flexible operation to secure the supply and to maximize their income.

Objectives and relevance of the work

- Assess how the operation of a pumped storage system react to different water availability scenarios (in terms of annual volume and seasonal pattern).
- Assess how the operation of a pumped storage system react to different electricity price scenarios (in terms of mean annual price and variance).

The results inform on the role of pumped storage systems under current and future climate conditions and electricity market situations.

Approach

We use a modeling framework for the integrated continuous simulation of streamflow regimes and of operation of HP systems composed of:

- Mass balance model of the hydropower system (reservoir module of Topkapi-ETH).
- Design of the hydropower system operations using optimization techniques (optimal policy of the hydropower operations)
- Simulation of the optimal hydropower operations with a spatial distributed hydrological model (hydrological module of Topkapi-ETH)

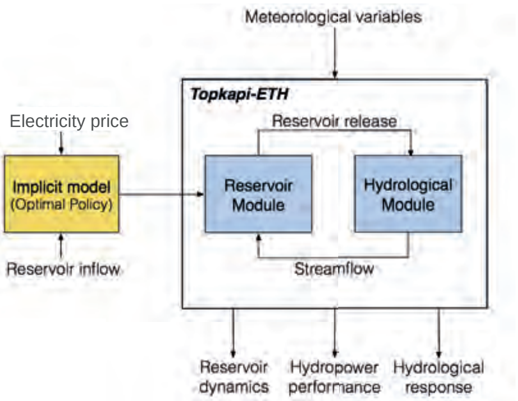

Figure 1: Scheme of the modeling framework combining optimization of the hydropower operations (yellow box) and simulation of the combined- human-natural system (blue boxes).

Water availability and electricity price scenarios

	Water availability	Electricity price
Current scenario	• Observed time series over the period 2008-2014.	• Observed time series over the period 2008-2014.
Future scenario	• Topkapi-ETH hydrological model • Emission Scenarios: A1B • Climate models: ECHAM5, RegCM3 • Stochastic Downscaling *(Bordoy Molina, 2013)*	• SWISSMOD model of the Swiss electricity market *(Schlecht and Weigt, 2014a,b)* • Swiss Energy Strategy 2050 scenarios (Prognos, 2012) • EU Energy Roadmap to 2050 (Capros 2013)

Study site

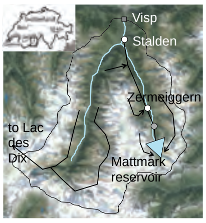

Mattmark hydropower system

Hydropower company: Kraftwerke Mattmark AG c/o Axpo Power AG

Mattmark storage: 100,101,000 m^3

Zermeiggern power plant: 38.8 MW

Zermeiggern pumping plant: 46 MW

Stalden power plant: 187 MW

Catchment area: 778 km^2

Figure 2: Study site hydrological catchment and hydropower system.

Preliminary results

The optimal reservoir operating policy is designed by maximizing the hydropower income. While the release patterns remain similar when considering the 3 different price scenarios (showing increasing volatility because of increasing shares of VRSs), the pumping patterns vary significantly as a consequence of price volatility, showing an increase of both intensity and frequency (Figure 3).

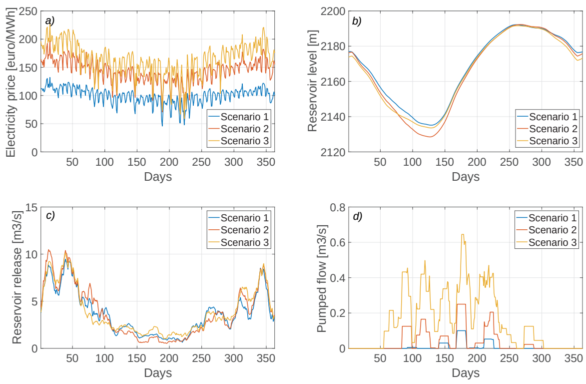

Figure 3: a) Future price scenarios relative to 2025, 2035, and 2045 (Scenario 1-3 respectively): they correspond to different electricity market formulations with increasing shares of VRSs and increasing electricity demand. b-d) Reservoir storage, release, pumping (mean over 10 simulated years).

References

- Bordoy Molina (2013). Spatiotemporal downscaling of climate scenarios in regions of complex geography. PhD. Thesis – ETH Zurich.
- Capros, P. (2013). The PRIMES Model 2013-2014: Detailed model description. E3MLab/ICCS at National Technical University of Athens.
- Prognos AG (2012). Die Energieperspektiven für die Schweiz bis 2050. Energienachfrage und Elektrizitätsangebot in der Schweiz 2000 - 2050.
- Schlecht and Weigt (2014a). Swissmod: A model of the Swiss electricity market. *Social Science Research Network.*
- Schlecht and Weigt (2014b). Linking Europe: The role of the Swiss electricity transmission grid until 2050. *Social Science Research Network.*

SCCER SoE
SWISS COMPETENCE CENTER for ENERGY RESEARCH
SUPPLY of ELECTRICITY

SCCER-SoE Annual Conference 2017

In cooperation with the CTI
Energy
Swiss Competence Centers for Energy Research
Swiss Confederation
Commission for Technology and Innovation CTI

Using streamflow forecasts to improve hydropower reservoir operations

D. Anghileri[1], S. Monhart[2], Z. Chuanyun[1], K. Bogner[2], A. Castelletti[1], P. Burlando[1], and M. Zappa[2]

1) Institute of Environmental Engineering ETH Zurich; 2) Mountain Hydrology and Mass Movements, Swiss Federal Research Institute WSL

Motivation

- Hydropower reservoir operation can be improved by considering streamflow forecasts when deciding how to operate the system, i.e., reservoir and power plant.
- Accurate and reliable streamflow forecasts are key to anticipate extreme events at different temporal scales, particularly on the short term (several hours ahead).
- Increased anticipation capability results into more flexible and adaptive hydropower operation over different time horizons from hourly operation, to weekly management, to monthly production planning.

Objectives and relevance of the work

The objective of the work is to develop a real time hydropower operation system for Alpine snow and rain dominated system, which includes:

i. an ensemble streamflow forecasting system;
ii. a real-time control system scheme.

The specific objectives are:

- to analyze the quality of a set of streamflow forecasts on a retrospective dataset;
- to improve the hydropower system operations;
- to assess the utility of pre-processing meteorological forcing and post-processing streamflow forecasts in terms of hydropower performance.

The results inform on how much reservoir operations can benefit by the consideration of ensemble streamflow forecasts.

Method and tools

We use a *forecast-based adaptive management framework* (see Figure 1) composed of:

i) Forecasting system

The forecasting system used is the one developed and adopted in the NRP70 HEPS4POWER project. See separate poster by Monhart et al..

This system is a further development of the one used by Jörg-Hess et al. (2015) for early detection of hydrological droughts in Switzerland.

The new implementation has been setup for the Verzasca river basin and has following features:

- hydrological model PREVAH forced by monthly IFS ensemble predictions (5 members for 1994-2014 and 51 members for 2014-2015);
- use of raw and pre-processed IFS forcing. Pre-processing make use of quantile mapping;
- use of post-processing techniques to refine the streamflow forecasts (Bogner et al., 2016).

ii) Real-time optimization system

We use a Model Predictive Control (MPC) scheme where the reservoir operations are periodically revised to include the most up-to-date streamflow forecasts.

We use a deterministic optimization on a rolling-horizon to define the operations for the following 30 days, we apply the reservoir release decision for the first day, and we re-optimize the operations for the following 30 days.

We repeat the optimization scheme for every forecast ensemble to estimate how the uncertainty in the forecasts translates into uncertainty in the reservoir operation performances. In so doing, we can assess how the buffering capacity of the reservoir can mitigate potential forecast inaccuracies.

Experimental approach

The assessment of the improvement in HP system performances will be based on the framework proposed in Anghileri et al., (2016).

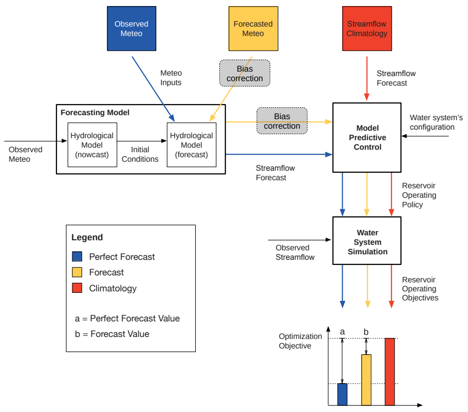

Figure 1: Forecast-based adaptive management framework composed of a forecasting model and a Model Predictive Control optimization scheme. The experimental setting consists of two benchmark (perfect forecast, climatology) which are compared with the forecast to determine the improvement of the HP performances as measured by the reservoir operating objective (modified from Anghileri et al., 2016).

Study site

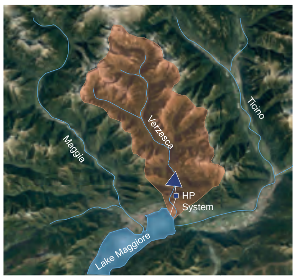

The forecast-based adaptive scheme is applied to the Verzasca hydropower system (Tessin).

<u>HP system features</u>

- Hydropower company: Verzasca SA
- Reservoir storage: 85 10^6 m^3
- Installed power: 105 MW

Figure 2: Study area in red and Verzasca hydropower system.

<u>Hydrological features</u>

The basin is characterized by mixed snow and rain.

At longer lead times the discrimination capability of hydrological predictions is better for low flow conditions (Figure 3). Only at early lead times higher flows show higher discriminative power. Predictions of flash floods remain challenging. The result confirms the findings by Jörg-Hess et al. (2015).

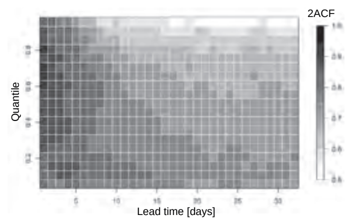

Figure 3: Two-alternative forced choice score (2AFC) for different streamflow quantiles. Values below 0.5 indicate that the forecasts have no discrimination, a value of 1 indicates perfect discrimination.

References

- Anghileri, D., N. Voisin, A. Castelletti, F. Pianosi, B. Nijssen, and D. P. Lettenmaier (2016), Value of long-term streamflow forecasts to reservoir operations for water supply in snow-dominated river catchments, Water Resour. Res., 52, doi:10.1002/ 2015WR017864.
- Jörg-Hess S, Griessinger N and Zappa M. 2015. Probabilistic Forecasts of Snow Water Equivalent and Runoff in Mountainous Areas. J. Hydrometeor, 16, 2169–2186. doi: http://dx.doi.org/10.1175/JHM-D-14-0193.1
- Bogner K, Liechti K, Zappa M. 2016. Post-Processing of Stream Flows in Switzerland with an Emphasis on Low Flows and Floods. Water, 8(4), 115; doi:10.3390/w8040115

SCCER-SoE Annual Conference 2017

In cooperation with the CTI

Evaluation de l'effet d'une crue artificielle et de l'augmentation de sédiments sur la morphologie dans une rivière avec débit résiduel

Anthony Maître, S. Stähly, M.J. Franca et A.J. Schleiss*
**auteur correspondant : anthony.maitre@epfl.ch*

Contexte

Les barrages ont l'inconvénient de représenter une barrière à la continuité des cours d'eau. Le **régime de débit est modifié**, la **migration des poissons est interrompue** et les **sédiments sont retenus à l'amont des barrages**. La rivière de la Sarine a été considérablement modifiée par l'implantation en 1948 du barrage de Rossens. Le **déficit de charriage** à entrainé l'incision de la rivière et le développement d'une végétation importante qui stabilise les berges et empêche donc les sédiments d'être remobilisés. Après la modification de la LEaux en 2011, le canton de Fribourg a entrepris un programme de **renaturation** de la Sarine pour réduire les effets négatifs de l'utilisation de la force hydraulique.

Solutions

Le canton de Fribourg et le groupe E, ont lâché une **crue artificielle de 24h** du 14 au 15 septembre 2016 pour nettoyer la rivière de ses algues. En parallèle, **des sédiments ont été ajoutés** par le LCH dans la rivière sous forme de **4 dépôts alternés**, selon (Battisacco, 2016).

Obectifs

Cette solution expérimentale vise à remobiliser les sédiments pour **réactiver une dynamique de charriage naturelle**. Une meilleure **diversité hydro-morphologique** de la rivière est attendue. Ceci devrait en outre, améliorer la qualité de vie des habitats pour la faune et la flore alluviales.

Méthodologie

Conditions initiales

- 4 dépôts de 250 m^3
- 489 sédiments équipés d'un système RFID (Radio Frequency Identification)
- Une crue artificielle pendant 24 h avec un débit de pointe Q = 195 m^3/s

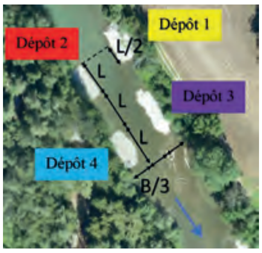

L : longueur des dépôts
B : largeur de la rivière

Déroulement de l'étude

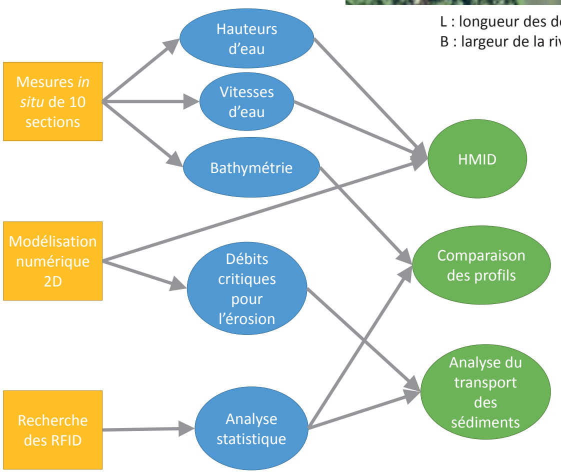

Transport des RFID

Un RFID est mis en mouvement au temps t_0 puis sort de la zone des dépôts après un temps t_1. Il est ensuite détecté par une antenne au temps t_2 et finalement déposé après un temps t_3. Les débits critiques pour l'érosion, permettent de connaître t_0 et t_3.

Hypothèse: Les RFID parcourent la distance x2 + x3 à une vitesse moyenne v = x3 / (t_3-t_2).

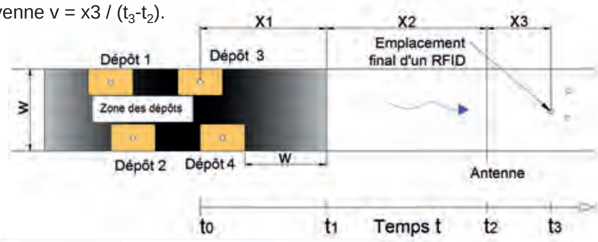

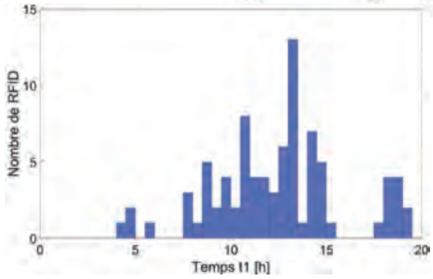

51 % des RFID retrouvés dans la rivière ont été retrouvés en aval de la zone des dépôts. Le temps nécessaire t_1 qu'il leur est nécessaire pour sortir de la zone des dépôts est présenté ci-contre (à gauche).

HMID (Indice hydro-morphologique de diversité)

Amélioration plus importante (+30%) du HMID dans la zone d'impact après la crue, suivant les mesures *in situ* et les résultats de la simulation numérique.

Résultats

Position des RFID et zone d'impact

277 RFID retrouvés sur 489, dont 166 retrouvés dans la rivière et 111 sur les dépôts. La zone d'impact s'étale sur environ **300 m**.

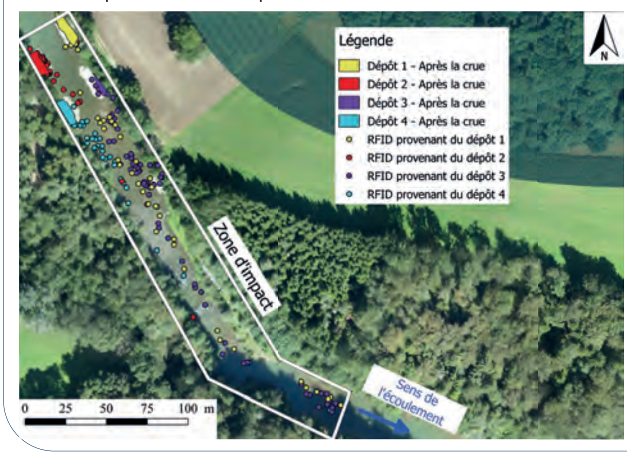

Conclusion

Le HMID indique une **amélioration de la diversité hydro-morphologique** dans la zone d'impact, due aux dépôts.
Selon (Battisacco, 2016), un **nouvel ajout de sédiments** avec une crue pourrait augmenter considérablement la longueur de la zone d'impact.
Les dépôts **1 et 3 profitent de l'écoulement secondaire** créé par la courbe juste à l'amont et sont donc plus érodés. Plus de sédiments pourraient donc être ajoutés sur ce type de dépôts.
Bien que basé sur des hypothèses qui méritent une vérification plus approfondie, le temps t_1 élevé, nécessaire aux sédiments pour quitter la zone des dépôts, représente une **borne supérieure** et peut être **une valeur de comparaison de l'efficacité de la crue** pour de prochaines experiences.

Références

Battisacco, E., Franca, M. J., & Schleiss, A. J. (2016). Sediment replenishment: Influence of the geometrical configuration on the morphological evolution of channel-bed. *Water Resources Research, 52*, 8879–8894

SCCER-SoE Annual Conference 2017

SCCER SoE
SWISS COMPETENCE CENTER for ENERGY RESEARCH
SUPPLY of ELECTRICITY

In cooperation with the CTI
Energy
Swiss Competence Centers for Energy Research
Commission for Technology and Innovation CTI

How does the HMID behave using numerical data?

Severin STÄHLY, Pierre BOURQUI, Christopher T. ROBINSON, Anton J. SCHLEISS*
severin.staehly@epfl.ch

Motivation

More than 15,000 km of the river network is categorized as strongly modified or artificial in Switzerland. In order to classify the natural state of a river, a solid method is needed. Commonly used methods, such as the Rapid Bio assessment Protocol (RBP, Barbour et al., 1999) based on **visual observations**, are sensitive to the person doing the survey.

The **Hydromorphological Index of Diversity** (short HMID, Gostner et al., 2013) can easily be combined with numerical 2D simulations and can serve as an **objective measure** in the geomorphological evaluation of a river before and after its modifications.

Based on a case study at the Sarine river, a **sensitivity analysis** of the HMID from numercial data was conducted, regarding:

- **Model calibration** (Strickler roughness values)
- **Extreme values**

Case study Sarine

Situation of the Sarine
Background: © swisstopo

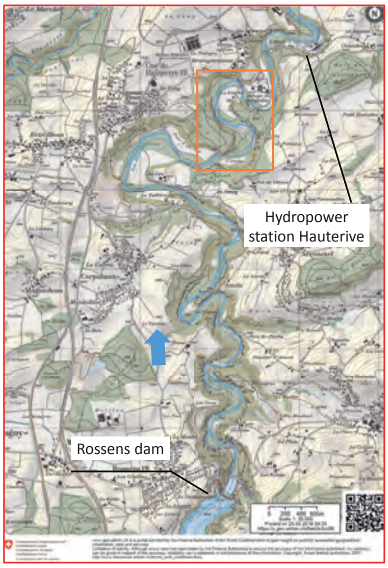

Fig. 1: Situation (top left), Sarine river (right) and the cross-sections taken for the numerical 2D model (bottom left)

Sarine River (Figure 1)

- Meandering river (wide canyon)
- Floodplain of national importance
- 2.5 m^3/s (residual flow reach)
- Average river width 30 m

Numerical model

- Numerical 2D model in BASEMENT with 2 m mesh size
- Based on 27 Cross-sections (80 m spacing) and LiDAR data

Index

The HMID uses flow depth *h* and velocity *v* from different points in the river and is defined by Gostner et al. (2013) as :

$$HMID_{Site} = \prod_i (1 + CV_i)^2 = \left(1 + \frac{\sigma_h}{\mu_h}\right)^2 \cdot \left(1 + \frac{\sigma_v}{\mu_v}\right)^2$$

CV = coefficient of variation [-]
μ = mean value of flow depth [m] or velocity [m/s]
σ = standard deviation of flow depth [m] or velocity [m/s]

Classifying in three different groups:

HMID < 3:	Channelized river with uniform cross-sections
3 < HMID < 5:	Limited habitat variabililty
HMID > 5 :	Full range of hydraulic habitats

Results model calibration

Based on the d_{90} measured in the river, a initial Strickler roughness value K = 30.4 $m^{1/3}/s$ was determined and applied. Table 1 shows that the optimal roughness based on the flow depth lies at K = 10 $m^{1/3}/s$.

Computing the HMID for the different roughness values one can observe in figure 2 that the HMID ranges from **8.4** (K = 10 $m^{1/3}/s$) to **12.1** (K = 30.4 $m^{1/3}/s$). The value measured with acoustic measurements in the field lies at 9.4 what was closest obtained with K = 14 $m^{1/3}/s$ (HMID(K=14) = 9.6).

If the same procedure is applied with a higher discharge, the dependence is significantly smaller.

Tab. 1: Calibration of Strickler roughness values and the difference in water levels compared to the in-stream measured

K [$m^{1/3}/s$]	MAX DIFFERENCE [m]	MEAN DIFFERENCE [m]
30.4	0.45	0.20
28	0.45	0.19
16	0.41	0.12
14	0.39	0.11
12	0.38	0.09
10	0.35	0.09

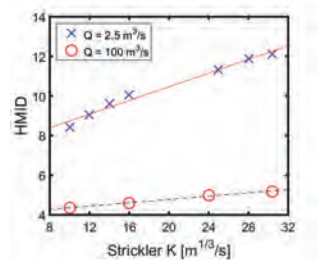

Fig. 2: Dependence of HMID on Strickkler roughness value

Results extreme values

Taking the example of K = 10 $m^{1/3}/s$, the influence of extreme values was investigated. The blue lines in figure 3 show the removal of the largest and the smallest 5% of the values. The HMID drops from 8.4 to **5.6**, what corresponds to a **decrease of 33%**.

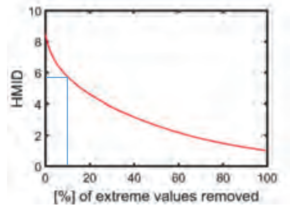

Fig. 3: Dependence of HMID on extreme values

Discussion and conclusion

- Analysis have shown that the calibration of a nurmerical model is important in regards to HMID computations. This effect is stronger at low discharges. In the Sarine the not calibrated model attains an HMID which is roughly **30% higher** than the best calibrated.
- A well calibrated model attains HMID values which are close to the one measured in the field.
- The HMID is largely influenced by extreme values. Therefore, data selection in the field has to ensure that **profiles with shallow as well as profound flow depths are accurately represented in the dataset**!
- In this analysis, the Manning-Strickler flow law was applied, which has been developed for uniform flow and giving one average flow velocity within a profile. Numerical 2D models are more complex and may be more accurate using different flow laws. **The study wants to bring the HMID closer to planning engineers who often use the Manning-Strickler approach.**

References

Barbour, M. T., Gerritsen, J., Snyder, B. D., & Stribling, J. B. (1999). *Rapid bioassessment protocols for use in streams and wadeable rivers: periphyton, benthic macroinvertebrates and fish* (2nd ed., p. 339). Washington, DC: US Environmental Protection Agency, Office of Water.

Gostner, W., Alp, M., Schleiss, A.J., & Robinson, C.T. (2013). The hydro-morphological index of diversity: a tool for describing habitat heterogeneity in river engineering projects. *Hydrobiologia*, 712(1), 43-60

Stähly, S., Bourqui, P., Robinson, C.T., & Schleiss, A. J. (2017). Sensitivity analysis of the hydromorphological index of diversity using numerical generated data. In *37th IAHR World Congress*.

70 NRP Energy Turnaround
National Research Programme

Work Package 3: Innovation Agenda

The objective of WP3 is to provide innovations both on the technical and the computational side for the two key technologies within the SCCER-SoE: hydropower and geo-energies.

Technical Highlights 2017

Expanding the operating range of hydraulic turbines and pump-turbines

In the framework of the FP7 HYPERBOLE project a new methodology to assess the stability of hydropower plants operating in off-design conditions has been developed and validated. Such operations are crucial to provide services to the grid and stay competitive with large hydropower plants. The developed methodology might lead to the revision of the scale-up relating to oscillating phenomena in the IEC 60193 standard for industrial model testing in the future.

Development of new turbines for existing infrastructure

A new turbine to harvest the energy of drinking water networks was developed. Five version of the prototype were tested, the final solution with encapsulated angular ball bearings guarantees lifetime and reliability. The installation of the first product on a pilot site is planned for 2018. A first 1 kW prototype of a kinetic turbine and a dedicated open-air platform have been installed in the tailrace channel of the Lavey hydropower plant. The experimental measurements of the turbine performances have confirmed the numerical predictions

Deep wells: towards long term durability seismometers

In order to allow for long term monitoring of induced seismicity, a borehole seismometer has been developed and installed in Lavey-les-Bains. Reliable operation at 85m depth, continuous data acquisition and transfer could be proven during two campaigns. Comparative performance analysis with SED borehole seismometers in different boreholes in Switzerland is under way.

Optimized workflow for drilling of deep geothermal wells

To improve borehole stability, a workflow to optimize the drilling direction has been developed. The focus is on taking rapid decisions because of the high costs of drill rig downtime. Decisions are based on the analysis of the already drilled vertical section in the crystalline basement prior to initiation of a kick-off angle. This workflow will be tested against various deep drilling data sets. Further improvements are expected from these tests.

Computational Highlights 2017

Prediction of silt-erosion in Pelton turbines

Most of the high head hydropower plants in Switzerland use Pelton turbines and the turbidity of water is high in alpine area. A novel multiscale model has been developed to handle the wide range of length and time scales involved in the sediment erosion phenomena. Several model improvements allow the efficient execution on large scale GPU clusters.

General tool for studying fluid structure interaction (FSI)

A new immersed boundary method has been developed and implemented. It is based on a flexible and general coupling library, with parallel variational transfer between non-matching meshes. It allows to couple existing fluid-dynamics and structural mechanics codes in a massively parallel setting. The new method has been tested for different FSI benchmarks and shows very good scaling behavior. Applications of this tool are foreseen mostly in the context of hydro-power. However, the application of this general approach in the context of reservoir stimulation is also possible.

Task 3.1

Title

Innovative technologies

Projects (presented on the following pages)

DuoTurbo: Mechanical Design
D. Biner, S. Luisier, L. Rapillard, L. Andolfatto, V. Berruex , V. Hasmatuchi, F. Avellan, C. Münch-Alligné

Workflow for managing deep deviated geothermal well stability
A. Dahrabou, B. Valley, F. Ladner, F. Guinot, P. Meier

Understanding the unstable off-design operation of Francis turbines for large scale NRE integration
A. Favrel, K. Yamamoto, A. Müller, F. Avellan

Prediction of hydro-acoustic resonances in hydropower plants operating in off-design conditions
A. Favrel, J. Gomes, C. Landry, S. Alligné, C. Nicolet, F. Avellan

Performance assessment of a new kinetic turbine prototype
A. Gaspoz, S. Richard, V. Hasmatuchi, N. Brunner, C. Münch-Alligné

Empirical models for Francis turbine performance estimation
J. Gomes, L. Andolfatto, F. Avellan

Impact of polymers in well cementing for geothermal wells
M. Palacios, R. K. Mishra, D. Sanz-Pont, R. J. Flatt

Extension of Francis turbine Operating Conditions by Controlling the Part Load Vortex Rope
S. Pasche, F. Gallaire, F. Avellan

Development of an experimental protocol to assess the new kinetic turbine performance
S. Richard, A. Gaspoz, V. Hasmatuchi, N. Brunner, S. Chevailler, C. Münch-Alligné

Expected Corrosion Issues in Geothermal Power Plants in Switzerland
A. Vallejo-Vitaller, U. Angst, B. Elsener

SCCER SoE
SWISS COMPETENCE CENTER for ENERGY RESEARCH
SUPPLY of ELECTRICITY

SCCER-SoE Annual Conference 2017

In cooperation with the CTI
Energy
Swiss Competence Centers for Energy Research
Swiss Confederation
Commission for Technology and Innovation CTI

DuoTurbo: Mechanical Design

D. Biner [1], S. Luisier [1], L. Rapillard [1], L. Andolfatto [2], V. Berruex [2], V. Hasmatuchi [1], F. Avellan [2], C. Münch-Alligné [1]

[1]HES-SO Valais//Wallis, School of Engineering, Hydroelectricity Group, Sion, daniel.biner@hevs.ch

[2]EPFL, Laboratory for Hydraulic Machines, Lausanne

Context

- Recovering hydraulic energy lost in **drinking water networks**
- Modular in-line "plug and play" turbine from **5 to 25 kW**
- No environmental impact
- Low investment costs

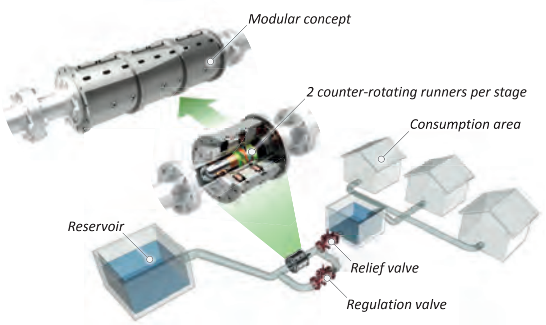

Project

DUO TURBO

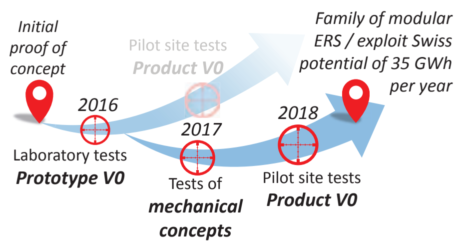

Technical challenges

The hydraulic and electrical concepts of the DuoTurbo prototype have successfully been validated by laboratory tests in 2016. The main issue that is still not entirely resolved, concerns the mechanical concept of the runner bearings. The given operating conditions and requirements make it difficult to find suitable technical solutions.

Operating conditions

- High **axial forces** > 3 kN possible
- High **rotational speed** up to 3500 min^{-1}
- Pipeline **pressure** > 20 bar possible
- Water contaminated with **abrasive particles**

Requirements

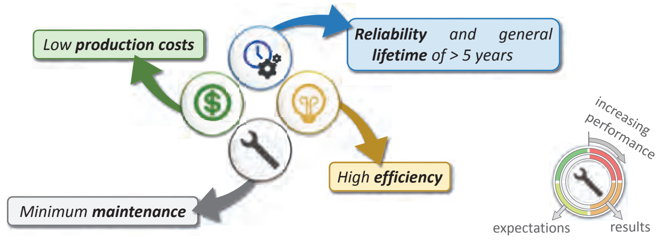

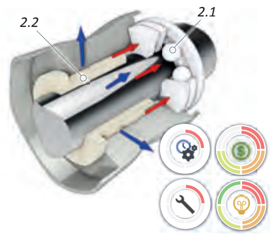

Version 0.2

Concept: Water lubricated axial ceramic ball bearing (*2.1*) combined with hydrodynamic radial plain bearing (*2.2*). Reduced mechanical losses and production costs.

Conclusion: Advanced stage of wear of ceramic ball bearings after laboratory tests. Water lubrication insufficient to ensure requested reliability.

Version 0.3

Concept: Hydrodynamic axial and radial plain bearings (*3.1*), ensuring low wear, low mechanical friction, low maintenance and production costs.

Conclusion: Different bearing materials and shapes tested on a test rig. Hydrodynamic effect too weak to support axial load of turbine runners. Failure during laboratory tests.

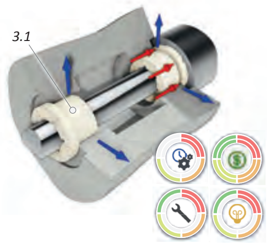

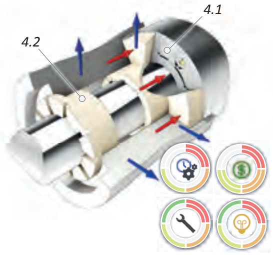

Version 0.4

Concept: Axial hydrostatic bearing (*4.1*) and radial hydrodynamic plain bearing (*4.2*), ensuring low mechanical friction, low wear and low maintenance costs. Hydrostatic bearing supplied by water pipeline pressure. Requires considerable precision of mechanical assembly.

Conclusion: Functionality of hydrostatic bearing validated on separate test rig. Low efficiency of labyrinth seals caused failure during laboratory tests, due to underestimated axial forces.

Tested mechanical concepts

The accomplishment of the given requirements is crucial for the realization of an industrial DuoTurbo turbine. Therefore, different mechanical solutions have been analyzed, designed and tested.

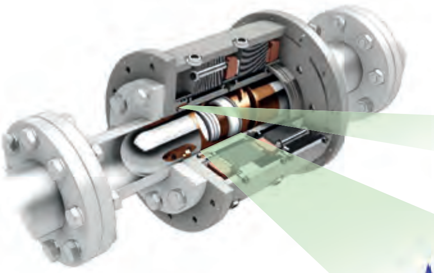

Labyrinth seals

...used to minimize volumetric losses and axial load on the runners.

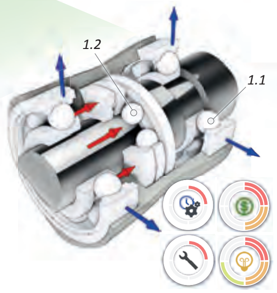

Version 0.1

Concept: Water lubricated radial (*1.1*) and axial (*1.2*) ceramic ball bearings with high corrosion resistance.

Conclusion: Successful for hydraulic and electrical laboratory tests (2016). Enlarged viscous friction and uncertain long time behaviour of submerged ceramic bearings.

Version 0.5

Concept: Encapsulated, grease lubricated angular ball bearings (*5.1*) guaranteeing requested lifetime and reliability. Tightness ensured by mechanical seal (*5.2*), typically used for pumps. Considerable maintenance costs due to regular replacement of the seal (1-2 years).

Actual state: First laboratory performance tests successful. Endurance test phase ongoing until end of 2017.

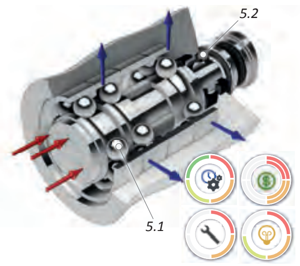

References

- D. Biner, V. Hasmatuchi, D. Violante, S. Richard, S. Chevailler, L. Andolfatto, F. Avellan, C. Münch, **"Engineering and Performance of DuoTurbo: Microturbine with Counter-Rotating Runners"**, *28nd IAHR Symposium - Grenoble*, July 2016.

Development team of Duo Turbo (CTI Nr. 17197.1 PFEN-IW)

HES-SO Valais//Wallis:
D. Biner, S. Luisier, S. Martignoni, D. Violante , V. Hasmatuchi, S. Richard, C. Cachelin, L. Rapillard, S. Chevailler, C. Münch-Alligné

EPFL LMH:
L. Andolfatto, V. Berruex, F. Avellan

Industrial partners:
Telsa SA, Jacquier-Luisier SA, Valelectric Farner SA

Jacquier & Luisier SA
Atelier mecanique

SCCER-SoE Annual Conference 2017

Workflow for managing deep deviated geothermal well stability

Asmae Dahrabou(1), Benoît Valley(1), Florentin Ladner(2), Frédéric Guinot(2), Peter Meier(2)
(1) Centre for Hydrogeology and Geothermics, University of Neuchâtel,Emile-Argand 11, 2000-Neuchâtel, Switzerland.
(2) Geo-Energie Suisse AG, Reitergasse 11, 8004 Zürich, Switzerland.

I- Project context and objectives

In the frame of a CTI-project, the CHYN and Geo-Energie Suisse AG are developing a workflow and associated software tools that allow a fast decision-making process for selecting an optimal well trajectory while drilling deep inclined wells for EGS-projects. The goal is to minimize borehole instabilities as it enhances drilling performance and maximize the intersection with natural fractures because it increases overall productivity or injectivity of the well. The specificity of the workflow is that it applies to crystalline rocks and includes an uncertainty and risk assessment framework.

II- Workflow development approach

A sensitivity study performed on data from the well BS-1 (DHM project Basel) showed that the most influential parameters on borehole stability are the magnitude of the maximum horizontal stress, S_{Hmax} the uniaxial compressive strength, UCS, and the internal borehole pressure P_{mud}

2.1- Model calibration

The understanding of borehole failure in deep crystalline well is lacunar because the strength and stress parameters are largely unknown independently. Moreover, there is no agreement on the appropriate failure model required to capture all characteristics of borehole failure

a. Calibration based on simple but consistent failure modeling approach

Different failure criteria were tested and it was shown that the purely cohesive criterion allows getting calibration that is more consistent across the studied failure indicators. This result is consistent with the literature that indicates that breakout formation is a cohesion weakening process.

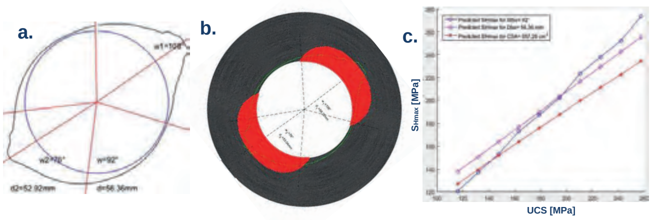

Figure 1. a) Failure observation in BS-1 hole at z=3509m. The blue circle corresponds to the bit size and the black envelop represents the geometry of the well. An average value of w= 92°, d= 56.36mm, CSA= 657.26 cm^2were observed for breakout width, depth and the cross sectional area respectively, b) Predicted failure using Mohr-Coulomb criterion in a simple elasto-brittle computation, c) Calibrated couples (S_{Hmax},UCS), for a vertical hole at z=3509m using the purely cohesive failure

b. Calibration based on independent data (sonic and density)

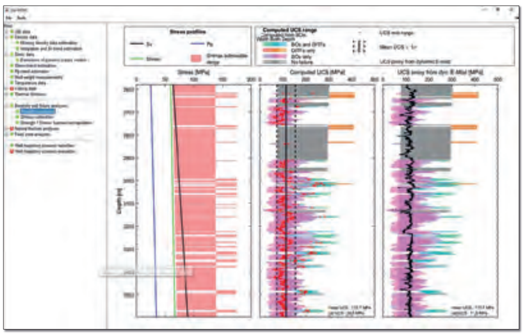

Figure 2. Output from the strength evaluation computations. This evaluation is performed in two main steps: a) realistic parameters ranges are computed based on frictional strength limit of the earth crust and observation of tensile failure in the well, then c) the strength is approximated using strength proxy and the strength/stress couple is calibrated.

• Extrapolating calibrated strength/stress profiles

The calibrated SHmax trend and UCS can be extrapolated to larger depth to anticipate condition when extending the borehole. In order to capture the variability associated with SHmax and UCS, a multipoint statistics direct sampling approached is used.

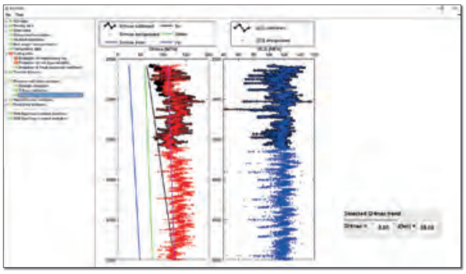

Figure 3. Computed extrapolated profiles of SHmax and UCS

2.2- Selection of wellbore trajectories scenarios

A summary of many decision factor in terms of stereographic projection is presented in order to help selecting potential scenario to be tested

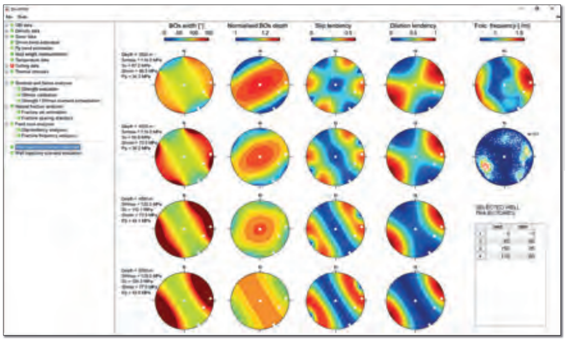

Figure 4. A set of stereographic projections in terms of many decision factors (Breakout width, breakout depth, slip tendency, dilation tendency and fracture frequency) that help selecting potential scenario. These results were performed for depth= 3500m, SHmax= 116 MPa, Sv= 87.2 MPa, Shmin= 66.5 MPa, Pp= 34.3 MPa. Four scenarios with different borehole orientation were selected (white points shown in the stereoplots)

III- Conclusions

- UCS and S_{Hmax} (maximum horizontal principal stresses) are the parameters the most influential on failure computation.
- In combination with an elastic solution for the computation of the stress concentration around the borehole, a purely cohesive failure criterion provides the most consistent prediction across failure indicators
- A pragmatic calibration approach was chosen: firstly, realistic ranges for both S_{Hmax} and UCS were computed based on admissible stress limits and secondly, independent data (sonic and density data) were used as a proxy to approximate the strength

IV- Perspectives

- Further develop the calibration approach adding some additional important parameters like well stability control with drilling mud
- Bring in some more systematic approach in selecting scenario based on identification of key drilling scenario using clustering analyses
- Further test and develop the simple failure model used so far against more advanced modeling approach
- Further test the workflow on existing deep geothermal drilling dataset (Soultz,…) and to new deep geothermal drilling site (Haute-Sorne)

References

Diederichs, M.S. 2007. The 2003 CGS Geocolloquium Address: Damage and spalling prediction criteria for deep tunnelling. Can. Geotech. J., Vol. 44: 9, pp. 1082-1116(35)

SCCER SoE
SWISS COMPETENCE CENTER for ENERGY RESEARCH
SUPPLY of ELECTRICITY

SCCER-SoE Annual Conference 2017

In cooperation with the CTI
Energy
Swiss Competence Centers for Energy Research
Swiss Confederation
Commission for Technology and Innovation CTI

Prediction of hydro-acoustic resonances in hydropower plants operating in off-design conditions

A. Favrel, J. Gomes, C. Landry, S. Alligné, C. Nicolet and F. Avellan

Context


Unsteady power output from renewable energies


Electrical grid is exposed to large fluctuations


Balancing by off-design operation of hydropower plants


High swirl and unstable cavitation flows

Research Project

The **HYPERBOLE** research project (ERC/FP7- ENERGY-2013-1-Grant 608532), consisting of leading European universities and turbine manufacturers, aims at making a decisive contribution towards the smooth integration of NRE by enabling the safe extension of Francis turbines operating range.

Objectives:

- Develop advanced 1D numerical model of cavitation flows in the draft tube of Francis turbines operating in off-design conditions
- Develop a complete methodology for predicting hydro-acoustic resonances in hydropower plants based on 1D numerical modelling and reduced scale model tests

Methodology

Reduced scale model test in laboratory

✓ Identification of the precession frequency and the natural frequency for a given σ – value and Froude number

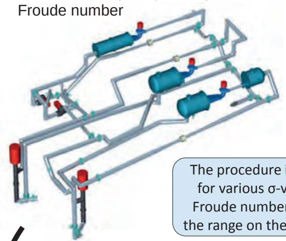

The procedure is repeated for various σ-values and Froude numbers covering the range on the prototype !

~~Direct prediction of resonance conditions~~

Frequencies versus Swirl number

✓ Influence of both the head and discharge on the precession and natural frequencies represented by a single parameter, the swirl number [2]:

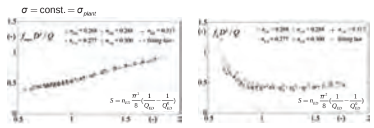

Identification of hydro-acoustic parameters [1]

✓ Wave speed in the draft tube at the model scale as a function of the swirl number:

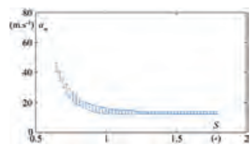

1D model of hydraulic test rig in off-design conditions [1]

1D simulation model

SIMSEN

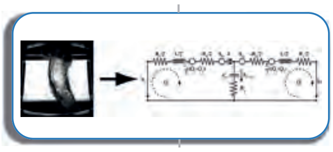

1D model of hydropower plant in off-design conditions [3]

Transposition of the hydro-acoustic parameters from model to prototype:

$$a^P = a^M \left(\frac{D^P_{ref}}{D^M_{ref}}\right)\left(\frac{n^P}{n^M}\right)$$

$$\mu''^P = \mu''^M \left(\frac{D^P_{ref}}{D^M_{ref}}\right)^2\left(\frac{n^P}{n^M}\right)^2\left(\frac{f^M_{natural}}{f^P_{natural}}\right)$$

Full-scale hydropower plant

Prediction of resonance conditions on the prototype

✓ Direct transposition of the precession frequency from model to prototype

✓ Computation of the prototype natural frequencies with 1D SIMSEN model of the hydropower plant unit

✓ Determination of the output power in resonance conditions, i.e. when $f_0 = f_{rope}$

Hydro-acoustic parameters at the prototype scale

✓ Wave speed in the draft tube at the prototype scale as a function of the swirl number:

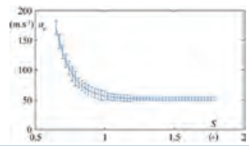

Results and validation by on-site measurements

✓ Very good agreement between predicted and experimental values for both the precession and natural frequencies, as well for the output power in resonance conditions

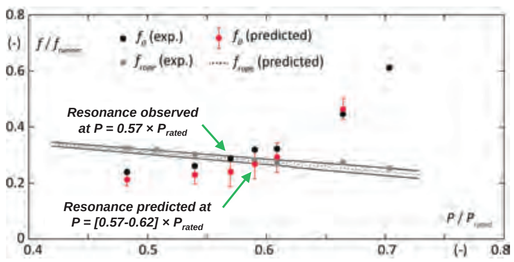

References

[1] Landry C. et al. (2016), «*Local wave speed and bulk flow viscosity in Francis turbines at part load operation*», Journal of Hydraulic Research, vol. 54(2)

[2] Favrel A. et al. (2017), «*New insight in Francis turbine cavitation vortex rope: Role of the runner outlet flow swirl number*», Journal of Hydraulic Research, accepted for publication (in press)

[3] Alligné et al. (2015), «*Francis turbine draft tube modelling for prediction of pressure fluctuations on prototype*», Journal of Physics: Conference Series, vol. 656(1)

HYPERBOLE
ERC/FP7-ENERGY-2013-1-Grant 608532
HYdropower plants PERformance and flexiBle Operation towards Lean integration of new renewable Energies

SCCER-SoE Annual Conference 2017

Understanding the unstable off-design operation of Francis turbines for large scale NRE integration

A. Favrel, K. Yamamoto, A. Müller, C. Landry and F. Avellan

Context

Unsteady power output from renewable energies

Electrical grid is exposed to large fluctuations

Balancing by off-design operation of hydropower plants

High swirl and unstable cavitation flows

Research Project

The HYPERBOLE research project (ERC/FP7- ENERGY-2013-1-Grant 608532), consisting of leading European universities and turbine manufacturers, aims at making a decisive contribution towards the smooth integration of NRE by enabling the safe extension of Francis turbines operating range.

Objectives:

- Reach a profound understanding of the underlying physical mechanisms leading to an unstable behaviour of hydropower unit operating in off-design conditions
- Enhance the accuracy of existing models for a comprehensive simulation of hydroelectric power plants over their whole operating range.

Flow instabilities in off-design conditions

Francis turbine units operating in off-design conditions experiences the development of flow instabilities, inducing cavitation and periodical / stochastic pressure pulsations in the hydraulic system:

FULL LOAD:

Self-oscillation of an axisymmetric cavitation vortex rope in the draft tube inducing pressure, torque and power pulsations

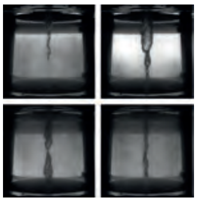

PART LOAD:

Precession of a cavitation vortex rope in the draft tube acting as a pressure excitation source with risk of resonance

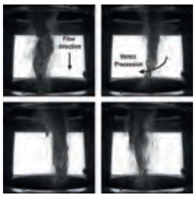

DEEP PART LOAD:

Cavitation vortices in the inter-blade channels (inter-blade vortices) with unknown draft tube flow interaction and erosive potential

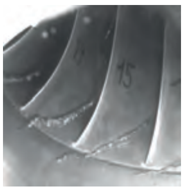

Investigative approach & Results

2D-LDV to determine the flow velocity fluctuations and identify the unstable fluid-structure interaction mechanisms at **full load**

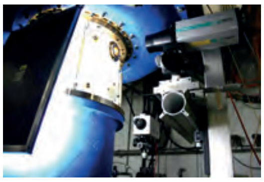

Variation of the flow swirl, pressure and torque over one instability period

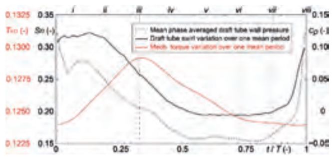

2D-PIV to identify the influence of the flow discharge on the vortex structure and parameters at **part load**

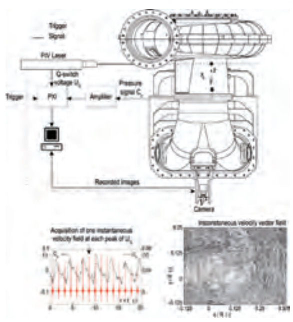

Evolution of the flow velocity field over one precession period

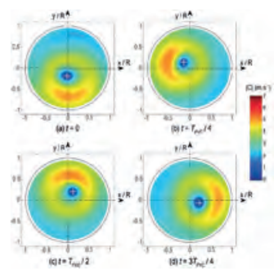

Visualizations with instrumented guide vanes & **CFD** simulation to capture the inter-blade vortices at **deep part load**

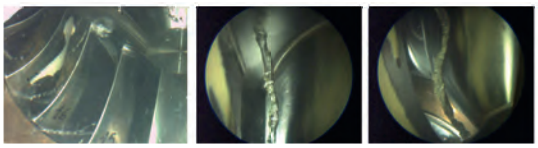

Flow structure inside blade channels

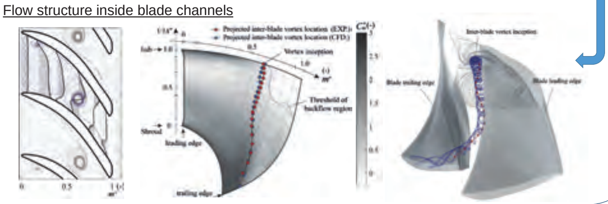

References

[1] Müller A. et al. (2017), "*Fluid–structure interaction mechanisms leading to dangerous power swings in Francis turbines at full load*", Journal of Fluids and Structures, vol. 69, 56-71.

[2] Favrel A. et al. (2015), "*Study of the vortex-induced pressure excitation source in a Francis turbine draft tube by particle image velocimetry*", Experiments in Fluids, 56(12)

[3] Yamamoto K. et al. (2017), "*Experimental evidence of inter-blade cavitation vortex development in Francis turbines at deep part load condition*", Experiments in Fluids, Article in press

SCCER SoE
SWISS COMPETENCE CENTER for ENERGY RESEARCH
SUPPLY of ELECTRICITY

SCCER-SoE Annual Conference 2017

Hes·so// VALAIS WALLIS
School of Engineering

In cooperation with the CTI
Energy
Swiss Competence Centers for Energy Research
Schweizerische Eidgenossenschaft
Confédération suisse
Confederazione Svizzera
Confederaziun svizra
Swiss Confederation
Commission for Technology and Innovation CTI

Performance assessment of a new kinetic turbine prototype

A. Gaspoz[1], S. Richard[1], V. Hasmatuchi[1], N. Brunner[2], C. Münch-Alligné[1]

[1]HES-SO Valais, School of Engineering, Hydroelectricity Group, CH-1950 Sion, Switzerland, anthony.gaspoz@hevs.ch
[2]Stahleinbau Gmbh, Talstrasse 30, CH-3922 Stalden, Switzerland

Objectives of this "pilot & demonstrator" project

- Design and construction of a first prototype of isokinetic turbine for artificial channels with a power of 1 kW
- Evaluation of its hydraulic performances in the tailrace canal of the Lavey run-of-river powerplant (Rhône river)
- Validation of the numerical simulation results
- Preparation of an industrialization phase to exploit this energetic potential in Switzerland and abroad

Pilot site

The pilot site to assess the performance of the first prototype is the tailrace channel of the run-of-the-river Lavey Hydropower plant in Switzerland. At the end of 2016, the open-air platform and the turbine have been installed in the tailrace channel.



Numerical investigations

Unsteady multiphase homogeneous flow numerical simulations of the turbine in the tailrace channel of Lavey have been performed using the ANSYS CFX software. The incompressible Reynolds Averaged Navier–Stokes equations are solved using a finite volume approach. The set of equations is closed-formed and solved using a two-equation turbulence model: the Shear Stress Transport (SST) model. A hybrid mesh of 13 Millions of nodes is used.

Numerical set up

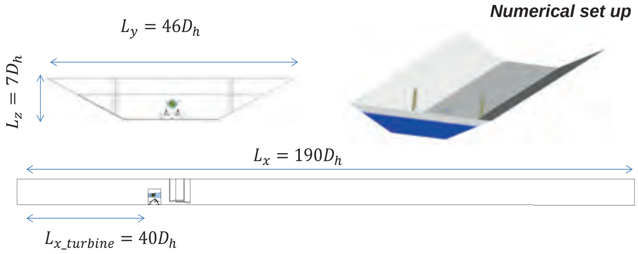

The numerical results have shown that the turbine has no impact on the available head of the Lavey powerplant. Moreover the Venturi effect of the duct and the specific design for the runner induce a strong acceleration of the flow inside the machine, as expected [1].

Free surface flow

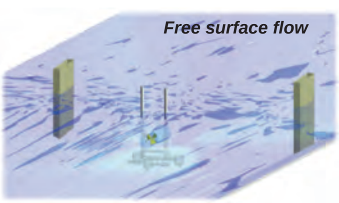

Axial flow velocity

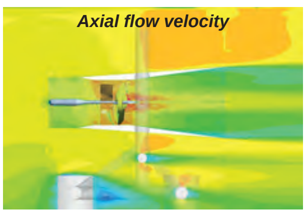

Experimental investigation

To measure the performance of the kinetic turbine on the pilot site, a specific instrumentation has been set up [2]:

- Acquisition/control system
- River boat equipped with an ADCP system
- Electrical multimeter
- Onboard instrumentation

Performance assessment

The turbine performance is obtained by measuring the produced electrical power compared to the available hydraulic power [3]. The objective of the project to reach 1kW with the turbine has been largely outshined with a maximal electrical power measured of 1.5 kW.

Electrical power production

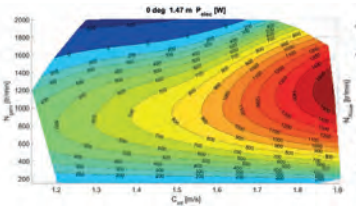

Power coefficient

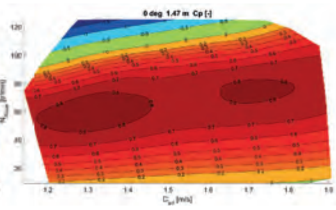

The numerical and experimental performances have been compared and a very good agreement is observed:

Numerical vs. experimental results

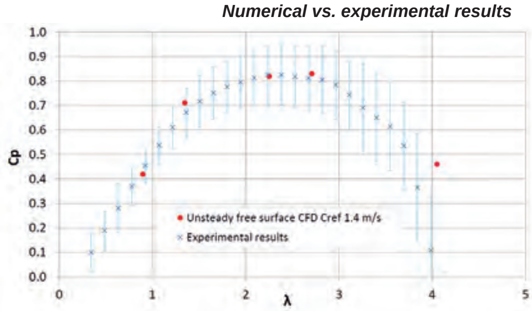

Conclusions and perspectives

These investigations have shown that:

- The objective of the project to produce 1kW with a new prototype of a kinetic turbine has been reached.
- Unsteady two phase flow numerical simulations allow to predict performance fairly accurately at BEP.
- The next step is the installation of a farm of kinetic turbines to investigate the influence of the machines between each other.

Acknowledgements

Schweizerische Eidgenossenschaft, Confédération suisse, Confederazione Svizzera, Confederaziun svizra — Office fédéral de l'énergie OFEN
the ark · STAHLEINBAU · SiL · SWISS VIT

References

[1] C. Münch, A. Gaspoz, S. Richard, V. Hasmatuchi, N. Brunner, 2017, "New prototype of a kinetic turbine for artificial channels" Simhydro Conference, Nice, 14-16 June.

[2] V. Hasmatuchi, A. Gaspoz, L. Rapillard, N. Brunner, S. Richard, S. Chevailler, C. Münch-Alligné, 2016, "Open-air laboratory for a new isokinetic turbine prototype", Annual conference, SCCER SoE, Sion.

[3] S. Richard, A. Gaspoz, V. Hasmatuchi, N. Brunner, S. Chevailler, C. Münch-Alligné, 2017, "Development of an experimental protocol to assess the new kinetic turbine performance", Annual conference, SCCER SoE, Zurich.

SCCER SoE
SWISS COMPETENCE CENTER for ENERGY RESEARCH
SUPPLY of ELECTRICITY

SCCER-SoE Annual Conference 2017

In cooperation with the CTI
Energy
Swiss Competence Centers for Energy Research
Swiss Confederation
Commission for Technology and Innovation CTI

Empirical models for Francis turbine performance estimation

J. Gomes, L. Andolfatto, F. Avellan

Motivation

- The **Energy Strategy 2050**: more energy generation from renewable sources;
- In Switzerland, **many hydropower plants can be upgraded or rehabilitated** therefore generating more power with the same amount of water **[1]**;
- Many feasibility studies, such as those for upgrading or rehabilitating the power plants, take the turbine's efficiency as a constant and don't check off-design or transient conditions.
- Being able to properly evaluate these other conditions and optimize the project from the very beginning is the added-value of this research work

Methods

- Representing the efficiency as a set of parameters **[2]**

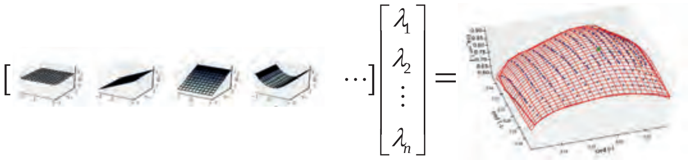

- For better precision, more complex efficiency surfaces may be achieved through a combination of low order polynomials and weighting functions

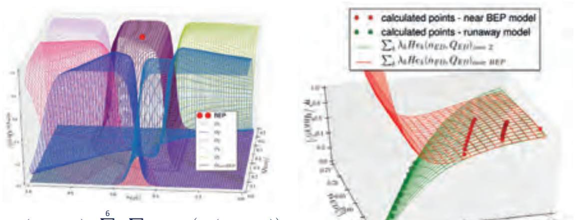

$$\eta(Q_{ED}, n_{ED}) = \sum_{i=1}^{6} \phi_i \sum_{j} \lambda_{i,j} He_j\left(g_i(Q_{ED}, n_{ED})\right)$$

- Available test data used to train the empirical models

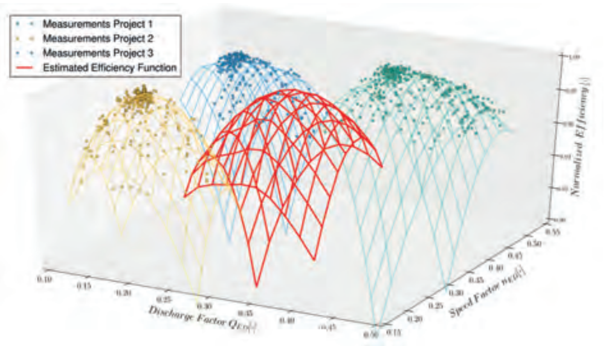

References

[1] – Association Suisse pour l'Aménagement des eaux, 2012 -*Droit de retour et renouvellement de concession des centrales hydroélectriques*

[2] – Andolfatto, L. et al., 2015. - *Analytical Hill Chart Towards the Maximisation of Energy Recovery in Water Utility Networks with Counter-Rotating Runners Micro-Turbine.* The Hague, 36th IAHR World Congress 2015

[3] – Gordon, J. L., 2001. - *Hydraulic Turbine Efficiency*. Canadian Journal of Civil Engineering, 28(2), pp. 238-253

RENOV Hydro

The RenovHydro CTI project no. 19343.1 PFIW-IW will create a **decision making assistant for hydropower project potential evaluation and optimization**.

- 3 years project, started in Dec. 2016;
- Empirical models for the turbine efficiency estimation is inside the Work Package 1 (Francis, Pelton and Kaplan turbine types);
- Partners: groupe e, Power Vision Engineering, FMV, EPFL

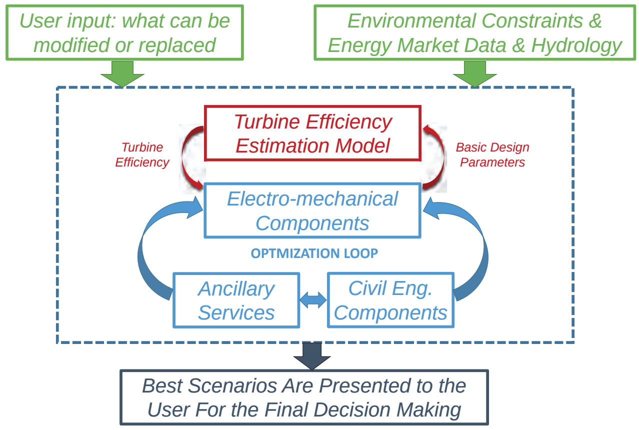

Generating efficiency estimation curves in 4 steps:

1-Peak Efficiency Estimation: based on an adaptation of a model developed by Gordon, J.L. [3], the peak effiency η_{BEP} is estimated according to the turbine's year of commissioning, size and specific speed:

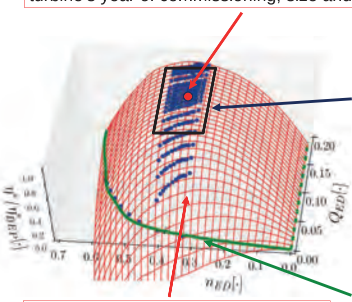

2- Typical operation zone: empirical model based on measurements performed at LMH-EPFL

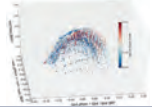

3-Runaway curve: empirical model. Curves are adjusted according to the turbine's specific speed

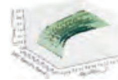

4- Transition zones: low order polynomials combined with weighting functions make the transition between runaway and operating zone values.

Conclusion

By means of a combination of empirical models trained with data obtained from efficiency measurements of Francis turbines through a spam of almost a hundred years [3], a methodology has been developed aimed to predict the performance of Francis turbines.

Inside the RenovHydro Project, an optimization loop that searches for the best combination of electro-mechanical, civil engineering components and ancillary services will make use of these turbine efficiency predictions to define the most suitable design parameters of the future Francis turbine.

A very good agreement has been observed between predictions and measurements, both for steady, typical operating conditions and for simulations of transient conditions such as an emergency shutdown.

LMH Laboratory for Hydraulic Machines
ÉCOLE POLYTECHNIQUE FÉDÉRALE DE LAUSANNE

SCCER SoE
SWISS COMPETENCE CENTER for ENERGY RESEARCH
SUPPLY of ELECTRICITY

SCCER-SoE Annual Conference 2017

In cooperation with the CTI
Energy
Swiss Competence Centers for Energy Research
Swiss Confederation
Commission for Technology and Innovation CTI

Impact of polymers in well cementing for geothermal wells

*M. Palacios, R. K. Mishra, D. Sanz-Pont, R. J. Flatt**

1. Introduction

Backfilling with cementitious material is essential for mechanical stability of deep wells. However, with increasing depth temperature rises involving many technological challenges such as poor rheological properties and quick setting of cement slurries. On site, a combination of different chemical admixtures including dispersants, set retarders and accelerators are normally used although a loss of performance is often found.

In the Group of Physical Chemistry of Building Materials, in the frame of WP3 Task 3.1 "Geo-energy technologies", we investigate the use of specific comb-copolymer superplasticizers to control cement hydration kinetics and rheological properties of cement slurries at the extreme conditions encountered in geothermal well. This will be done using an experimental and molecular modeling approach.

2. Methods

- **Isothermal calorimetry** to study the impact of polymer structure and dosage on cement reaction kinetics with the temperature.
- **Inductively Coupled Plasma – Optical Emission Spectrometry (ICP-OES)** and **Dynamic Light Scattering (DLS)** to analyze cement pore solutions.
- **High-end rheometer** to investigate the rheological properties of the superplasticized retarded mixes.
- **MD simulation** to understand the interaction between organic admixtures and the chemical species present in solution.

3. Highlights of the project

It has been demonstrated for first time that cement hydration can be delayed at high temperatures by specific dosages and structures of comb-copolymer superplasticizers (**Figure 1**).

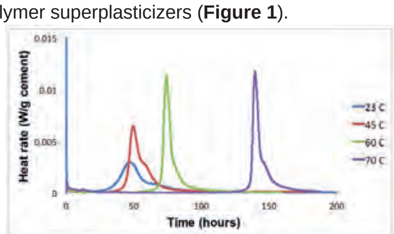

Figure 1. Calorimetry curves at different temperatures of cement pastes in presence of a specific comb-copolymer

The analysis of the chemical composition of the cement pore solution using ICP-OES method[1] has proved a dramatic increase in the concentrations of Si, Al, Fe and Mg, in admixed cement pastes hydrated at 23 °C (**Figure 2**). The formation of polymer aggregates involving intramolecular complexes between polymers and multivalent cations could explain the increase of these elements.

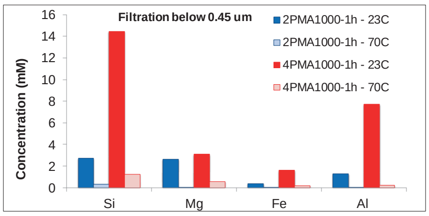

Figure 2. Analysis of pore solutions of admixed pastes by ICP-OES.

Distribution of Side Chains	Polymer	Carboxylate/ether (C/E)	Side chain (g/mol)
Irregular	4PMA1000	4	1000
Regular	2PMA1000	2	1000

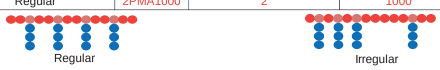

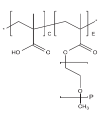

Figure 3. Structural details of comb-copolymer PCE superplasticizers.

The mechanisms behind molecular interactions between tricalcium silicate (main phase of cement) and aluminate ions has been firstly studied by molecular dynamics (MD) simulations using all-atom accurate force field models (**Figure 4**). Upon progress of hydration and at higher pH values, the binding strength of aluminates to the hydroxylated C_3S decreases so that its passivating effect, and retardation, are reduced (**Table 1**).[2] Furthermore, the interactions between the aluminate ions and PCE comb-copolymers have been investigated (**Figure 5**).

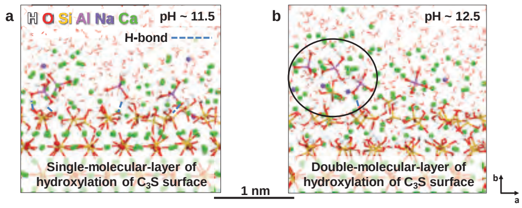

Figure 4. Interactions of aluminate ions with the hydroxylated C_3S surface. (a) Interactions of aluminate ions with the initially hydrated C_3S surface at pH ~ 11.5 involve strong bonding to calcium ions on the surface as well as interfacial hydrogen bonds (Al–OH···O⁻–Si and Al–OH···OH–Si). (b) Interactions of aluminate ions with the C_3S surface at pH ~12.5 are weaker. Dissolution of silicate ions and formation of ionic complexes between aluminate and calcium ions, aluminate ions and silicate ions (circular highlight) can be seen.

Table 1. Adsorption energy of $NaAl(OH)_4$ on the hydroxylated C_3S surface under ambient conditions for different hydration depth and added NaOH.

Type of C_3S surface	Adsorption energy (kcal/mol/molecule)	pH	Amount of hydration
Hyd.C_3S ($SiO(OH)_3^{1-}$)	–24 ± 6	11.5	Single molecular layer
Hyd.C_3S ($SiO(OH)_3^{1-}$)	–6 ± 3	12.5	Double molecular layer
Hyd.C_3S ($SiO(OH)_3^{1-}$) + NaOH	0	13.4	Single molecular layer

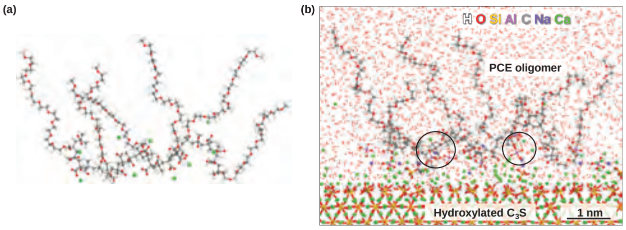

Figure 5. (a) Structure of PCE with six side chains.(b) MD snapshot of interaction between aluminate ions and polycarboxylate ether (PCE) admixture on the hyd. C_3S surface. Complex formations happen between carboxylate group and aluminate ions (circular highlight).

4. Ongoing research

The following studies will give new insights into the design of more robust cement grouts:

- Role of complex formation between polymer and multivalent (Al, Mg and Fe) cations
- Influence of the temperature on the adsorption of the polymer.
- Impact of PCE admixtures in presence of Mg and Fe ions

References

1. F. Caruso, S. Mantellato, M. Palacios, R. J. Flatt "ICP-OES method for the characterization of cement pore solutions and their modification by polycarboxylate-based superplasticizers" Cement and Concrete Research, **2017**, 91: 52-60,

2. E. Pustovgar, R. K. Mishra, M. Palacios, J.-B. d'Espinose de Lacaillerie, T. Matschei, A. S. Andreev, H. Heinz, R. Verel and R. J. Flatt "Influence of aluminates on the hydration kinetics of tricalcium silicate" Cement and Concrete Research, **2017**, 100: 245-262.

SCCER-SoE Annual Conference 2017

SCCER SoE
SWISS COMPETENCE CENTER for ENERGY RESEARCH
SUPPLY of ELECTRICITY

In cooperation with the CTI
Energy
Swiss Competence Centers for Energy Research
Swiss Confederation
Commission for Technology and Innovation CTI

Extension of Francis Turbine Operating Conditions by Controlling the Part Load Vortex Rope

Pasche S., Gallaire F., Avellan F.

Problematic

This project consists of applying the latest flow control theories to an important issue arising in hydraulic turbines: the development of a cavitation vortex rope at part load conditions in Francis turbines.

With the future massive introduction of renewable energy in the distribution systems, the operation of Francis turbines at off-design conditions, such as the part load regime, is thought to be one of the main solutions to mitigate large power fluctuations of the grid.

An intense cavitation rope is however known to appear in these conditions, which produces large pressure fluctuations at a well-defined frequency, with the associated hazards induced by the risks of operating instability and fatigue and resonance of the mechanical structures.

Objectives

Control the part load vortex rope to enable the extension of Francis turbine operating conditions and to further enhance the power generation flexibility of these generating units

Methods

Since the part load vortex rope is identified as an unstable eigenmode, a flow control strategy aiming at stabilizing this spatially developing mode is applied to obtain an optimal volume force controlling the part load vortex rope.

Francis turbine

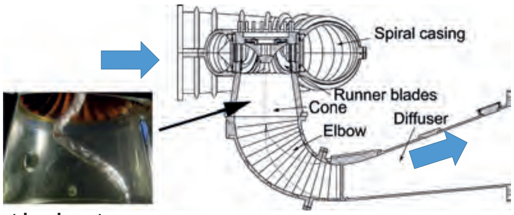

Part load vortex rope

Part load vortex rope eigenvalue spectrum and flow control strategy

Unstable eigenmode

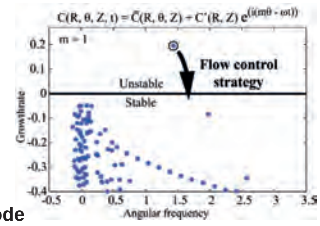

Results

Transient wall pressure signal of the part load vortex rope control

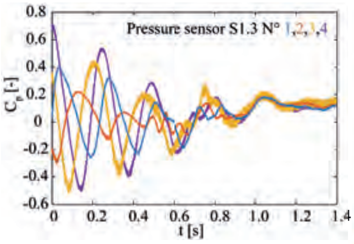

Part load vortex rope

Controlled flow distribution

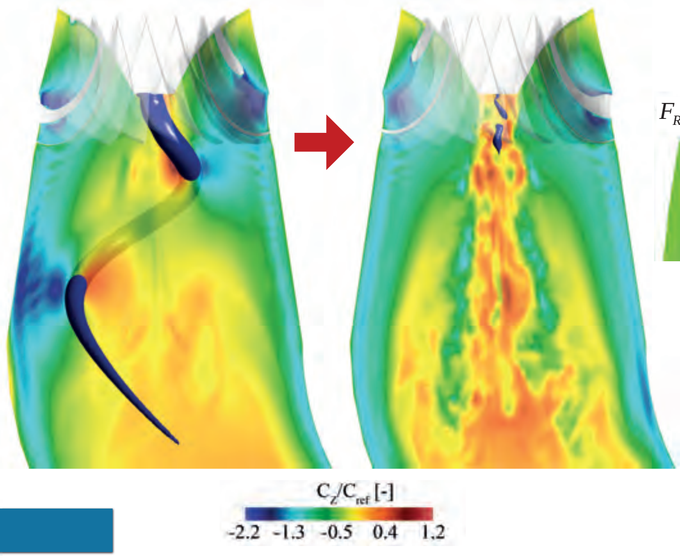

Optimal volume force

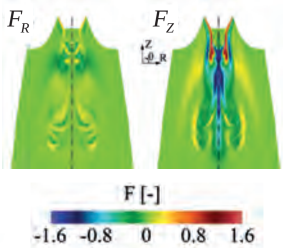

Conclusion

A new fluid flow control strategy aiming at stabilizing the development of self-sustained instabilities is applied to the Francis turbine vortex flow operating at part load conditions. This approach has led to the determination of the amplitude and the location of an optimal volume force, which successfully controls the part load vortex rope and can be, in a future work, realized by a passive control appendage. The enhancement of operation flexibility of Francis turbine is therefore numerically achieved in this project, which sheds a new light in the potential development of hydraulic turbines in mitigating electric power fluctuations.

.

FNSNF
LMH Laboratory for Hydraulic Machines
EPFL
ÉCOLE POLYTECHNIQUE FÉDÉRALE DE LAUSANNE

SCCER SoE
SWISS COMPETENCE CENTER for ENERGY RESEARCH
SUPPLY of ELECTRICITY

SCCER-SoE Annual Conference 2017

Hes·so Valais Wallis
School of Engineering

In cooperation with the CTI
Energy
Swiss Competence Centers for Energy Research
Commission for Technology and Innovation CTI

Development of an experimental protocol to assess the new kinetic turbine performance

S. Richard[1], A. Gaspoz[1], V. Hasmatuchi[1], N. Brunner[2], S. Chevailler[1], C. Münch-Allігné[1]
[1]HES-SO Valais/Wallis, School of Engineering, Hydroelectricity Group, CH-1950 Sion, Switzerland, sylvain.richard@hevs.ch
[2]Stahleinbau Gmbh, Talstrasse 30, CH-3922 Stalden, Switzerland

Context

- The first prototype of an isokinetic turbine for artificial channels with a power of 1 kW has been designed, optimised and manufactured [1].
- Its hydraulic performances have to be measured directly on a pilot site represented by the tailrace canal of the Lavey run-of-river powerplant (Rhône river) [2-3].

Objective:

- Development of an experimental protocol to assess the performance characteristics of the machine on the whole operating range using the available instrumentation.

Electro-mechanical concept

- Sealed bulb housing including the variable speed generator, the encoder, the speed multiplier and the mechanical coupling
- 1kW compact permanent magnet synchronous generator
- Coaxial gear speed multiplier with a factor of 1:16
- Mechanical shaft sealing: resistant to suspended sediment conditions

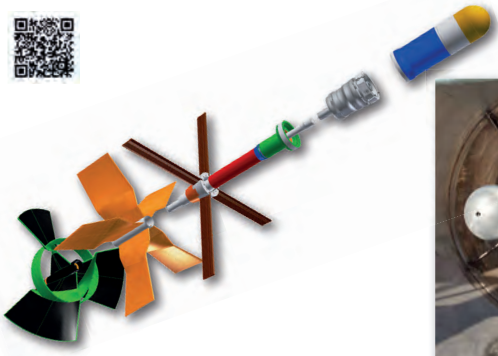

Performance tests of the generator

Main characteristics:

- Phase TK142-100-041-G-R0-pa synchronous machine
- 12 poles (permanent magnet)
- Water cooled
- Rated power: 2.39 kW
- Rated current: 6 A
- Rated/maximum speed: 1'000/2'000 rpm

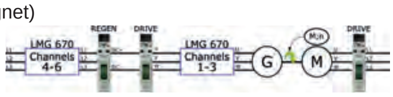

Components of the testing bench:

- Testing generator
- Torquemeter & encoder
- Entrainment motor unimotor fm 142U2E300
- Emerson M700 frequency converters

Instrumentation:

- Magtrol TMB 208 torquemeter
- Heidenhein ECN 1325 encoder
- Zimmer LMG 670 precision multimeter

Electrical performances

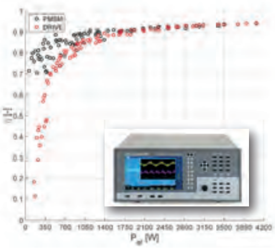

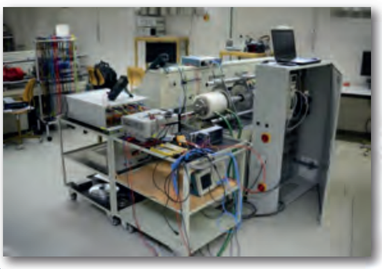

Torque-current constant

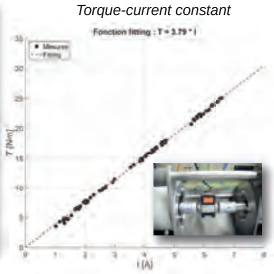

Performance tests of the gear box

Experimental methodology:

- Generator-gear box tested together
- Specific system allowing up to 260 N.m manual breaking torque
- Performance measurements based on synchronized dynamic acquisition of sensors signals

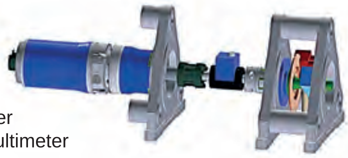

Instrumentation:

- NCTE 3000 torquemeter
- Heidenhein ECN 1325 encoder
- Zimmer LMG670 precision multimeter
- NI cDAQ-7124 signals digitizer

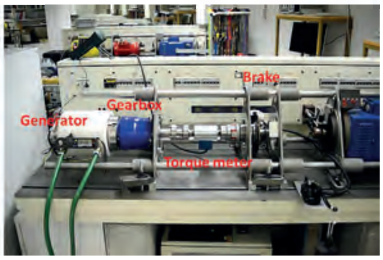

Main result:

- Dependency between the mechanical-to-electrical efficiency of the assembly generator-gear box and the measurements of the generator true-rms values of the current and the speed
- This methodology allows retrieving the hydraulic-to-mechanical efficiency of the turbine runner without torquemeter

Generator-gear box efficiency

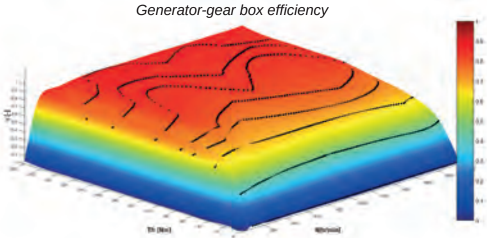

Conclusions

- Performances of the electrical generator successfully measured
- Performances of the assembly between the electrical generator and of the gear box successfully retrieved using the dynamic method
- The established experimental protocol enables the performance measurements of the new isokinetic turbine prototype directly in the tailrace canal of the Lavey powerplant

Acknowledgements

Office fédéral de l'énergie OFEN · the ark · STAHLEINBAU · SiL · SWISS VIT

References

[1] C. Münch, A. Gaspoz, S. Richard, V. Hasmatuchi, N. Brunner, 2017, "New prototype of a kinetic turbine for artificial channels" Simhydro Conference, Nice, 14-16 June.

[2] V. Hasmatuchi, A. Gaspoz, L. Rapillard, N. Brunner, S. Richard, S. Chevailler, C. Münch-Alligné, 2016, "Open-air laboratory for a new isokinetic turbine prototype", Annual conference, SCCER SoE, Sion.

[3] A. Gaspoz, S. Richard, V. Hasmatuchi, N. Brunner, C. Münch-Alligné, 2017, "Performance assessment of a new kinetic turbine prototype", Annual conference, SCCER SoE, Zurich.

SCCER-SoE Annual Conference 2017

SCCER SoE
SWISS COMPETENCE CENTER for ENERGY RESEARCH
SUPPLY of ELECTRICITY

In cooperation with the CTI
Energy
Swiss Competence Centers for Energy Research
Commission for Technology and Innovation CTI

Expected Corrosion Issues in Geothermal Power Plants in Switzerland

*A. Vallejo-Vitaller, U. Angst, B. Elsener **

1. Introduction

In Switzerland, the co-generation of electric power and heat from deep geothermal resources is gaining further attention. However, the expertise in operational issues and the knowledge of chemical properties of deep geothermal fluids (at depths of 4-5 km) is still limited. [1]

In this context, one of the main technical problems for the reliable and long-term operation of binary power plants is corrosion. Metallic materials, such as low-alloyed steels, are mainly subject to uniform corrosion, pitting corrosion, or stress corrosion cracking. The electrochemical reactions between the material and the environment lead to different types of corrosion products.

Therefore, the goal of this project is to contribute to a more detailed understanding of the corrosion mechanisms and the characterization of various metallic materials under various scenarios in Switzerland.

2. Experimental methods

An experimental setup consisting of a high temperature-high pressure test vessel has been used for the tests. The autoclave is heated from room temperature up to 200°C and subsequently cooled down. The heating and cooling cycles usually take ca. 15h.

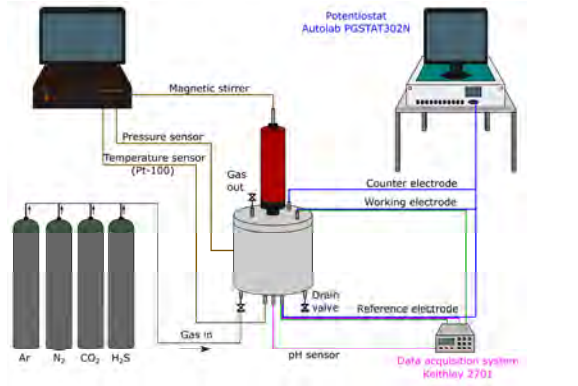

Electrochemical techniques

The open circuit potential (OCP) is measured continuously during the tests with a multimeter Keithley 2701. Linear polarization resistance (LPR) measurements are performed at given temperatures (usually at 80, 120, 160, and 200°C) with a potentiostat Autolab PGSTAT302N. The corrosion rate is then calculated as given by the Faraday's law:

$$Corrosion\ rate = \frac{M \cdot i_{corr}}{z \cdot F \cdot \rho}$$

M : molecular weight (g/mol)
i_{corr} : corrosion current density (A/cm^2)
z : valency of metal ion
F : Faraday's constant $(96485\ As/mol)$
ρ : density of metal (g/cm^3)

Materials

The steel grade L80 Type 1 (0.25%C, 1.02%Mn, 0.45%Cr) is a typical low-alloyed steel used for the casing of wells and produced according to the API specification (American Petroleum Institute).

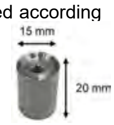

Synthetic fluids

Aqueous solutions were deaerated with N_2 gas for ca. 1-2h.

pH	*Ca^{2+}*	*Mg^{2+}*	*Na^+*	*K^+*	*HCO_3^-*	*SO_4^{2-}*	*Cl^-*
8.4-8.6	10.0	0.0	282.0	0.0	375.0	300.0	0.0

3. Results

Open Circuit Potential (OCP) evolution

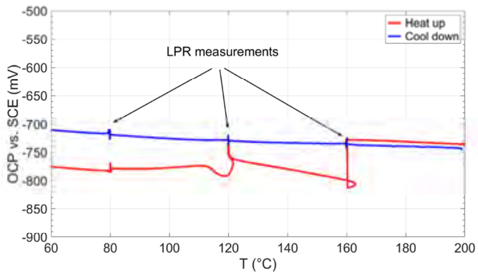

Linear Polarization Resistance (LPR) measurements

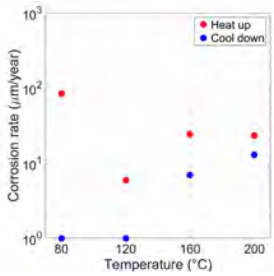

- Corrosion rates are lower during the cooling cycle
- Average corrosion rate is approx. 20µm/year

pH value

The pH value remains stable (8.2 ± 0.3 units) over the whole range of testing temperatures (20-200°C).

SEM and EDX analysis after test

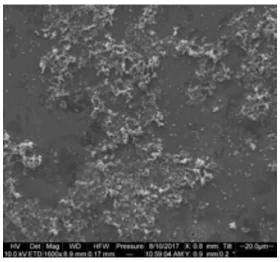

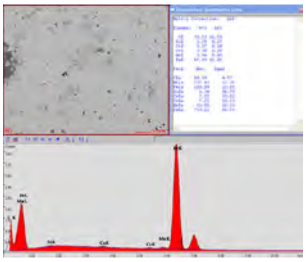

4. Conclusions and future work

- The OCP does not vary significantly with temperature (-750mV vs. SCE). According to the Pourbaix diagram of iron, the obtained value suggests that this element is in the oxidation state Fe^{2+}.
- Furthermore, the LPR measurements show that there is no dependency of the corrosion rate on temperature.
- From the SEM and EDX analysis, it can be seen that different oxides adhere to the metal surface (mostly carbonate components).
- Although the corrosion rate slightly changes with temperature (approx. 20µm/year), the corrosion behaviour of the material over longer time spans is still unknown. Further investigations on the protection provided by the corrosion products to the base metal are necessary.

5. References

[1] Sonney, R., & Vuataz, F. D. (2008). Properties of geothermal fluids in Switzerland: a new interactive database. Geothermics, 37(5), 496-509.

* Institute for Building Materials, ETH Zurich, 8092 Zurich, Switzerland; Corresponding author: ana.vallejo@ethz.ch

Task 3.2

Title

Computational energy innovation

Projects (presented on the following pages)

GPU-SPHEROS: A GPU-Accelerated Versatile Solver Based on the Finite Volume Particle Method
S. Alimirzazadeh, E. Jahanbakhsh, A. Maertens, S. Leguizamon, F. Avellan

Efficient Finite Element Simulation Methods for Fracture Networks
M. Favino, J. Hunziker, K. Hollliger, R. Krause

Parallel Methods for Contact Problems in Rough Rock Surfaces
R. Krause, M. Nestola, D. Vogler, C. von Planta, P. Zulian

A Multiscale Model for the Simulation of Sediment Impact Erosion
S. Leguizamón, E. Jahanbakhsh, A. Maertens, S. Alimirzazadeh, F. Avellan

Surface tension modeling: wetting and contact angle hysteresis
A. Maertens, E. Jahanbakhsh, F. Avellan

Reactive flow patterns in fractured media
J. Mindel, T. Driesner

Fictitious Domain Method for 3D FSI Simulations of Turbines
M. Nestola, P. Zulian, R. Krause

Investigating transport processes in 3D fractured reservoirs
P. Schaedle, A. Ebigbo, M. O. Saar

Sloshing motion of a water free surface in a Francis turbine operating in condenser mode
E. Vagnoni, A. Favrel, L. Andolfatto, F. Avellan

CSMP++GEM for reactive transport modelling with solid solutions
A. Yapparova, G.D. Miron, D.A. Kulik, T. Driesner

SCCER-SoE Annual Conference 2016

In cooperation with the CTI

GPU-SPHEROS: A GPU-Accelerated Versatile Solver Based on the Finite Volume Particle Method

Siamak Alimirzazadeh, Ebrahim Jahanbakhsh, Audrey Maertens, Sebastián Leguizamón, François Avellan

Introduction

GPU-SPHEROS is a **GPU-accelerated particle-based solver** based on Finite Volume Particle Method (**FVPM**) which inherits desirable features of both Smoothed Particle Hydrodynamics (SPH) and mesh-based Finite Volume Method (FVM) and is able to simulate the interaction between fluid, solid and silt [1]. With GPU-SPHEROS, the goal is to perform a industrial size setup simulations of hydraulic machines.

Software flowchart

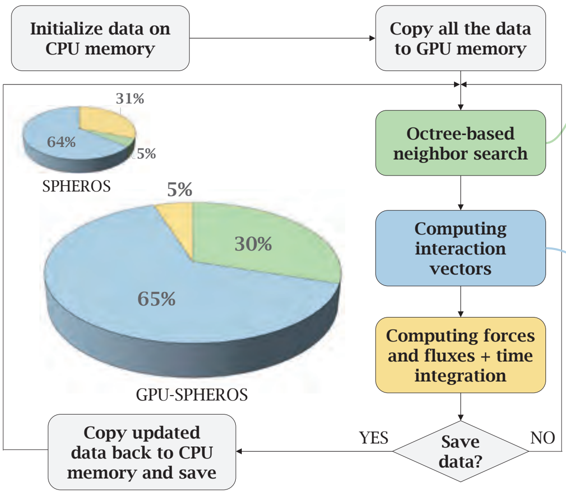

Speedup

- On NVIDIA Tesla P100, GPU-SPHEROS is **5.5x faster** than the CPU version running on a node with 2 x Intel® Xeon® E5-2660 v2 and also more than 6x faster compared to one Intel Broadwell based machine with 2 x Intel® Xeon® E5-2690 v4 CPUs.
- Throughput reaches **3x10⁵ particles per second** on Tesla P100.

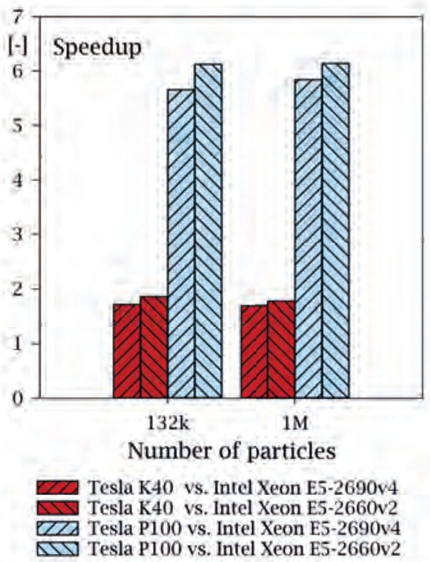

Octree-based neighbor search

- **Memory access efficiency** is a key point for GPU applications to be able to get a good performance.
- The data has been reordered using **space filling curves** (here, Morton curve) to improve memory access.
- An octree-based neighbor search algorithm has been implemented to find the neighbor particles.
- A highly optimized kernel has been implemented for parallel distance check between the particles.

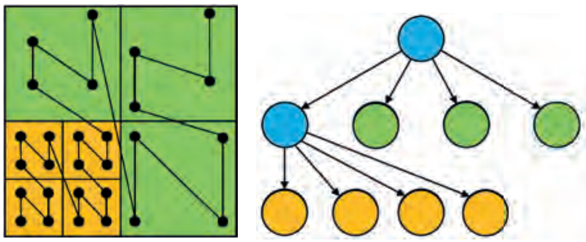

Computing interaction vectors

- FVPM can be interpreted as a generalization of conventional mesh-based FVM.
- In FVPM, control volumes are replaced by **overlapping particles** and the exchange occurs through the interfaces defined by overlapping regions.
- GPU-SPHEROS has been developed based on spherical-supported kernels.

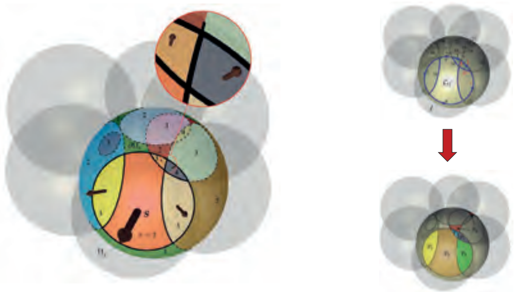

[1]

Case study

- Fluid jet impinging on a flat plate
- The pressure coefficient has been compared to experimental data.

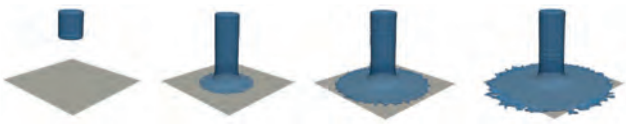

References

[1] E. Jahanbakhsh, A. Maertens, N. J. Quinlan, C. Vessaz, F. Avellan, Exact finite volume particle method with spherical-support kernels, *Comput. Methods Appl. Mech. Engrg*. 317 (2017) 102–127

SCCER-SoE Annual Conference 2017
Task 3.2: Computational Energy Innovation

SCCER SoE
SWISS COMPETENCE CENTER for ENERGY RESEARCH
SUPPLY of ELECTRICITY

In cooperation with the CTI
Energy
Swiss Competence Centers for Energy Research
Commission for Technology and Innovation CTI

Efficient Finite Element Simulation Methods for Fracture Networks

Marco Favino[1,2], Jürg Hunziker[2], Klaus Holliger[2], Rolf Krause[1]

[1]Institute of Computational Science, Università della Svizzera italiana
[2]Institute of Earth Sciences, University of Lausanne

Motivation

Numerical simulations of seismic waves in fractured rocks can result in significant advances for the indirect characterization of such environments. In fact, attenuation and modulus dispersion are due to fluid flow induced by pressure differences between regions of different compressibilities. Understanding these mechanisms in fractured rocks may provide information not only on fracture density but also on fracture connectivity. The main bottlenecks for these kinds of simulations are:

- mesh generation; this requires human interaction to generate meshes which follow the geometry, thus making the simulation of realistic fracture networks unfeasible,
- solution of the FE system due to its complicated structure, the large jumps in the material parameters, the complex nature of the variables in the frequency domain.

Methods

We developed a novel FE software called Parrot to study attenuation and modulus dispersion of seismic waves caused by fluid pressure diffusion in stochastic fracture networks. The new application has been developed inside the MOOSE framework. The latter has been extended in order to work with complex variables in order to simplify the form of the FE system and to speed-up the solution process when parallel direct solvers are employed. In Parrot, Biot's equation are solved in the time-frequency domain. The algorithm comprises the following steps:

1. Generation of a natural fracture networks, e.g. using a power-law distribution for fractures lengths

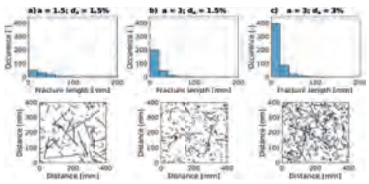

2. Adaptive mesh refinement (AMR) starting from a uniform coarse mesh

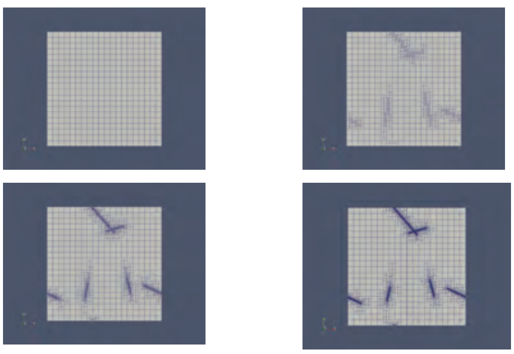

3. Solution of the linear system: the generated mesh is used to solve Biot's equations. The different levels can be employed in a multigrid solution process. The library MOONoLith allows for the parallel transfer between arbitrarily distributed meshes.

Validation

To show the effectiveness of our approach, we consider the problem of a spherically shaped inclusion. For this problem, an analytical solution has been provided by Pride et al. (2004). Starting from a coarse mesh 16x16x16, we applied 4 adaptive mesh refinement steps.

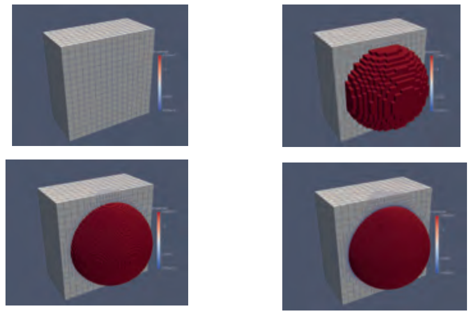

Convergence

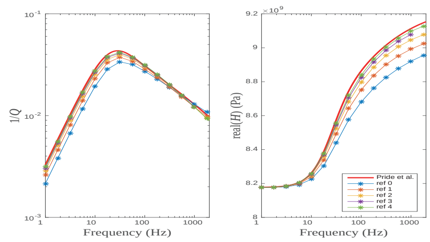

Scaling and speed-up

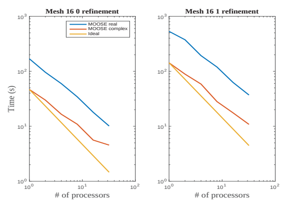

Discussion

The AMR approach allowed to reproduce the predicted attenuation and dispersion curves with a moderate number of unknowns (3M vs 135M of a uniform refinement approach). In particular, it confirmed the importance of having denser meshes at the interfaces where numerical inaccuracies are concentrated. The use of complex variables allowed to reduce the computational cost by a factor of 4 and the parallel direct solver MUMPS showed good scaling properties up to a moderate number of cores.

References

Biot, M. A., General theory for three-dimensional consolidation, Journal of Applied Physics, (1941), 12, 155–164.
Hunziker, J., Favino, M., Caspari, E., Quintal, B., Rubino, J. G., Krause, R., and Holliger, K., Seismic attenuation and modulus dispersion in porous rocks containing stochastic fracture networks, Journal of Geophysical Research (2017), under revision.
Pride, Berriman, Harris, Seismic attenuation due to wave-induced flow, Journal of Geophysical Research, (2004), vol. 109.

SCCER-SoE Annual Conference 2017
Task 3.2: Computational Energy Innovation

Parallel Methods for Contact Problems in Rough Rock Surfaces

Rolf Krause[1], Maria Nestola[1], Daniel Vogler[2], Cyrill von Planta[1], Patrick Zulian[1]

[1]*Institute of Computational Science, Università della Svizzera italiana*
[2] *Institute of Geophysics ETH Zurich*

Earthquakes, Friction and Contact Problems

Earthquakes occur along pre-existing faults which start slipping when the effective normal stress falls below a certain threshold and the frictional strength between the two sides of the rock is below the shear stresses. Understanding the extent of the contact area is key to understanding the overall frictional behavior of rock fractures and to predict at which hydraulic pressures the two sides of a fault will start moving against each other.

Rough Rock Surfaces

We use high resolution photogrammetry scans from granitic samples of the Grimsel test site in Switzerland. We then add three dimensional bodies around the surfaces and generate FEM meshes with non-matching surfaces.

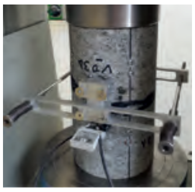

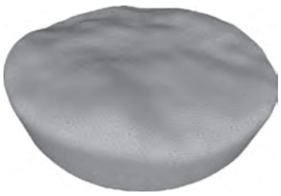

Figure: Left: Left: Rock sample with horizontal fracture in hydraulic press [3] Right: generated 3D mesh

Contact Formulation

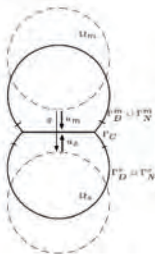

$$
\begin{aligned}
-\operatorname{div}\sigma(\mathbf{u}) &= f \quad \textit{in}\ \Omega := \Omega_s \cup \Omega_m \\
\mathbf{u} &= 0 \quad \textit{on}\ \Gamma_D^\alpha \\
\sigma_{ij}(\mathbf{u}) \cdot n_j &= p_i \quad \textit{on}\ \Gamma_N^\alpha \\
\sigma_n &\leq 0
\end{aligned}
$$

$$[\mathbf{u}\cdot\mathbf{n}] = \mathbf{u}^s \cdot \mathbf{n}^s + \mathbf{u}^m \cdot \mathbf{n}^m$$

$$
\begin{aligned}
-\sigma(\mathbf{u}^m) &= \sigma(\mathbf{u}^s) \\
[\mathbf{u}\cdot\mathbf{n}] &\leq g \\
([\mathbf{u}\cdot\mathbf{n}] - g)\sigma_n &= 0
\end{aligned}
$$

$$
\begin{aligned}
\mathbf{u}_T &= \mathbf{u} - u_n^\alpha \cdot \mathbf{n} \\
[\mathbf{u}_T] = 0 &\Rightarrow |\sigma_T| \leq \mathcal{F}|\sigma_n| \\
[\mathbf{u}_T] \neq 0 &\Rightarrow \sigma_T = -\mathcal{F}|\sigma_n|\frac{[\mathbf{u}_T]}{|[\mathbf{u}_T]|}
\end{aligned}
$$

Figure: Strong formulation of frictional contact between two bodies.

We use a finite element formulation of linear elasticity. A mortar method is used to transfer the contact constraints between the contact surfaces. The resulting constrained linear system is solved with a semismooth newton or a nonsmooth multilevel method. The later has the advantage that it is of optimal complexity and extends multigrid efficiency to contact problems: it neither requires a regularization parameter nor multiple outer iterations.

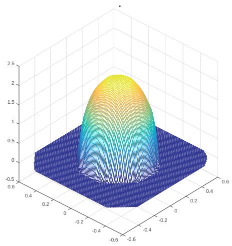

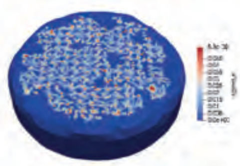

Figure: Left contact stresses for Hertzian contact. Right: contact stresses for rock sample.

Pseudo-L²-Projections

To transfer the information from the contact boundary of one body to another and also for the Galerkin assembly of the nested multilevel hierarchy for the non-smooth multilevel method we use pseudo-L²-projections.

$$T: V \longrightarrow W: \int_W (\mathbf{v} - T(\mathbf{v}))\,\mu\, d\omega = \int_W (\mathbf{v} - \mathbf{w})\,\mu\, d\omega = \mathbf{0}, \quad \forall \mu \in \mathbf{M}$$

Equation: The pseudo L²-formulation **T** is defined in a weak sense whereby the multiplier space **M** consists of biorthogonal basis functions.

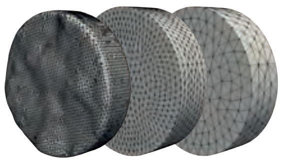

Figure: Multilevel hierarchy used for one body problem.

Implementation

For assembly of the finite element system we use MOOSE and for the solution of the system we use the PETSc SNES solver interface. The computation of the discrete L²-projection carried out using libmesh and MOONoLith [1].

Results

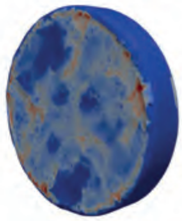

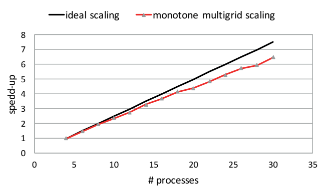

Figure: Left: one-body contact problem. Right: Strong scaling experiment.

We computed one- and two-body frictionless contact problems, and, for benchmark purposes, cubes with up to 2.1 million degrees of freedom. The method scales well up to 30 processes which were the limit of our test environment.

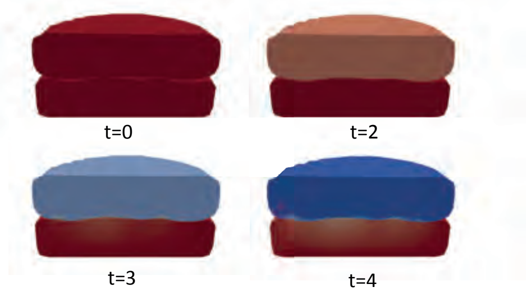

Figure: Cross section of the closing of two rocks in contact at timesteps t=0-4.

References

[1] Krause, Zulian SIAM 2016
[2] Dickopf, Krause Int. J. Numer. Meth. Engng 2008; 00:1–2
[3] Vogler, Settgast, Annavarapu, Madonna, Bayer and Amann, submitted

Energy Turnaround National Research Programme

SCCER SoE
SWISS COMPETENCE CENTER for ENERGY RESEARCH
SUPPLY of ELECTRICITY

SCCER-SoE Annual Conference 2017

LMH Laboratory for Hydraulic Machines

ÉCOLE POLYTECHNIQUE FÉDÉRALE DE LAUSANNE

In cooperation with the CTI
Energy
Swiss Competence Centers for Energy Research
Swiss Confederation
Commission for Technology and Innovation CTI

A Multiscale Model for the Simulation of Sediment Impact Erosion

Sebastián Leguizamón, Ebrahim Jahanbakhsh, Audrey Maertens, Siamak Alimirzazadeh, François Avellan

Motivation and Problem Description

The hydro-abrasive erosion of turbomachines is a **significant problem** worldwide. In the context of the Energy Strategy 2050, it is a problem which will become **more severe in the future** due to the retreat of glaciers and permafrost caused by **climate change**.

Our objective is to provide the **capability of simulating** the erosion process using the Finite Volume Particle Method [1]. Such simulations will become **advantageous** for both the **design** and the **operation** of the machines.

The erosion of hydraulic turbomachines is an **inherently multiscale process,** so its simulation is complicated. It demands a multiscale modeling approach.

Multiscale Nature of the Erosion Phenomenon

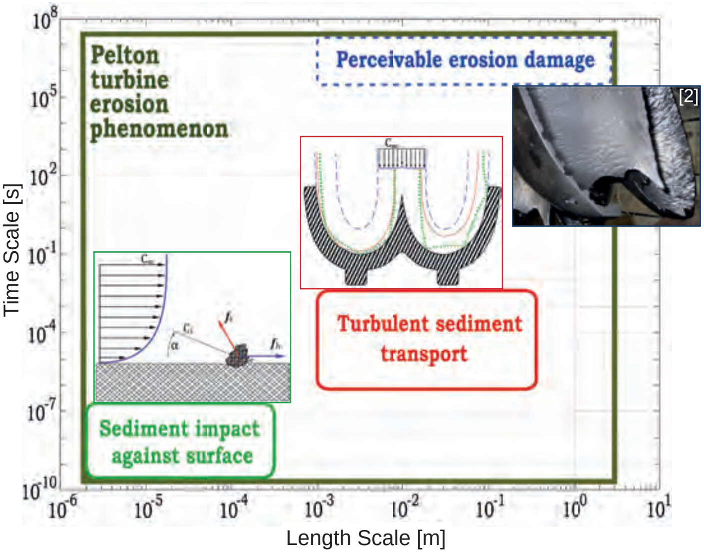

Multiscale Coupling and Validation

A sequential multiscale coupling algorithm is used to provide closure to the macroscale model based on the results of a finite set of microscale simulations.

Microscale output
- Erosion rate $f(\alpha_i, C_j)$
- Restitution coefficients $f(\alpha_i, C_j)$

Sequential coupling

Macroscale output
- Impact condition distributions
- Sediment flux against the surface
- Erosion distribution
- Global erosion rate

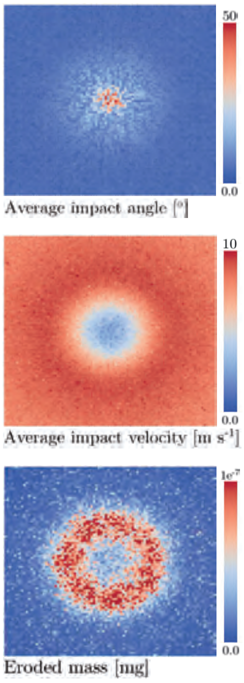

The slurry jet erosion of a flat plate is used to successfully validate the multiscale model.

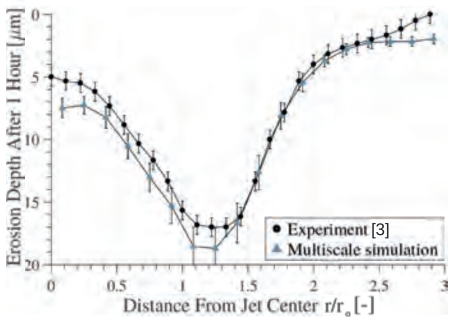

Macroscale Model: Sediment Transport

Turbulent sediment transport is computed in the macroscopic domain of interest.

- Finite Volume Particle Method
- Weakly compressible flow with k-ε turbulence closure
- Lagrangian sediment tracking accounting for drag, added mass, pressure gradient, turbulence dispersion, lift and interparticle contacts
- Arbitrary Weibull sediment size distribution at the inlet

Slurry Jet Erosion of a Flat Plate

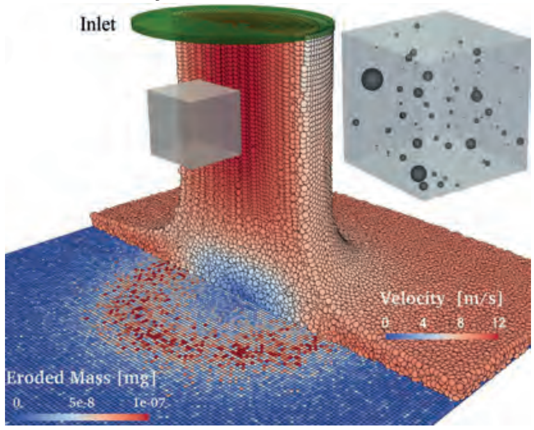

Microscale Model: Sediment Impacts

Detailed thermomechanical modeling of the sediment collisions under constant impact conditions.

- Elastoplastic solid with the Johnson-Cook constitutive and damage models
- Thermoplastic and frictional heating
- Temperature-corrected Mie-Grüneisen equation of state
- Arbitrarily shaped elastic or rigid sediments

Spherical Particle Impacts against Solid

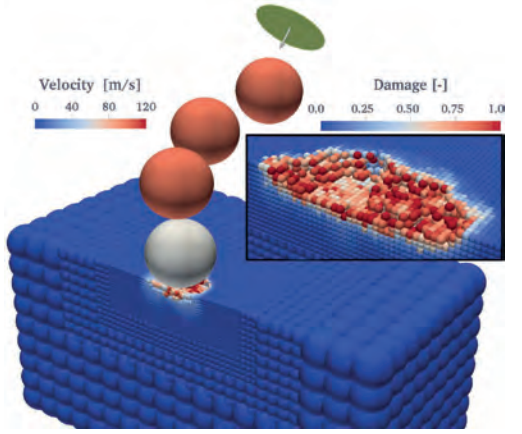

References

[1] E. Jahanbakhsh, A. Maertens, N. J. Quinlan, C. Vessaz, and F. Avellan, Exact finite volume particle method with spherical-support kernels, *Comput. Methods Appl. Mech. Engrg.*, 317: 02–127 (2017).

[2] K. Winkler, Understanding hydro-abrasive erosion for a sustainable future, *Hydro Vision India* (2011).

[3] K. Sugiyama, K. Harada, S. Hattori, Influence of impact angle of solid particles on erosion by slurry jet, *Wear* 265 (2008).

SWISS COMPETENCE CENTER for ENERGY RESEARCH
SUPPLY of ELECTRICITY

SCCER-SoE Annual Conference 2017

LMH Laboratory for Hydraulic Machines

ÉCOLE POLYTECHNIQUE FÉDÉRALE DE LAUSANNE

In cooperation with the CTI

Energy
Swiss Competence Centers for Energy Research

Commission for Technology and Innovation CTI

Surface tension modeling: wetting and contact angle hysteresis

Audrey Maertens, Ebrahim Jahanbakhsh, François Avellan

A versatile surface tension model for GPU-SPHEROS

- Finite Volume Particle Method ⇒ each particle represents a physical volume of fluid [1]
- Approach: analytical particle interaction derived from macroscopic force on free surface for spherical fluid particles
- Surface tension force on particle i from free-surface ($\mathcal{FS}$) elements $\mathcal{P}$ of surface area $S_{\mathcal{P}}$: $\boldsymbol{F}_i^{ST} = -\gamma \sum_{\mathcal{P}\in\mathcal{FS}} \frac{\mathrm{d}S_{\mathcal{P}}}{\mathrm{d}\boldsymbol{x}_i}$

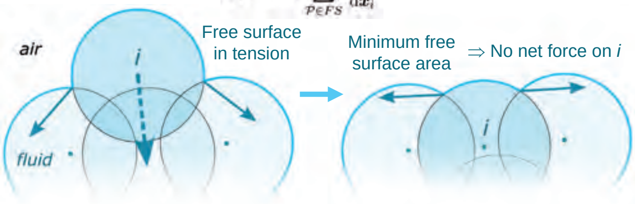

- A 2 mm wide cubic water drop evolves into a ball under the action of the surface tension force

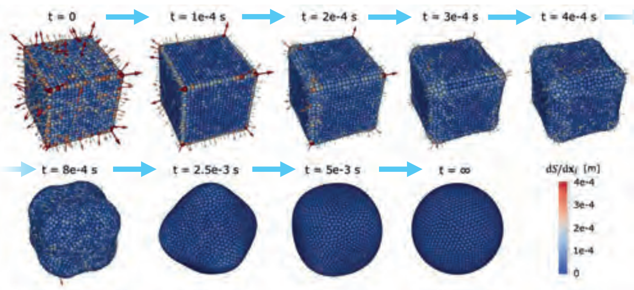

Wetting

- Same approach in the presence of three interfaces: fluid-air ($\mathcal{I}_{FA}$), fluid-wall ($\mathcal{I}_{FW}$) and wall-air: $\boldsymbol{F}_i^{ST} = -\gamma_{FA} \sum_{\mathcal{P}\in\mathcal{I}_{FA}} \frac{\mathrm{d}S_{\mathcal{P}}}{\mathrm{d}\boldsymbol{x}_i} + (\gamma_{WA}-\gamma_{FW}) \sum_{\mathcal{P}\in\mathcal{I}_{FW}} \frac{\mathrm{d}S_{\mathcal{P}}}{\mathrm{d}\boldsymbol{x}_i}$
- Wettability is controlled by the equilibrium contact angle θ_e. Young's equation: $\gamma_{WA}-\gamma_{FW}=\gamma_{FA}\cos\theta_e=\gamma\cos\theta_e$

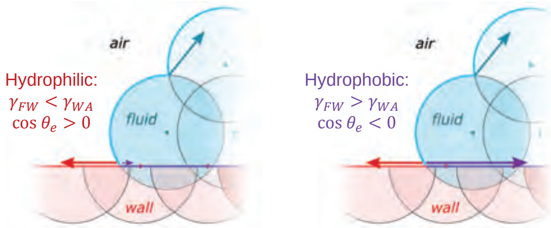

- Water drop shape on a flat surface and radius of wetted surface at equilibrium are a function of equilibrium contact angle

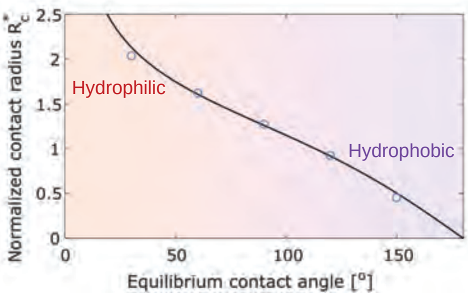

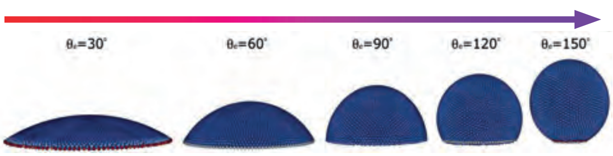

Properties and applications

- A symmetric force directly derived from macroscopic interactions
  - Conservative
  - Stable
  - No model fitting or tuning needed
  - Versatile: can also handle surface roughness and contact angle hysteresis
- Energy applications
  - Cavitation
  - Fracturing

Contact angle hysteresis

- In dynamic cases, advancing angle ≠ receding angle
- Contact angle hysteresis largely due to imperfect wall surface
- Approach: directly model surface roughness rather than dynamic angle
- Procedure for each wall particle:
  1. Pick a random vector **V**
  2. Rotate particle about **V** by predefined ε

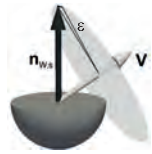

- Transforms a smooth surface into a surface of controlled roughness (here ε = 0.1 rad)

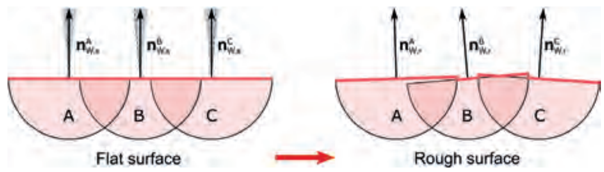

- The dynamics of a 3.6 mm diameter drop impacting a horizontal plane at 0.77 m/s is affected by contact angle hysteresis / surface roughness

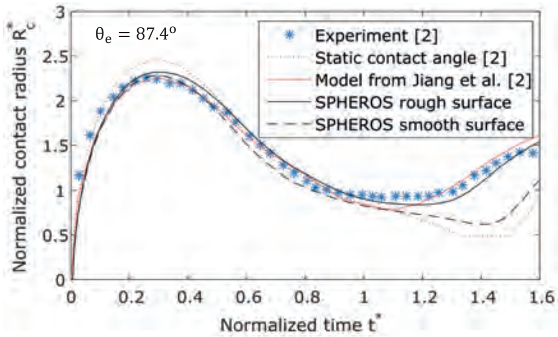

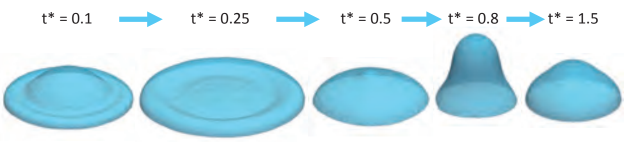

References

[1] E. Jahanbakhsh, A. Maertens, N. J. Quinlan, C. Vessaz, and F. Avellan, "Exact finite volume particle method with spherical-support kernels," *Comput. Methods Appl. Mech. Engrg*., 317: 02–127, 2017.

[2] Y. Guo, Y. Lian, and M. Sussman, "Investigation of drop impact on dry and wet surfaces with consideration of surrounding air," *Phys. Fluids*, 28(7):073303, 2016.

SCCER SoE SWISS COMPETENCE CENTER for ENERGY RESEARCH SUPPLY of ELECTRICITY
DESTRESS
SCCER-SoE Annual Conference 2017
In cooperation with the CTI
Energy Swiss Competence Centers for Energy Research
Commission for Technology and Innovation CTI

ETH zürich

Reactive flow patterns in fractured media

Julian Mindel and Thomas Driesner, Institute of Geochemistry and Petrology, ETH Zurich

Abstract / Background

Reactive transport through irregularly fractured rock masses is a key phenomenon in ore-forming hydrothermal systems, geothermal systems, and many other geological processes. Assuming modelling of most other processes is already in place, the addition of RT as a simulation capability represents a steep increase in overall system complexity and computational expense.
Our approach to this problem includes a combination of the finite element and finite volume capabilities of our in-house CSMP++ flow simulation platform [1] with the GEMS3K [2] chemical equilibration code. Our current improvements include implementations in terms of OpenMP parallelism, heat transport, front end, and the creation of a higher-level modular re-usable code design.

Methodology & key progress

Through operator splitting and a sequential solution approach we assume conductive heat transfer to take place mainly through rock while advective heat transport happens in the fluid. The resulting thermal-compressive effects are coupled to mass transport via a *mass correction source term*s detailed in [5]. Figures 1 and 2 present sample test simulations in 2D, and 3D respectively.

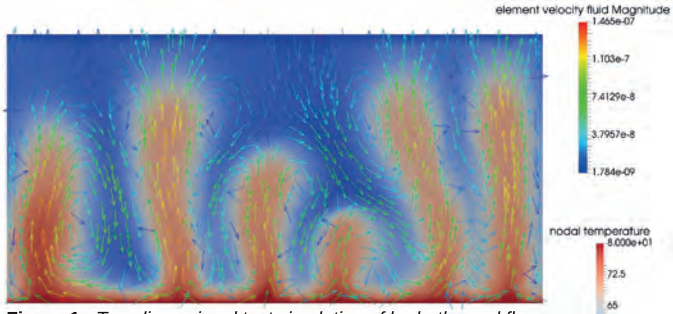

Figure 1: *Two dimensional test simulation of hydrothermal flow throw porous media. Heat is provided through the bottom boundary causing convective plumes to appear. Heat transport is modelled through the algorithm proposed in [5]*

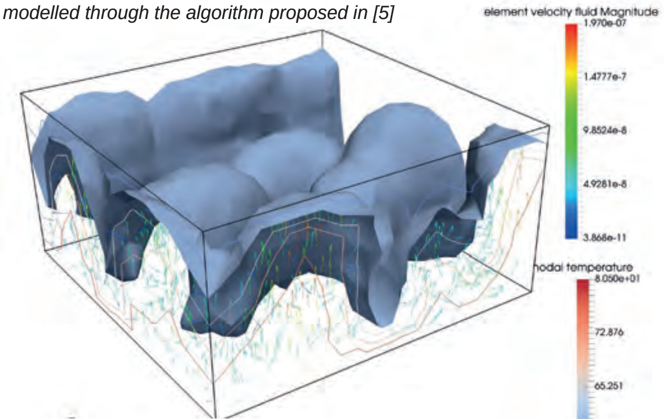

Figure 2: *3D test simulation of hydrothermal flow throw porous media. Heat is provided through the bottom boundary causing convective plumes to appear.*

Thin fractures and wells can be modelled via a lower-dimensional-element approach (LDE), allowing for complex networks that would otherwise incur prohibitive amounts of mesh resolution due to large scale differences. (Figure 3)

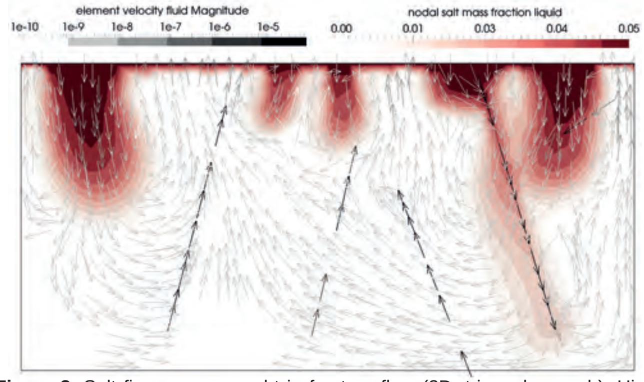

Figure 3: Salt fingers are caught in fracture flow (2D, triangular mesh). Higher flow velocities appear due to higher permeability assigned to line elements (LDEs) at the location of the fractures.

Honoring the governing equations for compressible porous media flow and chemical transport in our simulator, we also designed synthetic geometries (Figures 4 and 5) to study the propagation of a dolomitization front using the chemical conditions of the benchmark by Engesgaard and Kipp [3].
Conditions chosen in that benchmark minimize feedbacks resulting from porosity changes, etc.. The left sides of the simulation boxes are applied a Dirichlet boundary condition for aqueous Mg and a left to right pressure gradient is applied to induce flow.

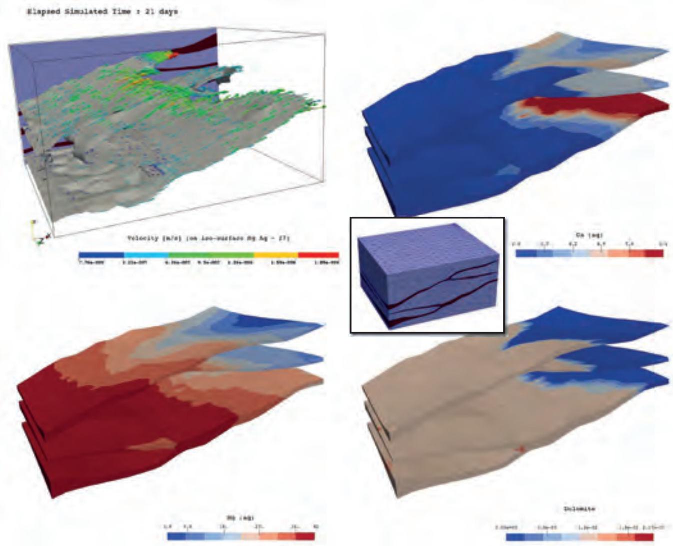

Figure 4 :*In the model setup, calcite is considered to form a thin coating on pore walls and reacts to dolomite with the incoming aqueous Mg chloride solution. Due to thickness variations inside the fracture zones, their orientation in the fluid pressure field, and the effects of branching on fluid pressure gradients, the chemical front advances heterogeneously*

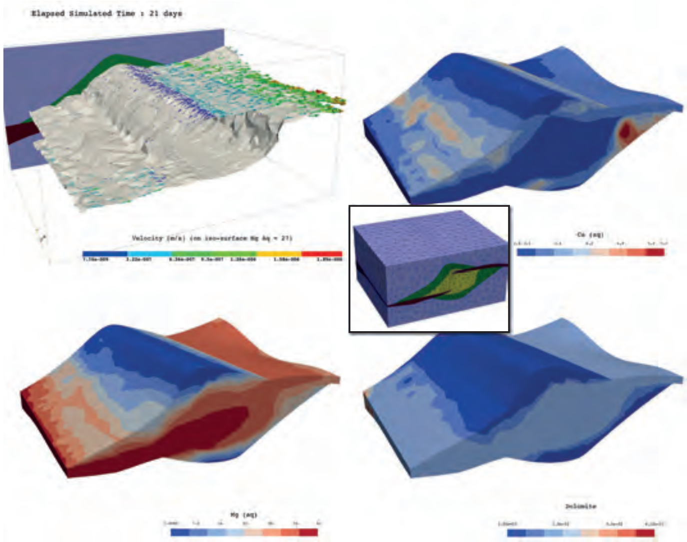

Figure 5: *Also here, non-uniformity of the geometry leads to heterogeneous advancement of the chemical front.*

Conclusions & Outlook

As sampled here, our approach is proving increasingly successful and is continuously tested on a variety of application problems. We are currently working towards adopting the CSMP++ "split node" approach [4] for reactive transport. Shifting focus on performance, we are also in the planning stages for CSMP++ native MPI functionality to be implemented and tested in combination with the GEMS library for simulations on distributed memory systems.

References

1. Matthai S.K. et al. (2012) ECMOR XIII, European Conf. Mathematics of Oil Recovery, Biarritz, France;
2. Kulik D.A. et al. (2013) Computational Geosciences 17,1-24; 3
3. Engesgaard, P., Kipp, K.L. (1992) Water Resour. Res. 28, 2829–2843; 4
4. Nick H.M. and Matthai S.K. (2011) Vadose Zone Journal 299-312
5. Weiss, P. et al. (2014) Geofluids 14, 347-371, 3

SCCER-SoE Annual Conference 2017
Task 3.2: Computational Energy Innovation

Fictitious Domain Method for 3D FSI Simulations of Turbines

Maria Giuseppina Chiara Nestola, Patrick Zulian, Rolf Krause

Institute of Computational Science, Università della Svizzera Italiana

Motivation

We present a completely parallel approach for Fluid-Structure Interaction (FSI) simulations.

Our approach is inspired by the fictitious domain method [1] and makes intensive use of variational transfer between the solid and the fluid grid.

For validation and evaluation of the accuracy of the proposed methodology, we present results for a benchmark configuration describing the deformations of two elastic beams in a flow channel.

We simulate the flow around a vertical axis turbine in order to show that the framework is suitable for industrial applications.

Mathematical Formulation

Find $(\mathbf{u}_f, p_f; \boldsymbol{\eta}_s, p_s; \boldsymbol{\lambda}) \subset (V_f \times Q_f \times V_s \times Q_s \times L)$ such that for every $(\mathbf{v}_f, q_f; \mathbf{v}_s, q_s; \boldsymbol{\mu}) \subset (V_f \times Q_f \times V_s \times Q_s \times L)$

$$\int_{\Omega_f} \rho_f \frac{\partial \mathbf{u}_f}{\partial t} \cdot \mathbf{v}_f dV + \int_{\Omega_f} \rho_f [(\mathbf{u}_f \cdot \nabla)\mathbf{u}_f] \cdot \mathbf{v}_f dV + \int_{\Omega_f} \sigma(\mathbf{u}_f, p_f) : \nabla \mathbf{v}_f dV - \int_{\mathcal{I}} \boldsymbol{\lambda} \cdot \mathbf{u}_f dV = 0$$

$$\int_{\Omega_f} q_f \nabla \cdot \mathbf{u}_f dV = 0$$

$$\int_{\mathcal{I}} \boldsymbol{\mu} \cdot \left(\frac{\partial \boldsymbol{\eta}_s}{\partial t} - \mathbf{u}_f\right) dV = 0$$

$$\int_{\widehat{\Omega}_s} \widehat{\rho}_s \frac{\partial^2 \widehat{\boldsymbol{\eta}}_s}{\partial t^2} \cdot \widehat{\mathbf{v}}_s + \int_{\widehat{\Omega}_s} \widehat{\mathbf{P}}(\widehat{\mathbf{F}}) : \nabla \widehat{\mathbf{v}}_s dV - \int_{\widehat{\Omega}_s} \widehat{p}_s \widehat{J} \widehat{\mathbf{F}}^{-T} : \nabla \widehat{\mathbf{v}}_s dV + \int_{\mathcal{I}} \boldsymbol{\lambda} \cdot \widehat{\mathbf{v}}_s dV = 0$$

$$\int_{\widehat{\Omega}_s} (\widehat{J} - 1) q_s dV = 0$$

$\widehat{\Omega}_s$: solid domain, Ω_f: fluid domain $\mathcal{I} := \widehat{\Omega}_s \cap \Omega_f$.

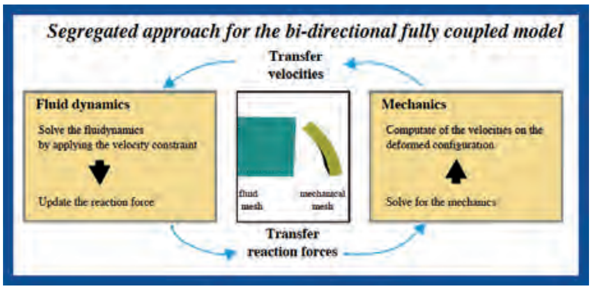

Coupling

- For coupling the fluid and the solid subproblems we adopt an inherently parallel approach for dealing with the L^2-projection operator. This approach includes a parallel search strategy, the computation of element intersections, and the parallel assembling of the transfer operator [2].

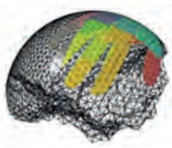

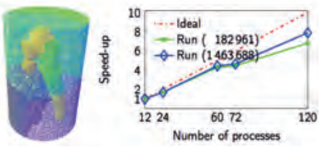

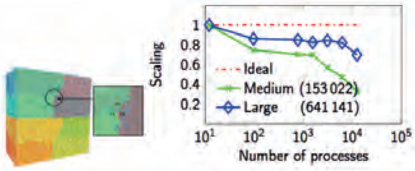

Results: Turbines Simulation

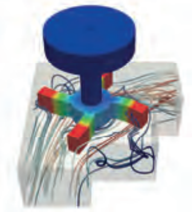

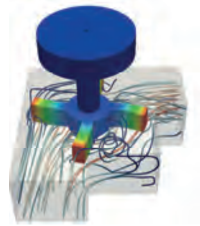

Energy Turnaround
National Research Programme

Results: Framework Validation

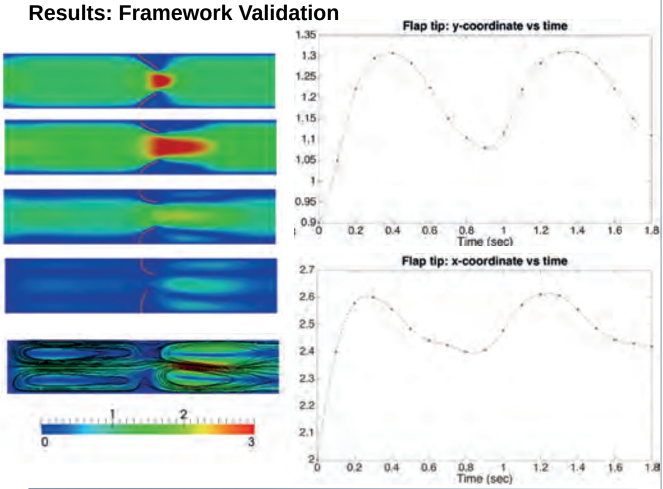

Discussion

We validate the framework by using a benchmark consisting of two nonlinear elastic flapping beams embedded into a two-dimensional Newtonian flow-channel. By analysing the displacement field of a point placed on the top beam, we get results in agreement with Gil [3].

The FSI framework is employed for simulating a cross-flow vertical-axis water turbine. More specifically, we use a linear elastic material for simulating the turbine blades, whereas the water is modelled as a Newtonian flow with a moderate high Reynolds number (~2000).

References

[1] Frank P T Baaijens. *International Journal for Numerical Methods in Fluids*, 35(7):743–761, 2001.

[2] Rolf Krause and Patrick Zulian. *SIAM Journal on Scientific Computing*, 38(3):C307–C333, 2016.

[3] Gil, Antonio J., et al. *Journal of Computational Physics* 229.22 (2010): 8613-8641.

SCCER-SoE Annual Conference 2017

SCCER SoE
SWISS COMPETENCE CENTER for ENERGY RESEARCH
SUPPLY of ELECTRICITY

ETHzürich

In cooperation with the CTI
Energy
Swiss Competence Centers for Energy Research
Schweizerische Eidgenossenschaft
Confédération suisse
Confederazione Svizzera
Confederaziun svizra
Swiss Confederation
Commission for Technology and Innovation CTI

GEO
Geothermal Energy & Geofluids

Investigating transport processes in 3D fractured reservoirs

Philipp Schädle, Anozie Ebigbo, Martin O. Saar
ETH Zurich, Zurich, Switzerland

Introduction

- Two key aspects are relevant for sufficient energy production from enhanced geothermal systems:
  1. Sufficiently high fluid production rates.
  2. Maximum effective **fracture surface area**.
- Flow and transport behavior in 3D fracture networks strongly depends on **network-scale** and **fracture-scale heterogeneities** [1,2].
- This work presents:
  1. Simulations of fluid flow and particle transport through **discrete fracture networks (DFNs)**.
  2. The influence of network-scale heterogeneity on transport and effective fracture surface area.

Conceptual model

DFN

- Domain size: 10 x 10 x 10 m
- Fracture orientation: Random
- Fracture size distribution: **Truncated power law**
- Length correlated aperture
- Aperture - permeability relation: Cubic law

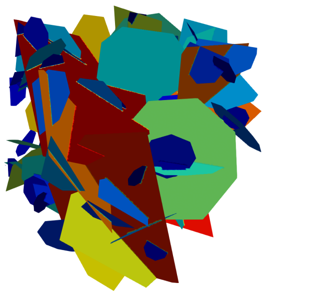

Figure: Example of a discrete fracture network; colors show the fracture permeability

Fluid flow simulation

- **Steady-state** flow
- Pressure difference between two Dirichlet boundaries: 0.01 MPa

Particle transport simulation

- A **Lagrangian** approach is used to calculate particle transport through the network.
- Particles are injected at high pressure boundary and exit at low pressure boundary.
- Particles are **instantaneously** injected at all fractures which intersect the domain boundary.
- At **each fracture** which intersects the domain boundary an **equal amount** of particles are equidistantly injected.

Effective surface area

Network-scale heterogeneity leads to preferential pathways for fluid flow and transport. Hence, the effective surface area depends on the network-scale heterogeneity.

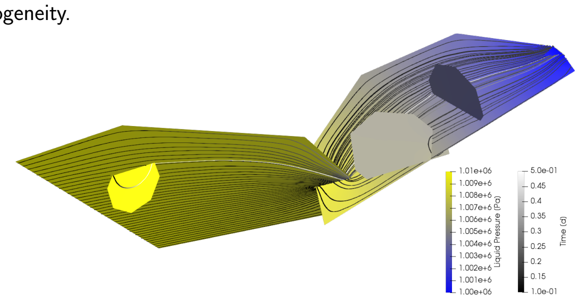

Figure: Pressure in fracture network consisting of five fractures. Trajectories of 40 particles with travel time [d]

The following observations can be made:

- **Dead-end fractures** are less affected by flow and transport.
- Particle transport is **delayed** by transport through hydraulically less transmissive fractures.
- Major parts of the particles are transported on **preferential pathways**.

Methods

Simulations are performed using *DFNworks* [3]. *DFNworks* is a code framework which allows to generate DFNs and model steady-state flow and particle transport. *PFLOTRAN* [4] is used to solve the flow part.

Calculation of the effective surface area

- Percentage of fracture surface area which is affected by transport.
- Calculated based on the grid cells of the DFN mesh.
- Grid cell is considered to be affected by transport, if:
  - a minimum of **n percent of all particles** is transported through the cell,
  - the particles intersecting the cell are not within the 10% particles with the largest travel time.

Preliminary Results

Two experiments have been performed:

1. Variing number of particles are injected in a single DFN.
2. Five different DFNs are generated based on equal network parameters. For each DFN, particle transport is simulated with 500 particles injected at each fracture.

For the two experiments the effective surface area is calculated for different percentage of considered particles.

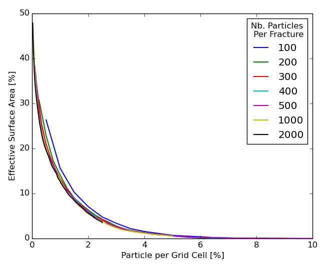

Figure: Effective surface area vs. percentage of considered particles. Different cases with varying number of injected particles at each fracture.

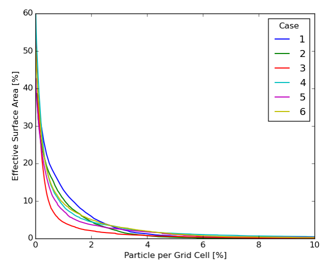

Figure: Effective surface area vs. percentage of considered particles. Realization of different DFNs with equal parameters. Injection of 500 particles per fracture

- The maximum effective surface area depends on the total number of injected particles.
- A minimum number of injected particles per grid cell at the domain boundary is required to calculate the effective surface area.
- If 1% of the particles are considered the effective surface area varies only over 2-3%, if a single DFN is considered.

Outlook

- Make stochastic investigations for multiple fracture network parameters.
- Investigate the influence of in-fracture variability on the effective surface area.
- Compare results for the effective surface area to borehole analysis methods.
- Investigate the influence of effective surface area on heat extraction rates.

References

1. de Dreuzy, J.-R., Meheust, Y., and Pichot, G. (2012). Influence of fracture scale heterogeneity on the flow properties of three-dimensional discrete fracture networks (DFN). Journal of Geophysical Research: Solid Earth, 117(B11):1-21.
2. Makedonska, N., Hyman, J. D., Karra, S., Painter, S. L., Gable, C. W., and Viswanathan, H. S. (2016). Evaluating the effect of internal aperture variability on transport in kilometer scale discrete fracture networks. Advances in Water Resources , 94(4):486-497.
3. Hyman, J.D., Karra, S., Makedinska, N., Gable, C.W., Painter, S.L., Viswanatha, H. (2015), dfnWorks: a discrete fracture network framework for modeling subsurface flow and transport. Computers & Geosciences, 84, pp. 10-19.
4. Lichtner, C.P., Hammond, G.E., Lu, C., Karra, S., Bisht, G., Andre, B., Mills, R.T., Kumar, J., Frederick, J.M., (2017). *PFLOTRAN* User Manual. http://www.documentation.pflotran.org

Contact: Philipp Schädle - philipp.schaedle@erdw.ethz.ch

SWISS COMPETENCE CENTER for ENERGY RESEARCH SUPPLY of ELECTRICITY

SCCER-SoE Annual Conference 2017

In cooperation with the CTI

Energy Swiss Competence Centers for Energy Research

Commission for Technology and Innovation CTI

Sloshing motion of a water free surface in a Francis turbine operating in condenser mode

E. Vagnoni, A. Favrel, L. Andolfatto and F. Avellan

Context and objectives

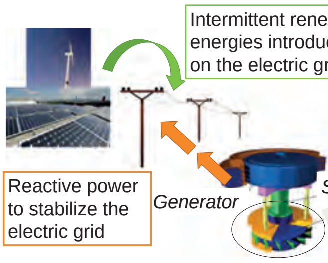

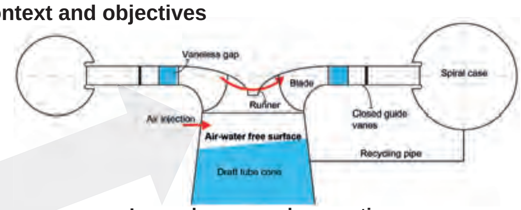

In condenser mode operation: Turbine spins in air to minimize the power consumption: compressed air is injected in the draft tube cone → **Air losses recorded**

Research objectives:
- *Study of the air-water interaction phenomena.*
- *Focus on the sloshing motion of the free surface in the draft tube cone.*
- *Relation between the sloshing motion and the air losses.*

Experimental set-up

Reduced scale physical model

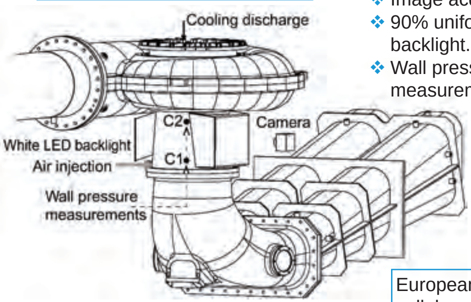

- Image acquisition at 30 Hz.
- 90% uniform white LED backlight.
- Wall pressure measurements at 3000 Hz.

European project in collaboration with BC-Hydro for investigating two-phase flow phenomena affecting turbine performance

Scaling law: $Fr_d = \sqrt{\frac{\rho_{air}}{\rho_{water}}} \frac{N\sqrt{D_e}}{\sqrt{g}}$

Methodology

Post-processing image method to evaluate the difference in elevation h of two sides of the free surface by image filtering and contrast detection

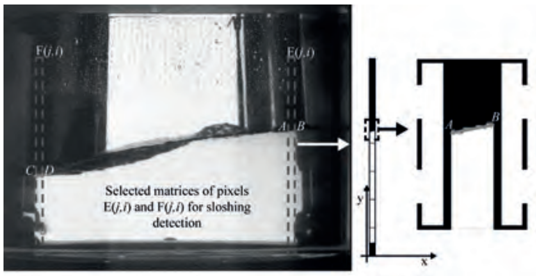

$$y_{AB,i} = \sum_j \left(E(j,i) = 255\right) \qquad y_{CD,i} = \sum_j \left(F(j,i) = 255\right)$$

Linear interpolation →

$$y_B = a x_B + b \qquad y_C = c x_C + d$$

$$\rightarrow h = y_B - y_C$$

Results

Study of the sloshing motion in time and frequency domain

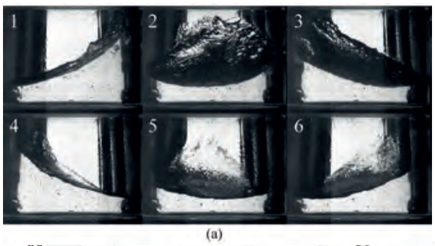

a. **Sequence of images** of the air-water oscillating free surface.
b. **Time resolved signals** of h.
c. **Corresponding spectrum magnitude.**

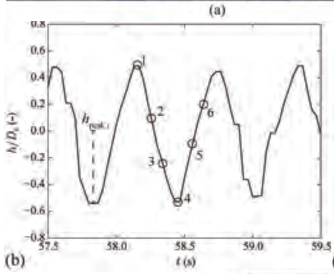

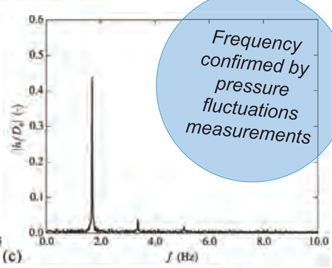

Frequency confirmed by pressure fluctuations measurements

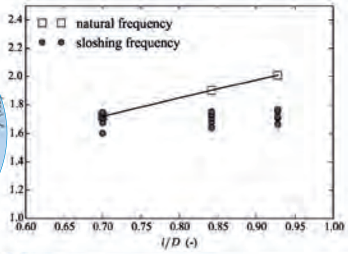

Resonance gravity wave excited at the first natural frequency of the water volume in the draft tube cone

Dependency of the sloshing amplitude and frequency by the densimetric Froude number

Mean amplitude peaks

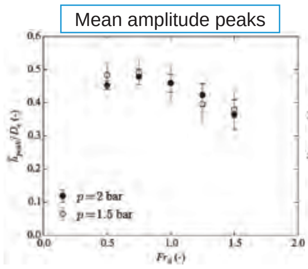

Frequency

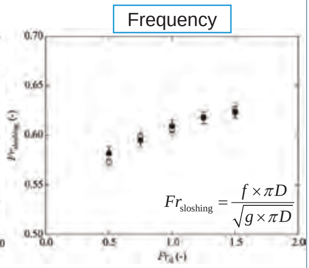

$$Fr_{sloshing} = \frac{f \times \pi D}{\sqrt{g \times \pi D}}$$

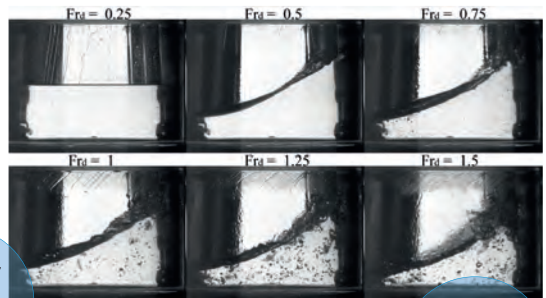

Fr_d key parameter of the sloshing motion

Increasing air-water mixing with Fr_d

E. Vagnoni et al., "Experimental investigation of the sloshing motion of the free surface in the draft tube of a Francis turbine operating in synchronous condenser mode", Experiments in Fluids (Submitted)

LMH Laboratory for Hydraulic Machines

ÉCOLE POLYTECHNIQUE FÉDÉRALE DE LAUSANNE

SCCER SoE
SWISS COMPETENCE CENTER for ENERGY RESEARCH
SUPPLY of ELECTRICITY

SCCER-SoE Annual Conference 2017

In cooperation with the CTI
Energy
Swiss Competence Centers for Energy Research
Swiss Confederation
Commission for Technology and Innovation CTI

CSMP++GEM for reactive transport modelling with solid solutions

A. Yapparova (ETHZ), G.D. Miron (PSI), D.A. Kulik (PSI), T. Driesner (ETHZ)

Motivation

- Reactive transport models (RTM) with non-ideal multicomponent solid solutions and mixed gaseous fluids are necessary for modelling natural magmatic-hydrothermal and geothermal systems
- Widely used LMA (law of mass action) codes (e.g. TOUGHREACT, PHREEQC) cannot model such chemical systems efficiently
- Feldspars are among the most abundant minerals in the Earth's crust. Alkali feldspar is a non-ideal ternary solid solution with end members K-feldspar, Albite, Anortite and a miscibility gap

Methods

The CSMP++GEM reactive transport code:

- Control volume finite element method (CVFEM) to solve PDEs for two-phase flow and heat transport in terms of pressure, enthalpy and salinity on unstructured grids (Weis et al., 2014).
- Accurate thermodynamic representation of fluid properties – Equation of state for a H2O-NaCl system (Driesner&Heinrich, 2007; Driesner, 2007).
- Chemical equilibrium calculations using the Gibbs energy minimisation method (GEM), implemented within the GEMS3K code (Kulik et al.,2013; Wagner et al., 2012).
- Sequential Non-Iterative Approach (SNIA) for transport-chemistry coupling for fast reactive transport calculations (compared to SIA and fully implicit methods).

Alkali Feldspar solid solution with non-ideal mixing

3 end-members:
- Albite (Na)
- Sanidine (K)
- Anorthite (Ca)

Multi-component Van Laar model (Holland & Powell, 2003) describes the mixing properties in an asymmetric system:

- one binary interaction parameter per pair of end-members,
- one scaling parameter (size parameter) per end-member.

Sanidine-Albite solvus at 1kbar

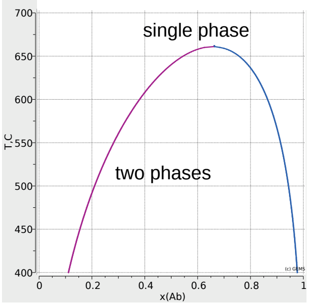

implemented in **TsolMod library** (Wagner et al., 2012)

1D model setup: Albitisation of K-feldspar

50 nodes

v=3*mm/yr* 5wt% NaCl → **K-feldspar, φ=10%**

5 cm

Isothermal simulations:
(1)300°C, 100bar – pure phases
(2)300°C, 100bar – solid solutions
(3)600°C, 1kbar – solid solutions

Secondary minerals:
boehmite, paragonite, muscovite, kaolinite

Results

(1) Pure phases vs (2) solid solutions at 300°C, 100bar

(1)

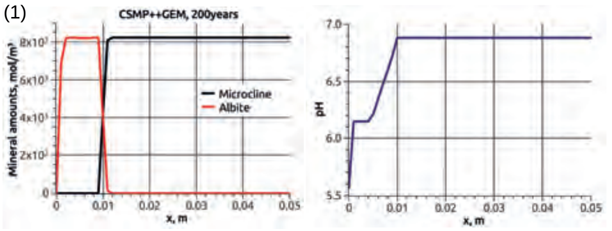

(2)

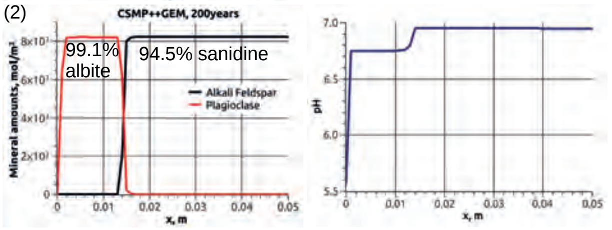

(3) Solid solutions at 600°C, 1kbar

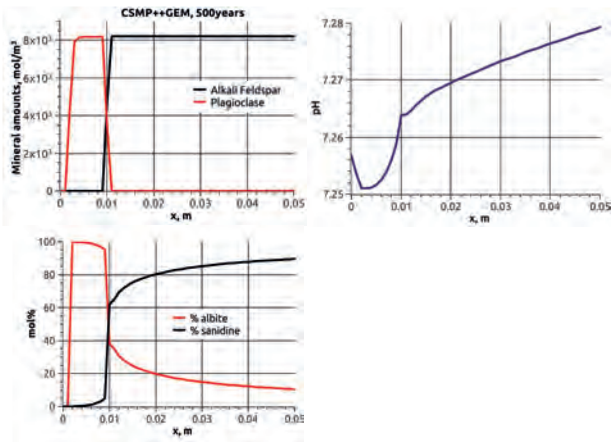

Conclusions

- Coupled RTM code CSMP++GEM can model reactive transport with non-ideal solid solutions and non-ideal fluids
- When modelling with pure phases instead of solid solutions, the speed of mineral replacement and the resulting pH evolution can be miscalculated
- At higher temperatures, it is especially important to consider solid solutions because of generally higher miscibility

References

[1] Weis et al., *Geofluids* **14** (2014)
[2] Driesner & Heinrich, *Geochimica et Cosmochimica Acta* **71** (2007)
[3] Driesner, *Geochimica et Cosmochimica Acta* **71** (2007)
[4] Kulik et al., *Computational Geosciences* **17** (2013)
[5] Wagner et al., *Canadian Mineralogist* **50** (2012)
[6] Holland & Powell, *Contribs.Mineral.Petrol*. **145** (2003)

Work Package 4: Future Supply of Electricity

The transformation of the Swiss energy system as envisaged within the Energy Strategy 2050 is far more than just a technological challenge for hydro power and geothermal energy. WP4 addresses therefore a variety of related aspects such as:

- risks, safety and societal concerns,
- new emerging energy technologies, and
- the integration within the overall energy system.

Within this broader perspective sustainability and security of supply aspects need to be considered, conflicting objectives and potential trade-offs analyzed and resolved by means of risk-cost benefit analysis, Multi-Criteria Decision Aiding processes and energy economic modeling.

Highlights 2017

Holistic concept of risk governance for deep geothermal energy

Since January 2017, a quantitative adaptive traffic light system based on a safety threshold has been refined, and a hierarchical Bayesian model for robust forecasting proposed. Based on statistical models, these tools can directly be employed in the industry during reservoir stimulation. Models and methods will later be improved by adding second-order physical aspects, which might provide improved mitigation strategies. Those aspects will be tested on the detailed data available from underground labs (e.g., Grimsel) and a dozen EGS projects. Transparency of the offered tools should be well received by the public concerned with EGS safety. However, based on an online survey, there is a trade-off between aiming for transparency by disclosing uncertainty and limited expert confidence, and thereby decreasing clarity and increasing concerns.

Technology assessment report finalized

The activity on technology assessment primarily focused on completion of the report on Assessment of the potentials, costs and environmental burdens of electricity generation technologies for Swiss electricity supply until 2050, which is a joint effort by the SFOE, SCCER-SoE and SCCER Biosweet. This report is currently awaiting final approval and will be released in Q4 of 2017. This comprehensive study represents an important contribution to the ongoing technology monitoring program of the SFOE, and the results will be used within the upcoming Swiss energy perspectives.

Progress on energy economic modelling

A bi-level electricity market model (BEM) was developed and used to understand price-formation and investments. BEM can run in different modes: (i) Investment and production decision on same level (ii) Single scenario (deterministic), and (iii) Social welfare maximization. For a better representation of the Swiss electricity sector in a European context improved long-term scenarios are developed. Global long-term sector development have been investigated with an updated scenario analysis in collaboration with the World Energy Council. Further studies were carried out on the interplay between mountain photovoltaic and wind energy in a fully renewable Switzerland.

Understanding socio-economic political drivers

This work is performed in close collaboration with the Joint Activity: Socio-political conditions of the extension of hydropower and geothermal energy. First results have been obtained on the sensitivity of residual load variability to renewables siting and demand response, and on regulatory, political and participatory perspectives of integrated development processes for hydropower and deep geothermal energy.

Task 4.1

Title

Risk, safety and societal acceptance

Projects (presented on the following pages)

Hierarchical Bayesian Modelling for Fluid-Induced Seismicity
M. Broccardo, A. Mignan, B. Stojadinovic, S. Wiemer, D. Giardini

Transformation of the Energy-related Severe Accident Database (ENSAD) into an interactive, web-based GIS application
Alternative: Task 4.2
P. Burgherr, W. Kim, M. Spada, A. Kalinina, S. Hirschberg

Probabilistic Damage Quantification for Unreinforced Masonry Walls Exposed to Induced Seismic Risk
M. Didier, M. Broccardo, G. Abbiati, F. Hefti, A. Gabbi, M. Petrovic, N. Mojsilovic, B. Stojadinovic

Developing dynamic context analysis procedures for DGE projects
Poster see task 4.3
O. Ejderyan, M. Stauffacher

One decade of induced seismicity in Basel, Switzerland: A consistent high-resolution catalog obtained by template matching
M. Herrmann, T. Kraft, T. Tormann, L. Scarabello, S. Wiemer

Generic cellular automaton for statistical analysis of landslides frequency-size distribution
A. Jafarimanesh, A. Mignan, D. Giardini

Uncertainty quantification of flood wave propagation resulting from a concrete dam break
A. Kalinina, M. Spada, P. Burgherr, C. T. Robinson

Where to site Enhanced Geothermal Systems (EGS)? Trading off heat benefits and induced seismicity risk from the investor’s and society’s perspective
T. Knoblauch, E. Trutnevyte

Communicating induced seismicity of deep geothermal energy and shale gas: low-probability high-consequence events and uncertainty
T. Knoblauch, M. Stauffacher, E. Trutnevyte

The price of public safety in EGS projects
A. Mignan, M. Broccardo, S. Wiemer, D. Giardini

Monitoring and imaging medium perturbations using the multiply scattered waves
A. Obermann, T. Planès, C. Hadziioannou, M. Campillo, S. Wiemer

Organizational ethnography›s contribution to the governance of a geothermal program: the Geneva example
Poster see task 4.3
F. Ruef, O. Ejderyan

SCCER SoE
SWISS COMPETENCE CENTER for ENERGY RESEARCH
SUPPLY of ELECTRICITY

SCCER-SoE Annual Conference 2017

In cooperation with the CTI
Energy
Swiss Competence Centers for Energy Research
Commission for Technology and Innovation CTI

Hierarchical Bayesian Modelling for Fluid-Induced Seismicity

Marco Broccardo, Arnaud Mignan, Bozidar Stojadinovic, Stefan Wiemer, and Domenico Giardini.

Abstract

A key component of the risk governance framework for induced seismicity arising from fluid-induced injections is the definition of a set of risk mitigation strategies. Among the possible strategies, Traffic Light Systems (TLS) are frequently used to mitigate induced seismicity risk by modifying the fluid injection profile. Shortly, a TLS defines one decision variable (event magnitude, peak ground acceleration, etc.) and a series of safety thresholds above which injection should be modified or eventually stopped. This poster presents the ground for a TLS based on a Bayesian Hierarchical model. Briefly stated, a hierarchical Bayesian model utilizes multistage prior distributions of the model parameters. A major strength of the Bayesian approach is that it allows uncertainties and information about parameters to be encoded into a joint prior distribution of the model parameters. Moreover, it allows the computation of posterior predictive distribution of the model parameters as soon as the project is started and information becomes available.

Probabilistic model

The recurrence of earthquake events is modeled with a non-homogeneous Poisson process (NHPP), defined by time varying rate $\lambda(t)$. The rate model is given as

$$\lambda(t;\boldsymbol{\theta}) = \begin{cases} 10^{a-bm_0}\dot{V}(t) & t \le t_s \\ 10^{a-bm_0}\dot{V}(t_s)\exp\left(-\frac{t-t_s}{\tau}\right), & t > t_s \end{cases}$$

where $\dot{V}(t)$ is the injection rate and t_s the shut in time, a the activation feedback, b the earthquake size ratio, and τ the mean relaxation time

Figure 1 shows samples of the NHPP for a given set of parameters

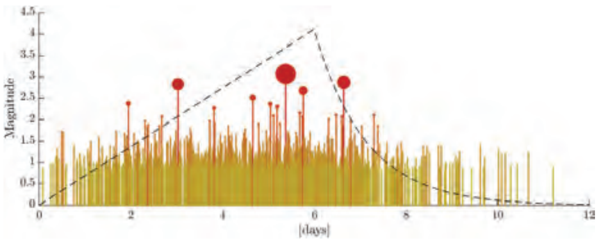

Figure 1 Sample of seismic induced sequence for given values of a, b and τ

Bayesian Hierarchical model, definition and inference

In a Bayesian approach, we consider a, b and τ as random variables adding an extra layer of uncertainty. The prior parameters distribution aim to reflect the relative likelihood of its possible outcomes, taking into account the uncertainties before gathering observations. We can represent models such as this one via Bayesian networks—also known as directed cyclic graph (DAG). Figure 1 shows the proposed model.

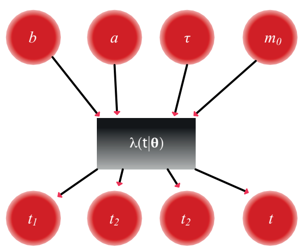

Figure 2 DAG for the proposed Bayesian hierarchical model

As standard practice in DAG, we denote with nodes the random variables, and with a box the model that encode the physics of the problem. From Figure 2, one can observe that the proposed framework is generalizable for any rate model different from the one recommended in this poster. The selection of the prior is the controversial part of Bayesian statistics since it is not unique and can be subject to personal interpretation. However, this can also be viewed as a strength since it allows experts to constrain the domain of the hyper-parameters by encoding physical principles and evidence. In this poster, we choose a subjective prior distribution, since the available data are limited to few past events, and we cannot gather in-situ information before a project take place. Figure 3 shows the three prior distributions, which are Beta distribution for a and b, and the Gamma distribution for τ. The classical Bayesian inference is used to update the probability distribution of the hyper-parameters when observations are available.

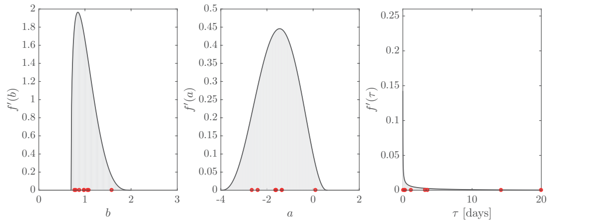

Figure 3 Prior distribution for a, b and τ

Given a set of observations, $D = [t_1, \ldots, t_N; m_1, \ldots, m_N]$, we update the probability distribution of the hyper-parameters as follo $f''_{\boldsymbol{\theta}}(\boldsymbol{\theta}|\mathcal{D}) = c\mathcal{L}(\mathcal{D}|\boldsymbol{\theta})f'(\boldsymbol{\theta})$
The likelihood is derived as:

$$\mathcal{L}(\mathcal{D}|\boldsymbol{\theta}) = \left[\prod_{n=1}^{N}\frac{\lambda(t_n|\boldsymbol{\theta})}{\Lambda(T)}f_M(m_n|b)\right]\Lambda^N(T|\boldsymbol{\theta})\exp[-\Lambda(T|\boldsymbol{\theta})]$$
$$= \left[\prod_{n=1}^{N}\lambda(t_n|\boldsymbol{\theta})f_M(m_n|b)\right]\exp[-\Lambda(T|\boldsymbol{\theta})]$$

where $\Lambda(t) = \int_0^t \lambda(t')dt'$

The small parameter space enable numerical integration. Figure 4 shows: in the diagonal the prior marginal distribution and the posterior marginal distribution of the parameters; in the lower triangular part, the prior pair-wise distribution; and in the upper triangular part, the posterior pair-wise di

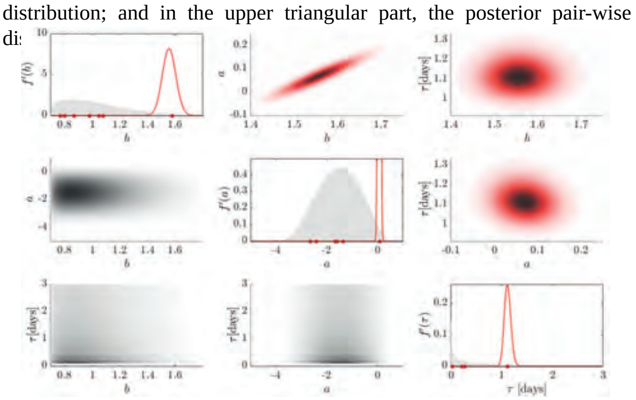

Figure 4 Posteriors distributions of a, b and τ

Anticipation model, predictive distribution

The proposed Bayesian model also allows a precise classification of the uncertainties. In particular, we separate epistemic (encoded in the parameter distributions) from aleatory uncertainty (encoded in the Poisson model). This separation is important in the prediction model which is derived as f

$$P(N(t \in [t+h]) = n|\mathcal{D}(t)) = \int_{\boldsymbol{\theta}}\left[\frac{\int_t^{t+h}\lambda(t'|\boldsymbol{\theta})dt'}{n!}\exp\left[-\int_t^{t+h}\lambda(t'|\boldsymbol{\theta})dt'\right]\right]f''_{\boldsymbol{\theta}}(\boldsymbol{\theta}|\mathcal{D}(t))d\boldsymbol{\theta}$$

Figure 5 shows prediction and true outcome for a window time of 4 hours

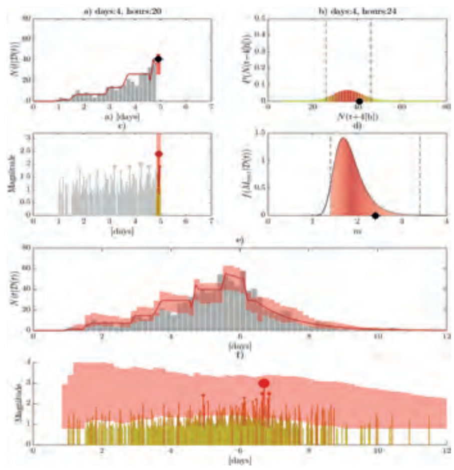

Figure 5 Anticipation model: left rates, right probability distribution of number of seismic events

SCCER-SoE Annual Conference 2017

SCCER SoE
SWISS COMPETENCE CENTER for ENERGY RESEARCH
SUPPLY of ELECTRICITY

70 NRP Energy Turnaround National Research Programme

PAUL SCHERRER INSTITUT PSI

In cooperation with the CTI
Energy Swiss Competence Centers for Energy Research

Schweizerische Eidgenossenschaft
Confédération suisse
Confederazione Svizzera
Confederaziun svizra
Swiss Confederation
Commission for Technology and Innovation CTI

(FRS) FUTURE RESILIENT SYSTEMS 未来韧性系统

Transformation of the Energy-related Severe Accident Database (ENSAD) into an interactive, web-based GIS application

P. Burgherr[1], W. Kim[2], M. Spada[1], A. Kalinina[1], S. Hirschberg[1]
[1]Technology Assessment Group, Paul Scherrer Institut, Villigen PSI, Switzerland
[2]Future Resilient Systems (FRS) , Singapore-ETH Centre, Singapore

Introduction

The **risk assessment of energy technologies** is a mature and established scientific field with a strong quantitative foundation (*Burgherr & Hirschberg, 2014*). Numerous important conceptual and methodological achievements since the 1980s continuously advanced its state-of-the-art. Particularly in the past two decades a more **integrated perspective** on risk assessment has emerged by combining it with several overarching concepts such as **sustainability**, **energy security**, **critical infrastructure protection** and **resilience**.

The systematic and **comprehensive collection of historical accidents** in the energy sector requires that complete energy chains are considered because accidents can occur at all stages and not just during the actual power and/or heat generation. However, such a dedicated and authoritative database became only available with the establishment of the **Energy-related Severe Accident Database** (**ENSAD**) by the Paul Scherrer Institut (PSI) in the 1990s (*Hirschberg et al., 1998*).

Current status of ENSAD

ENSAD has a number of advantages compared to general industrial and specialized ("narrow-scope") databases, including a **broad application range** with regard to accident risk assessment in the energy sector (*Burgherr et al., 2017*). Despite these obvious advantages, continuous improvements and developments, ENSAD has remained a static, non-spatial database in MS Access format. Therefore, a completely new, **interactive, web-based GIS database** – **ENSAD v2.0** – is developed with the following features:

1. **Spatial database** for accidents involving energy infrastructures.
2. Geo-referenced data based on **advanced geo-coding** technology.
3. **Web-based Geographic Information System** (GIS) to visualize and analyze the spatial and temporal characteristics of accidents.

Structure and Features of ENSAD v2.0

Figure 1 shows the system architecture and data flow of the new ENSAD v2.0, which is based on a **cloud server and open-source technologies**. The connection to a GIS server (GeoServer) generates the map content for the web client that meets the OGC (Open Geospatial Consortium) standard, i.e. WMS (Web Map Services), WFS (Web Feature Service), etc. ENSAD v2.0 is developed as a **responsive web application** so that a user can access it from a PC as well as a mobile device such as smartphone or tablet.

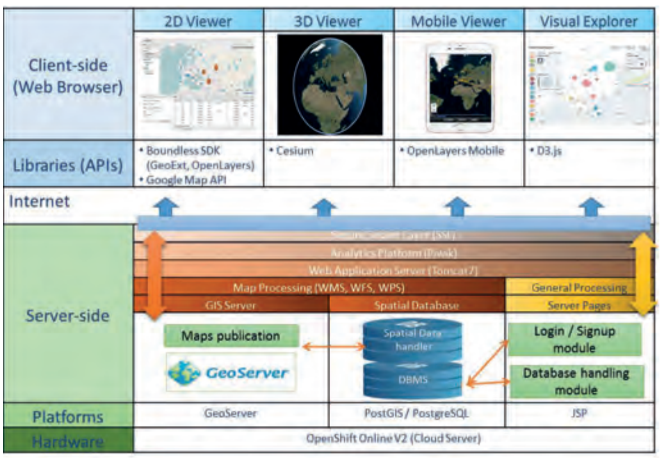

Figure 1: System architecture and data flow of ENSAD v2.0 (*Kim et al, 2017*).

On the client side, four ENSAD v2.0 versions are available. The **desktop version** provides the **complete information for all 32'963 accidents**, and data can be visualized either in 2D or 3D (**Figure 2, left**). Due to its limited screen size, the **mobile version focuses on displaying specific accident information** only. Users can also check for accident information at their current location using the positioning capabilities of their mobile device. Finally, the so-called **ENSAD Visual Explorer (EVE)** provides a **public version** of ENSAD v2.0 with access to a **limited number of data fields**, but all accident records can be viewed on a world map and pre-defined visualizations as well as limited analysis capabilities are available (**Figure 2, right**).

Figure 2: Main interfaces of ENSAD v2.0 desktop version (**left**), and ENSAD Visual Explorer (**right**) (*Kim et al., 2017*).

Selected Case Study Applications of ENSAD v2.0

Figure 3 shows two **case study examples using ENSAD v2.0**, namely **(left)** risk assessment of dam accidents, and **(right)** rough set analysis to develop classification models for natural gas accidents. Other ongoing activities include (1) the analysis of potential impacts of selected natural hazards and technical failures on the European natural gas transmission network and its recovery dynamics (e.g. *Kyriakidis et al., 2017*), and (2) the development of a web scraping tool to facilitate future updates of ENSAD with new energy accident data.

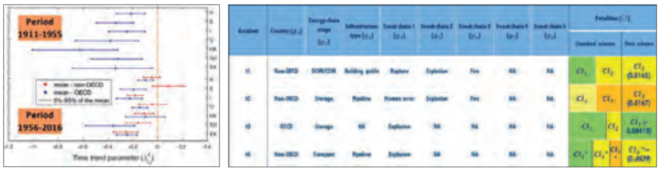

Figure 3: ENSAD v2.0 case study examples. (**left**) dam risk assessment (*Kalinina et al., 2016*), (**right**) rough set analysis (*Cinelli et al., 2017*).

Acknowledgments

This work has been carried out within the **Swiss Competence Center on Energy Research – Supply of Electricity** (concept, data management and preparation of data migration), the **Energy Turnaround National Research Programme (NRP70)** of the Swiss National Science Foundation (dam accident prototype), and the **Future Resilient Systems (FRS) program** of the Singapore-ETH Centre (SEC) (tool development and implementation, data migration).

References

- Burgherr, P., Hirschberg, S. (2014) Comparative risk assessment of severe accidents in the energy sector. Energy Policy, 74, S45-S56.
- Burgherr, P., Spada, M. Kalinina, A., Hirschberg, S., Kim., W., Gasser, P. & Lustenberger, P. (2017) The Energy-related Severe Accident Database (ENSAD) for comparative risk assessment of accidents in the energy sector. IN: Cepin, M. & Bris, R. (Eds.) Safety and Reliability - Theory and Applications. London, UK, CRC Press, Taylor & Francis Group.
- Cinelli, M., Spada, M., Miebs, G., Kadziński, M., Burgherr, P. (2017, forthcoming) Classification models for the risk assessment of energy accidents in the natural gas sector. The 2nd International workshop on Modelling of Physical, Economic and Social Systems for Resilience Assessment. Brussels, Belgium.
- Hirschberg, S., Spiekerman, G., Dones, R. (1998) Severe accidents in the energy sector – 1st ed. PSI Report No. 98-16. Villigen PSI, Switzerland.
- Kalinina, A., Spada, M., Burgherr, P., Marelli, S. & Sudret, B. (2016) A Bayesian hierarchical modelling for hydropower risk assessment. IN: Walls, L., Revie, M. & Bedford, T. (Eds.) Risk, Reliability and Safety – Innovating Theory and Practice. London, UK, CRC Press, Taylor & Francis Group.
- Kim, W. Burgherr, P., Spada, M., Hirschberg, S., Lustenberger, P., Gasser, P. (2017) Transformation of the Energy-Related Severe Accident Database to an Open Source, Interactive, Web-Based GIS Application for Risk Visualization and Decision-Support. Free Open Source Software For Geospatial (FOSS4G) 2017, Boston, USA.
- Kyriakidis, M., Lustenberger, P., Burgherr, P., Dang, V. & Hirschberg, S. (2017) The human element in infrastructure resilience – a quantitative analysis of natural gas network recovery dynamics in floods. Proceedings of the PSAM Topical Conference on Human Reliability, Quantitative Human Factors, and Risk Management, Munich, Germany.

SCCER SoE
SWISS COMPETENCE CENTER for ENERGY RESEARCH
SUPPLY of ELECTRICITY

SCCER-SoE Annual Conference 2017
70 NRP Energy Turnaround
National Research Programme

In cooperation with the CTI
Energy
Swiss Competence Centers for Energy Research
Swiss Confederation
Commission for Technology and Innovation CTI

Probabilistic Damage Quantification of Unreinforced Masonry Walls Exposed to Induced Seismic Risk

Max Didier, Marco Broccardo, Giuseppe Abbiati, Fiona Hefti, Adrian Gabbi, Milos Petrovic, Nebojsa Mojsilovic, Bozidar Stojadinovic

Objective

Sequences of low-magnitude induced earthquakes can cause non-structural damage to buildings, for example, to the plaster covering the surface of unreinforced masonry (URM) walls. This construction style is prominent in Switzerland, as well as in other European countries. Deep geothermal reservoir exploration and operation can induce such seismic events. Two types of possible damage need to be distinguished: damage due to larger, more rare events; and damage due to fatigue caused by repeated, smaller events. An experimental test campaign has been led at the Institute of Structural Engineering (IBK) of ETH Zurich to quantify the probabilities of both types. The findings can be used in combination with an appropriate seismic hazard and ground motion model to quantify the (financial) risk of deep geothermal projects.

Test Campaign

In total, 15 plastered URM walls have been tested at ETH Zurich. The 5 walls of the first phase were tested using the NAMC and BIN2_99 load protocols, representative of low to medium magnitude seismicity. The 10 following walls were tested using a load protocol representative of fatigue loads. All walls were tested in a 3-actuator quasi-static test setup. Data on the reaction of the walls was collected using a laser sensor, several LVDT sensors and a digital image correlation (DIC) system. The pictures obtained via DIC were then processed in the Vic2D and Matlab software to obtain displacement and von Mises strain maps of the plaster surface. These maps were then used to compute damage scores to estimate the expected damage.

Damage Scores

Two damage scores have been developed and evaluated using the obtained experimental data: the Normalized Crack Area (NCA) and the Normalized Crack Length (NCL).

The **NCA** is defined as:

$$NCA = \frac{damaged\ area\ of\ the\ plaster}{total\ area\ of\ the\ plaster} = \frac{number\ of\ white\ pixels\ on\ cum.\ von\ Mises\ strain\ map}{total\ number\ of\ pixels\ on\ cum.\ von\ Mises\ strain\ map}$$

and the **NCL** as:

$$NCL = \frac{sum\ of\ length\ of\ all\ cracks}{length\ of\ wall\ diagonal} = \frac{sum\ of\ crack\ perimeters/2}{length\ of\ wall\ diagonal}$$

Both metrics are computed from the von Mises strain maps of the plaster surface (Fig. 1a)). The maps need to be converted first into greyscale maps (Fig. 1b)) to compute, finally, cumulate binary von Mises strain maps (Fig. 1c)). From these, the number of white pixels and the sum of the crack perimeters can be derived.

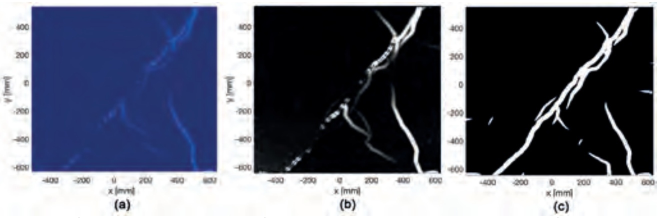

Fig. 1 a) von Mises strain map, b) greyscale von Mises strain map, and c) cumulate binary von Mises strain map

The computed damage scores can be correlated to the displacement amplitudes (Fig. 2). This allows to estimate the damage for a given displacement (e.g. imposed to the wall by an induced ground motion sequence at interest).

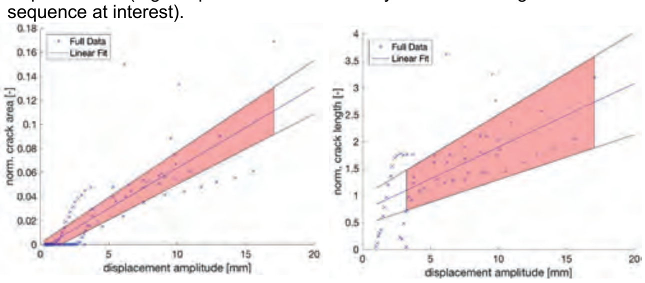

Fig. 2 Displacement amplitude and computed NCA and NCL

Damage States and Damage Probability

Three damage states have been defined to classify the damage of the walls:

- No damage: no visual damage detected on the picture;
- Visible crack: crack can be detected by visual inspection;
- Plaster fall-off: fall-off of parts of the plaster.

A survey has been conducted to correlate the calculated damage scores to the three damage states (Fig. 3). For a given NCA or NCL, the probability of observing a certain damage state can be estimated. In combination with Fig. 2, this allows to determine the probability of occurrence of damage to the plaster surface of an URM wall for a given displacement caused by an induced ground motion.

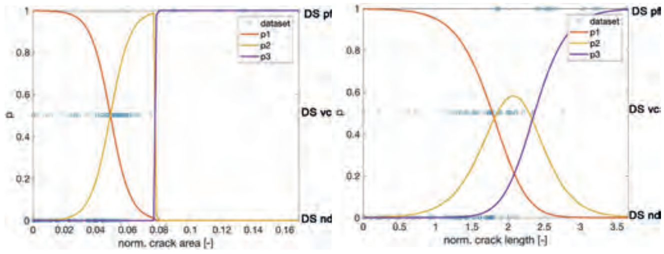

Fig. 3 Survey answers and multivariate logistic regression for NCA and NCL

Fatigue Damage

Experimental data obtained from applying fatigue-like load protocols on 10 walls was used to elaborate a fatigue damage model. Load sequences of amplitudes of 1mm, 3mm, 5mm and 7mm were applied up to 200 times to the same wall. The plaster surface was again analyzed by DIC. The NCA and the NCL were then computed for the progression of the fatigue tests (Fig. 4). An exponential regression was used to compute fatigue curves for plaster damage of the URM walls (Fig. 5).

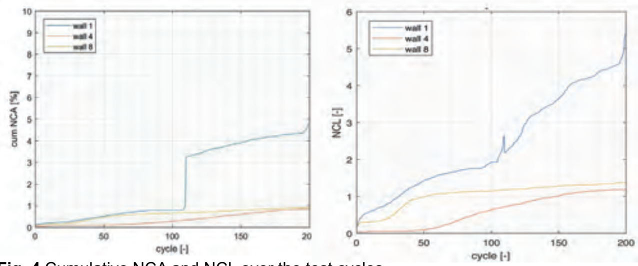

Fig. 4 Cumulative NCA and NCL over the test cycles

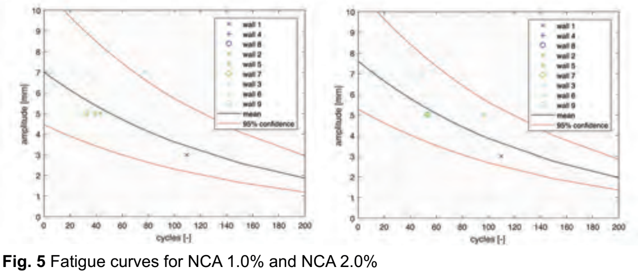

Fig. 5 Fatigue curves for NCA 1.0% and NCA 2.0%

Conclusion

Two damage scores have been developed using the data obtained from the experimental test campaign at ETH Zurich: the NCA, related to the damaged plaster surface; and the NCL, related to the length of the cracks on the plaster. Both metrics can be used to estimate the probability of observing a certain plaster damage state for a given displacement amplitude. The fatigue model allows to estimate the damage caused by long sequences of repeated induced ground motions. Combining the presented models with models for the expected induced seismicity of deep geothermal sites would allow to estimate the risk associated to such projects.

References

Didier, M., Abbiati, G., Broccardo, M., Beyer, K., Danciu, L., Petrovic, M., Mojsilovic, N., and Stojadinovic, B. (2017). Quantification of Non-Structural Damage in Unreinforced Masonry Walls Induced by Geothermal Reservoir Exploration using Quasi-Static Cyclic Tests. *Proceedings of 13th Canadian Masonry Symposium*, June 4-7, Halifax, Canada.

Mergos, P. E., & Beyer, K. (2014). Loading protocols for European regions of low to moderate seismicity. *Bulletin of Earthquake Engineering*, *12*(6), 2507-2530.

SCCER SoE
SWISS COMPETENCE CENTER for ENERGY RESEARCH
SUPPLY of ELECTRICITY

70 NRP Energy Turnaround
National Research Programme

ETH zürich

GEOBEST CH

SCCER-SoE Annual Conference 2017

One decade of induced seismicity in Basel, Switzerland: A consistent high-resolution catalog obtained by template matching

Marcus Herrmann[1], Toni Kraft[1], Thessa Tormann[1], Luca Scarabello[1], Stefan Wiemer[1]

[1] Swiss Seismological Service, ETH Zurich, Switzerland; ✉ marcus.herrmann@sed.ethz.ch

In cooperation with the CTI
Energy
Swiss Competence Centers for Energy Research
Schweizerische Eidgenossenschaft
Confédération suisse
Confederazione Svizzera
Confederaziun svizra
Swiss Confederation
Commission for Technology and Innovation CTI

Schweizerischer Erdbebendienst
Service Sismologique Suisse
Servizio Sismico Svizzero
Swiss Seismological Service

Background & Problem Statement

In December 2006, an extensive fluid injection was carried out below the city of Basel, Switzerland, to stimulate a reservoir for an Enhanced Geothermal System (EGS).
Some details:

- ~11'500 m³ water injected into crystalline rock, 5km deep
- After 6 days, M_L2.6 event exceeded safety threshold
  → reduced injection rate, then stopped completely
  → shut-in (closure of borehole)
- Hours later: widely felt M_L3.4 event
  → well opened; rapid decay of seismicity
- Originally detected ~13'000 EQs (located ~3,500)
- Dec. 2009: project canceled – a seismic risk study suggested substantial risk of further felt and potentially damaging events [*Baisch 2009*]
- Mid-2011: ultimate shut-in; pressure increase
- Mid-2012: **renewed increase** of seismicity (M_L>1.0)

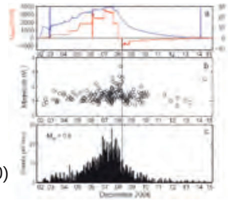

The well-monitored and well-studied induced sequence allowed many new insights in terms of reservoir creation. However, the **details of the long-term behavior** remained unexplored since a consistent catalog did not exist. We want to create one.

Highlights & Outlook

- Our newly obtained catalog …
  - spans more than ten years
  - contains **more than 130'000 events**
  - features a uniform detection threshold and consistent magnitude
  - decreased the detection limit by more than one magnitude unit
  - increased the spatiotemporal resolution
    → statistical analysis in great detail:
    - resolved variations of the a- and b-value
    - derived temporal development of the seismic hazard
    - …
- Detections confirm clearly the (re-)activity several years after injection; they tend to cluster
- Possible connection: pressure increase ↔ re-activation?
  - Since July 2017, the borehole is opened again periodically to reduce the pressure
  - ❑ How long do we have to monitor and maintain a closed EGS project?
- We hope to provide the basis for a better understanding of the processes that drive the induced seismicity in Basel
- We have also started to extend our analysis to other induced and natural sequences in Switzerland

Findings of a multi-template approach

We scanned the recordings of the **deepest installed borehole station** (2.7km). This station is very close (1.5–2.5km) to ~4.5km-deep reservoir, completely in the granite bedrock. It has the highest signal-to-noise ratio among all (borehole-)stations.

Technical details:
- Band-pass-filter of 5-80Hz; 500fps
- Removed 50Hz noise in the frequency domain
- The Z-channel failed in 2010. To be consistent, we only used the 2 horizontal channels. This might lead to wrong template associations.

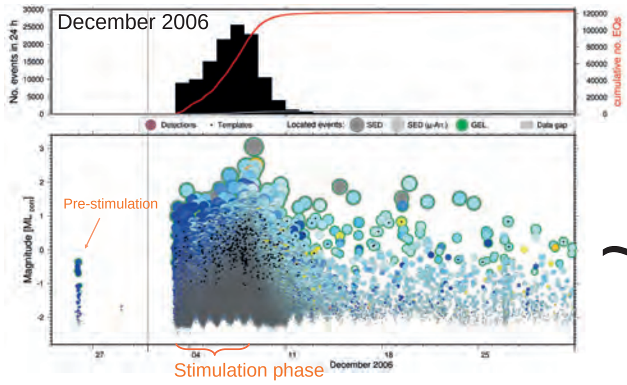

~

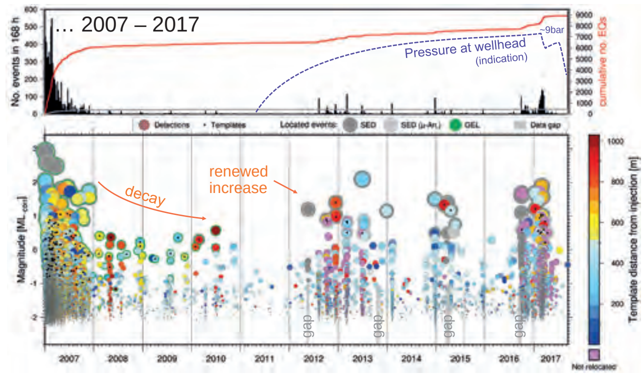

The **color** of a detection indicates to which template it is most similar. Later events tend to occur and cluster more outwards. But also older (inner) fault patches get reactivated again.

The orientation of the individual faults varies and deviates from the general orientation "seismic cloud" [*Deichmann et al. 2014*]. To reach an acceptable coverage of the complex seismicity in the stimulated volume, we selected **~500 templates** from >3'600 event waveforms and performed the scan in **parallel on ~600 cores** of the EULER high-performance computer. This scan over more than 10 years of data took ~36 hours.

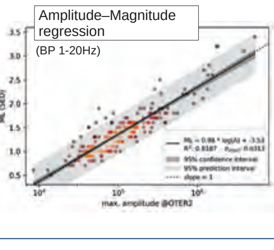

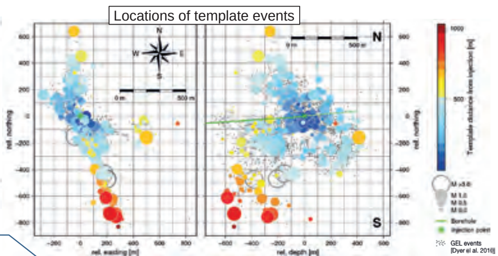

Earthquake statistics

The sampling of the seismic sequence in much closer detail significantly improved the completeness magnitude (*Mc*) of the catalog so that we can **resolve the *b*-value variation** and **thus the probability for a larger event** in unprecedented resolution. In particular, we can now assess the long-term evolution of the sequence even during periods when the rate of network-detected events is very low (e.g., 2010 – 2011).

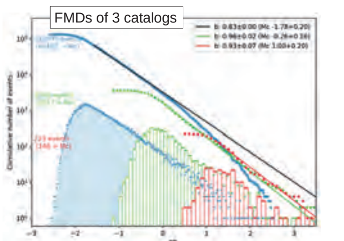

- our catalog based on template matching
- *Dyer et al. 2010*
- *Swiss Seismological Service (SED)*

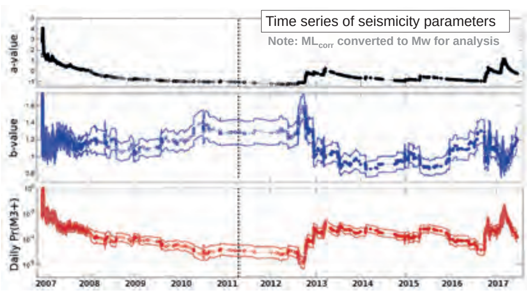

Acknowledgements

We thank GEOENERGIE SWISS AG and GEOEXPLORERS LTD. for providing the seismometer recordings of the Basel Geothermal Project. A special thanks goes to the team of the EULER high-performance computer (Swiss National Supercomputing Centre) for providing us plenty of computational power.
This work was conducted with the support of ENERGIESCHWEIZ in the framework of the project GEOBEST-CH. The research leading to these results has also received funding from the *European Community's Seventh Framework Programme* under grant agreement No. 608553 (Project *IMAGE*).

References

Baisch, S., Carbon, D., Dannwolf, U. S., Delacou, B., Devaux, M., Dunand, F., … Vörös, R. (2009). Deep Heat Mining Basel: Seismic Risk Analysis.
Dyer, B.C., et al., 2010. Application of microseismic multiplet analysis to the Basel geothermal reservoir stimulation events. Geophys. Prospect. 58.
Deichmann, et al., 2014. Identification of faults activated during the stimulation of the Basel geothermal project from cluster analysis and fault mechanisms for the larger magnitude events. Geothermics.

SCCER-SoE
SWISS COMPETENCE CENTER for ENERGY RESEARCH
SUPPLY of ELECTRICITY

ETH zürich

SCCER-SoE Annual Conference 2017

Generic cellular automaton for statistical analysis of landslides frequency-size distribution

Ahoura Jafarimanesh, Arnaud Mignan, and Domenico Giardini

In cooperation with the CTI
Energy
Swiss Competence Centers for Energy Research
Schweizerische Eidgenossenschaft
Confédération suisse
Confederazione Svizzera
Confederaziun svizra
Swiss Confederation
Commission for Technology and Innovation CTI
70 NRP Energy Turnaround
National Research Programme

Abstract:

This study presents a generic landslide cellular automaton (GLSCA) that is constructed based upon the rules of Self Organized Criticality (SOC) and is consistent with the broad range of values in nature. Despite different triggering mechanisms in landslides processes (e.g., rain, earthquakes, etc.), the related frequency-size distribution (FSD) appears to follow the power law probability function, with the power law exponent (α) valid for x ≥ xmin. Here, we study the role of various triggering mechanisms in addition to the soil characterization on α. The landslide activation is based on the factor of safety (FS), (e.g., Crosta, 1998 and references therein), and the dynamic of the model is controlled by the ground slope variation. We attempted to interpret the physical behaviour of the landslide (e.g., exponential roll over effect) based on α variation, and test other metrics such as the maximum extent per earthquake magnitude and landslide shape. In that, we demonstrated how our GLSCA compares to studies that have reported frequency distributions of landslides areas in the world.

Power law function and probability distributions:

Power law probability density function with the exponent (α) valid for x ≥ x_{min}

(1) $$p(x)=(\alpha-1)x_{min}^{\alpha-1}\,x^{-\alpha}$$

To study the roll over behaviour below x_{min}, double pareto (2) and inverse gama distribution (3) have been proposed:

(2) $$p(x)=\frac{\beta}{x_c}\left[\frac{(1+(\max x/x_c)^{-\alpha_2})^{\beta/\alpha_2}}{(1+(x/x_c)^{-\alpha_2})^{1+\beta/\alpha_2}}\right]\left(\frac{x}{x_c}\right)^{-\alpha_2-1}$$

(3) $$p(x)=\frac{1}{x_c\Gamma(\rho)}\left(\frac{x_c}{x-s}\right)^{\rho+1}\exp\left(-\frac{x_c}{x-s}\right)$$

Parameters (1) : **α** = **α_2**+1 ,**β** the power exponent below the rollover , ***x_c*** the corner size; Parameters (2) : **α =ρ+1**, ***s*** a parameter primarily controlling the exponential rollover, and ***x_c*** the corner size.

Landslide frequency size statistic and sampling:

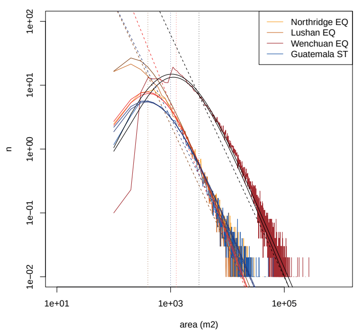

Fig. 1: The FSD of published landslide inventories. The power law exponent α ,(Eq. 1) for each case is equal to :

1:1994 Northridge earthquake (Harp and Jibson, 1995), α_1=2.4
2: 2013 Lushan earthquake (Xu et al., 2015), α_2=3
3: 2008 Wenchuan earthquake (Li et al., 2014), α_3=3
4: 1998 Hurricane Mitch (Bucknam et al., 2001) , α_4= 2.2

Updated table of α value correspondent to 50 landslide inventories shows α distribution with 2<α< 3 (Jafarimanesh et al., 2017- in preparation)

Generic Landslide Cellular Automaton (GLSCA):

A. Initiation phase: Landslide initiate when the factor of safety (Fs) is ≤ 1.

(4) $$FS=\frac{C}{\gamma h \sin\theta}+\frac{\tan\phi}{\tan\theta}-\frac{m\gamma_w\tan\phi}{\gamma\tan\theta}$$ (Jibson,1993) Earthquake triggered

(5) $$FS=\frac{\tan\phi}{\tan\theta}-\frac{-\Psi(Z,t)\gamma_w\tan\phi}{\gamma_s Z\sin\theta\cos\theta}+\frac{C}{\gamma_s Z\sin\theta\cos\theta}$$ (Iverson,2000) Rainfall triggered

Φ the effective internal friction angle, C the soil cohesion ,θ the slope angle, γ the soil unit weight, γ_w the water unit weight, h the slope-normal soil thickness, m the proportion of h that is saturated, γ_s is the depth-averaged soil unit weight, and ψ(Z,t) is the pressure head which determines the effect of the groundwater on slope stability.

B. **Propagation phase:** Altitude *z*(x,y) and soil depth *h*(x,y).

(6) $$\begin{cases} z(x,y)=z(x,y)-\Delta h \\ h(x,y)=h(x,y)-\Delta h \\ z(dir_{Moore}[\theta_{max}(x,y)])=z(dir_{Moore}[\theta_{max}(x,y)])+\Delta h \\ h(dir_{Moore}[\theta_{max}(x,y)])=h(dir_{Moore}[\theta_{max}(x,y)])+\Delta h \end{cases}$$

Input parameters are the initial topography (*z*, *h*) and soil properties (ϕ, *C*, ϒ, *m)*

and the mass movement is defined by Eq. 7:

(7) $$\Delta h=[z(x,y)-z(dir_{Moore}[\theta_{max}(x,y)])-\Delta s\tan(\theta_{stable})]/2$$

Algorithm, fractal topography modelling and the GLSCA application:

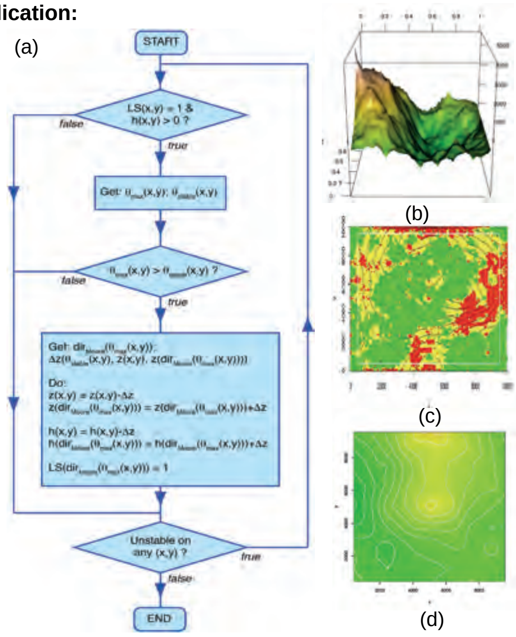

Fig. 2 : (a) Algorithm of the proposed CA method. (b): The example of fractal topography used in the modelling. (c) The factor of safety map, red cells are showing Fs<1 and yellow cells indicate 1≤Fs≤1.5 . (d) The new eroded topography after the analysis, the critical cells are removed.

Results :

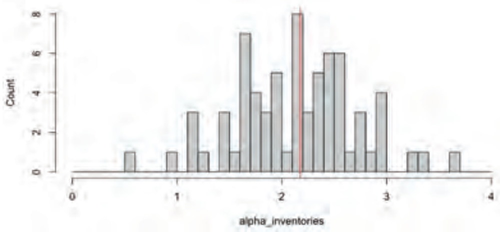

Fig. 3: The histogram of α values, correspondent to 50 frequency distribution of landslide areas worldwide (updated from Van Den Eeckhaut et al., 2007). The vertical red line shows the median of α values is around 2.1.

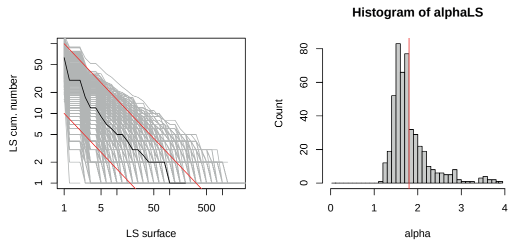

Fig. 4: (a) The FSD of CA method applied over 500 cases of fractal topographies. The Inclined red lines show the boundary of the analysis. (b) The histogram of non cumulated α values of analysis in (a); The vertical red line shows the median of the α values is approximately around 1.9.

Reference (Database):

- Van Den Eeckhaut, Miet, et al. "Characteristics of the size distribution of recent and historical landslides in a populated hilly region." Earth and Planetary Science Letters 256.3 (2007): 588-603.

SCCER SoE
SWISS COMPETENCE CENTER for ENERGY RESEARCH
SUPPLY of ELECTRICITY

SCCER-SoE Annual Conference 2017

70 NRP Energy Turnaround National Research Programme

PAUL SCHERRER INSTITUT PSI

In cooperation with the CTI
Energy Swiss Competence Centers for Energy Research
Swiss Confederation
Commission for Technology and Innovation CTI

Uncertainty quantification of flood wave propagation resulting from a concrete dam break

Anna Kalinina[1], Matteo Spada[1], Peter Burgherr[1], & Christopher T. Robinson[2]

[1]Technology Assessment Group, Paul Scherrer Institut, Villigen, Switzerland, [2] Department of Aquatic Ecology, Eawag, Dübendorf, Switzerland

Research scope and goal definition

Modelling of the dam-break event consists of 3 simulation Blocks:

Block 1: Dam-break outflow hydrograph → Block 2: Dam-break flood simulation → Block 3: Estimation of loss of life

Research scope: In the current phase of the PhD project, we focus on the model that evaluates the flow quantities reached downstream of the dam in case of a failure (**Block 1** and **Block 2)**

Research goals: **Metamodelling for uncertainty quantification and sensitivity analysis** is applied in the model of a large concrete dam break; Developing a generic model that can be used for analysis of any dam in Switzerland.

Generic physical model of flood wave propagation resulting from a concrete dam break

- The focus of the model is on large arch concrete hydropower dams located in the Alpine area of Switzerland;
- Complete and instantaneous failure of the dam is assumed; therefore, the dam-break is treated as a Riemann problem;
- The amount of water released from the dam is characterized using **4** parameters: *H, C, V,* B_{rel} (**Table 1**);
- Flood propagation is simulated for a generic model of the downstream valley characterized using **6** parameters: CL_{rel}, CW_{rel}, *shCH*, *BS*, *Mb*, & *Ms* (**Table 1**);
- A 1D model is then built in the BASEMENT software (ETHZ).

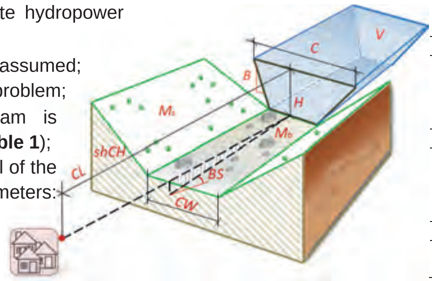

Table 1: Model Input Parameters

Par-r	Name	Unit
Physical characteristics of dam and reservoir		
H	Dam height	[m]
C	Length of dam crest	[m]
V	Reservoir volume	[10^3*m^3]
B_{rel}	Dam side slope (relative)	[m/m]
Physical characteristics of channel		
CL_{rel}	Channel length (relative)	[m/m]
CW_{rel}	Channel bed width	[m]
shCH	Shape parameter of channel cross section	[m^3]
BS	Slope of channel bed (relative)	[%/m]
Environmental characteristics		
Mb	Roughness coefficient of channel bed	[sec/$m^{1/3}$]
Ms	Rough. coeff. of channel embankments	[sec/$m^{1/3}$]

Framework for uncertainty quantification & sensitivity analysis

Modeled input uncertainty is propagated through the surrogate model created using **Polynomial Chaos Expansion (PCE)**:

$$Q_{peak} = \sum_{\alpha \epsilon A} y_\alpha \Psi_\alpha(X)$$

Q_{peak} - PCE response, X_i - input vector, y_α - coefficient, Ψ_α - polynomials

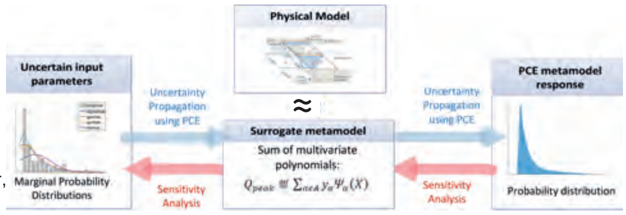

Sensitivity Analysis is performed using the linear correlation coefficient ρ_i between the i^{th} input and the model output Q_{peak}; and the Spearman rank correlation coefficient ρ_i^S.

Building a metamodel and sensitivity analysis are performed using UQLab (Marelli and Sudret, 2014).

Results for uncertainty & sensitivity of the model parameters

Model input uncertainty:

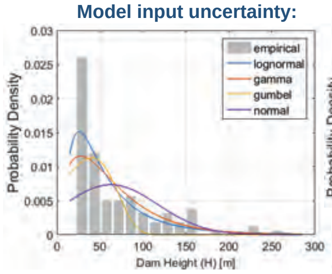

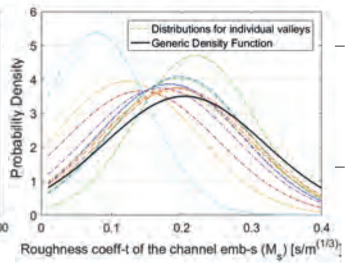

- Distributions of **4** input parameters (*H, C, V,* B_{rel}) are built using the data of 116 large dams in Switzerland (SwissCOD, 2016);
- Distributions of **6** other input parameters (CL_{rel}, CW_{rel}, *shCH*, *BS*, *Mb*, & *Ms*) are defined by classifying topographies downstream of 19 arch concrete dams in Switzerland. The classification is based on slopes and land cover data from GeoVITE (https://geodata4edu.ethz.ch/portal.jsp) & Rosgen, et al. (2013);
- Dependence between parameters was modelled by a Gaussian copula; certain distributions are truncated due to physical constrains.

Table 2: Marginal distributions of model inputs

Par-r	Distribution	Par-r	Distribution
H	$H \sim LN(3.83, 0.77)$	CW_{rel}	$CW_{rel} \sim \Gamma(0.013, 0.58)$
V	$V \sim LN(8.04, 2.76)$	shCH	$shCH \sim \Gamma(1.4e-4, 13.6)$
C	$C \sim \Gamma(0.007, 1.6)$	BS	$BS \sim LN(2.44, 0.57)$
B_{rel}	$B_{rel} \sim U(0,1)$	Mb	$Mb \sim LN(-2.63, 0.95)$
CL_{rel}	$CL_{rel} \sim \Gamma(0.04, 2.22)$	Ms	$Ms \sim N(0.20, 0.11)$

Model output uncertainty and sensitivity:

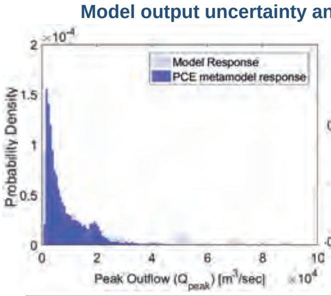

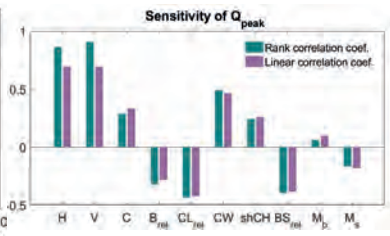

- **PCE** is calculated for the set of **flow quantities** at the location downstream of the dam, i.e., peak discharge Q_{peak} [m³/sec], the time to the Q_{peak} [sec], and water depth [m];
- **PCE** is built using a design sample of **111 runs** of the **original model**;
- The dam dimensions, channel bed width and its slope are **important** for the Qpeak; as well as it is important how far from the dam the inhabited locality, where the flow quantity need to be measured, is situated.

Conclusions: · The applied metamodelling approach can reproduce the original model, and allows **reducing computational efforts**.
· Sensitivity analysis can **support decision-making processes**, thus being **beneficial for the risk assessment field**.
· The generic model can be used for **analysis of any existing dam in Switzerland**, as well as dams **currently in design**.

Acknowledgement: This research project is part of the National Research Programme "Energy Turnaround" (NRP 70) of the Swiss National Science Foundation (SNSF). Further information on the National Research Programme can be found at www.nrp70.ch. It is also integrated with the activities of the Swiss Competence Center on Energy Research – Supply of Electricity (SCCER SoE).

The authors express their sincere thanks to Prof. Bruno Sudret and Dr. Stefano Marelli, ETHZ, and to Dr. David Vetsch, ETHZ, for valuable comments and assistance.

References
- Rosgen, et al. (2013). Waldo Canyon Fire Watershed Assessment: The WARSSS Results. Wildland Hydrology, 4 Appendices.
- ETH Zurich 2016. BASEMENT, Accessed in: http://www.basement.ethz.ch/.
- Marelli, S. & Sudret, B. 2014. UQLab: A framework for uncertainty quantification in Matlab 257 Vulnerability, Uncertainty, and Risk. 2nd ICVRAM2014, UK.
- SwissCOD 2016. Dams in Switzerland, Accessed in: http://www.swissdams.ch/index.php/en/swiss-dams/dams-in-switzerland.

SCCER-SoE Annual Conference 2017

Communicating induced seismicity of deep geothermal energy and shale gas: low-probability high-consequence events and uncertainty[1]

Theresa Knoblauch, Michael Stauffacher, Evelina Trutnevyte
ETH Zurich, Department of Environmental Systems Science (USYS), USYS Transdisciplinarity Lab

1 Motivation

- Deep geothermal energy (DGE) guidelines [2,3] recommend to communicate low-probability high-consequence (LPHC) events of induced seismicity (IS) to the public.
- However, risk communication literature lacks empirical evidence on how to communicate LPHC events of IS and whether to address related uncertainty.

2 Research questions

1) How do **different formats** of written risk communication of IS affect the public's perception of this risk communication in terms of **understandability, trust, and concern**? We distinguish between three formats (qualitative, qualitative and quantitative, qualitative and quantitative with risk comparisons).

2) How does **a statement of uncertainty and limited expert confidence** affect the public's perception of this risk communication in terms of understandability, trust, and concern?

3) How does the risk communication format affect the **public's perception of the risk** of IS?

4) To what extent does the technology, such as DGE and shale gas, affect the public's perception of the identical risk communication material?

3 Method

- Online survey August 2016
- Experimental design
- N = 590 participants
- German-speaking part of Switzerland

Table I Experimental conditions (C) of the survey

Format	Statement of uncertainty	Technology: DGE	Technology: Shale gas
Qualitative	Not included	C1	C7
	Included	C2	C8
Quantitative	Not included	C3	C9
	Included	C4	C10
Risk comparison	Not included	C5	C11
	Included	C6	C12

4 Technology framing

Figure 1 Detail of technology framing
Left: Near surface and deep geothermal energy [4,5]
Right: Conventional gas and shale gas with hydraulic fracturing[6,7]

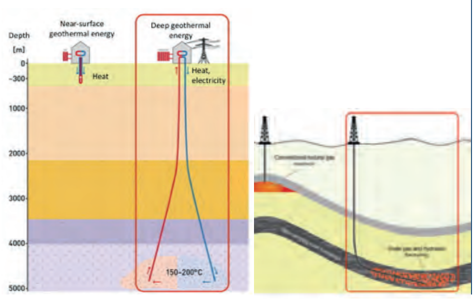

5 Risk communication for experimental conditions

Table II Examples of risk communication formats for different experimental conditions (C)

Qualitative format (C1, C7)

The risk study concluded for the week-long drilling and project operations in your community:
- Micro-earthquakes are virtually certain. These micro-earthquakes will be too small for humans to be felt.
- An earthquake that is lightly noticeable for humans is unlikely.
- An earthquake that is strongly felt and can cause slight damage (e.g. hair-line cracks or falling of small pieces of plaster) is exceptionally unlikely.
- An earthquake that is severely felt and can cause serious structural damage to average houses (e.g. large cracks in walls, falling of gable parts) is even more unlikely, thus also exceptionally unlikely.

Quantitative format with uncertainty and limited expert confidence (C4, C10)

The risk study concluded for the week-long drilling and project operations in your community:
- Micro-earthquakes are virtually certain. These micro-earthquakes will be too small for humans to be felt.
- An earthquake of magnitude 3 on the Richter scale that is lightly noticeable for humans has a probability of about 5%.
- An earthquake of magnitude 5 on the Richter scale that is strongly felt and can cause slight damage (e.g. hair-line cracks or falling of small pieces of plaster) is exceptionally unlikely. It has a probability of about 0.01%.
- An earthquake of magnitude 6 on the Richter scale that is severely felt and can cause serious structural damage to average houses (e.g. large cracks in walls, falling of gable parts) is even more unlikely, thus also exceptionally unlikely. It has a probability of about 0.001%.

The risk assessment is based on best available methods. Due to unpredictable reactions in the subsoil, such risk assessments carry uncertainty. Therefore, experts can disagree on the exact probabilities and the largest possible earthquake.

6 Main results

Figures II-IV: $\bar{\bar{x}}$: grand mean; significance level *p<0.05; ** p<0.01; ***p<0.001 for difference between conditions
Ratings range from 1= "do not agree at all" to 7= "completely agree". "Don't know" option coded as missing value.

1) Risk communication format
Figure II: Perception of different risk communication formats between conditions

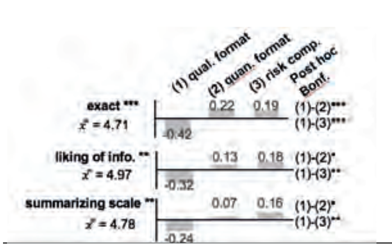

2) Including statement of uncertainty and expert confidence
Figure III: Effect of including a statement of uncertainty and expert confidence between conditions

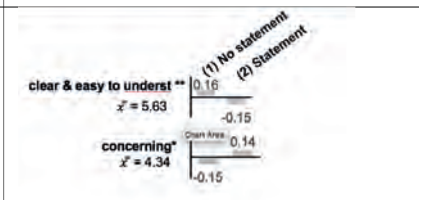

3) Perceived risk

- The format had no effect on respondents' risk perception of IS.
- The risk of IS seemed significantly less controllable when respondents read statement about uncertainty as compared to not reading about it (M 3.47, SD = 1.52 vs. M = 3.72, SD = 1.47), F(1,568)=3.91, p=0.048.
- Respondents perceived the risk of IS significantly higher for shale gas than for DGE (M = 4.81, SD = 1.13 vs. M = 4.19, SD = 1.14), F(1,589) = 43.83, p<0.001.

4) Technology framing
Figure IV: Effect of technology framing between conditions

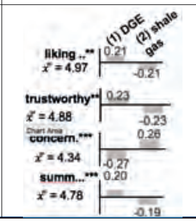

Respondents accepted shale gas projects in their region significantly less than DGE projects (M = 3.47, SD = 1.70 vs. M = 5.02, SD = 1.36), t(481)=11.41, p<0.001.

7 Conclusions

- Respondents perceived the quantitative and risk comparison format more exact and liked it more. They also found it easier to understand (n.s.).
- Respondents perceived risk communication including uncertainty and expert confidence as less clear and more concerning.
- Respondents perceived identical risk communication for shale gas as less trustworthy, more concerning and liked it less than for DGE.
- **Recommendation for practitioners:**

→The public appreciates careful elaboration of risk communication with numbers and suitable risk comparisons.

→The public might have difficulties in understanding information about uncertainty.

→Besides the careful wording of risk communication, the context matters!

References

[1] Knoblauch T., Stauffacher M., Trutnevyte E. (2017). Communicating low-probability high-consequence risk, uncertainty and expert confidence: Induced seismicity of deep geothermal energy and shale gas. Risk Analysis. Under review.
[2] Trutnevyte, E., & Wiemer, S. (2017). Tailor-made risk governance for induced seismicity of geothermal energy projects. *Geothermics*, *65*, 295–312.
[3] Majer, E. L., Nelson, J., Robertson-Tait, A., Savy, J., & Wong, I. (2012). *Protocol for addressing induced seismicity associated with enhanced geothermal systems*. *Geothermal Technologies Program*. U.S. Department of Energy.
[4] Department für Inneres und Volkswirtschaft Kanton Thurgau [Department for internal affairs and political economicy canton Thurgau]. (2009). Geothermie – die nachhaltige Energiequelle [Geothermal energy - the sustainable energy resource]. Retrieved April 4, 2016, from www.energie.tg.ch
[5] KBB Underground Technologies. (2016). Geothermie: Zuverlässige Energie aus den Tiefen unserer Erde [Geothermal energy: Reliable energy from our Earth's depths]. Retrieved April 4, 2016, from http://www.kbbnet.de/fachbereiche/geothermie/
[6] Europäisches Institut für Klima und Energie [European Institute for climate and energy]. (2010). Schiefergas als alternativer Energierohstoff – nur eine goldrauschähnliche Euphorie? [Shale gas as alternative resource - only a gold-rush-like euphoria]. Retrieved April 4, 2016, from http://www.eike-klima-energie.eu/climategate-anzeige/schiefergas-als-alternativer-energierohstoff-nur-eine-goldrauschaehnliche-euphorie/
[7] Bundesanstalt für Geowissenschaften und Rohstoffe [Federal Office for geoscience and resources]. (2016). Schieferöl und Schiefergas in Deutschland [Shale oil and shale gas in Germany].

SCCER SoE
SWISS COMPETENCE CENTER for ENERGY RESEARCH
SUPPLY of ELECTRICITY

SCCER-SoE Annual Conference 2017

FNSNF
SWISS NATIONAL SCIENCE FOUNDATION

Where to site Enhanced Geothermal Systems (EGS)? Trading off heat benefits and induced seismicity risk from the investor's and society's perspective

Theresa Knoblauch, Evelina Trutnevyte
ETH Zurich, Department of Environmental Systems Science (USYS), USYS Transdisciplinarity Lab

Introduction

There is a dilemma when siting EGS projects as siting influences both induced seismicity (IS) risk of EGS projects as well as their profitability [1,2].

On the one hand, when siting EGS in remote areas, building exposure and thus IS risk is reduced [3,4,5].

On the other hand, when siting EGS close to buildings, heat can be purposefully used by supplying it to a dense district heating network (DHN). This reduces costs of EGS projects and avoids CO_2 emissions by heat systems [6,7].

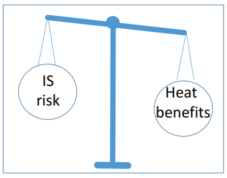

Figure 1 Trading off risk of IS and heat benefits when siting EGS.

Method

We use cost benefit analysis (CBA) to quantify this trade-off of siting EGS of different capacities in remote or in densely populated areas. We analyze 16 hypothetical scenarios that are combinations of different EGS and siting (Table 1).

We model the EGS plant and its heat and electricity production in detail and couple it to a stylized model of IS hazard and risk which is sufficient for CBA given high uncertainties and lack of data for IS [8].We distinguish between CBA from investor's and society's perspective [9]. CBA from investor's perspective includes Net Present Value (private) and Internal Rate of Return (IRR) as well as Levelized Cost of Electricity (LCOE) of the EGS in every scenario. CBA from society's perspective reflects costs and benefits to the society as a whole. In addition to direct costs and revenues, also damage due to IS and CO_2 savings with respect to conventional electricity and heat production are included to quantify NPV (social) and Benefit-to-Cost ratio (B/C ratio).

		Circulation rate [l/S]			
		50	**100**	**150**	**200**
Residents	**0**	S 1	S 2	S 3	S 4
	1'000	S 5	S 6	S 7	S 8
	10'000	S 9	S 10	S 11	S 12
	100'000	S 13	S 14	S 15	S 16

Table 1 EGS scenarios.

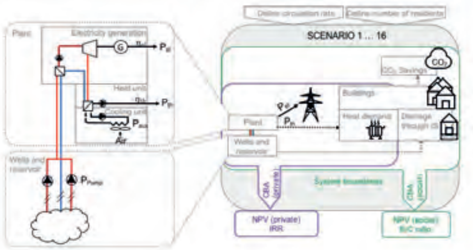

Figure 2 EGS framework for CBA from investors and society's perspectives.

Results of CBA from investor's perspective

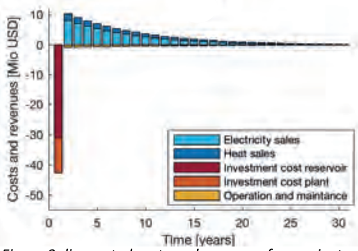

Figure 3 discounted costs and revenues from private perspective illustrated for EGS scenario 11.

Figure 3 shows direct costs and revenues, exemplarily depicted for EGS scenario 11 (150 l/s circulation rate, 10'000 residents). EGS come with high upfront investment costs followed by decreasing revenues from electricity during lifetime as EGS reservoir temperature declines due to thermal drawdown.

According to Figures 4 and 5, EGS are most profitable from investor's perspective when sited surrounded by large number of residents (10'000 or 100'000) and when operated with high circulation rate (150 l/s or 200 l/s).

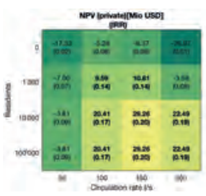

Figure 4 NPV (private) and IRR for EGS scenarios.

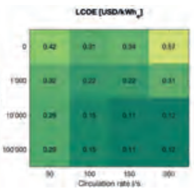

Figure 5 LCOE for EGS scenarios.

Results of CBA from society's perspective

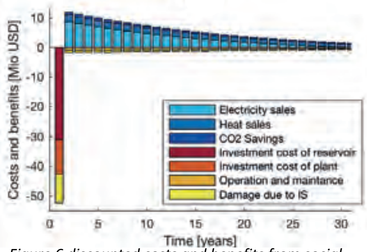

Figure 6 discounted costs and benefits from social perspective illustrated for EGS scenario 11.

Figure 6 presents direct and indirect costs and benefits for the wider society, exemplarily depicted for EGS scenario 11 (150 l/s circulation rate, 10'000 residents). Damage due to IS amounts to significant costs when creating the reservoir, whereas benefits of CO_2 savings are rather negligible.

According to Figures 7 and 8, EGS are most profitable from social perspective when sited surrounded by some residents (1 '000 or 10 '000) and when operated with medium circulation rate (100 l/s or 150 l/s).

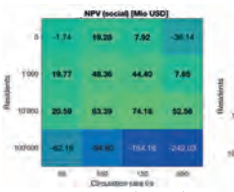

Figure 7 NPV (social) for EGS scenarios.

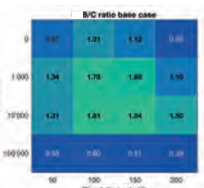

Figure 8 B/C ratio for EGS scenarios (base case).

Conclusions

- Results of CBA from investor's perspective suggest to preferably site EGS in areas where all remaining heat can be sold to a DHN, thus towns or cities with surrounding number of residents equal or larger than 10'000. In contrast, results of CBA from society's perspective suggest to site EGS where a fair amount of remaining heat can be sold but at the same time damage due to IS is limited, thus 1'000 or 10'000 surrounding residents. When considered jointly, CBA from both, investor's and society's perspectives suggests that EGS in remote areas are not as profitable as siting EGS surrounded by at least some residents due to lacking revenues from heat.

- CBA from both investor's and society's perspective suggests to implement an EGS of a certain circulation rate respecting two constraints: one, a minimum constraint of circulation rate ensures that EGS produces sufficient electricity and heat in order to compensate and ideally exceed high upfront investment costs. Two, a maximum constraint of circulation rate should ensure that pump power does not exceed net electricity output of EGS and thus prevents additional electricity supply from grid which would considerably decrease profitability. Plus, according to our model, damage due to IS also increases with circulation rate.

References

[1] T. Kraft, P. M. Mai, S. Wiemer, N. Deichmann, J. Ripperger, P. Kästli, C. Bachmann, D. Fäh, J. Wössner, and D. Giardini, "Enhanced Geothermal Systems: Mitigating Risk in Urban Areas," *Eos, Trans. Am. Geophys. Union*, vol. 90, no. 32, pp. 273–274, 2009.
[2] W. Schenler, "Economy," in *Energy from the Earth: Deep Geothermal as a Resource for the Future? TA Swiss Geothermal Project Final Report.*, S. Hirschberg, S. Wiemer, and P. Burgherr, Eds. Villingen, Switzerland: Paul Scherer Institute, 2015, pp. 155–182.
[3] E. L. Majer, R. Baria, M. Stark, S. Oates, J. Bommer, B. Smith, and H. Asanuma, "Induced seismicity associated with Enhanced Geothermal Systems," *Geothermics*, vol. 36, no. 3, pp. 185–222, 2007.
[4] J. J. Bommer, H. Crowley, and R. Pinho, "A risk-mitigation approach to the management of induced seismicity," *J. Seismol.*, vol. 19, no. 2, pp. 623–646, 2015.
[5] A. McGarr, B. Bekins, N. Burkhardt, J. Dewey, P. Earle, W. Ellsworth, S. Ge, S. Hickman, A. Holland, E. Majer, J. Rubinstein, and A. Sheehan, "Coping with earthquakes induced by fluid injection: Hazard may be reduced by managing injection activities," *Science.*, vol. 347, no. 6224, pp. 830–831, 2015.
[6] Department of Energy & Climate Change (DECC), "Deep geothermal review study. Final report," 2013.
[7] M. Beerepoot, "Technology roadmap - geothermal heat and power," 2011.
[8] E. Trutnevyte and I. L. Azevedo, "Expert agreements and disagreements on induced seismicity by Enhanced Geothermal Systems," *Manuscr. Submitt. Publ.*
[9] K. Blok and E. Nieuwlaar, "Economic analysis of energy technologies," in *Introduction to energy analysis*, Second edi., E. Nieuwlaar, Ed. London, New York : Routledge, Taylor & Francis Group, earthscan from Routledge, 2017, p. xxv, 310 pages

SCCER SoE
SWISS COMPETENCE CENTER for ENERGY RESEARCH
SUPPLY of ELECTRICITY

SCCER-SoE Annual Conference 2017

In cooperation with the CTI
Energy
Swiss Competence Centers for Energy Research
Swiss Confederation
Commission for Technology and Innovation CTI

The price of public safety in EGS projects

A. Mignan, M. Broccardo, S. Wiemer & D. Giardini

Abstract

The risk associated with seismicity caused by fluid injection in the deep underground in EGS projects can be faced using mitigation measures, such as traffic light systems (TLS), which impose a risk threshold criterion in order to ensure public safety. This infers that some wells may fail, which would tend to increase the EGS-generated electricity base price. We first estimate this increase as a function of borehole distance d to the nearest habitation considering a probability of fatality higher than 10^{-6} as unacceptable. Taking into account the underground feedback uncertainty (a- and b-values of the Gutenberg Richter law, maximum magnitude M_{max}), standard risk parameters and a reasonable economic model (base price of 0.20$/kWh), we find that the price increases to 0.23$/kWh above the borehole and rapidly decreases back to the base price at a distance d = 40km. Based on Cumulative Prospect Theory, we find the price to increase to 0.30$/kWh due to the risk aversion of uncertain well loss. The heat credit at short distances would compensate for this "cost of public safety" – *Disclaimer: All values are subject to modelling choices.*

Methods

- Project: triplet, depth z = 5km, stimulation of V = 30,000m^3
- Electricity generation (e.g., *Lacirignola & Blanc*, 2013): T_{prod} = 35z °C, T_{reinj} = 70°C, Q = 50l/s, ORC system (case 5), 8000hr/yr, P_{net} ≈ 2MW, E_{net} ≈ 15 GWh/yr, plant/well life of 20yr
- Costs (*Hirschberg et al.*, 2015): C_{well} = 20 million $, C_{frac} = 1 million $, C_{plant} = 4000$/kW
- Pricing = costs ($) / electricity generation (kWh) = **0.20 $/kWh**
- Induced seismicity risk model (*Mignan et al.*, 2015): RISK-UE method, intensity prediction equation, EMS98 class B building
- Risk mitigation TLS-based model (*Mignan et al.*, in rev.): p = **probability of fatality** curve crossing the **10^{-6} safety threshold**
- Price updating approach: additional cost per failed well = $p(C_{well}+C_{frac})$
- Risk aversion model: standard parameters of Cumulative Prospect Theory CPT (*Tversky & Kahneman*, 1992) with distortion of p, loss aversion amplification & different utility functions for losses/gains

Results

- Underground feedback uncertainty: M_{max} ambiguity turned into subjective probability (Pr(M_{max}=4)=Pr(M_{max}=7)=0.5); Worldwide (a, b) scattering assumed as true distribution & independent of well location

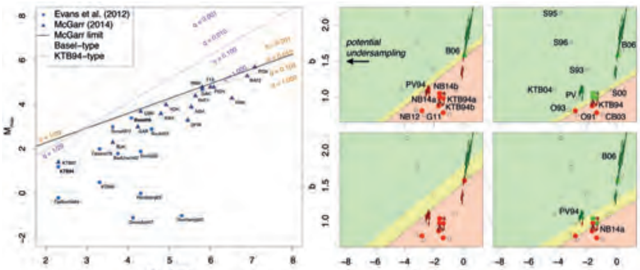

McGarr limit versus tectonic statistical limit (based on databases of Evans et al., 2012; McGarr, 2014)

(a,b) scattering versus TLS pass/fail for different Q and d (modified from Mignan et al., in rev.)

- Fatality curves & probability of TLS failure p:

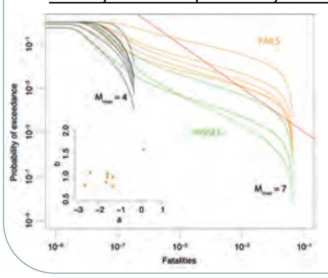

✓ d = 10 km from nearest building

✓ All M_{max} = 4 scenarios pass

✓ 5/8 M_{max} = 7 scenarios fail

✓ Yields p = (0+5)/16 ≈ 0.3

- Probability p & price changes versus distance to nearest habitation:

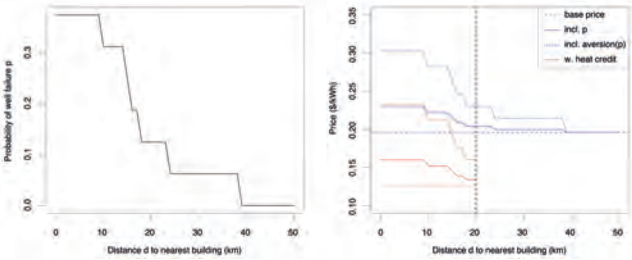

✓ Probability p decreases relatively fast with increasing distance d
✓ For maximum p (at d=0), the price increases from 0.20 to 0.23$/kWh
✓ Including risk aversion via CPT, the price increases to 0.30$/kWh
✓ A heat credit of 0.07$/kWh at short distances tends to compensate the increase, indicative of a trade-off between heat credit & seismic risk

Discussion

Advantages of the approach:
✓ Transparent actuarial approach, via TLS-based mitigation strategy
✓ Translates cost of seismic risk mitigation into electricity price
✓ To the public: Assured that a fixed safety threshold is respected
✓ To the industry: Decision making under uncertainty made possible
✓ To the authorities: Improved decisions based on clear rules. If the cost of failed wells becomes too high for the EGS industry, authorities may decide to decrease the safety threshold. E.g., for 10^{-5} probability of fatality, the original base price is reached at 5km

The additional cost of ambiguity:
✓ max(M_{max}) critical to probability of failure. Could be reduced if the underground was better known
✓ A 0.5 probability for max(M_{max}) is disputable (*Bommer & van Elk*, 2017). Whatever value used, ambiguity must be discussed in terms of a stress test (minimax option where the worst possible scenario is investigated)
✓ Reduction of uncertainties is costly & may not decrease risk
✓ Passing a stress test may be costly due to e.g., building retrofitting

Limitations:
✓ **All values and graphs shown here are subject to the modelling and parameter choices**
✓ Damage of potential earthquakes not considered & assumed insured
✓ (a,b) parameter set assumed independent of location. However if one well fails, e.g. due to high a-value, it is plausible that nearby wells would react in a similar way, meaning an increase of p

References

Bommer & van Elk (2017), about: Workshop on Maximum Magnitudes for Groningen, Bull. Seismol. Soc. Am. 107
Evans et al. (2012), A survey of the induced seismic response to fluid injection in geothermal and CO_2 reservoirs in Europe, Geothermics 41
Lacirignola & Blanc (2013), Environmental analysis of practical design options for EGS through life-cycle assessment, Renewable Energy 50
McGarr (2014), Maximum magnitude earthquakes induced by fluid injection, J. Geophys. Res. 119
Mignan et al. (2015), Induced seismicity risk analysis of the 2006 Basel, Switzerland, EGS project: Influence of uncertainties on risk mitigation, *Geothermics* 53
Mignan et al., Induced seismicity closed-form traffic light system for actuarial decision-making during deep fluid injections, Sci. Rep. (in rev.)
Hirschberg et al. (2015), Energy from the Earth, TA Swiss 62
Tversky & Kahneman (1992), Advances in Prospect Theory: Cumulative Representation of Uncertainty, J. Risk Unc. 5

SCCER-SoE Annual Conference 2017

SCCER SoE
SWISS COMPETENCE CENTER for ENERGY RESEARCH
SUPPLY of ELECTRICITY

In cooperation with the CTI
Energy
Swiss Competence Centers for Energy Research
Swiss Confederation
Commission for Technology and Innovation CTI

Monitoring and imaging medium perturbations using multiply scattered waves

Anne Obermann, Thomas Planès, Céline Hadziioannou, Michel Campillo, Stefan Wiemer

Context of the work

Changes in the seismic waveform between two perfectly reproducible acquisitions can be attributed to variations of elastic properties in the evolving medium. In mainly homogeneous lithologies, strong medium changes might be detected by direct waves, however, their sensitivity to weak changes is low. The **seismic coda**, the product of multiple scattering processes caused by heterogeneities, samples the propagation medium very densely, resulting in a high sensitivity to tiny modifications of the seismic properties in the medium. This sensitivity has been successfully used for monitoring purposes in different areas of seismology, among them the application to the deep geothermal ernergy projects in St. Gallen (Obermann et al. 2015) and Basel (Hillers et al. 2015), where additional information about the reservoir dynamics could be obtained.
Besides the **detection** of medium changes, an important aspectthe seismic is their **location** in space. The diffusive wave propagation in the seismic coda needs to be approximated in a probabilistic way. Based on the radiative transfer theory, we developed 2D and, recently, 3D probablistic sensitivity kernels to image the changes in space. The 3D kernels are successfully applied in numerical simulations to accurately determine the depth of the medium changes.

Detection of medium changes

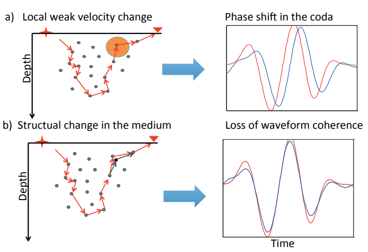

We compare a waveform of the seismic coda prior to a medium change (in blue) to waveforms affected by different kinds of changes (in red).
For this type of study we need perfectly reproducible acquisitions, depending on the scale (frequency), we use ambient noise cross-correlations (passive source) or active sources.

Application to the deep geothermal project in St. Gallen

In 2012, the project in St. Gallen targeted a hydrothermal resource at a depth of 3.5–5 km. Minor injection tests and acid stimulations showed low levels of micro seismicity. A sudden gas leakage into the well came as a surprise. Well rescue operations led to a ML 3.5 earthquake. Was there an aseismic response of the reservoir to the injections that could have alarmed operators?

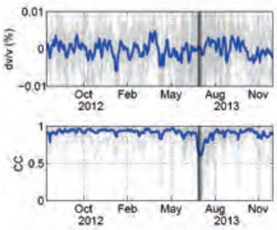

We calculate daily cross-correlations from the ambient seismic noise recordings and search the seismic coda (averaged over all station couples) for time-lapse changes. The vertical lines indicate the injection tests. You notice a clear waveform decoherence (CC), while there is no noticeable velocity change (dv/v).

a)

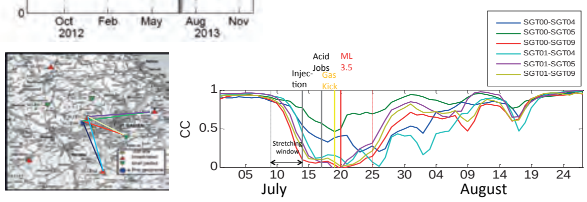

b)

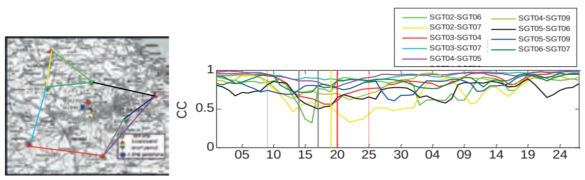

We zoom into the injection period and focus on the individual station pairs. Station pairs close to the injection well (a) noticed a waveform perturbation with the onset of the injections, while others did not (b). We interpret the massive loss of coherence as gas penetrating into the formation as a consequence of the injections and acid jobs.
Continuous monitoring with coda waves can provide additional information on aseismic reservoir processes that cannot be resolved with standard seismic analysis.

Location of the changes (St. Gallen)

(a)

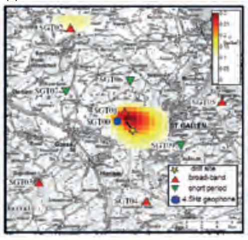

Horizontal location of the medium perturbation with an inversion procedure (a) based on 2D probabilistic approaches (Obermann et al. 2013). The medium perturbation can be confined within a few hundred meters of the injection well.
For the vertical location, we used a **spectral analysis**. The highest amount of coherence loss is found between 0.2-0.4 Hz (b). These frequencies are sensitive to the Malm layer where the injection occurred (c). Due to the nonuniform excitation of the ambient seismic field, a spectral analysis remains very approximative.

(b)

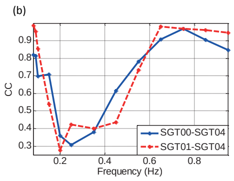

(c)

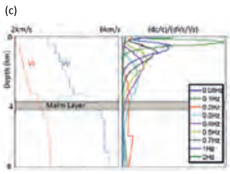

Development of 3D probabilistic kernels and numerical performance testing

We simulate coda waves in a heterogeneous model (a) with and without a cubic velocity perturbation. We developed 3D probabilistic sensitivity kernel (b) as a combination of bulk and surface wave sensitivity and successfully used them to locate the velocity perturbations at depth (c).

(a)

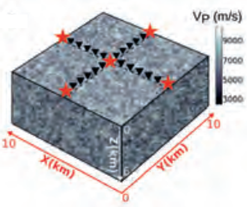

(c)

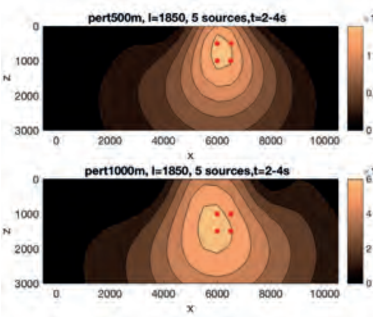

(b)

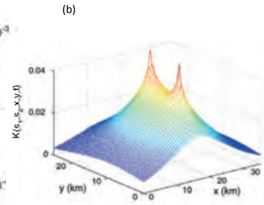

Imaging with such probabilistic 3-D kernels that are critical for depth location, could significantly improve our understanding of the nature of the medium variations revealed by seismic monitoring.

Next steps

Application of the 3D probabilistic kernels to real data sets (Basel, St. Gallen, Grimsel).
Further theoretical developments to accurately describe the elastic case.

References

Obermann et al. (2013) Imaging pre- and co-eruptive structural and mechanical changes on a volcano with ambient seismic noise, JGR, 118.
Obermann et al. (2015) Potential of ambient seismic noise techniques to monitor reservoir dynamics at the St. Gallen geothermal site. JGR, 120 (6).
Obermann et al. (2016) Lapse-time dependent coda wave depth sensitivity to local velocity perturbations in 3-D heterogeneous elastic media, GJI, 207.
Hillers et al. (2015) Noise based monitoring and imaging of aseismic transient deformations induced by the 2006 Basel reservoir stimulations, Geophysics, 80, 4.

SCCER-SoE Annual Conference 2017

SCCER SoE
SWISS COMPETENCE CENTER for ENERGY RESEARCH
SUPPLY of ELECTRICITY

PAUL SCHERRER INSTITUT PSI

In cooperation with the CTI
Energy
Swiss Competence Centers for Energy Research
Commission for Technology and Innovation CTI

A preliminary Spatial Multi-Criteria Decision Analysis for Deep Geothermal Systems in Switzerland

Matteo Spada, Peter Burgherr
Technology Assessment Group, Laboratory for Energy Systems Analysis, Paul Scherrer Institut (PSI)

Introduction

This study presents a preliminary application of a spatial Multi-Criteria Decision Analysis (sMCDA) to Deep Geothermal Energy (DGE) systems in Switzerland. sMCDA is a tool that combines Geographical Information Systems (GIS) capabilities with MCDA frameworks to take into account the spatial dimension, which is important for planning and decision-making purposes, etc. [1].

The scope of this work is to assess the most sustainable area for a hypothetical DGE plant in Switzerland. The focus is on the Molasse basin, Rhine Graben, and Jura mountains regions (i.e., not the Alpine region) where most of the Swiss DGE projects are planned. The proposed approach combines spatial information from both explicit data (e.g., heat flow) and calculated ones (e.g., risk indicators, environmental impact indicators, etc.) for specific *a priori* defined plant characteristics (e.g., capacities, number of drilled wells over lifetime). Results are then presented for different hypothetical preference profiles.

Method

The sMCDA framework consists of different steps. First, the characteristics of the technology to be used in the sustainability assessment has been selected. In this study, since no running DGE plants exist in Switzerland, an hypothetical power plant based on SCCER-SoE Phase 1 activities is considered (Table 1).

Table 1: Key physical parameters of the DGE plant capacity case considered in this study

Model Assumption	Unit	Value
Net Plant Capacity	MWe	1.47
Annual Generation	MWh/year	11849
Life Time	years	20
Number of Wells		2
Well Depth	km	5
Well Life Time	year	20

Next, criteria are established to cover all 3 pillars of sustainability (environment, economy and society). Furthermore, indicators are chosen for each criterion based on availability and potential spatial variability (Table 2).

Table 2: Selected criteria and indicators used in this study.

Criteria	Indicators	Unit
Environment	Climate Change	kg CO2 eq to air
	Human Toxicity	kg 1,4-DCB eq to urban air
	Particulate Matter Formation	kg PM10 eq to air
	Water Depletion	m3 (water)
	Metal Depletion	kg Fe eq
Economy	Average Generation Cost	rp/kWhe
Society	Non-seismic Accident Risk	Fatalities/kWh
	Natural Seismic Risk	Ordinal Scale [1-3]

Indicators are then quantified for the hypothetical plant in Table 1 and for a set of 31 potential areas defined using Heat Flux and Natural Seismic Risk maps (https://map.geo.admin.ch). Environmental and economic indicator values have been estimated based on the temperature gradient (ΔT) in the area of interest, since ΔT is the ratio between the HF and the thermal conductivity of rocks (on average 3 W/m*ºC in Switzerland [2]). On the other hand, the non-seismic accident risk indicator considers blow out risk and release of selected hazardous chemicals, which are related to the number of drilled wells [3]. The natural seismic risk indicator is considered in this study as a proxy of social acceptance, meaning that high risk is associated with lower social acceptance of a DGE system.

Once estimated, indicators are normalized to express them in a unit-less scale so they can be combined. Afterwards, they are weighted, based on individual stakeholder preferences. Finally, the indicators are aggregated using the weighted sum algorithm (WSA), which has been chosen due to its simplicity and transparency, for each area to receive a sustainability index for ranking purposes.

Results

No stakeholder interaction, e.g., through elicitation, has been performed in this study to assess weighting profiles of "real world" stakeholders. Instead, four artificial preference profiles have been defined:

- equal weights at all levels (both criteria and indicators in Table 2), which corresponds to the spirit of sustainability, where all pillars have the same weight.
- three weighting profiles that strongly favor one of the sustainability pillars (weight 80%), whereas the two other are both weighted 10%, and all indicators are equally weighted.

As an example, the results of the profile focusing on the Environment (80%) are shown in Figure 1. The lower the sMCDA score is in the figure, the better the area performs in terms of sustainability. From Figure 1a, the most sustainable areas are the ones in NE Switzerland. Furthermore, Figure 1b shows the contributions of each indicator to the final result. In particular, results for areas with highest values (e.g., 2) are strongly affected by the environment related indicators only, while the ones for areas with lower values (e.g., 17) are more a combination among the different indicators in Table 2.

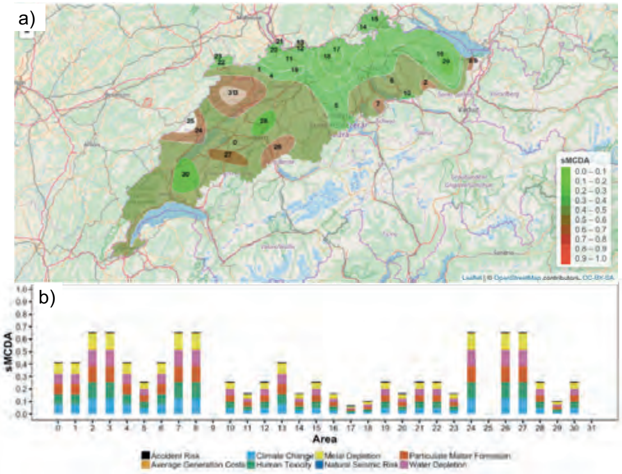

Figure 1: Environment-focused profile. a) Spatial distribution of the sMCDA results for Switzerland. b) Indicator contributions to each area.

Conclusions

- First application of sMCDA to DGE in Switzerland and its suitability as a decision-support tool has been demonstrated.
- Equal weighting generally leads to lower scores than preference profiles favoring a particular sustainability dimension.
- Rankings of profiles focusing on environment and economy are practically the same, but the indicator contributions differ. Generally, areas in NE Switzerland perform best.
- When focusing on social indicators, only few area have low sustainability scores, i.e. all areas along the basin are competitive, except for few in the North.

References

[1] Ferretti, V. & Montibeller, G. 2016. Key challenges and meta-choices in designing and applying multi-criteria spatial decision support systems. *Decision Support Systems,* 84**,** 41-52. doi: http://dx.doi.org/10.1016/j.dss.2016.01.005

[2] Bodmer Philippe H., (1982): Beiträge zur Geothermie der Schweiz. Diss. Naturwiss. ETH Zürich, Nr. 7034, 210 p.

[3] Spada, M., Burgherr, P. (2015). Chapter 6.1: Accident Risk. In Hirschberg S., Wiemer S. and Burgherr P.: Energy from the Earth. Deep Geothermal as a Resource for the Future? TA-SWISS Study TA/CD 62/2015, vdf Hochschulverlag AG, Zurich, Switzerland, pp. 229-262. http://dx.doi.org/10.3218/3655-8.

SCCER SoE
SWISS COMPETENCE CENTER for ENERGY RESEARCH
SUPPLY of ELECTRICITY

SCCER-SoE Annual Conference 2017

FNSNF
SWISS NATIONAL SCIENCE FOUNDATION

Building informed and realistic public preferences for Swiss electricity portfolios

Sandra Volken, Georgios Xexakis, Evelina Trutnevyte,
ETH Zurich, Department of Environmental Systems Science (USYS), USYS Transdisciplinarity Lab

Background

- Public debates about electricity generation as well as scientific studies usually focus on individual technologies[1,2,3,4].
- The public thus might neglect that electricity needs to be generated by a portfolio of technologies and that each technology comes with diverse risks and operational impacts to public health, safety, natural and built environment[5,6].
- We thus also know little about electricity portfolio preferences, even though we assume that also non-experts think of electricity generation as an interconnected system[7].
- Previous research shows that both group deliberation and targeted information can help formation of informed preferences [8,2,3]. We thus study such realistic electricity portfolio preferences for the first time for a sample of informed Swiss laypeople.

Research questions:

1. What are the public preferences for Swiss electricity generation, given balanced information on technology risks and operational impacts?
2. How do these informed preferences differ if the technologies are considered individually or if they need to be combined into realistic portfolios for Switzerland?
3. What is the short and longer-term effectiveness of different formats of information and deliberation on
   a) technology preferences and characteristics,
   b) revealed and self-rated knowledge, and
   c) willingness-to-act and interest in the energy topic, in the?
4. What is the usability and usefulness of information materials and how satisfied are participants with factsheets, Riskmeter, and workshops?

Methods and Materials

1. Invitation of 55 diverse laypeople to online survey #1 (Fig. 1) based on registration survey (demographics and technology preferences)
2. Homework: reading of factsheets (Fig. 2+3), containing tailor-made and comparable information about 13 technologies and 9 impact categories.
3. Participation of informed laypeople (N=46) in one of four workshops: discussing in small groups, submitting a portfolio created with the interactive web-tool Riskmeter (see Fig.4), and completing several paper-and-pencil surveys (#2-#5) (Fig 1).
4. Follow-up online survey (#6) after four weeks (Fig. 1).

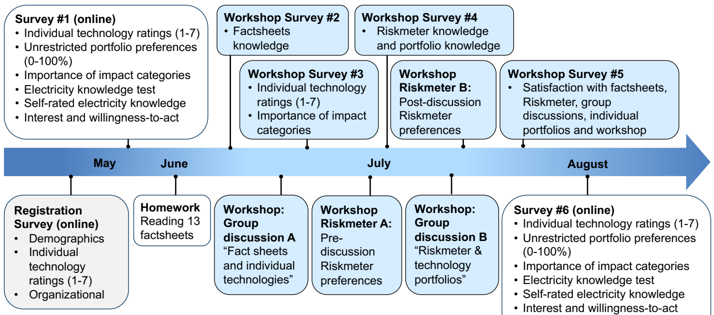

Fig. 1. Procedure: registration survey (grey), initial survey (#1), homework (white); workshop (blue); and follow-up survey (#6) after four weeks (white).

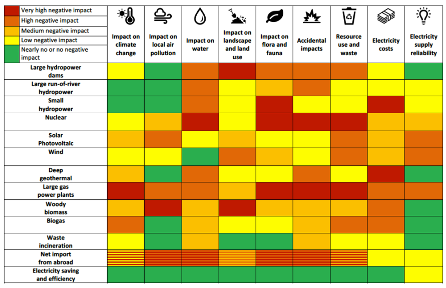

Fig. 2. Factsheet overview table: indicating severity of negative impacts of technologies, including net import and the electricity savings (rows), on different impact categories (columns). From dark red (= very high negative impact) to green (= no or negligible negative impact).

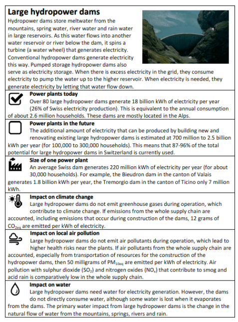

Fig. 3. Factsheet example: Large Hydro Dams (page 1/2).

Results

- We found highest support for low-carbon technologies: solar cells, electricity savings, waste incineration and all types of hydro power.
- Portfolio preferences (Fig. 4) complete individual technology ratings (see Fig. 5) in understanding public preferences.
- The impact of information on preferences (Fig. 5) depends on the type of measurement and technology. However, the longer-term influence remains unclear.
- We found a positive effect of information and workshops on electricity knowledge and self-rated knowledge.
- Participants were satisfied with and understood factsheets (Fig. 2+3) and Riskmeter (Fig. 4).
- Most important impact categories (Fig. 2) were climate change, local air pollution, and electricity supply reliability.

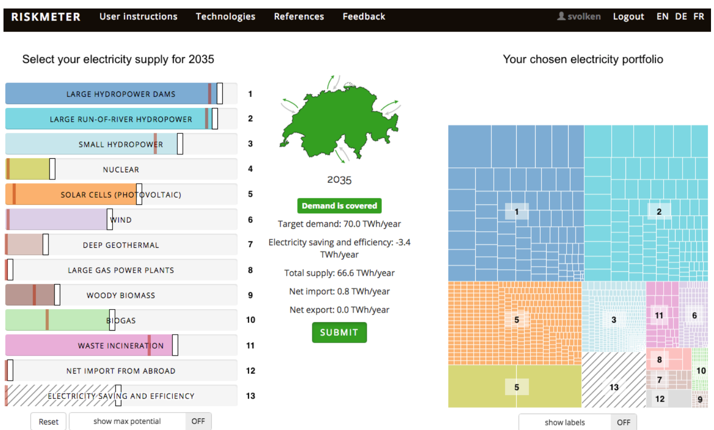

Fig. 4. Adaptation from the interactive-online tool RISKMETER (www.riskmeter.ethz.ch), showing the average portfolio selected by participants. Mean TWh/year and SD in decreasing order: Large hydro dams (20.3±1.1), large run-of-river hydropower (18.7± 1.0), solar cells (11.3±5.7), nuclear (5.0±8.0), small hydropower (4.5±0.9), electricity savings (3.7±2.5), waste incineration (2.7±0.5), wind (2.0±1.1), large natural gas (1.0±2.5), net import (0.9±3.4), deep geothermal (0.8±1.3), biogas (0.7±0.4), woody biomass (0.3±0.3). On the left: available potential and TWh/year selected for each technology, the red line indicates the initial position. Right: Portfolio in TWh/year out of selected technologies.

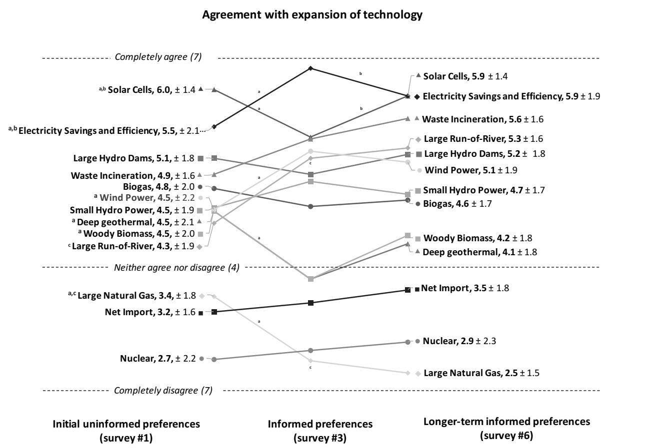

Fig. 5. Preferences for electricity generation technologies (7-point Likert scale ranging from 1= completely disagree to 7= completely agree with expansion of power plants until 2035). Significant (p <0.05) difference between: ᵃ initial preferences (left) and informed preferences (middle); ᵇ informed preferences (middle) and longer-term preferences (right); ᶜ initial (left) and longer-term (right) preferences.

References

[1] Demski C, Butler C, Parkhill KA, Spence A, Pidgeon NF. Public values for energy system change. Global Environmental Change. 2015;34:59-69.
[2] Fleishman LA, De Bruin WB, Morgan MG. Informed public preferences for electricity portfolios with CCS and other low-carbon technologies. Risk Anal. 2010;30(9):1399-410.
[3] Trutnevyte E, Stauffacher M, Scholz RW. Supporting energy initiatives in small communities by linking visions with energy scenarios and multi-criteria assessment. Energy Policy. 2011;39(12):7884-95.
[4] Pidgeon N, Demski C, Butler C, Parkhill K, Spence A. Creating a national citizen engagement process for energy policy. Proc Natl Acad Sci U S A. 2014;111 Suppl 4:13606-13.
[5] Sovacool BK, Andersen R, Sorensen S, Sorensen K, Tienda V, Vainorius A, et al. Balancing safety with sustainability: assessing the risk of accidents for modern lowcarbon energy systems. Journal of Cleaner Production. 2016;112:3952-65.
[6] Hirschberg S, Bauer C, Burgherr P, Cazzoli E, Heck T, Spada M, et al. Health effects of technologies for power generation: Contributions from normal operation, severe accidents and terrorist threat. Reliability Engineering & System Safety. 2016;145:373-87.
[7] Volken S., Wong-Parodi G., Trutnevyte E. 2017. Public awareness and perception of environmental, health and safety risks related to electricity generation: An explorative interview study in Switzerland. Under review.
[8] Mayer LA, Bruine de Bruin W, Morgan MG. Informed public choices for low-carbon electricity portfolios using a computer decision tool. Environ Sci Technol. 2014;48(7):3640-8.

SCCER SoE
SWISS COMPETENCE CENTER for ENERGY RESEARCH
SUPPLY of ELECTRICITY

SCCER-SoE Annual Conference 2017

FNSNF
SWISS NATIONAL SCIENCE FOUNDATION

Are Interactive Web-Tools for the Public Worth the Effort?
An Experimental Study on Public Preferences for the Swiss Electricity System Transition

Georgios Xexakis, Evelina Trutnevyte

ETH Zürich, Department of Environmental Systems Science (USYS), USYS Transdisciplinarity Lab

Introduction

Interactive web-tools is a recent trend in scientific communication (Spiegelhalter et al. 2011; Trutnevyte & Fuss 2017). They are often regarded as powerful methods to create engaging and personalized stories out of complex data, beyond the framing of static information (Grainger et al. 2016). In many fields, including environmental, climate and energy sciences, they are used as a solution for effective communication (McInerny et al. 2014; Parsons & Sedig 2011) and decision aids for the wider public (Aye et al. 2015; Bessette et al. 2014; Gong et al. 2017; Trutnevyte & Fuss 2017).

Nevertheless, including interactivity is much more resource consuming than traditional methods and, in some cases, may even undermine or complicate the communication further (Zikmund-Fisher 2012; Wong-Parodi et al. 2014). Although studies exist on how to design and assess interactive web-tools (Wong-Parodi et al. 2014), there is little empirical evidence whether they are more effective in communicating the messages, in comparison with more traditional methods (Zikmund-Fisher et al. 2011).

We study this effect in performance in the case of the Swiss electricity supply system transition to 2035 and specifically the elicitation of preferences from non-experts, given the information on health, safety, built and natural environment risks. This case study is considered appropriate as it involves a multidimensional and complex problem, i.e. a large number of possible transition strategies (Berntsen & Trutnevyte 2017) along with their aforementioned risks, that also generates interest and concern to the Swiss society, as shown by the recent votes for the Nuclear Phase-out and the Energy Strategy 2050.

Research questions

1. How do interactive and static formats of information perform in terms of making this information understandable, trustworthy and interesting for non-experts?
2. Is there a difference between a subjective and objective measurement of this performance?
3. Does the format affects the active mastery of the information?
4. In the case of informing non-experts for the health, safety, built and natural environment risks of the Swiss electricity supply system transition, does the format type affects the willingness to act on energy issues, the general interest in energy issues and the technology preference?

Methods and materials

We will conduct an experimental online survey with two groups (N=400 in total), where each group receives the same information on electricity supply technologies and strategies (Table 1), portfolios of these technologies and strategies, and associated impacts and risks (Table 2). The two groups will differ in the format of information: a static format (Figure 1), using text descriptions and static visualizations of four maximally different portfolios, and an equivalent interactive format (Figure 2), using a web-based RISKMETER tool we have developed (accessible at https://riskmeter.ethz.ch). Both groups will be asked to answer the same questions in the survey, including the questions on dependent variables (Table 3) as well as questions on demographic data, digital literacy, previous energy interest and understanding, to be used for experimental check.

Figure 1. Static format – four maximally different portfolios

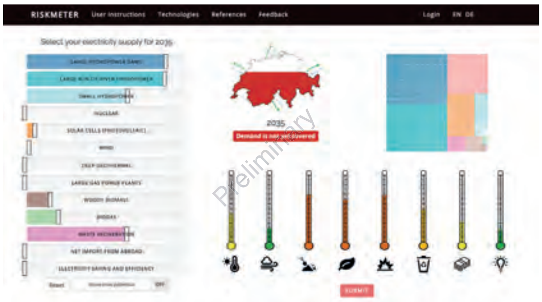

Figure 2. Interactive format – RISKMETER
(accessible at https://riskmeter.ethz.ch)

• Large hydropower dams	• Large gas power plants
• Large run-of-river hydropower	• Woody biomass
• Small hydropower	• Biogas
• Nuclear	• Waste incineration
• Solar cells (photovoltaic)	• Net import from abroad
• Wind	• Electricity saving and efficiency
• Deep geothermal	

Table 1. Electricity supply technologies and strategies

Criteria	Measurement
Impact on climate change	g $CO_{2\text{-}eq}$/kWh
Impact on local air pollution	mg PM_{10eq}/kWh, mg SO_2/kWh, mg NO_x/kWh
Impact on water	water withdrawal in m^3/kWh, water discharge temperature in ºC, water discharge effluents
Impact on landscape and land use	m^2/kWh
Impact on flora and fauna	PDF*m^2*a/kWh (ecosystem quality)
Accidental impacts	fatalities/kWh, fatalities/accident
Resource use and waste	mg solid waste/kWh, renewable and non-renewable primary energy equivalent in MJ-eq/kWh_{el}
Electricity costs	Rp/kWh
Electricity supply reliability	resource supply (0-10), flexibility (0-10)

Table 2. Criteria for health, safety, built and natural environment risks

Dependent variables	Measurement	
	Subjective	Objective
Understandability	Direct question(s)	True or false question(s) relying on given information
Interest	Direct question(s)	Time spent, completion rate
Trust	Direct question(s)	*Under discussion*
Active mastery	*Under discussion*	True of false question(s) requiring inferences on given information
Willingness to act on energy issues	Direct question(s)	*Under discussion*
Interest in energy issues	Direct question(s)	*Under discussion*
Technology preference	Direct question(s)	*Under discussion*

Table 3. Dependent variable measurement in the survey

Expected results

- We hypothesize that the non-expert users will be more interested and engaged with the interactive than with the static format.
- We are not expecting statistically significant differences of trust between the two formats but we cannot exclude the possibility that participants might perceive interactive tools more as games and less as tools, disregarding thus the significance of the information.
- We are expecting a difference between the subjective and the objective measurement of performance, especially in the understanding of the interactive format: participants might be overwhelmed by the higher information availability and the exploration freedom of this format, leading possibly to a lower objective measurement of understanding.

References

Aye, Z. et al., 2015. Prototype of a Web-based Participative Decision Support Platform in Natural Hazards and Risk Management. *ISPRS International Journal of Geo-Information*, 4(3), pp.1201–1224.
Berntsen, P.B. & Trutnevyte, E., 2017. Ensuring diversity of national energy scenarios: Bottom-up energy system model with Modeling to Generate Alternatives. *Energy*, 126, pp.886–898.
Bessette, D.L., Arvai, J. & Campbell-Arvai, V., 2014. Decision support framework for developing regional energy strategies. *Environmental Science & Technology*, 48(3), pp.1401–1408.
Gong, M. et al., 2017. Testing the scenario hypothesis: An experimental comparison of scenarios and forecasts for decision support in a complex decision environment. *Environmental Modelling and Software*, 91, pp.135–155.
Grainger, S., Mao, F. & Buytaert, W., 2016. Environmental data visualisation for non-scientific contexts: Literature review and design framework. *Environmental Modelling and Software*, 85, pp.299–318.
McInerny, G.J. et al., 2014. Information visualisation for science and policy: engaging users and avoiding bias. *Trends in Ecology & Evolution*, 29(3), pp.148–157.
Parsons, P. & Sedig, K., 2011. Human-information interaction: An emerging focus for educational cognitive tools. *Education in a technological world: communicating current and emerging research and technological efforts*, pp.245–251.
Spiegelhalter, D., Pearson, M. & Short, I., 2011. Visualizing Uncertainty About the Future. *Science*, 333(6048), pp.1393–1400.
Trutnevyte E., Fuss, G. 2017. Review of web-based interactive tools and decision aids for long-term energy transition, under preparation.
Wong-Parodi, G., Fischhoff, B. & Strauss, B., 2014. A method to evaluate the usability of interactive climate change impact decision aids. *Climatic Change*, 126(3–4), pp.485–493.
Zikmund-Fisher, B.J., 2012. The Right Tool Is What They Need, Not What We Have: A Taxonomy of Appropriate Levels of Precision in Patient Risk Communication. *Medical Care Research and Review*, 70, pp.1–23.
Zikmund-Fisher, B.J., Dickson, M. & Witteman, H.O., 2011. Cool but counterproductive: Interactive, web-based risk communications can backfire. *Journal of Medical Internet Research*, 13(3), pp.1–11.

Task 4.2

Title

Global observatory of electricity resources

Projects (presented on the following pages)

Transformation of the Energy-related Severe Accident Database (ENSAD) into an interactive, web-based GIS application
Poster see task 4.1
P. Burgherr, W. Kim, M. Spada, A. Kalinina, S. Hirschberg

Bi-level electricity market model (BEM)
M. Densing, E. Panos

Optimization of photovoltaic potential and its integration in Switzerland using genetic algorithm and optimal power flow
J. Dujardin, A. Kahl, B. Kruyt, M. Lehning

World Energy Scenarios 2016
T. Kober, E. Panos

A preliminary Spatial Multi-Criteria Decision Analysis for Deep Geothermal Systems in Switzerland
Poster see task 4.1
M. Spada, P. Burgherr

Marginal electricity supply mixes and their integration in version 3.4 of the ecoinvent database: results and sensitivity to key parameters
L. Vandepaer, K. Treyer, C. Mutel, C. Bauer, B. Amor

SCCER-SoE Annual Conference 2017

SCCER SoE
SWISS COMPETENCE CENTER for ENERGY RESEARCH
SUPPLY of ELECTRICITY

PAUL SCHERRER INSTITUT
PSI

In cooperation with the CTI
Energy
Swiss Competence Centers for Energy Research
Commission for Technology and Innovation CTI

Bi-level electricity market model (BEM)

Martin Densing (martin.densing@psi.ch), *Evangelos Panos*
Energy Economics Group, Laboratory for Energy Systems Analysis, PSI

Motivation

- Goal: Decision-support for policy makers (ES2050 and beyond): Improved understanding of investment, production and trading decisions of producers on the European electricity market, especially for Switzerland
- Focus: Electricity producer-side (not consumer-side)
- Oligopolistic market modelling is required, because producers (in corpore, or single utilities) influence prices: E.g.
  - Producers withhold production, or limit investment to drive prices up deliberately, or are forced by technical or regulator's outages
  - Market power may be exerted only in some sub-markets having scarcity effects (e.g. during peak-hours)
- **Research questions:**
  - How can we capture the **volatility of the electricity price** with a numerical model that is also suitable for academic purposes (without infeasible parametrization efforts, e.g. modelling each plant separately and each day's idiosyncratic market/demand situation)
  - Can we understand **profit-oriented investment** behaviour?
- Partners (Projects also with **BFE-SFOE** and with **VSE**):
  - Chair of Quantitative Business Administration, UZH
  - Energy Economics, Uni Basel (Data harmonization)

Method

- Multi-leader-follower game: Investment and subsequent production decision of several power producers
- Complements PSI's energy-system cost-optimization models
- Producers can influence prices by withholding investment or production capacity in certain load periods

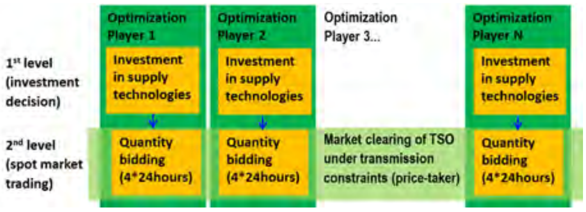

- Bi-level Nash-Cournot Game for electricity market
- General framework model with several operation sub-modes: (i) Investment-decision and production-decision on same level (ii) Single scenario (deterministic) (iii) Social welfare maximization (price-taker, marginal cost perspective)
- Transmission constraints between players: DC (linear) flow model
- Wholesale consumers represented via demand-price elasticity on spot market. Additional in-elastic perfect-competition market (OTC)
- Hourly trading over a day in four seasons of a future representative year: (24*4 = 96 trading hours = load periods)
- **Base configuration**: **Players are countries, i.e. each player has country specific generation portfolio**
- Input: CAPEX & OPEX per technology, seasonal availability, merit-order curves (=cumulative variable costs) per country, etc.

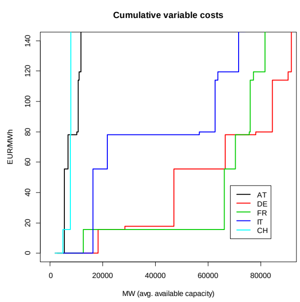

Results (Preliminary)

- Models with competitive market representation can explain price volatility better than (aggregated) social welfare maximization models:

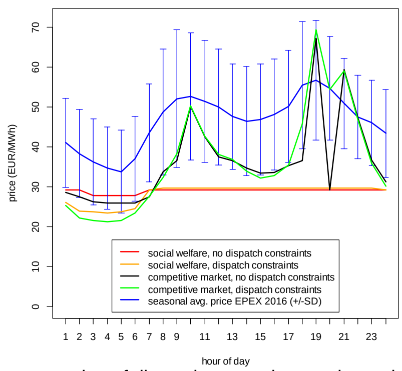

(single-level run)

- Representation of dispatch constraints on thermal generation is needed. Without such constraints, flexibility is overestimated, e.g. combined-cycle plants start freely without paying for start-up costs:

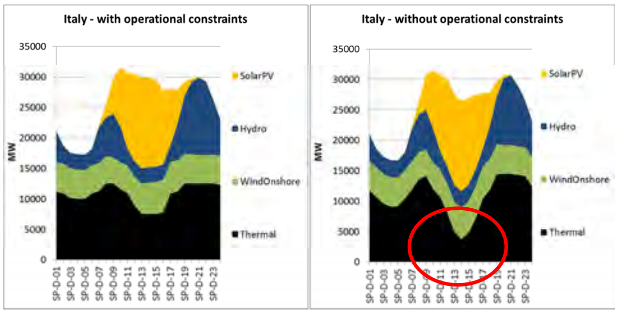

(Results from social welfare maximization, single-level run)

- Test of Bi-level game: What if the supply portfolio of the countries would acquire -in sequence- full Nash-Cournot market power:

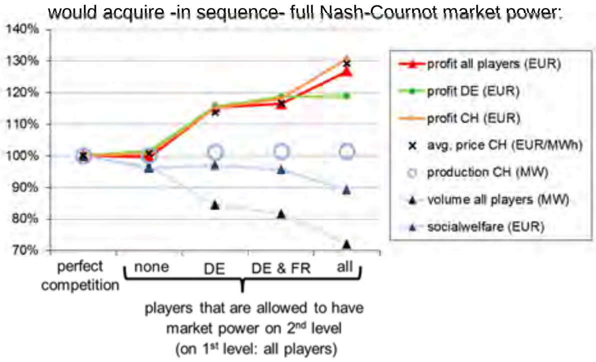

Outlook

- Status of project: Model operational, first results are obtained
- Stochasticity, geographical expansion (EU), several investment steps

References

- Densing, M., Panos. E., Schmedders K. (2017). Stochastic bi-level electricity market modeling, *2nd Workshop of SET-Nav WP10 Modelling Forum*, ETHZ
- Densing, M., Panos, E., Schmedders, K. (2015). Decision making in electricity markets: Bi-level games and stochastic programming, ESC *Workshop*, ETHZ
  https://www.psi.ch/eem/ConferencesTabelle/BilevelAndSP_MartinDensing_TALK.pdf
- Densing, M., Panos, E., Schmedders, K. (2015). Bilevel oligopolistic electricity market models: The case of Switzerland and surrounding countries, *OR2015,* Vienna

SCCER SoE
SWISS COMPETENCE CENTER for ENERGY RESEARCH
SUPPLY of ELECTRICITY

SCCER-SoE Annual Conference 2017

In cooperation with the CTI

Energy
Swiss Competence Centers for Energy Research

Commission for Technology and Innovation CTI

Optimization of photovoltaic potential and its integration in Switzerland using genetic algorithm and optimal power flow

Jérôme Dujardin [1], Annelen Kahl [1], Bert Kruyt [1,2], Michael Lehning [1,2]

[1] EPFL, Lausanne, Switzerland
[2] WSL, SLF, Davos, Switzerland

How to harvest solar energy effectively?

Given the natural resources? Given the transmission grid?

Fig.1. Annual solar irradiance and other electricity generation sources

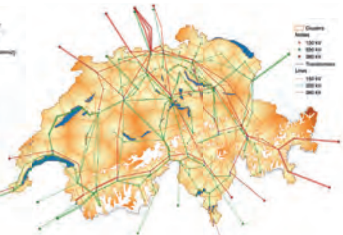

Fig.2. Transmission grid (as planned for 2025)

Hybrid deterministic / stochastic approach

1. Local photovoltaic (PV) configuration for **maximum yield**:
Differs from the classical setup (south at 39° tilt)

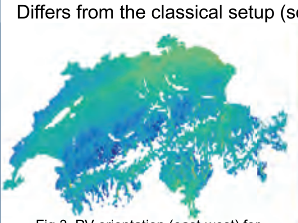

Fig.3. PV orientation (east-west) for maximum yield in each location

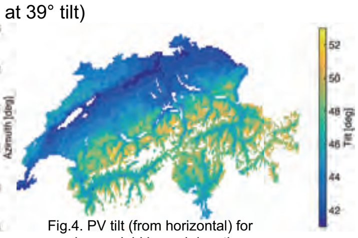

Fig.4. PV tilt (from horizontal) for maximum yield in each location

→ **Local settings** of PV panels are set, independently of the global configuration (locations within the country)

2. Local specificities of PV production:
- Annual yield
- Reduction of annual required import, due to higher winter production [1]
- Stability of annual production
- Stability of winter production

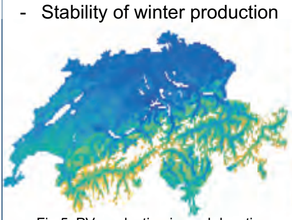

Fig.5. PV production in each location relative to the national average

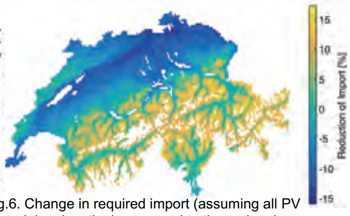

Fig.6. Change in required import (assuming all PV placed in a location) compared to the national average

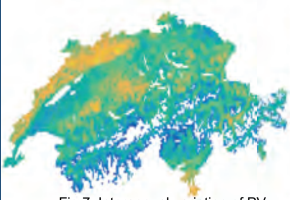

Fig.7. Interannual variation of PV production in each location

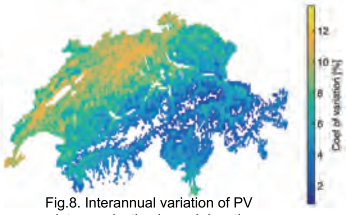

Fig.8. Interannual variation of PV winter production in each location

→ Multi-**objective function** for the genetic algorithm
→ Selection of the best locations within the clusters

3. Maximum PV coverage in each pixel based on CORINE land surface cover type.

Land type	Urban	Industry	Pasture	Agriculture	Open
Max coverage	10%	10%	5%	5%	5%

Constrained to altitudes below 2500m

→ Amounts to 670 km2 (~10 times the required PV area)
→ Leaves freedom to the genetic algorithm

→ **Constraints** on the solutions found by the genetic algorithm (upper limit of PV installed in each cluster)
→ Selection of the available locations within the clusters

4. Genetic algorithm

Initialization with a pool of homogenously spread PV + noise

Generation of a new solution from 2 random parents (random linear combination + random mutation)

Enough space in each cluster?

No / Yes

Test the solution with power flow model

Failure / Success

Solution added to the pool

Not enough solutions / Enough solutions

Reduction of the pool (best only)

Still improving / No more improvement

Best solution

Results

Fig.9. Optimal PV location

Optimization converges to a PV placement scenario that:

- **Increases the yield** (+18%) *
- **Reduces the interannual variations** (-37% yearly, -64% in winter) *

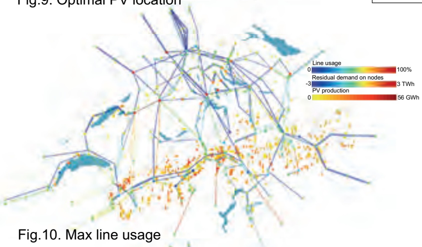

Fig.10. Max line usage

- **Never exceeds** the line capacity

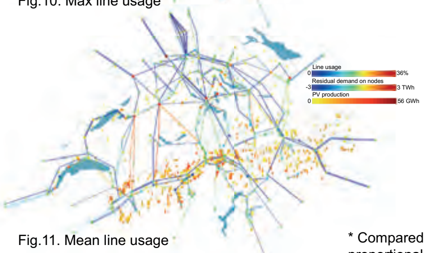

Fig.11. Mean line usage

- **Reduces the required import** (-17%) *

* Compared to a PV placement scenario proportional to population density

Perspectives

- Improvements on the definition of potential PV area by using more GIS products (access from road, complexity of the terrain).
- Increase resolution of topographic shading for better irradiance computation in **complex terrain**.
- Apply optimization strategies to **wind energy** as well.

References

[1] National energy balance model from:
J Dujardin et al. Interplay between photovoltaic, wind energy and storage hydropower in a fully renewable Switzerland. Energy, vol135, p513-525, 2017

Data

- PV production time series based on satellite-derived irradiance (MeteoSwiss)
- Wind production time series based on wind speed measurements (MeteoSwiss)
- Demand time series from Swissgrid (publicly available on their website)
- Run-of-the-river montlhy production and reservoirs' inflow from the Swiss Federal Office of Energy (SFOE) and PREVAH model (WSL)
- Storage / pumped hydropower characteristics from WASTA database (SFOE)

Acknowledgments

Stuart Bartlett, Pedro Manso, Massimiliano Zappa, Fabrizio Sossan

SCCER SoE
SWISS COMPETENCE CENTER for ENERGY RESEARCH
SUPPLY of ELECTRICITY

SCCER-SoE Annual Conference 2017

In cooperation with the CTI
Energy
Swiss Competence Centers for Energy Research
Swiss Confederation
Commission for Technology and Innovation CTI

World Energy Scenarios 2016

Tom Kober, Evangelos Panos

Energy Economics Group, Paul Scherrer Institute

Objectives of the study

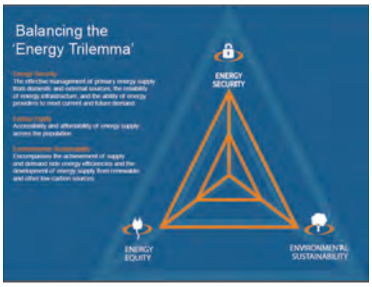

In partnership with the World Energy Council and Accenture, the Energy Economics Group in LEA PSI, quantified and analysed three scenarios (named **Modern Jazz, Unfinished Symphony** and **Hard Rock)** exploring alternative development pathways for the global energy system out to 2060.

The **Modern Jazz scenario** describes a market driven world oriented towards economic and affordable access to energy. The **Unfinished Symphony scenario** characterizes a more government driven world with coordinated international action to mitigate climate change. The **Hard Rock scenario** represents a rather fragmented world with low global cooperation and with priority on local energy security and exploitation of local energy resources.

The GMM global energy systems model

The scenario analysis was carried out by PSI using a **global MARKAL model**. This optimisation tool represents around 400 different energy technologies (e.g. power plants, heating devices, vehicles, etc.) and determines the least-cost configuration of the global **energy system for 15 world regions**, under specific boundary conditions.

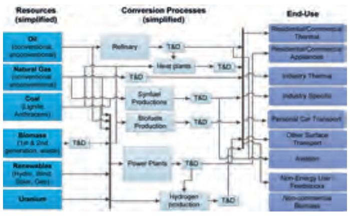

Selected results for the key elements of the **Energy Trilemma** are presented below.

Results

Dampened world primary energy growth and a peaking in per capita energy before 2030 due to unprecedented efficiencies created by new technologies and tightening policies

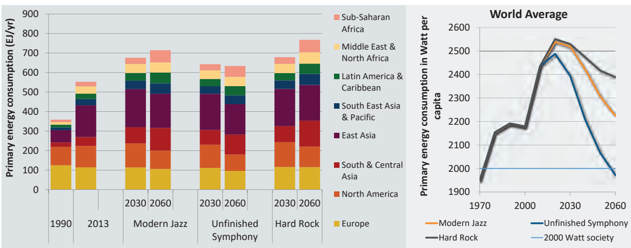

Demand for electricity to double to 2060, meeting this demand with cleaner energy sources requires substantial infrastructure investments and system integration to deliver benefits to all consumers

Global electricity generation

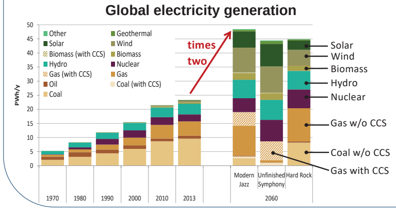

Global cumulative power generation investments (2011-2060) billion USD2010, undiscounted

	Modern Jazz	Unfinished Symphony	Hard Rock
Coal	2500	1600	4200
Oil	300	300	400
Gas	9800	8100	7600
Nuclear	2300	3500	3200
Hydropower	2800	3400	2700
Biomass	2500	3300	2300
Wind	12200	12900	8800
Solar	7700	10200	6600
Others	900	1300	60
Total	**41000**	**44600**	**36400**

Results (cont.)

Wind and solar continue to grow at an unprecedented rate and create new opportunities and challenges for energy systems

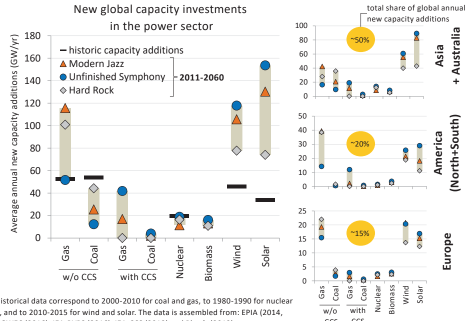

N.B.: Historical data correspond to 2000-2010 for coal and gas, to 1980-1990 for nuclear energy, and to 2010-2015 for wind and solar. The data is assembled from: EPIA (2014, 2016), GWEC (2016), IEA-PVPS (2016), IEA-CCS (2012) and Platt's (2013).

Transitioning global transport forms one of the hardest obstacles to overcome in order to decarbonise future energy systems

Global car fleet in 2060

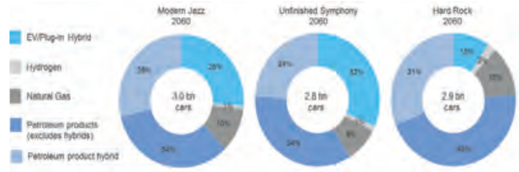

2ºC climate target will require an exceptional and enduring effort, far beyond already pledged commitments, and with high carbon prices

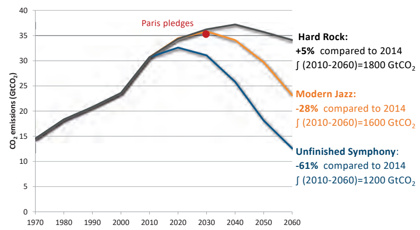

Performance of scenarios in view of the Energy Trilemma

Global cooperation, sustainable economic growth, and technology innovation are needed to balance the Energy Trilemma

	Modern Jazz	Unfinished Symphony	Hard Rock
Energy Security	• Higher energy production • Greater trading and diversity of international fossil energy suppliers	• Wider diversity of energy resource types • Government-promoted investment in infrastructure	• More domestic production • Lower capacity for funding infrastructure • Lower trade
Energy Equity	• Energy Access for all by 2060	• 0–0.5 bn people still lack access to energy	• 0.5–1 bn people still lack access to energy
Environmental Sustainability	• Surpass Carbon budget in early 2040s • Emissions fall 28% below 2014 volumes in 2060	• Surpass carbon budget in before 2060 • Emissions fall 61% below 2014 volumes in 2060	• Surpass carbon budget in early 2040s • Emissions are 5% above 2014 volumes in 2060

The challenge is to maintain the current integrity of energy systems worldwide while steering towards a new transformed future. This requires new policies and strategies, and consideration of novel and risky investments. The decisions taken in the next 10 years will have profound effects on the development of the energy sector. To this end, the WEC/PSI scenarios provide support to the robust development of medium to long-term strategies, government policies, investment and disinvestment decisions.

References

World Energy Scenarios 2016 – The Grand Transition

https://www.worldenergy.org/publications/2016/world-energy-scenarios-2016-the-grand-transition/

SCCER-SoE Annual Conference 2017

SCCER SoE
SWISS COMPETENCE CENTER for ENERGY RESEARCH
SUPPLY of ELECTRICITY

PAUL SCHERRER INSTITUT PSI

In cooperation with the CTI
Energy
Swiss Competence Centers for Energy Research
Swiss Confederation
Commission for Technology and Innovation CTI

Marginal electricity supply mixes and their integration in version 3.4 of the ecoinvent database : results and sensitivity to key parameters

Laurent Vandepaer[1,2], Karin Treyer[2], Chris Mutel[2], Christian Bauer[2] and Ben Amor[1]
[1]Université de Sherbrooke, Civil Engineering Department, Sherbrooke, Quebec, Canada, [2]Laboratory for Energy Systems Analysis, Paul Scherrer Institute, CH-5232 Villigen PSI, Switzerland

Introduction & objectives

- Marginal electricity supply mixes provided in previous versions of the ecoinvent database were based on historical data and limited by database features. This did not allow to capture accurately the consequences of additional demand for electricity given the complex nature of power markets.
- Objectives:
  - Provide long-term and consistent marginal electricity supply mixes based on energy scenarios to take into account future market trends and constraints.
  - Perform several sensitivity analyses to understand the influence of the key parameters and methodological choices on the mix composition and their corresponding environmental impacts.

Methodology

- The calculation method used to determine the marginal electricity supply mixes originates from (Schmidt et al. 2011; Muñoz 2015) :

$$Share_{i,TH} = 100 \cdot \frac{P_{i,TH} - P_{i,ref}}{\sum_i^n (P_{i,TH} - P_{i,ref})}$$

Where:
i: electricity producing technology
TH: the year chosen as time horizon
ref: the year chosen as a reference for the time of the decision
P: the quantity of electricity generated at time "TH" or "Ref" by technology i
n: includes all unconstrained electricity producing technologies with an increased production at TH with respect to ref
Share i: the percentage that supplier i contribute to the marginal mix

- The reference year is 2015 and time horizon is 2030.
- Public energy projections realized by national or supra-national official agencies are used as a source of data (e.g. European Commission, International Energy Agency, Energy Information Administration).
- Additional processes are created for missing activities.

Geographical coverage

- The long-term marginal electricity supply mixes of 40 countries are updated and integrated in version 3.4 of the ecoinvent database. These markets correspond to ~76.5 % of the global electricity production in 2015 (~76.9% in 2030).

Marginal mixes composition

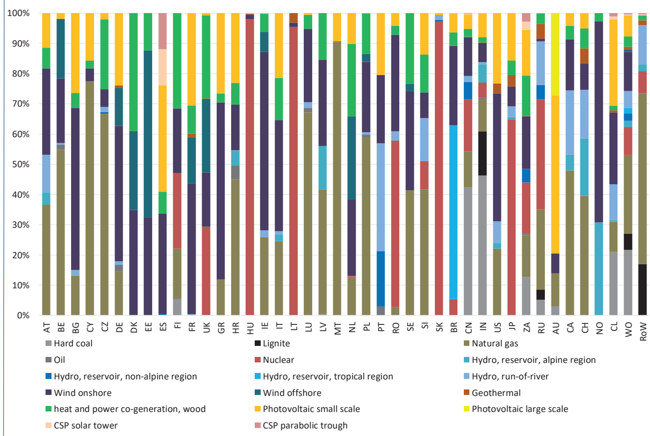

- The marginal mixes are composed on average by 29% fossil fuel power , 14% nuclear and 58% renewables

Meta-sensitivity analyses

- Different approaches to define the marginal mixes are tested : original v 3.3 approach, time horizon = 2020, reference year = 2020, average mix 2030.
- This compares the global warming potential (IPCC 2013, GWP 100a) of every activity of ecoinvent v.3.3 updated with v.3.4 marginal mixes to versions of ecoinvent v3.3 generated with the different approaches.

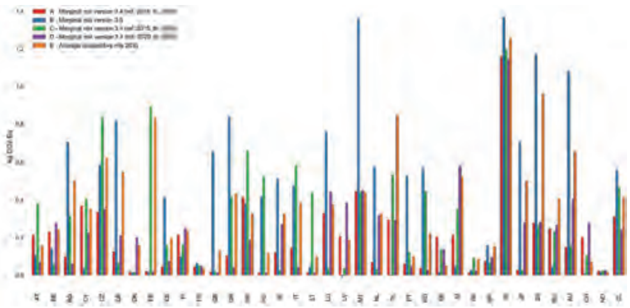

- This compares the global warming potential (IPCC 2013, GWP 100a) of every activity of ecoinvent v.3.3 updated with v.3.4 marginal mixes to versions of ecoinvent v3.3 generated with the different approaches.

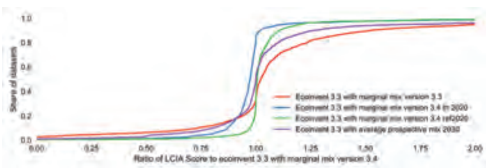

References

Muñoz I (2015) Example – Marginal Electricity in Denmark. In: consequential-lca.org. http://consequential-lca.org/clca/marginal-suppliers/the-special-case-of-electricity/example-marginal-electricity-in-denmark/. Accessed 15 Nov 2016

Schmidt JH, Thrane M, Merciai S, Dalgaard R (2011) Inventory of country specific electricity in LCA - consequential and attributional scenarios. Aalborg

Task 4.3

Title

Socio-economic-political drivers

Projects (presented on the following pages)

Developing dynamic context analysis procedures for DGE projects
Alternative: Task 4.1
O. Ejderyan, M. Stauffacher

Organizational ethnography›s contribution to the governance of a geothermal program: the Geneva example
Alternative: Task 4.1
F. Ruef, O. Ejderyan

SCCER-SoE Annual Conference 2017

SCCER SoE
SWISS COMPETENCE CENTER for ENERGY RESEARCH
SUPPLY of ELECTRICITY

In cooperation with the CTI
Energy
Swiss Competence Centers for Energy Research
Schweizerische Eidgenossenschaft
Confédération suisse
Confederazione Svizzera
Confederaziun svizra
Swiss Confederation
Commission for Technology and Innovation CTI

Developing dynamic context analysis procedures for DGE projects

Olivier Ejderyan, Michael Stauffacher - D-USYS TdLab, ETH Zürich

What is context?

Social acceptance plays an important role in the development of deep geothermal energy (DGE) in Switzerland. The literature on DGE stresses that large-scale deployment does not exclusively depend on technological innovation. It is crucial to take into account the context when planning DGE projects (Duijn, et al., 2013; Trutnevyte and Ejderyan 2017; Trutnevyte and Wiemer 2017).

This notion of context is commonly used in social science (Van Dijk 2008) to refer to the differences between situations in which social actors are engaged. Context is generally defined by two main dimensions:

1) Context is the setting or the environment in which an action takes place. As such it can be treated as a series of background variables that influence an action;
2) Context is what enables actors to give a meaning to a situation. As such it is an interpretative resource for the actors to make sense of a situation they are engaged in.

Tools and procedures for context analysis in DGE

The goal of this study is to identify relevant elements to take into account in the design of context analysis guidelines for DGE projects. Such guidelines will provide procedures to conduct a context analysis and respective operational tools derived from social science methods to collect information.

We conducted a review of context analysis guidelines for infrastructure development in the sectors of energy, planning, development aid, transport, and hydraulic engineering to identify how practitioners categorize elements of context. We specifically focused on existing guidelines for DGE and carbon capture and storage (CSS) to see which elements of context are addressed and how (see table below).

Petroleum museum in Pechelbronn, Northern Alsace. The historical context of oil extraction played an important role for the acceptance of nearby DGE plants of Soultz-sous Forêt and Rittershoffen (photo: O. Ejderyan, 2017)

All of the reviewed guidelines aim to address social aspects besides technical and environmental ones. Many of them distinguish different parts or elements of context such as stakeholder identification, public opinion or risk perception.

The reviewed guidelines identify general principles such as including stakeholders or the public and define what is in their view the best timing for addressing social aspects. Very few guidelines propose concrete tools and procedures to effectively analyse all the elements of context they have identified, with exception of Wade & Greenberg 2011 for CCS.

All guidelines address the context as a setting and consider the elements of context to be variables influencing the project. Only Duijn et al. 2013 mention the interpretative capacity of actors, but they do not propose tools for DGE developers to address it.

Elements of context		Brunstig et al. 2011	Creara Energy Experts 2014	Duijn et al. 2013	James et al. 2013	Trutnevyte, Wiemer 2017	Wade, Greenberg 2011
Spatial	Space	x		x			
	Environment	x		x	x		x
Actors	Stakeholders	x		x	x	x	x
	Population/ general public	x				x	x
Historical	Local history	x		x			
	Past projects	x				x	
Institutional	Legal	x	x	x	x		
	Formal political processes	x	x				
Socio-political	Social capital	x		x		x	x
	Socio-demographic	x	x	x	x	x	
	Discourse/perception	x		x			
Economic	Economic	x	x	x	x		x
Project related	Distribution of benefits/risks	x		x		x	
	Technology			x	x		
	Organisational	x					

Elements of context cited in guidelines for context analysis for DGE and CCS projects

Discussion

Context analysis is essential for DGE as it informs siting processes and public engagement. As such it can have an impact on social acceptance The results of the review indicate that context analysis guidelines for practice address the context as a set of variables influencing the project. In such a view, the context is something static. This explains why many guidelines recommend to conduct a context analysis prior to planning or in early phases. Thus in DGE, context analysis is used in the siting phase to select locations or to set up of a strategy to foster project acceptance.

However, static context analyses do not account for the changes that occur once a project altering its context. An initially “good” social context can suddenly become hostile to a DGE project depending on how this project is interpreted. Research in social science have underlined the importance of the interpretative dimension of context both theoretically and in practice (Van Dijk, 2008). This dimension of the context of DGE requires further research in order to develop dynamic context analysis tools and procedures.

References

Brunstig, S., et al. 2011. *Qualitative and Quantitative Social Site Characterisations*. SiteChar. Characterisation of European CO2 Storage. Deliverable N° D8.1. Amsterdam

Duijn, M et al. 2013. *Laying the Groundwork for Public Acceptance of Enhanced Geothermal Systems*. EC FP7 Project GEISER. Delft.

Jammes, L. et al. 2013. *Social Site Characterization & Stakeholder Engagement*. Global CCS Institute. Brussels.

Trutnevyte, E., & Ejderyan, O. 2017. Managing geoenergy-induced seismicity with society. *Journal of Risk Research*, (online first), 1–8. https://doi.org/10.1080/13669877.2017.1304979

Trutnevyte, E. & Wiemer, S., 2016. Tailor-made risk governance for induced seismicity of geothermal energy projects: An application to Switzerland. *Geothermics*, 65, pp.295–312.

Van Dijk, T. A. 2008. *Discourse and Context: A Sociocognitive Approach*. Cambridge: Cambridge University Press.

Wade, S., & Greenberg, S. 2011. *Social Site Characterisation: From Concept to Application*. CSIRO/Global CCS Institute

SCCER SoE
SWISS COMPETENCE CENTER for ENERGY RESEARCH
SUPPLY of ELECTRICITY

SCCER-SoE Annual Conference 2017

In cooperation with the CTI
Energy
Swiss Competence Centers for Energy Research
Schweizerische Eidgenossenschaft
Confédération suisse
Confederazione Svizzera
Confederaziun svizra
Swiss Confederation
Commission for Technology and Innovation CTI

Organizational ethnography's contribution to the governance of a geothermal program: the Geneva example

Franziska Ruef, Olivier Ejderyan – D-USYS TdLab, ETH Zürich

Research Context

In the context of geothermal energy, social science studies make a valuable contribution to public engagement procedures for siting, planning and risk governance. As there is no uniform perception of geothermal technology across a territory, it is important to take into account multiple scales, actors and contexts in order to gain an insight of the **local characteristics** of each site (Majer et al. 2012; Trutnevyte & Ejderyan, 2017).

Drilling site in Meyrin, GE (July 2017, by OE)

GEOTHERMIE 2020

This study takes place in the context of the Geneva program for geothermal energy, **GEothermie 2020**, which is funded by the public utilities *SIG* and the canton of Geneva. The program launched in 2014 started with an extensive prospection and exploration campaign that has now already led to the selection of first sites for concrete heat projects.

Research goals and methods

The goal of this research is to analyse how GEothermie 2020 can contribute to embed geothermal energy in the cantonal territory. This implies finding ways to relate geothermal energy to the local social reality. For this purpose we will:

- Identify contextual factors affecting decision-making and develop reflexive procedures to monitor and address them.
- Understand the effects of participation not only on the stakeholders and the public, but also on decision makers.
- Analyse public values in energy transition contexts and show how their identification can contribute to embed DGE in a regional context.

Public information event on Plainpalais in Geneva (October 2016, by OE)

As a highly transdisciplinary research, our study intends to create **"knowledge that is solution-oriented, socially robust, and transferable to both scientific and societal practice"** (Lang, et al. 2012). Tasks directly linked to project needs are conveyed to the researcher by the practitioners and are part of the research model and data at the same time. Thus, participating in this transdisciplinary project means that knowledge is **co-produced by research and practice** in close collaboration of different actors.

Organizational Ethnography – what does it mean for this study?

Organizational Ethnography was chosen as research method in order to follow the program on a regular basis and thus being responsive to changing priorities and upcoming topics. As an ethnographic method it is enable to take into account the context of the object of study.

We mobilize a range of Organizational ethnography's methods within three research axes that contribute to reach our research goal:

- **Decision-making:** Decision-making within the GEothermie 2020 program is studied by means of participant observation of weekly management meetings, as well as attendance of public events

- **Participation:** We intend to identify the effect participation has on participants on one side and on decision makers and their strategies on the other. We use participant observation of participatory processes and public events as well as interviews with stakeholders and representatives of the program.

- **Context Analysis:** We analyse documents and conduct focus groups to identify public values from which we can develop indicators for context analysis.

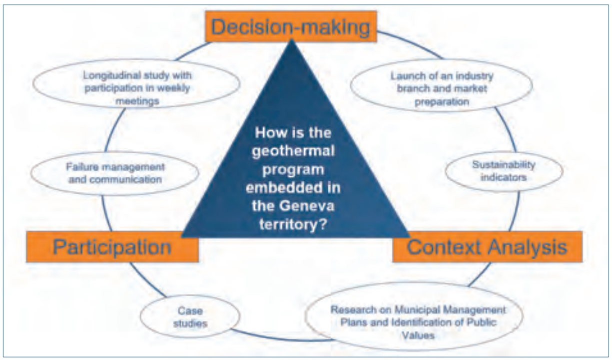

Research Framework with main axes and topics of interest

First challenges identified (since project start in May 2017):

First observations and document analysis enabled us to identify the following challenges for embedding DGE in Geneva:

Program vs. Project:
GEothermie2020 proposes a **global** planning approach at the regional level rather than one single project. As such, it offers opportunities but as well new challenges in terms of governance, communication, and inclusion of stakeholders.

Participation at multiple scales:
Participation implies communication and interaction with a broad range of stakeholders and the public. Ethnographic methods applied simultaneously in the Cantonal administration and on selected sites will provide crucial information on how to develop such **multi-scale participative procedures.**

Coordinating actors:
Establishing a complete value-chain of DGE introduces new actors to the field of energy in Geneva. The research will contribute to respond to challenges linked to **coordination of actors** and formalize exchange among actors them.

Developing new tools and procedures for governance
Building a new branch from scratch asks for the consideration of a number of new procedures, frameworks and regulations. The research contributes to the elaboration of **governance tools** as part of the transdisciplinary process.

References

Lang, D. J. et al. (2012). Transdisciplinary research in sustainability science: Practice, principles, and challenges. *Sustainability Science*, 7(SUPPL. 1), 25–43.

Majer, E. et al. (2013). *Best Practices for Addressing Induced Seismicity Associated With Enhanced Geothermal Systems (EGS). Draft May 2013.* Washington DC.

Trutnevyte, E., & Ejderyan, O. (2017): Managing geoenergy-induced seismicity with society, *Journal of Risk Research, 9877(April), 1–8.*

Task 4.4

Title

Joint Activity Scenarios & Modeling (JA-S&M)

Project (presented on the following page)

Impact of EU Electricity Policies on Long-term Electricity Supply in Switzerland
A. Singh, R. Kannan, T. Kober

SCCER SoE
SWISS COMPETENCE CENTER for ENERGY RESEARCH
SUPPLY of ELECTRICITY

SCCER-SoE Annual Conference 2017

In cooperation with the CTI
Energy
Swiss Competence Centers for Energy Research
Commission for Technology and Innovation CTI

Impact of EU Electricity Policies on Long-term Electricity Supply in Switzerland

Antriksh Singh, Ramachandran Kannan, Tom Kober
Energy Economics Group, Laboratory for Energy Systems Analysis,
Paul Scherrer Institut, 5232 Villigen PSI, Switzerland
Email: antriksh.singh@psi.ch

PAUL SCHERRER INSTITUT PSI

The sustainability of Switzerland's electricity system in the mid- to long-term can be highly influenced by technical, economic and political developments in Europe, in particular the neighboring countries. In capacity of the Task 4.2, the European Swiss TIMES Electricity Model (EUSTEM) is used to assess the impacts of key EU policies on the Swiss electricity system. EUSTEM is a multi-region, long-term capacity expansion model with high temporal resolution. We assess a range of Switzerland's electricity supply up to year 2050 in framework of the EU policies of nuclear decommissioning and decarbonization, to understand potential pathways for energy transition in Switzerland to meet the goals of the 2050 Swiss Energy Strategy. Outputs from EUSTEM will be used to develop a novel Bi-level Electricity Market Model (BEM).

European Swiss TIMES model (EUSTEM)

EUSTEM is a cost optimization framework of the whole electricity system with long time horizon (2050+) and an hourly representation of inter annual variabilities. The model covers 96% of EU-28 electricity supply (Fig. 1) with a detailed representation of Switzerland. From a social planner's perspective, economic dispatch and international electricity trades, along with intermittent renewables generation, are assessed to satisfy given electricity demand. The model is suitable to assess long-term electricity supply using what-if type scenario. To illustrate its strengths, we present two exemplary scenarios.

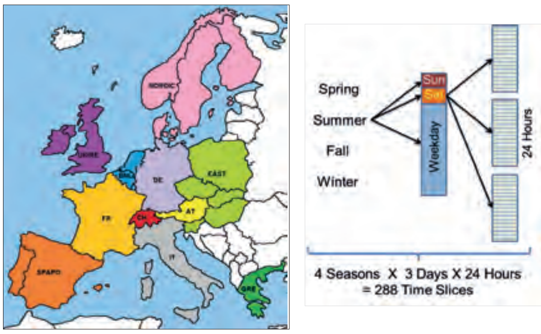

Fig 1. Regions in EUSTEM (Left); and definition of temporal details (Right)

European Electricity Scenarios

Reference shows the least cost electricity supply for the electricity demands from the EU reference scenario. Some of the existing EU policies, for example, nuclear phase-out, renewable targets, etc. are implemented.

Climate scenario aim for 95% CO_2 emissions reduction from 1990 levels in the whole EU electricity system by 2050.

Electricity Supply in the EU

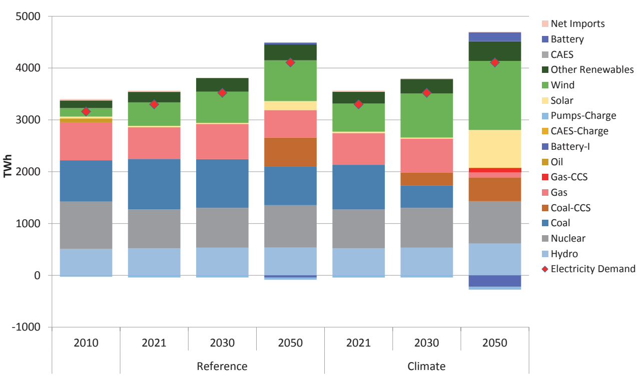

Fig 2. Generation profile in EU 2030 in and 2050

In **Reference** scenario, bulk of baseload electricity is generated by nuclear and coal power plants. Supply from wind and solar PV reaches 21% by 2050. In **Climate** scenario, 45% of the 2050 generation is from solar PV and wind. Additionally, adoption of storage technologies (to cope with increased share of variable renewables generation) become prominent. For base load, 2030 onwards, in addition to the hydro and nuclear, carbon capture and storage (CCS) technologies gain traction and replace conventional gas/coal power plants.

Impacts on Switzerland's Electricity System

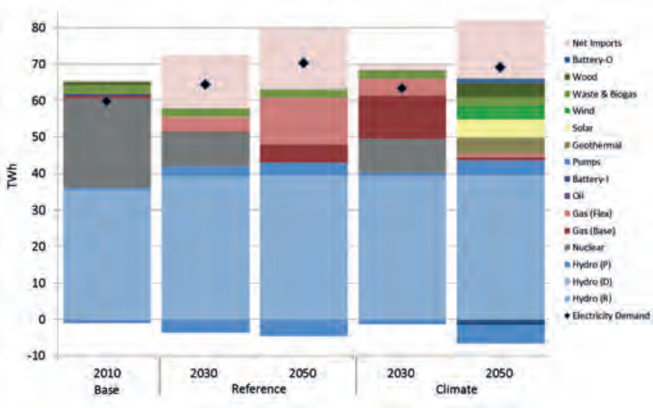

Fig 3. Electricity supply in Switzerland in Reference and Climate scenarios

By 2050, **Reference** scenario shows substitution of nuclear primarily by gas electricity generation (in absence of low-cost renewable alternatives), with greater reliance on low-cost imports (limited by interconnection capacity) and pumped hydro storages.

In **Climate** scenario more than 25% of the generation is from a diverse portfolio of new renewables (Fig. 3). While the level of electricity import in Switzerland in 2050 is similar in the two scenarios, the electricity imports in **Reference** case constitute of low-cost coal based generation whereas in **Climate** scenario has greater share of renewables.

In 2050, cost of electricity generation in **Climate** scenario is 65% higher compared to **Reference** scenario due to significant investments in new renewables generation capacity and costly imports.

Conclusions and Outlook

Climate targets lead to mass adoption of variety of renewables in EU, albeit at a higher cost. In Switzerland, electricity generation from gas and imports from neighboring countries emerge as cost effective supply options due to limited renewable potential and higher costs of renewables electricity generation in the near future. In both the scenarios new investments in cross-border interconnections are needed. Additionally, more new storage capacity is required in **Climate** scenario.

EUSTEM is continuously developed, within the scope of SCCER-SoE and other projects. The model is being updated in terms of future technology cost, renewable resource potentials and their variability, dispatch features, etc. Eventually, understanding of pathways for development of electricity system derived from EUSTEM will be utilized for development of new market models in the coming years.

References

Shivakumar, A., C. Taliotis, P. Deane, J. Gottschling, R. Pattupara, R. Kannan, D. Jakšić, K. Stupin, R. V. Hemert, B. Normark and A. Faure-Schuyer, 'Need for Flexibility and Potential Solutions. Europe's Energy Transition - Insights for Policy Making', Academic Press, 2017

R. Pattupara, 'Long-term Evolution of the Swiss Electricity System Under a European Electricity Market', Ph.D. Thesis, ETH Zürich, 2016

Work Package 5: Pilot & Demonstration Projects

The key objective of the SCCER-SoE in Phase II is the initiation and in some case completion of pilot & demonstration (P&D) projects, which will be executed in close collaboration with industrial partners. The new WP5 combines the integrated approaches developed for geo-energies (WP1), hydropower (WP2), and the innovative technologies of WP3 in a series of seven P&D projects. The successful completion of these projects is a key milestone to deliver in 2025 a portfolio of tested solutions, which shall enable Switzerland to reach the targets of the Energy Strategy 2050. Status and highlights are summarized below.

The seven demonstrator projects are:
Demo-1: Flagship stimulation experiment in the Deep UnderGround Laboratory
Demo-2: Reservoir engineering for heat exchange in Haute Sorne
Demo-3: Geneva basin-scale hydrothermal play for heat extraction and storage
Demo-4: CO_2 geological storage pilot
Demo-5: Small Hydro-Power Plant
Demo-6: Controlled fine sediment release from a reservoir by a hydrodynamic mixing device
Demo-7: Complex large hydropower scheme

Demo-1: Flagship stimulation experiment in the Deep UnderGround Laboratory

The project aims at a better understanding of the hydroseismo-mechanical coupled processes that are associated with high pressure fluid injections in a crystalline rock mass. Experiments are carried out at various scales ranging from centimeters to hundreds of meters. Intermediate experiments at ten-meter scale are carried out at the Grimsel Test Site, Switzerland. All stimulation activities have been completed in May 2017 and the circulation phase will be performed in Oct-Dec 2017. Subsequently, all personnel and funding will move to the DUGLab Bedretto Pilot Project in 2018 which will demonstrate hydraulic stimulation at hundred-meter scale.

Demo-2: Reservoir engineering for heat exchange in Haute Sorne

GeoEnergie Suisse AG is developing a pilot and demonstration project for deep petrothermal electricity generation in the village of Haute-Sorne (Jura). The system aims at depths of 4000 – 5000 m and is projected to deliver up to 5 MW electricity and/or heat for industrial processes as well as district heating. For the first time, the project will implement the so-called multi-fracture system in a granitic environment. Enabling the success of the Haute-Sorne project is one of the highest priorities within the SCCER-SoE. Many activities will be targeted towards enabling the technology but also in using the data from Haute-Sorne for calibration, upscaling and validation of methods and results, such as strategies for adaptive traffic light seismic monitoring systems, underground heat exchanger design, construction, and optimization, as well as research on optimal fluid circulation and associated heat extraction strategies.

Demo-3: Geneva basin-scale hydrothermal play for heat exchange and storage

This demonstration project will be implemented as part of the “Geothermie 2020” program of the Canton of Geneva. A step-wise approach including drilling wells (production and storage) at progressively increasing depths (650-1500m) will be performed by SIG during Phase II (Q4 2017-2018). This will provide the opportunity to test and validate the effectiveness of exploration concepts and models developed within WP1 as well as proof the feasibility of direct heat production and subsurface storage potential in sedimentary basins at relatively shallow depths. The project is already approved and in advanced stage of realization.

Demo-4: CO_2 Geological Storage Pilot

According to IEA, IPCC and COP21, (Carbon Capture & Storage) CCS has to be implemented to keep global warming within 2°C. ELEGANCY, an SFOE funded P&D project, embedded in a larger European framework, has the mission to provide clean hydrogen for heat and mobility based on steam-methane-reforming. CCS is an essential part of this concept. Underground experiments at the Mt Terri Lab will study the potential CO_2 migration through a fault in the caprock and the effects of fault activation. This is complemented by lab experiments on rock samples, modelling of injection and CO_2 migration, and the identification of regions in the Swiss sedimentary basin that are suitable for a future CO_2-storage pilot site.

Demo-5: Small Hydro-Power Plant

Research performed by SCCER-SoE partners will be implemented in a new small HP plant to be installed/ built in the coming 2 to 3 years. This demonstrator will show the ability produce clean, sustainable and renewable energy while producing ancillary services. Several topics will be addressed such as: the now-casting and seasonal forecasts of discharge to the water intake as a basis for sediment management and for a flexible power production scheme; a critical review of the implemented operation practice, in view of efficiency improvements considering multi-sectorial objectives; a technical optimization of the hydro electrical equipment operating conditions allowing a flexible control and set up of a predictive maintenance; an investigation of the ecosystem (metabolism, food web), fish migration and biodiversity; an assessment of the new regulation for small hydropower plant and the possible financial models.

Demo-6: Controlled fine sediment release from a reservoir by a hydrodynamic mixing device

Following the preliminary implementation carried out in the Mauvoisin reservoir in Valais, we will implement a project with HP industry with the goal of demonstrating the effectiveness of technologies to artificially stir the water stored in a dam reservoir to prevent sediment from settling and allow for the sediment to be conveyed downstream at acceptable rates through the turbines. The mobile mixing device will be tested at a few dams to show its efficiency in different conditions. The expected outcome is (i) to validate the flushing efficiency as compared to laboratory development conditions; (ii) to characterize the dependence from local conditions; (iii) to identify practical difficulties and shortcomings of field implementation; (iv) to control the modifications to the sediment regime in the river downstream of the powerhouse as well as in the residual flow strength, and the resulting environmental impacts. We will seek funding for industry and SFOE to initiate the demonstrator in 2017.

Demo-7: Complex large hydropower scheme

FLEXSTOR will test a set of innovative tools for flexible operation of storage hydropower plants in changing environment and market conditions at a complex hydropower scheme. This demostrator is motivated by the main hydropower challenge in Switzerland, namely the need for flexible operation targeting premium remuneration hours, for which comprehensive methodologies for hydropower upgrading projects are still missing. Specific goals of FLEXSTOR are to demonstrate how to: concentrate production in less hours, while mitigating negative impacts (e.g. river up/down surges); manage reservoir sedimentation to expand storage capacity while complying with the Waters Protection Act; address mountain slope instability risks in periglacial zone, avoiding non-optimal “preventive reservoir lowering”; identify the changing demand structure and the required adaptation of the storage management; extend the operating range of hydraulic machinery, whilst avoiding instabilities; optimally manage a compensation basin in order to minimize the ecological impacts of hydropeaking in the downstream river reach. All these developments, which are at the core of the WP2 efforts, will be validated in the complex system of KWO Oberhasli, which allows later replication to other hydropwer schemes in Switzerland.

Projects (presented on the following pages)

Hydro-economic Consequences of Hydro-peaking Removal
Poster see task 2.3
L. E. Adams, P. Meier, J. Lund

Demonstrator 6: SEDMIX Fine sediment evacuationthroughthe power intakes at Trift reservoir
A. Amini, N. Lindsay, P. Manso, A. Schleiss

Fine sediment settling under pumped-storage operations in Räterichsboden
A. Baldin, S. Guillén Ludeña, P. Manso, A. J. Schleiss

Development of a real-time nowcasting and short range forecasting system of inflows to a small alpine hydropower plant
K. Bogner, M. Buzzi, M. Schirmer, M. Zappa

Cross-borehole characterization of permeability enhancement & heat transport in stimulated fractured media: preliminary results from the ISC experiment at the Grimsel Test Site
Poster see task 1.2
B. Brixel, M. Klepikova, M. Jalali, F. Amman, S. Loew

Influence of the angle of the jet-inflow on sediment settling in Räterichsboden»
M. Carbonne, S. Guillén Ludeña, P. Manso, A. J. Schleiss

Impacts of Future Market Conditions on Hydropower Storage Operations
Poster see task 2.2
L. Chambovey, J. P. Matos, P. Manso, A. J. Schleiss, H. Weigt, I. Schlecht, F. Jordan

CFD investigation of a Francis turbine to help the experimental measurements and the definition of start-up procedures
J. Decaix, V. Hasmatuchi, M. Titzschkau, F. Avellan, C. Münch-Alligné

Injection Protocol and First Results of Hydraulic Fracturing Experiments at the Grimsel Test Site
Poster see task 1.2
N. Dutler, B. Valley, L. Villiger, H. Krietsch, M. Jalali, V. Gischig, J. Doetsch, F. Amann

A comparison of the seismo-hydro-mechanical observations during two hydraulic stimulations at the Grimsel Test Site
Poster see task 1.2
V. Gischig, J. Doetsch, M. Jalali, F. Amann, H. Krietsch, L. Villiger, N. Dutler, B. Valley

Sediment balance of a system of alpine reservoirs in cascade
S. Guillén Ludeña, P. Manso, A. J. Schleiss

Challenging onboard measurements in a 100 MW high-head Francis turbine prototype
V. Hasmatuchi, M. Titzschkau, J. Decaix, F. Avellan, C. Münch-Alligné

Permeability Changes Induced by Hydraulic Stimulation at the Grimsel Test Site
Poster see task 1.2
M. Jalali, V. Gischig, J. Doetsch, H. Krietsch, L. Villiger, N. Dutler, B. Valley, K. F. Evans, F. Amann

Tracer based characterization of the connected fracture volume in the DUG Lab at the Grimsel Test Site
Poster see task 1.2
A. Kittilä, K. Evans, M. Jalali, M. Willmann, M. O. Saar

Geological characterization and in-situ stress state of the ISC experimental volume
Poster see task 1.2
H. Krietsch, V. Gischig, F. Amann, J. Doetsch, M. Jalali, B. Valley

Deformation and tilt measurements during the ISC experiment at the Grimsel Test Site
Poster see task 1.2
H. Krietsch, V. Gischig, B. Valley, F. Amann

Hydropeaking attenuation: how can revitalized rivers contribute?
A. Mark, P. Manso, S. Stähly, A. J. Schleiss, P. Meier

Operation changes of a complex hydropower system over decades
Poster see task 2.2
J. P. Matos, P. Manso, B. Schaefli, A. Schleiss

Augmentation de la flexibilité d'exploitation d'aménagements hydroélectriques de haute-chute au fil de l'leau en Valais
G. Morand, N. Adam, P. Manso, A. J. Schleiss

SmallFlex: Demonstrator for flexible Small Hydropower Plant
C. Münch, P. Manso, M. Staehli, M. Schmid, C. Nicolet, F. Avellan, A. Schleiss, J. Derivaz

Demonstration of new solutions for an upcoming small alpine HP plant (Adont, Surses)
M. Stähli, K. Bogner, M. Schirmer, A. Amini, M. Klauenbösch

Pico-seismicity during hydraulic stimulation experiments at the Grimsel Test Site
Poster see task 1.2
L. Villiger, V. Gischig, J. Doetsch, H. Krietsch, M. Jalali, N. Dutler, B. Valley, K. Evans, F. Amann, S. Wiemer

SWISS COMPETENCE CENTER for ENERGY RESEARCH
SUPPLY of ELECTRICITY

SCCER-SoE Annual Conference 2017

In cooperation with the CTI
Energy
Swiss Competence Centers for Energy Research
Commission for Technology and Innovation CTI

Demonstrator 6 : SEDMIX
Fine sediment evacuation through the power intakes at Trift reservoir

Azin Amini, Nicole Lindsay, Pedro Manso, Anton Schleiss
Ecole Polytechnique Fédérale de Lausanne, Corresponding author: azin.amini@epfl.ch

Introduction

Taking advantage of the withdrawal of some glaciers, several new dams will eventually be constructed in Switzerland in the coming years as a part of the 2050 energy strategy. The Trift dam, is one of these new projects. However, sedimentation is a key issue for reservoir sustainability as it results in a loss of capacity storage thus also affecting the hydropower production capacity [1].
A recent study by Jenzer-Althaus (2011) shed light on an innovative system, (called SEDMIX) allowing to keep in suspension or resuspend the fine particles near the outlets and the dam thanks to specific water jet arrangements and to avoid reservoir silting. The SEDMIX demonstrator aims to identify the possibility of controlled sediment release through power waterways.

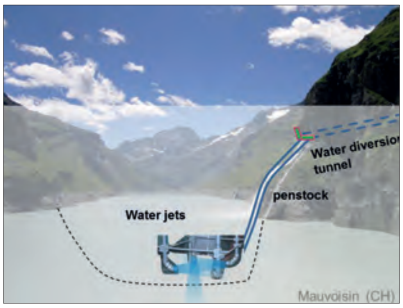

Concept of SEDMIX device implemented in Mauvoisin reservoir [2]

The project of a new dam reservoir in the Trift Valley currently being developed by *Kraftwerke Oberhasli SA (KWO)* is an opportunity to implement the SEDMIX device for the first time in a real case.

Numerical model

The current study aims at creating a three dimensional numerical model of the Trift reservoir and evaluating the effect of SEDMIX device on mitigation on the reservoir sedimentation. For this purpose The ANSYS-CFD three-dimensional finite volume model for multiphase flows is used.
The key physical parameters that will be tested are the geometry and mass inertia of the reservoir (which vary with the water level as function of the seasonal inflows and hydropower operation), the position, orientation and discharge of the SEDMIX jets, as well as the characteristics of the suspended sediments such as initial concentration and grain size.

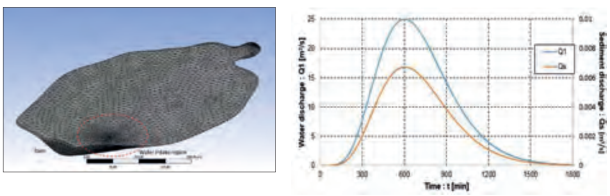

Numerical model mesh (left) and the inflow hydrograph and solidograph (right)

To design the device in the case of the Trift reservoir, the optimal values found empirically by Jenzer-Althaus (2011) are upscaled in order to define the dimension of jet nuzzles, the distance between jets, as well as the jet's discharge. The upscaling relies on Froude similarity. As such, jets with a distance of 20 m and a total discharge of 1 m^3/s are considered.

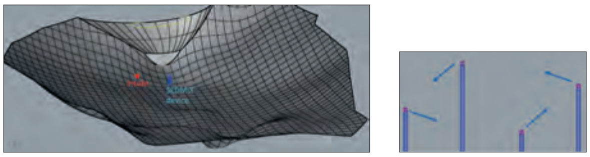

Water intake and SEDMIX jets location in the Trift reservoir [2] (left) details of SEDMIX jets (right)

In a preliminary phase, many simulations have been done with/without sediments both in steady state and transient flow conditions. Once the model parameters have been adjusted, the SEDMIX device is implemented into the model. It is placed close to the dam in a distance of about 100m from the water intake. The results are then compared to the reference case, i.e. simulation without jets.

Results

The numerical model highlights the influence of SEDMIX device in producing rotational flow in the reservoir, that can eventually keep fine sediments in suspension.

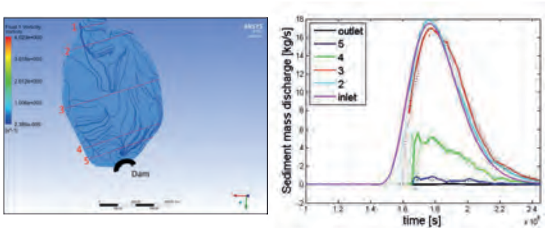

Flow pattern in the reservoir due to jet effect (left) sediment discharge at sections 1 to 5 (right)

The evacuated sediment ratio, the ratio between the total evacuated sediment weight and the initially supplied sediment weight [3], is equal to 14% for the reference case without SEDMIX jets. However, the presence of SEDMIX device increase the evacuation rate up to about 70%. This results brings out the efficiency of SEDMIX device in increasing the sediment release to downstream.

Conclusions

Moreover, at the current stage and with a preliminary choice of the jets position, this study shows high contribution of jets in keeping fine sediments in suspension and evacuation through the water intakes during normal operation of the hydropower plant. Numerical simulations have been successfully launched. However, due to the complex morphology of the reservoir, the hydrodynamic behavior needs further investigations.

References

[1] A.J. Schleiss, C. Oehy. Verlandung von Stausen und Nachhaltigkeit. Wasser, Energie, Luft, Heft 7/8:227-234, 2002.
[2] J. Jenzer Althaus, Sediment evacuation from reservoirs through intakes by jet induced flow. PhD thesis EPFL-LCH, communication 45, 2011.
[3] J. Jenzer-Althaus, G. De Cesare & A.J.Schleiss. Sediment evacuation from reservoirs through intakes by jet-induced flow. Journal of Hydraulic Engineering, 141 (2).2014
[4] A. Amini, P. A. Manso, S. Venuleo, N. Lindsay, C. Leupi, A.J. Schleiss "Computational hydraulic modelling of fine sediment stirring and evacuation through the power waterways at the Trift reservoir", Conf. Hydro 2017, Seville.

SCCER-SoE Annual Conference 2017

SCCER SoE
SWISS COMPETENCE CENTER for ENERGY RESEARCH
SUPPLY of ELECTRICITY

FlexSTOR

In cooperation with the CTI
Energy
Swiss Competence Centers for Energy Research
Schweizerische Eidgenossenschaft
Confédération suisse
Confederazione Svizzera
Confederaziun svizra
Swiss Confederation
Commission for Technology and Innovation CTI

Fine sediment settling under pumped-storage operations in Räterichsboden

Andrea Baldin, Sebastián Guillén-Ludeña, Pedro Manso, Anton J. Schleiss*
Laboratory of Hydraulic Construction (LCH), École Polytechnique Fédérale de Lausanne (EPFL), Switzerland
**Corresponding author: sebastian.ludena@epfl.ch*

EPFL ÉCOLE POLYTECHNIQUE FÉDÉRALE DE LAUSANNE

LCH LABORATOIRE DE CONSTRUCTIONS HYDRAULIQUES

Framework

Reservoir sedimentation is, at present, one of the main concerns in the operational management of dams. The reduction of the reservoir capacity due to sedimentation has negative impacts on the hydropower production, flood protection and availability of water for irrigation and human consumption. The most efficient and sustainable measure to cope with reservoir sedimentation consists in guaranteeing the sediment balance between upstream and downstream of the reservoir.
The main purpose of this poster is to describe the study of the interaction between pumped-storage operations (PSO) and the sedimentation process in the Räterichsboden reservoir.

The goals can be summarized as listed below:
- Characterize the hydrodynamics of the reservoir under PSO;
- Analyze the influence of the PSO on the reservoir sedimentation process;
- Determine the region of in- and out-flow sequences.

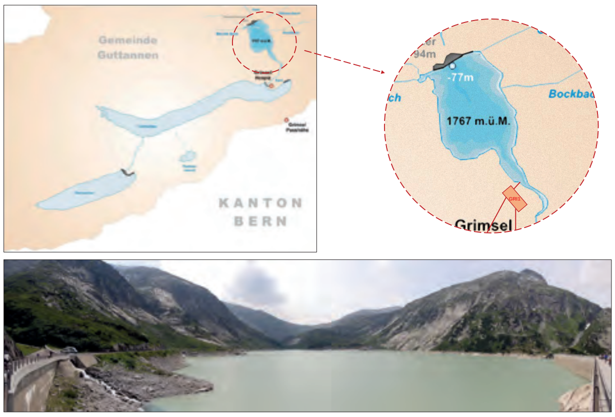

Figg. 1 – Plant of Raterichsboden reservoir and view of the lake from the dam (source of pictures: Wikimedia)

Methods

This study is based on a 3D numerical modelling using ANSYS CFX. However, in order to complete it, different programs were used as reported below:

Tab. 1 – Software used for the analysis of Räterichsboden reservoir

GEOMETRY (Qgis, Rhino, Design Modeler) → MESH (Ansys Meshing) → NUMERICAL SIMULATION (Ansys CFX) → POST-PROCESSING (CFX-POST, Excel, MATLAB)

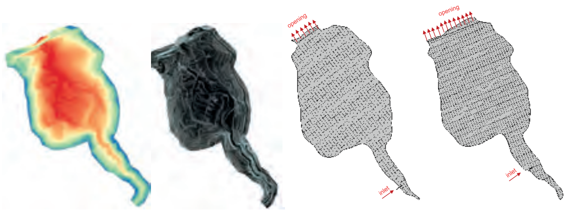

Fig. 2 – From the left to the right: Qgis DEM, countour lines, Rhino geometry 1753 m a.s.l. and 1767 m a.s.l.

Different parameters were taken into account and were varied for checking how they influence the hydrodynamic and the sedimentation process inside the reservoir.

Tab. 2 – Parameters taken into account for this study

Water level	Maximum supply level (1767 m a.s.l.)		Operating level (1753 m a.s.l.)
Volume	Minimum volume	Mean volume	Maximum volume
In- and outflow rates	Constant hydrograph		Oscillating hydrograph
Sediment concentration at the inlet	0 mg/L (inflow of water)		75 mg/L (75% of the initial concentration of the reservoir)

Tab. 3 – Mesh statistics for the two models

Mesh statistics	Model Min Operating Level	Model Max Supply Level
Total Number of Nodes	69445	87962
Total number of Elements	209849	271142

Sand particles (density equal to 2600 kg/m^3) with a diameter of 4.37 μm were chosen for all the simulations.
For a better understanding of the influence of the different models (in terms of mass-momentum and turbulence transfer between the two phases) inside ANSYS CFX, a large number of tests was carried out with a simply geometry (a cylinder).
Finally, an analysis of the results let us choose the best models for this study.

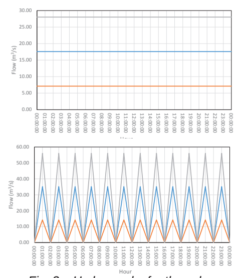

Fig. 3 – Hydrographs for the volumes

In the end, the simulations which were launched and completed for this study were 26.

Tab. 4 – Table summarizing the experiment schedule

TRANSIENT	Water level	Volume	In- and outflow rates	Sediment concentration at the inlet	TOTAL
Hydrodynamics	2	3	2		12
Sediment	2	2	1	2	8

STEADY STATE	Water level	Volume	In- and outflow rates	Sediment concentration at the inlet	TOTAL
Hydrodynamics	2	3	1		6

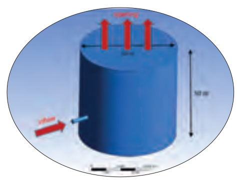

Fig. 4 – Cylinder used for the tests

Results

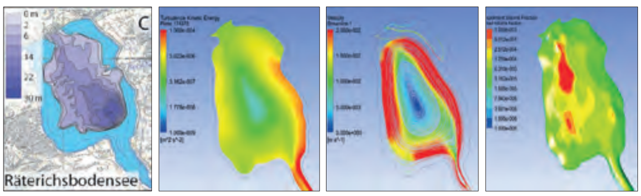

Fig. 5 – From the left: sediment isopach[1], main parameters for hydrodynamic and sediment studies

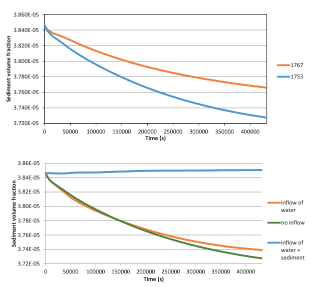

Fig. 6 – From the top: sediment volume fraction vs time (no inflow) and sediment volume fraction vs time for the different conditions (minimum operational level)

By analysing the results from the simulations, it was possible to conclude that:

- Low water TKE and velocities areas correspond to areas with thicker sediments (delta).
- The graphs show the results expected: by increasing the inflow (and consequently the velocity of the fluid) or the concentration of sediment in the inlet, the particles require more time to settle down.

Conclusion

- Numerical simulations provide predictive information about the behaviour of the flood inside the reservoir. These results must be validated by physical experiments. However, if we compare the influence zones from previous studies and from the analysis following the simulations, it' s clear how there are several similarities.
- From CFD simulations it was possible to characterize the hydrodynamics of the reservoir, the influence of PSO on the sedimentation process and to determine the region of in- and outflow sequence.

References

Anselmetti, F.S., Bühler, R., Finger, D., Girardclos, S., Lancini, A., Rellstab, C., and Sturm, M. (2007). Effects of Alpine hydropower dams on particle transport and lacustrine sedimentation. *Aquatic Sciences*, 69(2), 179-198.
Bonalumi, M., Anselmetti, F.S., Kaegii, R., and Wüest, A. (2011). Particle dynamics in high-Alpine proglacial reservoirs modified by pumped-storage operation. *Water Resources Research*, 47(9), n/a-n/a.
Möeller, G., Boes, R., Theiner, D., Fankhause, A., De Cesare, G., and Schleiss, A. J. (2011). Hybrid modelling of sediment management during drawdown of Räterichsboden reservoir. *Dams and Reservoirs under Changing Challenges*, 421. [1]
Müller, M., De Cesare, G., and Schleiss, A. J. (2014). Continuous Long-Term observation of Suspended Sediment Transport between Two Pumped-Storage Reservoirs. Journal of Hydraulic Engineering, 140(5), 5014003.
Schleiss, A. J., Franca, M.J., Juez, C., and De Cesare, G. (2016). Reservoir sedimentation. Journal of Hydraulic Research, 54(6), 595-614.

SCCER SoE
SWISS COMPETENCE CENTER for ENERGY RESEARCH
SUPPLY of ELECTRICITY

SCCER-SoE Annual Conference 2017

In cooperation with the CTI
Energy
Swiss Competence Centers for Energy Research
Commission for Technology and Innovation CTI

Development of a real-time nowcasting and short range forecasting system of inflows to a small alpine hydropower plant

K. Bogner[1], M. Buzzi[2], M. Schirmer[3], M. Zappa[1]
[1] WSL, [2] MeteoSwiss, [3] SLF

Motivation

In order to highlight the possibilities of increasing the flexibility in managing Small Hydropower Plants (SHP) with very limited storage capacities high resolution forecasts will be adapted to the small alpine catchment at Gletsch. Up to now the COSMO-E meteorological forecasts with a spatial resolution of ~ 2.2 km have been implemented in an operational hydrological forecast chain, which produce hourly inflow forecasts for the next 5 days. For the first six hours the INCA-CH nowcast system will be implemented at next with a resolution of ~ 1 km. All produced inflow forecasts will be post-processed in order to minimize modelling errors and to improve the reliability in real-time by the use of novel statistical methodologies, like machine learning methods.

Study area

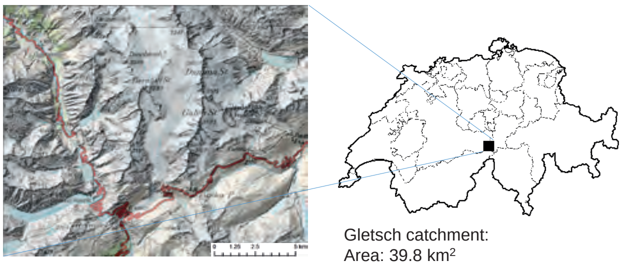

Gletsch catchment:
Area: 39.8 km²
Glaciation: 52%
Mean elevation: 2719 m a.s.l.

Methods

The forecast chain under development consists of :

- Meteorological forecasts
  → **Seamless forecast chain:** 0-6h INCA-CH, 6-24h COSMO-1, 24-120h COSMO-E

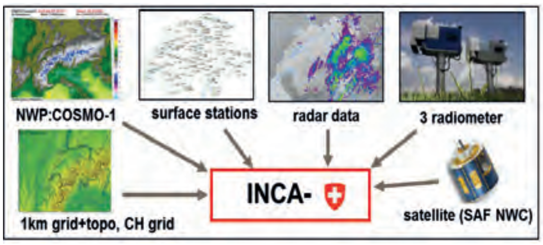

INCA-CH model set up

- Hydrological model PREVAH + Post-Processing of the inflow forecasts

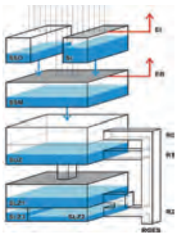

PREVAH model scheme

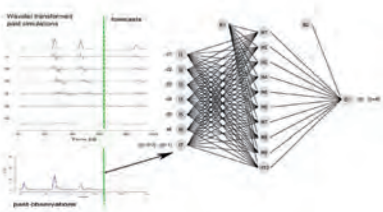

Novel statistical error correction methods

Preliminary results

- The hydrological model PREVAH has been calibrated for the Gletsch catchment and the COSMO forecasts have been set up for producing inflow forecasts to the Gletsch Small Hydropower Plant (SHP), which is under construction. The runoff from the Gletch catchment is heavily influenced by glacier melt. During the winter period the runoff is very low (close to zero), only at the late Spring time, when the temperature increases, the runoff starts to react. This will be one of the crucial periods to forecast. Below you can see the forecasts one day ahead and one day after the melting period starts.

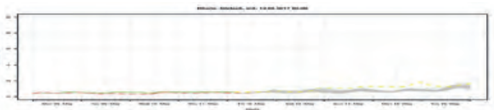

Forecast example one day before the glacier melt starts (mid of May)

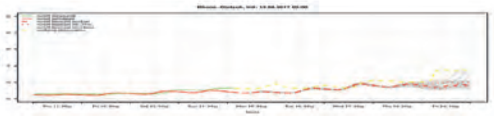

One day after the start of the melting season

- Post-processing methods have been adapted to the operational forecasts

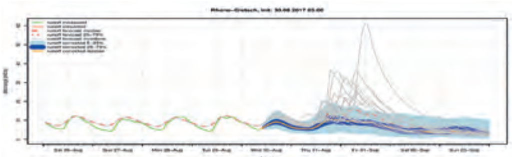

Post-processed forecast applying the Quantile Regression Neural Network (QRNN) method

- INCA-CH forecasts are retrieved every 10 min with forecasts for the next 6 hours with 10 min resolution. These high-resolution forecasts will be incorporated into the forecast chain at next. An ensemble nowcast system, which is under development at MeteoSwiss, will be included in the next year in order to derive the total predictive uncertainty.

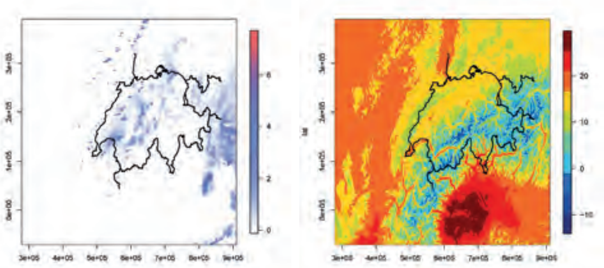

Example of INCA precipitation and temperature forecast from the 12th of September 2017

Outlook

Besides the development of a seamless forecast chain and the derivation of the predictive uncertainty including the hydrological and the meteorological uncertainty, possible improvements in the forecast quality will analysed by integrating novel snow hydrology models developed at SLF.

References

Bogner, K., Liechti, K., and Zappa, M.: *Post-Processing of Stream Flows in Switzerland with an Emphasis on Low Flows and Floods,* Water, *8, 115, 2016.*
Haiden, T., Kann, A., Wittmann, C., Pistotnik, G., Bica, B., and Gruber, C.: *The Integrated Nowcasting through Comprehensive Analysis (INCA) system and its validation over the Eastern Alpine region*, Weather Forecast., 26, 166–183, 2011.
Nerini, D., Besic, N., Sideris, I., Germann, U., and Foresti, *L.: A non-stationary stochastic ensemble generator for radar rainfall fields based on the short-space Fourier transform,* Hydrol. Earth Syst. Sci., *21, 2777-2797, 2017.*
Viviroli D, Zappa M, Gurtz J and Weingartner R.: *An introduction to the hydrological modelling system PREVAH and its pre- and post-processing-tools.* Environmental Modelling & Software. 24(10): 1209–1222, 2009.

SCCER SoE
SWISS COMPETENCE CENTER for ENERGY RESEARCH
SUPPLY of ELECTRICITY

SCCER-SoE Annual Conference 2017

FlexSTOR

In cooperation with the CTI
Energy
Swiss Competence Centers for Energy Research
Schweizerische Eidgenossenschaft
Confédération suisse
Confederazione Svizzera
Confederaziun svizra
Swiss Confederation
Commission for Technology and Innovation CTI

Influence of the jet-inflow angle on sediment settling in Räterichsbodensee

Maximilien Carbonne, Sebastián Guillén-Ludeña, Pedro Manso, Anton J. Schleiss*
Laboratory of Hydraulic Construction (LCH), École Polytechnique Fédérale de Lausanne (EPFL), Switzerland
**Corresponding author: sebastian.ludena@epfl.ch*

Framework

Reservoir sedimentation is, at present, one of the main concerns in the operational management of dams. The reduction of the reservoir capacity due to sedimentation has negative impacts on the hydropower production, flood protection and availability of water for irrigation and human consumption. The most efficient and sustainable measure to cope with reservoir sedimentation consists in guaranteeing the sediment balance between upstream and downstream of the reservoir.
The main purpose of this poster is to describe the study of the interaction between pumped-storage operations (PSO) and the sedimentation process in the Räterichsboden reservoir.

The aims of the study can be summarized as listed below:

- Characterize the hydrodynamics of the reservoir under PSO under different jet-inflow angles
- Analyze the influence of the PSO on the reservoir sedimentation process

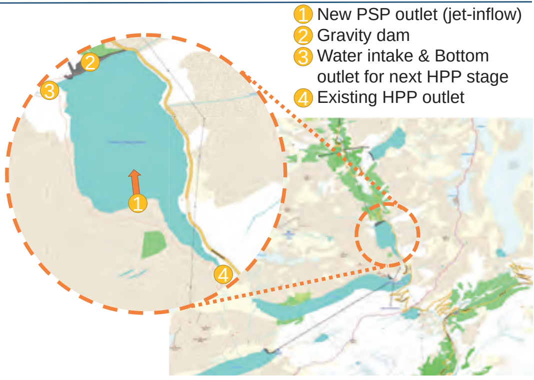

Figure 1: Location plan of Räterichsbodensee

Methods

The study was carried out with 3D numerical modelling using Ansys CFX as well as some other software to prepare the geometry.
There were several parameters in this study : water level, jet angle (**alpha**), discharge (**Q**), initial sediment concentration in the lake, **concentration ratio** (ratio between inflow concentration and initial sediment concentration in the lake).

Geometry
- A custom software was used to create the basic geometry from the terrain elevation data
- Rhino 3D was used to simplified the geometry
- Design Modeler

Mesh
- Ansys Meshing
- Inflation layers at the bottom

Numerical Simulation
- Ansys CFX
- Outlet at the water surface near the dam

Results post-processing
- Ansys CFD-Post
- Libreoffice Calc
- Custom coding (python, matplotlib)

Figure 2: 3D model obtained from terrain elevation data

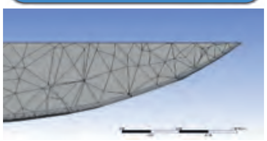

Figure 3: cutaway of the mesh, we can see inflation layers

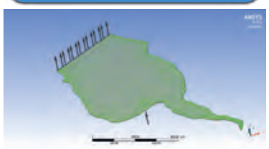

Figure 4: overview of the model, once set up

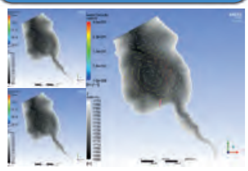

Figure 5: velocity field for different angles (clockwise from top left : +30°, 0°, -30°)

Results

The first main result is obviously the change in the velocity field. On Figure 5, the velocity field in the reservoir is plotted for different jet-inflow angles (the tunnel is drawn in pink). The number of vortexes also depends on the inflow angle. But our concern is the sediment settling, and I had to find a link between velocity field and sedimentation. In order to find a correlation between sediment settling and the velocity field (and thus the jet angle) I proposed several indicators to quantify the different phenomena :

agitationta : volume average of time-averaged velocity in the whole reservoir

sed : volume average of sediment volume fraction in the whole reservoir

depta : area average of time-averaged sediment volume fraction on the bottom surface of the reservoir

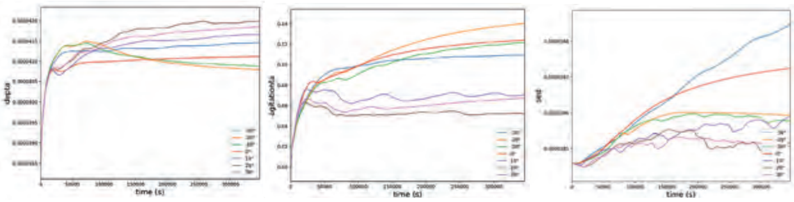

Figure 6: jet-inflow angle influence on main indicators
*Evolution of **depta**, **agitationta** and **sed** in time for Q = 90 m³/s, water level at 1767 m.a.s.l, and alpha = -30º to +30º (from left to right)*

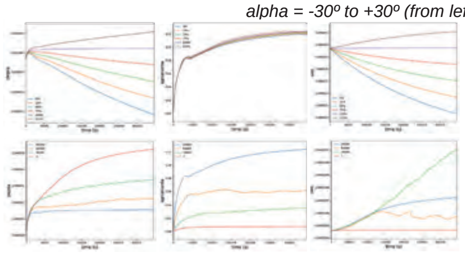

*Figure 7: influence of discharge level (Q) and concentration ratio : Evolution of **depta**, **agitationta** and **sed** in time for*

- *Q = 90 m³/s, water level at 1767 m.a.s.l and concentration ratio = 0% to 125% (first line)*
- *Q = 0 m³/s to 90 m³/s, water level at 1767 m.a.s.l and concentration ratio = 100% (second line)*

Conclusion

With this study, I tried to show the influence of the jet-inflow angle. I can conclude that for alpha lower than -20º, the inflow impacts on the sediment bar located near the inlet. This impact is associated with a local energy dissipation and thus, favors the sediment settling within the reservoir. It also seems that a good range is between -20° and -10°. Nevertheless, a finer study in this range would be appreciated. In fact, due to lack of time and computational resources, we decided to limit the number of simulations. Finally, results should be taken with caution : this study is mainly based on global indicators and is aimed to study the global trend. I recommend further studies and taking in account erosion.

References

Anselmetti, F.S., Bühler, R., Finger, D., Girardclos, S., Lancini, A., Rellstab, C., and Sturm, M. (2007). Effects of Alpine hydropower dams on particle transport and lacustrine sedimentation. *Aquatic Sciences*, 69(2), 179-198.
Bonalumi, M., Anselmetti, F.S., Kaegii, R., and Wüest, A. (2011). Particle dynamics in high-Alpine proglacial reservoirs modified by pumped-storage operation. *Water Resources Research*, 47(9), n/a-n/a.
Möeller, G., Boes, R., Theiner, D., Fankhause, A., De Cesare, G., and Schleiss, A. J. (2011). Hybrid modelling of sediment management during drawdown of Räterichsboden reservoir. *Dams and Reservoirs under Changing Challenges*, 421.
Müller, M., De Cesare, G., and Schleiss, A. J. (2014). Continuous Long-Term observation of Suspended Sediment Transport between Two Pumped-Storage Reservoirs. Journal of Hydraulic Engineering, 140(5), 5014003.
Schleiss, A. J., Franca, M.J., Juez, C., and De Cesare, G. (2016). Reservoir sedimentation. Journal of Hydraulic Research, 54(6), 595-614.

SCCER SoE
SWISS COMPETENCE CENTER for ENERGY RESEARCH
SUPPLY of ELECTRICITY

SCCER-SoE Annual Conference 2017

FlexSTOR

In cooperation with the CTI
Energy
Swiss Competence Centers for Energy Research
Commission for Technology and Innovation CTI

CFD investigation of a Francis turbine to help the experimental measurements and the definition of start-up procedures

J. Decaix[1], V. Hasmatuchi[1], M. Titzschkau[2], F. Avellan[3], C. Münch-Alligné[1]

[1]HES-SO Valais, School of Engineering, Hydroelectricity Group, Sion, jean.decaix@hevs.ch [2]Kraftwerke Oberhasli AG, Grimsel Hydro, Innertkirchen [3]EPFL, Laboratory for Hydraulic Machines, Lausanne

Motivation

Due to the development and the integration of renewable energies, the electrical grid undergoes instabilities [1]. Hydraulic turbines and pump-turbines are a key technology to stabilize the grid. However to reach this objective, the hydraulic machines have to extend their operating range. Such an extension requires to deal with start-up and stand-by operation, which often leads to a reduction of the lifespan of the machines [2].
Nowadays, numerical simulations reached a robustness allowing to investigate unstable operating points such as rotor/stator interaction, low head operating condition and start-up [3].
By coupling numerical and measurements investigations, several features can be drawn and solutions can be found to extend the operating range of the machine whilst the lifespan is weakly affected.

Test Case

The machines of hydropower plant Grimsel 2 is equipped with horizontal ternary units with a complete motor-generator coupled with a Francis turbine on one hand and a single stage radial pump on another hand.
The Francis turbine undergoes cracks at the junction between the trailing edge of the blades and the shroud. The cracks appeared after the operating conditions of the turbine changes from few stop and start per day to a large number of stop and start per day.
The origin of the cracks is however not yet understood.
The phenomenon responsible for the development of the cracks is investigated using numerical simulations to complete the experimental approach.

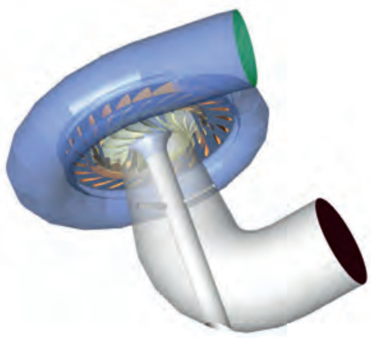

Numerical Set Up

The computational domain takes into account the spiral case, the distributor, the runner and the draft tube. The tripod inside the draft tube is also considered.
An hexahedral mesh is generated for each part of the turbine and then put together.
Reynolds-Averaged Navier-Stokes simulations are performed using the SST k-ω model.
The operating points investigated are clustered around the best efficiency point. Both inlet flow rate or inlet total pressure boundary conditions have been considered.

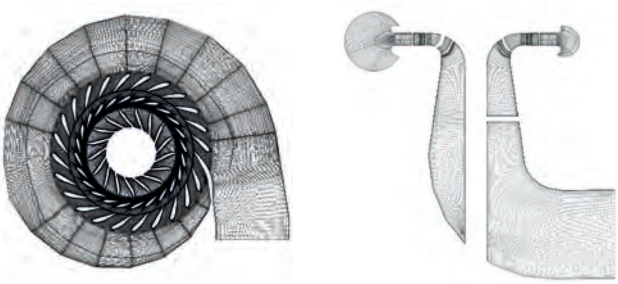

Results

The performance of the turbine predicted by the simulations are plotted on the hillchart of the Francis turbine. The agreement between the simulations and the measurements is good, whatever the operating points considered.

Pressure field

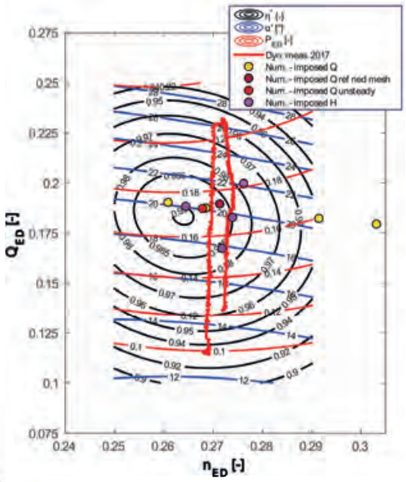

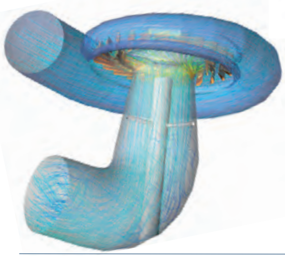

Blades Pressure field

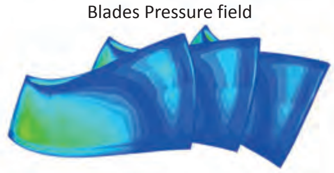

Conclusions & Perspectives

The numerical simulations are able to predict the performance of the turbine for different operation points clustering the best efficiency point with a good agreement compared to the measurements.
Therefore, the confidence in the simulations will allow the investigation of unstable operating points mainly those corresponding to the start-up procedure of the turbine in order to determine the phenomenon responsible of the blade cracks.

References

[1] Vu, T. L., & Turitsyn, K. 2016, 'Robust transient stability assessment of renewable power grids'. In IEEE International Conference on Sustainable Energy Technologies (ICSET) (pp. 7–12).
[2] M Gagnon et al, 2010, 'Impact of startup scheme on Francis runner life expectancy', IOP Conf. Ser.: Earth Environ. Sci. 12 012107
[3] J Nicolle et al 2012, 'Transient CFD simulation of a Francis turbine startup', IOP Conf. Ser.: Earth Environ. Sci. 15 062014

Acknowledgements

Schweizerische Eidgenossenschaft
Confédération suisse
Confederazione Svizzera
Confederaziun svizra
Swiss Confederation
Commission for Technology and Innovation CTI

FlexSTOR

Partners of the FLEXSTOR - WP6 project (17902.3 PFEN-IW-FLEXTOR)

Hes·so Valais Wallis
EPFL École Polytechnique Fédérale de Lausanne
KWO Grimselstrom

SCCER-SoE Annual Conference 2017

FlexSTOR

In cooperation with the CTI

Sediment balance of a system of alpine reservoirs in cascade

Sebastián Guillén-Ludeña, Pedro Manso, Anton J. Schleiss*
Laboratory of Hydraulic Construction (LCH), École Polytechnique Fédérale de Lausanne (EPFL), Switzerland
**Corresponding author: sebastian.ludena@epfl.ch*

Scope of work

Reservoir sedimentation is, at present, one of the main concerns in the operational management of dams. The reduction of the reservoir capacity due to sedimentation has negative impacts on the hydropower production, flood protection, and availability of water for irrigation and human consumption.

This study aims firstly at determining the sediment balance of a system of reservoirs in cascade. Secondly, this study aims at determining the percentage of fine sediments (d_m < 10 μm) contained in the overall volume of sediment deposited annually in each reservoir.

For those purposes, this study analyzes the system formed by the reservoirs of Oberaar, Grimsel, and Räterichsboden in the Swiss Alps (Figure 1).

Figure.1 Aerial view of the system formed by the reservoirs of Oberaar, Grimsel, and Räterrichsboden

Methods

The methodology followed in this study to determine the sediment balance of the system of reservoirs in cascade consists in quantifying the in- and outfluxes of sediments for each reservoir. These fluxes are:

- V_A: Annual sediment yield produced by the catchment computed by the formula of Beyer-Portner et al. (1998):
  $$V_A = 93\cdot10^{-15}\cdot H^{0.052}\cdot SE^{0.091}\cdot SV^{8.108}\cdot \Delta LG^{0.082}+274$$
  where H stands for the average precipitation in mm registered from June to September, SE is the percentage of erodible soil (not including the glacier), SV is the percentage of surface non covered by vegetation (including the glacier), and ΔGL is the annual variation of the glacier length in percentage.
- *PSE*: Volume of sediments exchanged between reservoirs as a results of pump-storage operations. These fluxes are computed as the product of the volume of water exchanged annually and the suspended sediment concentration of the reservoirs.
- *SR:* Annual sedimentation rate estimated from periodic bathymetric surveys and compared to those estimated by Anselmetti et al (2007).

The formula proposed by Bonalumi et al (2011) was used to compute the annual volume of fine sediments deposited annually:

$$SRF = \frac{1}{t_2 - t_1}\int_{t_1}^{t_2} w_s\cdot SSC(t)\cdot A(t)\cdot dt$$

where w_s is the settling velocity of the suspended particles (0.5 m/day), *SSC* is the suspended sediment concentration for each reservoir (Figure 2d), and A(t) is the evolution of the surface of the reservoirs.

Data

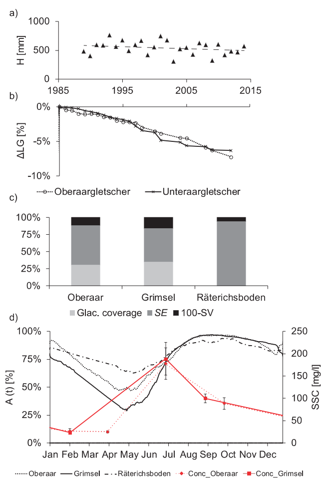

Figure.2 a) Annual average precipitation measured at Grimsel-Hospiz. b) Accumulated variation of the glacier s' length. c) Percentage of glacier coverage, erodible soil (SE), and vegetated surface (100-SV) for each catchment. d) Daily average evolution of the surface of the reservoir and the suspended sediment concentration within the reservoirs

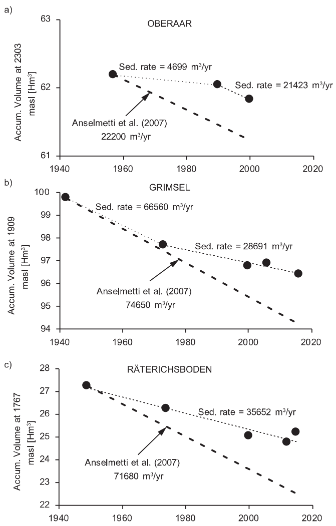

Figure.3 Annual sedimentation rates estimated by means of bathymetric surveys, and those reported by Anselmetti et al (2007) for: a) Oberaar, b) Grimsel, and c) Räterichsboden

Results

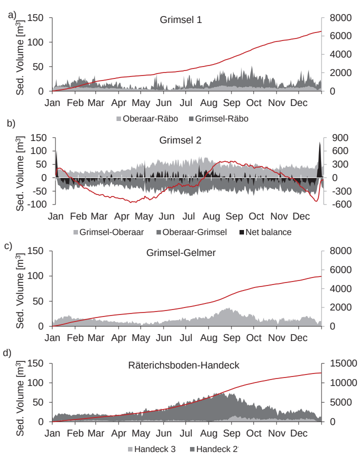

Figure.4 Daily average and annually - accumulated volumes of sediment exchanged by pump-storage operations (PSE) in: a) Grimsel 1, b) Grimsel 2, c) Grimsel –Gelmer, and d) Räterichsboden-Handeck

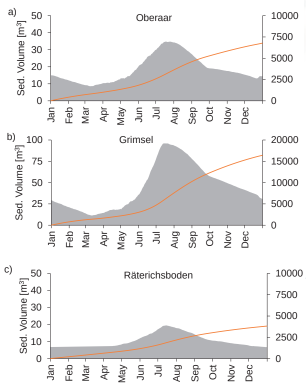

Figure.5 Daily average and annually - accumulated volumes of fine sediments deposited in: a) Oberaar, b) Grimsel , and c) Räterichsboden

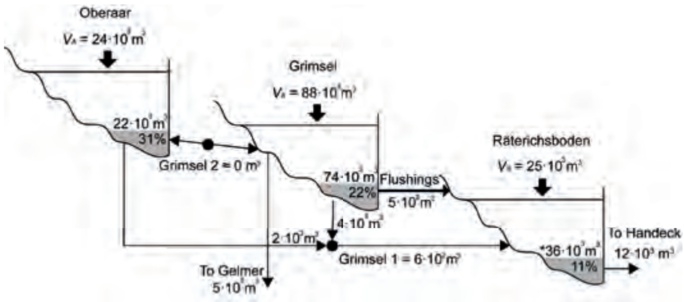

*Figure.6 Sediment balance of the system of reservoirs in cascade. The percentage indicate the portion of fine sediments deposited with respect to the total sedimentation rate (SR). * The sedimentation rate of Räterichsboden might be affected by periodic flushing operations in Grimsel.*

Conclusion

The sediment balance of the system of reservoirs in cascade formed by Oberaar, Grimsel, and Räterichsboden was determined by quantifying the in and outfluxes of sediments of each reservoir. The sedimentation rate estimated for fine sediments is not negligible with respect to the total sedimentation rate, since it may reach up to 30% of the total sedimentation rate of Oberaar.

References

- Anselmetti, Flavio S., Raphael Bühler, David Finger, Stéphanie Girardclos, Andy Lancini, Christian Rellstab, and Mike Sturm. 2007. "Effects of Alpine Hydropower Dams on Particle Transport and Lacustrine Sedimentation." Aquatic Sciences 69 (2): 179–98. doi:10.1007/s00027-007-0875-4.
- Bonalumi, Matteo, Flavio S. Anselmetti, Ralf Kaegi, and Alfred Wüest. 2011. "Particle Dynamics in High-Alpine Proglacial Reservoirs Modified by Pumped-Storage Operation." Water Resources Research 47 (9). doi:10.1029/2010WR010262.
- Beyer Portner, N, and Anton J. Schleiss. 1998. Erosions Des Bassins Versants Alpins Par Ruissellement de Surface. Communication 6 (Laboratoire de Constructions Hydrauliques, Ecole Polytechnique Fédérale de Lausanne). Lausanne: EPFL-LCH.

SCCER SoE
SWISS COMPETENCE CENTER for ENERGY RESEARCH
SUPPLY of ELECTRICITY

SCCER-SoE Annual Conference 2017

FlexSTOR

In cooperation with the CTI
Energy
Swiss Competence Centers for Energy Research
Schweizerische Eidgenossenschaft
Confédération suisse
Confederazione Svizzera
Confederaziun svizra
Swiss Confederation
Commission for Technology and Innovation CTI

Challenging onboard measurements in a 100 MW high-head Francis turbine prototype

V. Hasmatuchi[1], M. Titzschkau[2], J. Decaix[1], F. Avellan[3], C. Münch-Alligné[1]

[1]HES-SO Valais/Wallis, School of Engineering, Hydroelectricity Group, Sion, vlad.hasmatuchi@hevs.ch
[2]Kraftwerke Oberhasli AG, Grimsel Hydro, Innertkirchen [3]EPFL, Laboratory for Hydraulic Machines, Lausanne

Motivation

- Pumped-storage power plants: key components of a successful integration of renewable energy sources into electrical grid.
- Hydraulic turbines and pump-turbines:
  - operation in a wide range to offer power regulation flexibility
  - subject to frequent start-up and/or stand-by operating regimes
  - facing harsh structural loadings with impact on their lifetime.

Objectives:

- Establishment of a hydrodynamic instability level hill-chart of the machine based on several experimental monitoring parameters;
- Proposal of an alternative less-harmful start-up path and stand-by position with direct effect on the long-term maintenance costs;
- Elaboration of a diagnosis protocol to draw hydrodynamic instability level hill-charts on different hydropower units, using only a simplified instrumentation set.

Experimental instrumentation

Methodology:

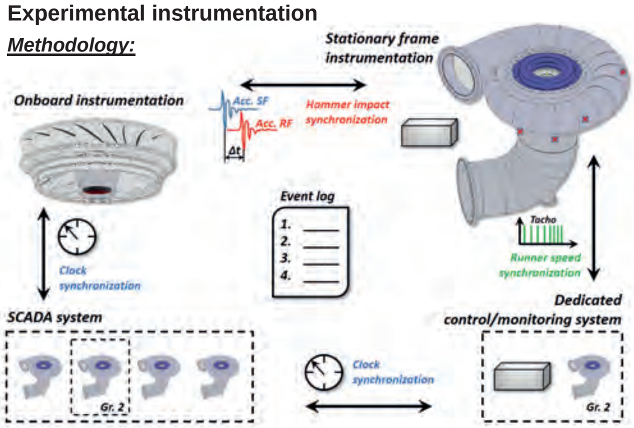

Onboard instrumentation:

1x Gantner Q.brixx acquisition system
2x 21 Ah, 22.2 VDC LiPo batteries
1x power supply protection electronics
8x quarter bridge strain gauges
2x single-axis IEPE accelerometers
2x inductive tachometers

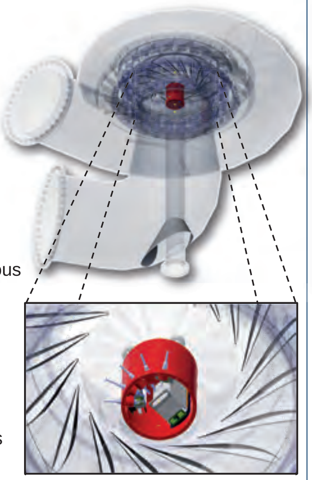

Main features:

- Autonomous multichannel synchronous 10 kHz continuous acquisition
- Data storage capacity: 2xUSB 16GB
- Autonomy of power supply : > 20h
- Protection relay against deep discharge of the batteries
- Possibility of data downloading, fast controlled recharging of batteries and system power switch on/off

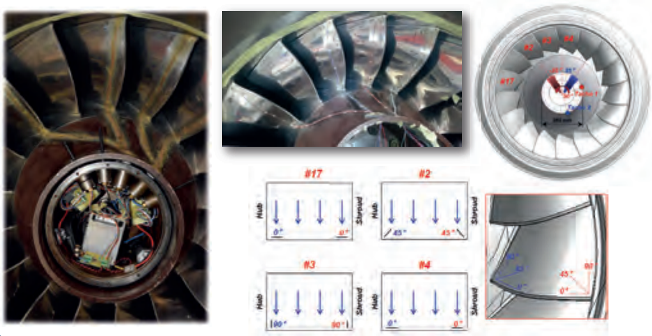

Preliminary results

- Conducted tests focused on normal turbine operation, deep part-load, turbine normal start-up, modified slower turbine start-up and pump start-up

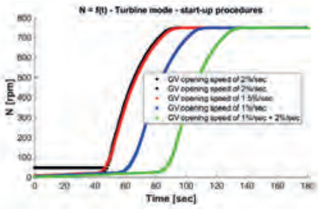

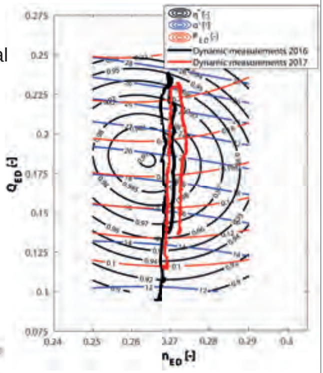

- Evidence of harmful structural loading of the turbine runner blades during the normal start-up and shut down procedures – signals recorded with the onboard instrumentation

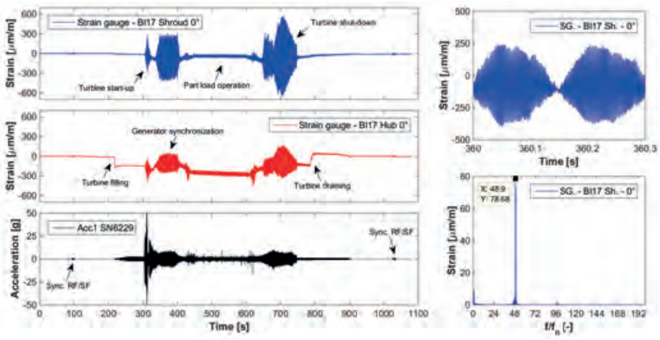

Conclusions & Perspectives

- Two experimental campaigns conducted in a 100 MW high-head Francis turbine prototype
- Onboard measurements successful, post-processing ongoing
- Seek for a feasible simple technical solution to reduce the turbine head for the start-up and shut down procedures
- Setup of a 3rd experimental campaign using only simplified instrumentation to test the new proposed start-up method(s)
- Driving the 3rd experimental campaign and analysis of results
- Establishment of a diagnosis protocol based on a simplified instrumentation set to identify harsh operating conditions on a different hydropower unit.

References

[1] Egusquiza E., Valentín D., Presas A., Valero C., 2017, "*Overview of the experimental tests in prototype*", IOP Conf. Series: Journal of Physics: Conf. Series **813**, doi:10.1088/1742-6596/813/1/012037.
[2] Drefs W., Greck A., Koutnik J., Loefflad J., Krantzsch A., 2016, "Online residual life assessment of power unit components", Hydro 2016, Montreux, Switzerland.
[3] Hasmatuchi V., 2012, "*Hydrodynamics of a Pump-Turbine Operating at Off-Design Conditions in Generating Mode*", EPFL Thesis No. 5373, Lausanne, Switzerland.
[4] Gagnon M., Tahan S.A., Bocher P., Thibault D., 2010, "*Impact of startup scheme on Francis runner life expectancy*", IOP Conf. Series: Earth and Environmental Science **12**, doi:10.1088/1755-1315/12/1/012107.

Acknowledgements

Schweizerische Eidgenossenschaft
Confédération suisse
Confederazione Svizzera
Confederaziun svizra
Swiss Confederation
Commission for Technology and Innovation CTI

FlexSTOR

Partners of the FLEXSTOR - WP6 project (CTI no. 17902.3 PFEN-IW-FLEXSTOR)

Hes·so VALAIS WALLIS
EPFL ÉCOLE POLYTECHNIQUE FÉDÉRALE DE LAUSANNE
KWO GRIMSELSTROM

SCCER-SoE Annual Conference 2017

SCCER SoE
SWISS COMPETENCE CENTER for ENERGY RESEARCH
SUPPLY of ELECTRICITY

FlexSTOR

In cooperation with the CTI
Energy
Swiss Competence Centers for Energy Research
Commission for Technology and Innovation CTI

Hydropeaking attenuation: how can revitalized rivers contribute?

Mark[1] A., Manso[1] P. A., Stähly[1] S., Schleiss[1] A.J. and Meier[2] P.
1) EPFL-LCH; 2) Eawag

Motivation

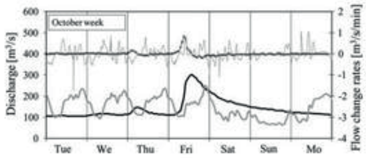

Hydropeaking, the sudden starting and stopping of turbines, lead to highly unsteady flow regimes in the river downstream of the restitution points of hydropower plants. Powerplants mainly operate during peak hours, when the selling price is at it's highest due to an important energy demand. Therefore a restrictive turbine mode, which would efficiently reduce the hydropeaking effect, would not be an economically nor and energy efficient or sustainable option for the operating company. The strict restrictions in these up and down surges (hydropeaking) can be controlled either with construction measures before the water is released, either by morphological features in the river itself or combining both. This work aims at assessing the contribution of different geomorphic river features in attenuating the hydropeaking effects. The Hasliaare, river in the Canton of Bern, operated by KWO, is analysed and used as a benchmark for other Alpine rivers. It's morphology is varied and therefore adequate for this analysis.

Method

Our *scientific hypothesis* is that varied river morphology is more prone to attenuate hydropeaking up-/down-ramps, in particular if it provides for lateral inundation, water storage and therefore somewhat delayed wave routing. Testing this hypothesis is done through the following methodology:

1. Establish a 2D river model (Figure 1)
2. Through field measurements, calibrate the model and then let hydrographs pass through the model to obtain the variation in the hydrograph, assessing the contribution of different geomorphic features.
3. Compare the present attenuation factors (lumped factors per each section, see below) with observed attenuation for variable discharges.

Following first field tests carried out in 2008/09 [2] between Innertkirchen and the Lake of Brienz, *lumped attenuation factors* (one value per river cross section for all discharges) have been obtained with the methodology presented below (applies to all three places if not mentioned otherwise).

Input hydrographs (modified for Meiringen, probably due to an unstable section)
↓
Adjusting baseflow to the estimated values
↓
Adjusting high discharges in respect to sub catchment areas
↓
Imposing a maximal up-ramping rate
↓
Imposing a minimal down-ramping rate
↓
Calculate mean up- and down-ramping rates

Figure 1: Resulting mesh from groin field with a DTM recording with a vertical exaggeration factor of 3; 3D mesh representation done with Basement (dry bed).

Figure 2: Aerial photo of the river reach of figure 1 (Flow rate estimated at 17 m³/s).

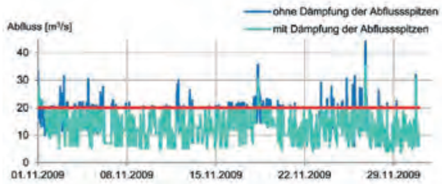

Figure 3: Attenuation due to the compensation basin (Limnex, 2009).

Results

A preliminary attempt to assess wave attenuation in the groin field reach is done using Meile's attenuation parameter for macro-roughness elements in a prismatic channel [1]. This method can only be applied to real size channels with certain restrictions, such as geometric ratios of the macro-roughness elements and the flow regime; It applies when groins are not submerged. Applying such methodology to the Innertkirchen groin field reach (figure 4) indicates that attenuations of up to 40% of the wave height can be obtained in the main channel within 400 m, and up to 20% in few dozen meters at the upstream side of the river reach, as shown in the graph 1 below. This results set a (state-of-the-art) reference for future analysis, which includes numerical modelling and field tests.

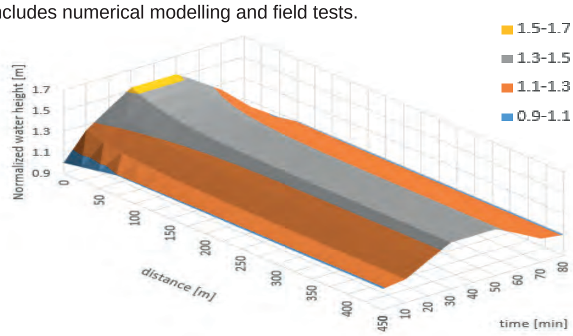

Graph 1: Hydrograph going through a groin field in a prismatic channel, without taking into account the time the wave takes to travel the distance. (Normalized water height: water height of the wave divided by the normal water height)

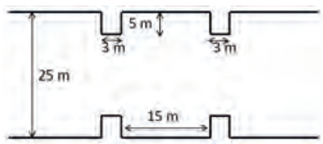

Figure 4: Idealized geometry of the river reach used to obtain the results from graph 1.

Outlook

The output of the work is to develop a methodology and a tool to characterise the spatial variation of hydropeaking mitigation as a function of the travelling distance and of a riverbank configuration.
Furthermore, we aim at adapting the current attenuation assessment methods expressed in terms of discharge variation into water levels variations instead.

References

[1] Meile, T. (2007). Influence of macro-roughness of walls on steady and unsteady flow in a channel.
[2] Limnex (2009): Schwall-Sunk in der Hasliaare. Gewässerökologische Untersuchung con Hasliaare und Lütschine und Beurteilung der Schwall-Auswirkungen in je zwei Strecken un Szenarien. Bericht im Auftrag der KWO (Baumann P., Wächter K. and Vogel U.)
[3] Meier P., Manso P., Bieri M. Schleiss A., Schweizer S., Fankhauser A., Schwegler B. (2016) "Hydro-peaking mitigation measures: performance of a complex compensation basin considering future system extensions", Conference Hydro 2016 Montreux.

We acknowledge KWO team, for the great help with the work and the very usefull documents.

SCCER SoE

SWISS COMPETENCE CENTER for ENERGY RESEARCH
SUPPLY of ELECTRICITY

SCCER-SoE Annual Conference 2017

In cooperation with the CTI
Energy
Swiss Competence Centers for Energy Research
Swiss Confederation
Commission for Technology and Innovation CTI

Augmentation de la flexibilité d'exploitation d'aménagements hydroélectriques de haute-chute au fil de l'eau en Valais

Grégory MORAND, Nicolas ADAM[1], Pedro MANSO[1], Anton J. SCHLEISS[1]
[1] Laboratoire de Constructions Hydrauliques (LCH), Ecole Polytechnique Fédérale de Lausanne (EPFL), Station 18, CH-1015 Lausanne

Introduction

En Suisse et ailleurs dans les Alpes, plusieurs aménagements hydroélectriques de haute chute fonctionnent sans retenue amont. Cela oblige à turbiner les apports captés au fil de l'eau par manque de capacité de stockage. Il n'est donc pas possible d'adapter la production hydroélectrique selon la demande. En hiver, les débits d'apport des rivières alpines sont largement inférieurs au débit équipé. Il arrive parfois même qu'il ne soit plus possible de turbiner tant les débits sont faibles. Le but de ce projet est donc de trouver des solutions innovatrices permettant d'exploiter ces aménagements en hiver.

Méthodologie

L'augmentation de la flexibilité d'exploitation passe par l'utilisation de volumes de stockage intra-journalier (dessableur, galerie en charge, galerie d'accès). La recherche de ces volumes se fait de manière systématique.

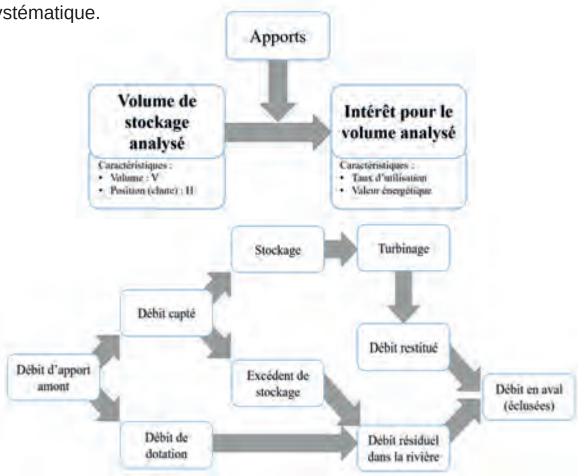

Résultats

Six modules de stockage ont été identifiés. On les combine de manière progressive en ajoutant aux modules déjà utilisés un nouveau module.

Modules	Volume [m³]	Volume cumulé [m³]
Galerie en charge 1/3	3075	3075
Galerie en charge 2/3	3075	6150
Galerie en charge 3/3	3075	9225
Dessableur	2355	11580
Galerie d'accès	609	12189
Stockage extérieur (barrage-mobile)	4795	16984

Le graphe ci-dessous montre la hauteur de chute en fonction du volume ainsi que le coefficient énergétique de chaque combinaison de modules.

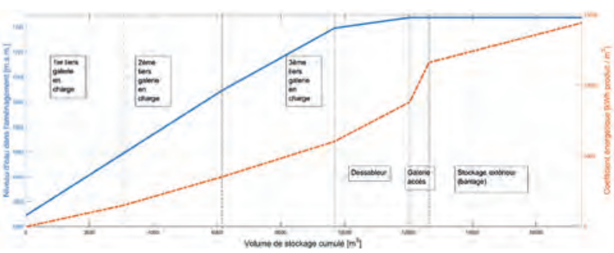

Cas d'étude : Kraftwerk Rhône-Oberwald (KWRO)

Cet aménagement hydroélectrique au fil de l'eau est situé sur le Rhône entre les villages de Gletsch et d'Oberwald en Valais.

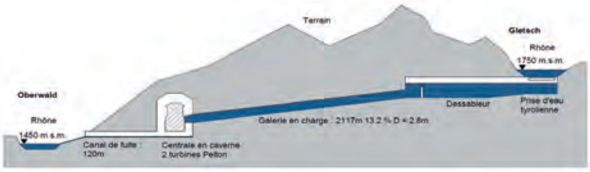

• Chute brute	287.85 m
• Débit nominal	5.7 m³/s
• Puissance installée	14.4 MW
• Puissance annuelle moyenne	4.6 MW (reçoit la RPC)
• Production annuelle prévue	39 GWh

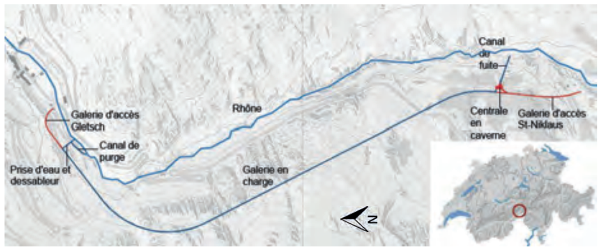

Discussions

D'après les résultats obtenus, les modules de stockage les plus intéressants d'un point de vue économique et flexibilité sont :

1. Dessableur : bon rendement économique de par sa hauteur de chute constante (grande valeur énergétique) et faibles investissements nécessaires.
2. Galerie en charge inclinée : valeur énergétique plus faible que celle de autres modules mais grand volume de stockage, ce qui rend l'exploitation plus flexible. Investissements faibles.

La galerie d'accès et le barrage mobile ont une grande valeur énergétique mais leur rentabilité économique est moins bonne.

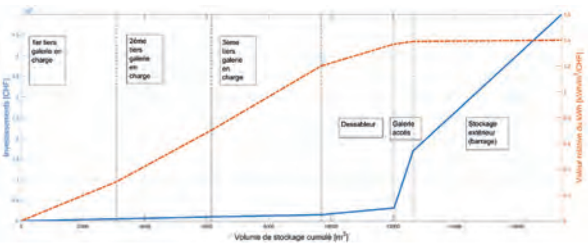

Conclusion

La démarche entreprise peut également s'appliquer à d'autres aménagements de haute chute au fil de l'eau (en Suisse, 175 petites centrales de puissance entre 1 et 30 MW avec des débits inférieurs à 5 m³/s) [WASTA, 2015]. Les modes d'exploitation flexible appliqués au cas d'étude permettent d'augmenter de 169% la production d'électricité hivernale de KWRO, ce qui équivaut à 2.8% de la production annuelle (gain de 1.09 GWh par an).

Enfin, ce type de projet s'inscrit parfaitement dans la stratégie énergétique suisse et dans le marché d'un futur proche sans RPC où l'énergie de pointe sera fortement valorisée. Ce type d'aménagement est aussi appelé à remplir de nouvelles fonctions comme la stabilisation du réseau.

SCCER SoE
SWISS COMPETENCE CENTER for ENERGY RESEARCH
SUPPLY of ELECTRICITY

SCCER-SoE Annual Conference 2017

In cooperation with the CTI
Energy
Swiss Competence Centers for Energy Research
Swiss Confederation
Commission for Technology and Innovation CTI

SmallFlex: Demonstrator for flexible Small Hydropower Plant

C. Münch[1], P. Manso[2], C. Weber[3], M. Staehli[4], M. Schmid[3], C. Nicolet[6], F. Avellan[5], A. Schleiss[2], J. Derivaz[7]

1 HES SO Valais, School of Engineering, Hydroelectricity Group, Sion ; 2 EPFL, Laboratory of Hydraulic Constructions, Lausanne ;
3 EAWAG, Department of Surface Water – Research and Management, Kastanienbaum ; 4 WSL, Birmensdorf ;
5 EPFL Laboratory for Hydraulic Machines, Lausanne ; 6 Power Vision Engineering Sàrl, Ecublens ; 7 FMV, Sion

Context

The current project is integrated in the activities of the SCCER-SoE, which include for the period 2017-2020 **a demonstrator on small hydropower schemes** (SHPs). Small hydropower plants are expected to provide a large share of the production increase planned in the 2050 energy transition strategy.

Summary

The aim of this project is to investigate how small-hydropower plants (SHP) can provide winter peak energy and ancillary services, whilst remaining eco-compatible.

The outcome of recent research by SCCER-SoE partners will be applied to a pilot facility provided by FMV with the goal of providing operational flexibility to the SHP owner and therefore harvest additional revenues.

The addition of flexibility will be done by testing infrastructure and equipment or operational adaptation measures, assessing their impact in terms of outflows, electricity output and revenues.

The lessons learned from this Demonstrator will be publically presented and used as a benchmark for the SHP sector.

Project activities & organisation

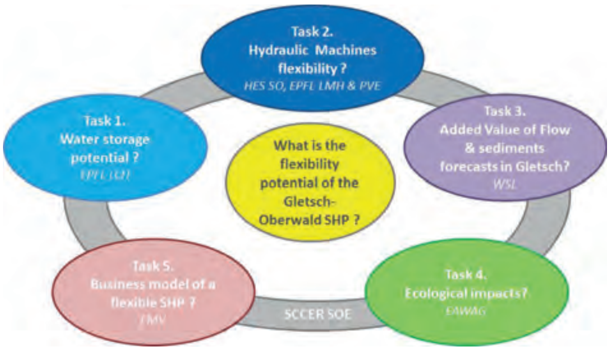

Overarching questions

- How can intra-day, intra-week or intra-monthly storage be added to a given run-of-the-river scheme, on the headrace side, on the tailrace side or both, in order to allow the scheme to generate peak energy and eventually contribute to grid regulation?
- What are the consequences of enlarging the operational range of the Pelton turbines in case of large head variations ?
- What's the added value of short and extended range inflow forecasts in Gletsch for the flexible operation of the new HP plant and for the management of sediments at the basins of decantation?
- What are the effects of short-term hydropeaks/ inter-dial fluctuations in discharge on the structure and function of alpine river ecosystems?
- What is the business model of the flexibility for small hydropower plants even in case of run-of-the-river plants with a priori small storage capacity?

Demonstrator site : The Gletsch-Oberwald SHP Project

With a installed discharge of 5.7 $m^3.s^{-1}$ and a net head of 288 m, this future SHP will produce 41 GWh with a mean gross capacity of 4.68 MW. The SHP is equipped with two Pelton turbines of 7 MW

1. **Zugangstollen Fassung** *Galerie d'accès à la prise d'eau*
2. **Installationsplätze Gletsch** *Place de chantier de Gletsch*
3. **Wasserfassung** *Prise d'eau*
4. **Triebwasserstollen** *Centrale souterraine*
5. **Zentrale unterirdisch** *Centrale souterraine*
6. **Rückgabestollen** *Galerie en charge*
7. **Zugangsstollen Zentrale** *Galerie d'accès à la centrale*
8. **Installationsplatz St. Niklaus** *Place de chantier de St. Niklaus*
9. **Umweltmassnahmen** *Mesures de compensation environnementale*
10. **Materialaufbereitung Kieswerk** *Valorisation des matériaux à la gravière*
11. **Ablagerung Grie** *Dépôt des matériaux*


Pictures of demonstrator site

Expected results

The methods developed in this project may be applicable to affect positively **several hundred high-head plants** with no or little storage, resulting in an annual revenue increase of 5-10% from increased value of the winter production. A small increase in energy production (< 5%) is foreseen, due to an improved use of excess waters at high-altitude intakes above the residual discharge releases.

Research partners :

FMV, HES-SO, EPFL, WSL, eawag aquatic research, Power Vision Engineering

SCCER SoE
SWISS COMPETENCE CENTER for ENERGY RESEARCH
SUPPLY of ELECTRICITY

SCCER-SoE Annual Conference 2017

In cooperation with the CTI
Energy
Swiss Competence Centers for Energy Research
Schweizerische Eidgenossenschaft
Confédération suisse
Confederazione Svizzera
Confederaziun svizra
Swiss Confederation
Commission for Technology and Innovation CTI

Demonstration of new solutions for an upcoming small alpine HP plant (Adont, Surses)

Manfred Stähli, Konrad Bogner, Michael Schirmer (WSL), Azin Amini (EPFL), Martin Klauenbösch (ewz)

Background

With the **aim** of testing new solutions for a productive and sustainable operation of new small HP plants (< 10 MW) *SCCER SoE* and *ewz* have started a joint research collaboration in central Grisons. Here, the implementation of a new diversion plant in the Adont-catchment (commune Surses) is in the planning stages. The case poses particular challenges as it is located in an inner-alpine area with relatively small amounts of precipitation and water demand for different purposes. In addition, the terrain is highly erosive requiring a smart sediment management.

Description of the planned small HP plant

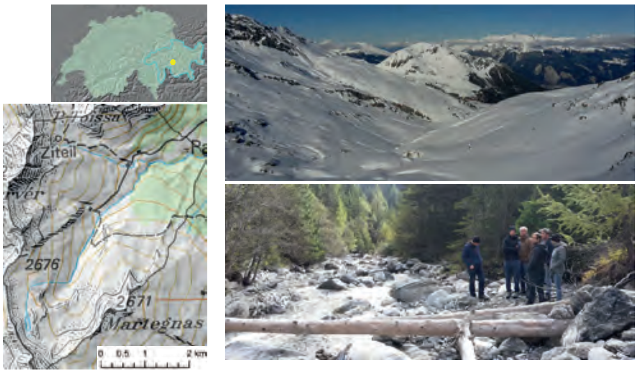

- Hydropower plant type: Run-of-the-river SHP (~3 MW, 11 GWh/a)
- Location: in the Adont-catchment, commune Surses, Grisons
- Small alpine catchment of 17 km², 1'500 – 2'700 m asl.
- Planned turbine : Peltonen (6 nozzles)

Current state of project implementation by ewz

- Construction permit has been obtained from commune and canton
- Depending on available feed-in remuneation at cost, tenders for implementation will be invited soon.

Research questions

Researchers and representatives from *ewz* have discussed and identified the following key-questions:

- Availability of water with current and future climate (special focus on specific extreme events)
- Short-term (<24 hours) forecasts of snowmelt and runoff for intra-day operation
- Winter-time operation (winter turbine?)
- Implication of the large erosion in the channel for the sediment management
- Synergies with other water users (snow production, meadow irrigation)

High resolution modelling of snow melt processes

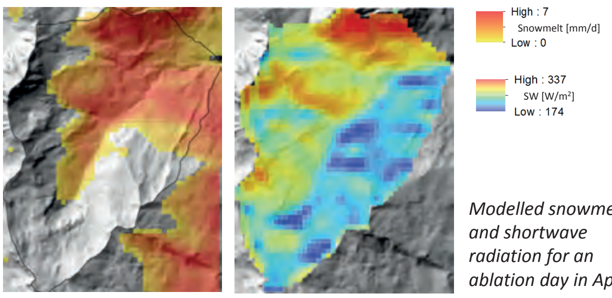

Modelled snowmelt and shortwave radiation for an ablation day in April

- Snow melt has a crucial role for the hydrology of this alpine catchment
- Resolving small-scale processes is mandatory to capture the spatial variability of snowmelt dynamics
- Allows for a realistic depiction of the amount and timing of runoff in small mountain catchments
- Outlook: Coupling with a weather generator (see related poster) and a gridded hydrological model for future runoff simulations

Flexible operation of a small HP plant with limited storage

To optimize the benefit of a small HP plant – both for the consumers and the producer – it could be an option to store the water during some hours of the day with low electricity demand and turbine it during hours of peak demand. Such a flexible operation requires a) an operational hydrological forecast system that predicts the water inflow of the coming few hours at very high accuracy, and b) storage capacities.

Operational hydrological forecast system

A well-established hydrological model (PREVAH) has been set up for the Adont catchment. The model uses a digital terrain model at a resolution of 200 m to represent the alpine topography and hourly meteorological input fields to simulate within-day variability in runoff. The forecast system will be run in real-time to facilitate the intra-day management of the plant. In addition, it will be used for calculating the climate change impact on the water availability in this catchment.

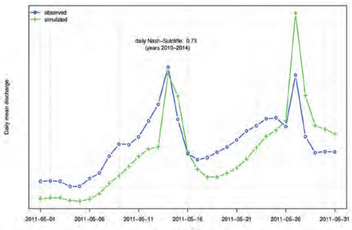

Example of the results of the model calibration with daily resolution for one month and 200m spatial resolution

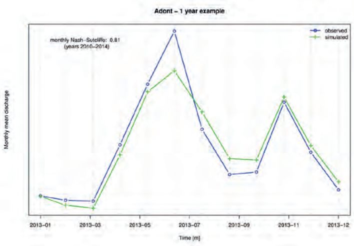

First results of the model calibration for one year of monthly aggregates and 200m spatial resolution

Storage capacities

Similar to many other small run-of-the river HP plants, no reservoir is available, and consequently the water cannot be retained easily. This issue can mainly lead to decrease of power generation during times when available flow is less than minimum design flow. From mid-November to the beginning of April the river discharge is very low and accordingly difficult to be turbined. However, by providing intra-day storage capacity, the water can be stocked, and HP operation can be launched once a certain volume of water is available.

To this end, the following possibilities can be considered:

1. Modification of hydraulic structures (e.g. penstock, sand trap, access gallery to the sand trap or headrace channel) and using them for water storage.
2. Building an external basin close to the water intake
3. Constructing a small dam at the intake place

Different storage/operation cycles will be simulated and compared in order to achieve the optimal solution.
However, providing the extra storage capacity is costly and needs extra investment. Furthermore, using the hydraulic structures to retain water may increase the risk of damage for such structures. The following points will therefore be considered thoroughly:

- Constructive modifications and investment increase;
- Eventual need for changing the concession;
- Risk of air entrainment into the penstock;
- Risk of sediment entrainment into the penstock;
- Operational range of the machines (variable head);
- Environmental impacts;

In view of the elevated altitude of the catchment special attention will be paid to the risk of water freezing in the penstock or other structures.

(Note: The consideration of a small dam at the intake location has not been put forward by ewz, and there are no plans for implementation.)

Academic Research Partners

Cooperation Partners